

Bahman Zohuri

Heat Pipe Design and Technology

Modern Applications for Practical
Thermal Management

Second Edition

 Springer

Heat Pipe Design and Technology

Bahman Zohuri

Heat Pipe Design and Technology

Modern Applications for Practical Thermal
Management

Second Edition



Springer

Bahman Zohuri
Galaxy Advanced Engineering, Inc.
Albuquerque, NM, USA

ISBN 978-3-319-29840-5 ISBN 978-3-319-29841-2 (eBook)
DOI 10.1007/978-3-319-29841-2

Library of Congress Control Number: 2016932886

© Springer International Publishing Switzerland 2011, 2016

This work is subject to copyright. All rights are reserved by the Publisher, whether the whole or part of the material is concerned, specifically the rights of translation, reprinting, reuse of illustrations, recitation, broadcasting, reproduction on microfilms or in any other physical way, and transmission or information storage and retrieval, electronic adaptation, computer software, or by similar or dissimilar methodology now known or hereafter developed.

The use of general descriptive names, registered names, trademarks, service marks, etc. in this publication does not imply, even in the absence of a specific statement, that such names are exempt from the relevant protective laws and regulations and therefore free for general use.

The publisher, the authors and the editors are safe to assume that the advice and information in this book are believed to be true and accurate at the date of publication. Neither the publisher nor the authors or the editors give a warranty, express or implied, with respect to the material contained herein or for any errors or omissions that may have been made.

Printed on acid-free paper

This Springer imprint is published by Springer Nature
The registered company is Springer International Publishing AG Switzerland

*This book is dedicated to my wife Firouzeh,
my daughters Natasha and Natalie, and son
Sasha*

*I am also dedicating this book to my mother
Marzieh and father Akbar
without their individual encouragement, this
book would not have been written.*

Preface for the Second Edition

Now that the second edition of this book is out, the reader will need to know additional information and improvements that are in this edition. First of all, the errors found in the first edition were corrected and certain sections were eliminated when there was no need for them based on the input from kind readers such as Mahboobe Mahdavi and Saeed Tiari.

A complete section was added to Chap. 4 entitled “Heat Pipe Applications in Thermal Energy Storage Systems” including all the subsections, which were graciously provided by Mahboobe Mahdavi and Saeed Tiari of the Mechanical Engineering Department of Temple University at Philadelphia, Pennsylvania, where further applications of heat pipes are identified along with Concentrated Solar Power (CSP) system. CSP recently has shown a great potential as part of renewable energy infrastructure.

The heat pipe is one of the remarkable achievements of thermal physics and heat-transfer engineering in this century because of its unique ability to transfer heat over large distances without considerable losses. The main applications of heat pipes deal with the problems of environmental protection and energy and fuel savings.

Heat pipes have emerged as an effective and established thermal solution, particularly in high heat flux applications and in situations where there is any combination of non-uniform heat loading, limited airflow over the heat-generating components, and space or weight constraints. This book will briefly introduce heat pipe technology and then highlight its basic applications for passive thermal control.

After a review of heat and mass transfer theory relevant to heat pipe performance, mathematical models are developed for calculating heat-transfer limitations of high-temperature heat pipes and heat-transfer limitations and temperature gradient of low-temperature heat pipes. Calculated results are compared with the available experimental data from various sources to increase confidence in the present mathematics models.

For the convenience of the users of the present theory, a few computer codes and their application are mentioned and they are available from Galaxy Advanced Engineering, Inc. These codes are designed to handle interactive input from users of the codes, and two computer programs for high- and low temperature heat pipes respectively are reported. These programs enables the performance of wrapped-screen heat pipes, rectangular-groove heat pipes, or screen-covered rectangular-groove wick to be predicted. These codes are especially helpful in design of steady-state heat pipe and are executable on Window/PC computing platforms.

Additionally, whenever the author finds the need to understand the basic physics and mathematics and for those readers to refresh their knowledge, sections of Wikipedia are presented in this book to further clarify certain complexities and advanced approaches for different equations and description of various topics on physics of fluid mechanics, heat transfer, and gas dynamics.

Heat pipe technology is pertinent to the design and application of self-controlled, variable conductance heat pipes for spacecraft thermal control is discussed. Investigations were conducted to (1) provide additional confidence in existing design tools, (2) to generate new design tools, and (3) to develop superior variable conductance heat pipe designs. A computer program for designing and predicting the performance of the heat pipe systems was developed.

Within this book a comprehensive review and analysis of all aspects of heat pipe technology pertinent to the design of self-controlled, variable conductance devices for spacecraft thermal control is also presented. Subjects considered include hydrostatics, hydrodynamics, heat transfer into and out of the pipe, fluid selection, materials compatibility, and variable conductance control techniques. Also included is a discussion of VCHP design techniques.

A variable-conductance heat pipe system (VCHPS) and its design have been discussed, and various references have been identified for further information to provide a thermal control for a transmitter experiment package (TEP) to be flown on the Communications Technology Satellite. The VCHPS provides heat rejection during TEP operation and minimizes the heat leak during power down operations. The VCHPS described features a unique method of aiding priming of arterial heat pipes and a novel approach to balancing heat pipe loads by staggering their control ranges.

This book introduces operational and design principles for heat pipes. A heat pipe is essentially a passive device that can quickly transfer heat from one point to another. They are often referred to as the “superconductors” of heat as they possess an extraordinary heat-transfer capacity and rate with almost no heat loss. The heat transferred from the hot source evaporates the fluid in the wick, causing the vapor to expand into the center core of the heat pipe. The latent heat of vaporization is carried with the vapor to the cold end of the tube, where it is removed by transference to the heat sink as the vapor condenses. The condensate is then carried back in the wick to the hot end of the tube by capillary action and by gravity (if the tube is tilted from the horizontal), where it is recycled. This two-phase heat-transfer mechanism results in heat-transfer capabilities from 100 to several thousand times that of an equivalent piece of copper.

The heat pipe is compact and efficient because (1) the finned-tube bundle is inherently a good configuration for convective heat transfer in both ducts and (2) the evaporative-condensing cycle within the heat pipes is a highly efficient method of transferring heat internally.

The effects of different factors on the performance of the heat pipe—compatibility of materials, operating temperature range, diameter, power limitations, thermal resistances, and operating orientation— will be considered in the book.

Heat pipes can be designed to operate over a very broad range of temperatures from cryogenic (less than 30 K) applications to high temperature systems (more than 2000 K). Until recently, the use of heat pipes has been mainly limited to space technology due to its cost-effectiveness and complex wick construction. There are several applications of heat pipes in this field, such as spacecraft temperature equalization component cooling, temperature control, and radiator design in satellites. Currently heat pipe technology has been integrated into modern thermal engineering designs, such as terrestrial thermal control systems, solar energetic, etc.

The increasing power and shrinking size of electronic components presents growing thermal management challenges. While solid metal conductors such as aluminum extrusions may provide acceptable cooling for individual components in certain situations, broad-level solutions with more advanced cooling technologies are needed in a growing number of applications.

After a review of heat and mass transfer theory, relevant to heat pipe performance, math models are developed for calculating heat-transfer limitations of high-temperature heat pipes and heat-transfer limitations and temperature gradient of low-temperature heat pipes. Calculated results are compared with the available experimental data from various sources to increase confidence in the present math models.

For the convenience of the users of the present theory, complete listings of two computer programs for high- and low-temperature heat pipes respectively are appended to the book.

These programs enables the performance of wrapped-screen heat pipes, rectangular-groove heat pipes, or screen-covered rectangular-groove wick to be predicted.

Few more computer programs are also mentioned, and some are obtainable either from US government organization or from Galaxy Advanced Engineering, Inc. or from other commercial companies that help in the design of steady-state heat pipe and, most of them, are executable on Window/PC computing platform. These codes are additional help for readers to calculate working fluid properties. They also assist heat-transfer analysis for design of fins for both constant and variable heat pipes. In addition, Excel spreadsheets that evaluate analytical solutions of four view factor geometries (perpendicular and rectangular shape with a common edge, coaxial parallel disks, coaxial cylinders, and aligned parallel rectangles) may be downloaded from Galaxy Advanced Engineering website at www.gaeinc.com, please contact this company.

A variable-conductance heat pipe system (VCHPS) has been designed to provide thermal control for a transmitter experiment package (TEP) to be flown on the

Communications Technology Satellite. The VCHPS provides for heat rejection during TEP operation and minimizes the heat leak during power down operations. The VCHPS described features a unique method of aiding priming of arterial heat pipes and a novel approach to balancing heat pipe loads by staggering their control ranges.

This book introduces operational and design principles for heat pipes. A heat pipe is essentially a passive device that can quickly transfer heat from one point to another. They are often referred to as the “superconductors” of heat as they possess an extraordinary heat-transfer capacity and rate with almost no heat loss. The heat transferred from the hot source evaporates the fluid in the wick, causing the vapor to expand into the center core of the heat pipe. The latent heat of vaporization is carried with the vapor to the cold end of the tube, where it is removed by transference to the heat sink as the vapor condenses. The condensate is then carried back in the wick to the hot end of the tube by capillary action and by gravity (if the tube is tilted from the horizontal), where it is recycled. This two-phase-heat transfer mechanism results in heat-transfer capabilities from 100 to several thousand times that of an equivalent piece of copper.

The heat pipe is compact and efficient because (1) the finned-tube bundle is inherently a good configuration for convective heat transfer in both ducts and (2) the evaporative-condensing cycle within the heat pipes is a highly efficient method of transferring heat internally.

The effects of different factors on the performance of the heat pipe—compatibility of materials, operating temperature range, diameter, power limitations, thermal resistances, and operating orientation—will be considered in the lecture.

Heat pipes can be designed to operate over a very broad range of temperatures from cryogenic (less than 30 K) applications to high-temperature systems (more than 2000 K). Until recently, the use of heat pipes has been mainly limited to space technology due to its cost-effectiveness and complex wick construction. There are several applications of heat pipes in this field, such as spacecraft temperature equalization component cooling, temperature control, and radiator design in satellites. Currently, heat pipe technology has been integrated into modern thermal engineering designs, such as terrestrial thermal control systems, solar energetic, etc. The increasing power and shrinking size of electronic components presents growing thermal management challenges. While solid metal conductors such as aluminum extrusions may provide acceptable cooling for individual components in certain situations, broad-level solutions with more advanced cooling technologies are needed in a growing number of applications. Heat pipes have emerged as an effective and established thermal solution, particularly in high heat flux applications and in situations where there is any combination of non-uniform heat loading, limited airflow over the heat-generating components, and space or weight constraints. This lecture will briefly introduce heat pipe technology and then highlight its basic applications for passive thermal control.

Preface for the First Edition

The heat pipe is one of the remarkable achievements of thermal physics and heat transfer engineering in this century because of its unique ability to transfer heat over large distances without considerable losses. The main applications of heat pipes deal with the problems of environmental protection and energy and fuel savings.

Heat pipes have emerged as an effective and established thermal solution, particularly in high heat flux applications and in situations where there is any combination of non-uniform heat loading, limited airflow over the heat-generating components, and space or weight constraints. This book will briefly introduce heat pipe technology and then highlight its basic applications for passive thermal control.

After a review of heat and mass transfer theory, relevant to heat pipe performance, mathematical models are developed for calculating heat-transfer limitations of high-temperature heat pipes and heat-transfer limitations and temperature gradient of low-temperature heat pipes. Calculated results are compared with the available experimental data from various sources to increase confidence in the present mathematics models.

For the convenience of the users of the present theory, a few computer codes and their application are mentioned, and they are available at Galaxy Advanced Engineering, Inc. These codes are designed to handle interactive input from users of the codes, and two computer programs for high- and low-temperature heat pipes respectively are reported. These programs enable the performance of wrapped-screen heat pipes, rectangular-groove heat pipes, or screen-covered rectangular-groove wick to be predicted. These codes are especially helpful in the design of steady-state heat pipe and are executable on Window/PC computing platforms.

Additionally, wherever the author find the need to understand the basic physics and mathematics and for those readers to refresh their knowledge, an extra annotations boxes of text or sections are presented in this book, to further clarify certain complexity and advance approaches for different equations and description of various topics on physics of fluid mechanics, heat transfer, and gas dynamics.

Heat pipe technology pertinent to the design and application of self-controlled, variable-conductance heat pipes for spacecraft thermal control is discussed. Investigations were conducted to (1) provide additional confidence in existing design tools, (2) to generate new design tools, and (3) to develop superior variable-conductance heat pipe designs. A computer program for designing and predicting the performance of the heat pipe systems was developed.

Within this book, a comprehensive review and analysis of all aspects of heat pipe technology pertinent to the design of self-controlled, variable-conductance devices for spacecraft thermal control is also presented. Subjects considered include hydrostatics, hydrodynamics, heat transfer into and out of the pipe, fluid selection, materials compatibility, and variable-conductance control techniques. Also included is a discussion of VCHP design techniques.

A variable-conductance heat pipe system (VCHPS) and its design have been discussed, and various references have been identified for further information about thermal control for a transmitter experiment package (TEP) to be flown on the communications technology satellite. The VCHPS provides heat rejection during TEP operation and minimizes the heat leak during power down operations. The VCHPS described features a unique method of aiding priming of arterial heat pipes and a novel approach to balancing heat pipe loads by staggering their control ranges.

This book introduces operational and design principles for heat pipes. A heat pipe is essentially a passive device that can quickly transfer heat from one point to another. They are often referred to as the “superconductors” of heat as they possess an extraordinary heat-transfer capacity and rate with almost no heat loss. The heat transferred from the hot source evaporates the fluid in the wick, causing the vapor to expand into the center core of the heat pipe. The latent heat of vaporization is carried with the vapor to the cold end of the tube, where it is removed by transference to the heat sink as the vapor condenses. The condensate is then carried back in the wick to the hot end of the tube by capillary action and by gravity (if the tube is tilted from the horizontal), where it is recycled. This two-phase heat-transfer mechanism results in heat-transfer capabilities from 100 to several thousand times that of an equivalent piece of copper.

The heat pipe is compact and efficient because (1) the finned-tube bundle is inherently a good configuration for convective heat transfer in both ducts and (2) the evaporative-condensing cycle within the heat pipes is a highly efficient method of transferring heat internally.

The effects of different factors on the performance of the heat pipe—compatibility of materials, operating temperature range, diameter, power limitations, thermal resistances, and operating orientation—will be considered in the book.

Heat pipes can be designed to operate over a very broad range of temperatures from cryogenic (less than 30 K) applications to high-temperature systems (more than 2000 K). Until recently, the use of heat pipes has been mainly limited to space technology due to its cost-effectiveness and complex wick construction. There are several applications of heat pipes in this field, such as spacecraft temperature equalization, component cooling, temperature control, and radiator design in

satellites. Currently heat pipe technology has been integrated into modern thermal engineering designs, such as terrestrial thermal control systems, solar energetic, etc.

The increasing power and shrinking size of electronics components presents growing thermal management challenges. While solid metal conductors such as aluminum extrusions may provide acceptable cooling for individual components in certain situations, broad level solutions with more advanced cooling technologies are needed in a growing number of applications.

After a review of heat and mass transfer theory, relevant to heat pipe performance, math models are developed for calculating heat-transfer limitations of high-temperature heat pipes and heat-transfer limitations and temperature gradient of low-temperature heat pipes. Calculated results are compared with the available experimental data from various sources to increase confidence in the present math models.

For the convenience of the users of the present theory, complete listings of two computer programs for high- and low-temperature heat pipes respectively are appended to the report.

These programs enables the performance of heat pipes with wrapped screen, rectangular groove or screen-covered rectangular-groove wick to be predicted.

Few more computer programs are also mentioned, and some are obtainable either from US government organization or from Galaxy Advanced Engineering, Inc. or from other commercial companies that help design steady-state heat pipe, and most of them are executable on Window/PC computing platform. These codes are additional help for readers to calculate working fluid properties. They also assist heat-transfer analysis for design of fins for both constant and variable heat pipes. In addition, Excel spreadsheets that evaluate analytical solutions for four view factor geometries (perpendicular rectangles with a common edge, coaxial parallel disks, coaxial cylinders, and aligned parallel rectangles) may be downloaded from Galaxy Advanced Engineering Company Site. Please contact this company.

A variable-conductance heat pipe system (VCHPS) has been designed to provide thermal control for a transmitter experiment package (TEP) to be flown on the Communications Technology Satellite. The VCHPS provides for heat rejection during TEP operation and minimizes the heat leak during power down operations. The VCHPS described features a unique method of aiding priming of arterial heat pipes and a novel approach to balancing heat pipe loads by staggering their control ranges.

This lecture introduces operational and design principles for heat pipes. A heat pipe is essentially a passive device that can quickly transfer heat from one point to another. They are often referred to as the “superconductors” of heat as they possess an extraordinary heat-transfer capacity and rate with almost no heat loss. The heat transferred from the hot source evaporates the fluid in the wick, causing the vapor to expand into the center core of the heat pipe. The latent heat of vaporization is carried with the vapor to the cold end of the tube, where it is removed by transference to the heat sink as the vapor condenses. The condensate is then carried back into the wick to the hot end of the tube by capillary action and by gravity (if the tube is tilted from the horizontal), where it is recycled. This two-phase heat-transfer

mechanism results in heat-transfer capabilities from 100 to several thousand times that of an equivalent piece of copper.

The heat pipe is compact and efficient because (1) the finned-tube bundle is inherently a good configuration for convective heat transfer in both ducts and (2) the evaporative-condensing cycle within the heat pipes is a highly efficient method of transferring heat internally.

The effects of different factors on the performance of the heat pipe—compatibility of materials, operating temperature range, diameter, power limitations, thermal resistances, and operating orientation— will be considered in the lecture.

Heat pipes can be designed to operate over a very broad range of temperatures from cryogenic (less than 30 K) applications to high temperature systems (more than 2000 K). Until recently, the use of heat pipes has been mainly limited to space technology due to its cost-effectiveness and complex wick construction. There are several applications of heat pipes in this field, such as spacecraft temperature equalization, component cooling, temperature control, and radiator design in satellites. Currently heat pipe technology has been integrated into modern thermal engineering designs, such as terrestrial thermal control systems, solar energetic, etc. The increasing power and shrinking size of electronic components presents growing thermal management challenges. While solid metal conductors such as aluminum extrusions may provide acceptable cooling for individual components in certain situations, broad-level solutions with more advanced cooling technologies are needed in a growing number of applications. Heat pipes have emerged as an effective and established thermal solution, particularly in high heat flux applications and in situations where there is any combination of non-uniform heat loading, limited airflow over the heat-generating components, and space or weight constraints. This lecture will briefly introduce heat pipe technology and then highlight its basic applications for passive thermal control.

Albuquerque, NM, USA

Bahman Zohuri

Acknowledgment

I am indebted to the many people who aided, encouraged, and supported me beyond expectation. Some of those who are not around to see the end result of their encouragement, I hope they can see this acknowledgment. My many thanks go to Joe Rogers of NASA, one of my best friends who helped me with most of the computer codes that are presented in this book, to bring them to its present status from their legacy stages.

I am also indebted to Hal Brand of Lawrence Livermore National Laboratory, who also was there to provide assistance with my computer programming needs. I thank my other friends such as Dr. Patrick Burns of Colorado State University and Dr. David Glass of NASA Langley Research Center. They provided me with their research papers and computers codes. In addition, I acknowledge Leonardo Tower, the best person whom I got the honor of knowing during the write up of this book. He provided me with his newly developed computer code of the subject. My many thanks to Darryl Johnson, David Antoniuk, and Dr. Bruce Marcus of North Grumman (TRW), as well as to Mark North of Thermacore Incorporation. I appreciated most their seamless support, since they all had their own share of effort to publish this book and bring to this end.

I thank my other best friend William Kemp of Air Force Weapons Laboratory at Albuquerque, New Mexico, who is really a true friend and remains to be one. Finally my many thanks to Mrs. Tiffany Gasbarrini, senior editor of Mechanical, Aerospace, and Nuclear and Energy Engineering of Springer, who made all of this happen. Finally, I am also indebted to the individuals and organizations that granted permission to reproduce copyrighted materials and published figures.

I am also thankful to David Saunders of NASA Ames in the Aerothermodynamics Branch at ARC under contract to ELORET Corporation. He is always very supportive of me. I am also grateful to Mrs. Kimberly Hoffman of the Catholic University of America for her endless support in obtaining few documents from the works of Chi, which I needed so much.

I also take this opportunity to thank Mahboobe Mahdavi and Saeed Tiari for their valuable inputs to the improve the second edition of this book.

Above all, I offer very special thank to my mother, father while he was alive, wife, and children. They provided constant interest and encouragement, without which this book would not have been written.

Their patience with my many absences from home and long hours in front of computer during preparation of the manuscript is especially appreciated.

Contents

1	Basic Principles of Heat Pipes and History	1
1.1	Introduction	1
1.2	History	3
1.3	Description and Technology of Heat Pipes	4
1.4	Principle of Operation	16
1.4.1	Container	16
1.4.2	Working Fluid	16
1.4.3	Wicker or Capillary Structure	17
1.4.4	Sintered Power Metal	18
1.4.5	Grooved Tube	19
1.4.6	Wire Screen Mesh	19
1.5	How the Heat Pipe Is Working	20
1.5.1	Heat Pipe Assemblies Design Guidelines	21
1.5.2	Orientation with Respect to Gravity	23
1.5.3	Temperature Limits	23
1.5.4	Heat Removal	23
1.5.5	Reliability	23
1.5.6	Forming or Shading	24
1.5.7	Effects of Length and Pipe Diameter	24
1.5.8	Wick Structure	24
1.6	How Heat Pipe Works	25
1.7	Constraints	27
1.8	Lesson(s) Learned	32
1.9	Applications	33
1.10	Summary	37
	References	40
2	Heat Pipe Theory and Modeling	43
2.1	Heat Pipe Theory	43
2.2	Fundamental Considerations	44

- 2.3 Operating Characteristics of Heat Pipes 47
- 2.4 Operating Limits 50
- 2.5 Capillary Pressure Differences or Balance 50
 - 2.5.1 Normal Hydrostatic Pressure 60
 - 2.5.2 Axial Hydrostatic Pressure 61
 - 2.5.3 Capillary Pressure at the Liquid–Vapor Interface 61
- 2.6 Turbulent and Laminar Flow of the Vapor 64
- 2.7 One-Dimensional Two-Phase Flow 67
 - 2.7.1 What Is a Two-Phase Flow? 69
- 2.8 Flow Regime 69
- 2.9 Heat Transfer 71
- 2.10 Condensation of a Pure Vapor 75
- 2.11 Sonic Limit or Choking 76
 - 2.11.1 Sonic Limitation and Startup Problem of Heat Pipes 83
- 2.12 Entrainment Limit 84
- 2.13 Wicking/Capillary or Circulation Limit 88
 - 2.13.1 Liquid Pressure Drop 91
 - 2.13.2 Vapor Pressure Drop 96
 - 2.13.3 Capillary or Wick Limitation Analysis on Heat Transport 106
 - 2.13.4 Characteristic of Wick 112
 - 2.13.5 Single-Layer Wick 114
 - 2.13.6 Two-Layer Wick 115
 - 2.13.7 Artery Wick 116
 - 2.13.8 Monogroove Wick 118
 - 2.13.9 Variable Thickness Wick 120
 - 2.13.10 Wick Structure and How Does It Affect the Performance of the Heat Pipes 121
 - 2.13.11 Wick Structure for Low-Temperature and Higher Heat Transfer in Heat Pipes 122
 - 2.13.12 Effective Thermal Conductivity of Wick Structure 125
- 2.14 Boiling Limit 129
- 2.15 Viscous Limit 133
- 2.16 Condenser Limit 135
- 2.17 Transport Limitations 135
- 2.18 The Working Fluid 144
 - 2.18.1 The Operating Temperature Range 144
 - 2.18.2 Heat Transfer Requirements 144
 - 2.18.3 Expecting Body-Force Field 146
 - 2.18.4 Tolerance of Wick Structure to Boiling 146
 - 2.18.5 Conventional or Variable Conductance Heat Pipe 148
 - 2.18.6 Special Requirements 150
 - 2.18.7 Materials Compatibility and Stability 150

2.19	Heat Pipe Startup Characteristic and Control	152
2.19.1	Transient of Heat Pipe Startup Characteristic and Control	153
2.19.2	Normal Startup Characteristic	158
2.19.3	Frozen and Startup Characteristic	158
2.20	Summary	160
	References	163
3	Mathematical Modeling and Available Computer Codes	167
3.1	One-Dimensional Models	168
3.2	Overview of Heat Pipes	169
3.2.1	Selection of the Working Fluid	170
3.2.2	Selection of the Wick or Capillary Structure	171
3.2.3	Selection of the Container	173
3.3	Design Guide and Heat Pipe Selection Criteria	173
3.3.1	Fluid Inventory	178
3.3.2	Priming Heat Pipe	180
3.4	How to Select a Heat Pipe	182
3.5	What Materials Can Be Used to Construct a Heat Pipe	184
3.6	When to Consider a Heat Pipe	185
3.7	Things to Consider, When Designing a Heat Pipe	185
3.7.1	What the Four Heat Transport Limitations of a Heat Pipe Are	185
3.7.2	Heat Pipe Diameter	186
3.7.3	Heat Pipe Containers Design	189
3.7.4	Heat Pipe Material Selection	192
3.8	Entrainment and Boiling Limitations	195
3.9	What the Common Heat Pipe Wick Structure Is	201
3.9.1	Wick Design	202
3.10	Steady-State and Transient Regime	207
3.11	Heat Pipe Steady-State and Transient Analysis	209
3.11.1	Solution of the Steady-State Equation	220
3.11.2	Solution of the Transient Equation	225
3.12	Design Criteria and Constraints	228
3.12.1	Heat Source Characteristics	228
3.12.2	Heat Sink Characteristics	229
3.12.3	Heat Pipe Thermal Resistance	250
3.12.4	Effective Thermal Conductivity and Heat Pipe Temperature Difference	255
3.12.5	Heat Pipe Operating Environments	258
3.12.6	Wick Structures	261
3.12.7	Multicomponent Fluids	262
3.12.8	Maximum Heat Flux	266
3.12.9	Size and Weight Constraints	268
3.12.10	Temperature Constraints	269

3.12.11	Fabrication and Cost Constraints	269
3.12.12	Heat Pipe Area–Temperature Relations	270
3.12.13	Heat Pipe Manufacturing	275
3.13	Optimal Heat Pipes	279
3.14	Design Examples	282
3.15	Computer Codes for Designing Heat Pipes	285
3.15.1	SINDA/FLUINT Computer Codes for Loop Heat Pipe Analysis	286
3.15.2	LERCHP NASA Glenn Steady-State Heat Pipe Code	293
3.15.3	Los Alamos (HTPIP) Steady-State Heat Pipe Analysis Program Codes	296
3.15.4	ANLHTP: A Computer Code for the Simulation of Heat Pipe Operation	297
3.15.5	Heat Pipe Fluid (HPF) Properties Program	299
3.15.6	Groove Analysis Program (GAP) Computer Program	300
3.15.7	GASPIPE 2 Computer	301
3.15.8	Computer Program GRADE	302
3.15.9	Extended Development of Variable Conductance Heat Pipes	303
3.15.10	SODART Program	303
3.16	Computer Codes for Heat Transfer and Fin Designs and Materials Composite	305
3.16.1	Existing Computer Codes	306
3.16.2	TOPAZ2D Finite Element Computer Codes and Its Pre- and Post-processors	306
3.16.3	TOPAZ3D Finite Element Computer Codes and Its Pre- and Post-processors	307
3.16.4	FACET Computer Code	308
3.16.5	MONTE2D Computer Code	309
3.16.6	MONTE3D Computer Code	311
3.16.7	VIEW Radiation View Factor Computer Code	312
3.16.8	ALE3D (Arbitrary Lagrange/Eulerian Multiphysics 3D) Computer Code	313
3.16.9	NASTRAN Computer Code	317
3.16.10	NASA TRASYS Computer Code	318
3.17	Piping Stress Analysis Software	319
3.17.1	Piping Stress Analysis Software Availability	320
3.18	Other Heat Pipe Analysis Codes	320
3.18.1	VCHPDA: A Computer Program Subroutine Usage Code	321
3.18.2	HPMAIN Computer Code	322

3.18.3	SMLBUB Spherical Bubble Model Computer Program	323
3.19	COMSOL Multiphysics Software	326
3.19.1	COMSOL Multiphysics Software Availability	331
	References	331
4	Application of Heat Pipe in Industry	335
4.1	Application of Heat Pipe in Industry	335
4.2	Overview	337
4.2.1	Cooling of Electronic Components	339
4.2.2	Spacecraft	340
4.2.3	Energy Conservation	340
4.2.4	Heat Pipe Heat Exchanger	340
4.2.5	Preservation of Permafrost	341
4.2.6	Snow Melting and Deicing	341
4.2.7	Heat Pipe Inserts for Thermometer Calibration	341
4.2.8	High-Temperature Heat Pipe Furnace	342
4.2.9	Miscellaneous Heat Pipe Applications	343
4.3	Energy-Dependent Boundary Equations	343
4.4	Heat Pipe in Space	345
4.4.1	Radioisotope Systems	347
4.4.2	Fission Systems: Heat	348
4.4.3	Fission Systems: Propulsion	349
4.4.4	Heat Pipe Power System	350
4.4.5	Space Reactor Power Systems	351
4.4.6	Project Prometheus 2003	351
4.5	Space Shuttle Orbiter Heat Pipe Applications	354
4.6	Heat Pipe in Electronics	356
4.7	Heat Pipe in Defense and Avionics	359
4.7.1	On the Ground	360
4.7.2	On the Sea	361
4.7.3	In the Air	362
4.7.4	In Space	362
4.8	Heat Pipe as Heat Exchanger	363
4.9	Heat Pipe in Residential Building	366
4.10	Heat Pipe Applications in Thermal Energy Storage Systems	368
4.10.1	Energy Storage Methods	369
4.10.2	Latent Heat Thermal Storage Materials	371
4.10.3	PCM Classification	372
4.10.4	Latent Heat Thermal Energy Storage Systems Assisted by Heat Pipes	374
	References	392
5	Heat Pipe Manufacturing	395
5.1	Manufacturing of Heat Pipes	395
5.1.1	Envelope	396
5.1.2	End Cap	397

- 5.1.3 Fill Tube 399
- 5.1.4 Wick 399
- 5.1.5 Working Fluid 401
- 5.2 Heat Pipe Manufacturing Procedures 401
- 5.3 Cleaning of Parts 402
- 5.4 Assembly of Heat Pipes 408
 - 5.4.1 Summary of Assembly of Heat Pipes Procedures 413
- 5.5 Evacuation and Charging 416
 - 5.5.1 Fluid Charging 418
 - 5.5.2 Fluid Purity and Inventory 418
 - 5.5.3 Analysis of Gas Blockage 420
 - 5.5.4 Effect of Heat Pipe Design and Operating Conditions on Gas Blockage 422
- 5.6 Full Tube Closure 427
- 5.7 Heat Pipe Testing Techniques 427
 - 5.7.1 Mechanical Sounders 427
 - 5.7.2 Wick Wetting 428
 - 5.7.3 Performance Versification 428
- References 430
- 6 Other Types of Heat Pipes 431**
 - 6.1 Other Types of Heat Pipes 431
 - 6.2 Thermosyphon 432
 - 6.3 Loop Heat Pipes/Capillary Pumped Loop 433
 - 6.4 Pulsating Heat Pipes 433
 - 6.5 Micro-heat Pipes (MHPs) 435
 - 6.6 Constant Conductance Heat Pipes (CCHPs) 439
 - 6.7 Variable Conductance Heat Pipes (VCHP) 439
 - 6.7.1 Variable Conductance with Gas-Loaded Heat Pipes 443
 - 6.8 Rotating and Revolving Heat Pipes 444
 - 6.9 High-Temperature Heat Pipes (Liquid-Metal Heat Pipes) 444
 - 6.10 Cryogenic Heat Pipes 446
 - References 448
- Erratum E1**
- Appendix A: Dimensional Equivalents and Physical Constants 451**
- Appendix B: Properties of Solid Materials 453**
- Appendix C: Properties of Fluids 461**
- Appendix D: Different Heat Pipe Design Examples 479**
- Index 511**

About the Author

Dr. Bahman Zohuri is currently at the Galaxy Advanced Engineering, Inc., a consulting company that he started himself in 1991 when he left both semiconductor and defense industries after many years working as a chief scientist. After graduating from the University of Illinois in the field of physics and applied mathematics and the University of New Mexico's nuclear engineering department, he joined Westinghouse Electric Corporation where he performed thermal-hydraulic analysis and natural circulation for inherent shutdown heat removal system (ISHRS) in the core of a liquid metal fast breeder reactor (LMFBR) as a secondary fully inherent shut system for secondary loop heat exchange. All these designs were used for Nuclear Safety and Reliability Engineering for Self-Actuated Shutdown System. At around 1978, he designed the mercury heat pipe and electromagnetic pumps for large pool concepts of LMFBR for heat rejection purpose for this reactor, where he received a patent for it. He later on, he was transferred to defense division of Westinghouse, where he was responsible for the dynamic analysis and method of launch and handling of an MX missile out of canister. The results are applied to MX launch seal performance and muzzle blast phenomena analysis (i.e., missile vibration and hydrodynamic shock formation). He also was involved in analytical calculation and computation in the study of Nonlinear Ion Wave in Rarefying Plasma. The results are applied to the propagation of "soliton wave" and the resulting charge collector traces, in the rarefaction characteristic of the corona of a laser-irradiated target pellet. As part of his graduate research work at the Argonne National Laboratory, he performed computation and programming of multi-exchange integral in surface physics and solid-state physics. He holds different patent in areas such as diffusion processes and design of diffusion furnace while he was a senior process engineer working for different semiconductor industries such as Intel, Varian, and National Semiconductor. Later on, he joined Lockheed Missile and Aerospace Corporation as a senior chief scientist and was responsible for the research and development (R&D), the study of vulnerability, survivability, and both radiation and laser hardening of different components of the Strategic Defense Initiative, known as Star Wars. This is

comprised of a payload (i.e., IR Sensor) for Defense Support Program (DSP), Boost Surveillance and Tracking Satellite (BSTS), and Space Surveillance and Tracking Satellite (SSTS) against laser or nuclear threat. While in there, he also studied and performed the analysis of characteristics of laser beam and nuclear radiation interaction with materials, transient radiation effects in electronics (TREE), electromagnetic pulse (EMP), system-generated electromagnetic pulse (SGEMP), single-event upset (SEU), blast and thermomechanics, hardness assurance, maintenance, and device technology.

He did few years of consulting under his company Galaxy Advanced Engineering, Inc., with Sandia National Laboratories (SNL), where he was supporting development of operational hazard assessments for the Air Force Safety Center (AFSC) in connection with other interest parties. Intended use of the results was their eventual inclusion in Air Force Instructions (AFIs) specifically issued for Directed Energy Weapons (DEW) operational safety. He completed the first version of a comprehensive library of detailed laser tools for Airborne Laser (ABL), Advanced Tactical Laser (ATL), Tactical High-Energy Laser (THEL), Mobile/Tactical High-Energy Laser (M-THEL), etc.

He also was responsible on SDI computer programs involved with Battle Management C³ and artificial intelligence and autonomous system. He is author of few publications and holds various patents such as Laser Activated Radioactive Decay and Results of Thru-Bulkhead Initiation.

Recently he has published one book with CRC and Francis Taylor and seven books with Springer on the following subjects:

1. Heat Pipe Design and Technology: A Practical Approach 1 edition, Published by CRC Publishing Company, 2011, First Edition.
2. *Dimensional Analysis and Self-Similarity Methods for Engineering and Scientist*, published by Springer Publishing Company.
3. *High Energy Laser (HEL): Tomorrow's Weapon in Directed Energy Weapons Volume I*, Published by Trafford Publishing Company.
4. *High Energy Laser (HEL): Tomorrow's Weapon in Directed Energy Weapons Volume II*, published by Trafford Publishing Company.
5. *Thermodynamics In Nuclear Power Plant Systems*, published by Springer Publishing Company.
6. *Thermal-Hydraulic Analysis of Nuclear Reactors*, published by Springer Publishing Company.
7. *Application of Compact Heat Exchangers for Combined Cycle Driven Efficiency in Next Generation Nuclear Power Plants: A Novel Approach*, published by Springer Publishing
8. *Nuclear Energy for Hydrogen Generation through Intermediate Heat Exchangers: A Renewable Source of Energy* 1st ed. 2016 Edition, published by Springer Publishing Company.
9. *Directed Energy Weapons: Physics of High Energy Lasers (HEL)*, Springer Publisher 2016

Purpose

A detailed overview of heat pipes is presented in this book, including a historical perspective, principles of operations, types of heat pipes, heat pipe performance characteristics, heat pipe limitations, heat pipe frozen startup and shutdown, heat pipe analysis and simulations, and various applications of heat pipes. Over the last several decades, several factors have contributed to a major transformation in heat pipe science and technology. The first major contribution was the development and advances of new heat pipes, such as loop heat pipes, micro and miniature heat pipes, and pulsating heat pipes. In addition, there are now many new commercial applications that have helped contribute to the recent interest in heat pipes, especially related to the fields of electronic cooling and energy. For example, several million heat pipes are now manufactured each month since all modern laptops use heat pipes for CPU cooling. Numerical modeling, analysis, and experimental simulation of heat pipes have also significantly progressed due to a much greater understanding of various physical phenomena in heat pipes, as well as advances in computational and experimental methodologies.

This text covers the fundamentals of heat pipes and what a heat pipe is all about. The book shows the understanding of heat pipe as a simple device that can quickly transfer heat from one point (evaporator) to another (condenser). They are often referred to as the “superconductors” of heat as they possess an extraordinary heat-transfer capacity and rate with almost no heat loss.

The book describes the heat pipe as a closed evaporator-condenser system consisting of a sealed, hollow tube whose inside walls are lined with a capillary structure or wick. Thermodynamic working fluid, with substantial vapor pressure at the desired operating temperature, saturates the pores of the wick in a state of equilibrium between liquid and vapor. When heat is applied to the heat pipe, the liquid in the wick heats and evaporates. As the evaporating fluid fills the heat pipe hollow center, it diffuses throughout its length. Condensation of the vapor occurs wherever the temperature is even slightly below that of the evaporation area. As it condenses, the vapor gives up the heat it acquired during evaporation. This effective

high thermal conductance helps maintain near-constant temperatures along the entire length of the pipe.

This book shows the heat pipe basic cooling solution which usually weighs less while moving more heat at a lower delta than traditional cooling solutions, increasing components and product lifetimes and operation reliability.

Throughout the book, we show how the heat pipes enable passive cooling solutions for high heat load and high-temperature equipment, lacking moving parts and boasting extraordinary lifetimes as a result.

Chapter 1

Basic Principles of Heat Pipes and History

The heat pipe is one of the remarkable achievements of thermal physics and heat transfer engineering in this century because of its unique ability to transfer heat over large distances without considerable losses. The main applications of heat pipes deal with the problems of environmental protection and energy and fuel savings.

Heat pipes have emerged as an effective and established thermal solution, particularly in high heat flux applications and in situations where there is any combination of nonuniform heat loading, limited airflow over the heat-generating components, and space or weight constraints. This chapter will briefly introduce heat pipe technology and then highlight its basic applications as a passive thermal control device.

1.1 Introduction

The original idea of heat pipe was considered in 1944 by Gaugler [1] and in 1962 by Trefethen [2]. Although Gaugler patented a very lightweight heat transfer device, that was essentially a very basic presentation of heat pipe. During that time period, the technology did not require a need for such sophisticated yet constructively simple two-phase and passive heat transfer device, and there was not much attention that was paid to it. First suggested by Trefethen [2] in 1962 and then was appeared through a patent application of heat pipe again in 1963 by Wyatt [3]. It was not widely considered and publicized until 1964 when George Grove [4] and his co-worker at the Los Alamos National Laboratory independently reinvented the same concept for their existing space program and its application. He is the one who named this most satisfactory and simplistic heat transmission device “heat pipe” and developed its applications.

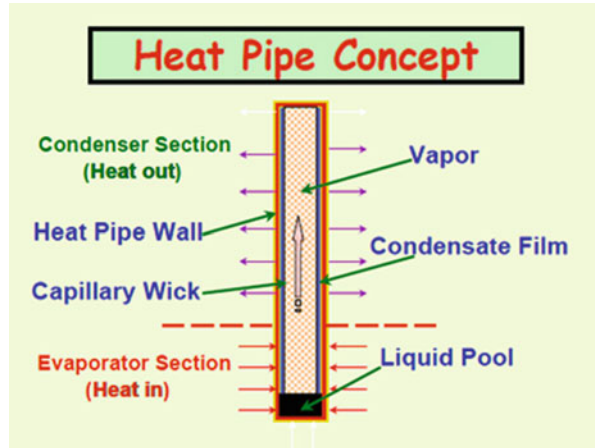
Heat pipes are two-phase flow heat transfer devices where a process of liquid to vapor and vice versa circulates between evaporator and condenser with high effective thermal conductivity. Due to the high heat transport capacity, heat

exchanger with heat pipes has become much smaller than traditional heat exchangers in handling high heat fluxes. With the working fluid in a heat pipe, heat can be absorbed on the evaporator region and transported to the condenser region where the vapor condenses releasing the heat to the cooling media. Heat pipe technology has found increasing applications in enhancing the thermal performance of heat exchangers in microelectronics; energy saving in classical heating, ventilating, and air conditioning (HVAC) systems for operating rooms, surgery centers, hotels, clean rooms, etc.; temperature regulation systems for the human body; and other industrial sectors including spacecraft and various types of nuclear reactor technologies as a fully inherent cooling apparatus. The heat pipe is a self-contained structure which achieves very high thermal energy conductance by means of two-phase fluid flow with capillary circulation. A heat pipe operates within a two-phase flow regime as an evaporation–condensation device for transferring heat in which the latent heat of vaporization is exploited to transport heat over long distances with a corresponding small temperature difference.

Heat added to the evaporator is transferred to the working fluid by conduction and causes vaporization of the working fluid at the surface of the capillary structure. Vaporization causes the local vapor pressure in the evaporator to increase and vapor to flow toward the condenser, thereby transporting the latent heat of vaporization. Since energy is extracted at the condenser, the vapor transported through the vapor space is condensed at the surface of the capillary structure, releasing the latent heat. Closed circulation of the working fluid is maintained by capillary action and/or bulk forces. An advantage of a heat pipe over other conventional methods to transfer heat such as a finned heat sink is that a heat pipe can have an extremely high thermal conductance in steady-state operation. Hence, a heat pipe can transfer a high amount of heat over a relatively long length with a comparatively small temperature differential. Heat pipe with liquid-metal working fluids can have a thermal conductance of a thousand or even tens of thousands folds better than the best solid metallic conductors, silver or copper. In a heat pipe energy is transported by utilizing phase change of the working substance instead of a large temperature gradient and without external power. Also, the amount of energy transferred through a small cross section is much larger than that by conduction or convection. Heat pipes may be operated over a broad range of temperatures by choosing an appropriate working fluid (Fig. 1.1).

However, this useful device has some operating limitations such as the sonic, the capillary, the entrainment, and finally the boiling limit, which will be discussed throughout the book. When any of these limitations is encountered, the capillary structure may dry out leading to failure of the heat pipe. In addition to these limitations, when liquid metal is used as the working fluid, startup difficulty may take place due to possible solid state of the working fluid and extremely low vapor density.

Fig. 1.1 Heat pipe concept



1.2 History

Early research in heat pipes conducted at Los Alamos was directed to applications in space-based thermionic energy conversion systems operating in excess of 1500 K. Heat pipes were considered for heating thermionic emitters, for cooling thermionic collectors, and for the ultimate radiation of heat to space fluids, and materials were tailored to this temperature regime. Experiments with a Nb-1%Zr heat pipe, with lithium operating at 1573 K, 207 W/cm² evaporator radial heat flux; a 1.95 kW/cm² axial heat flux, and an Ag-Ta operating at 2273 K, 410 W/cm² evaporator radial heat flux; and a 4 kW/cm² axial heat flux are reported in Deverall and Kemme [5]. The results of early thermionic-related heat pipe fluid-wall compatibility and life test studies with systems of In-W at 2173 K for 75 h, Ag-Ta at 2173 K for 100 h, Cs-Ti at 673 K in excess of 2000 h, Na-stainless steel at 1073 K for 500 h, and Li-Nb-1%Zr at 1373 K for 4300 h are summarized in Grover et al. [6], Deverall and Kemme [5], Grover et al. [7], Cotter et al. [8], and Ranken and Kemme [9]. A study characterizing both potassium and sodium heat pipes with various wick structures and a treatment of the limitations to heat pipe startup and operation is contained in Kemme [10].

On July 24, 1963, George Grover made the following entry into his laboratory notebook: "Heat transfer via capillary movement of fluids. The "pumping" action of surface tension forces may be sufficient to move liquids from a cold temperature zone to a high-temperature zone (with subsequent return in vapor form using as the driving force the difference in vapor pressure at the two temperatures) to be of interest in transferring heat from the hot to the cold zone. Such a closed system, requiring no external pumps, may be of particular interest in space reactors in moving heat from the reactor core to a radiating system. In the absence of gravity, the forces must only be such as to overcome the capillary and the drag of the returning vapor through its channels."

Thus, began heat pipe research at Los Alamos. Later that year, Grover submitted the results of “heat pipe” experiments with water and sodium as working fluids to the *Journal of Applied Physics* [6]. The sodium heat pipe, 90 cm long with a 1.9 cm outer diameter (OD), operated at 1100 K with 1 kW heat input. This paper reviews 28 years of space power-related liquid-metal heat pipe research that has been conducted at Los Alamos since the invention of the heat pipe.

1.3 Description and Technology of Heat Pipes

A heat pipe is essentially a passive heat transfer device with an extremely high effective thermal conductivity. It is a simple closed-loop device that can quickly transfer heat from one point to another using a two-phase flow schema. It is a high thermal conductance device as well which transfers heat by two-phase fluid circulation. The operating temperature range of a heat pipe is determined by the type of working fluid used and its optimum design envelope. They are often referred to as the “superconductors” of heat as they possess an extraordinary heat transfer capacity and rate with almost no heat loss. Of the various means of transmitting heat, the heat pipes are known as one of the most satisfactory devices to carry on such a task. In a simple form of its structure, this device is transporting heat from one point to another via evaporation and condensation, and the heat transport fluid is recirculated by capillary forces which automatically develop as induction of the heat transport process.

This closed loop of heat pipe is consisting of a sealed hollow tube with two zones, namely, evaporator and condenser, in a very simple case of such device whose inside walls are lined with a capillary structure known as wick. A thermodynamic working fluid having a substantial vapor pressure at the desired operating temperature saturates the pores of the wick. When heat is applied to any portion of the heat pipe evaporator, this fluid is heated and it evaporates, readily filling the hollow center of the pipe. The vapor then diffuses throughout the heat pipe. Condensation of the vapor occurs on the pipe wall whenever the temperature is even slightly below that of the evaporation area. As it condenses, the liquid gives up the heat it acquired and returns to the evaporator section or heat source by means of capillary action within the wick. This tends to produce isothermal operation and a high effective thermal conductance. When a heat sink is attached to a portion of the heat pipe, condensation takes place preferentially at this point of heat loss, and a vapor flow pattern is then established.

The system, proven in aerospace application, transmits thermal energy at rates hundreds of times greater than the most efficient solid conductor does and at a far superior energy-to-weight ratio.

In terms of thermal conduction, a heat pipe is designed to have very high thermal conductance.

Heat is transported from the heat source (evaporator section of the heat pipe) to the heat sink (condenser section of the heat pipe) by means of a condensable fluid contained in a sealed chamber.

Liquid is vaporized, absorbing heat in the evaporator section. Then the vapor flows to the condenser section, where it condenses and releases its latent heat. The liquid is drawn back to the evaporator section by capillary action, where it is re-vaporized to continue the cycle. The temperature gradient along the length of pipe is minimized by designing for a very small vapor pressure drop as the vapor flows from the evaporator section to the condenser section. Thus, the saturation temperatures (temperatures at which evaporation and condensation takes place) are very nearly the same in both sections.

The idea of heat pipes was first suggested by Gaugler in 1942 [1]. However, it was not until 1962, when Grover et al. [4] invented it, that its remarkable properties were appreciated and serious development began. It consists of a sealed aluminum or copper container whose inner surfaces have a capillary wicking material. A heat pipe is similar to a thermosyphon. It differs from a thermosyphon by virtue of its ability to transport heat against gravity by an evaporation–condensation cycle with the help of porous capillaries that form the wick. The wick provides the capillary driving force to return the condensate to the evaporator. The quality and type of wick usually determines the performance of the heat pipe, for this is the heart of the product. Different types of wicks are used depending on the application for which the heat pipe is being used.

The spectrum of heat pipe working fluids extends from cryogenics to liquid metals, the choice of fluid being such that its saturation temperature, at the heat pipe operating pressure, be compatible with the heat pipe's application. Also, the fluid is chosen to be chemically inert when wetting the pipe and capillary wick. Ideally, the fluid would have a high thermal conductivity and latent heat. It should have a high surface tension and low viscosity.

Heat transfer in a heat pipe is limited by: the rate at which liquid can flow through the wick; “choking” (the inability to increase vapor flow with increasing pressure differential, also called “sonic limit”); entrainment of liquid in the vapor stream, such that liquid flow to the evaporator is reduced; and the rate at which evaporation can take place without excessive temperature differentials in the evaporator section.

Isothermalizer heat pipes will transport heat in either direction, and for a given configuration, the heat flow will depend entirely on the temperature difference between the heat source and heat sink. The isothermalizer heat pipe is therefore a basically passive device with a fixed conductance, provided that none of its limiting conditions are exceeded (sonic, entrainment, capillary, and boiling limits (see Figs. 1.2 and 1.3)). The isothermalization function of a heat pipe can be modified to produce active devices in two ways: diode heat pipes, where the pipe operates as an isothermalizer in the forward mode and shuts off in the reverse mode, or variable conductance heat pipes, where the conductance in the forward mode can be actively controlled and again shuts down in the reverse mode.

Fig. 1.2 A traditional heat pipe schematic. A traditional heat pipe is a hollow cylinder filled with a vaporizable liquid. (A) Heat is absorbed in the evaporating section. (B) Fluid boils to vapor phase. (C) Heat is released from the upper part of cylinder to the environment; vapor condenses to liquid phase. (D) Liquid returns by gravity to the lower part of cylinder (evaporating section)

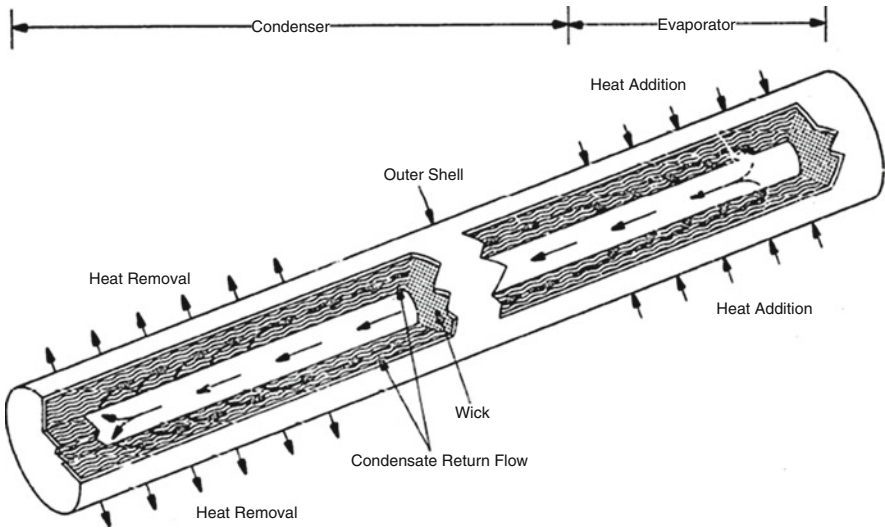
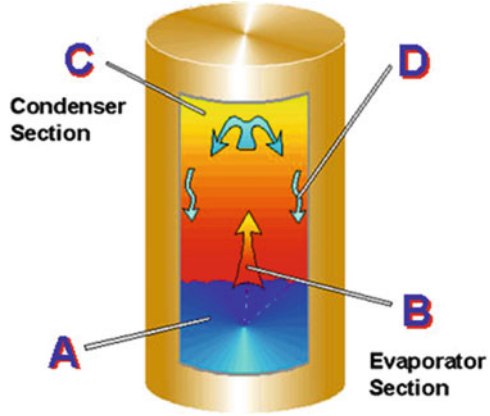


Fig. 1.3 Parts and functions of basic heat pipe

But today's heat pipes can work both vertically and horizontally as well as arbitrary angle of installation and operation of its application. Recent applications of them in zero gravity in particular in satellite are enhanced and proven by NASA and Air Force in collaboration with Los Alamos National Laboratory and other contractors such as TRW and Honeywell and others. Figures 1.2, 1.3, and 1.4 are some examples of such applications.

Figure 1.5 shows application of loop heat pipe containing two parallel evaporators and two parallel condensers with passive and self-regulating as well as heat load sharing between evaporators. This configuration was implemented to NASA's New Millennium Program, The Space Technology [13] (ST8) mission. Part of the new spacecraft has been illustrated in Fig. 1.6 where the loop heat pipe was used.

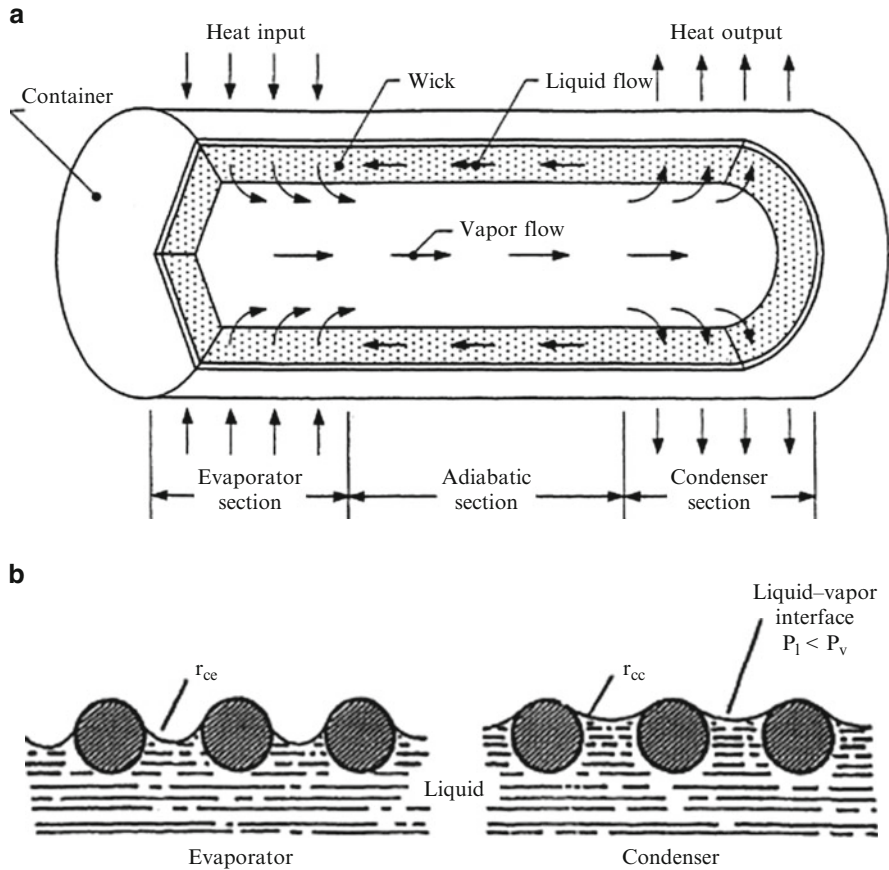


Fig. 1.4 (a) Components and principle of operation of a conventional heat pipe; (b) radii of curvature of the liquid–vapor interface in the condenser and evaporator [11]

Depending on its applications in particular in the nuclear reactor industry where these reactors are a source of electric power generation, heat pipes are used as a cooling part of secondary loop of inherent shutdown system, which typically you see them as liquid heat pipe (i.e., mercury or sodium as cooling environment within heat pipe); there might be some consideration for a section of heat pipe that is known as adiabatic zone where heat pipe is cast into structure of cooling assembly. A typical example of such approach could be seen in the early study of companies such as Westinghouse Electric on their core design of liquid-metal fast breeder reactor (LMFBR); the mercury heat pipe was considered as part of a fully inherent shutdown system of this particular reactor design (where the author was involved with such design and Westinghouse was awarded few patents). This sort of approach was giving better safety factor for any incidental meltdown of reactor and was providing better tool to release excessive heat and help to reduce the core temperature below critical point without any operator within the loop. Modern

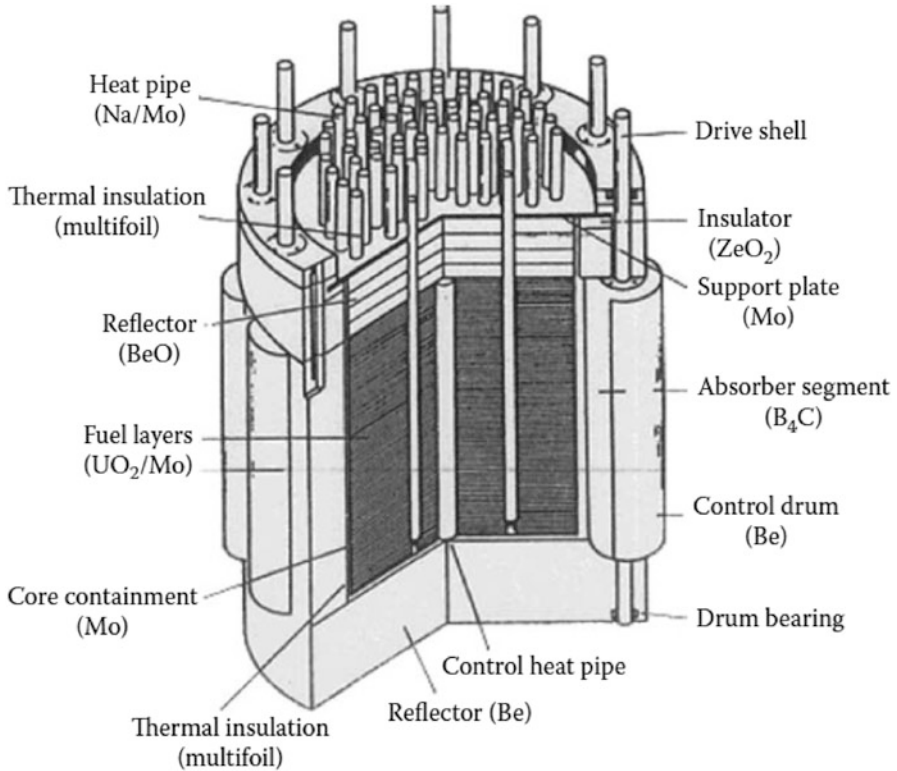


Fig. 1.5 Usage of sodium/molybdenum heat pipes in the thermal control of nuclear power reactor [12]

design and new generation of LMFBR reactor such as French-built Phoenix are utilizing such heat pipes. A typical conventional heat pipe with its adiabatic section is depicted in Fig. 1.4. These types of heat pipes with their adiabatic zone are designed for use in thermal control of nuclear reactor cores that are used in the form of convection, conduction, and radiation heat transfer device and they are shown in Fig. 1.5. In case of rapid reduction of core temperature, additional radiation surface area in the form of fin is built on top of evaporation section of heat pipe, or variable heat pipes are utilized which are described in the later part of this section

This type of loop heat pipe has been utilized as part of new NASA series of experiments for space-worthy value of heat pipe studies.

Loop heat pipe operation involves complex physical processes such as:

- Fluid dynamics, heat transfer, and thermodynamics
- Gravitational, inertial, viscous, and capillary forces

The first orbital test demonstrating heat pipe operation under zero-gravity conditions took place in 1967. The launch vehicle for the ATS-A satellite carried

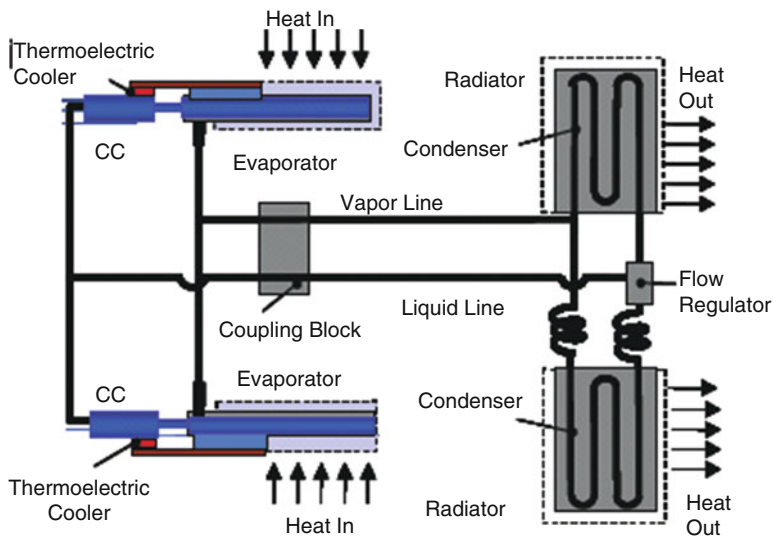


Fig. 1.6 Loop heat pipe (LHP) containing two parallel evaporators and two parallel condensers

a heat pipe with thermocouples to determine its temperature uniformity and performance under varying heat loads throughout different portions of its Earth orbit. This successful demonstration was followed 1 year later by the launching of GEOS-2, using heat pipes designed by Johns Hopkins. GEOS-2 was the first satellite designed to use heat pipes as an integral part of its overall thermal control system (see Fig. 1.7).

The large-scale satellite and the International Space Station have made great progress in the past several decades. One of the problems urgent to be solved is the heat dissipation. There exists a large amount of heat that should be transferred and radiated into the outer space. Single-phase liquid loops were the major method used in large-scale spacecrafts for heat transfer and dissipation in the past decade. Since the 1980s researches worldwide have focused their efforts on two-phase liquid loop technology to be used in the spacecraft thermal control systems on the International Space Station, telecommunication, and technological satellites. Space nuclear systems require large area radiators to reject the unconverted heat to space. A conceptual design of a waste heat radiator has been developed for a thermoelectric space nuclear power system [13]. The basic shape of the heat pipe radiator was a frustum of a right circular cone. The design included stringer heat pipes to carry reject heat from the thermoelectric modules to the radiator skin that was composed of small-diameter, thin-walled cross heat pipes. The stringer heat pipes were armored to resist puncture by a meteoroid. The cross heat pipes were designed to provide the necessary unpunctured radiating area at the mission end with a minimum initial system mass. Several design cases were developed in which the individual stringer survival probabilities were varied and the radiator system mass was calculated. Results are presented for system mass as a function of individual

Spacecraft Bus built by Orbital Sciences

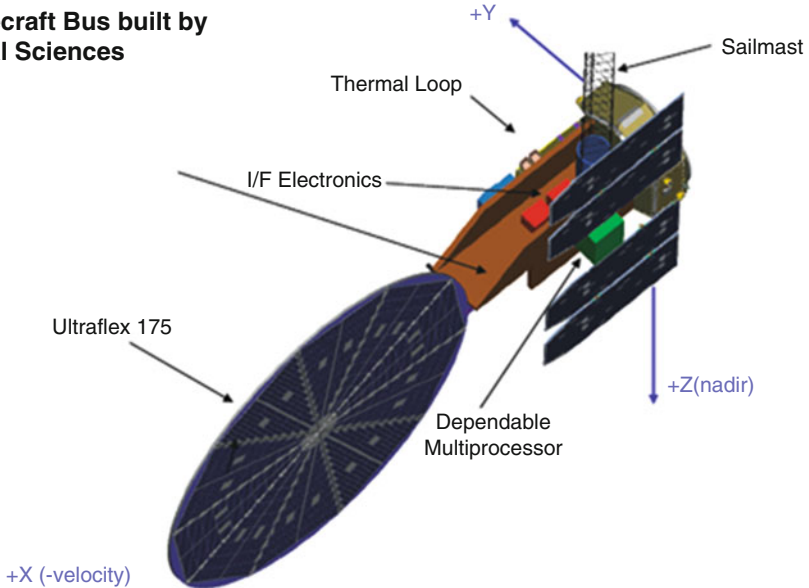


Fig. 1.7 Part of NASA's New Millennium Program satellite

stringer survival probability for six candidate container materials, three candidate heat pipe fluids, two radiator operating temperatures, two meteoroid shield types, and two radiating surface cases. Results are also presented for radiator reject heat as a function of system mass, area, and length for three system sizes. We will discuss this in later chapters.

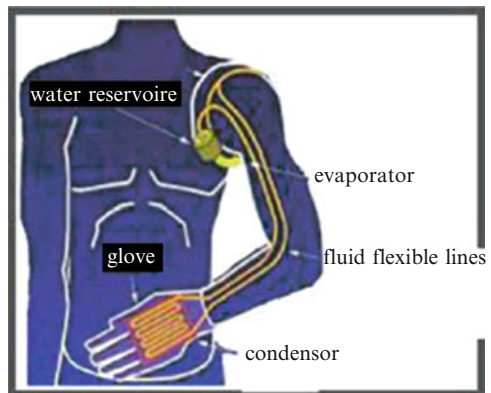
Heat pipe operation on Earth is dominated by the force of gravity, which makes it difficult to predict the performance of a heat pipe in space and requires thermal system engineers to adopt conservative designs and ground-test programs to reduce the risks of systems failures after launch. A heat pipe is a very efficient heat transfer device commonly used for cooling electronic components and sensors. Recently, the results from a heat pipe performance experiment have led to the development and validation of an improved analytical heat pipe model. The accuracy of this computer model, known as GAP, now allows engineers to be less conservative in their designs, which leads to fewer heat pipes per spacecraft, thereby achieving significant cost and weight savings.

Loop heat pipe (LHP) and capillary pumped loop (CPL) with “natural” circulation of two-phase flow are used on satellites to ensure the thermal transfer from core module equipments to a radiator. LHP and CPL are considered as reliable thermal management devices that are able of operating at any orientation in a gravitational field, and heat can be transported over long distances. The main components of

LHP and CPL are evaporator that is responsible for the generation of capillary forces that drive the working fluid via a porous structure and condenser [14].

Electric blankets are also well known but often provide uneven heating and subject the user to low-level electromagnetic radiation. Nonetheless, whether used for heating or cooling, such suits and blankets generally disadvantageously require external connections and/or require external power sources. Numerous devices have been developed for regional, therapeutic heat transfer. Faghri's invention [15] meets the need for lightweight, comfortable suits and blankets for body temperature regulation by using heat pipes to redistribute body heat and to provide supplemental heat from external sources. A temperature regulation system for the human body will result, taking the form of garments, blankets, and pads. This invention further provides for an improved pad incorporating heat pipes for use in regional, therapeutic heat transfer. The heat pipes are positioned to provide heat transfer between one or more separate portions of the body. A garment for use in cold environments, such as a body suit, pants, or jacket, may, thus, include heat pipes which extend from the torso of the body, which is typically warmer, to an extreme level. For example, in a garment such as a body suit, this fourth embodiment provides a means to overcome problems with damage to heat-sensitive organs when whole body hyperthermia is induced for medical treatment. Heat may be applied to major portions of the body to induce hyperthermia with one heat exchanger having means for heating, while portions of the body facing heat-sensitive organs may be cooled with another heat exchanger having means for cooling (Fig. 1.8). Temperature control is of particular interest where the present invention is used for deliberate inducement of hyperthermia for medical treatment or to provide controlled heating or cooling for hypothermia or hyperthermia patients.

Fig. 1.8 A method for temperature regulation in hand



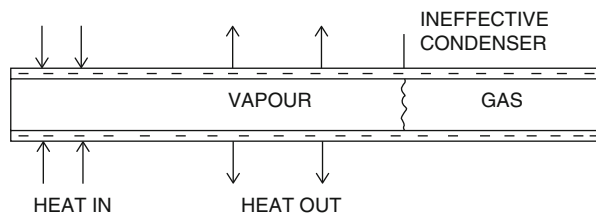
Note that:

Heat transfer mechanisms can be grouped into three broad categories	
Conduction	Regions with greater molecular kinetic energy will pass their thermal energy to regions with less molecular energy through direct molecular collisions, a process known as conduction. In metals, a significant portion of the transported thermal energy is also carried by conduction-band electrons
Convection	When heat conducts into a static fluid, it leads to a local volumetric expansion. As a result of gravity-induced pressure gradients, the expanded fluid parcel becomes buoyant and displaces, thereby transporting heat by fluid motion (i.e., convection) in addition to conduction. Such heat-induced fluid motion in initially static fluids is known as free convection For cases where the fluid is already in motion, heat conducted into the fluid will be transported away chiefly by fluid convection. These cases, known as forced convection , require a pressure gradient to drive the fluid motion, as opposed to a gravity gradient to induce motion through buoyancy
Radiation	All materials radiate thermal energy in amounts determined by their temperature, where the energy is carried by photons of light in the infrared and visible portions of the electromagnetic spectrum. When temperatures are uniform, the radiative flux between objects is in equilibrium, and no net thermal energy is exchanged. The balance is upset when temperatures are not uniform, and thermal energy is transported from surfaces of higher to surfaces of lower temperature

Generally speaking, typically, there are two classes of heat pipes, variable conductance heat pipe (VCHP) or “conventional” heat pipe also known as constant conductance heat pipe (CCHP) or fixed conductance heat pipe (FCHP). A typical conventional heat pipe is illustrated in Fig. 1.9, while a variable conductance heat pipe is depicted in Fig. 1.8. The distinctive feature of these types of heat pipes from conventional ones are their abilities and functionality to operate in a specific desired temperature range along certain portions of the pipe, in spite of variations in the source and sink conditions. When such conditions are desired based on the application of heat pipe, it is important to actively or passively control the heat pipe so that the desired temperature range can be maintained.

Figure 1.9 is the simple form of variable heat pipe structure with gas-buffered section on the condenser part of the pipe. Later on there was an add-on reservoir structured to give a downstream form of condenser (Fig. 1.10) which was allowing the heat pipe to have adequate effective length on condenser side of the pipe to operate at maximum of its capability and provide more accurate control of the vapor temperature [11].

Fig. 1.9 Equilibrium state of gas-loaded heat pipe [11]



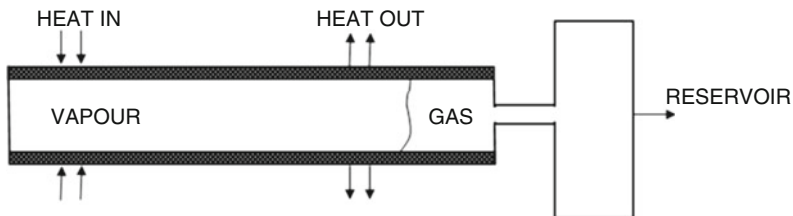


Fig. 1.10 Cold-reservoir variable conductance heat pipe [11]

In the early days of designing the cold-reservoir variable conductance heat pipe (VCHP), there was a problem associated with diffusion of vapor into the reservoir, followed by condensation. We will discuss more about variable heat pipe in later chapters and some approaches taken by the designer of such heat pipes to improve their structure and applications in the industry. Computer codes were generated to have better feeling for these types of heat pipes, and of the most known computer code, “GASPIPE” was developed by Marcus [16] and associates at TRW where they studied and developed VCHP for NASA in the early days of the 1970s.

A new type of variable conductance heat pipe, the liquid-controlled heat pipe (LCHP), has been developed. While the gas-controlled heat pipe is able to stabilize the temperature of the heating zone, the LCHP limits the temperature of the cooling zone to a certain adjustable value. The physical principle is to regulate the heat transfer capability by regulating the amount of liquid inside the heat pipe. The liquid is partly stored in a reservoir with a variable volume, as, for example, a bellows. The temperature of the cooling zone, corresponding to the vapor pressure inside the heat pipe, can be adjusted by the outer pressure (gas or spring) on the bellows. The LCHP is applicable where heat is needed at a constant temperature or where the vapor pressure inside a heat pipe has to be limited.

In Fig. 1.11a, a gradual increase in working temperature is accompanied by a rapid increase in saturated vapor pressure of the working fluid. In contrast there is only a slight increase in the temperature on the noncondensable gas, and, since the relationship between pressure and cubic capacity is constant, the boundary surface is pushed out by the working fluid so that the “condenser section that is effective for radiation with admixture of working fluid” migrates toward the gas reservoir. In Fig. 1.11b, the region occupied by the working fluid is reduced, and the internal heat transfer rate is still small. If the temperature is further increased, the condenser section that is effective for radiation becomes larger, and the heat radiation rate increases. At the point of maximum heat radiation, the noncondensable gas is totally contained within the gas reservoir. In Fig. 1.11c, if the heat radiation rate is greater than the maximum heat input to the evaporator section by the heat source, sufficient heat radiation can be obtained, and the temperature of the evaporator section will not increase further [15].

Constant Conductance Heat Pipe (CCHP) Also Known as Fixed Conductance Heat Pipe (FCHP)

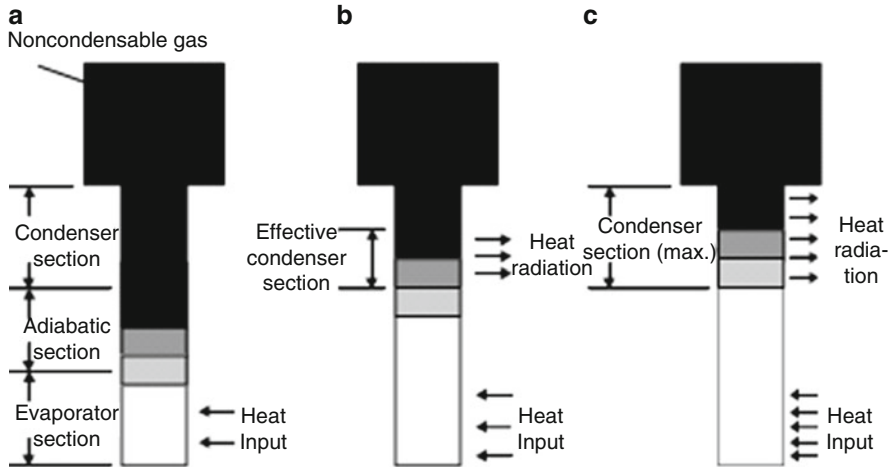


Fig. 1.11 Heat transfer during VCHP operation. (a) QL: no heat radiation. (b) Boundary surface migration. (c) QH: maximum heat transfer

Constant conductance heat pipes (CCHPs) transport heat from a heat source to a heat sink with a very small temperature difference. Axial groove capillary wick structures are utilized because of the relative ease of manufacturing (aluminum extrusions) and their demonstrated heritage in spacecraft and instrument thermal control applications. CCHPs can transport heat in either direction and are typically used to transfer heat from specific thermal loads to a radiator panel or as part of an integrated heat pipe radiator panel. Common working fluids include: ammonia, propylene, ethane, and water.

Fixed conductance heat pipes (FCHPs) filled with working fluid at low or moderate temperatures develop a volume of excess liquid when operated at high temperatures. The excess liquid forms as either a puddle or a slug at the coldest end of the condenser and creates a temperature differential between the evaporator and the condenser end cap. Simple algebraic expressions are presented for predicting the thermal performance of an FCHP operating with a liquid slug formed by the combined influence of liquid density temperature dependence and meniscus depression. Both differential and two-node models are developed to account for condensation modeled either as a constant flux processor based on an isothermal vapor with a constant internal film coefficient. Numerical examples are included to illustrate the behavior of two axially grooved pipes operating over a range of heat loads with both real and ideal fluids. Prediction of evaporator temperature and liquid slug length is observed to have a weak dependence on the choice of model and mode of condensation and a strong dependence on real fluid effects.

Figure 1.12 shows a structural comparison of a conventional heat pipe and the variable conductance heat pipe (VCHP). In the conventional type, a small volume of working fluid is sealed into an evacuated metal container. The working fluid repeatedly vaporizes and condenses as a result of the small temperature difference

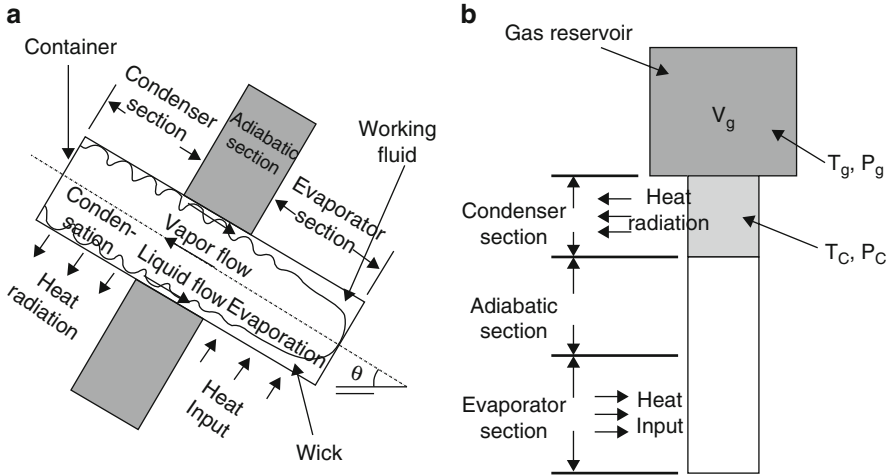


Fig. 1.12 Structural comparison of conventional and variable conductance heat pipes [14]

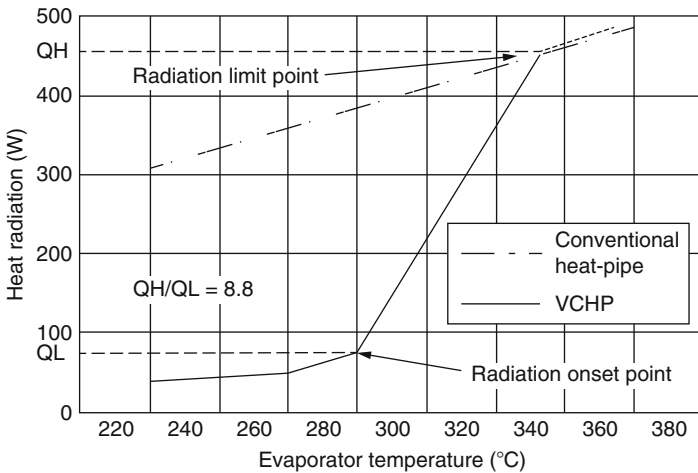


Fig. 1.13 Heat radiation characteristics of conventional and variable conductance heat pipes [14]

(or temperature gradient) between the evaporator and condenser sections, and heat is transferred by the latent heat of the working fluid. The heat pipe comprises an evaporator section, an adiabatic section, and a condenser section, and a wick or mesh is provided in the container to facilitate the circulation of the working fluid. The maximum heat transfer rate, which is the measure of heat pipe performance, is determined by the wick, the volume of working fluid, and so on, while the working temperature is determined passively by the external heat source, the temperature of the heat radiator (condenser) section, and so on [15].

Figure 1.13 compares the heat radiation characteristics of conventional and variable conductance heat pipes. Unlike the conventional heat pipe, in which the

heat radiation rate has a constant gradient relative to temperature, the radiation rate in the VCHP increases rapidly from a given temperature (the radiation onset temperature) until the radiation limit is reached. When the radiation limit is exceeded, it traces a constant gradient, like a conventional heat pipe. The term “variable conductance” has its origin in this characteristic, and the slope of the line between the radiation onset point and the radiation limit point (hereinafter referred to as the radiation gradient) is an important characteristic of the VCHP [15].

1.4 Principle of Operation

The three basic components of a heat pipe are:

1. The container
2. The working fluid
3. The wick or capillary structure

1.4.1 *Container*

The function of the container is to isolate the working fluid from the outside environment. It has to therefore be leakproof, maintain the pressure differential across its walls, and enable transfer of heat to take place from and into the working fluid.

Selection of the container material depends on many factors. These are as follows:

- Compatibility (both with working fluid and external environment)
- Strength to weight ratio
- Thermal conductivity
- Ease of fabrication, including welding, machineability, and ductility
- Porosity
- Wettability

Most of the above are self-explanatory. A high strength to weight ratio is more important in spacecraft applications. The material should be nonporous to prevent the diffusion of vapor. A high thermal conductivity ensures minimum temperature drop between the heat source and the wick.

1.4.2 *Working Fluid*

A first consideration in the identification of a suitable working fluid is the operating vapor temperature range. Within the approximate temperature band, several possible working fluids may exist, and a variety of characteristics must be examined in

order to determine the most acceptable of these fluids for the application considered. The prime requirements are:

- Compatibility with wick and wall materials
- Good thermal stability
- Wettability of wick and wall materials
- Vapor pressure not too high or low over the operating temperature range
- High latent heat
- High thermal conductivity
- Low liquid and vapor viscosities
- High surface tension
- Acceptable freezing or pour point

The selection of the working fluid must also be based on thermodynamic considerations which are concerned with the various limitations to heat flow occurring within the heat pipe such as viscous, sonic, capillary, entrainment, and nucleate boiling levels.

In heat pipe design, a high value of surface tension is desirable in order to enable the heat pipe to operate against gravity and to generate a high capillary driving force. In addition to high surface tension, it is necessary for the working fluid to wet the wick and the container material, i.e., contact angle should be zero or very small. The vapor pressure over the operating temperature range must be sufficiently great to avoid high vapor velocities, which tend to set up large temperature gradient and cause flow instabilities.

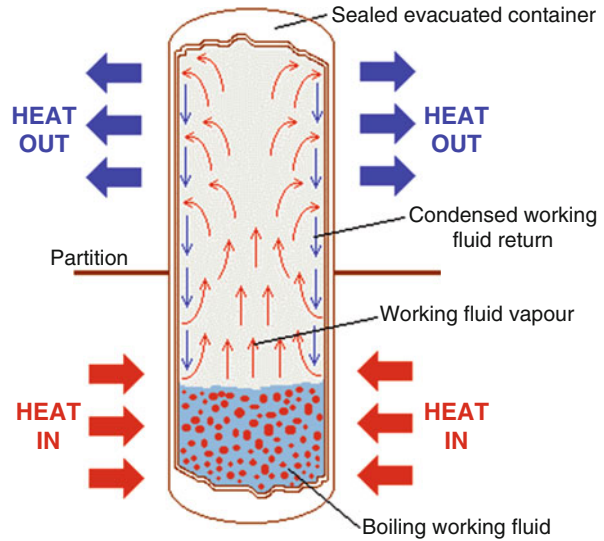
A high latent heat of vaporization is desirable in order to transfer large amounts of heat with minimum fluid flow and hence to maintain low-pressure drops within the heat pipe. The thermal conductivity of the working fluid should preferably be high in order to minimize the radial temperature gradient and to reduce the possibility of nucleate boiling at the wick or wall surface. The resistance to fluid flow will be minimized by choosing fluids with low values of vapor and liquid viscosities. Tabulated below are a few mediums with their useful ranges of temperature (Fig. 1.14).

1.4.3 Wick or Capillary Structure

It is a porous structure made of materials like steel, aluminum, nickel, or copper in various ranges of pore sizes. They are fabricated using metal foams and more particularly felts, the latter being more frequently used. By varying the pressure on the felt during assembly, various pore sizes can be produced. By incorporating removable metal mandrels, an arterial structure can also be molded in the felt.

Fibrous materials, like ceramics, have also been used widely. They generally have smaller pores. The main disadvantage of ceramic fibers is that they have little stiffness and usually require a continuous support by a metal mesh. Thus while the fiber itself may be chemically compatible with the working fluids, the supporting

Fig. 1.14 Schematic representation of the heat pipe



materials may cause problems. More recently, interest has turned to carbon fibers as a wick material. Carbon fiber filaments have many fine longitudinal grooves on their surface, have high capillary pressures, and are chemically stable. A number of heat pipes that have been successfully constructed using carbon fiber wicks seem to show a greater heat transport capability.

The prime purpose of the wick is to generate capillary pressure to transport the working fluid from the condenser to the evaporator. It must also be able to distribute the liquid around the evaporator section to any area where heat is likely to be received by the heat pipe. Often these two functions require wicks of different forms. The selection of the wick for a heat pipe depends on many factors, several of which are closely linked to the properties of the working fluid.

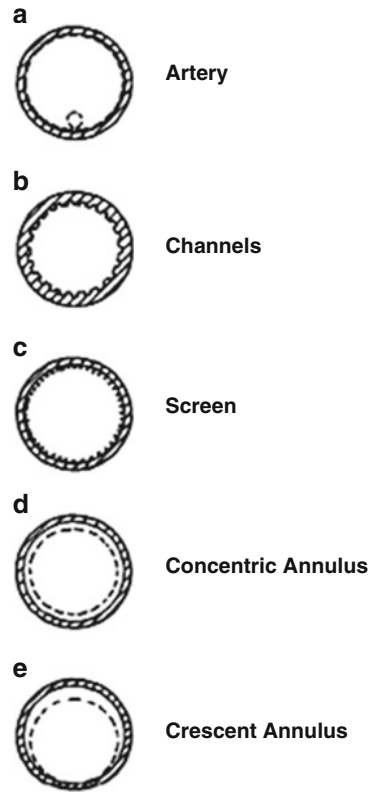
The maximum capillary head generated by a wick increases with decrease in pore size. The wick permeability increases with increasing pore size. Another feature of the wick, which must be optimized, is its thickness. The heat transport capability of the heat pipe is raised by increasing the wick thickness. The overall thermal resistance at the evaporator also depends on the conductivity of the working fluid in the wick. Other necessary properties of the wick are compatibility with the working fluid and wettability.

The most common types of wicks that are used are as follows:

1.4.4 Sintered Power Metal

This process will provide high-power handling, low-temperature gradients, and high capillary forces for antigravity applications. Figure 1.15 shows a complex sintered wick with several vapor channels and small arteries to increase the liquid flow rate. Very tight bends in the heat pipe can be achieved with this type of structure.

Fig. 1.15 Cross section of various wick structures [17]



1.4.5 Grooved Tube

The small capillary driving force generated by the axial grooves is adequate for low-power heat pipes when operated horizontally or with gravity assistance. The tube can be readily bent. When used in conjunction with screen mesh, the performance can be considerably enhanced.

1.4.6 Wire Screen Mesh

This type of wick is used in the majority of the products and provides readily variable characteristics in terms of power transport and orientation sensitivity, according to the number of layers and mesh counts used (see Fig. 1.16).

Figure 1.17 demonstrates several common wicking structures presently in use, along with more advanced concepts under development [18].

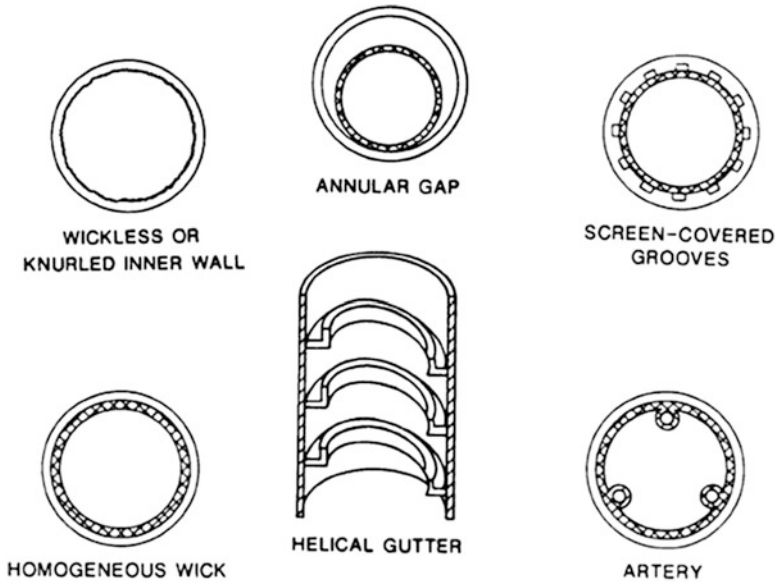


Fig. 1.16 Heat pipe liquid return geometries [18]

1.5 How the Heat Pipe Is Working

Inside the container is a liquid under its own pressure that enters the pores of the capillary material, wetting all internal surfaces. Applying heat at any point along the surface of the heat pipe causes the liquid at that point to boil and enter a vapor state. When that happens, the liquid picks up the latent heat of vaporization. The gas that then has a higher pressure moves inside the sealed container to a colder location where it condenses. Thus, the gas gives up the latent heat of vaporization and moves heat from the input to the output end of the heat pipe (Fig. 1.18).

Heat pipes have an effective thermal conductivity many thousands of times that of copper. Its “Axial Power Rating (APR)” specifies the heat transfer or transport capacity of a heat pipe. It is the energy moving axially along the pipe. The larger the heat pipe diameter, the greater is the APR. Similarly, the longer the heat pipe, the lesser is the APR. Heat pipes can be built in almost any size and shape. A simple Heat Pipe Assemblies Design Guidelines can be found in so many manufacture of heat pipe. Figure 1.19 is the best that the author has found.

Web site of Aavid Engineering, which was founded in 1964 as subsidiary of Aavid Thermal Technologies, Inc., is recommending certain and simple criteria as role of thump for any Heat Pipe Assemblies Design as follows:

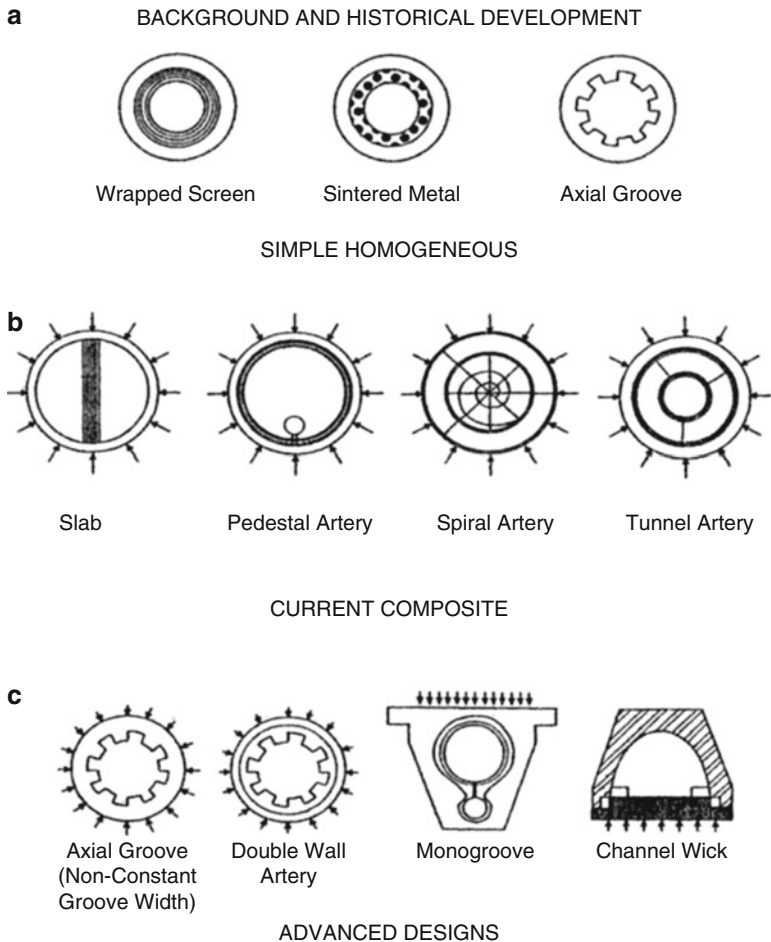


Fig. 1.17 Typical heat pipe wicking configurations and structures [19]

1.5.1 Heat Pipe Assemblies Design Guidelines

The following approach is sort of a quick and back-of-the-envelope-type analysis of choosing your design before you model your heat pipe for best optimum point of your design that falls within the constraint and limit of operating range of heat pipe such as sonic, entrainment, wicking, and boiling limits.

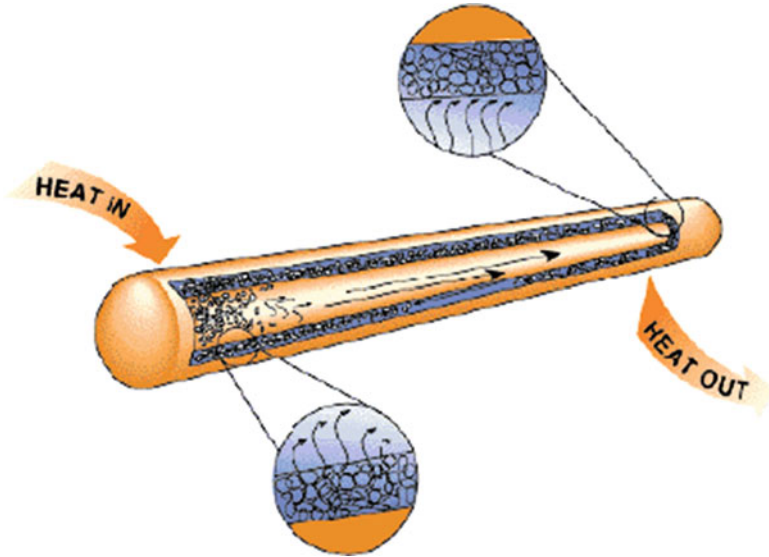


Fig. 1.18 Principal of conserved energy and heat transfer in heat pipe

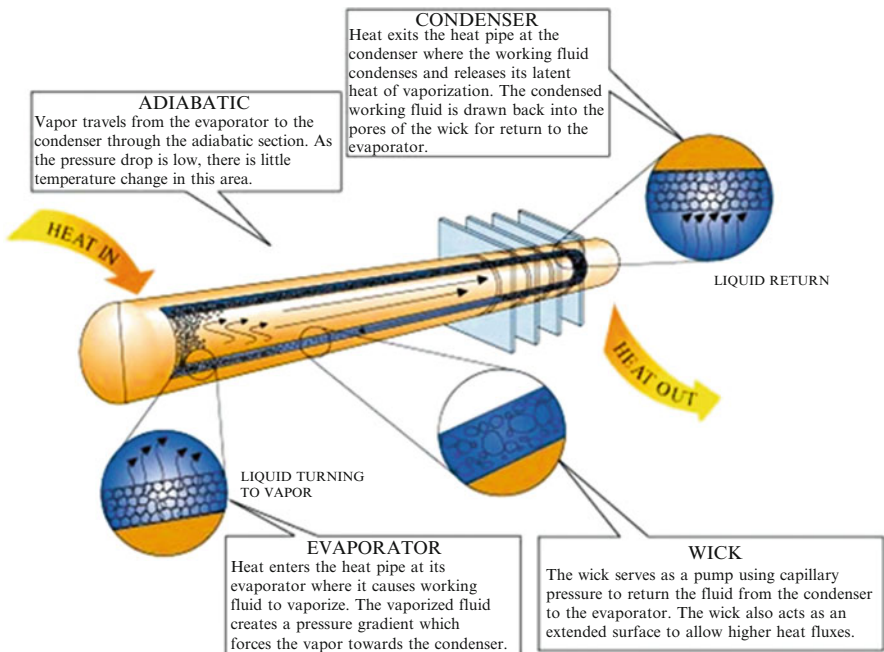


Fig. 1.19 Heat pipe operation

1.5.2 Orientation with Respect to Gravity

For the best performance, the application should have gravity working with the system; that is, the evaporator section (heated) should be lower, with respect to gravity, than the condenser (cooling) section. In other orientations where gravity is not aiding the condensed liquid return, the overall performance will be degraded. Performance degradation depends on a number of factors including wick structure, length, and working fluid of the heat pipe along with heat flux of the application. Careful design can minimize the performance loss and allow an accurate prediction performance.

1.5.3 Temperature Limits

Most pipes use water and methanol/alcohol as the working fluids. Depending on the wick structure, pipes will operate in environments with as low as $-40\text{ }^{\circ}\text{C}$. Upper temperature limits depend on the fluid, but $60\text{--}80\text{ }^{\circ}\text{C}$ is the average limit.

1.5.4 Heat Removal

Heat can be removed from the condenser using air cooling in combination with extrusion, bonded-fin heat sinks, or flat-fin stock. Enclosing the condenser in a cooling jacket allows liquid cooling.

1.5.5 Reliability

Heat pipes have no moving parts and have demonstrated life of over 20 years. The largest contributor to heat pipe reliability comes from control of the manufacturing process. The seal of the pipe, purity of the materials used in the wick structure, and cleanliness of the internal chamber have measurable effect on the long-term performance of a heat pipe. Any leakage will eventually render the pipe inoperable. Contamination of the internal chamber and wick structure will contribute to the formation of noncondensable gas (NCG) that will degrade performance over time. Well-developed processes and rigorous testing are required to ensure reliable heat pipes.

1.5.6 Forming or Shading

Heat pipes are easily bent or flattened to accommodate the needs of the heat sink design. Forming heat pipes may affect the power handling capability as the bends and flattening will cause a change in fluid movement inside the pipe. Therefore, design rules that take heat pipe configurations into consideration and the effect on thermal performance ensure the desired solution performance.

1.5.7 Effects of Length and Pipe Diameter

The vapor pressure differential between the condenser end and the evaporator end controls the rate at which the vapor travels from one end to the other. Diameter and length of the heat pipe also affect the speed at which the vapor moves and must be considered when designing with heat pipes. The larger the diameter, the more cross-sectional area available to allow vapor to move from the evaporator to the condenser. This allows for greater power carrying capacity. Conversely, length when in opposition to gravity has a negative effect on heat transport as the rate at which the working fluid returns from the condenser end to the evaporator end is controlled by the capillary limit of the wick, which is an inverse function of the length of the pipe. Therefore, shorter heat pipes carry more power than longer pipes when used in application not assisted by gravity.

1.5.8 Wick Structure

Heat pipe inner walls can be lined with a variety of wick structures. The four most common wicks are:

- (a) Groove tube
- (b) Wire screen mesh
- (c) Sintered powder metal
- (d) Fiber/spring

Among the above common ones, the three most common ones that are used in the industry to fabricate heat pipes are grooved tube and wire screen mesh that were describe and presented in Sects. 1.4.5–1.4.6 or a to c here.

The wick structure provides a path for liquid to travel from condenser to the evaporator using capillary action. Wick structures have performance advantages and disadvantages depending on the desired characteristics of the heat sink design. Some structures have low capillary limits making them unsuitable for applications where they must work without gravity assist. The plots of Fig. 1.20a, b are demonstration standard operating range of simple heat pipe.

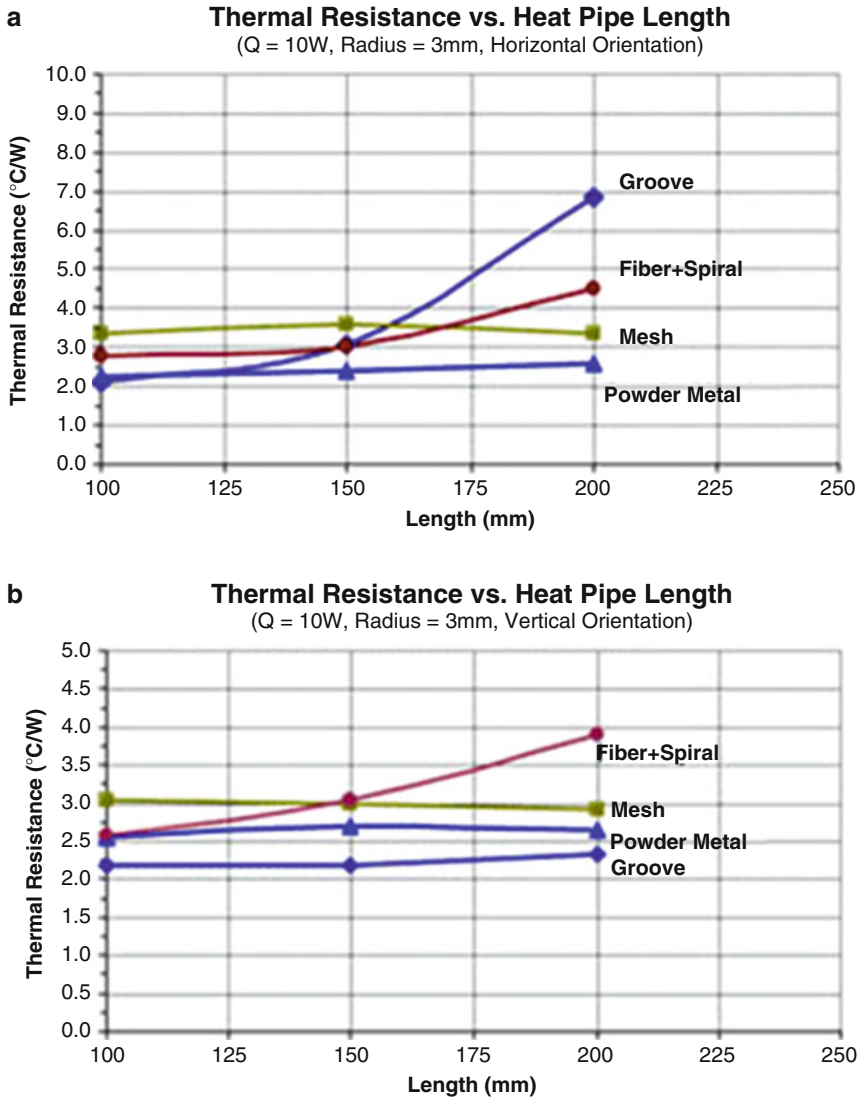


Fig. 1.20 (a and b) Standard operating range of simple heat pipe

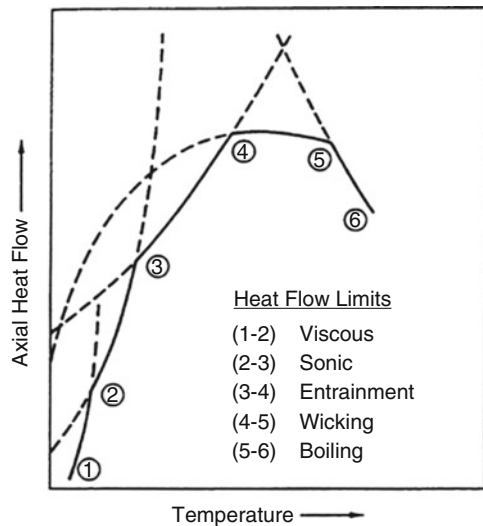
1.6 How Heat Pipe Works

No matter what type of application you may consider the heat pipe for, there are certain limitations that one has to look upon it for the heat pipe to operate properly and be able to perform the requirements that are imposed on the heat pipe and its application in that environment. These limitations are briefly described below:

1. *Viscous limit*: In long pipes and at low temperatures, the vapor pressure is low, and the effect of viscous friction on the vapor flow may dominate over the inertial forces. In this situation, the circulation of the working fluid is limited, which, consequently, limits the heat transfer through the pipe.
2. *Sonic limit*: At low vapor pressures, the velocity of the vapor at the exit of the evaporator may reach the speed of sound. Then the evaporator cannot respond to further decrease in the condenser pressure. That is, the vapor flow is choked, which limits the vapor flow rate.
3. *Capillary limit*: A capillary structure is able to provide circulation of a given fluid up to a certain limit. This limit depends on the permeability of the wick structure and the properties of the working fluid.
4. *Entrainment limit*: The vapor flow exerts a shear force on the liquid in the wick which flows opposite the direction of the vapor flow. If the shear force exceeds the resistive surface tension of the liquid, the vapor flow entrains small liquid droplets (Kelvin–Helmholtz instabilities). The entrainment of liquid increases the fluid circulation but not the heat transfer through the pipe. If the capillary force cannot accommodate the increased flow, dry out of the wick in evaporator may occur.
5. *Boiling limit*: At high temperatures, nucleate boiling may take place which produces vapor bubbles in the liquid layer. The bubbles may block the wick pores and decrease the vapor flow. Furthermore, the presence of the bubbles decreases the conduction of heat through liquid layer which limits the heat transfer from the heat pipe shell to the liquid which is by conduction only (Fig. 1.21).

Later chapters will show how to calculate each of these limits and its mathematical modeling. These analyses will allow the designer to plot the above curves,

Fig. 1.21 Typical limit of heat pipe operating limits



and the best design and fabrication of a heat pipe is where it operates within these envelope limits which is the area below all the curves. This area is known as best optimum design of heat pipe for the particular application of designer.

1.7 Constraints

There are many parameters which affect the performance of a heat pipe like compatibility of materials, operating temperature range, heat transport limitation, thermal resistance, operating orientation, dimension and geometric constraints, etc. For example, in miniature heat pipes, the maximum heat transport capacity was found to be primarily governed by the capillary pressure [18].

All heat pipes have three physical elements in common. These include an outer container, a small amount of working fluid, and a capillary wick structure. In addition to these basic components, heat pipes may also include gas reservoirs (variable conductance/diode heat pipes) and liquid or gas traps (diodes). Functionally, the heat pipe consists of three sections: evaporator, condenser section, and adiabatic regions. The evaporator section is mounted to the heat-producing components, while the condenser is thermally coupled to a heat sink or radiator. The adiabatic section allows heat to be transferred from the evaporator to the condenser with very small heat losses and temperature drops. Figure 1.22 depicts the basic heat pipe.

Heat pipes can operate in the fixed conductance, variable conductance, or diode mode. The fixed conductance heat pipe can transfer heat in either direction and operates over broad temperature ranges, but has no inherent temperature control capability. Constant conduction heat pipes allow isothermalization of shelves, radiators, and structures; spread heat from high heat dissipating components; and conduct heat away from heat-producing devices embedded within instruments and

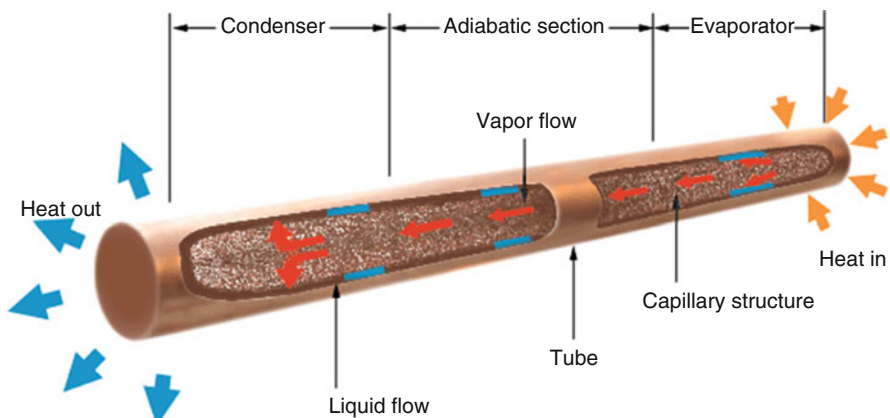


Fig. 1.22 Depicts the basic heat pipe

satellites. In the variable conductance heat pipe (VCHP), a small quantity of noncondensable gas (NCG) is loaded into the heat pipe. The VCHP can be used to control the temperature of equipment within very narrow limits; control is possible to less than 1 K by using careful design techniques. This is accomplished by controlling the location of the NCG/vapor interface within the condenser end of the heat pipe, thereby varying the active length of the condenser and causing a modulation in the condenser heat rejection capability. Temperature control of the attached device is achieved by an active feedback system consisting of a temperature sensor at the heat source and a controller for a heater at the NCG reservoir. The heater causes the gas in the reservoir to expand, thus moving the gas/vapor interface. Diode heat pipes permit heat to flow in one direction and inhibit heat flow in the opposite direction.

Specific benefits of heat pipes are:

1. Heat pipes have enormously more heat transfer capability than other methods on a weight and size basis.
2. Heat pipes permit configuration flexibility in contact areas with heat sources and heat sinks.
3. Heat can be transported over considerable distances with insignificant temperature drop.
4. Capillary pumping in the wick is generated by the heat transfer process and requires no other power or moving parts to pump the condensate.
5. Heat pipes operate satisfactorily in a zero gravity environment.

The choice of working fluid is dictated by several considerations, including operating temperature, latent heat of vaporization, liquid viscosity, toxicity, chemical compatibility with container material, wicking system design, and performance requirements. Figures 1.23 and 1.24 and Table 1.1 depict some of the above characteristics for several fluids. The highest performance from a heat pipe is

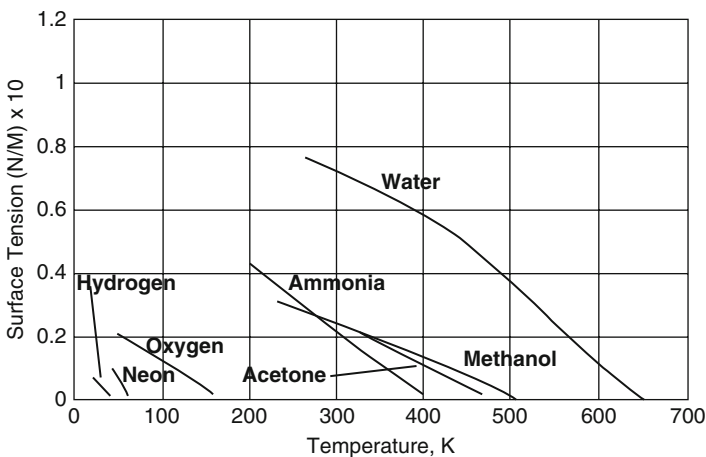


Fig. 1.23 Surface tension for typical heat pipe fluid

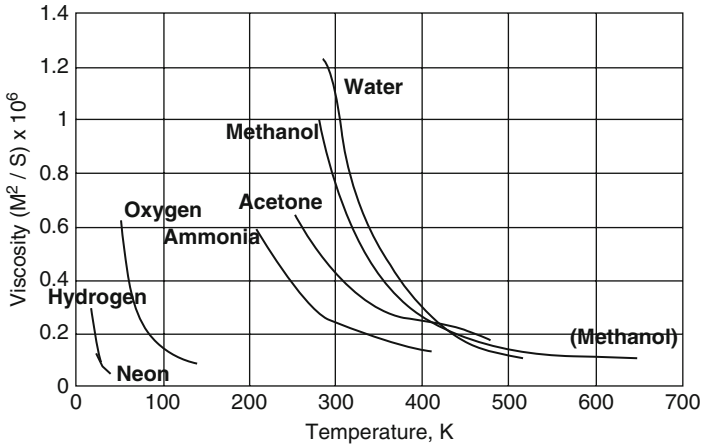


Fig. 1.24 Viscosity for typical heat pipe fluid

Table 1.1 Comparison of latent heat to specific heat for typical heat pipe fluids

Fluid properties				
Fluid	Boiling point K	Latent heat (kJ/kg) h_{fg}	Specific heat (kJ/kg K) c_p	Ratio (K) h_{fg}/c_p
Helium	4	23	4.60	5
Hydrogen	20	446	9.79	46
Neon	27	87	1.84	47
Oxygen	90	213	1.90	112
Nitrogen	77	198	2.04	97
Argon	87	162	1.14	142
Propane	231	425	2.20	193
Ethane	184	488	2.51	194
Methane	111	509	3.45	147
Toluene	384	363	1.72	211
Acetone	329	518	2.15	241
Heptane	372	318	2.24	142
Ammonia	240	1180	4.80	246
Mercury	630	295	0.14	2107
Water	373	2260	4.18	541
Benzene	353	390	1.73	225
Cesium	943	49	0.24	204
Potassium	1032	1920	0.81	2370
Sodium	1152	3600	1.38	2608
Lithium	1615	19,330	4.27	4526
Silver	2450	2350	0.28	8393

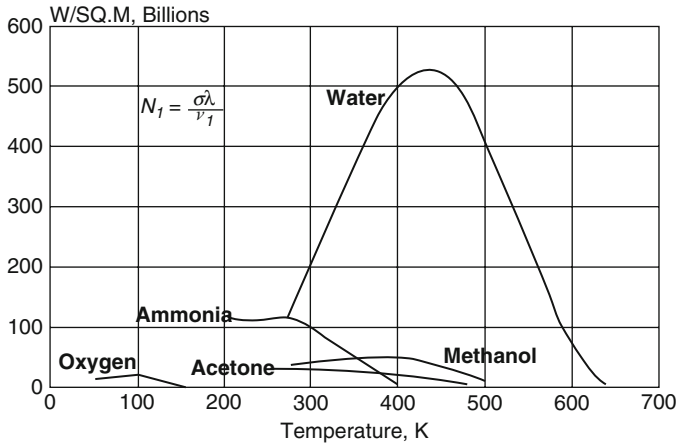


Fig. 1.25 Comparison of liquid transport factor for typical heat pipe working fluids

obtained by utilizing a working fluid that has a high surface tension (σ), a high latent heat (l), and a low liquid viscosity (n_1). These fluid properties are contained in the parameter N_1 , the liquid transport factor. Figure 1.25 is a plot of N_1 for five typical heat pipe working fluids. These data are used as selection criteria for heat pipe working fluids. Once an application is defined, the heat pipe designer reviews the requirements and selects the best working fluid. Below the freezing point of water and above about 200 K, ammonia is an excellent working fluid. Regardless of the fluid chosen, minimum purity must be at least 99.999%. A careful analysis of the purity of the ammonia should be obtained from an independent laboratory prior to use.

The outer container usually consists of a metal tube to provide mechanical support and pressure containment. The chosen design and processing of the container are extremely important in selecting the metal, because they can affect the useful life of the heat pipe. In addition, a compatibility must exist between the pipe material and the working fluid. For heat pipes, working fluid/container compatibility issues encompass any chemical reactions or diffusion processes occurring between the fluid and wall/wick materials that can lead to gas formation and/or corrosion. Table 1.2 lists the compatibilities of several metals and working fluids. Along with the metal/fluid compatibility, other considerations in the metal selection are ease of working the material, extrusion capability of the material, and its weldability. Proper container cleaning and heat pipe processing procedures are of extreme importance, since residual contamination within the heat pipe may also lead to gas generation. Steps must also be taken to ensure the purity of the fluid charge; trace amounts of water in ammonia can lead to a reaction with the aluminum container and the formation of hydrogen gas. Chi [11] and B & K Engineering list standard cleaning and filling methods for a variety of working fluid/wall material combinations. Special consideration must be given to the processing of heat pipes to be used at temperatures below 250 K. As the

Table 1.2 Material composite for heat pipe/fluid combinations

	Aluminum	Stainless steel	Copper	Nickel	Titanium
Water	I	C*	C	C	
Ammonia	C	C		C	
Methanol	I	C	C	C	
Acetone	C	C	C		
Sodium		C		C	I
Potassium				C	I

C, Compatible; I, Incompatible; *, Sensitivity to cleaning

A column of six fluid names is on the left of the table

The fluid names are separated by horizontal lines that extend to the right

In descending order, the fluid names are “water,” “ammonia,” “methanol,” “acetone,” “sodium,” and “potassium”

Five columns are on the right of the table. Each column is headed by a name of a metal. The names of the metals are separated by vertical lines that extend downward. From left to right, the names of the metals are “aluminum,” “stainless steel,” “copper,” “nickel,” and “titanium”

The extended horizontal lines and the extended vertical lines intersect to form boxes. There are five boxes in a horizontal line adjacent to each fluid name. Each box contains one to two symbols or is left blank

The symbols are identified as follows:

C = compatible

I = incompatible

* = sensitivity to cleaning

The fluid names and the contents of the horizontal row of boxes adjacent to them are as follows:

“Water” aluminum—I, stainless steel—C*, copper—c, nickel—C, titanium—blank

“Ammonia” aluminum—C, stainless steel—C, copper—blank, nickel—C, titanium—blank

“Methanol” aluminum—I, stainless steel—C, copper—C, nickel—C, titanium—blank

“Acetone” aluminum—C, stainless steel—C, copper—C, nickel—blank, titanium—blank

“Sodium” aluminum—blank, stainless steel—C, copper—blank, nickel—C, titanium—I

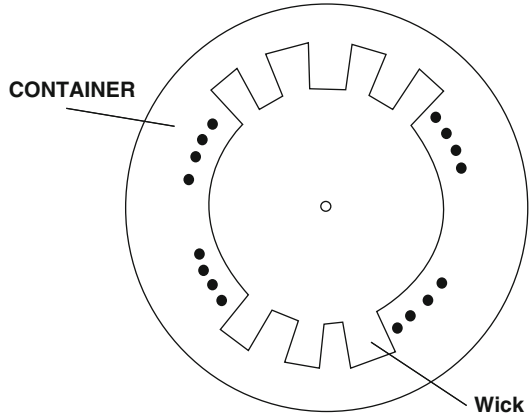
“Potassium” aluminum—blank, stainless steel—blank, copper—blank, nickel—C, titanium

temperature drops, the vapor pressure of the fluid falls off. This allows any noncondensable gas created by contamination to expand, thus creating an even larger problem.

The heat pipe wick structure provides a porous medium for the formation of liquid menisci (which cause the capillary pumping action) and a vehicle for returning the working fluid from the condenser to the evaporator. To accomplish these wick functions effectively, the designer must provide pores, cavities, or channels of the right size, shape, quantity, and location. An optimization technique is used in wick design to find the desired combination of ultimate heat transfer capacity, pumping capability, and temperature drop. The designer must also consider ease of wick fabrication, compatibility with the working fluid, wetting angle, and permeability of the selected wick material. Figure 1.26 depicts a cross-sectional view of an axial groove wick; this design probably is the most commonly used for space application.

In addition, X-ray certification of all welds at the end caps and fill tube is required to ensure good weld penetration and the absence of voids. The heat pipe container must be pressure tested to at least twice its maximum expected operating

Fig. 1.26 Axially grooved wick



pressures (MEOP) prior to filling [20]. Other qualification procedures include performance tests at adverse tilt angles to demonstrate proper wick function, and gas pocket tests performed with the heat pipe in the reflux mode. Heat pipes should be handled with care, especially those that contain ammonia or other high vapor pressure fluids. They should be treated as any other pressure vessel, and appropriate safety precautions must be exercised. Exposure to ammonia vapor can cause severe irritation to eyes and other mucous membranes. Exposure to ammonia liquid can cause severe burns to the skin. Whenever possible, heat pipes should be stored in a cold, dry environment. This will inhibit any internal chemical reactions which produce noncondensable gas.

1.8 Lesson(s) Learned

Heat transfer by means other than the heat pipe can have the following impacts:

1. A price paid with respect to weight and size of the heat transfer equipment
2. Significant heat lost in transfer over considerable distances
3. Electromotive devices, such as liquid pumps, required to move the heat
4. Possible problems presented by operation in zero gravity

Nonadherence to the implementation methods presented above could result in the following possible impacts: improper cleaning and processing of the aluminum container could result in contaminants reacting with the ammonia to form NCG, which will interfere with the flow of vapor and reduce the heat transfer effectiveness. Contaminants reacting with ammonia normally produce hydrogen, and the gas collects in the condenser region. As more and more of the condenser is blocked, the surface area available for heat rejection decreases, reducing the heat transfer effectiveness; ultimately, the heat pipe may cease to function. Failure to certify welds at the end caps and the fill tube could result in improper or defective welds

permitting leaks or catastrophic failure of the pressure vessel. For long-term space missions, working fluids in the appropriate temperature range, such as methanol and water, exhibit an incompatibility with aluminum and should not be used.

1.9 Applications

There are many applications for heat pipes, which are well proven and may now be regarded as routine. In conventional use, heat pipes are integrated into a total thermal subsystem to transport heat from the heat source to remote areas. The heat pipes' ability to act as a primary heat conductive path allows engineers to solve thermal problems in applications with space constraints or other limitations. Thus, you can use heat pipes to carry heat away from the heat-sensitive components to the finned array or a heat sink located in an area where more space for heat dissipation is allowed—leaving room for electronic layout flexibility.

A high-capacity power electronic cooler is an example of a thermal solution where no sufficient space is available to mount directly a finned heat sink to the heat source.

In addition to acting as a heat conductive path and aiding in remote heat transfer, heat pipes can improve thermal solution efficiency. You can accomplish this by embedding heat pipes into the heat sink base or passing the heat pipes through the fins. In most cases, embedding heat pipes into the conventional thermal solution results in size or weight reduction.

The most appropriate application for heat pipe integration into the heat sink base is when the base is large compared with the heat source. In such applications, the heat source location produces the highest temperature. The smaller the heat source, the more spreading has to occur over the heat sink base, resulting in a greater temperature rise in the center of the base. Integrating heat pipes into the base of the heat sink decreases the temperature gradient across the base, yielding a more efficient solution.

You can also improve heat sink fin efficiency with heat pipe integration. Fin efficiency is related to the rate at which the fin can dissipate heat energy. The maximum rate at which the fin can dissipate energy is the rate that would exist if the fin were at base temperature. Therefore, the efficiency of the fin can be improved by passing a heat pipe through the fin. Compared with the traditional finned heat sink, the use of a heat pipe configuration with implementation of fin as part of condenser reduces footprint area of the power heat sink and improves heat dissipation capability.

While external factors such as shock, vibration, force impact, thermal shock, and corrosive environment can affect heat pipe life, its integration into a thermal solution also delivers many benefits. If manufactured and designed properly, heat pipes are highly reliable and have no moving parts. In addition, heat pipes are economical, having little effect on the overall cost of the total thermal.

The heat pipe itself is not a heating or cooling device. Heat pipe assemblies are used for moving heat away from the input area (cooling—the most common application) or for moving heat into the output area (heating). Heat pipe assemblies typically have three parts:

1. The heat input assembly
2. The heat transport assembly (the heat pipe)
3. The heat output assembly

Heat pipe assemblies provide thermal management solutions in all mediums: liquid, solid, and gas. Compared to heat pipes, the traditional methods of cooling (extruded metal heat sinks, fans, water, air conditioning, etc.) all have inherent limitations in size, weight, and efficiency. More and more, the limiting factor in systems of all kinds is the inability to dissipate heat. The desire for more power in smaller packages with less weight often cannot be achieved because of excess heat.

Use of heat pipes in high-power (>150 W) cooling applications has been limited to custom applications requiring either low thermal resistance or having a severely restricted enclosure area. The cost of these larger diameter heat pipes was high due to a limited number of manufacturers and handmade assembly times.

A new and valuable addition to the heat transfer community, a heat transport device known as a loop heat pipe (LHP), is discussed in this work. This body of research is very important as the LHP is becoming increasingly prevalent in heat transfer applications. US commercial use of the loop heat pipe will begin on the next generation of communications satellites being developed and built by Hughes Space and Communications Company. These satellites take advantage of the passive nature of the LHP, requiring no external means of pumping, along with its ability to transport large quantities of heat over significant distances. This device comes to the heat transfer community at an ideal time, as the aerospace industry is demanding higher and higher power payloads and this increasing power must be handled by the most efficient means possible. The LHP is also being investigated for uses in ground-based applications such as solar collectors and computer cooling. This dissertation focuses on experimentation conducted with a space-based satellite application in mind; however, results are applicable to other implementations as well. The LHP is a descendant of the conventional heat pipe. The LHP utilizes the advantages of the conventional heat pipe while overcoming some of the conventional heat pipe's inherent disadvantages. This dissertation serves as a complete body of work on this new device, from background and literature review on the development and history of the LHP to important computer simulation and experimental work, both ground based and space based, performed on the LHP in an effort to gain a thorough understanding of the workings of the loop heat pipe and to investigate novel new applications for the LHP such as the ability to control the temperature of an entire spacecraft payload with a minute fraction of the heater power once required. The LHP introduces important new opportunities to the heat transfer community, and the research presented here furthers the knowledge and understanding of this breakthrough device.

The application of heat pipes can be as diverse as their structure and shapes. We can claim these unique heat transfer devices are used in many fields in the industry, and they have played very important roles from simple heat exchanger to electronic, space application, nuclear reactor, oil lines, and even for constructing ice pontoons through marshes and the foundations of drilling towers, as well as roads in permafrost regions. Reference [21] has a variety of flavors of heat pipe applications in the industry and the companies and manufacturers who are involved with their unique design and application of such devices.

For example, within the USA, there are applications and development in progress in a drill for ultra deep drilling of a bore in the form of a miniature fast-neutron reactor cooled by means of heat pipes.

Other application of heat pipe can be seen in centrifugal heat pipe shapes that are used for cooling asynchronous motors with short-circuited cast rotors. Such motors are used mainly in mechanical engineering. With the use of centrifugal heat pipes in a rotor, it has become possible to control the motor speed electrically, eliminating the need for complex transmissions and gear trains [21]. Investigations are currently in progress in the USSR to explore the possible use of heat pipes to cool transformers, both air filled and oil filled, miniature, and high power, and for cooling of electrical busbars.

The West German firm Brown Boveri Corporation has developed a system of electronic devices with heat pipes.

1. Thyristor systems of power greater than 1 kW; the thermal resistance R of the heat pipe is 0.035 K/W and the cooling air velocity is $V = 6$ m/s.
2. A device for a portable current rectifier system (700 W, thermal resistance; 0.055~, cooling air; velocity, $V = 6$ m/s).

Heat pipes have proved adaptable to the incorporation of electronic equipment, thereby increasing the cooling effect by factors of 10.

Products of the British SRDE laboratory (Signal Research and Development Establishment) include the following: heat pipes in the form of planar electrical insulators, a heat pipe of very small diameter, and various combinations of heat pipes and thermally insulating modules.

Very interesting possibilities have opened up for producing static batteries and thermal energy converters based on heat pipes, thermal diodes, vapor chambers, etc., and materials which vary their aggregate state (fused salts, metals, sulfur with halogens, etc.); operating temperature is 500–800~, the material of the heat pipes is stainless steel, and the heat transfer agent is sodium. The thermal power stored can be up to 10–100 kW/h. High-temperature heat pipes using alkali metals can be employed successfully as electrodes in plasma generators.

In the energy industry, there is a trend to build electric stations using solar energy and hot springs. At present, an electric station of power of at least 100 kW is under construction in the southern USA; it takes the form of a battery of high-temperature heat pipes, heated by the sun, and working into water vapor generators or thermo-electric converters. Such batteries of heat pipes, linked to heat-storage units, will

make it possible to develop electrical energy around the clock. There are plans to use heat pipes as electric cables and distribution lines.

On October 4, 1974, a sounding rocket was launched into space (the Black Brant Sounding Rocket), which carried heat pipes made by the NASA/Goddard Space Flight Center, ESRO, GFW, Hughes Aircraft Company, and NASA/Ames:

1. ESRO constructed two aluminum heat pipes of length 885 mm and diameter 5 mm. The wick was a single layer of stainless steel mesh with an artery diameter of 0.5 mm. One pipe was filled with ammonia and the other with acetone. The acetone heat pipe transmitted 8.4 W of power, and the ammonia pipe transmitted 21 W. The heat sink was an aluminum block.
2. GFW (Gesellschaft für Weltraumforschung) of the West German Ministry of Technology constructed a flat aluminum heat pipe in the form of a disk of diameter 150 mm and a titanium heat pipe of length 600 mm, charged with methanol, with its end face joined to the disk by an aluminum tube. The flat heat pipe was filled with acetone, and the other end was joined to a heat-storage device (a canister with a molten substance)—“Eicosane”—with a fusion temperature of 35 °C. This system transmitted 26 W of power.
3. The Hughes Aircraft Company constructed two flexible heat pipes made of stainless steel (6.4 mm in diameter; 270 cm in length). The working liquid is methanol, and the wick is a metal mesh.
4. NASA/Ames constructed two stainless steel heat pipes of length 910 mm and diameter 12.7 mm. The liquid is methanol, and the inert gas is nitrogen. The wick is a screw thread on the body, and the artery is a wafer of metallic felt. This kind of artery is insensitive to the presence of noncondensable gas.
5. NASA constructed a cryogenic heat pipe made of aluminum with longitudinal channels of length 910 mm and diameter 16 mm, charged with methanol.

Thus, in the international experiment on October 4, 1974, the organizations NASA/GSFC (Grumman and TRW), NASA/Ames (Hughes), Hughes (Hughes), ESRO (the IKE Institute in Stuttgart), and GFW (Dornier) took part in the testing of heat pipes in space. Of these, Grumman constructed five different groups of heat pipes, and TRW constructed three.

In addition to the sounding rockets, NASA has used a number of satellites for testing heat pipes, to evaluate the effect of long-term weightless conditions on heat pipe parameters (the spacecraft Skylab, OAO-III, ATS-6, CTS, etc.).

The French National Center for Space Research, CNS, independently of the American and European Space Center (USA), developed and operated a program of space experiments with heat pipes, constructed by the Aerospatiale and SABCA companies. In November, 1974, the French sounding rocket ERIDAN 214 was launched, carrying a radiator of heat pipes. The aim of the experiment was to verify the operational capability of heat pipes under weightless conditions, to verify that the heat pipes would be ready to operate at the start of a rocket flight, and to select various heat pipe structures for spacecraft equipment.

Three types of heat pipe were investigated:

1. A curved heat pipe made by SABCA, of length 560 mm and diameter 3.2 mm, made of steel stairs, the filter being a stainless steel mesh, with ammonia as the heat transfer agent. The transmitted power was 4 W. The pipe was flexible.
2. A heat pipe made by the CENG organization (the atomic center in Grenoble) of length 270 mm and diameter 5 mm, made of copper, with a wick made of sintered bronze powder. The heat transfer agent was water. The transmitted power was 20 W.
3. A SABCA heat pipe, similar to No. 1, but straight. The transmitted power was 5 W. The heat sink was a box with a variable-phase fusible substance $T_f = 28.5\text{ }^\circ\text{C}$ (n-octadecane). The energy source was an electric battery with $U = 27\text{ V}$. The total weight of the experimental equipment was 2.3 kg.

These investigations point very clearly to positive gains at present, and we can confidently assert that heat pipes will find wide applications in space in the near future. For example, the USA plans to use heat pipes for thermal control and thermal protection of the reusable shuttle and also for the Spacelab space laboratory.

For these, the heat-sensitive equipment will be located in boxes or canisters within which the temperature will be held constant by means of heat pipes located in the walls of the enclosure.

Reference [21] provides a vast variety application of heat pipes in the present industry and future trend of it.

1.10 Summary

Heat pipes

General

A heat pipe is a passive energy recovery heat exchanger that has the appearance of a common plate-finned water coil except the tubes are not interconnected. Additionally, it is divided into two sections by a sealed partition. Hot air passes through one side that is known as evaporator, and it is cooling while cooler air passes through the other side that is known as condenser. While heat pipes are sensible heat transfer exchangers, if the air conditions are such that condensation forms on the fins, there can be some latent heat transfer and improved efficiency (Fig. 1.27)

Heat pipes are tubes that have a capillary wick inside running the length of the tube, are evacuated and then filled with a refrigerant as the working fluid, and are permanently sealed. The working fluid is selected to meet the desired temperature conditions and is usually a Class I refrigerant. Fins are similar to conventional coils—corrugated plate, plain plate, spiral design. Tube and fin spacing are selected for appropriate pressure drop at design face velocity. HVAC systems typically use copper heat pipes with aluminum fins; other materials are available

Advantages

- Passive heat exchange with no moving parts
 - Relatively space efficient
 - The cooling or heating equipment size can be reduced in some cases
-

(continued)

Heat pipes

- The moisture removal capacity of existing cooling equipment can be improved
 - No cross-contamination between airstreams
-

Disadvantages

The use of the heat pipe:

- Adds to the first cost and to the fan power to overcome its resistance
 - Requires that the two airstreams be adjacent to each other
 - Requires that the airstreams must be relatively clean and may require filtration
-

Applications

Heat pipe heat exchanger enhancement can improve system latent capacity. For example, a 1 °F dry bulb drop in air entering a cooling coil can increase the latent capacity by about 3 %. The heat pipe's transfer of heat directly from the entering air to the low-temperature air leaving the cooling coil saves both cooling and reheating energy. It can also be used to precool or preheat incoming outdoor air with exhaust air from the conditioned spaces

Best applications

- Where lower relative humidity is an advantage for comfort or process reasons, the use of a heat pipe can help. A heat pipe used between the warm air entering the cooling coil and the cool air leaving the coil transfers sensible heat to the cold exiting air, thereby reducing or even eliminating the reheat needs. Also the heat pipe precools the air before it reaches the cooling coil, increasing the latent capacity and possibly lowering the system cooling energy use
 - Projects that require a large percentage of outdoor air and have the exhaust air duct in close proximity to the intake can increase system efficiency by transferring heat in the exhaust to either precool or preheat the incoming air
-

Possible applications

- Use of a dry heat pipe coupled with a heat pump in humid climate areas
 - Heat pipe heat exchanger enhancement used with a single-path or dual-path system in a supermarket application
 - Existing buildings where codes require it or they have "sick building" syndrome and the amount of outdoor air intake must be increased
 - New buildings where the required amount of ventilation air causes excess loads or where the desired equipment does not have sufficient latent capacity
-

Applications to avoid

- Where the intake or exhaust air ducts must be rerouted extensively; the benefits are likely not to offset the higher fan energy and first cost
 - Use of heat pipe sprays without careful water treatment. Corrosion, scale, and fouling of the heat pipe where a wetted condition can occur need to be addressed carefully
-

Technology types (resource)

Hot air is the heat source, flows over the evaporator side, is cooled, and evaporates the working fluid. Cooler air is the heat sink, flows over the condenser side, is heated, and condenses the working fluid. Vapor pressure difference drives the evaporated vapor to the condenser end, and the condensed liquid is wicked back to the evaporator by capillary action. Performance is affected by the orientation from horizontal. Operating the heat pipe on a slope with the hot (evaporator) end below horizontal improves the liquid flow back to the evaporator. Heat pipes can be applied in parallel or series

Efficiency

Heat pipes are typically applied with air face velocities in the 450–550 ft/min range, with four to eight rows deep and 14 fins per inch, and have an effectiveness of 45–65 %. For example, if entering air at 77 °F is cooled by the heat pipe evaporator to 70 °F and the air off the cooling coil is reheated from 55 to 65 °F by the condenser section, the effectiveness is 45 % $[(65 - 55)/(77 - 55) = 45 \%$]. As the number of rows increases, effectiveness increases but at a declining rate. For example,

(continued)

 Heat pipes

doubling the rows of a 48 % effective heat pipe increases the effectiveness to 65 %

Tilt control can be used to:

- Change operation for seasonal changeover
 - Modulate capacity to prevent overheating or overcooling of supply air
 - Decrease effectiveness to prevent frost formation at low outdoor air temperatures
- Tilt control (six maximum) involves pivoting the exchanger about its base at the center with a temperature-actuated tilt controller at one end. Face and bypass dampers can also be used
-

 Manufacturers

Heat pipes

1. American Heat Pipes, Inc.

6914 E. Fowler Ave.

Suite E

Tampa, FL 33617

1-800-727-6511

2. Dectron Inc.

4300 Blvd. Poirier

Montreal, PQ H4R 2C5

Canada

(514) 334-9609

mail@dectron.com

3. Des Champs Laboratories Inc.

P.O. Box 220

Douglas Way

Natural Bridges Station, VA 24579

(703) 291-1111

4. EcoTech Consultants, Inc.

3466 Holcombe Bridge Road

Suite 1000

Norcross, GA 30092

(404) 723-6564

5. Heat Pipe Technology Inc.

P.O. Box 999

Alachua, FL 32615-0999

1-800-393-2041

6. Munters DryCool

16900 Jordan Rd.

Selma, TX 78154-1272

1-800-229-8557

moreinfo-dc@americas.munters.com

7. Nautica Dehumidifiers, Inc.

9 East Carver St.

Huntington, NY 11743

(516) 351-8249

dehumidify@aol.com

8. Octagon Air Systems

1724 Koppers Road

Conley, GA 30288

(404) 609-8881

(continued)

 Heat pipes

9. Power-Save International
 P.O. Box 880
 Cottage Grove, OR 97424
 1-800-432-5560

10. Seasons 4 Inc.
 4500 Industrial Access Road
 Douglasville, GA 30134
 (770) 489-0716

11. Temprite Industries
 1555 Hawthorne Lane
 West Chicago, IL 60185
 1-800-552-9300

12. Venmar CES
 2525 Wentz Ave.
 Saskatoon, SK S7K 2K9
 Canada
 1-800-667-3717
 customerservice@venmarvent.com

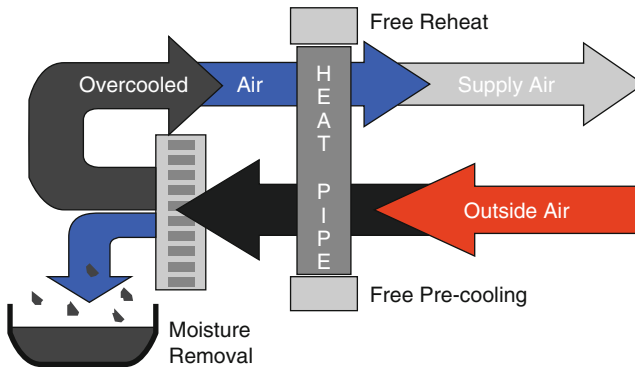


Fig. 1.27 Heat pipe application concept

References

1. Gaugler, R. S. (1944, June 6). *Heat transfer device*. U.S. Patent 2,350,348.
2. Trefethen, L. (1962, February). *On the surface tension pumping of liquids or a possible role of the candlewick in space exploration*. G. E. Tech. Info., Ser. No. 615 D114.
3. Wyatt, T. (Johns Hopkins/Applied Physics Lab.). (1963). *Satellite temperature stabilization system. Early development of spacecraft heat pipes for temperature stabilization*. U.S. Patent No. 3,152,774 (October 13, 1964), application was filed June 11, 1963.
4. Grove, G. M., Cotter, T. P., & Erikson, G. F. (1964). Structures of very high thermal conductivity. *Journal of Applied Physics*, 35, 1990.
5. Deverall, J. E., & Kemme, J. E. (1964, October). *High thermal conductance devices utilizing the boiling of lithium and silver*. Los Alamos Scientific Laboratory report LA-3211.

6. Grover, G. M., Cotter, T. P., & Erickson, G. F. (1964). Structures of very high thermal conductance. *Journal of Applied Physics*, 35(6), 1990–1991.
7. Grover, G. M., Bohdansky, J., & Busse, C. A. (1965). *The use of a new heat removal system in space thermionic power supplies*. European Atomic Energy Community—EURATOM report EUR 2229.
8. Cotter, T. P., Deverall, J., Erickson, G. F., Grover, G. M., Keddy, E. S., Kemme, J. E., et al. (1965). *Status report on theory and experiments on heat pipes at Los Alamos*. Proceedings of the International Conference on Thermionic Power Generation, London, September 1965.
9. Ranken, W. A., & Kemme, J. E. (1965). *Survey of Los Alamos and EURATOM heat pipe investigations*. Proc. IEEE Thermionic Conversion Specialist Conf., San Diego, California, October 1965, Los Alamos Scientific Laboratory, report LA-DC-7555.
10. Kemme, J. E. (1966). *Heat pipe capability experiments*. Proc. of Joint AEC Sandia Laboratories report SC-M-66-623, 1, October 1966. Expanded version of this paper, Los Alamos Scientific Laboratory report LA-3585-MS (August 1966), also as LA-DC-7938. Revised version of LA-3583-MS, Proc. EEE Thermionic Conversion Specialist Conference, Houston, Texas, (November 1966).
11. Chi, S. W. (1976). *Heat pipe theory and practice*. New York: McGraw-Hill.
12. Dunn, P. D., & Reay, D. A. (1982). *Heat pipes* (3rd ed.). New York: Pergamon.
13. Bennett, G. A. (1977, September 1). *Conceptual design of a heat pipe radiator*. LA-6939-MS Technical Report, Los Alamos Scientific Lab., N.Mex. (USA).
14. Gerasimov, Y. F., Maidanik, Y. F., & Schegolev, G. T. (1975). Low-temperature heat pipes with separated channels for vapor and liquid. *Journal of Engineering Physics*, 28(6), 957–960 (in Russian).
15. Watanabe, K., Kimura, A., Kawabata, K., Yanagida, T., & Yamauchi M. (2001). Development of a variable-conductance heat-pipe for a sodium-sulfur (NAS) battery. *Furukawa Review*, 20.
16. Marcus, B. D. (1971). *Theory and design of variable conductance heat pipes: Control techniques*. Research Report No. 2, July 1971, NASA 13111-6027-R0-00.
17. Kemme, J. E. (1969, August 1). *Heat pipe design considerations*. Los Alamos Scientific Laboratory report LA-4221-MS.
18. Woloshun, K. A., Merrigan, M. A., & Best, E. D. (1988). *HPIPE: A steady-state heat pipe analysis program, A User's Manual*.
19. Peterson, G. P. (1994). *An introduction to heat pipes: Modeling, testing, and applications* (pp. 175–210). New York: John Wiley & Sons.
20. Brennan, P. J., & Kroliczek, E. J. (1979). *Heat pipe design handbook*. Towson, MD: B & K Engineering, Inc.
21. MIL-STD-1522A (USAF). (1984, May). *Military standard general requirements for safe design and operation of pressurized missile and space systems*.

Chapter 2

Heat Pipe Theory and Modeling

In this chapter, we will discuss the theory of heat pipe with an approach that our readers have no knowledge of advanced mathematics, physics, and heat pipe. We cover the basic science and technology behind the heat pipe. Whenever we had to refer to basic knowledge of physics, fluid mechanics, and gas dynamics, Wiki site or very basic physics books to give the reader some general idea of specific topics of discussion in the particular section of this chapter along with heat pipe science were utilized. This section covers the fundamental theory behind the heat pipe based on different research papers and books available at present time in order to open a clear path for reader to design and fabricate their required heat pipe within their applications.

2.1 Heat Pipe Theory

Heat transport has been one of the most difficult and inefficient tasks in thermal management. It often results in costly heat transfer losses and reduced overall efficiencies. Performance of mechanical and electronic components inside automobiles is now governed by efficiency of cooling system [1]. Heat transfer by heat pipes is one of the fastest and most efficient methods for thermal management. Heat pipes are highly conductive heat transfer device. They use the latent heat of the working fluid for efficient heat transfer over very small temperature drop. They have been a subject of numerous studies since the early 1950s and are commercially available in a variety of forms. The heat pipe is a promising technology that has received significant research interest since the early 1950s.

2.2 Fundamental Considerations

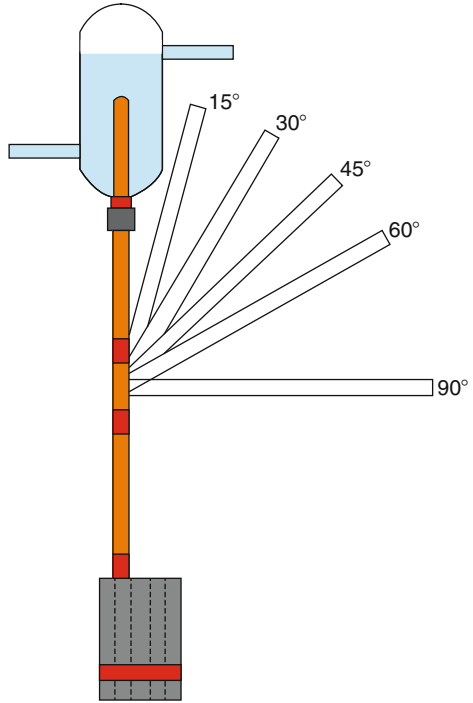
A heat pipe is a very efficient heat conductor. A typical heat pipe consists of a vessel in which its inner walls are lined with a wick structure. The heat pipe vessel is first vacuumed, then charged with a working fluid, and hermetically sealed. When the heat pipe is heated at one end, the working fluid evaporates from liquid to vapor (phase change). The vapor travels through the hollow core of the heat pipe to the other end of the heat pipe. Here, the vapor condenses back to liquid and releases heat at the same time. The liquid then travels back to the original end of the heat pipe via the wick by capillary action.

The energy required to change phase from liquid to gas is called the latent heat of evaporation. The heat pipe can be bent and flattened in order to meet the needs of different structure, which need no base and can get powerful heat conduction. References [1, 2] are about the investigation of the effect bending has on the performance of heat pipes. Flexible and prebent heat pipes have been studied and successfully demonstrated in the past. Bendable heat pipes, which can be bent after fabrication as needed, are a novel device developed during this study. The effect of bending on temperature drop, performance, and performance limits was investigated. The early studies mostly concentrated on heat pipes used in straight configurations. However, many practical designs demand heat pipes in contorted shapes [2, 3]. This thesis investigates the feasibility of bendable heat pipes. These heat pipes can be bent after fabrication without affecting their performance.

The heat fluxes from electronic components are steadily increasing and have now, in some applications, reached levels where air cooling is no longer sufficient. One alternative solution, which has received much attention during the last decade, is to use heat pipes or thermosyphons for transferring or spreading the dissipated heat. In this chapter, two-phase thermosyphon loops are discussed. Especially, the choice of fluid and its influence on the design and performance is treated. The discussion is supported by results from simulations concerning heat transfer and pressure drop. In general, it is found that high-pressure fluids will give better performance and more compact designs as high-pressure results in higher boiling heat transfer coefficients and smaller necessary tube diameter.

A heat pipe is a very efficient heat conductor. A typical heat pipe consists of a vessel in which its inner walls are lined with a wick structure. The heat pipe vessel is first vacuumed, then charged with a working fluid, and hermetically sealed. When the heat pipe is heated at one end, the working fluid evaporates from liquid to vapor (phase change). The vapor travels through the hollow core of the heat pipe to the other end of the heat pipe. Here, the vapor condenses back to liquid and releases heat at the same time. The liquid then travels back to the original end of the heat pipe via the wick by capillary action. The energy required to change phase from liquid to gas is called the latent heat of evaporation. A flexible heat pipe was developed and built by Bliss et al. [4] to analyze its operating characteristics for varying degrees of bend and under vibration in an unbent mode. The flexible heat pipes have received regular attention over the years, and not surprisingly many of

Fig. 2.1 Schematic of bending configurations for [1] HP01



the problems were put forth by the aerospace industry. Figure 2.1 is a demonstration of a typical flexible heat pipe.

The heat pipe can be bent and flattened in order to meet the needs of different structures. The short and thick ones are called heat column, which need no base and can get powerful heat conduction. Heat pipes are used to perform several important heat transfer roles in the chemical and closely allied industries. Examples include heat recovery, the isothermalizing of processes, and spot cooling in the molding of plastics. In its simplest form, the heat pipe possesses the property of extremely high thermal conductance, often several hundred times that of metals. As a result, the heat pipe can produce nearly isothermal conditions, making an almost ideal heat transfer element. In another form, the heat pipe can provide positive, rapid, and precise control of temperature under conditions that vary with respect to time.

The heat pipe is self-contained, has no mechanical moving parts, and requires no external power other than the heat that flows through it.

- **Heat Pipe Heat/Sink Module with Penetrated Fin**

The ones use thick-gap fins (Cu or Al) on the condensation end of heat pipes. There are two methods, which are oppressively match and soldering process, to assemble the fins and heat pipes. Now these types of heat sinks are widely used in telecommunication, note books, industry control equipments, etc. They greatly reduce the size and improve thermal performance effectively.

- **Heat Pipe Heat/Sink Module with Embedded Heat Pipe**

Heat pipes embedded in the base of the heat sink can balance the temperature distributing and raise thermal efficiency. Especially under the conditions of limited heat area but expanse base area, this kind of heat sink can bring a better, homogenized temperature distribution.

Modern-day electronic systems are compact and often include one or more high-power, high-density devices, such as microprocessors. As the functionality of these microprocessors increases, they are becoming denser, operating at higher speeds, and are, thus, producing more heat. The heat-generating devices are typically incorporated into one or more integrated circuits. Each integrated circuit, or die, is housed in a relatively flat circuit package, or housing. As used hereinafter, the term “chip” refers to the circuit package and the included die. The high-power, high-density chips frequently cannot be adequately cooled by the conventional forced air-cooling system used to cool the overall electronic system. Instead, these chips require their own, i.e., dedicated, cooling systems. One type of dedicated cooling system uses a liquid coolant that changes phase as it absorbs and dissipates heat. The coolant changes from liquid to vapor as heat is transferred to it from the chip and changes from vapor back to liquid as it dissipates the heat to the surrounding environment. The coolant may be housed in a conventional heat pipe, which has one end that acts as an evaporator and an opposing end that acts as a condenser. The end of the pipe that acts as the evaporator is placed in thermal contact with the chip and conducts heat, through its walls, from the chip to the coolant. This causes the coolant to vaporize. The vapor then travels to the condenser end of the pipe. At this end, heat is dissipated from the vapor to the surrounding environment and the vapor condenses. A wick or other capillary device draws the condensed coolant back through the pipe to the evaporator, where heat is again transferred to it from the chip. Conventional heat pipes are relatively rigid and may include expandable bellows that are also relatively rigid. These heat pipes can be bent, but large bending radii are required and thick effective cross-sections result. These conventional heat pipes thus cannot be readily deformed, either elastically or plastically, to match the space constraints of the electronic system. If the heat pipe is, for example, metal, it generally cannot be flexed or bent, even to facilitate installation. Accordingly, accessible space within the system, that is, the size and shape of the pipe and proximate to the heat-generating chip, must be created to accommodate the pipe. As consumers demand smaller, more powerful systems, providing space for these rigid heat pipes becomes more and more of a problem. Components other than those incorporated into the relatively flat circuit housings, for example, power transistors, which are generally cylindrical, may also require cooling. The conventional, rigid heat pipes are not readily configurable, and thus, custom, shaped pipes must be specifically manufactured for these components. Such custom pipes are generally more expensive to produce. What is needed is a heat pipe that can fit into relatively narrow spaces and can be readily shaped, elastically or plastically, to conform to existing space within a system and/or to the components that are not incorporated into the circuit housings. It is expected

that the high-power chips will be included in more and more devices, to accommodate consumer demand for faster, more powerful electronic systems. Accordingly, heat pipes will be included in more and more of these systems. The cost of manufacture of these heat pipes thus becomes a significant factor in the cost of manufacture and the pricing of the systems. Thus, what is needed is a heat pipe that is inexpensive to manufacture.

2.3 Operating Characteristics of Heat Pipes

A heat pipe is broadly divided in three sections, namely, evaporator, adiabatic, and condenser. A typical heat pipe as shown in Fig. 2.1 has one evaporator section that takes heat from a source. The heat absorbed in the evaporator causes change of phase of the working fluid from liquid to vapor. The increased vapor pressure in the evaporator causes the vapor to exit from the evaporator section and travel through the adiabatic section. Traveling through the adiabatic section, the vapor reaches the condenser region where condensation rejects the latent heat of the fluid to the sink. The condensed liquid is pumped back against an adverse pressure gradient to the evaporator by a combination of the capillary pumping action and/or bulk forces. This fluid circuit is repeated during the normal operation of the heat pipe and can continue as long as there is sufficient vapor pressure and capillary pressure to support its operation.

At the evaporator end, the liquid recedes into the wick pores, and hence the menisci in the pores at the vapor interface are highly curved, whereas the liquid menisci at vapor interface in the condenser end are almost flat. This difference in the interface curvature of the menisci at the vapor interface coupled with the surface tension of the working fluid causes a capillary pressure gradient at the liquid–vapor interface along the length of the pipe. This capillary pressure gradient pumps the working fluid against various pressure losses such as friction and inertia and against bulk body forces [5]. This axial variation of pressure is illustrated in Figs. 2.2 and 2.3.

Heat pipes transport heat by two-phase flow of a working fluid [5]. Shown in Fig. 2.4, a heat pipe is a vacuum-tight device consisting of a working fluid and a wick structure. The heat input vaporizes the liquid working fluid inside the wick in

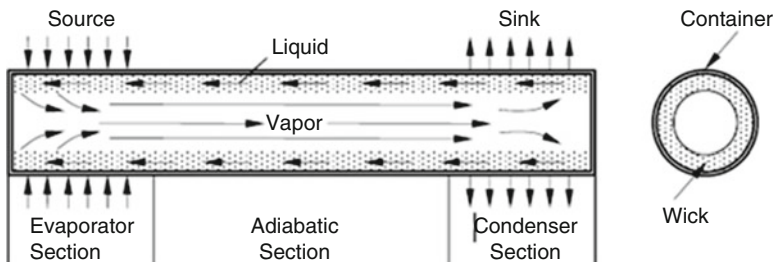


Fig. 2.2 Schematic of construction and operation of a typical heat pipe

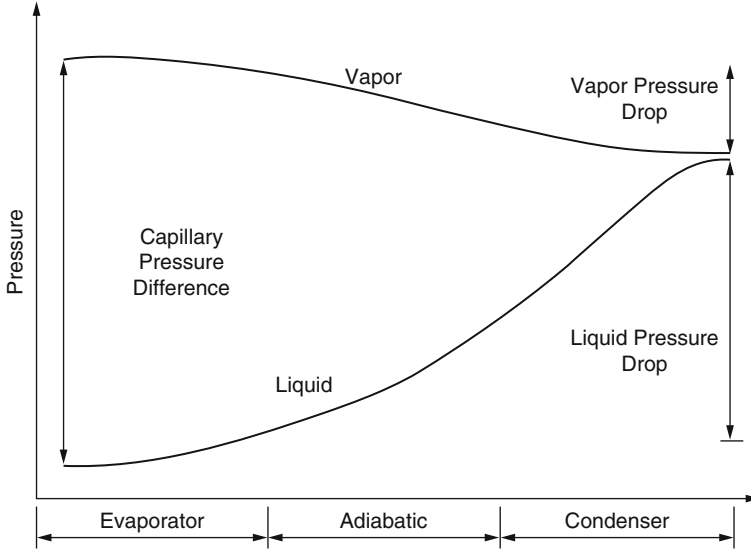
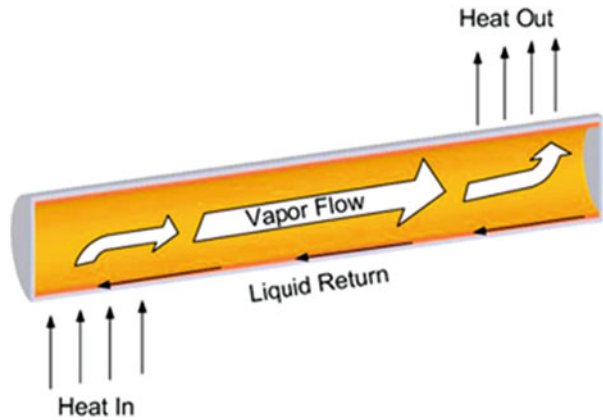


Fig. 2.3 Pressure variation along a heat pipe

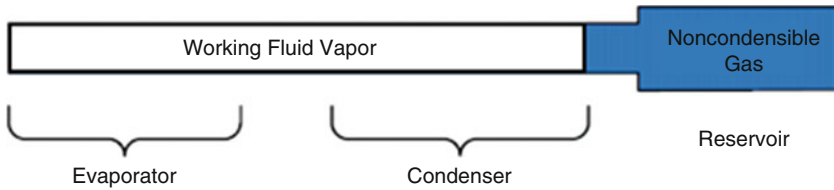
Fig. 2.4 Basic heat pipe operation



the evaporator section. The saturated vapor, carrying the latent heat of vaporization, flows towards the colder condenser section. In the condenser, the vapor condenses and gives up its latent heat. The condensed liquid returns to the evaporator through the wick structure by capillary action. The phase change processes and two-phase flow circulation continue as long as the temperature gradient between the evaporator and condenser is maintained.

Variable conductance heat pipes, or VCHPs, can passively maintain a relatively constant evaporator temperature over a wide range of input powers [6–8]. Shown in Fig. 2.5, a VCHP is similar to a conventional heat pipe but has a reservoir and

High Heat Load - NCG Compresses



Low Heat Load - NCG Expands

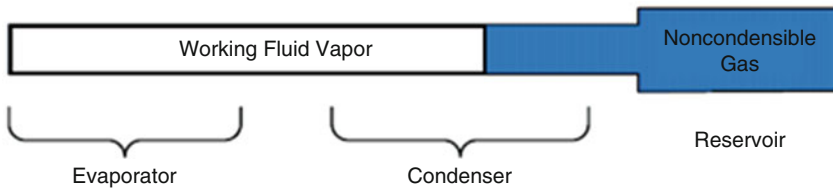


Fig. 2.5 Variable conductance heat pipes (VCHP) operation

controlled amount of non-condensable gas (NCG). When the heat pipe is operating, the gas is swept toward the condenser end of the heat pipe by the flow of the working fluid vapor. The NCG then blocks the working fluid from reaching a portion of the condenser. The VCHP works by varying the amount of condenser available to the working fluid. As the evaporator temperature increases, the vapor temperature rises, the NCG compresses (Fig. 2.5 top part), and more condenser is exposed to the working fluid. This increases the effective thermal conductivity of the heat pipe and drives the temperature of the evaporator down. Conversely, if the evaporator cools, the vapor pressure drops and the NCG expands (Fig. 2.5 bottom part). This reduces the amount of available condenser, decreases the heat pipe thermal conductivity, and drives the evaporator temperature up.

For the simple VCHP shown in Fig. 2.5, the degree of control depends primarily on two factors: the slope of the working fluid vapor pressure curve and the ratio of reservoir and condenser volumes. Working fluids having steeper vapor pressure curves at the particular operating temperature result in tighter temperature control. Small changes in temperature result in large changes in pressure and subsequently large changes in the NCG volume. Similarly, large reservoir volumes improve control because a given pressure change results in a larger change in the position of the gas/vapor interface in the condenser. Smaller reservoirs contain less gas and can provide less change in the position of the gas/vapor interface. Typical turndown ratios of between 5:1 and 10:1 are possible depending upon reservoir size. Temperature control can be as close as ± 3 °C for some combinations of working fluid and operating temperature.

2.4 Operating Limits

As with any other system, the performance and operation of a heat pipe is limited by various parameters. Physical phenomena that might limit heat transport in heat pipes include capillary forces, choked flow, interfacial shear, and incipient boiling. The heat transfer limitations depend on the size and shape of the pipe, working fluid, wick parameters, and operating temperature. The lowest limit among these constraints defines the maximum heat transport limitation of a heat pipe at a given temperature [9].

2.5 Capillary Pressure Differences or Balance

The difference in the capillary pressure across the liquid–vapor interfaces governs the operation of the heat pipes. This is one of the most important parameters that affect the performance and operation of a heat pipe. It is usually a major limiting factor in the working of low-temperature heat pipes. The capillary limit is encountered when the capillary pressure is not sufficient to pump the liquid back to evaporator, causing the dryout of the wick of the evaporator end. The physical structure of the wick is one of the most important reasons for this limit and the type of working fluid also affects it. Once limit is encountered, any further increase in heat input may cause serious damage to the heat pipe [9].

When a heat pipe is operating in steady state, there is a continuous flow of vapor from the evaporator section to the condenser section and liquid from the condenser section to the evaporator section through the wick. These flows are possible because of the vapor pressure gradient (Δp_v) and the liquid pressure gradient (Δp_l) along the length of the heat pipe (Fig. 2.6). There exists a capillary pressure due to the menisci formed at the liquid–vapor interface; this capillary pressure ($\Delta p_{\text{cap,max}}$) is necessary for the flow of liquid back to the evaporator. In addition, there are pressure gradients due to phase change taking place at the evaporator ($\Delta p_{\text{e,phase}}$) and the condenser ($\Delta p_{\text{c,phase}}$) ends and due to gravity (Δp_g). The capillary limit is expressed as

$$\Delta p_{\text{cap,max}} \geq \Delta p_l + \Delta p_v + \Delta p_{\text{e,phase}} + \Delta p_{\text{c,phase}} + \Delta p_g \quad (\text{Eq.2.1a})$$

Another form of Eq. (2.1a) can be established bases on operating inclination angle of heat pipe [10]:

$$\Delta p_{\text{cap,max}} \geq \Delta p_l + \Delta p_v \pm \Delta p_g \quad (\text{Eq.2.1b})$$

where Δp_l is the pressure drop required to return the liquid from the condenser to the evaporator, Δp_v is the pressure drop necessary to cause the vapor to flow from the evaporator to the condenser, and Δp_g is the gravitational head which is a

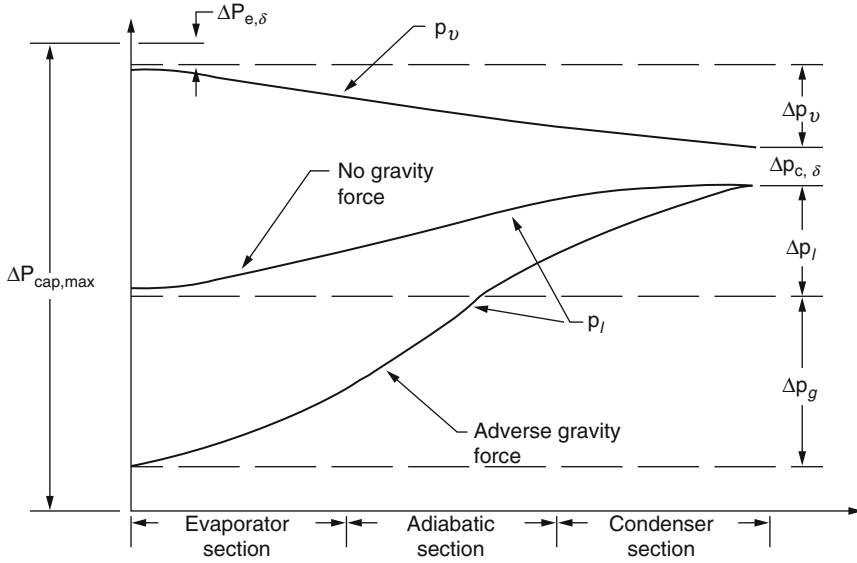


Fig. 2.6 Pressure balance in a heat pipe

function of the inclination angle of the heat pipe. If the evaporator section lies above the condenser section, Δp_g represents a pressure drop (a positive sign in Eq. (2.1b)), which the reverse orientation will yield a pressure rise (a negative sign in Eq. (2.1b)).

In order for the heat pipe to operate properly, the above equation must be satisfied for the pressure balance and the maximum capillary head can be calculated by [9]

$$\Delta p_{\text{cap,max}} = \frac{2\sigma}{r_{\text{eff}}} \tag{Eq.2.2}$$

where r_{eff} is the effective pore or capillary radius corrected by the factor $l/\cos\theta_{\text{max,min}}$. In Eq. (2.1), Δp_v should be considered as absolute vapor pressure along the heat pipe and Δp_g is considered as pressure drop in the liquid due to influence of gravitational forces in the direction of the heat pipe axis and expressed as

$$\Delta p_g = \rho_l g L_t \sin \phi \tag{Eq.2.3}$$

where ϕ is the inclination angle of the heat pipe in respect to horizontal direction. Both $\Delta p_{\text{le,phase}}$ and $\Delta p_{\text{c,phase}}$ are the pressure drops due to the evaporation and condensation at the liquid–vapor interfaces, respectively, and usually can be neglected. Δp_l is the major factor which causes the capillary limit and presents the pressure drop of the liquid flow in a heat pipe wick structure due to frictional drag [9].

For the heat pipe to work normally, the capillary pressure should be greater than the entire pressure gradient across the liquid–vapor path. For a heat pipe to function properly, the capillary pressure must be greater or equal to the sum of the pressure drops due to inertial, viscous, and hydrostatic forces, as well as, pressure gradients. If it is not, then the working fluid is not supplied rapidly enough to the evaporator to compensate for the liquid loss through vaporization. If this occurs, there is dryout in the evaporator.

In order to derive Eq. (2.2), we assume a meniscus is formed at the liquid–vapor interface whiting a normal heat pipe operation range and as shown in Fig. 2.6, and the capillary pressure defined as $(P_v - P_l)$ can be calculated using Laplace and Young as follows:

$$P_{\text{Capillary}} = P_c = \sigma \left(\frac{1}{R_1} + \frac{1}{R_2} \right) \quad (\text{Eq.2.4})$$

In this equation, R_1 and R_2 are the principal radii of curvature of the meniscus and σ is the surface tension coefficient of the liquid [11].

Note that constraint or limitation to use Young–Laplace equation (2.4) is typical when the liquid–vapor interface is static. This is because under normal operation of heat pipe, the driving potential for working fluid circulation in a capillary action is provided by the curvature difference between the evaporator and condor parts of the heat pipe in case of one-dimensional two-phase flow of liquid and vapor interfaces. We can translate these interfaces into macroscopic and microscopic scales, respectively, and say that in macroscopic scale, this interface between liquid and vapor is modeled as a surface of discontinuity and characterized by the property of surface tension. However, the microscopic scale of these two interfaces is a volumetric transition region across which molecule number density varies continuously. The surface tension of macroscopic scale can be defined thermodynamically as the change in surfaces excess of free energy (or work required) per unit increase in interfacial area and can be shown as Eq. (2.5)

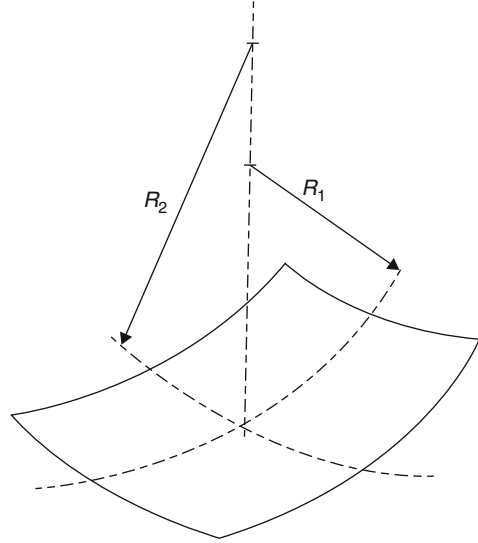
$$\sigma = \left(\frac{\partial E}{\partial A_s} \right)_{T,n} \quad (\text{Eq.2.5})$$

As depicted in Fig. 2.7, the capillary pressure at this interface is driven by the curvature of the menisci and the property surface tension of working fluid which is derived by the Laplace–Young equation [12] that is shown as follows:

$$\Delta P_c = \sigma \left(\frac{1}{R_1} - \frac{1}{R_2} \right) \quad (\text{Eq.2.6})$$

where R_1 and R_2 are defined radii of meniscus as depicted in Fig. 2.7 and σ is the surface tension of working fluid within heat pipe. Note again that the limitation of this equation is based on assumption that the liquid–vapor interface is static and

Fig. 2.7 Geometry of meniscus at liquid–vapor interface



interfacial mass fluxes (in heat pipe case evaporation) are low and disjoining pressure effects are negligible. In case of very thin film, a technique has been provided by Wayner [12] where he reviewed and showed that disjoined pressure effects must be included in order to predict a physically correct and accurate capillary pressure across an interface.

At this point, our interest is toward calculation of maximum value for $\left(\frac{1}{R_1} + \frac{1}{R_2}\right)$ considering various types of wick structures, therefore the maximum capillary pressure, $p_{\text{capillary,max}}$. In form of cylindrical pore, both R_1 and R_2 are equal to each other, and they can be set equal to R and it can be calculated to be

$$R = \frac{r}{\cos \theta} \quad (\text{Eq.2.7a})$$

where

r is the radius of the cylindrical pore and

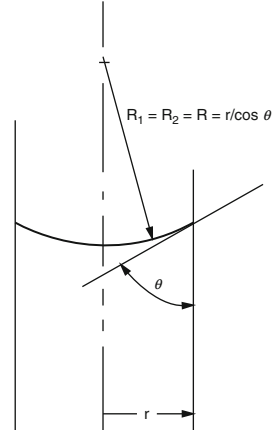
θ is the wetting angle.

Substituting for R from Eq. (2.7a) into Eq. (2.7) results to an expression of capillary pressure for the cylindrical pore as follows (see Fig. 2.8):

$$P_c = \frac{2\sigma \cos \theta}{r} \quad (\text{Eq.2.7b})$$

The maximum capillary takes place if in Eq. (2.7b) the value of $\cos \theta = 1$ for the wetting angle of $\theta = 0$. As a result, the maximum capillary pressure for cylindrical pores can be calculated by Eq. (2.7c)

Fig. 2.8 Depiction of meniscus in cylindrical pore



$$P_{\text{capillary}_{\text{max}}} = \frac{2\sigma}{r_{\text{capillary}}} \quad (\text{Eq.2.7c})$$

In this case, $r_{\text{capillary}} = r_{\text{eff}}$ is effective capillary radius or pores of the wick in Eq. (2.7c) and is defined such that $\frac{2\sigma}{r_{\text{capillary}}}$ can represent maximum value of $\left(\frac{1}{R_1} + \frac{1}{R_2}\right)$ for different wick structures. More often this value can be determined theoretically for wick prose of simple geometry and liquid–vapor interface, and for a complex geometry, experimental results are needed [13–15].

In summary, if one of the radii of curvature in Fig. 2.7 is infinity and the other, at wetting angle being zero for maximum capillary pressure, is equal to half of the groove width so long as the groove depth is greater than half of the groove width and it easily can be shown for rectangular grooves,

$$r_c = w \quad (\text{Eq.2.7d})$$

where

w is the groove width.

For a triangular groove where half the included angle is β and the width is w , and again one of the radii of curvature is equal to infinity and the other at zero wetting angle, then we have

$$R = \frac{w}{2 \cos \beta} \quad (\text{Eq.2.7e})$$

Hence, the effective capillary radius for this type of geometry can be analyzed by the following equation:

$$\frac{2}{r_c} = \frac{1}{R} = \frac{2 \cos \beta}{w} \quad (\text{Eq.2.7f})$$

Table 2.1 Expressions for the effective capillary radius $r_{\text{capillary}} = r_c$ for several wick structures

Structure	r_c	Data
Circular cylinder (artery or tunnel wicks)	$r_{\text{eff}} = r$	$r =$ radius of liquid flow passage
Rectangular groove	$r_{\text{eff}} = w$	$w =$ groove width
Triangular groove	$r_{\text{eff}} = \frac{w}{\cos \beta}$	$w =$ groove width $\beta =$ half-included angle
Parallel wires	$r_{\text{eff}} = w$	$w =$ wire spacing
Wire screens	$r_{\text{eff}} = \frac{w + d_w}{2} = \frac{1}{2N}$	$N =$ screen mesh number $w =$ wire spacing $d_w =$ wire diameter
Packed spheres	$r_c = 0.41r_s$	$r_s =$ sphere radius

Source: Chi [18], with permission

Thus,

$$r_c \frac{\cos \beta}{w} \tag{Eq.2.7g}$$

For a wick structure that consists of a series of parallel wires, it can be readily shown that

$$r_c = w \tag{Eq.2.7h}$$

In Table 2.1, expression of $r_{\text{capillary}} = r_c$ for different wicks are demonstrated along with their sources.

In physics, the **Laplace–Young equation** is a nonlinear partial differential equation that describes the capillary pressure difference sustained across the interface between two static fluids, such as water and air, due to the phenomenon of surface tension. It relates the pressure difference to the shape of the surface, and it is fundamentally important in the study of static capillary surfaces. It is a statement of normal stress balance for static fluids meeting at an interface, where the interface is treated as a surface (zero thickness):

$$\begin{aligned} \Delta p &= \gamma \nabla \cdot \hat{n} \\ &= 2\gamma H \\ &= \gamma \left(\frac{1}{R_1} + \frac{1}{R_2} \right) \end{aligned}$$

where Δp is the pressure difference across the fluid interface, γ is the surface tension, \hat{n} is a unit normal to the surface, H is the mean curvature, and R_1 and R_2 are the principal radii of curvature. (Some authors refer inappropriately to the factor $2H$ as the total curvature). Mathematically the **mean curvature**

(continued)

H of a surface S is an *extrinsic* measure of curvature that comes from differential geometry and that locally describes the curvature of an embedded surface in some ambient space such as Euclidean space.

The concept was introduced by Sophie Germain in her work on elasticity theory.

Note: Only normal stress is considered; this is because it can be shown that a static interface is possible only in the absence of tangential stress.

Definition: Let p be a point on the surface S . Consider all curves C_i on S passing through the point p on the surface. Every such C_i has an associated curvature R_i given at p . Of those curvatures R_i , at least one is characterized as maximal R_1 and one as minimal R_2 , and these two curvatures R_1, R_2 are known as the *principal curvatures* of S .

The **mean curvature** at $p \in S$ is the average of curvatures (Spivak, Volume 3, Chapter 2) [16], hence the name

$$H = \frac{1}{2}(R_1 + R_2)$$

More generally (Spivak, Volume 4, Chapter 7) [16], for a hypersurface T , the mean curvature is given as

$$H = \frac{1}{n} \sum_{i=1}^n R_i$$

More abstractly, the mean curvature is (times) the trace of the second fundamental form (or equivalently, the shape operator).

Additionally, the mean curvature H may be written in terms of the covariant derivative ∇ as $H\vec{n} = g_{ij}\nabla_i\nabla_j X$, using the *Gauss–Weingarten relations*, where $X(x,t)$ is a family of smoothly embedded hypersurfaces, \vec{n} a unit normal vector, and g_{ij} the metric tensor. A surface is a minimal surface if and only if the mean curvature is zero. Furthermore, a surface, which evolves under the mean curvature of the surface S , is said to obey a heat-type equation called the mean curvature flow equation.

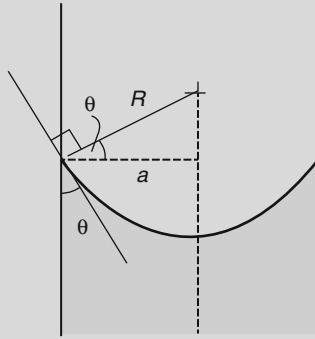
The sphere is the only surface of constant positive mean curvature without boundary or singularities.

Capillary Pressure in a Tube

In a sufficiently narrow (i.e., low Bond number) tube of circular cross section (radius a), the interface between two fluids forms a meniscus that is a portion of the surface of a sphere with radius R . The pressure jump across this surface is

$$\Delta p = \frac{2\gamma}{R}$$

(continued)



Spherical meniscus with wetting angle less than 90°

This may be shown by writing the Laplace–Young equation in spherical form with a contact angle boundary condition and also a prescribed height boundary condition at, say, the bottom of the meniscus. The solution is a portion of a sphere, and the solution will exist *only* for the pressure difference shown above. This is significant because there is not another equation or law to specify the pressure difference; existence of solution for one specific value of the pressure difference prescribes it.

The radius of the sphere will be a function only of the contact angle, θ , which in turn depends on the exact properties of the fluids and the solids in which they are in contact:

$$R = \frac{a}{\cos \theta}$$

so that the pressure difference may be written as:

$$\Delta p = \frac{2\gamma \cos \theta}{a}$$

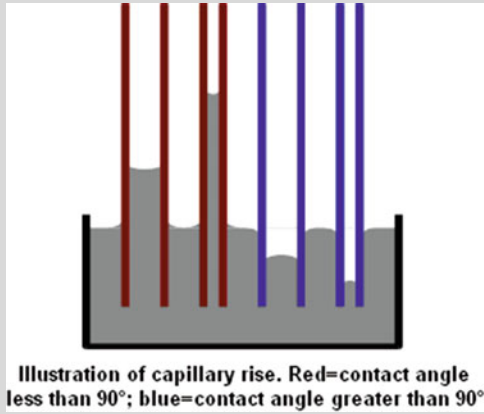
In order to maintain hydrostatic equilibrium, the induced **capillary pressure** is balanced by a change in height, h , which can be positive or negative, depending on whether the wetting angle is less than or greater than 90° . For a fluid of density ρ :

$$h = \frac{2\gamma \cos \theta}{\rho g a}$$

where g is the gravitational acceleration. This is sometimes known as the **Jurin rule** or **Jurin height** after **James Jurin** who studied the effect in 1718.

(continued)

For a water-filled glass tube in air at sea level,



$\gamma = 0.0728 \text{ J/m}^2$ at 20 °C	$\theta = 20^\circ$ (0.35 rad)
$\rho = 1000 \text{ kg/m}^3$	$g = 9.8 \text{ m/s}^2$

and so the height of the water column is given by

$$h \approx \frac{1.4 \times 10^{-5}}{a} \text{ m}$$

Thus, for a 2-mm-wide (1 mm radius) tube, the water would rise to 14 mm. However, for a capillary tube with radius 0.1 mm, the water would rise to 14 cm (about 6 in.).

Capillary Action in General

In the general case, for a free surface and where there is an applied “over-pressure,” Δp , at the interface in equilibrium, there is a balance between the applied pressure, the hydrostatic pressure, and the effects of surface tension. The **Young–Laplace** equation becomes

$$\Delta p = \rho g h - \gamma \left(\frac{1}{R_1} + \frac{1}{R_2} \right)$$

The equation can be nondimensionalized in terms of its characteristic length scale, the capillary length

$$L_c = \sqrt{\frac{\gamma}{\rho g}}$$

and **characteristic pressure**

$$p_c = \frac{\gamma}{L_c} = \sqrt{\gamma \rho g}$$

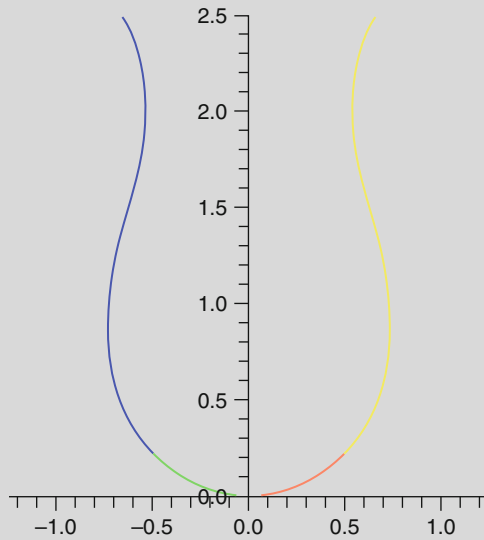
(continued)

For clean water at standard temperature and pressure, the **capillary length** is ~2 mm.

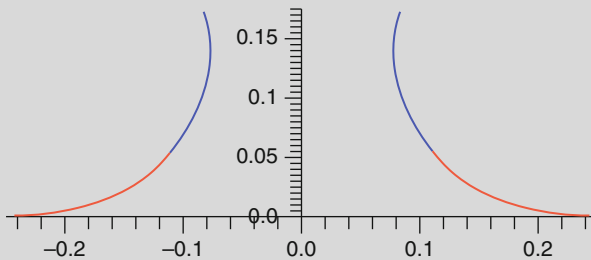
The nondimensional equation then becomes

$$h^* - \Delta p^* = \left(\frac{1}{R_1^*} + \frac{1}{R_2^*} \right)$$

Thus, the surface shape is determined by only one parameter, the overpressure of the fluid, Δp^* and the scale of the surface is given by the **capillary length**. The solution of the equation requires an initial condition for position and the gradient of the surface at the starting point.



A pendant drop is produced for an overpressure of $\Delta p^* = 3$ and initial condition $r_0 = 10^{-4}$, $z_0 = 0$, $dz/dr = 0$



A liquid bridge is produced for an overpressure of $\Delta p^* = 3.5$ and initial condition $r_0 = 0.25^{-4}$, $z_0 = 0$, $dz/dr = 0$

(continued)

Axisymmetric Equations

The (nondimensional) shape, $r(z)$ of an axisymmetric surface can be found by substituting general expressions for curvature to give the hydrostatic **Laplace–Young** equations

$$\frac{r''}{(1+r'^2)^{\frac{3}{2}}} - \frac{1}{r(z)\sqrt{1+r'^2}} = z - \Delta p^*$$

$$\frac{z''}{(1+z'^2)^{\frac{3}{2}}} + \frac{z'}{r\sqrt{1+z'^2}} = \Delta p^* - z(r)$$

Equation for minimum capillary pressure [17]

$$(\Delta P_c)_m \geq \int_{L_{\text{eff}}} \frac{\partial P_v}{\partial x} dx + \int_{L_{\text{eff}}} \frac{\partial P_l}{\partial x} dx + \Delta P_{\text{ephase}} + \Delta P_{\text{cphase}} + \Delta P_{\perp} + \Delta P_{\parallel} \quad (\text{Eq.2.8a})$$

where $(\Delta P_c)_m$ = maximum capillary pressure difference generated within capillary wicking structure between wet and dry points,

$\frac{\partial P_v}{\partial x}$ = sum of inertial and viscous pressure drops occurring in vapor phase,

$\frac{\partial P_l}{\partial x}$ = sum of inertial and viscous pressure drops occurring in liquid phase,

ΔP_{ephase} = pressure gradient across phase transition in evaporator,

ΔP_{cphase} = pressure gradient across phase transition in condenser,

ΔP_{\perp} = normal hydrostatic pressure drop, and

ΔP_{\parallel} = axial hydrostatic pressure drop.

The driving force that transports the condensed working liquid through the wick to the evaporator is provided by capillary pressure. Working fluids that are employed in heat pipes have concave facing menisci (wetting liquids) as opposed to convex facing menisci (non-wetting liquids) [9].

Contact angle is defined as the angle between the solid and vapor regions. Wetting fluids have angles between 0 and 90°. Non-wetting fluids have angles between 90° and 180° [9].

2.5.1 Normal Hydrostatic Pressure

Within a heat pipe, the hydrostatic pressure gradient takes place when the heat pipe is exposed to gravitational or body forces within the vapor and liquid phases.

The *normal hydrostatic pressure* drop ΔP_{\perp} occurs only in heat pipes in which circumferential communication of the liquid in the wick is possible. It is a result of the component of the body force acting perpendicular to the longitudinal axis of the heat pipe. The normal hydrostatic pressure drop can be expressed as follows [17]:

$$\Delta P_{\perp} = \rho_1 g d_v \cos \psi \quad (\text{Eq.2.8b})$$

where

- ρ_1 = liquid density,
- g = gravitation acceleration,
- ψ = inclination angle of heat pipe, and
- d_v = diameter of the vapor portion of the heat pipe.

2.5.2 Axial Hydrostatic Pressure

The *axial hydrostatic pressure* drop ΔP_{\parallel} results from the component of the body force acting along the longitudinal axis. It can be presented as follows [17]:

$$\Delta P_{\parallel} = \rho_1 g L \sin \psi \quad (\text{Eq.2.8c})$$

where

- ρ_1 = liquid density,
- g = gravitation acceleration,
- ψ = inclination angle of heat pipe, and
- L = overall length of the heat pipe.

2.5.3 Capillary Pressure at the Liquid–Vapor Interface

As discussed in the above section, the capillary pressure difference at a single liquid–vapor interface is defined as $P_v - P_l$ or $\Delta P_{\text{capillary}} = \Delta P_c$ (Figs. 2.9 and 2.10) and can be represented by form of the Laplace–Young equation that is represented in Eq. (2.6) of the form $\Delta P_c = \sigma \left(\frac{1}{R_1} - \frac{1}{R_2} \right)$, where R_1 and R_2 are defined radii of meniscus as depicted in Fig. 2.7 and σ is the surface tension of working fluid within heat pipe [17].

For many heat pipe wicking structures, the maximum capillary pressure could be written in terms of a single radius of curvature, r_c . In this fashion, the maximum capillary pressure between the wet and dry points can be presented as the difference between the capillary pressure across the meniscus at the wet point, or

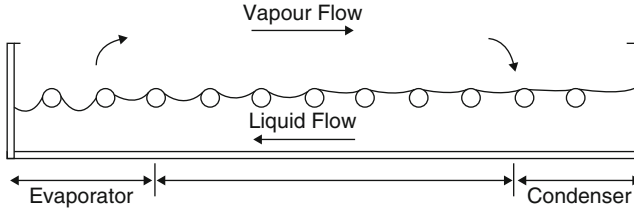


Fig. 2.9 Variation of meniscus curvature as a function of axial position

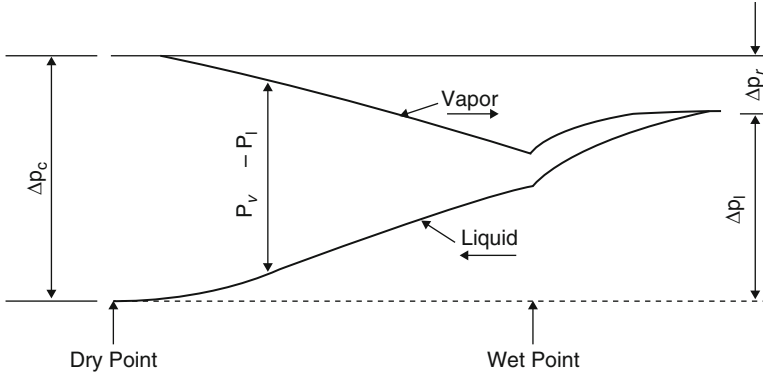


Fig. 2.10 Typical liquid and vapor pressure distribution in a heat pipe

$$\Delta P_c = \frac{2\sigma}{r_{\text{Cevaporator}}} - \frac{2\sigma}{r_{\text{Ccondenser}}} \quad (\text{Eq.2.9})$$

As we discussed in previous section and using Fig. 2.9, the vaporization occurring in evaporator causes the liquid meniscus to recede into the wick, reducing the local capillary radius $r_{\text{Cevaporator}}$, and in condenser section, condensation causes flooding of the wick, which in turn increases the local capillary radius $r_{\text{Ccondenser}}$. The resulting difference in the two radii of curvature causes a pressure difference and, hence, pumping of the liquid from the condenser to the evaporator [17]. In steady-state operation of heat pipe, it is generally assumed that the capillary radius in the condenser or at the wet point, $r_{\text{Ccondenser}}$, approaches infinity, so that the maximum capillary pressure for a heat pipe operating at this state in many cases can be presented as a function of only the effective capillary radius of evaporator wick as shown in Eq. (2.7) and can be expressed in different forms here as Eq. (2.10):

$$\Delta P_{\text{capillary}_{\text{max}}} = \frac{2\sigma}{r_c} \quad (\text{Eq.2.10})$$

Table 2.1 gives values for the effective capillary radius r_c for some of the more common wicking structures by Chi [18]. For other simple geometries, values for the

effective capillary radius can be found theoretically using the methods proposed by Chi [18] and reflected in Sect. 2.13.1 of this book as well as reflecting Chi’s approach. Experimentally methods described by Ferrell and Alleavitch, Freggens [19], or Eninger [20] can show pores or structures of more complex geometries. In addition, limited information on the transient behavior of capillary structures is also available (Colwell and Chang) [21].

Example 2.1 (from Peterson [17] book) A method often used to increase the transport capacity of a given heat pipe design is to substitute a higher mesh number screen (i.e., one with smaller capillary) to increase the maximum capillary pressure. However, this also increases the liquid flow resistance. Using the dimensions for copper screen obtained from handbooks, plot the capillary pressure wick versus the mesh number. How does varying the mesh number affect the maximum transport capacity [17]? This problem is from Peterson book Ref. [17].

Solution The maximum capillary pressure is given by (assuming that the correct angle is zero)

$$\Delta P_{\text{capillary,max}} = \frac{2\sigma}{r_{\text{Cevaporator}}} \quad \text{where} \quad r_c = \frac{1}{2N} \quad \text{for wire screens}$$

The permeability and porosity are obtained from Eqs. (2.52) and (2.53), respectively, as

$$K = \frac{d^2 \epsilon^3}{122(1 - \epsilon)^2} \quad \text{and} \quad \epsilon = 1 - \frac{\pi S N d}{4}$$

Assuming the fluid is water at 33 °C such as $\sigma = 70.9 \times 10^{-3}$ N/m and the mesh dimensions are as shown below, the individual values for capillary pressure, porosity, and permeability can be tabulated as follows (Table 2.2).

Table 2.2 Mesh dimension for water as working fluid

Mesh/in.	Mesh/m	dw (in.)	dw (m)	P_c (Pa)	ϵ	K
8.0000	314.96	0.0280	0.00071	89.32	0.8153	6.58×10^{-8}
12.0000	472.44	0.0230	0.00058	133.98	0.7724	2.49×10^{-8}
16.0000	629.92	0.0180	0.00046	178.65	0.7625	1.35×10^{-8}
18.0000	708.66	0.0170	0.00043	200.98	0.7477	1.00×10^{-8}
24.0000	944.88	0.0140	0.00036	267.97	0.7229	5.10×10^{-9}
30.0000	1181.10	0.0135	0.00034	334.96	0.6660	2.55×10^{-9}
40.0000	1574.80	0.0100	0.00025	446.61	0.6701	1.46×10^{-9}
50.0000	1968.50	0.0090	0.00023	558.27	0.6289	7.74×10^{-10}
60.0000	2362.20	0.0075	0.00019	669.92	0.6289	5.37×10^{-10}
80.0000	3149.60	0.0055	0.00014	893.23	0.6371	3.14×10^{-10}
100.0000	3937.00	0.0045	0.00011	1116.53	0.6289	1.93×10^{-10}

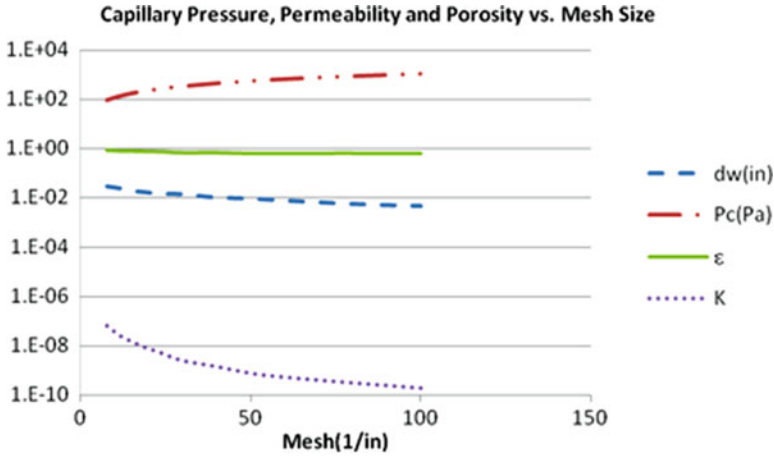


Fig. 2.11 Capillary heat transport versus adiabatic temperature

These values can be represented graphically as shown in Fig. 2.11 for British unit.

Looking at the graph of capillary pressure and permeability versus mesh number, the two values are seen to be inversely proportional [17]. Thus, by increasing the mesh number, the capillary pressure is correspondingly increased. However, the permeability decreases, and thus the liquid frictional pressure drop increases. To determine exactly whether changing the mesh number will increase the maximum heat transport capability, the length of the heat pipe must be considered. For a “short” heat pipe, the gain in capillary pressure will be much greater than the increased liquid pressure drop. The opposite will be true for a “long” heat pipe [17].

2.6 Turbulent and Laminar Flow of the Vapor

In this section, briefly we discuss the difference between laminar and turbulent flow which should be known to majority of readers here how, as an introduction to fundamental of these two types flow, the following definitions do apply.

Laminar flow: sometimes known as streamline flow, occurs when a fluid flows in parallel layers, with no disruption between the layers. In fluid dynamics, laminar flow is a flow regime characterized by high momentum diffusion, low momentum convection, pressure, and velocity independent from time. It is the opposite of turbulent flow. In nonscientific terms, laminar flow is “smooth,” while turbulent flow is “rough.”

So, basically, slow fluid flow is tending to be laminar, and as it speeds up a transition occurs; hence, it crinkles up into complicated random turbulent flow. But even slow flow coming from a large orifice can be turbulent; this is the case with

smoke stacks. Since turbulence is altogether a different type of fluid flow to laminar flow, it is desirable to be able to quantify under what conditions it occurs. As the speed U [(m/s) in SI units] increases, transition to turbulent will take place. Assuming you could provide a large enough pressure, even for fast flow the motion would remain laminar. However, any experiments in the fluid mechanics laboratory suggest that laminar flow occurs for low speeds, small diameters, low densities, and high viscosities, while turbulent flows occur for the opposite conditions: high speeds, large diameters, high densities, and low viscosities.

Now viscosity is a measurable fluid property as is its density, temperature, etc. We often use “kinematic viscosity ν ” which is the dynamic viscosity μ kg/m s divided by the density, and the kinematic viscosity unit is m^2/s . Notice its dimensions are the same as a length multiplied by a velocity. If the fluid speed is U (m/s) and the orifice diameter is D (m), then we can write the following dimensionless ratio that is known as Reynolds number as part of dimensionless group of numbers in fluid:

$$\text{Re} = \frac{\rho U D}{\mu} = \frac{U D}{\nu} \quad (\text{Eq.2.11})$$

Turbulent flow: In fluid dynamics, **turbulence** or **turbulent flow** is a fluid regime characterized by chaotic, stochastic property changes. This includes low momentum diffusion, high momentum convection, and rapid variation of pressure and velocity in space and time. Flow that is not turbulent is called laminar flow. The (dimensionless) Reynolds number characterizes whether flow conditions lead to laminar or turbulent flow; e.g., for pipe flow, a Reynolds number above about 4000 (a Reynolds number between 2100 and 4000 is known as transitional flow) will be turbulent. At very low speeds, the flow is laminar, i.e., the flow is smooth (though it may involve vortices on a large scale).

As the speed increases, at some point, the transition is made to turbulent flow. In turbulent flow, unsteady vortices appear on many scales and interact with each other. Drag due to boundary layer skin friction increases. The structure and location of boundary layer separation often changes, sometimes resulting in a reduction of overall drag. Because laminar–turbulent transition is governed by Reynolds number, the same transition occurs if the size of the object is gradually increased, or the viscosity of the fluid is decreased, or if the density of the fluid is increased.

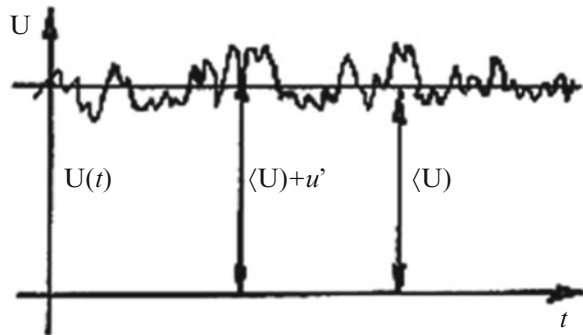
Turbulence causes the formation of eddies of many different length scales. Most of the kinetic energy of turbulent motion is contained in large-scale structures. The energy “cascades” from these large-scale structures to smaller-scale structures by an inertial and essentially inviscid mechanism. This process continues, creating smaller and smaller structures, which produces a hierarchy of eddies. Eventually this process creates structures that are small enough that molecular diffusion becomes important and viscous dissipation of energy finally takes place. The scale at which this happens is the Kolmogorov length scale.

Figure 2.12 below is a presentation of laminar flow (foreground near bow) and turbulent flow (to the stern) over an atomic submarine hull.

Fig. 2.12 Schematic of laminar and turbulent flow combined



Fig. 2.13 Velocity profile versus time in turbulent flow schema



As we expressed above, turbulent flow is characterized by unsteady eddying motions that are in constant motion with respect to each other. At any point in the flow, the eddies produce fluctuations in the flow velocity and pressure. If we were to measure the stream-wise velocity in turbulent pipe flow, we would see a variation in time as shown in Fig. 2.13 here.

Observation in Fig. 2.13 reveals that the velocity has a time-averaged value $\langle U \rangle$ and a fluctuating value u' , so that $\langle U \rangle$ is not a function of time, but u' is.

Note that in two-dimensional analytical treatment of vapor flow in a heat pipe, it is safe to assume that the vapor flow remains laminar, even for radial Reynolds number much larger than 1. Inertial forces are then dominant and viscous forces are negligible. Condition like this normally leads to the development of turbulent flow

when the flow rate is constant. Therefore, the question of flow stability in the vapor of heat pipes could be answered, by expressing that the stability of fluid through a tube at a constant mass flow rate without the radial injection or removal of fluid is characterized by the *axial Reynolds number* which is define as

$$\text{Re}_a = \frac{\rho U D}{\mu} \quad (\text{Eq.2.12})$$

where ρ is the fluid density, μ is the fluid dynamic viscosity, U is the average fluid velocity, and D is the flow average passage diameter. Two distinct flow regimes can exist depending on the value of Re_a .

Based on Eq. (2.12) description here, when $\text{Re}_a < 2000$, the flow is remaining in laminar flow regime, and under this regime, all the fluid particles move parallel to the flow passage axis. The radial velocity distribution at any axial is parabolic, falling from a maximum value at the axis to zero at the wall [22].

When $\text{Re}_a > 4000$, the flow falls in turbulent regime, and its character changes drastically, and extensive random interchanging activity between all the flow particles adjacent to each other takes place. The velocity distribution becomes relatively flat over most of the flow passage cross section, falling off sharply to zero in a thin boundary layer near the interior wall of the pipe or tube. The frictional resistance during turbulent flow is considerably larger than what takes place for the flow conditions that remain laminar. Finally for the Reynolds number of $2000 < \text{Re}_a < 4000$, the flow is in transition between laminar and turbulent and may exhibit both laminar and turbulent flow behavior and characteristic simultaneously [22].

2.7 One-Dimensional Two-Phase Flow

The subject of two or multiphase flow has become increasingly important in a wide variety of engineering systems for their optimum design and safe operations. It is, however, by no means limited to today's modern industrial technology and multiphase flow phenomena which require better understandings. Some of the important applications are listed below:

Heat pipes including two-phase closed thermosyphons are two-phase heat transfer devices with an effective thermal conductance hundreds of times higher than that of copper. As part of heat pipe modeling, one has to consider the following principal physical processes:

1. Energy conduction through evaporator/condenser wall
2. The diffusion of the vapor–gas interface
3. Wick–liquid dynamics
4. Boiling in the heat pipe evaporator's wick and movement of resulting vapor away from the evaporator through the heat pipe vapor space and into the condenser
5. Two-phase presence inside the vapor space

The process of liquid reaching the evaporator end of the heat pipe from the condenser must be modeled in such a manner that takes into consideration wick–liquid dynamics. This required some type of numerical analysis that must take slow nature of transient solutions with restricted numerical stability and constrained accuracy. Several attempts at modeling heat pipe transient have been made over the last few years. These analyses deal only with single phase. But in fact these analyses should be done for the two-phase flow inside the heat pipe. A similar work has been published using the numerical calculation of mist flows consisting of vapor, and water droplets are made on the assumption that particle reflection from the surface is perfectly elastic [23].

Under one-dimensional, two-phase flow condition, analysis within operational circumstances of heat pipe indicates that the stability of vapor flow in a heat pipe is far less certain than for the constant flow rate situation in a tube of similar situations. The flow rate increases continuously in the evaporator section, remains constant in the adiabatic region of the heat pipe, while it decreases continuously in condenser section. There is also experimental evidence and observation that the continuous suction of fluid from a flow stream maintains the flow in a laminar state for axial Reynolds numbers at which the flow normally was anticipated to be turbulent [24].

In any operating heat pipe under normal conditions, the abrupt transition from injection of vapor from the evaporator side to the removal of heat from vapor at the condenser junction could disturb the stability of what on the other hand might be a laminar flow pattern, inducing turbulence. If the axial Reynolds number Re_a that is given in Eq. (2.12) leaves the evaporator for values greater than 4000, turbulence would be expected to develop in a following adiabatic section, persist well into the adjacent condenser section, and may fail constraint of sonic limit as well as possibly propagate partially back into the evaporation section, which eventually may possibly result in burnup of heat pipe.

The axial Reynolds number Re_a of the vapor at the evaporator exit is shown in Table 2.3 for the case in which the heat transfer rate is 20 % of the sonic heat transport limit which is known as sonic limit. Re_a is observed to be greater than 4000 for all of the heat pipe fluids except lithium. Thus, the potential for turbulent vapor flow exists for many heat pipe fluids during operation at high heat transfer rates.

The table shows the friction factor for vapor flow in the evaporator section of heat pipe referred to as the Poiseuille friction, and it is a constant equal to 64 ($f_{Po} = 64$), while $\Omega_{Po} = 4/3$ is designated as the momentum factor and the subscript Po denotes the Poiseuille flow.

Table 2.3 Variation of friction factor and momentum factor with radial Reynolds number

Radial Reynolds number Re_r	f/f_{Po}	Ω/Ω_{Po}
$\ll 0.1$	1.000	1.000
0.1	1.010	0.998
1.0	1.068	0.984
10.0	1.202	0.947
100.0	1.245	0.929
$\gg 100.00$	–	0.926

2.7.1 What Is a Two-Phase Flow?

A *phase* is simply one of the states of matter and can be a gas, a liquid, or a solid. *Multiphase flow* is the simultaneous flow of several phases. *Two-phase flows* are the simplest cases of multiphase flows.

The term *two component* is sometimes used to describe flows in which the phases do not consist of the same chemical substance. For example, steam–water flows are two phase, while air–water flows are two component. Some two-component flows (mostly liquid–liquid) consist of a single phase but are often called two-phase flows in which the phases are identified as the continuous or discontinuous components. Since the mathematics, which describes two-phase or two-component flows, is identical, it does not really matter which definitions are chosen. The two expressions will therefore be treated as synonyms in most developments. There are many common examples of two-phase flows. Some, such as fog, smog, smoke, rain, clouds, snow, icebergs, quick sands, dust storms, and mud, occur in nature. Others, such as boiling water, tea making, egg scrambling, etc., are good examples of such status [25].

2.8 Flow Regime

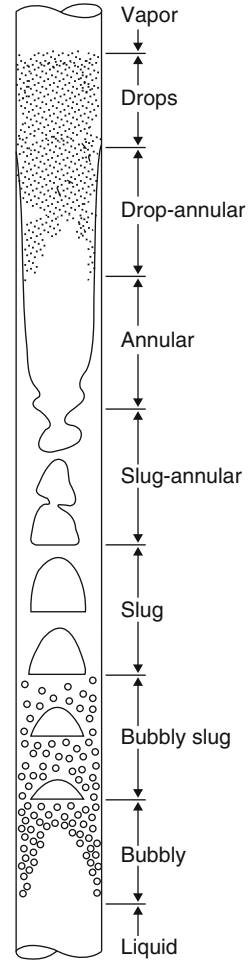
The prediction for greater accuracy results in greater complexity of any given problem, in particular facing a two-phase flow in heat pipe. In two-phase flow, the amount of knowledge that is needed in order to perform a granule analysis is often surprisingly great. For example, in studying the motion of a single gas bubble rising in a stagnant liquid, one should be concerned with all of the following effects:

- Inertia of the gas and the liquid
- Viscosity of the gas and the liquid
- Density difference and buoyancy
- Surface tension and surface contamination

The latest item above is by itself extremely complicated since “contamination” can take the form of dirt, dissolved matter, or surface-active agents that have serious impact on heat transfer within that system. Heat transfer and mass transfer to the bubble also alter its motion. Perhaps the first step in rendering this hydra-like problem tractable is to break it up into various regimes, which are each governed by certain dominant geometrical or dynamic parameters. Part of the definition of the flow regime is a description of the morphological arrangement of the components, or *flow pattern*.

An example of the complexity of two-phase flows is depicted in Fig. 2.14 that shows a sequence of flow pattern taking place in an evaporator of heat pipe as more

Fig. 2.14 Approximate sequence of flow patterns in a vertical heat pipe evaporator



and more liquid is getting converted to vapor. Complexity of the problem arises in different parts of the evaporator that requires different methods of analysis, and the problem of how one regime develops from another has to be considered too.

Many presentations of flow pattern and flow regime are mapped out by numerous authors which indicate two-independent coordinates on a graph. For a given apparatus and specific components, this is done in terms of the flow rates, as shown in Figs. 2.15 and 2.16. However, since the flow regime is governed by about a dozen variables, a two-dimensional plot is quite inadequate for general representation.

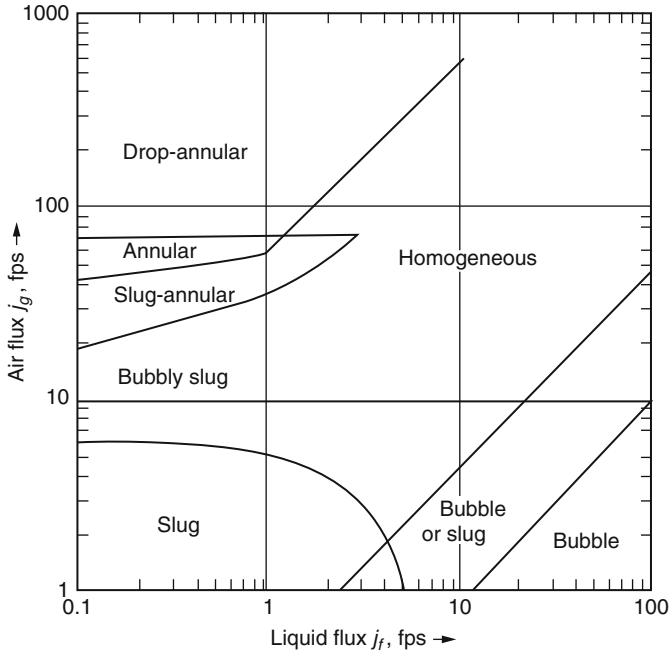


Fig. 2.15 Flow-pattern boundaries for vertical up flow of air and water at 15 psi in a 1" diameter tube deduced from equations in Ref. [25]

2.9 Heat Transfer

The transfer of heat is normally from a high-temperature object to a lower-temperature object. Heat transfer changes the internal energy of both systems involved according to the first law of thermodynamics. Heat may be defined as energy in transit from a high-temperature object to a lower-temperature object. An object does not possess "heat"; the appropriate term for the microscopic energy in an object is internal energy. The internal energy may be increased by transferring energy to the object from a higher-temperature (hotter) object—this is properly called heating. A convenient operational definition of temperature is that it is a measure of the average translational kinetic energy associated with the disordered microscopic motion of atoms and molecules. The flow of heat is from a high-temperature region toward a lower-temperature region. The details of the relationship to molecular motion are described in kinetic theory. The temperature defined from kinetic theory is called the kinetic temperature. Temperature is not directly proportional to internal energy since temperature measures only the kinetic energy part of the internal energy, so the two objects with the same temperature do not in

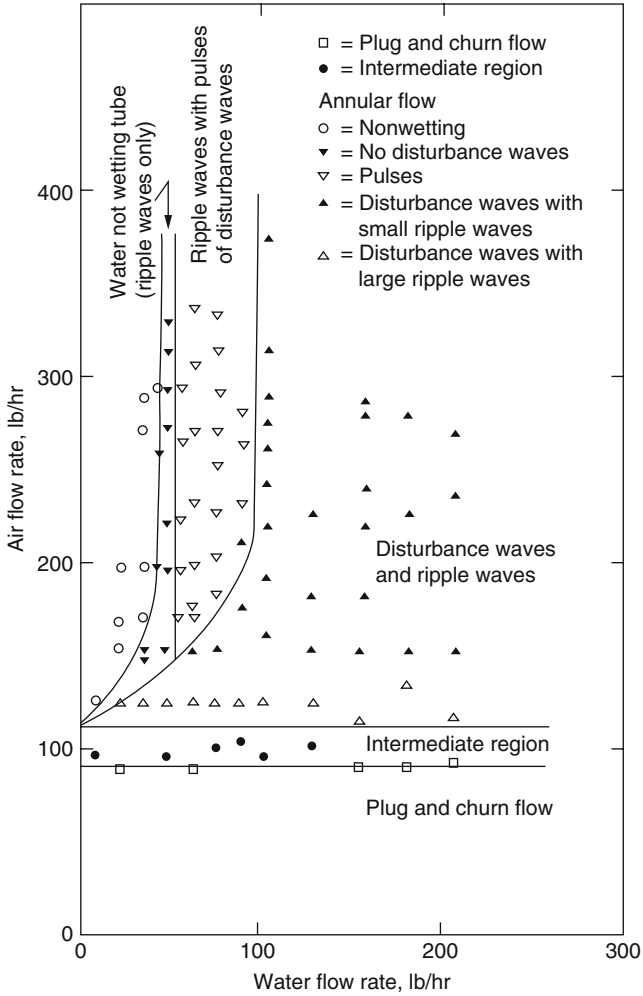


Fig. 2.16 Various regime or subdivisions of the annular flow pattern for current upward flow of air and water in a 1^{1/4}-in.-diameter pipe at 15 psi. (Hall-Taylor and Hewitt AERE-R3952, UKAEA, 1962)

general have the same internal energy (see water–metal example). Temperatures are measured in one of the three standard temperature scales (Celsius, Kelvin, and Fahrenheit). There are three mechanisms by which thermal energy is transported:

1. Convection
2. Conduction
3. Radiation

- **Convection:** Energy is transferred by the mass motion of groups of molecules resulting in transport and mixing of properties. When heat conducts into a static fluid, it leads to a local volumetric expansion. As a result of gravity-induced pressure gradients, the expanded fluid parcel becomes buoyant and displaces, thereby transporting heat by fluid motion (i.e., convection) in addition to conduction. Such heat-induced fluid motion in initially static fluids is known as **free convection**. For cases where the fluid is already in motion, heat conducted into the fluid will be transported away chiefly by fluid convection. These cases, known as **forced convection**, require a pressure gradient to drive the fluid motion, as opposed to a gravity gradient to induce motion through buoyancy.

1. Free convection:

Similar to forced convection, heat transfer due to free convection is described by Newton's law of cooling,

$$\dot{Q} = hA(T_w - T_\infty) = hA \cdot \Delta T$$

The rate of heat \dot{Q} transferred to the surrounding fluid is proportional to the object's exposed area A and the difference between the object temperature T_w and the fluid free-stream temperature T_∞ . *The constant of proportionality h is termed the convection heat transfer coefficient. Other terms describing h include film coefficient and film conductance.*

2. Force convection:

The essential ingredients of forced convection heat transfer analysis are given by Newton's law of cooling:

$$\dot{Q} = hA(T_w - T_\infty) = hA \cdot \Delta T$$

The rate of heat \dot{Q} transferred to the surrounding fluid is proportional to the object's exposed area A , and the difference between the object temperature T_w and the fluid free-stream temperature T_∞

The constant of proportionality h is termed the convection heat transfer coefficient. Other terms describing h include film coefficient and film conductance.

Example: holding your hand over a stove burner. In meteorology, we speak of convection predominantly as that caused by rising currents of warm air. We refer to all other mass motions of air as advection.

- **Conduction:**

Energy is transferred by the direct contact of molecules, not by the movement of the material. Regions with greater molecular kinetic energy will pass their thermal energy to regions with less molecular energy through direct molecular collisions, a process known as conduction. In metals, a significant portion of the transported thermal energy is also carried by conduction-band electrons.

Example: Putting your hand on a stove burner. The amount of energy transferred depends on how conductive the material is. Metals are good

conductors, so they are used to transfer energy from the stove to the food in pots and pans. Air is the best insulator, so good insulating products try to trap air and not allow it to move.

- **Radiation:**

Energy is transferred by the direct contact of molecules, not by the movement of the material. All materials radiate thermal energy in amounts determined by their temperature, where the energy is carried by photons of light in the infrared and visible portions of the electromagnetic spectrum. When temperatures are uniform, the radiative flux between objects is in equilibrium, and no net thermal energy is exchanged. The balance is upset when temperatures are not uniform, and thermal energy is transported from surfaces of higher to surfaces of lower temperature.

Example: Heat felt when standing away from a large fire on a calm night. Everything that has a temperature above absolute zero radiates energy. Radiation is not “felt” until it is absorbed by a substance. It does not require a medium to transfer energy through, as do conduction and convection.

- **Specific heat:**

specific heat is the amount of heat needed to raise the temperature of one gram of a substance to 1°Celsius. The specific heat of water is very high compared to other substances, so water can store energy longer than most other substances. For example, the Gulf of Mexico remains warm during the night, when air and soil temperatures decrease rapidly.

Why is the Southern Hemisphere summer generally not warmer than the Northern Hemisphere summer? Although Earth is closer to the sun during the Southern Hemisphere summer, most of the Southern Hemisphere is water, which regulates the seasonal temperature.

- **Energy**

Energy is the ability or capacity to do work on some form of matter. There are several forms of energy, including the following:

- **Potential energy** is the energy which a body possesses as a consequence of its position in a gravitational field (e.g., water behind a dam).
- **Kinetic energy** is the energy which a body possesses as a consequence of its motion (e.g., wind blowing across a wind generator). It is dependent upon an object’s mass and velocity (e.g., moving water vs. moving air).
- **Internal energy** is the total energy (potential and kinetic) stored in molecules.
- **Heat (or thermal) energy** is kinetic energy due to motion of atoms and molecules. It is energy that is in the process of being transferred from one object to another because of their temperature difference.
- **Radiant energy** is the energy that propagates through space or through material media in the form of electromagnetic radiation.

The first law of thermodynamics states that energy lost during one process must equal the energy gained during another.

- **Latent heat:**

Latent heat is the heat energy required to change a substance from one state to another. There are basically three states of matter: solid, liquid, and gas. The difference between them is how the molecules are arranged. Solids have tightly packed molecules, liquids are still bound together but not strongly enough to keep them from flowing, and gas molecules are free flowing, not bound to one another at all. Energy is required to change from one state to another because bonds must be loosened, broken, tightened, or made. Energy must be given to the molecules if bonds are to be loosened or broken and taken from the molecules if they are to be tightened or made. Energy is required to change from solid to liquid, liquid to gas (evaporation), or solid to gas (sublimation). Energy will be released to change from liquid to solid (fusion), gas to liquid (condensation), or gas to solid.

Basically the quantity of heat absorbed or released when a substance changes its physical state at constant temperature, e.g., from a solid to a liquid at its melting point or from a liquid to a gas at its boiling point. The release of *latent heat of condensation* in the rising air of a hurricane is the chief force fuelling that meteorological phenomenon.

Evaporation is a cooling process, and latent heat of evaporation is the energy used to change liquid to vapor.

Condensation is a warming process, and latent heat of condensation is energy released when water vapor condenses to form liquid droplets.

Latent heat of fusion describes both changing from solid to liquid and from liquid to solid.

Latent heat of sublimation describes both changing from solid to gas and gas to solid.

2.10 Condensation of a Pure Vapor

Many factors are involved in determining the vapor-to-condenser surface heat transfer coefficient during condensation. The problem is even more complex when the vapor contains different molecular species which may or may not condense. In summary, the term “pure vapor” implies that only one species is present.

In industrial condensers, vapor and condensate flows are, in general, three-dimensional and involve effects of gravity, shear stress at the condensate surface due to vapor velocity, and interface temperature difference due to nonequilibrium and inundation, i.e., condensate from higher or upstream surfaces impinging on lower or downstream surfaces. For profiled surfaces (e.g., finned tubes), surface tension effects are also important. Condensate and vapor flows may be either laminar or turbulent. The condensate may form a continuous film on the surface or, when the surface is not wetted by the condensate, form discrete droplets (i.e., dropwise condensation occurs when a vapor condenses on a surface not wetted by the condensate). Condensation may occur on external surfaces, e.g., on the outside

of the tubes in a shell-and-tube condenser or on internal surfaces, e.g., in-tube condensation. In “direct contact” condensation, liquid at a temperature below the saturation temperature is brought into contact with the vapor. The extent to which the condensation process is understood and the accuracy with which heat transfer coefficients can be calculated depend on the circumstances. After almost 100 years of research, accurate predictions can now be made for relatively simple geometry (e.g., flat plate or single horizontal tube) and for well-defined flow conditions.

2.11 Sonic Limit or Choking

This sonic limit is the first among several limitations encountered, and the performance of the heat pipe is restricted until the vapor temperature increases accordingly until the velocity of the vapor leaving the evaporator is less than the sonic velocity. The vapor leaves the evaporator at a sonic speed. The vapor flow is “choked” and the maximum heat transfer rate is therefore limited. Both of these effects are typically important during the heat pipe startup. The evaporator and condenser sections of the heat pipe undergo addition and removal of mass due to the circulation of the working fluid. They act like a nozzle where vapor flows from the adiabatic section into or out of the end sections. The converging–diverging nozzle-like nature of the vapor flow path imposes a choking flow condition on the vapor velocity. The velocity at a choke point cannot be greater than the local speed of sound. This is called the sonic limit, and the heat transfer can now only increase by increasing the operating temperature of the heat pipe. Although, the operation of a heat pipe under such condition causes a substantial temperature drop across the heat pipe, it is not considered a serious risk [9]. Sonic limit occurs when the vapor velocity reaches sonic speed at the evaporator, and any increase in pressure difference will not speed up the flow like choked flow in converging–diverging nozzle. At the sonic limit, there is a maximum axial heat transport rate due to the choked flow and a fixed axial temperature drop along the evaporator associated with any given evaporator entrance temperature. The sonic limit usually occurs in liquid–metal heat pipe during startup or low-temperature operating requirement associated with very low vapor densities under this condition. Also increasing the heat rejection rate beyond the sonic limit (by lowering the condenser temperature) induces supersonic vapor flow that accounts for compressibility, friction, vapor velocity profile, nonuniform mass suction, and temperature dependency. A well-calculated procedure has been developed for the supersonic flow of vapor in the condensation zone of high-temperature heat pipes [26]. In this reference, an equilibrium two-phase flow model describes the vapor state. The method is tested for a supersonic vapor flow in sodium heat pipes with various cooling intensities, and a good agreement has been established between calculation results and experimental data. For this condition, ultimately, the vapor velocity at the condenser entrance reaches the sonic velocity and choked flow conditions will be introduced. Under such condition, any continuation of heat reduction in condenser region helps to

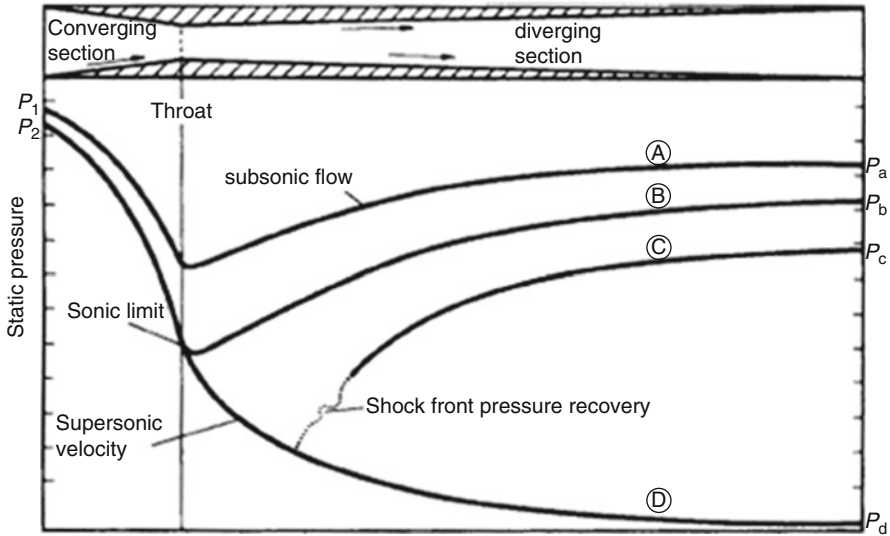


Fig. 2.17 Pressure profiles in a converging–diverging nozzle [27]

decrease the temperature in this zone within heat pipe and has no effect on the vapor temperature in the evaporator section of pipe. As explained by Cotter [26], during the startup phase of heat pipe, the vapor undergoes a transition from continuum flow to molecular flow that gradually works its way through the condenser zone. Once the continuum flow regime reaches the end of the condenser, a shock wave is formed. This shock wave then slowly progresses upstream and grows weaker until it eventually disappears at the exit to the evaporator [17]. Under this circumstance, the entire flow regime will be restored to a subsonic condition. Figure 2.17 is a good illustration of such relationship between the vapor temperature and the axial position in a heat pipe. In this illustration, the following definitions are valid:

1. Curve A is a representation of temperature for a heat pipe with subsonic conditions and partial pressure recovery.
2. Curve B is a demonstration of increasing the heat rejection rate and lowering the condenser temperature, which results decrease in the evaporator temperature, and the vapor velocity at the exit becomes sonic, and critical and choked flow conditions exist. Further increasing the heat rejection rate only lowers the condenser temperature because the heat transfer rate of the section cannot be increased due to the presence of choked flow. In this case, change in condenser temperature will not have any effect upon the evaporator because the vapor is moving at the speed of sound at the evaporator exit and changes in condenser conditions will not be transmitted upstream to the evaporator section of the pipe.
3. As before, the velocity will reduce during travel through the diverging section, and there will be some pressure recovery. If the outlet pressure is further reduced, the flow rate will remain constant and the pressure profile will follow curve C.

4. Curve D shows that for a certain exit pressure, the gas can be caused to accelerate throughout the diverging region. Further pressure reduction will not affect the flow pattern in the nozzle region. It should be noted that after curve C, pressure reduction does not affect the flow pattern in the converging section; hence, the mass flow did not increase after the throat velocity has attained the sonic value. This condition is referred to as choked flow [27].

Unlike the other previous discussion around transport limitation of heat pipe, sonic limitation actually serves as an upper limit to the axial heat transport capacity and does not necessarily result in dryout condition of the heat pipe evaporator wick or total failure of it. But any attempt to exceed the sonic limit will result in increases in the axial temperature gradient along the heat pipe and will eliminate or reduce the isothermal characteristics that are typically found in the vapor flow region.

Kemme [13] has shown very clearly that a heat pipe can operate in a very similar manner to the diverging nozzle. His experimental arrangement is shown in Fig. 2.15. Kemme used sodium as the working fluid and maintained a constant heat input of 64 kW. He measured the axial temperature variation, but since this is related directly to pressure, his temperature profile can be considered to be the same as the pressure profile.

Per David Reay and Peter Kew [27] on heat pipe, Kemme [13] arranged to vary the heat rejection at the condenser by means of a gas gap, the thermal resistance of which could be altered by varying the argon/helium ratio of the gas. Kemme's results are shown in Fig. 2.18. Curve A demonstrates subsonic flow with pressure recovery; curve B, obtained by lowering the condenser temperature, achieved sonic velocity at the end of the evaporator and hence operated under choked flow conditions. Further decrease in the thermal resistance between the condenser and the heat sink simply reduced the condenser region temperature but did not increase the heat flow that was limited by the choked flow condition and fixed axial

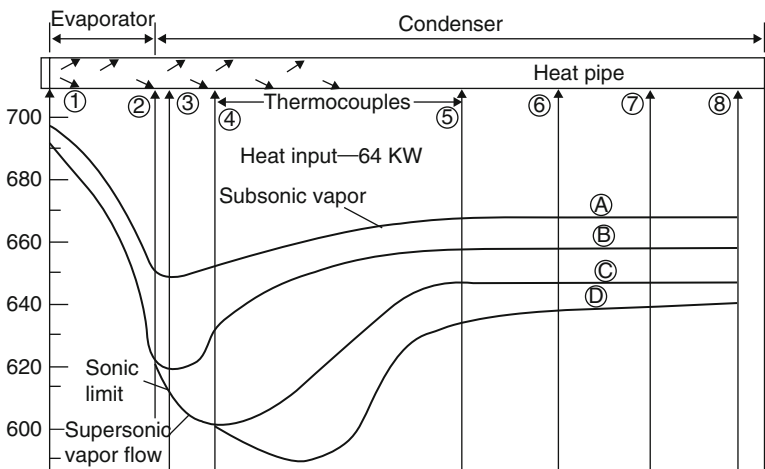


Fig. 2.18 Temperature as a function of axial position [13]

temperature drop in the evaporator. It should be noted that under these conditions of sonic limitation, considerable axial temperature and pressure changes will exist, and the heat pipe operation will be far from isothermal [28].

It can be shown analytically [11] that there is a correspondence between constant area flow in a heat pipe: with mass addition (evaporator) and removal (condenser) and constant mass flow in a converging–diverging nozzle. The end of the evaporator section in the heat pipe corresponds to the throat of the nozzle. Consequently, just as there is a sonic (MACH 1) limitation on the flow velocity through a nozzle throat, there is a similar limit on the flow velocity at the heat pipe evaporator exit. For a given evaporator exit temperature and working fluid, this choked flow condition is a fundamental limitation on the axial heat flux capacity of the heat pipe. To increase the axial heat transfer capacity of the heat pipe, one must increase the vapor flow area.

A closed-form expression for the sonic limitation can be derived based on the one-dimensional vapor flow theory under the following assumptions:

1. The properties of the vapor follow the ideal gas law.
2. The inertial effects dominate.
3. The frictional effects may be neglected.

All these assumptions are very reasonable since the sonic limitation generally occurs when a heat pipe is operating at low vapor density and high vapor velocity [11, 18]. Under the first assumption above, the ideal gas law states that

$$\frac{P_0}{\rho_0 T_0} = \frac{P_v}{\rho_v T_v} \quad (\text{Eq.2.13})$$

Within Eq. (2.13) the subscripts 0 and v are indications of stagnation and static states of the vapor within ideal gas. Neglecting the friction effects and considering the conservation of energy and momentum requires that

$$\frac{T_0}{T_v} = 1 + \frac{V_0^2}{2C_p T_v} \quad (\text{Eq.2.14})$$

$$\frac{P_0}{P_v} = 1 + \frac{\rho_v V_0^2}{P_v} \quad (\text{Eq.2.15})$$

Additionally, a heat pipe axial vapor flux density is proportional to the axial heat flux through Eq. (2.16):

$$\dot{m}_v'' = \frac{Q}{A_v \lambda} = \rho_v V_v \quad (\text{Eq.2.16})$$

This means the sonic limit is calculated by setting the vapor flow velocity equal to the sonic velocity in the continuity equation and multiplying by the latent heat of vaporization as follows:

$$\frac{Q_s}{A_v} = \lambda \rho_v V_s \quad (\text{Eq.2.17})$$

Equation (2.17) is valid for local Mach number of 1, and when using this equation to calculate the sonic limit, the parameters must be evaluated at the local conditions where choking takes place at the exit of the evaporator. In this equation, the following parameters are valid:

$$\frac{Q_s}{A_v} = \text{Axial heat flux at MACH 1 conditions.}$$

V_s = Sonic velocity of vapor at the exit of evaporator.

Sometimes it is more convenient to calculate this limit in terms of conditions at the beginning of the evaporator. This can be done using an equation developed by Levy [11]:

$$\frac{Q_s}{A_v} = \frac{\lambda \rho_v V_s}{\sqrt{2(\gamma + 1)}} \quad (\text{Eq.2.18})$$

where γ is the ratio of specific heats $\left(\gamma = \frac{C_p}{C_v}\right)$.

But Chi [18] has derived Eq. (2.16) by taking the local Mach number M_v and the sonic velocity, defined as $\sqrt{\gamma_v R_v T_v}$, and then Eqs. (2.14) through (2.16) can be written, respectively, as

$$\frac{T_0}{T_v} = 1 + \frac{\gamma_v - 1}{2} M_v^2 \quad (\text{Eq.2.19})$$

$$\frac{P_0}{P_v} = 1 + \gamma_v M_v^2 \quad (\text{Eq.2.20})$$

$$\dot{m}_v'' = \frac{Q}{A_v \lambda} = \rho_v M_v \sqrt{\gamma_v R_v T_v} \quad (\text{Eq.2.21})$$

In the above equations, γ_v is the ratio of specific heats whose magnitude for monoatomic vapor is 5/3, for diatomic is 7/5, or for polyatomic is 4/3. The term R_v is the vapor constant, which defines the universal gas constant divided by the molecular weight of the vapor. Substituting Eqs. (2.19) and (2.20) into Eq. (2.14) will result in Eq. (2.22) as follows:

$$\frac{\rho_0}{\rho_v} = \frac{1 + \gamma_v M_v^2}{1 + \frac{\gamma_v - 1}{2} M_v^2} \quad (\text{Eq.2.22})$$

Substituting T_v and ρ_v from Eqs. (2.19) and (2.22), respectively, into Eq. (2.21), we obtain

$$Q = \frac{A_v \rho_0 \lambda (\gamma_v R_v T_v)^{1/2} M_v \left(1 + \frac{\gamma_v - 1}{2} M_v^2\right)^{1/2}}{1 + \gamma_v M_v^2} \quad (\text{Eq.2.23})$$

When the Mach number at the evaporator exit is equal, the unity and then the vapor velocity reaches the sonic limit and the sonic limitation at evaporator takes place. In this case, Eq. (2.23) will reduce to its sonic limit and will be represented by Eq. (2.24) which is considered to be $Q_{S_{\max}}$ and presents the sonic limit within heat pipe:

$$Q_{S_{\max}} = A_v \rho_0 \lambda \left[\frac{\gamma_v R_v T_v}{2(\gamma_v + 1)} \right]^{1/2} \quad (\text{Eq.2.24})$$

There exists a relationship between axial distribution of the vapor Mach number, for a heat pipe, and operation at its sonic limit through the following equation:

$$\frac{Q}{Q_{S_{\max}}} = \frac{M_v \left[2(\gamma_v + 1) \left(1 + \frac{\gamma_v - 1}{2} M_v^2\right) \right]^{1/2}}{1 + \gamma_v M_v^2} \quad (\text{Eq.2.25})$$

which can be derived by dividing Eq. (2.22) by Eq. (2.23). The axial distribution of the liquid–vapor interface temperature T_v can be calculated by Eq. (2.19) with the value of M_v obtained from Eq. (2.25).

Equation (2.24) originally was derived by Levy and is often referred to as Levy [11] equation for the calculation of a heat pipe's maximum heat transport rate at its sonic limit. Equation (2.19) together with Eqs. (2.24) and (2.25) can be used to evaluate the liquid–vapor interface temperature along the evaporator section of heat pipe.

Levy [11] developed a closed-form expression for the sonic limit derived from a one-dimensional vapor flow theory by treating the one-dimensional two-phase flow approach. In this analysis, the frictional effect was assumed negligible; therefore, inertial effects dominate, and the vapor behaves as a perfect gas.

Busse [23] later on presented an alternative approach by assuming that only inertial effects are present in one-dimensional flow. In this case, the momentum equation yields

$$\frac{dP}{dx} = -\frac{d}{dx} \rho v^2 \quad (\text{Eq.2.26})$$

Integrating both sides of Eq. (2.26) with combination with the continuity equation and assuming that vapor behaves like an ideal gas results to an expression for the

maximum heat transport capacity as a function of the thermophysical and geometric properties as follows:

$$Q = \lambda \left(\frac{\rho_v P_v}{A} \right)^{1/2} \left[\frac{P}{P_v} \left(1 - \frac{P}{P_v} \right) \right]^{1/2} \quad (\text{Eq.2.27})$$

A determination of the point where the first derivative, $\frac{dQ}{dP}$, vanishes will result in a relationship for the sonic limit within heat pipe:

$$Q_s = 0.474 \lambda A_v (\rho_v P_v)^{1/2} \quad (\text{Eq.2.28})$$

where both ρ_v and P_v are vapor density and pressure at the evaporator exit of heat pipe. The most difficult aspect of determining the sonic limit depends on determining these two quantities along with the inlet pressure of the condenser within heat pipe that is under consideration.

Further steps were taken to describe the sonic limit from idealizing one-dimensional vapor flow of a perfect gas with negligible frictional effect to a two-dimensional approach using Navier–Stokes equations. Several attempts were achieved to show such solutions using numerical methods by different authors. Bankstone and Smith [29] and Rohani and Tien [30] all used such methods. The former study indicated that axial flow reversal occurred for high condensation rates at the end of the condenser. Comparison with the predicted results of a one-dimensional model developed by Busse [23] indicated good agreement for high condensation rates in the condenser region deposit this flow is reversal [30].

It is interesting to compare the results for the viscous limit and sonic limit where a relationship between the two exists with respect to the quantity $\rho_v P_v$. Inertial effects are found to vary with the product $(\rho_v P_v)^{1/2}$, while the viscous effects vary linearly with respect to $\rho_v P_v$. As a result, when this product is small, viscous effects typically limit the transport capacity, but with increasing $\rho_v P_v$, inertial effects begin to dominate and a transition occurs from the viscous to the sonic limit. The boundary between these two limits can be determined by setting these two equations equal to each other and solving for the combined terms as a function of temperature (Ivanovskii et al. [31] and Busse [23]). The results indicate that the transition temperature is dependent on the thermophysical properties of the working fluid, the geometry of the heat pipe, and the length of the evaporator and condenser regions. Experimental work by Vinz and Busse [32] verified that this transition compared quite well with predicted values. These studies indicate that axial flow reversal occurs for $Re_r < -2.3$ at the end of the condenser during conditions of high evaporation and condensation.

Example 2.2 (from Chi book) Determine the maximum heat transport rate at the sonic limit of a conventional sodium vapor within a heat pipe with core diameter of 0.75 in. (1.91×10^{-2} m). Assume that the vapor temperature at the upstream end of the evaporator is 800 °F (700 K).

Solution As the vapor velocity at the upstream end of the evaporator is zero, 800 °F (700 K) is the vapor stagnation temperature. Properties of sodium vapor at 800 °F (700 K), relevant to sonic limitations [18], are as follows:

Vapor density $\rho_0 = 2.6 \times 10^{-5} \text{ lbf/ft}^3 = 4.17 \times 10^{-4} \text{ kg/m}^3$.

Latent heat of vaporization $\lambda = 1800 \text{ Btu/lbf} = 4.18 \times 10^6 \text{ J/kg}$.

Specific heat ratio for monoatomic vapor $\gamma_v = 5/3 = 1.67$.

Universal gas constant $\bar{R} = 1545 \text{ (ft lbf/lbfm mol R)} = 8.314 \times 10^3 \text{ J/kg mol K}$.

Vapor constant $R_v = 1545/23 \text{ (ft lbf/lbfm R)} = 67.17 \text{ (ft lbf/lbfm R)} = 2163$
(ft lbf/slug R (361 J/kg K))

Vapor core cross-sectional area is

$$A_v = \frac{\pi d_v^2}{4} = \frac{\pi(0.75)^2}{4(144)} = 3.07 \times 10^{-3} \text{ ft}^2 \quad (2.85 \times 10^{-4} \text{ m}^2)$$

Sonic limit

$$\begin{aligned} Q_{S_{\max}} &= A_v \rho_0 \lambda \left[\frac{\gamma_v R_v T_v}{2(\gamma_v + 1)} \right]^{1/2} \\ &= (3.07 \times 10^{-3}) (2.6 \times 10^{-5}) (1800) \left[\frac{(1.67)(2163)(1260)}{2(1.67+1)} \right]^{1/2} \\ &= 0.1326 \text{ Btu/s} \\ &= 478 \text{ Btu/s} \\ &= 140 \text{ W} \end{aligned}$$

Hence, the sonic heat transport limit of the heat pipe is 468 Btu/h (140 W). The actual heat transport limit will of course be dependent upon wick structures. If 478 Btu/h is less than any of the other three limits (i.e., capillary, entrainment, or boiling), then 478 Btu/h will be the actual maximum heat transport limit of this heat pipe operating at 800 °F (700 K).

2.11.1 Sonic Limitation and Startup Problem of Heat Pipes

In the design of heat pipes, consideration must be given not only to the internal structure and fluid dynamics of the pipe but also to the external conditions imposed upon it. By *fully operational steady characteristics* of heat pipe up to now, we have assumed a steady-state heat pipe, with heat being added to and removed from the heat pipe at a constant rate. Under this condition, we mean that the heat pipe is relatively *isothermal* and heat is being dissipated over the entire length of the condenser. If the heat pipe input and output rates are then equal, the heat pipe will be functioning in the steady-state condition. If an imbalance between the heat

input and output rates take place, then the temperature of the fully operational heat pipe will continue to change with time to a level at which the balance between heat input and output rates is restored [22].

The vapor pressure and physical state of the heat pipe liquid at ambient temperature, as well as the thermal resistance between the condenser and the adjacent heat sink, has significant influence on the startup behavior of a heat pipe.

Prior to startup, the temperature of a heat pipe is equal to the ambient temperature, and its internal pressure is equal to the vapor pressure of the heat pipe liquid at ambient temperature. Also depending on its freezing point, the heat pipe liquid may be in the liquid or the solid state. The transient behavior and problems of heat pipe startup have been studied by Cotter [26] and Deverall et al. [14]. Tests results reported by the latter indicate that the transient behavior of a heat pipe depends on the circumstances mentioned above [14].

Analyzing Fig. 2.14, when sufficient continuum flow reaches the condenser end of the pipe to start raising its temperature, the evaporator entrance temperature gradually moved away from the sonic curve, indicating a decrease in vapor velocity and an increase in vapor density [13]. Eventually the temperature drop along the evaporator approaches zero, and isothermal operation is achieved. This indicates that a startup with sonic vapor flow is possible with carefully controlled heat input and rejection rates. However, there are some heat pipe applications where the pipe might have to start up with full design heat input and a closely coupled heat sink, which could make startup difficult or, in some cases, impossible [26].

2.12 Entrainment Limit

As liquid and vapor move in opposite directions, the vapor exerts a shearing force on the liquid at the liquid–vapor interface. If this shear force exceeds the surface tension of the liquid, liquid droplets are entrained into the vapor flow and are carried towards the condenser section. The magnitude of this shear force depends on the thermophysical properties of the vapor and its velocity, and if it becomes large enough, it causes dryout of the evaporator [5, 17]. Entrainment limit at high vapor velocities, droplets of liquid in the wick are torn from the wick and sent into the vapor, which results in dryout. An abrupt wick dryout will take place when entrainment begins, and there is a sudden substantial increase in fluid circulation to the point that return liquid system cannot accommodate this flow increase [18]. This limit was identified by Kemme [28] when he discovered the sounds that were made by droplets from media liquid within the heat pipe striking the condenser end of the heat pipe and through the abrupt overheating of the evaporator [28]. The entrainment limit is also known as an axial heat flux, the heat transport rate per unit of vapor space cross-section area. Under this condition, the fluid velocities increase so as drag force as the heat transport rate through the heat pipe increases. The drag force on the heat pipe liquid is proportional to the liquid surface area in the wick pores, whereas the resisting surface tension force is proportional to the pore

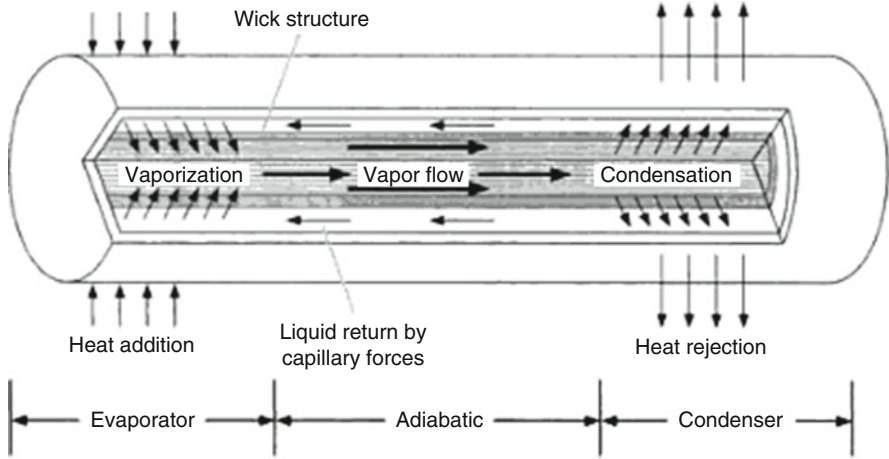


Fig. 2.19 Schematic of heat pipe

width normal to the drag force [22]. Consequently, the ratio of the drag force to the surface tension force is proportional to the pore size and decreases as the pore size diminishes (Fig. 2.19).

In this case, a higher vapor velocity is then needed to increase the drag force and cause entrainment. The entrainment limit is therefore an inverse function of the wick pore size. If the wick is partially filled with liquid, the liquid–vapor interface will lie within the wick structure. The vapor in contact with the liquid should then be relatively stagnant, and the viscous shear stress on the liquid surface will be quite small. The entrainment limit would then be expected to be considerably large than when the liquid–vapor interface lies at the edge of the wick structure. In general, raising the entrainment limit can only be considered for a composite or two-layer wick, in which the flow channel layer remains full and liquid recession is confined to the capillary pumping layer. In single-layer wick structures consisting of open grooves cut into the heat pipe wall, even a slight degree of underfilling can severely reduce heat transport capability [33, 34]. Since the liquid vapor never reaches the evaporator, it cannot contribute to the heat transferred by the heat pipe. However, it does contribute to the liquid flow loss. Thus, the maximum axial heat transfer in the heat pipe is no longer equal to the maximum fluid circulation rate times the latent heat of vaporization, but is some lower value which defines the entrainment limit. The vapor velocity in a heat pipe is generally much larger than the liquid velocity. F_s represents the shear force at the liquid–vapor interface [18] and tends to tear the liquid from the surface of the wick, and it is proportional to the product of dynamic pressure of the moving vapor $\frac{\rho_v V_v^2}{2}$ and the area A_s of individual surface pores of the wick and can be shown in terms of Eq. (2.29):

$$F_s = K_1 \frac{\rho_v V_v^2 A_s}{2} \tag{Eq.2.29}$$

The force F_t is representing the surface force which holds the liquid in the wick, is proportional to the product of the surface tension coefficient σ and the wetted perimeter C_s of the individual surface pores of the wick, and is shown in terms of Eq. (2.29) as follows:

$$F_t = K_2 C_s \sigma \quad (\text{Eq.2.30})$$

In both Eqs. (2.29) and (2.30), the constant proportionality is given by K_1 and K_2 respectively.

The conditions leading to entrainment are expressed in terms of the ratio of vapor inertial forces to liquid surface tension forces, called the Weber number, and it is the ratio of F_s and F_t that can be shown as We:

$$\text{We} = \frac{\rho_v \bar{V}_v^2 z}{\sigma} \quad (\text{Eq.2.31})$$

where

ρ_v = vapor density,

\bar{V}_v = average vapor velocity,

σ = liquid surface tension, and

z = characteristic dimension associated with liquid surface and is representing the form of $z = \frac{K_1 A_s}{2K_2 C_s}$

where

A_s = individual surface pores of the wick and

C_s = wetted perimeter of the individual surface pores of the wick.

At present time, there are limited experimental data that is available with screen wicks, indicating a Weber number of unity which is a representation of the entrainment condition when z is set approximately equal to the screen wire diameter. Note that some authors argue that the wire-to-wire spacing is a more appropriate value for z [35], which requires additional experimental data to validate such claims. Subsequently this suggest that by using finer mesh screen, entrainment can be inhibited—a hypothesis which has been verified at Los Alamos heat pipe programs.

For wick structures that do not involve screens, any construction that reduces interaction between the vapor and liquid will save to raise the entrainment limit. On the other hand, open wick structures such as axial grooves cut in the wall are particularly susceptible to the effects of vapor–liquid drag [10].

When the Weber's number reaches unity that is given by Eq. (2.32),

$$\text{We} = \frac{K_1 \rho_v \bar{V}_v^2 A_s}{2K_2 C_s \sigma} = 1 \quad (\text{Eq.2.32})$$

Data [28, 35] is given by Kemme and Busse for the value of K_1/K_2 ; although limited at the present time, it appears to indicate that K_1/K_2 is of the order of 8. Hence, Eq. (2.32) for entrainment limitation can be written as

$$We = \frac{2r_{h,s}\rho_v V_v^2}{\sigma} = 1 \quad (\text{Eq.2.33})$$

where $r_{h,s}$ is the hydraulic radius of the wick surface pores and is defined as [18]

$$r_{h,s} = \frac{2A_s}{C_s} \quad (\text{Eq.2.34})$$

This radius is equal to 0.5 of the wire spacing for screen wick, the width of the groove for groove wicks, and 0.41 of the sphere radius for a packed sphere.

The vapor velocity of a heat pipe is related to the axial heat flux by Eq. (2.35) as follows:

$$V_v = \frac{Q}{A_v \rho_v \lambda} \quad (\text{Eq.2.35})$$

Substituting Eq. (2.33) into Eq. (2.35) for V_v will yield the following expression for the entrainment heat transport limit:

$$Q_{e_{\max}} = A_v \lambda \left(\frac{\sigma \rho_v}{2r_{h,s}} \right)^{1/2} \quad (\text{Eq.2.36})$$

Example 2.3 (from Chi book) An axially grooved sodium heat pipe has the following characteristics:

Vapor core radius, $r_v = 0.75$ in. (1.91×10^{-2} m).

Number of rectangular grooves, $n = 120$.

Groove width, $w = 0.02$ in. (5.08×10^{-4} m).

Groove depth, $\delta = 0.05$ in. (1.27×10^{-3} m).

Determine the entrainment heat transport limit of the heat pipe when it is operating at 800 °F (700 K).

Pertinent properties of sodium at 800 °F (700 K).

Solution Surface tension coefficient, $\sigma = 1.1 \times 10^{-2}$ lbf/ft (1.605×10^{-1} N/m).

Vapor density, $\rho_v = 2.6 \times 10^{-5}$ lbfm/ft³ = 8.07×10^{-7} slug/ft³ = (4.17×10^6 kg/m³).

Latent heat of vaporization, $\lambda = 1800$ Btu/lbm = 5.8×10^4 Btu/slug = (4.18×10^6 J/kg).

Pertinent pipe dimensions:

Surface pore hydraulic radius, $r_{s,h} = w = 0.02$ in. = 1.667×10^{-3} ft = (5.1×10^{-4} m).

Vapor core cross-sectional area, $A_v = \pi r_v^2 = 1.227 \times 10^{-2} \text{ ft}^2 = (1.14 \times 10^{-3} \text{ m}^2)$.

Entrainment limit, Eq. (2.34) yields

$$\begin{aligned} Q_{e_{\max}} &= A_v \lambda \left(\frac{\sigma \rho_v}{2r_{h,s}} \right)^{1/2} \\ &= (1.227 \times 10^{-2}) (5.8 \times 10^4) \left[\frac{(1.1 \times 10^{-2}) 8.07 \times 10^{-7}}{2(1.667 \times 10^{-3})} \right]^{1/2} \\ &= 1.16 \text{ Btu/s} \\ &= 4180 \text{ Btu/h} \\ &= 1224 \text{ W} \end{aligned}$$

Hence, the entrainment limit of this heat pipe at 800 °F (700 K) is 4180 Btu/h (1224 W).

2.13 Wicking/Capillary or Circulation Limit

The “wicking limit” or “capillary limit” is the best understood. This condition is occurring when an applied heat flux causes the liquid in the wick structure to evaporate faster than it can be supplied by capillary pumping power of the wick. Once this event takes place, the meniscus at the liquid–vapor interface continues to withdraw and move back into the wick until all of the liquid has been depleted. This action will result the wick to become dry, and heat pipe container temperature may continue to rise at the evaporator until a “burnout” condition is reached [36]. The difference in the capillary pressure across the liquid–vapor interfaces governs the operation of the heat pipes. This is one of the most important parameters that affect the performance and operation of a heat pipe. It is usually a major limiting factor in the working of low-temperature or cryogenic heat pipes.

The capillary limit is encountered when the capillary pressure is not sufficient to pump the liquid back to evaporator, causing the dryout of the wick of the evaporator end. The physical structure of the wick is one of the most important reasons for this limit, and the type of working fluid affects it. Once limit is encountered, any further increase in heat input may cause serious damage to the heat pipe [17].

The performance and operational characteristics for a given heat pipe and thermosyphons as a function of the mean adiabatic or operating temperature and envelope of these operating limits have been discussed in various sections of this book and are depicted here as well (see Fig. 2.20).

Any design of heat pipe that falls within the operation envelope of its function (red color) is essentially considered as a good design and will work within specific function of operating temperature that is defined for that design.

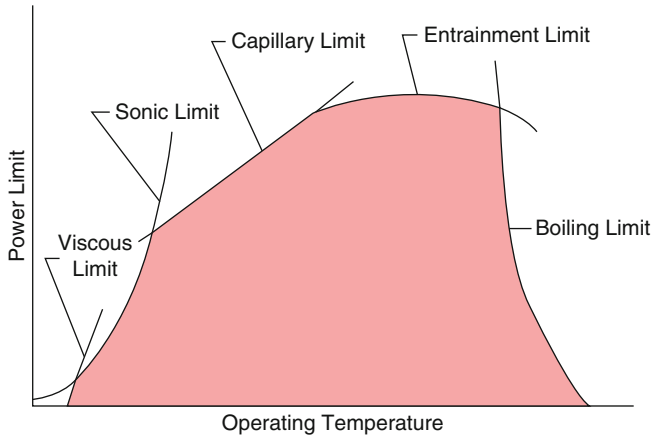


Fig. 2.20 Typical heat pipe performance map

Note: Thermosiphon (alternately, **thermosyphon**) refers to a method of passive heat exchange based on natural convection which circulates liquid without the necessity of a mechanical pump.

Any modeling of heat pipe even with the simplest configurations requires two-dimensional axisymmetric geometries that involve two-phase constitutive relationships, and at minimum, a one-dimensional two-phase flow analysis assuming the vapor flow at high Mach number is compressible, and the model should compensate for the effects of vaporization and condensation at the liquid–vapor and solid–vapor interfaces accordingly [37]. Knowledge of liquid flow in porous media is required for a high vapor flow which may result to some interfacial instability through the wick structures [38]. And finally other complicated issues and problems such as fluid property degradation, freezing [39], or corrosion [40] as well as chemical reactions between working fluid, wick, and internal material structure of heat pipe [41] will impact the simplest steady-state flow modeling of heat pipe. Typically as part of procedure to design a heat pipe, we begin with the calculation of wick or capillary limit since wick structure and materials as we said play a big role in this. This is due to the fact that equations used to analyze both Reynolds number and the Mach number are functions of the heat transport capacity and most solutions that are commonly used assumes a laminar, incompressible vapor flow within the heat pipe internal structure [17].

Chi [18] has shown a great detail of how to obtain the maximum heat transport capacity $Q_{c_{max}}$ using the expression for the vapor Reynolds number and the Mach number with the help of Eq. (2.8a) to determine the accuracy of the above assumption. Here we can use the detailed derivation of the $Q_{c_{max}}$ for a heat pipe that is given by Chi [18]. (Note: Chi’s book is no longer in publication circulation; for the readers who are interested to obtain their own personal copy, they should try to purchase a used copy. This is the main reason the details of his derivation are shown here.)

When a heat pipe is operating in steady state, there is a continuous flow of vapor from the evaporator section to the condenser section and liquid from the condenser section to the evaporator section through the wick. These flows are possible because of the vapor pressure gradient (Δp_v) and the liquid pressure gradient (Δp_l) along the length of the heat pipe (see Sect. 2.5 for more details). Considering the circulation of vapor flow between evaporator and condenser, there exists a liquid pressure gradient along the vapor flow passage. The same argument is valid for liquid pressure gradient as the condensed liquid flows back from the condenser to the evaporator side of the heat pipe. The balance of pressure that is required along the entire heat pipe length and the difference between the two sides of liquid–vapor interface is called the capillary pressure, and it is established by the menisci that form at the interface. Mathematically the pressure balance can be expressed as follows:

$$[P_v(x_{ref}) - P_v(x)] + [P_v(x) - P_l(x)] + [P_l(x) - P_l(x_{ref})] + [P_l(x_{ref}) - P_v(x_{ref})] = 0 \tag{Eq.2.37}$$

Introducing the capillary pressure of P_c that is presenting the pressure at the vapor side of the liquid–vapor interface minus (two-phase situation) that at the liquid side results in

$$P_c(x) = P_c(x_{ref}) + \Delta P_v(x - x_{ref}) + \Delta P_l(x_{ref} - x) \tag{Eq.2.38}$$

where

P_c = capillary pressure at position, x along the heat pipe = $P_v(x) - P_l(x)$,

$P_c(x_{ref})$ = capillary pressure at a reference position, $x_{ref} = P_v(x_{ref}) - P_l(x_{ref})$,

$\Delta P_v(x - x_{ref})$ = vapor pressure drop on flowing from x to $x_{ref} = P_v(x_{ref}) - P_v(x)$, and

$\Delta P_l(x_{ref} - x)$ = liquid pressure drop on flowing from x_{ref} to $x = P_l(x_{ref}) - P_l(x)$.

This pressure difference is equal to zero where this difference is at its minimum (Fig. 2.21). So if the reference position, x_{ref} , is chosen to be at x_{min} where the

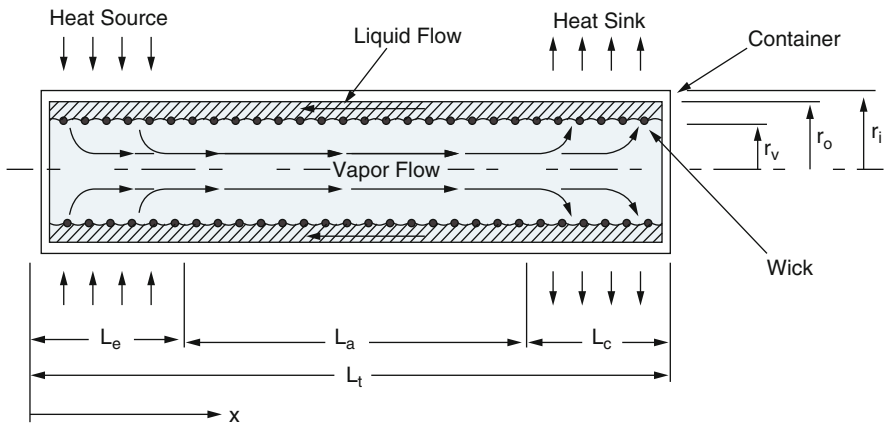


Fig. 2.21 Schematic of a heat pipe showing circulation of working fluid (Chi [18])

capillary pressure is minimum and equal to zero, then Eq. (2.36) reduces into Eq. (2.39) as follows:

$$P_c(x) = \Delta P_v(x - x_{\min}) + \Delta P_1(x_{\min} - x) \quad (\text{Eq.2.39.})$$

Generally speaking, the pressure drop terms ΔP_v and ΔP_1 on right-hand side of Eq. (2.35) increase with heat load during operation of heat pipe, and as a result, the capillary pressure P_c increases accordingly. However, there exists a maximum capillary pressure that can be introduced for a liquid–wick pair, and the detail analysis of such development is presented in Sect. 2.5. For a heat pipe to operate properly and continuously without any dryout within the wick region, then the required capillary should not exceed the maximum possible capillary pressure at any point along the heat pipe (see Eq. (2.7)). This limitation on the heat transport capability of a heat pipe is known as the wick or capillary limitation.

2.13.1 Liquid Pressure Drop

Per Chi [18], the pressure drop of the liquid in wick structures can be obtained by integrating the liquid gradient

$$\begin{aligned} \Delta P_1(x_{\min} - x) &= P_1(x_{\min}) - P_1(x) \\ &= - \int_{x_{\min}}^x \frac{dP_1}{dx} dx \end{aligned} \quad (\text{Eq.2.40})$$

where $\frac{dP_1}{dx}$ is the liquid gradient in the direction of liquid flow.

For a steady-state mode (constant heat addition and removal) and little manipulation and integration over the length of heat pipe, another form of Eq. (2.40) can be written as the following form:

$$\Delta P_1 = \left(\frac{\mu_1}{K A_w \rho_1 \lambda} \right) L_{\text{eff}} q \quad (\text{Eq.2.41})$$

where

μ_1 = the liquid viscosity,

V_1 = the liquid velocity,

ρ_1 = the liquid density,

λ = the latent heat of vaporization,

A_w = the wick cross-sectional area

K = permeability represents a property of the wick structure since, and

L_{eff} = effective heat pipe length.

In this scenario, the dynamic pressure can be neglected, since liquid velocity in heat pipe wicks is generally very low. For steady-state condition, this is related to the frictional drag and gravitational force by the following equation:

$$\frac{dP_1}{dx} = -\frac{2\tau_1}{r_{h_1}} \pm \rho_1 g \sin \psi \quad (\text{Eq.2.42})$$

where

r_{h_1} = hydraulic radius for liquid flow. The hydraulic radius defined as twice the cross-sectional area divided by the wetted perimeter,

τ_1 = the frictional stress at the liquid–solid interface,

ψ = the angle of inclination of the heat pipe measured from the horizontal direction,

ρ_1 = the liquid density, and

g = the gravitational acceleration.

Note: The gravitational force may be positive or negative depending upon whether the liquid is flowing in a direction with or against g .

Now we can introduce two other parameters into this analysis known as drag coefficient of f_1 and the dimensionless Reynolds number of Re_1 and they both can be shown as follows:

$$Re_1 = \frac{2r_{h_1}\rho_1 V_1}{\mu_1} \quad f_1 = \frac{2\tau_1}{\rho_1 V_1^2} \quad (\text{Eq.2.43})$$

where

μ_1 = the liquid viscosity and

V_1 = the liquid velocity.

The liquid velocity V_1 is related to the local axial Q :

$$V_1 = \frac{Q}{\varepsilon A_w \rho_1 \lambda} \quad (\text{Eq.2.44})$$

where

λ = the latent heat of vaporization,

A_w = the wick cross-sectional area, and

ε = the wick porosity.

Substituting Eqs. (2.40) and (2.41) into Eq. (2.39) yields the following expression for the liquid pressure gradient:

$$\frac{dP_1}{dx} = -\frac{(f_1 Re_1)\mu_1}{2\varepsilon A_w r_{h_1}^2 \rho_1 \lambda} Q \pm \rho_1 g \sin \psi \quad (\text{Eq.2.45})$$

Or we can rearrange the above equation as follows:

$$\frac{dP_1}{dx} = -F_1 Q \pm \rho_1 g \sin \psi \quad (\text{Eq.2.46})$$

where F_1 is representing the frictional coefficient for the liquid flow and is defined as

$$F_1 = \frac{\mu_1}{KA_w \lambda \rho_1} \quad (\text{Eq.2.47})$$

And wick permeability is calculated from Eq. (2.48) down below

$$K = \frac{2\epsilon r_{hi}^2}{(f_1 \text{Re}_1)} \quad (\text{Eq.2.48})$$

In Eq. (2.46) the permeability K represents a property of the wick structure since:

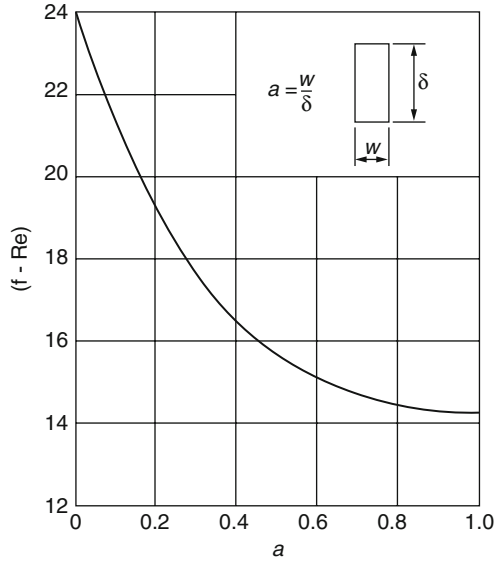
1. The flow of liquid in the heat pipe wick structure is laminar due to the generally low liquid velocity.
2. For laminar flow, $(f_1 \text{Re}_1)$ is a constant whose magnitude depends only on the geometry of wick structure as do the other quantities in Eq. (2.48). Several methods to evaluating K is suggested by Chi [18] for several common wicks, and the reader should refer to his book in pages 40–42. But here we present Table 2.4 by him for different wick structures as follows.

Note that the hydraulic radius is equal to the radius of the liquid flow passage r and the porosity is equal to unity for a wick structure that is molded in a circular passage, e.g., artery wick or tunnel shape. In this case, the term $(f_1 \text{Re}_1)$ is equal to 16 for a laminar tube flow using the well-known Hagen–Poiseuille solution [42]:

Table 2.4 Expressions of wick permeability K for several wick structure

Wick structures		K expressions
Circular artery	$K = \frac{r^2}{8}$	
Open rectangular grooves	$K = \frac{2\epsilon r_{hi}^2}{(f_1 \text{Re}_1)}$	$\epsilon = \text{porosity} = \frac{w}{s}$ $s = \text{groove pitch}$ $r_{hi} = \frac{2w\delta}{w + 2\delta}$ $w = \text{groove width}$ $\delta = \text{groove depth}$ $(f_1 \text{Re}_1)$ from Fig. 2.22
Circular annular wick	$K = \frac{2\epsilon r_{hi}^2}{(f_1 \text{Re}_1)}$	$r_{hi} = r_1 - r_2$ $(f_1 \text{Re}_1)$ from Fig. 2.23 $d = \text{wire diameter}$
Wrapped screen wick	$K = \frac{d^2 \epsilon^3}{122(1 - \epsilon)^2}$	$\epsilon = 1 - \frac{1.05\pi Nd}{4}$ $N = \text{mesh number}$
Packed sphere	$K = \frac{r_s^2 \epsilon^3}{37.5(1 - \epsilon)^2}$	$r_s = \text{sphere radius}$ $\epsilon = \text{porosity (value depends on packing mode)}$

Fig. 2.22 Frictional coefficients for laminar flow in rectangular tubes



$$K = \frac{r^2}{8} \tag{Eq.2.49}$$

Laminar fluid flow solutions in rectangular passages exhibit a relationship between $(f_1 Re_1)$ and the passage aspect ratio of α (see Fig. 2.22). Using Eq. (2.48) the permeability K for a covered rectangular groove wick of known aspect ratio ($\alpha = \frac{w}{\delta}$) and porosity ε can be calculated. The term $(f_1 Re_1)$ is read from Fig. 2.22 with r_{hi} equal to $\frac{w\delta}{w+\delta}$. For a wick with open rectangular grooves of known porosity, K can be calculated by Eq. (2.48) also. However, the wick's aspect ratio should first be calculated by the following equation:

$$a = \frac{w}{2\delta} \tag{Eq.2.50}$$

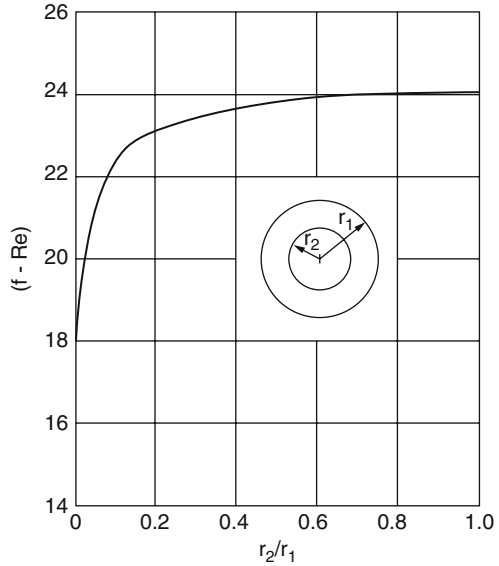
In this case, the value of $(f_1 Re_1)$ can be obtained using Fig. 2.22 and the wick's hydraulic radius calculated using Eq. (2.51):

$$r_{hi} = \frac{2w\delta}{w + 2\delta} \tag{Eq.2.51}$$

On the other hand, Fig. 2.23 determines the theoretical values of $(f_1 Re_1)$ for a family of circular annular flow passages [42]. For annular wicks of known r_1, r_2 and K the permeability value can be calculated by again using Eq. (2.48). Under this assumption, the following values are valid:

$$\varepsilon = 1$$

Fig. 2.23 Frictional coefficients for laminar flow in circular annuli



$$r_{hi} = r_1 - r_2$$

and $(f_1 Re_1)$ is read from Fig. 2.23.

For the wrapped-screen wick, the permeability varies widely since it is a function of the wrap tightness. But for a loosely wrapped wick, K can be approximated by a series of parallel annular passages.

Marcus [43] with his report “Theory and Design of Variable Conductance Heat Pipes” of April 1972 has shown that experimental data on tightly wrapped wicks have been correlated by a modified Blake–Kozeny equation (see Appendix A):

$$K = \frac{d^2 \varepsilon^3}{122(1 - \varepsilon)^2} \tag{Eq.2.52}$$

where in Eq. (2.52), d is the wire diameter and ε can be calculated by the equation

$$\varepsilon = 1 - \frac{\pi S N d}{4} \tag{Eq.2.53}$$

where N is the mesh number and S is the crimping factor (≈ 1.05) [44]. The crimping factor accounts for the fact that screens are not simply crossed rods. Per Chi [18] if the degree of wrapping tightness is uncertain, then using the formula for a tightly wrapped wick (Eqs. 2.52 and 2.53) provides a conservative approach since the tightly wrapped wicks have higher flow resistance than their loosely wrapped counterparts.

Using approximation by the Blake–Kozeny [45, 46] equation for a packed spherical bed, the permeability of sintered metal can be calculated using the following equation:

$$K = \frac{r_s^2 e^3}{37.5(1 - e)^2} \quad (\text{Eq.2.54})$$

Note that again the liquid flow in heat pipe wick is generally characterized by very low flow velocities and Reynolds number (laminar flow) [43]. Consequently, inertial effects can be neglected for steady-state operation, and the flow losses attributed only to viscous shear.

Associated with above arguments, the two following figures that are present by Chi [18] are depicted here.

2.13.2 Vapor Pressure Drop

Similarly the vapor pressure drop in the heat pipe vapor flow is calculated by integrating the vapor pressure gradient as follows:

$$\begin{aligned} \Delta P_v(x - x_{\min}) &= P_v(x) - P_v(x_{\min}) \\ &= - \int_{x_{\min}}^x \frac{dP_v}{dx} dx \end{aligned} \quad (\text{Eq.2.55})$$

where $\frac{dP_v}{dx}$ is the vapor pressure gradient in the direction of vapor flow.

Chi found that upon integration of the vapor pressure gradient, the dynamic pressure effects cancel, and another result of Eq. (2.55) can be represented as follows:

$$\Delta P_v = \left(\frac{C(f_v \text{Re}_v)\mu_v}{2(r_{h_v})^2 A_v \rho_v \lambda} \right) L_{\text{eff}} q \quad (\text{Eq.2.56})$$

where

- r_{h_v} = hydraulic radius of the vapor space,
- C = a constant that depends on the Mach number,
- A_v = cross-sectional area of vapor control volume with width of dx ,
- f_v = drag coefficient for vapor flow,
- Re_v = Reynolds number for vapor flow,
- μ_v = vapor dynamic viscosity,
- ρ_v = vapor density,
- λ = latent heat of vaporization,
- q = heat transferred, and
- L_{eff} = effective heat pipe length.

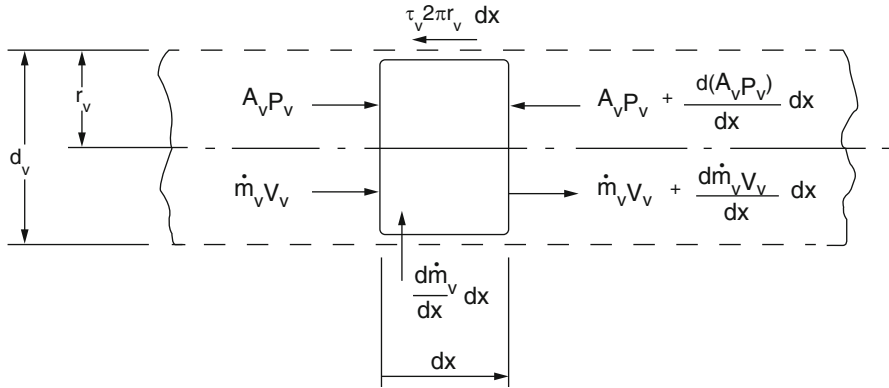


Fig. 2.24 An elementary control volume for vapor flow (Chi [18])

Calculating of the vapor pressure drop in a heat pipe is often considerably more difficult than liquid pressure analysis. In addition to viscous shear, one has to take into account the analysis for momentum effects and possibly turbulent flow and compressibility [43]. This calculation gets more complicated due to the fact that mass addition in the evaporator and its removal from the condenser side of heat pipe can significantly alter the velocity profiles and, hence, the local pressure gradient. In the steady state, the mass flow rate for the vapor is equal to that for the liquid at the same axial position. However, because of the low density for the vapor in comparison with that for liquid, the vapor velocity can be considered much larger than the liquid velocity. Under these circumstances, the vapor pressure gradient results not only from the frictional drag but also from the dynamic effect, and the flow of vapor may be laminar or turbulent [18]. The compressibility of the vapor may also become important. Therefore, the theory that describes the vapor pressure drop depends on whether the flow is laminar or turbulent and can be analyzed mainly on either the parabolic or the one-seventh power law of vapor velocity profiles.

Using Fig. 2.24, this analysis starts with a consideration of the stationary vapor in a control volume of the cross-sectional area with A_v , width dx , and with a mass flux per unit width at the liquid–vapor interface of $d\dot{m}_v/dx$. Neglecting the effects of gravitational force due to the low vapor density as per our assumption and using the definition of the principle of conservation of axial momentum result in Eq. (2.57) as follows:

$$\frac{dP_v}{dx} = \frac{-(f_v Re_v)\mu_v \dot{m}_v}{2A_v r_{h_v}^2 \rho_v} - \beta \frac{2\dot{m}_v}{A_v \rho_v} \frac{d\dot{m}_v}{dx} \tag{Eq.2.57}$$

Again this is as result of the condition that laminar flow exists throughout the heat pipe and the vapor pressure gradient can be approximated by the sum of two terms which is the viscous shear and that is due to momentum gradients in the evaporator and condenser side of the heat pipe.

In Eq. (2.57) the first term on the right-hand side represents the vapor pressure gradient due to frictional drag, and the second term is the pressure gradient due to variation of dynamic pressure, where f_v is representing the frictional drag coefficient and β is defined by the following equation:

$$\beta = \frac{\rho_v^2 A_v}{\dot{m}_v^2} \int_{A_v} V_v^2 dA \quad (\text{Eq.2.58})$$

Equation (2.58) accounts for the effects of changes in vapor velocity across the section [18]. On the other hand, the mass flux \dot{m}_v is related to the axial heat flux at same point x , ($\dot{m}_v = Q/\lambda$) and then Eq. (2.57) can be written in a different form as follows:

$$\frac{dP_v}{dx} = -F_v Q - D_v \frac{dQ^2}{dx} \quad (\text{Eq.2.59})$$

where

F_v = frictional coefficient for the vapor flow and
 D_v = dynamic pressure coefficient for the vapor flow,
 and they are defined in the following forms:

$$F_v = \frac{(f_v \text{Re}_v) \mu_v}{2r_{h_v}^2 A_v \rho_v \lambda} \quad (\text{Eq.2.60})$$

$$D_v = \frac{\beta}{A_v^2 \rho_v \lambda^2} \quad (\text{Eq.2.61})$$

where

A_v = vapor cross-section area,
 D_v = dynamic pressure coefficient,
 f_v = drag coefficient for vapor flow,
 Re_v = Reynolds number for vapor flow,
 r_{h_v} = hydraulic radius for vapor flow,
 β = profile coefficient for momentum flux,
 μ_v = vapor dynamic viscosity,
 ρ_v = vapor density, and
 λ = latent heat of vaporization.

The value of $(f_v \text{Re}_v)$ in Eq. (2.60) can be evaluated using the same manner as liquid pressure drop analysis, and it is equal to 16 for a circular vapor flow passage. For further value of $(f_v \text{Re}_v)$ rectangular passages of different aspect ratio, refer to Table 2.5, and for annular passages of different radius ratio, refer to Fig. 2.23. The value of β can be calculated by Eq. (2.58), assuming a parabolic velocity profile. β is equal to 1.25, 1.33, and 1.44, respectively, for annular passages of radius ratio close to unity, circular tubes, and rectangular passages [18].

If the values of f_v and β which depend upon the flow conditions, are known, then one can evaluate the value of F_v and D_v and we need to specify the flow conditions by nondimensional quantities, namely, the vapor Reynolds number and Mach number and they are defined as follows:

$$\text{Re}_v = \frac{2r_{h_v}Q}{A_v\mu_v\lambda} \quad (\text{Eq.2.62})$$

$$M_v = \frac{Q}{A_v\rho_v\lambda\sqrt{\gamma_v R_v T_v}} \quad (\text{Eq.2.63})$$

where γ_v is the vapor-specific heat ratio, which is equal to 1.6, 1.4, or 1.33 for monoatomic, diatomic, or polyatomic vapor, respectively, and the rest of the variables are defined as follows [18]:

R_v = gas constant for vapor.

M_v = Mach number for vapor flow.

Re_v = Reynolds number for vapor flow.

Q = heat-flow rate.

T_v = vapor temperature.

A_v = vapor cross-section area.

r_{h_v} = hydraulic radius for vapor flow.

β = profile coefficient for momentum flux.

μ_v = vapor dynamic viscosity.

ρ_v = vapor density.

λ = latent heat of vaporization.

γ_v = vapor-specific heat ratio.

The vapor can be considered to be laminar and incompressible when the condition for values of $\text{Re}_v = 2300$ and $M_v = 0.2$ could be met. Under the circumstances where $\text{Re}_v < 2300$ and $M_v > 0.2$, the flow is still laminar and the values of β in Eq. (2.60) will still be approximately applicable [18]. In accordance with Ref. [47] (Von Karman), the ratio of the drag coefficient for compressible laminar flow $f_{v,c}$ to that for incompressible laminar flow $f_{v,i}$ at the same Reynolds number (based upon the bulk fluid properties) can be adequately correlated by the following equation:

$$\frac{f_{v,c}}{f_{v,i}} = \left(1 + \frac{\gamma_v - 1}{2} M_v^2\right)^{-1/2} \quad (\text{Eq.2.64})$$

By substituting Eq. (2.64) into Eq. (2.60), a new form of equation can be established to present the vapor frictional coefficient F_v as follows:

$$F_v = \frac{(f_v \text{Re}_v)\mu_v}{2r_{h_v}^2 A_v \rho_v \lambda} \left(1 + \frac{\gamma_v - 1}{2} M_v^2\right)^{-1/2} \quad (\text{Eq.2.65})$$

In this equation, the value of $(f_v \text{Re}_v)$ is the same as that for the incompressible laminar flow as above. For flow at large Reynolds number $\text{Re}_v > 2300$, the value of f_v and β can be calculated from the one-seventh power law of velocity profiles [18], and for a circular tube flow, the value of β is being very close to unity for this case ($\beta = 1.02$) and yields the following relationship for the drag coefficient for incompressible turbulent flow:

$$f_v = \frac{0.038}{\text{Re}_v^{0.25}} \quad (\text{Eq.2.66})$$

In that case, the frictional and dynamic coefficients for the vapor pressure for the pressure gradient of Eq. (2.58) are, respectively,

$$F_v = \frac{0.019\mu_v}{r_{h_v}^2 A_v \rho_v \lambda} \left(\frac{2r_{h_v} Q}{A_v \lambda \mu_v} \right)^{3/4} \quad (\text{Eq.2.67})$$

$$D_v = \frac{1}{A_v^2 \rho_v \lambda^2} \quad (\text{Eq.2.68})$$

Also per Von Karman [47] the drag coefficient for compressible turbulent flow is related to the drag coefficient for incompressible flow for the same Reynolds number and presented by the following equation:

$$f_{v,c} = f_{v,i} \left(1 + \frac{\gamma_v - 1}{2} M_v^2 \right)^{-3/4} \quad (\text{Eq.2.69})$$

Therefore, when the Reynolds number is greater than 2300 and for Mach number than 0.2, the vapor pressure can be calculated by Eq. (2.59) with F_v and D_v as follows:

$$F_v = \frac{0.019\mu_v}{r_{h_v}^2 A_v \rho_v \lambda} \left(\frac{2r_{h_v} Q}{A_v \lambda \mu_v} \right)^{3/4} \left(1 + \frac{\gamma_v - 1}{2} M_v^2 \right)^{-3/4} \quad (\text{Eq.2.70})$$

$$D_v = \frac{1}{A_v^2 \rho_v \lambda^2} \quad (\text{Eq.2.71})$$

In summary, the vapor pressure drop in heat pipe can be calculated by integrating the vapor pressure gradient using Eq. (2.59). The values of the frictional coefficient F_v and dynamic coefficient D_v for the pressure gradient was described and also detailed out in Table 2.5 below for different vapor flow conditions.

Table 2.5 Expression of vapor frictional coefficient F_v and dynamic coefficient D_v for circular vapor cross section

Flow conditions	F_v	D_v
$Re_v \leq 2300$ $M_v \leq 0.2$	$\frac{8\mu_v}{r_{hv}^2 A_v \rho_v \lambda}$	$\frac{1.33}{A_v^2 \rho_v \lambda^2}$
$Re_v \leq 2300$ $M_v > 0.2$	$\left(\frac{8\mu_v}{r_{hv}^2 A_v \rho_v \lambda}\right) \left(1 + \frac{\gamma_v - 1}{2} M_v^2\right)^{-1/2}$	$\frac{1.33}{A_v^2 \rho_v \lambda^2}$
$Re_v > 2300$ $M_v \leq 0.2$	$\left(\frac{0.019\mu_v}{r_{hv}^2 A_v \rho_v \lambda}\right) \left(\frac{2r_{hv} Q}{A_v \lambda \mu_v}\right)^{3/4}$	$\frac{1}{A_v^2 \rho_v \lambda^2}$
$Re_v > 2300$ $M_v > 0.2$	$\left(\frac{0.019\mu_v}{r_{hv}^2 A_v \rho_v \lambda}\right) \left(\frac{2r_{hv} Q}{A_v \lambda \mu_v}\right)^{3/4} \left(1 + \frac{\gamma_v - 1}{2} M_v^2\right)^{-3/4}$	$\frac{1}{A_v^2 \rho_v \lambda^2}$

Example 2.4 (from Peterson book) A simple horizontal copper–water heat pipe is constructed from a 1.5 cm internal diameter, 0.75 m long tube. The vapor and condenser lengths of the heat pipe are 0.25 m each. The wicking structure consists of two wraps of 100 mesh copper screen. Given that the maximum heat transport capacity of the heat pipe at 30 °C is 24.5 W, plot the vapor and liquid pressures as a function of axial position for the heat pipe. For the vapor pressure, use both the one-dimensional approximation and the two-dimensional results and compare the results.

Solution

1. *One-dimensional vapor:* The pressure gradient is given by Eq. (2.57) (Fig. 2.25):

$$\frac{dP_v}{dx} = \frac{-(f_v Re_v) \mu_v \dot{m}_v}{2A_v r_{hv}^2 \rho_v} - \beta \frac{2\dot{m}_v}{A_v^2 \rho_v} \frac{d\dot{m}_v}{dx}$$

Assume that $\beta \approx 1$ and

$\frac{d\dot{m}}{dx} = 4.04 \times 10^{-5} \text{ kg/s}$	Evaporator
$\frac{d\dot{m}}{dx} = 0$	Adiabatic
$\frac{d\dot{m}}{dx} = -4.04 \times 10^{-5} \text{ kg/s}$ Condenser	Condenser: the length of condenser and evaporator are the same as a result $L_c = L_e$
$f_v Re_v = 16$	Laminar and incompressible flow and with the assumption of uniform mass additional and rejection; the mass flow rate is $P_x(x) = \int_0^x \frac{dP_v}{dx}$

Evaporator:

$$P_x(x) = \int_0^x \left(-F_{v,1} \dot{m}_v - F_{v,2} \dot{m}_v \frac{d\dot{m}_v}{dx} \right) dx$$

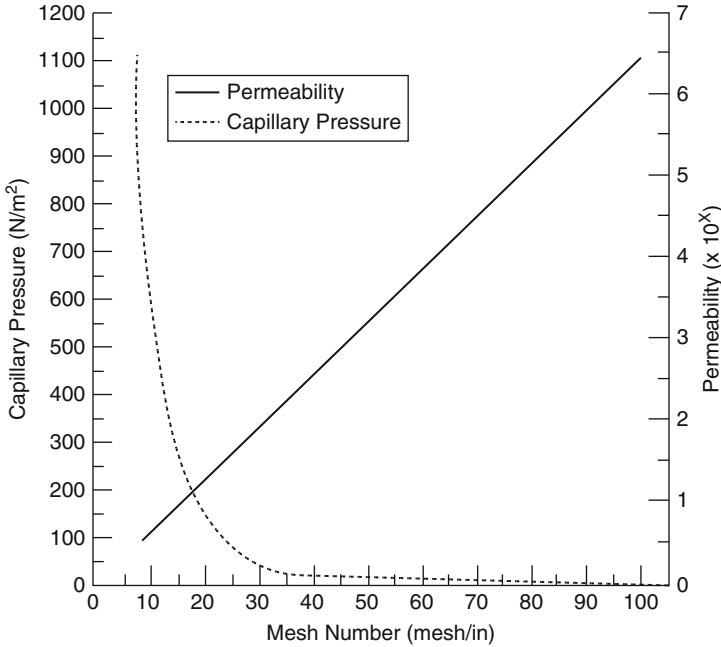


Fig. 2.25 Permeability and capillary pressure versus mesh

where

$$F_{v,1} = \frac{f_v \text{Re}_v \mu_v}{2A_v r_{h_v}^2 \rho_v} = \frac{16(9.29 \times 10^{-6})}{2(1.56 \times 10^{-4})(0.00705)^2(0.035)} = 2.739 \times 10^5$$

$$F_{v,2} = \frac{2}{A_v^2 \rho_v} = \frac{2}{(1.56 \times 10^{-4})^7(0.035)} = 2.35 \times 10^9$$

$$P_x(x) = \int_0^x -2.739 \times 10^5 (1.62 \times 10^{-4}x) - 2.35 \times 10^9 (4.04 \times 10^{-5}) \times (1.62 \times 10^{-4})$$

$$P_x(x) = \int_0^x -59.75x dx = -29.88x^2 \Big|_0^x$$

$$P(x=0) - 29.88x^2$$

Adiabatic:

with $\dot{m}_v = \text{constant}$ and $\frac{d\dot{m}_v}{dx} = 0$

$$P_v(x) = P(x=L_e) - F_{v,1} \dot{m}_v (x - L_e) = P(x=L_e) - 11.06(x - L_e)$$

Condenser:

$$P_v(x) = P_v(x = L_e + L_a) + 29.88(x^2 - (L_e + L_a)^2) - 44.98(x - L_e - L_a)$$

2. Two-dimensional vapor

Evaporator (Eq. 3.12 of Peterson book) [17]:

$$P(x) \simeq P(x = 0) - 4\mu \frac{\bar{v}L_e}{r_o^2} \left[1 + 0.61\text{Re}_r + \frac{0.61\text{Re}_r}{3.6 + \text{Re}_r} \right] \frac{x^2}{L_e^2}$$

\bar{v} = average velocity

$$\text{Re}_r = \frac{\rho_v u_v r_o}{\mu_v} = \frac{1}{2\pi\mu_v} \frac{d\dot{m}}{dx}$$

where

Re_r = radial Reynolds number,

u_v = radial component of velocity for vapor (m/s),

r_o = outer radial,

μ_v = vapor absolute viscosity (N s/m²), and

\dot{m}_v = vapor mass flow rate (kg/s).

From reference Peterson [17], we have

$$\bar{v} = \frac{\dot{m}}{\rho_v A_v} = \frac{Q}{\lambda \rho_v A_v} = \frac{24.5}{(2425 \times 10^3)(0.035)(1.56 \times 10^{-4})} = 1.85 \text{ m/s}$$

and Re_r is calculated from the overall mass flow rate divided by the length of the evaporator wall area (assuming that mass addition is uniform throughout the evaporator):

$$\frac{d\dot{m}}{dx} = \frac{\dot{m}}{L_e} = \frac{Q}{\lambda L_e} = \frac{24.5w}{(2425 \times 10^3)(0.25)} = 4.04 \times 10^{-5} \text{ kg/s m}$$

and

$$\text{Re}_r = \frac{1}{2\pi(9.29 \times 10^{-6} \frac{\text{Ns}}{r^2})} \times 4.04 \times 10^{-5} \text{ kg/s m} = 0.692$$

Thus,

$$P(x) = P(x = 0) - 4(9.29 \times 10^{-6}) \frac{1.85(0.25)}{(0.00705)^2} \\ \times \left[1 + 0.61(0.692) + \frac{0.61(0.692)}{3.6 + 0.692} \right] \frac{x^2}{(0.25)^2}$$

or

$$P(x) = P(x=0) - 8.4x^2(\text{Pa}) \quad \text{and} \quad \frac{dP}{dx} = -16.8x$$

Adiabatic section (Eq. 3.13 of Peterson's book) [17]:

$$P(x) \simeq P(x=0) - \frac{8\mu\bar{v}x}{r_o^2} \left[1 + \frac{0.106\text{Re}_r}{18 + 5\text{Re}_r} \frac{1 - e^{(-30x/\text{Re}_a r_o)}}{x/\text{Re}_a r_o} \right]$$

where

$$\text{Re}_a = \frac{4\dot{m}}{\pi q_v \mu_v} = 97.9$$

and $x = 0$ is the entrance of the adiabatic section:

$$\begin{aligned} P(x) &\simeq P(x=0) - \frac{8(9.29 \times 10^{-6})(1.85)x}{(0.00705)^2} \\ &\quad \times \left[1 + \frac{0.106(0.692)}{18 + 5(0.692)} \frac{1 - e^{1-30x/(97.9)(0.00705)}}{x/(97.9)(0.00705)} \right] \\ P(x) &\simeq P(x=0) - 2.76x \left[1 + 0.00236 \frac{1 - e^{(-43.4x)}}{x} \right] \end{aligned}$$

or

$$P(x) \simeq P(x=0) - 2.76x - 0.0065 \left[1 - e^{(-43.4x)} \right]$$

Condenser section (Eq. 3.14 of Peterson's book) [17]:

$$P(x) = P(x=L_c) + \frac{4\mu\bar{v}L_c}{r_o^2} \left[1 - \text{Re}_{\text{capillary}} \left(\frac{7}{9} - \frac{8a}{27} + \frac{23a^2}{405} \right) \right] \times \left(1 - \frac{x}{L_c} \right)^2$$

The value of a is a velocity profile correction factor that compensates for the deviation from the *Poiseuille* flow [48].

In the evaporator section, the velocity profile correction factor a takes the form

$$a = 0.68 \left\{ \left(5 + \frac{18}{\text{Re}_r} \right) - \left[\left(5 + \frac{18}{\text{Re}_r} \right) - 8.8 \right]^{1/2} \right\}$$

and varies from $a=0$ for the Poiseuille velocity profile where the radial Reynolds number approaches zero to $a=0.665$ for radial Reynolds numbers approaching

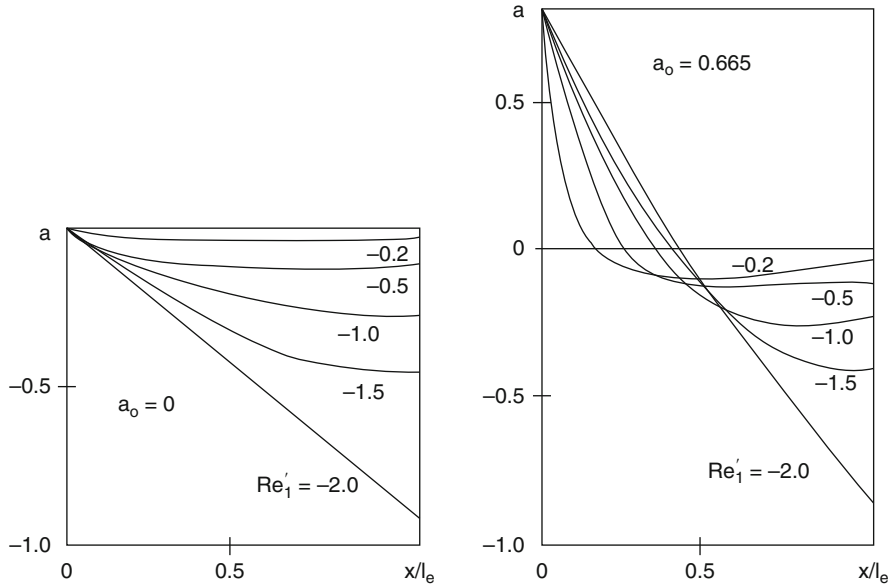


Fig. 2.26 Correction to the velocity profile along the length of the condenser [48]

infinity [48]. In the adiabatic region, this correction factor is dependent upon the velocity profile at the entrance to the adiabatic region [18].

In case of the above example (Example 2.4), the value of $a = 0.142$ (relatively low value) can be determined from Fig. 2.26, in the evaporator and $L_a = 0.25$ m, the vapor flow may be assumed to return a Poiseuille velocity profile such that $a_0 = 0$. Thus, with $a_0 = 0$, $Re_r = -0.692$:

$$0 > a > -0.15$$

from Fig. 2.26:

$$\begin{aligned}
 P(x) &= P(x = L_c) + \frac{4(9.29 \times 10^{-6})(1.85)(0.25)}{(0.00705)^2} \\
 &\times \left[1 - (-0.692) \left(\frac{7}{9} - \frac{89}{27} + \frac{23a^2}{405} \right) \right] \left(1 - \frac{x}{L_c} \right)^2 \\
 &= P(x = L_c) + 0.346 \left[1 + 0.692 \left(\frac{7}{9} - \frac{8a}{27} \right) \right] \left(1 - \frac{x}{L_c} \right)^2
 \end{aligned}$$

Note:

Differentiation of this term requires the knowledge of the function $a(x)$.

3. Liquid Channel

The pressure gradient is given by Eq. (2.57) with the substitution $\dot{m}\lambda = 1$, and then we have

$$\begin{aligned}\frac{dP_1}{dx} &= \frac{\mu_1 \dot{m}_1}{KA_w \rho_1} = \frac{(769 \times 10^{-6}) \dot{m}}{1.94 \times 10^{-10} (2.057 \times 10^{-5}) (995.3)} \\ &= 1.94 \times 10^8 \dot{m}_1\end{aligned}$$

Thus, by substituting and integration, we have

$$\begin{aligned}P_1(x) &= P_1(x=0) + 1.57 \times 10^4 x^2 \quad (\text{Evaporator}) \\ P_1(x) &= P_1(x=L_e) + 7.84 \times 10^3 (x-L_e) \quad (\text{Adiabatic}) \\ P_1(x) &= P_1(x=L_a) - 1.571 \times 10^4 (x^2 - (L_e + L_a)^2) \\ &\quad + 2.37 \times 10^4 (x - L_e - L_a) \quad (\text{Condenser})\end{aligned}$$

2.13.3 Capillary or Wick Limitation Analysis on Heat Transport

We did talk about liquid and vapor pressure drop in Sects. 2.13.1 and 2.13.2, respectively, as well as describe the minimum capillary pressure balance in Sect. 2.13 which is well defined by Eq. (2.37). The capillary pressure along the entire length of the heat pipe is required to solve the following equation:

$$P_c(x) = \Delta P_1(x_{\min} - x) + \Delta P_v(x - x_{\min}) \quad (\text{Eq.2.72})$$

Substituting for both terms of $\Delta P_1(x_{\min} - x)$ and $\Delta P_v(x - x_{\min})$ from Eqs. (2.41) and (2.55), respectively, into Eq. (2.72), we have

$$P_c(x) = \int_{x_{\min}}^x \left(\frac{dP_v}{dx} - \frac{dP_1}{dx} \right) dx \quad (\text{Eq.2.73})$$

If exists a maximum possible capillary pressure for any liquid–wick combination (see Sect. 2.4 and Eq. (2.7)) and in addition if a heat pipe is operating in a gravitational field along with circumferential condition of liquid within the liquid is possible, then maximum effective capillary pressure $P_{\text{capillary,max, evaporator}}$ available for axial transport of fluid will be smaller than the maximum capillary pressure calculated by Eq. (2.7). This drop in pressure is due to the effect of the gravitational force perpendicular to the direction to the heat pipe axis given:

$$P_{\text{capillary,max, evaporator}} = \frac{2\sigma}{r_{\text{capillary}}} - \Delta P_{\perp} \quad (\text{Eq.2.74})$$

For a heat pipe with inclination ψ in respect to the horizontal direction and with diameter d , the maximum effective capillary pressure $P_{\text{capillary}_{\text{max, evaporator}}}$ would be calculated by the following equation:

$$P_{\text{capillary}_{\text{max, evaporator}}} = \frac{2\sigma}{r_{\text{capillary}}} - \rho_l g d_v \cos \psi \quad (\text{Eq.2.75})$$

As it can be seen from both Eqs. (2.74) and (2.75) for a given heat pipe operating at a known temperature and orientation, the maximum effective capillary pressure is essentially a constant. However, the integral of Eq. (2.73), in general, increases with the heat load since the fluid circulation increases with the heat load [18].

In integral of Eq. (2.73) at x equal to maximum effective capillary pressure of Eq. (2.74), x_{max} , the wick will begin to dryout.

The general equation for the capillary or wick limitation on head load of heat pipe will be the result when Eqs. (2.73) and (2.74) are combined as follows:

$$\frac{2\sigma}{r_{\text{capillary}}} - \Delta P_{\perp} = \int_{x_{\text{min}}}^{x_{\text{max}}} \left(\frac{dP_v}{dx} - \frac{dP_l}{dx} \right) dx \quad (\text{Eq.2.76})$$

The steps for calculating specific solution for this limit for conventional heat pipe are shown below per Chi [18] reference. For a conventional heat pipe, see Fig. 2.27.

A conventional heat pipe is considered as a fixed heat pipe rather than a variable one; generally speaking, it is straight with uniform cross section, with three sections consisting of the evaporator, adiabatic, and condenser, in which the evaporator and the condenser are located in each opposing end, while the adiabatic section is in the middle and located between the other two sections. When this device operates under normal heat pipe mode, then the assumption is that the evaporator is on a

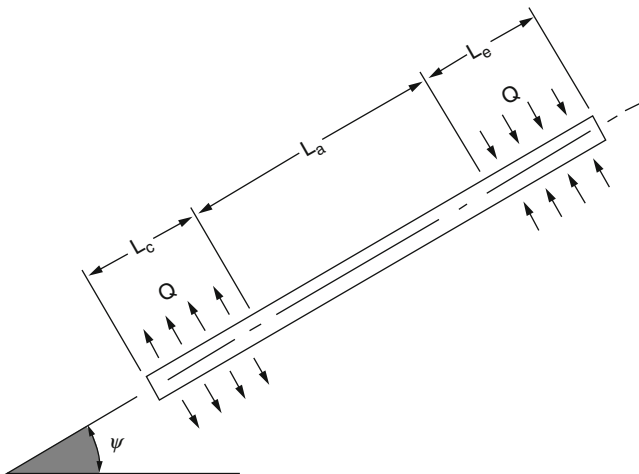


Fig. 2.27 Sketch of a conventional heat pipe operating in a heat pipe mode

level with or above the condenser as shown in Fig. 2.26. Under these circumstances, it can be easily seen, by following the path of circulation of the working fluid, that the maximum vapor pressure occurs at the end of the evaporator and the minimum vapor pressure occurs at the end of the condenser. Likewise, the maximum liquid pressure occurs at the end of the condenser and the minimum liquid pressure occurs at the end of the condenser. This results that for a conventional heat pipe which is operating in its normal cycle mode, the minimum capillary pressure occurs at the end of the condenser (i.e., at $x_{\min} = x = 0$) and the maximum capillary pressure occurs at the end of the evaporator (i.e., at $x_{\max} = x = L_{\text{total}}$ total length of heat pipe), and Eq. (2.74) can be reduced to

$$\frac{2\sigma}{r_{\text{capillary}}} - \Delta P_{\perp} = \int_0^{L_{\text{total}}} \left(\frac{dP_v}{dx} - \frac{dP_l}{dx} \right) dx \quad (\text{Eq.2.77})$$

where again L_{total} represents the total length of heat pipe under normal operating heat pipe mode.

Using Eqs. (2.46) and (2.59) and substituting for dP_v/dx and dP_l/dx respectively, into Eq. (2.77), we obtain the following result:

$$\frac{2\sigma}{r_{\text{capillary}}} - \Delta P_{\perp} = \int_0^{L_{\text{total}}} \left(F_v Q - D_v \frac{dQ^2}{dx} + F_l Q + \rho_l g \sin \psi \right) dx \quad (\text{Eq.2.78})$$

where

ΔP_{\perp} = hydrostatic pressure in direction perpendicular to pipe axis,

L_t = total length of heat pipe,

ψ = heat pipe inclination measured from horizontal position,

Q = heat-flow rate,

F_l = frictional coefficient for liquid flow,

D_v = dynamic pressure coefficient,

F_v = frictional coefficient for vapor flow,

g = gravitational acceleration,

ρ_l = liquid density,

σ = surface tension coefficient, and

$r_{\text{capillary}}$ = effective capillary radius.

What we are using are frictional terms in gradient in both Eqs. (2.44) and (2.58) with negative in the direction of fluid flow. As a result, the vapor is flowing in opposite direction for the integration in Eq. (2.79) from 0 to L_{total} . Therefore, the frictional terms $F_v Q$ and $F_l Q$ are both positive in Eq. (2.80). Additionally substituting for D_v from Eq. (2.70) and knowing that Q is equal to zero at both ends of the heat pipe, we have

$$\int_0^{L_{\text{total}}} D_v \frac{dQ^2}{dx} = \int_0^{L_{\text{total}}} \frac{2\beta Q}{A_v^2 \rho_v \lambda^2} dQ \frac{\beta}{A_v^2 \rho_v \lambda^2} Q^2 \Big|_0^{L_t} = 0 \quad (\text{Eq.2.79})$$

Hence, Eq. (2.79) can be written as

$$\frac{2\sigma}{r_{\text{capillary}}} - \Delta P_{\perp} - \rho_1 g L_{\text{total}} \sin \psi = \int_0^{L_{\text{total}}} (F_1 + F_v) dx \quad (\text{Eq.2.80})$$

This equation can generally be used to analyze the capillary limitation for a conventional heat pipe as was described above operating under heat pipe mode since the frictional coefficient for the liquid and vapor flows, F_1 and F_v have been derived in Sects. 2.13.1 and 2.13.2, respectively, as well as supporting Tables 2.4 and 2.5. In particular, we are interested in a case where the vapor flow is laminar and incompressible with Reynolds number of Re_v less than 2300 and Mach number of M_v less than 0.2 as well. Under this circumstances, the value for F_1 and F_v are independent of heat transfer rates, and they can be calculated by Eqs. (2.47) and (2.60) accordingly. Consequently, expression for capillary limitation on the heat transport factor $(QL)_{\text{capillary}_{\text{max}}}$ can be obtained as follows:

$$(QL)_{\text{capillary}_{\text{max}}} = \int_0^{L_{\text{total}}} Qx = \frac{\frac{2\sigma}{r_c} - \Delta P_{\perp} - \rho_1 g L_{\text{total}} \sin \psi}{F_1 + F_v} \quad (\text{Eq.2.81})$$

where again both Eqs. (2.47) and (2.60) can be reminded as follows:

$$F_1 = \frac{\mu_1}{KA_w \lambda \rho_1} \quad (\text{Eq.2.46})$$

$$F_v = \frac{(f_v Re_v) \mu_v}{2r_{\text{hv}}^2 A_v \rho_v \lambda} \quad (\text{Eq.2.57})$$

This follows with the fact that capillary limitation on the heat transport rate, namely, $Q_{\text{capillary}_{\text{max}}}$, can be derived from the heat transport factor $(QL)_{\text{capillary}_{\text{max}}}$ if we specify the heat flux distribution along the heat pipe. For example, if the heat pipe in Fig. 2.27 has uniform heat flux distributions along its evaporator and condenser section, the axial heat flux distribution will be as follows [17]:

$$\begin{aligned} \text{At } 0 \leq x < L_c & \quad Q = \frac{x}{L_c} Q_{\text{capillary}_{\text{max}}} \\ \text{At } L_c \leq x < (L_c + L_a) & \quad Q = Q_{\text{capillary}_{\text{max}}} \\ \text{At } (L_c + L_a) \leq x < L_{\text{total}} & \quad Q = Q_{\text{capillary}_{\text{max}}} \end{aligned}$$

As result $Q_{\text{capillary}_{\text{max}}}$ and $(QL)_{\text{capillary}_{\text{max}}}$ will be associated by the equation

$$(QL)_{\text{capillary}_{\text{max}}} = \int_0^{L_t} Q dx = (0.5L_c + L_a + 0.5L_e) Q_{\text{capillary}_{\text{max}}} \quad (\text{Eq.2.82})$$

And finally maximum capillary or wicking limitation for a conventional heat pipe operating under normal heat pipe mode is given by

$$Q_{\text{capillary}_{\text{max}}} = \frac{(QL)_{\text{capillary}_{\text{max}}}}{(0.5L_c + L_a + 0.5L_e)} \quad (\text{Eq.2.83})$$

Chi [18] has done an excellent job to analyze this limitation in his book that was repeated here for those readers that do not have access of his book. He also has elaborated on the fact that if the vapor flow is turbulent and its compressibility effect may not be neglected, then integration of Eq. (2.77) becomes such a tedious exercise that use of a computational analysis via computer is recommended. However, most heat pipes have been manufactured in a way to have vapor flows within the range of incompressible laminar flow and to have a frictional coefficient for vapor flow F_v that is much smaller than that for liquid flow F_l . For such heat pipes, Eq. (2.82) is generally used to evaluate their capillary limitation. Some of his examples using this equation have been shown here as well.

Example 2.5 (from Chi's book) [18] A 20-in. (0.508 m) ammonia heat pipe with rectangular axial grooves has the following characteristics:

Aluminum tube O.D., $d_0 = 0.5 \text{ in.} = 4.167 \times 10^{-2} \text{ ft}$ (0.00127 m)

Groove depth, $\delta = 0.03 \text{ in.} = 2.5 \times 10^{-3} \text{ ft}$ ($7.62 \times 10^{-4} \text{ m}$)

Groove width, $w = 0.018 \text{ in.} = 1.5 \times 10^{-3} \text{ ft}$ ($4.57 \times 10^{-4} \text{ m}$)

Number of grooves, $n = 36$

Vapor core diameter, $d_v = 0.36 \times 10^{-2} \text{ ft}$ ($9.14 \times 10^{-3} \text{ m}$)

Heat pipe inclination, $\psi = 0 \text{ rad}$

Condenser length, $L_c = 5 \text{ in.}$ (0.127 m)

Adiabatic length, $L_a = 10 \text{ in.}$ (0.254 m)

Evaporator length, $L_e = 5 \text{ in.}$ (0.127 m)

Determine its capillary limitation on the heat transport factor $(QL)_{\text{capillary}_{\text{max}}}$ and on the heat transport rate $Q_{\text{capillary}_{\text{max}}}$. Assume a uniform heat flux distribution along the evaporator as well as the condenser. Let the average temperature of the working fluid be 80°F (300 K).

Solution Properties of Ammonia at 80°F (300 K) (see Appendix C):

Liquid density, $\rho_l = 37.5 \text{ lbm/ft}^3 = 1.165 \text{ slugs/ft}^3$ (601 kg/m^3).

Liquid viscosity, $\mu_l = 0.516 \text{ lbm/ft h} = 4.451 \times 10^{-6} \text{ slug/ft s}$ ($2.13 \times 10^{-4} \text{ kg/ms}$).

Liquid surface tension, $\sigma = 1.35 \times 10^{-3} \text{ lbf/ft}$ ($1.97 \times 10^{-2} \text{ N/m}$).

Latent heat of vaporization, $\lambda = 499 \text{ Btu/lbm} = 1.607 \times 10^4 \text{ Btu/slug}$ ($1.16 \times 10^6 \text{ J/kg}$).

Vapor density, $\rho_v = 0.512 \text{ lbm/ft}^3 = 1.59 \times 10^{-2} \text{ slug/ft}^3$ (8.2 kg/m^3).

Vapor viscosity, $\mu_v = 2.67 \times 10^{-2} \text{ lbm/ft h} = 2.3 \times 10^{-7} \text{ slug/ft s}$ ($1.104 \times 10^{-5} \text{ kg/ms}$).

Maximum available pumping pressure, $P_{P_{\max}}$.

Capillary radius (Table 2.1), $r_c = w = 1.5 \times 10^{-3}$ ft (4.572×10^{-4} m).

Maximum capillary pressure (Eq. 2.7), $P_{\text{Capillary}_{\max}} = P_{c_{\max}} = 2\sigma/r_c = 1.8$ lbf/ft² (86.2 N/m²).

Normal hydrostatic pressure (note: for axial grooves, there is no circumferential communication of liquid), $\Delta P_{\perp} = 0$.

Axial hydrostatic pressure, $\rho_1 g L_t \sin \psi = 0$.

Maximum effective pumping pressure, $P_{P_{\max}} = P_{c_{\max}} - \Delta P_{\perp} - \rho_1 g L_t \sin \psi = 1.8$ lbf/ft² (86.2 N/m²).

Liquid frictional coefficient, F_1 :

Mean radius of liquid-flow passage, $r_m = d_v + \delta/2 = 0.195$ in. = 1.625×10^{-2} ft (4.95×10^{-3} m).

Wick cross-sectional area, $A_w = 2\pi r_m \delta = 2.55 \times 10^{-4}$ ft² (2.37×10^{-5} m²).

Wick porosity, $\varepsilon = nw/2\pi r_m = 0.529$.

Groove aspect ratio, $\alpha = w/\delta = 0.6$.

Groove hydraulic radius (Table 2.4), $r_{h_1} = 2w\delta/(w + 2\delta) = 1.154 \times 10^{-3}$ ft (3.52×10^{-4} m).

Coefficient of drag (Fig. 2.22), $f_1 \text{Re}_1 = 15$.

Permeability (Table 2.4), $K = 2\varepsilon r_{h_1}^2 / f_1 \text{Re}_1 = 9.393 \times 10^{-8}$ ft (8.73×10^{-9} m²).

Liquid frictional coefficient (Eq. 2.44), $F_1 = 9.924$ (lbf/ft²) (Btu ft/s) [1.479(N/m²)/W m].

Vapor frictional coefficient, F_v :

Hydraulic radius, $r_{h_v} = d_v/2 = 1.5 \times 10^{-2}$ ft (4.57×10^{-3} m).

Vapor flow area, $A_v = \pi d_v^2/4 = 7.068 \times 10^{-4}$ ft² (6.57×10^{-5} m²).

Coefficient of drag, $f_v \text{Re}_v = 16$.

Vapor frictional coefficient (Eq. 2.59), $F_v = 0.045$ (lb/ft²) (Btu ft/s) [6.71×10^{-3} (N/m²)/W m].

Capillary limitation, $(QL)_{\text{capillary}_{\max}}$ and $Q_{\text{capillary}_{\max}}$:

Maximum heat transport factor (Eq. 2.81),

$$\begin{aligned} (QL)_{\text{capillary}_{\max}} &= \frac{1.8}{9.924 + 0.045} \text{Btu ft/s} \\ &= 0.181 \text{Btu ft/s} \\ &= 650 \text{Btu ft/h} \\ &= 2285 \text{W in. (58 W m)} \end{aligned}$$

Maximum heat transport (Eq. 2.84),

$$\begin{aligned} Q_{\text{capillary}_{\text{max}}} &= \frac{2285}{(0.5 \times 5) + 10 + (0.5 \times 5)} \text{W} \\ &= 152 \text{ W} \\ &= 520 \text{ Btu/h (152 W)} \end{aligned}$$

Checking the results:

Maximum Reynolds number for vapor flow (Eq. 2.59),

$$\text{Re}_v = \frac{2r_{\text{hv}} Q_{\text{capillary}_{\text{max}}}}{A_v \mu_v \lambda} = 1657 (\text{i.e., } < 2300)$$

Maximum Mach number (Eq. 2.62),

$$M_v = \frac{Q_{\text{capillary}_{\text{max}}}}{A_v \rho_v \lambda \sqrt{\gamma_v R_v T_v}} = 5.5 \times 10^{-4} (\text{i.e., } < 0.2)$$

Vapor to liquid frictional ratio, $\frac{F_v}{F_l} = 0.45\%$.

Per Chi [18] and his example here, values for the capillary limitations on heat transport factor and heat transport rate, in several different units, have been calculated above. In particular, $(QL)_{\text{capillary}_{\text{max}}}$ and $Q_{\text{capillary}_{\text{max}}}$ in units of W in. and Btu/h, respectively, are the most common forms found in the heat pipe literature. Particularly in NH_3 heat pipe $(QL)_{\text{capillary}_{\text{max}}}$ was found to be equal to 2285 W in. (58 W m) and $Q_{\text{capillary}_{\text{max}}}$ was found to be equal to 520 Btu/h (152 W). The maximum vapor flow Reynolds number Re_v and Mach number M_v were found to be 1657 and 5.5×10^{-4} , respectively; hence, the flow can be considered laminar and incompressible. In addition, it was found that the frictional ratio for vapor-to-liquid flow was only 0.45%. Such low values of M_v and F_v/F_l are usually the case for cryogenic (very low temperature) and moderate-temperature heat pipes, when the vapor pressure is high and the hydraulic radius for vapor flow is much larger than that for liquid flow. For the NH_3 heat pipe under consideration, the vapor pressure is at 153 psi ($1.055 \times 10^6 \text{ N/m}^2$) and the ratio of r_{hv} and r_{hl} is equal to 13.

2.13.4 Characteristic of Wick

Heat pipes are well-established two-phase devices used in the electronics cooling industry to transport heat from the point it is generated to the place where it is extracted from the system. Three wick structures are most commonly used to

provide the capillary path for the liquid return to evaporation section; these are sintered powder, screen mesh, and grooved pipes. Although the sintered heat pipe is the most common in the commodity product market including laptop computers, servers, and desktop products, the grooved heat pipe is used primarily in space applications. The screen mesh heat pipe has, to date, not achieved the popularity of the other designs.

Screen mesh, one of the oldest wick structures used for heat pipes, has been used since 1964 when Cotter and Grover [49] first published articles about heat pipes as they are known today. However, with today's requirements of higher-power handling and reduced space available, mesh heat pipes are becoming a more attractive option for certain demanding military and medical/analytical applications.

Heat pipe inner walls can be lined with a variety of wick structures. The four most common wicks are:

- (a) Groove
- (b) Wire mesh
- (c) Sintered powder metal
- (d) Fiber/spring

The wick structure provides a path for liquid to travel from the condenser to the evaporator using capillary action. Wick structures have performance advantages and disadvantages depending on the desired characteristics of the heat sink design. Some structures have low capillary limits, making them unsuitable for applications where they must work without gravity assist.

A number of processes that are vital and important to the transport of heat through a heat pipe take place in the wick structure. The heat pipe working fluid evaporates from and condenses on the inner wick surface. Condensate vapors in form of liquid return to the evaporator section through the wick as well.

Another process that takes place is when capillary pressure necessary to sustain circulation of the heat pipe fluid is generated at the inner wick surface. The surface tension barrier that prevents liquid in the wick from being entrained by adjacent high-velocity vapor also develops at the inner wick surface [22]. Characterization of the liquid flow channel relatively is defined by coarse pore structure in order to minimize resistance to liquid flow. On the other hand, relatively fine pores are desired to maximize the capillary pressure that balances the liquid–vapor pressure difference throughout the heat pipe. A relative tick wick structure is also desirable to minimize the axial resistance to liquid flow, whereas resistance to heat flow across the wick increases with thickness [22]. Figure 2.28 is a depiction of the basic types of wick that are used in a heat pipe for its normal operations.

Generally speaking, a design requirement of a heat pipe for its particular application use is driven by the factor for selection of a particular type of wick. The simplest wick structure that is suitable to a particular design situation is most preferable. Under certain design where the porous wick structure is used, the wick may be formed from a variety of small elements, including screens, particles, and fibers. The wick structure may also be formed from grooves cut into the inner heat pipe wall. A variant on the grooved wick is a roughened wall or a geometric pattern knurled or engraved in the wall [22] (see Fig. 2.29).

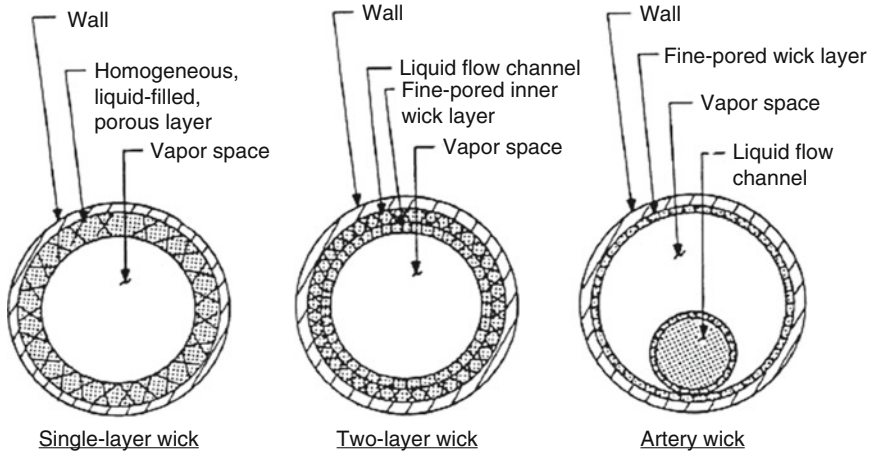
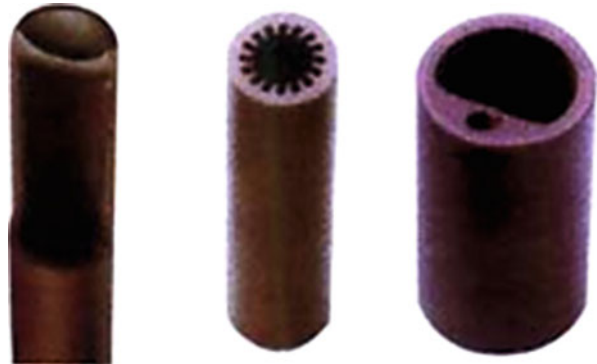


Fig. 2.28 Basic wick type for heat pipes applications [22]

Fig. 2.29 A variant grooved wick



A slotted sheet or layers of screen may also be used to form multiple liquid flow channels without the necessity of cutting groove in the heat pipe wall (see Fig. 2.30).

2.13.5 Single-Layer Wick

The single-layer wick shown in Fig. 2.28 is of simple wick construction, consisting of a relatively homogeneous assemblage of elements such as screens, fibers, or particles. The heat transport capability of a heat pipe with a single-layer wick is generally limited by the need to select a single wick pore size that can accommodate both liquid flow channel and capillary pressure requirements. The conflicting

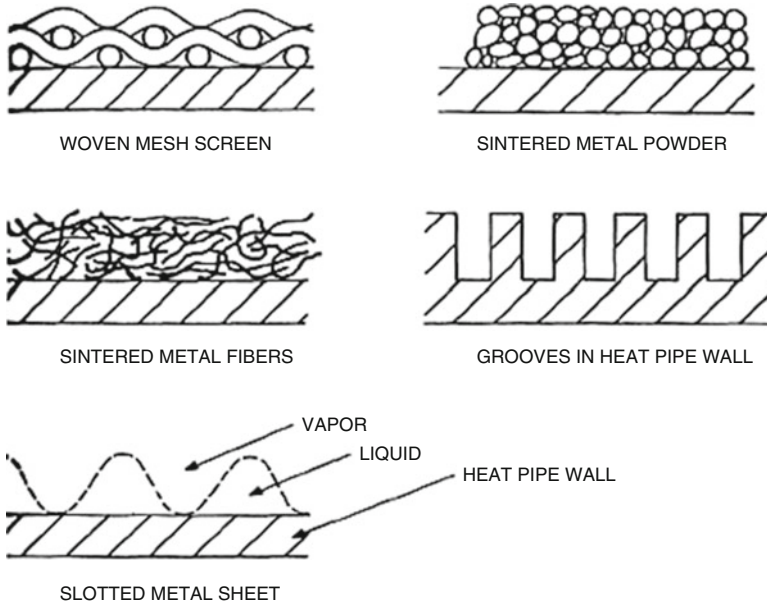


Fig. 2.30 Heat pipe capillary wick structure [22]

requirements of large pore size to minimize frictional flow resistance and small pore size to maximize capillary pressure capability may be difficult to reconcile with a single-layer, homogeneous wick structure. Consequently, the single-layer wick heat pipe may be unsuitable for an application involving one of or more of the following conditions [22]:

1. A relatively small liquid heat pipe transport parameter
2. A high heat transport rate
3. A relatively long heat pipe length

2.13.6 Two-Layer Wick

If a distinct function of liquid flow path and capillary pressure generation are assigned to separate wick layers as shown in Fig. 2.28, then a two-layer or composite wick structure can be employed. In this case, the flow channel can be characterized by coarse pores to minimize frictional resistance to flow of the heat pipe liquid. This can be done without any concern for the effect of the pores on capillary pressure capability. A separate wick layer adjacent to the vapor flow passage provides the requisite fine pore structure needed to develop adequate capillary pressure. Naturally a two-layer wick within a heat pipe has substantially greater heat transport capability than a single-layer wick, since the pore sizes of the liquid flow channel and capillary pumping layer are established independently of

each other. In fact, the internal pore structure in the liquid flow channel of two-layer wick can be completely eliminated to produce a completely open annular channel of minimum frictional resistance. Usage of annular open liquid flow channel generally permits high heat transport rates with a relatively thin wick. For more details, refer to Silverstein [22].

2.13.7 Artery Wick

A significant limitation on the amount of heat that a heat pipe can transfer in a given time is its power capability and that is the amount of power that can be accommodated at the heat transfer surface where the capillary action is moving liquid to or from the surface while heat transfer is taking place. One method of overcoming this limitation is the use of internal tunnel arteries within a sintered wick structure with high thermal conductivity. Such a structure is described in US Pat. No. 4,196,504 by George Y. Eastman that is introduced using a method of constructing such tunnels. The conflicting requirements of a relatively thick wick to minimize frictional resistance in the liquid flow direction and a relatively thin wick to minimize thermal resistance across the wick thickness can be reconciled through use of an artery wick. With an artery wick, the liquid flow channel is displaced from its usual position next to the heat pipe wall, so that the heat transferred into and out of the heat pipe is not required to traverse the thickness of the liquid flow passage. The thermal resistance to heat flow is then limited to a wick layer of minimal thickness along the wall in which capillary pressure is generated (i.e., the capillary pumping layer) [22]. The artery may be formed as an integral part of the wall capillary pumping layer. It may be in contact with the capillary pumping layer, as shown in Fig. 2.26, or connected via a stem of the same fine-pored materials. More details are provided by Silverstein [22].

In another study in modulated wick heat pipe by Hwang et al. [50], in heat pipes, modulation of evaporator wick thickness provides extra cross-sectional area for enhanced axial capillary liquid flow and extra evaporation surface area, with only a moderate increase in wick superheat (conduction resistance). This modulated wick (periodic stacks and grooves over a thin, uniform wick) is analyzed and optimized with a prescribed, empirical wick superheat limit. A thermal hydraulic heat pipe figure of merit is developed and scaled with the uniform wick figure of merit to evaluate and optimize its enhancement. The optimal modulated wick for the circular and flat heat pipes is found in closed-form expressions for the viscous-flow regime (low permeability), while similar results are obtained numerically for the viscous-inertial flow regime (high permeability which is also gravity sensitive). The predictions are compared with the experimental result of a prototype (low permeability, titanium/water pipe with the optimal design) heat pipe which gives a scaled merit of Fig. 2.2. Good agreement is found between the predicted and measured performance. The maximum enhancement is limited by the pipe inner

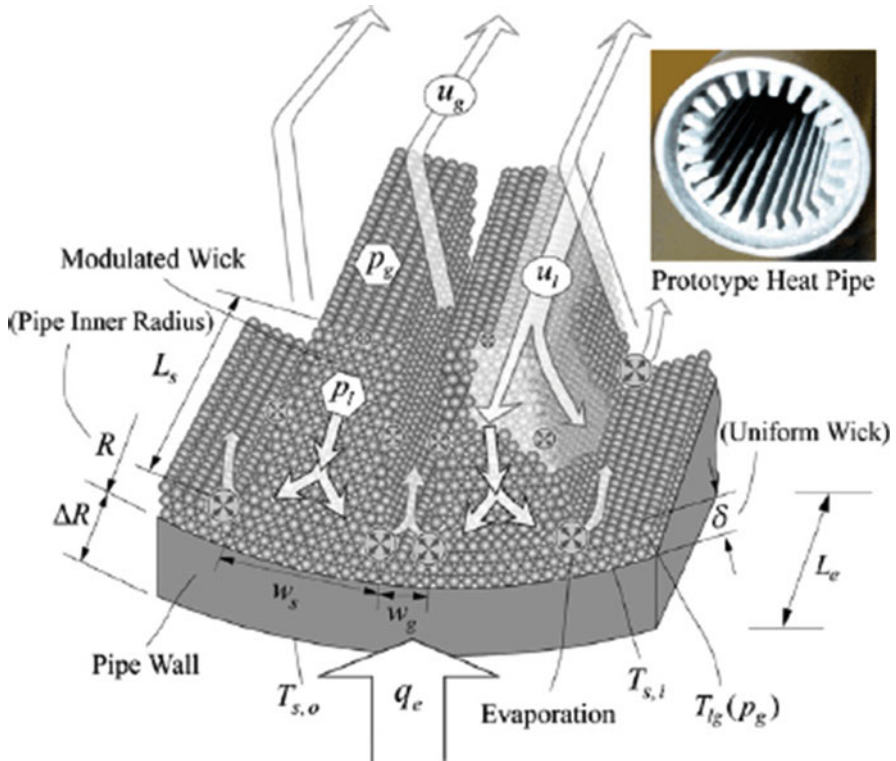


Fig. 2.31 Schematic of the modulated wick geometry in the evaporator and the liquid/vapor flow paths and evaporation surface (sites). The photograph of the prototype-modulated wick heat pipe is also shown [50]

radius (tapering of the stacks), the wick effective thermal conductivity, and the prescribed wick superheat limit.

Figure 2.31 shows the modulated wick structure with heat and liquid flow paths in the evaporator, evaporation surface (sites), and a prototype-modulated wick heat pipe. The thick wick portion of the modulated wick (stacks) decreases the liquid flow resistance, and the thin wick portion (i.e., grooves) reduces the wick superheat. This modulation of the evaporator is used to design high-performance heat pipes for microgravity applications [51, 52]. The modulated wick has capillary arteries (with an azimuthally regular interval) connected to a thin, uniform wick lining the tube, which feeds liquid to the evaporator. The liquid is vaporized on the entire surface of the modulated wick where the influx heat is exhausted and moves back to the condenser as vapor phase to make a circulation loop.

A new method for making a heat pipe wick and arteries includes drilling radial holes around the circumference of the heat pipe container at its ends and stringing monofilament polymer lines inside the container between corresponding holes. The container is rotated at a slow rate, while a slurry of nickel powder mixed into a

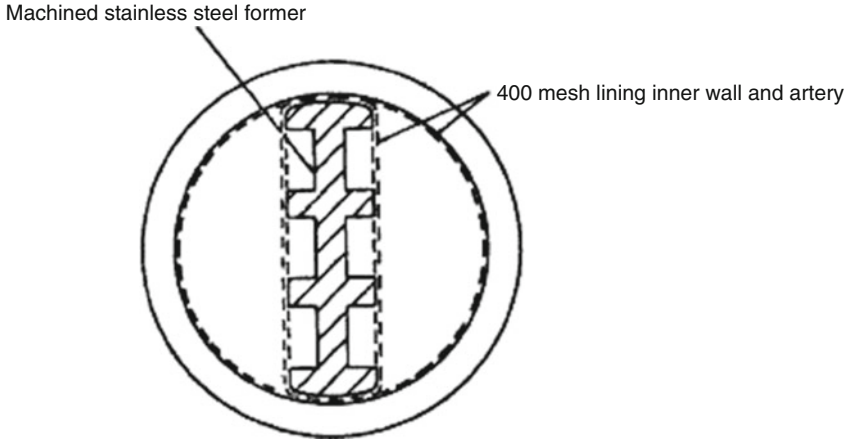


Fig. 2.32 Arterial wick developed at NEI-IRD [27]

viscous binder of water, Polyox and Methocel, is injected inside the container to cover the inside surface of the container and the lines. The rotational rate of the container is then increased to force the slurry to level out to a uniform depth set by the thickness of sleeves attached at each end of the container. Forced air is blown through the inside of the rotating pipe to dry the slurry and form a green wick. After stopping rotation of the pipe, it is then heated inside a sintering oven in a reducing atmosphere to disintegrate the binder and polymer lines and to leave a sintered metal wick having hollow longitudinal arteries. For more information, refer to method of manufacturing heat pipe wicks and arteries US Patent 4929414.

In summary, arterial wicks are necessary in high-performance heat pipes for spacecraft, where temperature gradients in the heat pipe have to be minimized to counter the adverse effect of what are generally low-thermal conductivity working fluids. An arterial wick that is developed for this purpose by NEI-IRD is shown in Fig. 2.32.

2.13.8 Monogroove Wick

Recent monogroove heat pipe developments have produced high-performance heat pipes with tested heat transport performances in excess of 14,000 W m and theoretical capacities in excess of 25,000 W m. These improvements represent an increase in heat transport capacity of better than two orders of magnitude over other currently existing heat pipes designed to operate at near-ambient temperatures.

The basic monogroove heat pipe design incorporates two relatively large, independent axial channels, a larger one for vapor and a smaller one for liquid. These provide for handling the axial transport of the fluids (liquid and vapor) independently from the radial transfer of the heat, the latter being facilitated by liquid-conducting circumferential wall grooves in the vapor channel. A small capillary slot separates (interconnects) the otherwise independent channels and

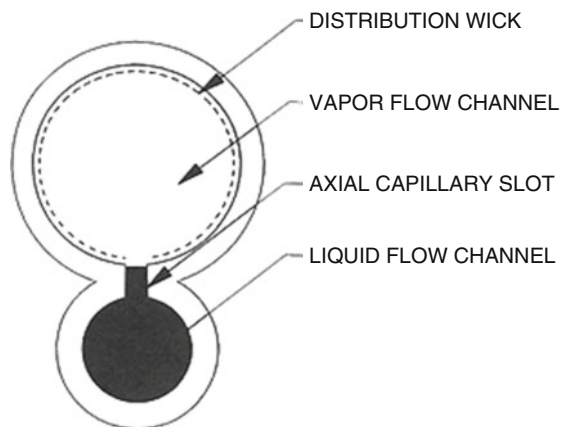
provides for the passage of fluid in between. The small slot sustains a high capillary pressure difference which, coupled with the minimized flow resistance provided by the two separate channels, results in the high axial heat transport capacity of the monogroove heat pipe design. The overall design also provides high evaporation and condensation film coefficients for the working fluid by means of the circumferential grooves in the walls of the vapor channel, while not interfering with the overall heat transport capability of the axial groove.

Such a monogroove heat pipe design has particular utility in zero gravity environments, for example, for meeting the heat rejection requirements for large space platforms or space stations, and wherein capillary forces alone entirely control the working fluids in the heat pipe operation, no moving parts or auxiliary equipment are being required.

As is recognized in this type of design, a continuous liquid flow path between the primary axial channel or groove and the circumferential wall grooves in the evaporation section of the vapor channel must be assured. This continuity must be maintained even with both groove menisci realistically depressed to reflect maximum heat flux conditions. One particular advantage of the monogroove heat pipe design is its inherent resistance to nucleate boiling within the axial liquid flow channel under high loads. In current designs, this is largely a consequence of separating the liquid channel and the heat input zone by locating the heat input zone at the top side of the vapor channel, opposite the liquid channel. Should gas bubbles form or become entrapped within the liquid channel, a particular advantage of the separate liquid and vapor channels is that such gas bubbles can readily be vented into the vapor channel through the common monogroove slot. A disadvantage is that the heat load usually has to be temporarily reduced to re-prime the liquid channel.

Figure 2.33 shows a variation on the artery wick concept in which the artery is now located completely outside the vapor space and this concept is known as the monogroove heat pipe [53, 54]. In the artery concept of Fig. 2.28, the pressure difference between the vapor and the artery liquid is balanced by capillary pressure over the entire periphery of the artery. In the monogroove heat pipe, the vapor–liquid

Fig. 2.33 The monogroove heat pipe concept [56]



pressure difference is balanced by the capillary pressure that develops in a single fine groove. Just as in the case with the artery wick, liquid is distributed over the inner circumference of the evaporator and condenser sections by a thin, fine-pored wick layer. This wick layer can be simply an array of the fine circumferential grooves [22].

The Space Constructible Radiator (SCR) Life Test heat pipe performance testing is currently conducted at NASA/Johnson Space Center as part of the Advanced Technology Development Program to show employment of such heat pipe. The SCR is a dual passage, monogroove heat pipe radiator designed and manufactured by Grumman Aerospace for NASA. The heat pipe has many aerospace applications since it can transport a large amount of heat with a compact lightweight design. As the micrometeoroid/orbital debris environment worsens, it may be advantageous to add the heat pipe radiator to the space station's thermal control system. The SCR Life Test has been operating over the last 10 years and will continue until the year 2000. The overall heat transfer coefficient has decreased from 792 W/K (1500 Btu/h-mDF) to 475 W/K (900 Btu/h-mDF) but appears to have stabilized [55].

The application of heat pipes to space systems includes the thermal control of space station and satellites and the radiator design of large space power systems. Although many advances have been made in the past few years in the development of high heat transfer performance heat pipes, the heat pipe modeling efforts are not in step with the technological requirements.

2.13.9 Variable Thickness Wick

A simpler alternative to the artery wick for reconciling the conflicting wick thickness needs of the liquid and heat transfer flow paths involves the use of a variable thickness wick (see Fig. 2.34). In this region of the evaporator where the

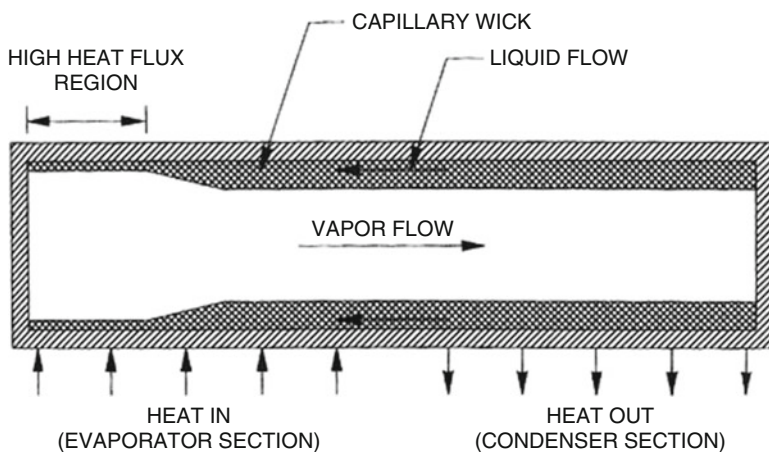


Fig. 2.34 Variable-thickness wick [22]

heat flux is highest, the liquid flow channel is made thin to minimize the temperature drop and superheat across the wick thickness. In other regions of the heat pipe, a thicker liquid flow channel is used to reduce the overall liquid pressure drop.

2.13.10 Wick Structure and How Does It Affect the Performance of the Heat Pipes

For the best performance, the application should have gravity working with the system; that is, the evaporator section (heated) should be lower, with respect to gravity, than the condenser (cooling) section. In other orientations where gravity is not aiding the condensed liquid return, the overall performance will be degraded. Performance degradation depends on a number of factors including wick structure, length, and working fluid of the heat pipe along with heat flux of the application. Careful design can minimize the performance loss and allow an accurate prediction of performance.

The orientation of a heat pipe plays an important role in its performance. The performance of a heat pipe under specific orientations is directly related to its wick structure. Wick structures with low capillary limit work best under gravity-assisted conditions, where the evaporator is located below the condenser. There are numerous published studies that explore heat pipe performance limits; however, none of them explicitly looked into the effect of orientation on heat pipe performance with different wick structures. But a study paper by Loh et al. [57] conducts a comparative study on heat pipe performance with different wick structures subjected to different orientations. The published results may serve as a reference for mechanical and electrical engineers when they try to incorporate heat pipes into their thermal solutions [57]. Also a study by Roger R. Riehl and Nadjara dos Santos [58] presents an investigation of loop heat pipes (LHPs) that operate with acetone as working fluid, for maximum operational heat loads of 80 W, where the results of tests performed in laboratory conditions are presented. Two identical LHPs were tested, where one presents the capillary evaporator primary wick with axial grooves, while the other presents the design of circumferential grooves and both evaporators present microgrooves in their internal diameter. For the same active length, there has been a gain of 20 % on the contact area when using circumferential grooves on the primary wick. When the LHP operates at its maximum operational heat load, the heat source temperatures for the evaporator with the primary wick with circumferential grooves are kept at levels 50 % lower than when using the one with axial grooves. Besides the fact that an increase on the contact area has been achieved, other factors related to the design of the capillary evaporator have also resulted in the overall improvement, which were also verified with the results obtained from a mathematical model. This represents a possibility of using the new designed LHPs operating at higher heat loads while keeping the source temperatures at lower levels.

The conventional heat pipe includes a wick structure on an internal sidewall of a tubular member. The wick structure typically includes a woven mesh or sintered powder to aid in transmission of working fluid. However, the woven mesh or the sintered powder each has advantages and drawbacks. For example, the fine and dense structure of the sintered powder wick structure provides better capillary force for reflow of the liquid-state working fluid. However, during fabrication, an axial rod has to be inserted into the tubular member to serve as a support member of the wick structure during the sintering process, so as to avoid collapse of the powdered which has not been sintered yet. Therefore, the width of the sintered powder wick structure is thicker. Consequently, the capillary thermal resistance is increased to be disadvantageous to the heat transmission. Further, requirement of the axial rod hinders the mass production of the heat pipe and causes fabrication and quality issues of the heat pipe.

A composite wick structure fabricated from a woven mesh and sintered powder attached to an internal sidewall of a tubular member does not require the axial rod; while the sintered powder coated at least on one side of the internal sidewall can enhance the heat transmission efficiency. This will take place due to better capillary force provided by the sintered powder, and the liquid-phase working fluid can reflow to the bottom of the heat pipe much better. Further, the problems of poor capillary effect of the woven mesh and the problems caused by usage of an axial rod during the process of applying sintered powder can be resolved [59].

2.13.11 Wick Structure for Low-Temperature and Higher Heat Transfer in Heat Pipes

High-temperature electronics require innovative thermal management devices. Copper water heat pipes are a well-established solution for many conventional electronics cooling applications; however, they have several problems when applied to high-temperature electronics. The high vapor pressure of the working fluid combined with the decreasing strength of an already soft material leads to excessive wall thickness, high mass, and an inability to make thermally useful structures such as planar heat pipes (vapor chambers) or heat pipes with flat input surfaces. Another significant technical challenge associated with the high-temperature water heat pipe technology is the design and manufacture of the wicks for high performances at the elevated temperatures. Water's surface tension drops off quickly as the temperature increases, placing increasing burdens on the capillary wick design. Figure 2.35 below shows the photos of various wicks, designed, manufactured, and tested in high-temperature water heat pipes. These include clockwise, axial grooves, mesh screen, sintered metal powders, sintered metal powder grooves (fine grooves), sintered slab, and sintered metal powder grooves (large grooves).



Fig. 2.35 Various wicks for high-temperature water heat pipes

Recent work [60] has shown that titanium/water and Monel/water heat pipes can overcome the disadvantages of copper/water heat pipes and produce a viable thermal management solution for high-temperature electronics. The study has shown that water remains the fluid of choice due to its favorable transport properties. Monel and titanium offer much higher strength and result in reasonable wall thickness and mass. Testing has shown compatibility at high temperature. Presented in this chapter are a survey of potential replacement fluids, results from high-temperature life testing of water in Monel and titanium envelopes, and comparison of mass and performance with competing approaches such as copper/water. A variety of wick structures have been produced in both titanium and Monel. As shown in Fig. 2.36, the simplest wick structure is a layer of screen that was spot-welded to the interior wall of the heat pipe. Sintered powder metal structures include plain circumferential wicks, axial grooves produced from sintered powder, and a so-called slab or I-beam wick which consists of a circumferential wall wick and a large central slab in the center of the heat pipe. The slab wick is a practical structure when vapor pressure and density are high. Only a small amount of area is needed for vapor flow, so the rest of the heat pipe section can be dedicated to liquid flow. Both sintered and solid axial grooves have been produced in titanium and Monel heat pipes. Sintered axial grooves both enhance fluid flow in the heat pipe condenser by reducing pressure drop and increase heat flux capability in the evaporator by serving as extended surfaces. One of the methods used to produce the solid axial grooves can result in grooves with tapered sidewalls as shown in the cross section. This can provide freeze tolerance by allowing solidified working fluid to eject itself from the grooves [60].



Fig. 2.36 Survey of wick structures produced in titanium and Monel which shows equivalence to structures currently produced in copper

Recent study by Hwang et al. [50] shows that, in heat pipes, modulation of evaporator wick thickness provides extra cross-sectional area for enhanced axial capillary liquid flow and extra evaporation surface area, with only a moderate increase in wick superheat (conduction resistance). This modulated wick (periodic stacks and grooves over a thin, uniform wick) is analyzed and optimized with a prescribed, empirical wick superheat limit. A thermal–hydraulic heat pipe figure of merit is developed and scaled with the uniform wick figure of merit to evaluate and optimize its enhancement. The optimal modulated wick for the circular and flat heat pipes is found in closed-form expressions for the viscous-flow regime (low permeability), while similar results are obtained numerically for the viscous-inertial flow regime (high permeability which is also gravity sensitive). The predictions are compared with the experimental result of a prototype (low permeability, titanium/water pipe with the optimal design) heat pipe which gives a scaled merit of Fig. 2.2. A good agreement is found between the predicted and measured performance. The maximum enhancement is limited by the pipe inner radius (tapering of the stacks), the wick effective thermal conductivity, and the prescribed wick superheat limit.

2.13.12 Effective Thermal Conductivity of Wick Structure

The most initial heat transfer mechanism for hear pipes are as follows [18]:

1. Heat conduction across the container wall and the liquid-saturated wick at the evaporator section with subsequent evaporation at the liquid–vapor interface of that section
2. Convective transport of latent heat by vapor from the evaporator to the condenser
3. Heat conduction across the liquid-saturated wick and the container wall at the condenser section with subsequent condensation at the liquid–vapor interface of that section

Values of the thermal conductivity for homogeneous materials such as solids or liquids are available from various sources (see Appendices B and C). Effective thermal conductivities for heterogeneous liquid-saturated wicks will be dealt with below in some detail.

Several heat transfer models for heterogeneous materials have been formulated by Gorring and Churchill [61], most of which can be modified for application to the liquid-saturated wicks. Figure 2.35 is the simplest configuration that consists of wick materials and liquid either in series or parallel. The exact solutions for these cases are, respectively,

$$k_e = \frac{k_1 k_w}{\varepsilon k_w + k_1(1 - \varepsilon)} \quad (\text{Eq.2.84})$$

and

$$k_e = \varepsilon k_1 + (1 - \varepsilon)k_w \quad (\text{Eq.2.85})$$

where

ε is the volume fraction of liquid, i.e., the volume of the liquid divided by the total volume of the liquid-saturated wick,

k_1 is the effective thermal conductivity of the liquid-saturated wick, and

k_w is the thermal conductivity of the wick materials.

Thermal conductivities for the liquid-saturated wick of either distributed cylinders or of spheres have been correlated, respectively, by the equations

$$k_e = \frac{k_1[(k_1 + k_w) - (1 - \varepsilon)(k_1 - k_w)]}{[(k_1 + k_w) + (1 - \varepsilon)(k_1 - k_w)]} \quad (\text{Eq.2.86})$$

and

$$k_e = \frac{k_1[(2k_1 + k_w) - 2(1 - \varepsilon)(k_1 - k_w)]}{[(2k_1 + k_w) + (1 - \varepsilon)(k_1 - k_w)]} \quad (\text{Eq.2.87})$$

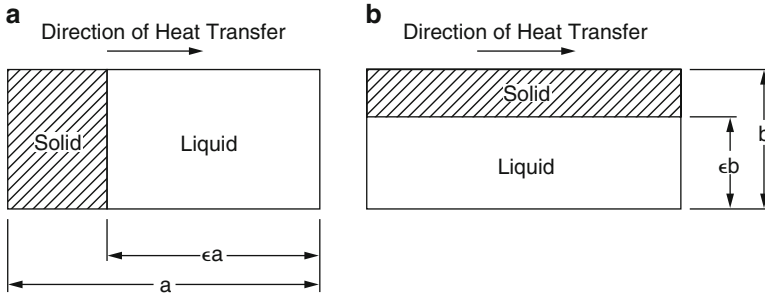


Fig. 2.37 Heat transfer model for series or parallel arrangement of liquid-saturated wick structure [18]. (a) Solid and liquid in series. (b) Solid and liquid in parallel

The statement of effective thermal conductivities can be for various common heat pipe wicks. For example, Eq. (2.85) can be used for the condenser section of the rectangular-grooved wicks, while Eq. (2.86) is for the wrapped-screen wicks, and finally Eq. (2.87) can be used for the packed-sphere wicks. Equation (2.87) can also deal with approximation effectiveness of thermal conductivity for liquid-saturated, porous-material wicks. However, this equation's accuracy decreases as the radius of contact among adjacent particles increases (see Fig. 2.37). Therefore, k_e for a sintered metal wick with a large contact radius should be calculated by the following equation [18]:

$$k_e = \frac{\pi}{8} \left(\frac{r_c}{r_s} \right)^2 k_w + \left[1 - \frac{\pi}{8} \left(\frac{r_c}{r_s} \right)^2 \right] \left[\frac{k_l k_w}{\epsilon' k_w + k_l (1 - \epsilon')} \right] \quad (\text{Eq.2.88})$$

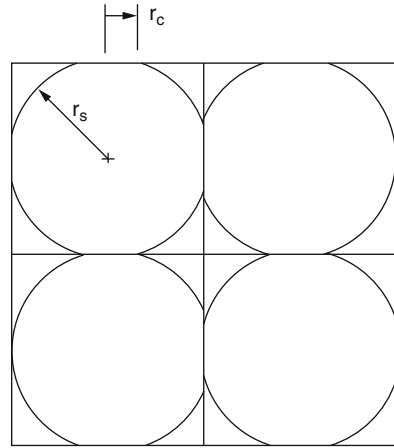
where

$$\epsilon' = \frac{\epsilon}{1 - \frac{\pi}{8} \left(\frac{r_c}{r_s} \right)^2} \quad (\text{Eq.2.89})$$

According to Chi [18], this equation has been derived by considering two parallel heat-flow paths for sintered-porous wicks. One of the paths involves homogeneous wick materials, and the other involves both liquid and wick materials in series. Additionally, in the absence of data for the contact radius, r_c (Fig. 2.38) can be estimated by means of a material balance for the idealized geometry. The result is the following equation:

$$\epsilon = \frac{\pi}{6 \left[1 - \left(\frac{r_c}{r_s} \right)^2 \right]^{2/3}} \left\{ 1 - \left(\frac{r_c}{r_s} \right)^2 \left[2 - \sqrt{1 - \left(\frac{r_c}{r_s} \right)^2} \right] \right\} \quad (\text{Eq.2.90})$$

Fig. 2.38 Heat transfer model for cubic array of truncated sphere [18]



r_s = Radius of Spherical Particles
 r_c = Contact Radius

It should be noted that at the condenser section, the effective conductivity for rectangular-grooved wicks can be calculated by considering the groove fins and the liquid to be in parallel and Eq. (2.85) should be used. Eq. (2.85) is in the form of Eq. (2.91), since the porosity for rectangular-grooved wick is equal to the width of the grooves over the sum of the groove width and the fin width:

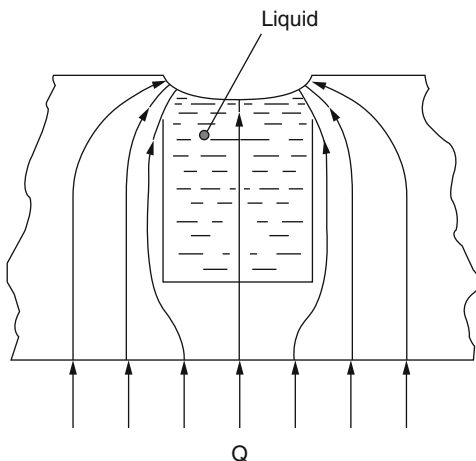
$$k_e = \frac{wk_l + w_f k_w}{w + w_f} \tag{Eq.2.91}$$

where

- k_e = effective thermal conductivity,
- k_w = thermal conductivity of wick material,
- k_l = liquid thermal conductivity,
- ϵ = wick porosity,
- w_f = groove fin thickness,
- w = groove thickness, and
- δ = groove depth.

The heat transfer mode across the groove wicks at the evaporator is somewhat different from that at the condenser. This difference occurs because condensation takes place at the fin tips as well as the liquid–vapor interface, whereas evaporation takes place solely at the liquid–vapor interface. A section view of rectangular-grooved wicks (Fig. 2.39) at the evaporator section is demonstrated in Fig. 2.37 with heat-flow paths indicated [18]. The figure shows that heat travels from the inner wall of the heat pipe container to the liquid–vapor interface through two parallel paths. Heat travels:

Fig. 2.39 Sketch of evaporative heat transfer mechanism for groove wicks [18]



1. Directly through the liquid film
2. Through a series path consisting of the groove fin and a thin film of liquid adjacent to the tip of the liquid–fin interface

Under these circumstances, the thermal conductivity for the first parallel path is simply equal to the thermal conductivity of the liquid, which can be seen as the following equation:

$$k_1 = k_l \quad (\text{Eq.2.92})$$

Chi [62] reported mathematical models for predicting performance of heat pipes of various wick structures (e.g., wrapped-screen, open-groove, and screen covered-groove wicks) and temperatures ranging from cryogenic to liquid–metal temperatures. As far as possible, the confidence in theoretical predictions was to establish a way of comparison of theory with available experimental data. There are two computer codes reported in this reference that we will talk about later on in Chap. 3. Also Chi [62] has shown that the film heat transfer coefficient for the liquid–fin interface with respect to the fin width is equal to $k_l/(0.185w_f)$. As a result, the equivalent thermal conductivity for the second path, consisting of groove fin and the liquid film at liquid–fin interface, can be calculated by the following equation that is given by Chi [18]:

$$k_2 = \frac{k_l k_w \delta}{0.185 w_f k_w + \delta k_l} \quad (\text{Eq.2.93})$$

Per Chi [18], combining the two parallel paths having widths equal to those of the grooves and fins, respectively, with their corresponding thermal conductivities, that is represented by Eqs. (2.92) and (2.93), respectively, the values of the effective

Table 2.6 Expressions of effective thermal conductivity k_e for liquid-saturated wicks

Wick structure	k_e Expressions
Wick and liquid in series	$k_e = \frac{k_1 k_w}{\epsilon k_w + k_1(1 - \epsilon)}$
Wick and liquid in parallel	$k_e = \epsilon k_1 + (1 - \epsilon)k_w$
Wrapped screen	$k_e = \frac{k_1[(k_1 + k_w) - (1 - \epsilon)(k_1 - k_w)]}{[(k_1 + k_w) + (1 - \epsilon)(k_1 - k_w)]}$
Packed sphere	$k_e = \frac{k_1[(2k_1 + k_w) - 2(1 - \epsilon)(k_1 - k_w)]}{[(2k_1 + k_w) + (1 - \epsilon)(k_1 - k_w)]}$
Rectangular grooves	$k_e = \frac{(w_f k_1 k_w \delta) + (w k_1)(0.185 w_f k_w + \delta k_1)}{(w + w_f)(0.185 w_f k_w + \delta k_1)}$

Source: Chi [18]

thermal conductivity for the groove wicks at the evaporator section can be derived by the following equation:

$$k_e = \frac{(w_f k_1 k_w \delta) + (w k_1)(0.185 w_f k_w + \delta k_1)}{(w + w_f)(0.185 w_f k_w + \delta k_1)} \tag{Eq.2.94}$$

For easy reference, equations for these wick structures are collected in Table 2.6 from Chi [18]. These equations are recommended for use in heat pipe calculation unless the experimental data are available for a particular liquid–wick combination where

- k_e = effective thermal conductivity,
- k_w = thermal conductivity of wick material,
- k_1 = liquid thermal conductivity,
- ϵ = wick porosity,
- w_f = groove fin thickness,
- w = groove thickness, and
- δ = groove depth.

2.14 Boiling Limit

A typical cylindrical heat pipe receives heat at the evaporator end where it is transferred to the working fluid radially. When the input flux is sufficient, nucleation sites are formed inside the wick and bubbles are trapped in the wick, blocking liquid return that results in evaporator dryout [17]. As compared to other heat pipe limits, boiling limit is a radial flux constraint and not an axial flux constraint. For liquid–metal heat pipes, the boiling limit is not very common [9]. The boiling limit is due to excessive radial heat flux; all the other limits are due to axial heat flux. The maximum heat flux beyond which bubble growth will occur resulting in dryout is given by [17]

$$Q_{\text{Evaporator}} = \left(\frac{2\pi L_e k_{\text{eff}} T_v}{\lambda \rho_v \ln(r_i/r_v)} \right) \left(\frac{2\sigma}{r_n} - \Delta P_{c,m} \right) \quad (\text{Eq.2.95})$$

where $\Delta P_{c,m}$ = maximum difference in capillary pressure, σ = surface tension (function of fluid and temperature), r_n = nucleation site radius (assume to be between 2.54×10^{-5} m and 2.54×10^{-7} m), T_v = vapor temperature, L_e = length of vapor, r_v = vapor space (radius of open heat pipe allowing vapor to pass through), r_i = inner radius of heat pipe, ρ_v = density of vapor, λ = latent heat of vaporization, and k_{eff} = effective conductivity.

Heat flux or boiling limit is determined by nucleate boiling theory and is comprise of two separate phenomena [17]—bubble formation and the subsequent growth or collapse of the bubbles [18]. Bubble formation obeys and is ruled by the number and size of nucleation sites on a solid surface and the temperature difference between the heat pipe wall and the working fluid. This temperature difference, termed the *superheat*, governs the formation of the bubbles and can typically be defined in terms of maximum heat flux as [17]

$$q_m = \left(\frac{k_{\text{eff}}}{T_w} \right) \Delta T_{\text{cr}} \quad (\text{Eq.2.96})$$

where k_{eff} is the effective thermal conductivity of the liquid–wick combination and ΔT_{cr} is the critical superheat, defined by Marcus as [63]

$$\Delta T_{\text{cr}} = \left(\frac{T_{\text{sat}}}{\lambda \rho_v} \right) \left(\frac{2\sigma}{r_n} - \Delta P_{i,m} \right) \quad (\text{Eq.2.97})$$

Here T_{sat} is the saturation temperature of the fluid and r_n is the critical nucleation site radius, which according to Dunn and Reay [27], can be assumed to be from 2.54×10^{-5} to 2.54×10^{-7} m for conventional metallic heat pipe case materials.

As presented by Brennan and Kroliczek [44], this model yields a very a very conservative estimate of the amount of superheat required for bubble formation. This is true even when the lower bound for the critical nucleation site radius is used. Some scientists and researchers attribute this to the absence of absorbed gases on the surface of the nucleation sites caused by the degassing and cleaning procedures used in the preparation and charging of heat pipe for starting up.

The growth or collapse of given bubble once established on a flat or planar surface is dependent upon the liquid temperature and corresponding pressure difference across the liquid–vapor interface caused by the vapor pressure and surface tension of the liquid. By performing a pressure balance on any given bubble and using the Clausius–Clapeyron equation to relate the temperature and pressure, an expression for the heat flux beyond which bubble growth will occur may be

developed [18]. This expression, which is a function of the fluid properties, can be written as illustrated in Eq. (2.84)

$$Q_{\text{Evaporator}} = \left(\frac{2\pi L_e k_{\text{eff}} T_v}{\lambda \rho_v \ln(r_i/r_v)} \right) \left(\frac{2\sigma}{r_n} - \Delta P_{c,m} \right) \quad (\text{Eq.2.98})$$

where k_{eff} is the effective thermal conductivity of the liquid–wick combination (give in Table 2.6), r_i is the inner radius of the heat pipe wall, and r_n is again the nucleation site radius.

There are more detailed information given by G.P. Peterson in his book *An Introduction to Heat Pipes Modeling, Testing, and Application* [17].

Analysis of the boiling limitation is well defined by Chi [18] and involves the theory of nucleate boiling. This involves two separate processes as follows:

1. The formation of bubbles (nucleation)
2. The subsequent growth and motion of these bubbles

All these processes are also well defined in Sect. 2.7 under one-dimensional two-phase flow and can be also found in references by Graham [64] and Busse [23].

If we assume a vapor bubble sphere at vicinity of wick structure rising while it is interfacing the wick and it is in equilibrium state, then the following equation is a valid expression:

$$\pi r_b^2 (P_{\text{pw}} - P_1) = 2\pi r_b \sigma \quad (\text{Eq.2.99})$$

where

P_{pw} = saturation vapor pressure at heat pipe wick interface,

P_1 = liquid pressure,

r_b = radius of vapor bubble, and

σ = surface tension coefficient.

At the interface between liquid and vapor, the liquid pressure P_1 is equal to the difference between vapor pressure P_v and capillary pressure P_c at the same spot and can be shown as

$$P_1 = P_v - P_c \quad (\text{Eq.2.100})$$

By substituting Eq. (2.100) into Eq. (2.99), we have the following:

$$\pi r_b^2 (P_{\text{pw}} - P_v + P_c) = 2\pi r_b \sigma \quad (\text{Eq.2.101})$$

Utilizing the Clausius–Clapeyron equation relates T and P along the saturation line as follows:

$$\frac{dP}{dT} = \frac{\lambda \rho_v}{T_v} \quad (\text{Eq.2.102})$$

Now combine Eq. (2.102) with Eq. (2.103) along with assumption of

$$P_{pw} - P_{wv} \approx (T_{pw} - T_{wv})dP/dT \quad (\text{Eq.2.103})$$

to get the following result:

$$T_{pw} - T_{wv} = \frac{T_v}{\lambda\rho_v} \left(\frac{2\sigma}{r_b} - P_c \right) \quad (\text{Eq.2.104})$$

But $(T_{pw} - T_{wv})$ is the temperature drop across the wick structure at the evaporator section. Utilize conduction theorem for a heat pipe with uniform heat flux distribution along the evaporator length L_e . Equation (2.105) can be reduced and rearranged to the following form:

$$(T_{pw} - T_{wv}) = \frac{Q \ln(r_i/r_v)}{2\pi L_e k_e} \quad (\text{Eq.2.105})$$

where

Q = total heat Transfer at the evaporator,

r_i = inner radius of the pipe,

r_v = vapor core radius,

L_e = evaporator length, and

k_e = effective thermal conductivity of the liquid-saturated wick.

Substituting the $(T_{pw} - T_{wv})$ from Eq. (2.92) into Eq. (2.104), we have the following:

$$Q = \frac{2\pi L_e k_e T_v}{\lambda\rho_v \ln(r_i/r_v)} \left(\frac{2\sigma}{r_b} - P_c \right) \quad (\text{Eq.2.106})$$

This recent equation is representing the heat transfer rate required to maintain equilibrium vapor bubbles of radius r_b in the heat pipe wick.

Depending on the surface conditions and affected by the presence of dissolved gas in the liquid, the nucleation radius of the vapor bubbles, r_n (the initial radius of the vapor bubbles at its formation), has finite values [18]. Replacing r_b with r_n in Eq. (2.106), the vapor bubbles, if ever formed and will collapse if

$$Q < \frac{2\pi L_e k_e T_v}{\lambda\rho_v \ln(r_i/r_v)} \left(\frac{2\sigma}{r_n} - P_c \right) \quad (\text{Eq.2.107})$$

The vapor bubbles, if ever formed, will collapse if:

$$Q > \frac{2\pi L_e k_e T_v}{\lambda\rho_v \ln(r_i/r_v)} \left(\frac{2\sigma}{r_n} - P_c \right) \quad (\text{Eq.2.108})$$

The vapor bubbles will be formed and grow in the wick structures. Therefore, final expression for the boiling heat transport limit is given by the equation

$$Q_{b_{\text{Max}}} = \frac{2\pi L_e k_e T_v}{\lambda \rho_v \ln(r_i/r_v)} \left(\frac{2\sigma}{r_n} - P_c \right) \tag{Eq.2.109}$$

Here, $Q_{b_{\text{Max}}}$ is the boiling limit on heat transfer rate and to evaluate it, the value of r_n is required. For more details, see Griffith and Walls [65] as well as Rohsenow and Choi [66].

2.15 Viscous Limit

The vapor-pressure limitation (or viscous limitation) in heat pipes develops when the pressure drop in the vapor core reaches the same order of magnitude as the vapor in the evaporator. Under these conditions, the pressure drop due to flow through the vapor core creates an extremely low vapor pressure in the condenser, preventing the vapor from flowing in the condenser (Fig. 2.40). A general expression for the vapor-pressure limitation is given by Dunn and Reay [27].

Viscous forces at low operating temperatures are dominated in the vapor flow down the pipe. The vapor pressure difference between the condenser and the evaporator of a heat pipe or thermosyphon may not be enough to overcome viscous forces. As a result, the vapor from the evaporator does not move to the condenser and the thermodynamic cycle does not occur. This no-flow or low-flow condition in the vapor portion of a heat pipe is known as viscous limitation. Since the vapor

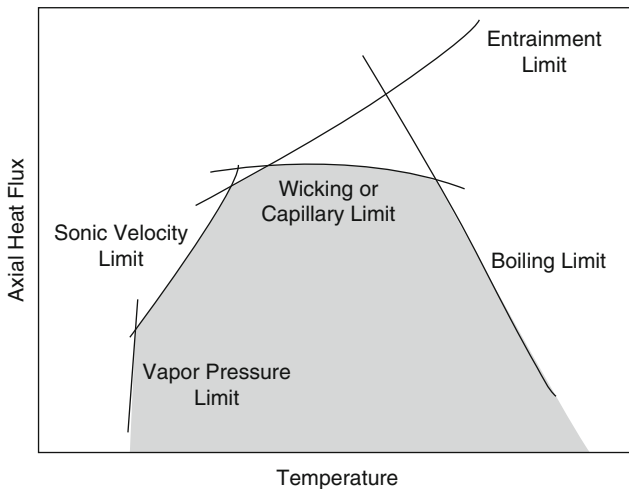


Fig. 2.40 Heat transfer limitations in heat pipes

pressure typically must be very low for this to occur, the viscous limit most often takes place in cryogenic-type heat pipes, heat pipes with very long condenser section, and/or heat pipes undergoing startup process from a frozen state:

$$Q_{\text{vapor,max}} = \frac{\pi r_v^4 h_{fg} \rho_{ve} P_{ve}}{12 \mu_{ve} l_{\text{eff}}} \quad (\text{Eq.2.110})$$

where

- r_v is the cross-sectional radius of the vapor core (m),
- h_{fg} is the latent heat of vaporization (J/kg),
- ρ_{ve} is the vapor density in the evaporator (kg/m^3),
- P_{ve} is the vapor pressure in the evaporator (Pa),
- μ_{ve} is the vapor viscosity in the evaporator N s/m^2 , and
- l_{eff} is the effective length of heat pipe at the lower end of the working-fluid temperature range (m).

Equation (2.107) was established by Buss [67] and has shown that the axial heat flux increases as the pressure in the condenser is reduced, the maximum heat flux occurring when the pressure is reduced to zero. He carried out a two-dimensional analysis, finding that the radial velocity component had a significant effect, and he derived Eq. (2.110). Another version of Eq. (2.110) is also presented below as for Eq. (2.111) that is denoted by other heat pipe text books and papers

$$Q_{\text{vapor,max}} = \frac{r_v^2 L \rho_{ve} P_{ve}}{16 \mu_{ve} l_{\text{eff}}} \quad (\text{Eq.2.111})$$

where

- P_{ve} is the vapor pressure in evaporator (Pa),
- ρ_{ve} the vapor density in evaporator (kg/m^3),
- r_v the cross-sectional radius of the vapor core (m),
- μ_{ve} the vapor viscosity in the evaporator (N s/m^2),
- l_{eff} the effective length of heat pipe at the lower end of the working-fluid temperature range (m), and
- L the latent heat of vaporization (J/kg).

Or it can be seen as the following form:

$$Q_{\text{vapor,max}} = \frac{A_v r_0^2 \lambda \rho_{ve} P_{ve}}{16 \mu_{ve} L_{\text{eff}}} \quad (\text{Eq.2.112})$$

where

- P_{ve} is the vapor pressure in evaporator (Pa),
- ρ_{ve} the vapor density in evaporator (kg/m^3),

- r_v the cross-sectional radius of the vapor core (m),
- μ_{v_e} the vapor viscosity in the evaporator (N s/m^2),
- L_{eff} the evaporator length (m),
- A_v the vapor cross section area (m^2), and
- λ the latent heat of vaporization (J/kg).

2.16 Condenser Limit

In general, heat pipe condensers and the method of cooling the condenser should be designed such that the maximum heat rate capable of being transported by the heat pipe can be removed. However, in exceptional cases with high-temperature heat pipes, appropriate condensers cannot be developed to remove the maximum heat capability of the heat pipe. In other cases, during continuous operation due to the presence of non-condensable gases, the effective length of the heat pipe is reduced and therefore the condenser is not to its full capacity. In such cases, the heat transfer limitation can be due to the condenser limit [9].

Also usage of fins at the condenser side of the heat pipe will assist heat dissipation for removing additional heat from the condenser side of the pipe. The fin usage will be an element to increase limit in particular for short-length heat pipe. A fin unit located above the base plate and having a plurality of fins stacked together and at least a heat pipe having an evaporating section thermally engaging with the base plate and a pair of condensing sections extending through the fins. Each of the fins may have a plurality of parallel and protruding flanges on a top face thereof. The protruding flanges of the fins should be of equal height and parallel to short sides of the fins. Each protruding flange then has a length equal to that of the short sides of the fins. A distance between the two neighboring ones of the protruding flanges located between the condensing sections in this case is the same. The protruding flanges may be provided for increasing a heat dissipation area of the fin.

2.17 Transport Limitations

The most important heat pipe design consideration is the amount of power the heat pipe is capable of transferring. Heat pipes can be designed to carry a few watts or several kilowatts, depending on the application. Heat pipes can transfer much higher powers for a given temperature gradient than even the best metallic conductors. If driven beyond its capacity, however, the effective thermal conductivity of the heat pipe will be significantly reduced. Therefore, it is important to assure that the heat pipe is designed to safely transport the required heat load.

The maximum heat transport capability of the heat pipe is governed by several limiting factors which must be addressed when designing a heat pipe. There are five

primary heat pipe heat transport limitations. These heat transport limits, which are a function of the heat pipe operating temperature, include viscous, sonic, capillary pumping, entrainment or flooding, and boiling. Figure 2.8 is showing theoretical envelope of these limits, while Figs. 2.40, 2.41, and 2.42 show a computer run of graphs of the axial heat transport limits as a function of operating temperature for typical powder metal and screen-wicked heat pipes.

Each limit has its own particular range in which it is important for design of a good operational heat pipe without any failure. However, in practical operation, the capillary and boiling limits are the most important. The figure below is an example of these ranges.

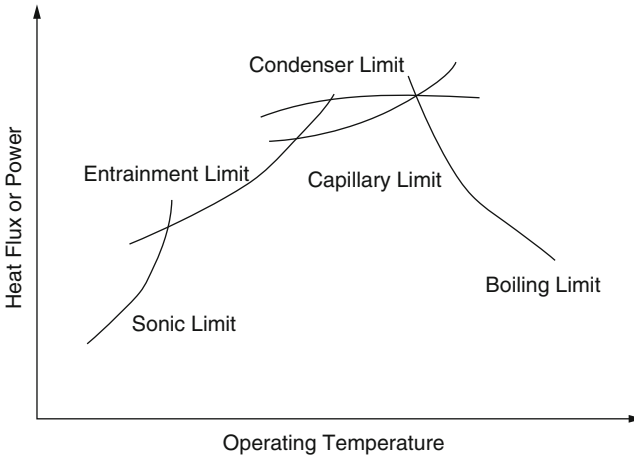


Fig. 2.41 Operating limits for a heat pipe

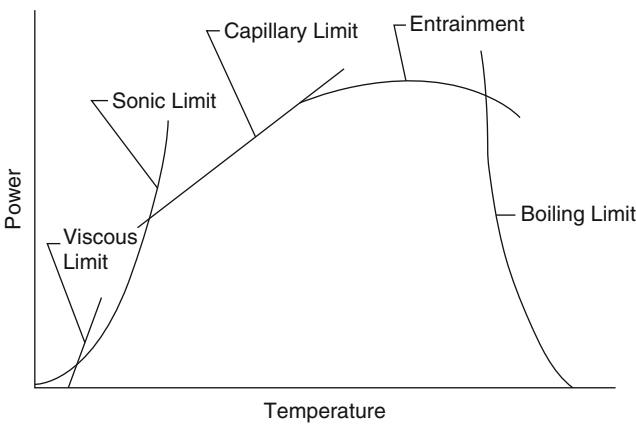


Fig. 2.42 Heat pipe performance map

The maximum limitations of input heat that may be transported by a heat pipe are divided into two classifications. These two classifications or categories are based on the following:

1. Complete success of heat pipe operation under envelope and configuration of heat pipe based on its operating limitation
2. The failure of such operation. For the limitations that result to the failure of the heat pipe, known as heat pipe *burn out* or *dry out*, driven by insufficient liquid flow from the condenser to the evaporator for a given parameter of heat input and output, wick structure has played a role as well.

There exists functionality between input heats of Q versus the mass flow rate (\dot{m}) of the working fluid within the heat pipe that is circulating between the evaporator and condenser side and the latent heat of h_{fg} of that working fluid as shown in Eq. (2.113)

$$Q = \dot{m} h_{fg} \quad (\text{Eq.2.113})$$

Note that more complexities will be introduced into these limitations if the heat pipe is a constant or a variable device or is operating in the absence of gravity or the heat pipe is not in the appropriate angle of inclination of installation within its environment. As a result of such complexity, the limitations of heat pipe, failure, or success of its operation will be summarized in Fig. 2.42, known as the heat pipe performance map or the optimum operating envelope. This is the envelope where a designer or manufacturer of that heat pipe has to take under consideration in order to guarantee the success of heat pipe operation.

Actual performance curves, viscous limit, sonic limit, capillary or wicking limit, entrainment limit, and finally boiling limit are the limiting factors. The three major limitations that should be considered for a heat pipe not to operate successfully and fail their operating envelopes are (1) *capillary/wicking limit*, (2) *boiling limit*, and (3) *entrainment limit*, and each one of them are briefly described here.

1. *Capillary or wicking limit*. This limit is the fundamental governing phenomenon for heat pipe operating parameter which is a function of capillary pressure difference across liquid–vapor interface between evaporator and condenser of such pipe.
2. *Boiling limit*. This limit is driven by sufficient heat flux that is causing nucleate boiling in the evaporator wick of heat pipe. In this case, the vapor bubbles that are created cause partial blockage of returned liquid from the condenser to evaporator and leads to the dryout of wick. This limit is also known as *heat flux limit*.
3. *Entrainment limit*. This limit is driven by high shear forces that are developed as the vapor passes in counterflow direction over the liquid-saturated wick. This is because the liquid may be entrained by the vapor and returned to the condenser, leading to insufficient liquid flow to the wick structure.

The summary on a non-failure limitation is also described below as well as graphically plotted in Fig. 2.39.

1. *Viscous limit.* The viscous limit also is known as *vapor pressure* limit. This limit takes place when a very low operating temperature exists, where the saturation vapor pressure is the same order of pressure drop necessary to drive the vapor flow in the heat pipe.
2. *Sonic limit.* The sonic limit is driven by the fact that at low vapor densities, associated mass flow rate in the heat pipe may result in very high vapor velocities, and the choking condition in vapor flow of vapor passage may take place.
3. *Condenser limit.* This limit is based on cooling limitations such as the radiation or natural convection at the condenser. For radiative case, the heat pipe transport is governed by the condenser surface area, emissivity, and operation temperature. Calculation of this limitation for either constant or variable heat pipe may change.

In addition, the capillary, viscous, entrainment, and sonic limits are axial heat flux limits. These limits are a function of the axial heat transport capacity along the heat pipe. However, the boiling limit is a radial heat flux limit taking place in the evaporator [68].

Using various computational or analysis techniques for each of these operation limits independently yields an envelope of operation limit such as in Fig. 2.40. In this figure, the heat transport capacity depicted as a function of the mean operating temperature or known as adiabatic vapor temperature can be determined. Effectively these operational range defines envelope or optimum design of any given heat pipe based on its performance and operational requirements. The region under this envelope or region defines the combination of temperature and maximum transport capabilities at which the heat pipe will function properly from startup pointing to full operation cycle. This will assure that the heat pipe will operate under required thermal condition and can transport the load or allow adjusting the design to best optimum operational functions. It should be said that it has a lot to do with the operating temperature of the heat pipe. Naturally the conditions will change if the heat pipe is a variable heat pipe or operates in the absence of gravity, or if fins are considered as part of the overall design of the pipe on the condenser side or may be the adiabatic region is considered for the heat pipe in question.

A heat pipe is essentially a passive heat transfer device with an extremely high effective thermal conductivity. The two-phase heat transfer mechanism results in heat transfer capabilities from one hundred to several thousand times that of an equivalent piece of copper.

As shown in Fig. 2.43, the heat pipe in its simplest configuration is a closed, evacuated cylindrical vessel with the internal walls lined with a capillary structure or wick that is saturated with a working fluid. Since the heat pipe is evacuated and then charged with the working fluid prior to being sealed, the internal pressure is set by the vapor pressure of the fluid.

From this a designer can have some optimum design parameters for his specific heat pipe requirement. The upper limitation of each separate limit with their joint point designs the envelope that will represent the performance limit of heat pipe design. This envelope can be calculated easily and plotted with power as a function of operation temperature (Figs. 2.44 and 2.45).

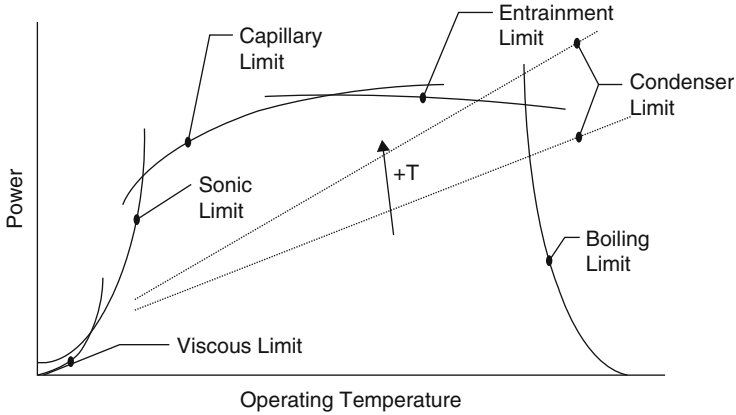


Fig. 2.43 Typical heat pipe performance map

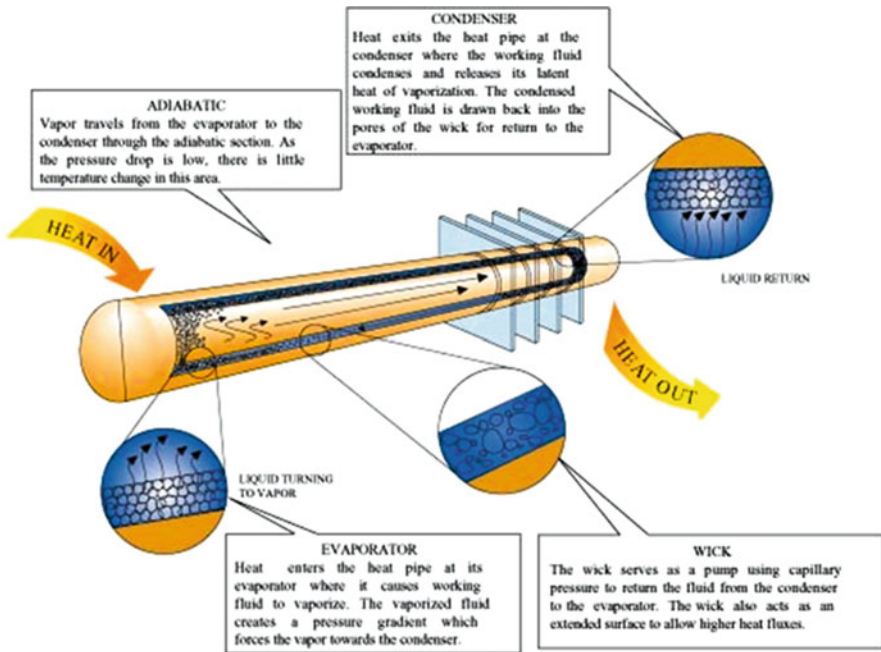


Fig. 2.44 Heat pipe operation process

As shown in Figs. 2.46 and 2.47, the capillary limit is usually the limiting factor in a heat pipe design. The capillary limit is set by the pumping capacity of the wick structure. As it is shown in Fig. 2.46, the capillary limit is a strong function of the operating orientation and the type of wick structure.

The two most important properties of a wick are the pore radius and the permeability. The pore radius determines the pumping pressure the wick can develop. The permeability determines the frictional losses of the fluid as it flows

Fig. 2.45 Wick structures

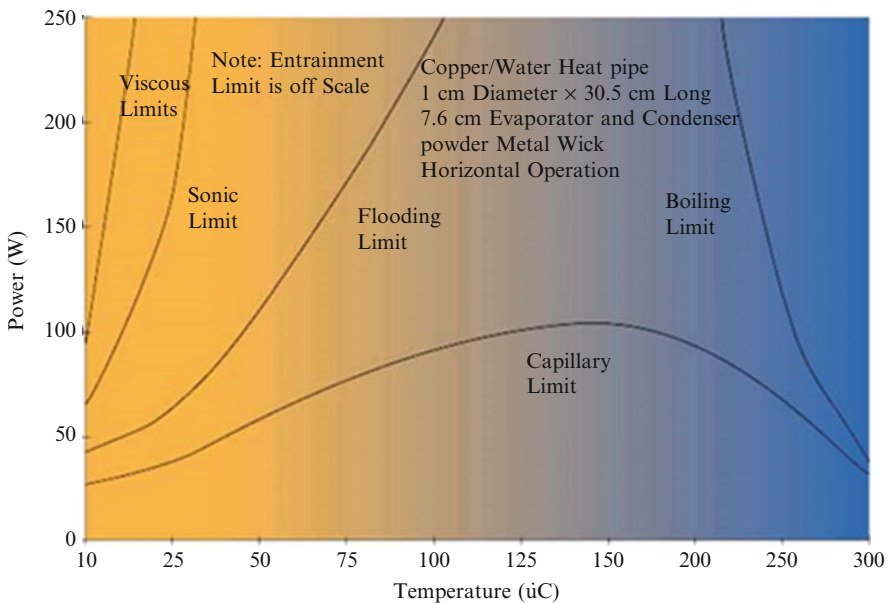
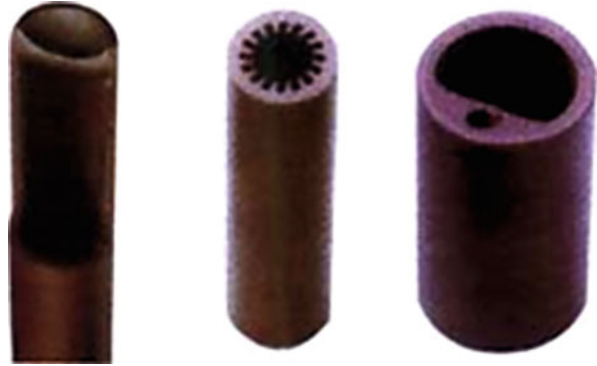


Fig. 2.46 Predicted heat pipe limits

through the wick. There are several types of wick structures available including grooves, screen, cables/fibers, and sintered powder metal. Figure 2.45 shows several heat pipe wick structures.

It is important to select the proper wick structure for your application. The above list is in order of decreasing permeability and decreasing pore radius. Grooved wicks have a large pore radius and a high permeability; as a result, the pressure losses are low, but the pumping head is also low. Grooved wicks can transfer high heat loads in a horizontal or gravity-aided position, but cannot transfer large loads against gravity. The powder metal wicks on the opposite end of the list have small pore radii and relatively low permeability. Powder metal wicks are limited by pressure drops in the horizontal position but can transfer large loads against gravity [69] (Fig. 2.48).

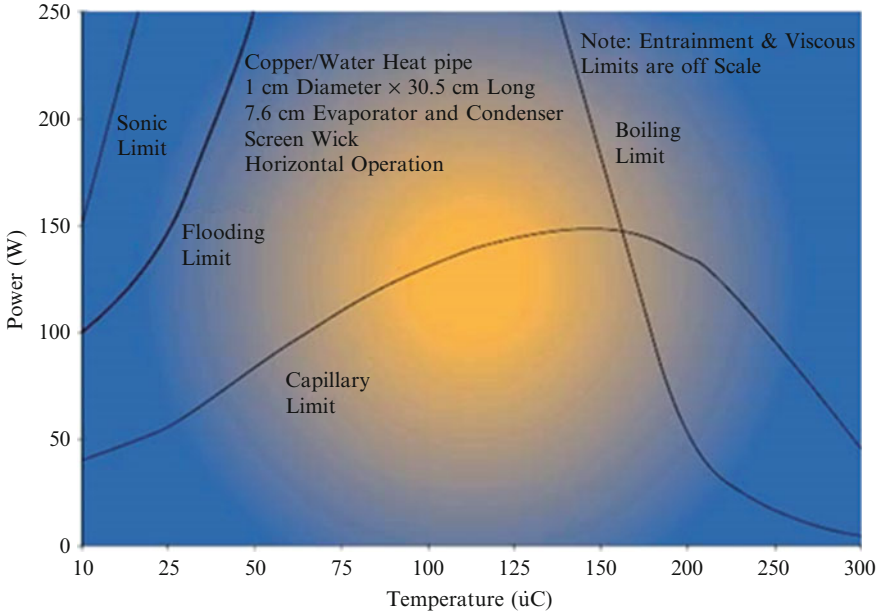


Fig. 2.47 Predicted heat pipe limitations

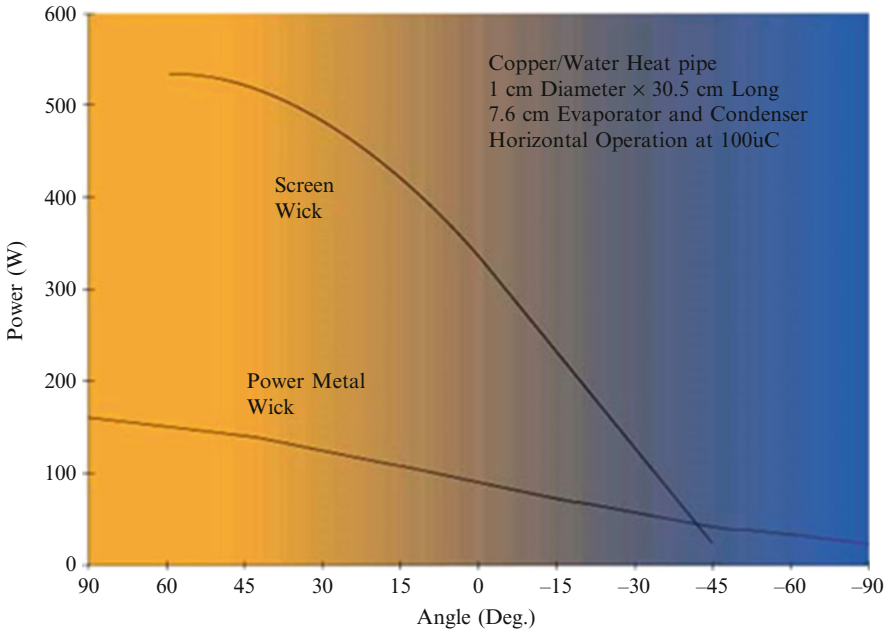


Fig. 2.48 Capillary limits versus operating angle

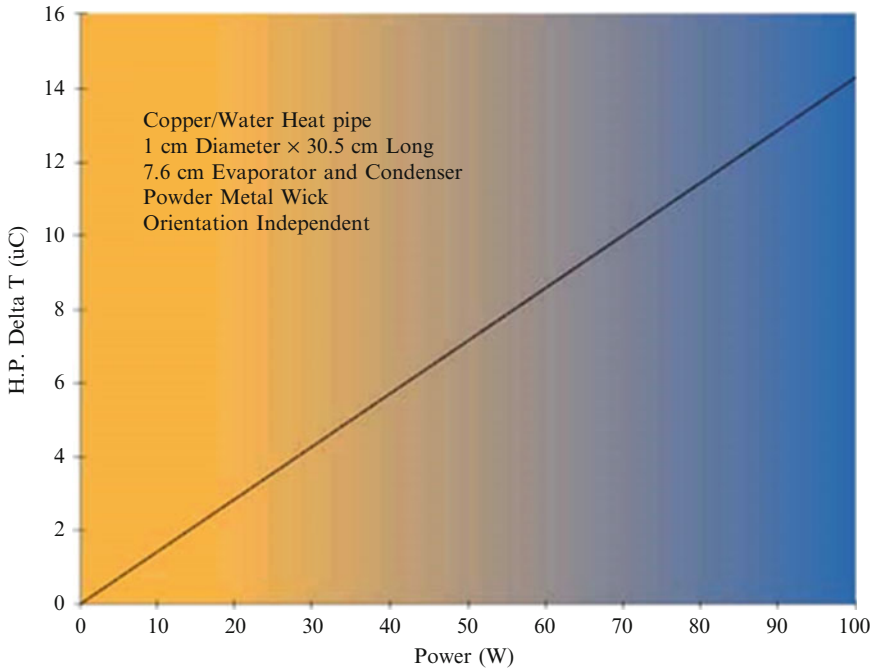


Fig. 2.49 Predicted heat pipe ΔT

The other primary heat pipe design consideration is the effective heat pipe thermal resistance or overall heat pipe ΔT at a given design power. As the heat pipe is a two-phase heat transfer device, a constant effective thermal resistance value cannot be assigned. The effective thermal resistance is not constant but a function of a large number of variables, such as heat pipe geometry, evaporator length, condenser length, wick structure, and working fluid.

The total thermal resistance of a heat pipe is the sum of the resistances due to conduction through the wall, conduction through the wick, evaporation or boiling, axial vapor flow, condensation, and conduction losses back through the condenser section wick and wall. Figure 2.49 shows a power versus ΔT curve for a typical copper/water heat pipe.

The detailed thermal analysis of heat pipes is rather complex. There are, however, a few rules of thumb that can be used for first-pass design considerations. A rough guide for a copper/water heat pipe with a powder metal wick structure is to use $0.2 \text{ }^\circ\text{C/W/cm}^2$ for thermal resistance at the evaporator and condenser and $0.02 \text{ }^\circ\text{C/W/cm}^2$ for axial resistance [69].

The evaporator and condenser resistances are based on the outer surface area of the heat pipe. The axial resistance is based on the cross-sectional area of the vapor space. This design guide is only useful for powers at or below the design power for the given heat pipe.

For example, to calculate the effective thermal resistance for a 1.27 cm diameter copper/water heat pipe 30.5 cm long with a 1 cm diameter vapor space, the

following assumptions are made. Assume the heat pipe is dissipating 75 W with a 5 cm evaporator and a 5 cm condenser length. The evaporator heat flux (q) equals the power divided by the heat input area ($q = Q/A_{\text{evap}}$; $q = 3.8 \text{ W/cm}^2$). The axial heat flux equals the power divided by the cross-sectional area of the vapor space ($q = Q/A_{\text{vapor}}$; $q = 95.5 \text{ W/cm}^2$).

The temperature gradient equals the heat flux times the thermal resistance:

$$\begin{aligned}\Delta T &= q_{\text{evap}} \times R_{\text{evap}} + q_{\text{axial}} \times R_{\text{axial}} + q_{\text{cond}} \times R_{\text{cond}} \\ \Delta T &= 3.8 \text{ W/cm}^2 \times 0.2^\circ\text{C/W/cm}^2 + 95.5 \text{ W/cm}^2 \times 0.02^\circ\text{C/W/cm}^2 \\ &\quad + 3.8 \text{ W/cm}^2 \times 0.2^\circ\text{C/W/cm}^2 \\ \Delta T &= 3.4^\circ\text{C}\end{aligned}$$

It is important to note that the equations given above for thermal performance are only rule-of-thumb guidelines. These guidelines should only be used to help determine if heat pipes will meet your cooling requirements, not as final design criteria. More detailed information on power limitations and predicted heat pipe thermal resistances are given in the heat pipe design books listed in Ref. [69].

Each heat transport limitation is summarized in Table 2.7.

Table 2.7 Heat pipe heat transport limitations

Heat transport limit	Description	Cause	Potential solution
Viscous	Viscous forces prevent vapor flow in the heat pipe	Heat pipe operating below recommended operating temperature	Increase heat pipe operating temperature or find alternative working fluid
Sonic	Vapor flow reaches sonic velocity when exiting heat pipe evaporator resulting in a constant heat pipe transport power and large temperature gradients	Power/temperature combination, too much power at low operating temperature	This is typically only a problem at startup. The heat pipe will carry a set power and the large T will self-correct as the heat pipe warms up
Entrainment/flooding	High velocity vapor flow prevents condensate from returning to evaporator	Heat pipe operating above designed power input or at too low an operating temperature	Increase vapor space diameter or operating temperature
Capillary	Sum of gravitational, liquid, and vapor flow pressure drops exceed the capillary pumping head of the heat pipe wick structure	Heat pipe input power exceeds the design heat transport capacity of the heat pipe	Modify heat pipe wick structure design or reduce power input
Boiling	Film boiling in heat pipe evaporator typically initiates at 5–10 W/cm ² for screen wicks and 20–30 W/cm ² for powder metal wicks	High radial heat flux causes film boiling resulting in heat pipe dryout and large thermal resistances	Use a wick with a higher heat flux capacity or spread out the heat load

2.18 The Working Fluid

Considering that heat pipe is a closed-loop heat exchanger and the primary mode of its operation is based on vaporization and condensation of the working fluid, then selection of a suitable working fluid is one the most important aspect of the heat pipe design and its manufacturing process for given application.

The selection of the appropriate working fluid for a given application is based on many considerations. These include [63]:

- (a) Operating temperature range
- (b) Heat transfer requirements
- (c) Expected body-force field (e.g., 0 g, 1 g, etc.)
- (d) Tolerance of wick structure to boiling
- (e) Type of heat pipe (conventional or variable conductance)
- (f) Special requirements
- (g) Materials compatibility and stability

Brief discussions of these considerations follow.

2.18.1 *The Operating Temperature Range*

Clearly, a heat pipe cannot be operated below the freezing point or above the thermodynamic critical point of its working fluid. Thus, the first criterion for selection of a fluid is that these two thermodynamic conditions fall within the required operating temperature range.

These conditions, however, actually represent lower and upper bounds which are seldom approached. Most often, the low end of a given fluid's operating temperature range is established by adverse vapor dynamics (sonic limit, entrainment limit, or simply excessive ΔP_v) due to low vapor densities and corresponding high vapor velocities. The high end of the temperature range is frequently set by the mechanical aspects of containing the fluid vapor pressure.

2.18.2 *Heat Transfer Requirements*

The axial heat transport requirement can have a major impact on the choice of working fluid. Different fluids will yield different capillary pumping limits for the same wick structure. Thus, the case can easily arise where a simple homogeneous wick design can be substituted for a complex arterial wick design by the choice of fluid.

To determine the best fluid for a given application, one must theoretically examine the optimal designs for each fluid by integrating the loss equations to

determine their respective capillary pumping limit (see Sect. 2.13.3). Sometimes this is actually necessary since, in the general case, there is no simple grouping of fluid properties which serves as a basis for selection. However, there exist such groupings for special cases which at least provide some general guidelines. Thus, for a heat pipe operating in the absence of body forces and for which the vapor pressure drop is negligible, the capillary pumping limit can be shown to be proportional to the grouping $(\sigma\rho_1\lambda/\nu_1)$, sometimes referred to as the “liquid transport factor” or “0 g figure of merit.” Figure 2.50 shows the liquid transport factor for the principal fluids of interest in spacecraft thermal control as a function of operating

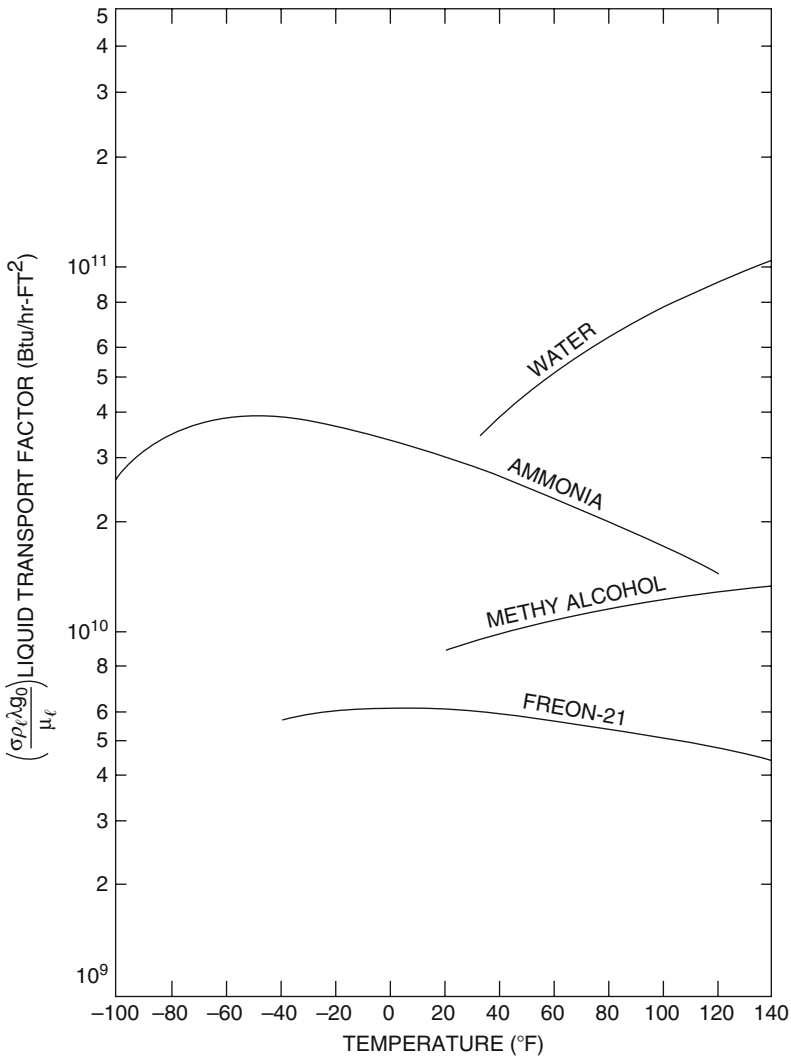


Fig. 2.50 Liquid transport factor for heat pipe working fluids

temperature. Additional curves for many other fluids can be found in the literature [35, 70, 71].

Although this grouping applies to the special case of negligible body forces and vapor pressure drop, those conditions do pertain to many spacecraft thermal control applications so that this is a valid basis of comparison for such heat pipes. However, as mentioned previously, it is not of general value. As Joy [72] has shown, the presence of even small body forces (e.g., acceleration fields) can render this basis of comparison invalid for cryogenic fluids.

2.18.3 *Expecting Body-Force Field*

As pointed out in the last section, the presence of body forces can have a major impact on the relative performance of various fluids. This situation is due to two phenomena:

1. The body-force head is subtracted from the maximum capillary head in establishing the pumping head available to overcome flow losses
2. The body-force head must be overcome by surface tension effects in order to prime arteries, etc.

Since, in both cases, the problem is one of the surface tension forces working against body forces, the ratio of these forces represents a basis of fluid comparison. In terms of fluid properties, this ratio is proportional to the grouping (σ/ρ_l) . Thus, to minimize adverse body-force effects, one should select a fluid with a high value of this parameter. Figure 2.51 shows the variation in (σ/ρ_l) with operating temperature for the principal spacecraft thermal control fluids.

2.18.4 *Tolerance of Wick Structure to Boiling*

In Sects. 2.19.2 and 2.19.3, fluids were compared on the basis of their hydrodynamic and hydrostatic properties. However, as has been emphasized in this report, one must also consider radial heat transfer in the evaporator, especially if boiling would seriously degrade hydrodynamic performance (e.g., nucleation with arteries). The criteria for nucleation were discussed and shown by Marcus [49, 73]. Assuming the critical radius (r_n) in Eq. (3.14) for the critical superheat is equal to the wick pore size, the pertinent fluid property grouping for superheat tolerance is $(\sigma/\lambda\rho_v)$. Multiplying this grouping by the thermal conductivity of the liquid yields a measure of the fluids' radial heat transfer tolerance with respect to nucleation. Figure 2.50 shows the variation of this parameter ($k\sigma/\lambda\rho_v J$) with operating temperature for the principal spacecraft thermal control fluids; gas control scheme provides additional selection criteria based on the slope of the vapor pressure curve:

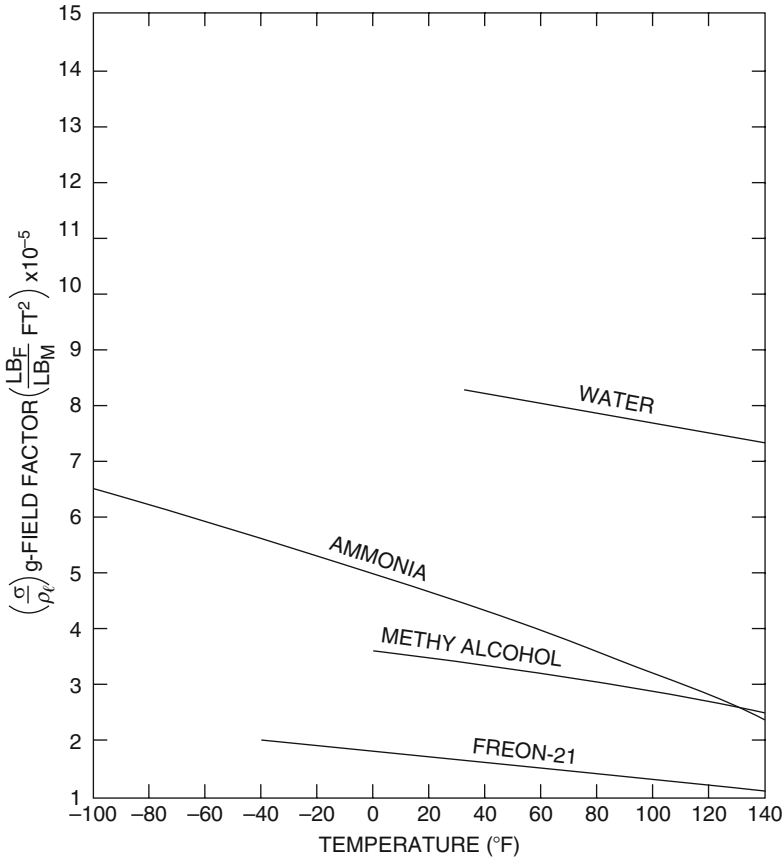


Fig. 2.51 Gravity field figure of merit for heat pipe working fluids

$$\Delta T_{\text{critical}} = \frac{T_{\text{saturation}}}{J\lambda\rho_v} \left[\frac{2\sigma}{r_n} - \Delta P_c^* \right] \tag{Eq.2.114}$$

where

$T_{\text{saturation}}$ = saturation temperature of the fluid,

J = mechanical equivalent of heat,

r_n = effective radius of critical nucleation cavity, and

ΔP_c^* = maximum value of capillary head along the evaporator.

Note that ΔP_c^* does not equal to $\Delta P_{c_{\text{max}}}$ as given in Eq. (2.10) unless the heat pipe is operating at the capillary pumping limit [63]. Rather, it is the maximum value of ΔP_c as given below by Eq. (2.111) along the evaporator section of the heat pipe [63]:

$$\Delta P_c = \Delta P_l + \Delta P_v \pm \Delta P_b \quad (\text{Eq.2.115})$$

where

$$\begin{bmatrix} \text{net} \\ \text{capillary} \\ \text{head} \end{bmatrix} = \begin{bmatrix} \text{liquid} \\ \text{pressure} \\ \text{drop} \end{bmatrix} + \begin{bmatrix} \text{vapor} \\ \text{pressure} \\ \text{drop} \end{bmatrix} \pm \begin{bmatrix} \text{body force} \\ \text{head} \\ \text{(if any)} \end{bmatrix}$$

For more detail, refer to Marcus report [63].

Generally, all of the terms on the right-hand side of Eq. (2.116) are known except r_n , which is a function of the boiling surface finish. To establish the appropriate value of r_n , one should first establish its value assuming cavities of all sizes were present on the surface and then impose appropriate limits. This can be done using the nucleation theory of Rohsenow and Bergles [73]. Their equation for r_n is given by

$$r_n = \left[\frac{2\sigma T_{\text{saturation}} k_l v_{lg}}{\lambda q_r''} \right]^{1/2} \quad (\text{Eq.2.116})$$

where

k_l = thermal conductivity of liquid,

v_{lg} = difference in specific volume of vapor and liquid, and

q_r'' = radial heat flux into evaporator.

The value of r_n given in Eq. (2.116) is the appropriate one to use in Eq. (2.115), assuming that cavities of such size exist on the surface and are potential nucleation sites. For more details, refer to Marcus [63] report.

Note that a potential nucleation site is a cavity which contains a preexisting gaseous phase.

2.18.5 Conventional or Variable Conductance Heat Pipe

The fluid selection criteria discussed so far apply to all heat pipes. However, if one is designing variable conductance heat pipe (VCHP), additional criteria may be involved, depending on the control scheme. Thus, heat pipes which employ vapor throttling as a control mechanism require low pressure working fluids. Similarly, the non-condensable gas (NCG) control scheme provides additional selection criteria based on the slope of the vapor pressure curve (see Fig. 2.52).

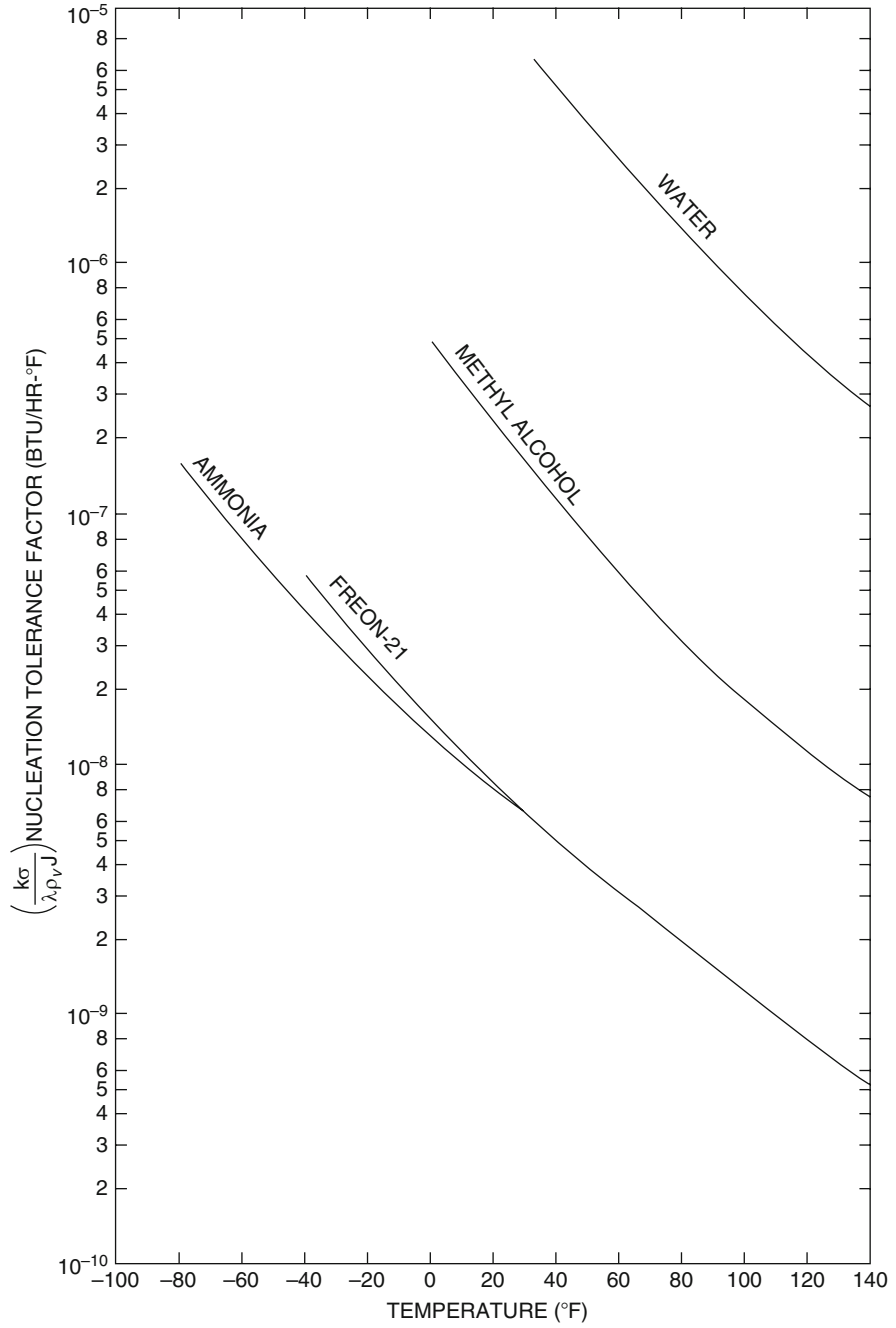


Fig. 2.52 Nucleation tolerance parameter for heat pipe working fluids

2.18.6 *Special Requirements*

In addition to properties which affect the thermodynamic and hydrodynamic performance of heat pipes, there are other factors which can impose severe constraints on fluid selection for particular applications. For example:

- Many applications wherein the heat pipe concept is integrated into the packaging of electronic equipment will require the use of dielectric working fluids.
- Applications of heat pipes on-board manned spacecraft or aircraft may require the use of nontoxic and/or nonflammable working fluids.

2.18.7 *Materials Compatibility and Stability*

A major factor in selection of working fluids is their stability and compatibility with other materials in the heat pipe system. Certain low-temperature heat pipes, of the type applicable to spacecraft thermal control, are subject to continuous performance degradation as a result of:

1. Chemical reaction or decomposition of the working fluid
2. Corrosion or erosion of the container and wick

Chemical reaction or decomposition of the working fluid may result in non-condensable gas evolution (e.g., H_2 , N_2 , O_2). A specific example of this is the hydrolysis of water-yielding hydrogen gas when one attempts to build a water–aluminum heat pipe. In an ordinary heat pipe, all non-condensable gas is swept to the condenser end, forming a diffusion barrier to vapor flow and effectively reducing the available condenser area. In gas-controlled, variable conductance heat pipes, the generation of additional, non-condensable gas raises the operating temperature of the heat pipe above design conditions. Similar effects can result from a change in the chemical composition of the working fluid by virtue of a change in its vapor pressure as a function of temperature.

Corrosion and erosion of the container and wick can be manifested as a change in the wetting angle of the working fluid as well as the permeability, porosity, or capillary pore size of the wick. Solid precipitates resulting from corrosion and erosion are transported by the flowing liquid to the evaporator region where they are deposited when the liquid vaporizes. This leads to an increased resistance to fluid flow in the evaporator, resulting in a decrease in the heat transport capacity of the heat pipe.

At this point in time, there does not appear to exist any generally satisfactory way to predict stability or compatibility under arbitrary operational conditions. Consequently, faced with the need for such information, many heat pipe laboratories have run extensive test programs to empirically establish stable material combinations and processing variables. For more details, refer to Marcus [63] report.

In summary, the first consideration in the identification of a suitable working fluid is the operating vapor temperature range. Within the approximate temperature band, several possible working fluids may exist, and a variety of characteristics

must be examined in order to determine the most acceptable of these fluids for the application considered. The prime requirements are:

- Compatibility with wick and wall materials
- Good thermal stability
- Wettability of wick and wall materials
- Vapor pressure not too high or low over the operating temperature range
- High latent heat
- High thermal conductivity
- Low liquid and vapor viscosities
- High surface tension
- Acceptable freezing or pour point

The selection of the working fluid must also be based on thermodynamic considerations which are concerned with the various limitations to heat flow occurring within the heat pipe like viscous, sonic, capillary, entrainment, and nucleate boiling levels.

In heat pipe design, a high value of surface tension is desirable in order to enable the heat pipe to operate against gravity and to generate a high capillary driving force. In addition to high surface tension, it is necessary for the working fluid to wet the wick and the container material, i.e., contact angle should be zero or very small. The vapor pressure over the operating temperature range must be sufficiently great to avoid high vapor velocities, which tend to set up large temperature gradient and cause flow instabilities.

A high latent heat of vaporization is desirable in order to transfer large amounts of heat with minimum fluid flow and hence to maintain low pressure drops within the heat pipe. The thermal conductivity of the working fluid should preferably be high in order to minimize the radial temperature gradient and to reduce the possibility of nucleate boiling at the wick or wall surface. The resistance to fluid flow will be minimized by choosing fluids with low values of vapor and liquid viscosities. Tabulated below are a few mediums with their useful ranges of temperature.

Medium	Melting pt. (°C)	Boiling pt. at atm. pressure (°C)	Useful range (°C)
Helium	-271	-261	-271 to -269
Nitrogen	-210	-196	-203 to -160
Ammonia	-78	-33	-60 to 100
Acetone	-95	57	0-120
Methanol	-98	64	10-130
Flutec PP2	-50	76	10-160
Ethanol	-112	78	0-130
Water	0	100	30-200
Toluene	-95	110	50-200
Mercury	-39	361	250-650
Sodium	98	892	600-1200
Lithium	179	1340	1000-1800
Silver	960	2212	1800-2300

2.19 Heat Pipe Startup Characteristic and Control

Predicting the heat pipe startup behavior is not a very easy procedure to do and may vary based on many factors such as working fluid and wick structure and its configuration. The effect of these factors has been studied by many researchers and startup performance has been identified qualitatively, while a general description of this phenomenon has been obtained [14, 26, 48].

During startup, vapor must flow at a relatively high velocity to transfer heat from the evaporator to the condenser side of the heat pipe, and the pressure drop through the central channel of it will be large. Since the axial temperature gradient in a heat pipe is determined by the vapor pressure drop, the temperature of the evaporator will be initially much higher than that of the condenser. The temperature level reached by the evaporator will be driven by fluid that has been used as part of design criteria for working fluid. If the heat input is large enough, a temperature front will gradually move towards the condenser section. During normal heat pipe startup, the temperature of the evaporator will increase by a few degrees until the front reached the end of the condenser. At this point, the condenser temperature will increase until the pipe structure becomes almost isothermal (when lithium or sodium is used as working fluids, this process occurs at temperature levels where the heat pipe becomes red hot, and the near isothermal behavior is visible).

Heat pipes with screen-covered channels behave normally during startup as long as heat is not added too quickly. Kemme [74] found that heat pipes with open channels did not exhibit straightforward startup behavior. Very large temperature gradients were measured, and the isothermal state was reached in a peculiar manner.

In some instances during startup, when the vapor density is low and its velocity is high, the liquid can be prevented from returning to the evaporator. This is more likely to occur when open return channels are used for liquid transfer than when porous media are used.

Further work by van Andel [75] on heat pipe startup has enabled some quantitative relationships to be obtained which assist in ensuring that satisfactory startup can occur. This is based on the criterion that burnout does not occur, i.e., the saturation pressure in the heated zones should not exceed the maximum capillary force. If burnout is allowed to occur, drying of the wick results, inhibiting the return flow of liquid.

A relationship that gives the maximum allowable heat input rate during the startup condition is

$$Q_{\max} = 0.4\pi r_c^2 \times 0.73(P_E \rho_E) \quad (\text{Eq.2.117})$$

where

- r_c = vapor channel radius,
- L = latent heat of vaporization,
- P_E = vapor pressure in the evaporator, and
- ρ_E = vapor density in the evaporator.

It is important to meet the startup criteria when a heat pipe is used in an application that may involve numerous starting and stopping actions, for example, in cooling a piece of electronic equipment or cooling brakes. One way in which the problem can be overcome is to use an extra heat source connected to a small branch heat pipe when the primary role of cooling is required, thus reducing the number of startup operations [5]. The startup time of gas-buffered heat pipes is quicker.

Busse [76] has made a significant contribution to the analysis of the performance of heat pipes, showing that before sonic choking occurs, a viscous limitation that can lie well below the sonic limit can be met. Where it is required to calculate transient behavior of heat pipes during startup and in later transient operation, time constants and other data may be calculated using equations presented in Ref. [77].

2.19.1 Transient of Heat Pipe Startup Characteristic and Control

An important problem of the all two-phase thermal transport devices is their startup characteristics. In the design of heat pipes, consideration must be given not only to the internal structure and fluid dynamics of the pipe but also to the external conditions imposed upon it. An understanding of both the conditions under which a heat pipe may be successfully started and of the various phenomena that may inhibit startup is important in the practical use of the heat pipes under normal operation. The transient behavior and problems of heat pipe startup have been studied and tested by different authors [14, 26, 78, 79].

The transient behavior of a heat pipe depends on the pipe structure, the vapor pressure of the working fluid at sink temperature, and the thermal resistance between the pipe and its heat sink at the condenser. Common modes of the startup can best be described by considering a heat pipe starting at sink temperature with a heat load increasing slowly from zero. Under these conditions, the characteristics of the heat pipe at different times can be approximated by those that occur at the steady state. Figure 2.53 below shows schematically the failure of a heat pipe at startup when the vapor pressure of the pipe working fluid at the temperature of the heat sink and interface thermal resistance at the condenser are both very low [18]. Because of the low thermal resistance of the interface, the increase in heat load with time fails to raise the temperature (and consequently the pressure and density) of the vapor at the condenser. Low vapor density results in sonic flow at the evaporation exit and supersonic flow and compression shock in the condenser. With the increase in heat load, these high vapor velocities eventually sweep the liquid out of the wick structure, causing the evaporator to dryout and overheat.

A second mode of startup is presented in Fig. 2.54, and it occurs when the vapor pressure is high at the sink temperature. The high vapor pressure results in both a small vapor velocity and temperature drop. For a two-phase heat pipe system, the temperature is related to the pressure. Hence, temperature of the heat pipe remains

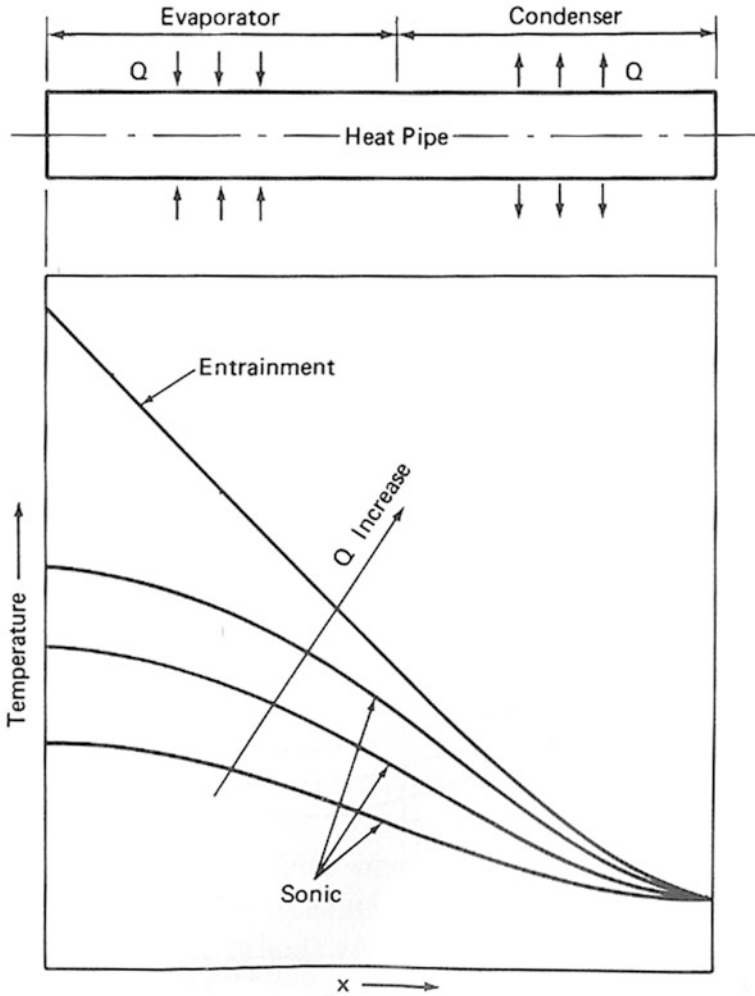


Fig. 2.53 Startup failure due to low vapor pressure at the sink temperature and low condenser thermal resistance [18]

essentially uniform at the startup and increases with time and the heat load. Under these conditions, the heat load of the pipe can, therefore, always be increased until the designed operating condition is achieved.

A third mode of startup is shown in Fig. 2.54. Here, the vapor pressure at the sink temperature is low, but the interface thermal resistance between the condenser and heat sink is high. In this case, the sonic and supersonic flow may exit at initial stages of the setup, because of low vapor pressure at sink temperature. As heat load increases, the condenser temperature and consequently vapor pressure also rises because of high interface resistance. The increase in vapor pressure reduces the vapor velocity at the evaporator exit. This enables the heat pipe to move through the

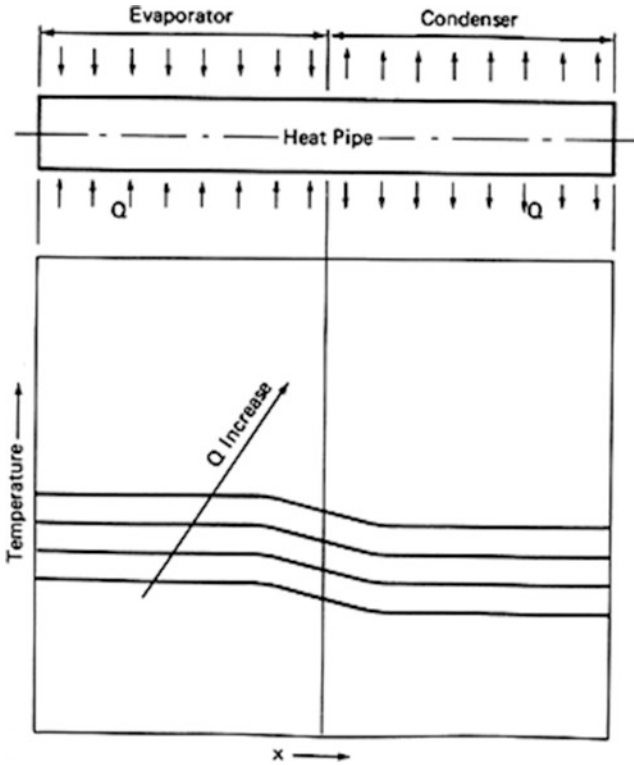


Fig. 2.54 Successful startup of a heat pipe with high vapor pressure at the sink temperature [18]

sonic regime toward the isothermal regime of Fig. 2.55. Thereafter as the heat load increases, the temperature of the pipe remains essentially uniform and rises in magnitude. Hence, the design heat load can be achieved for the pipe in this case. The presence of non-condensable gas in a heat pipe has the effect of increasing the interface thermal resistance at the condenser section of the heat pipe. With further increases in the heat load resulting to vapor temperature and pressure, the non-condensable gas is compressed more toward the end of the pipe condenser. The heat pipe operation remains essentially isothermal except for the portion blocked by the gas. This produces a startup in the form of a wave front moving along the heat pipe as the heat load is increased. With the non-condensable gas (variable heat pipe), successful startup can be achieved even though the heat sink is closely coupled to the condenser with small interface thermal resistance [18].

The four modes of startup shown in Figs. 2.53, 2.54, 2.55, and 2.56 are described above with reference to the working fluid in the liquid phase at startup. For the startup of a water heat pipe from subzero temperatures or an alkali metal heat pipe from ambient temperature, the working fluid will be in the solid state. A startup from the pipe working fluid in the solid state is again a function primarily of the sink temperature and interface thermal resistance at the condenser. The thermal

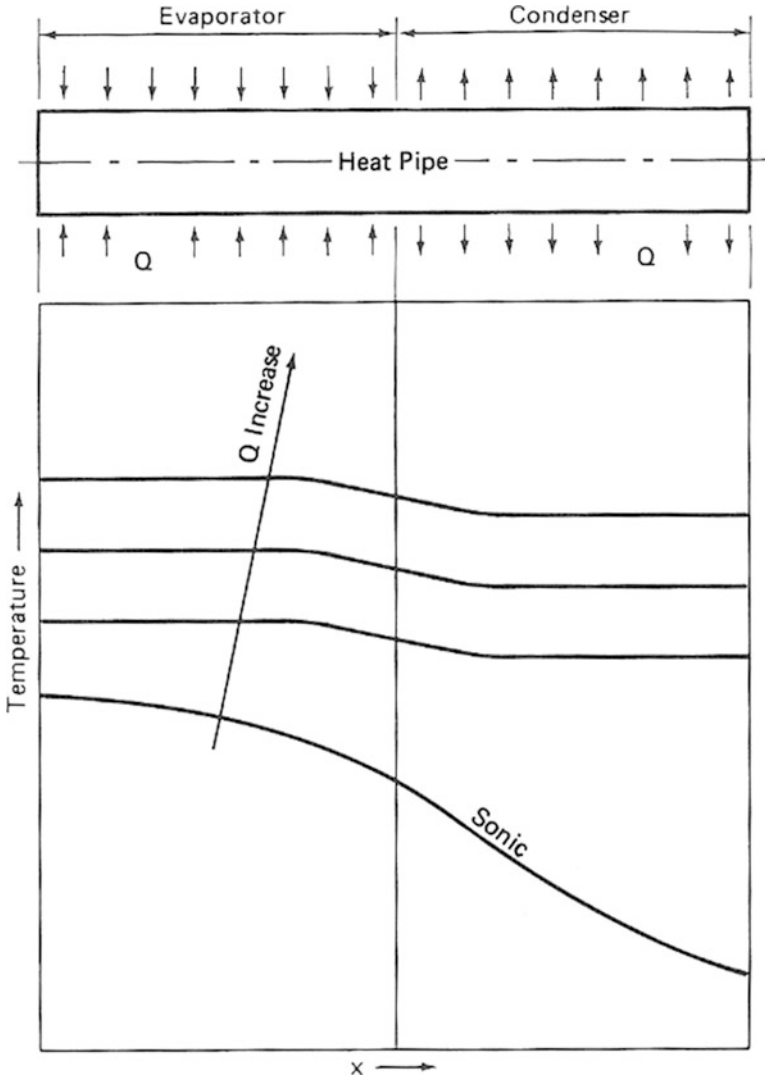


Fig. 2.55 Successful startup of a heat pipe with lower vapor pressure at the sink temperature but high condenser thermal resistance [18]

resistance must be high enough to enable the heat that is transferred to melt the fluid in the condenser and allow liquid to return through the wick structure before the evaporator is depleted of fluid. A small amount of non-condensable gas in the heat pipe also aids in the startup by retarding the vapor flow so that melting of the solid is done progressively along the heat pipe [18].

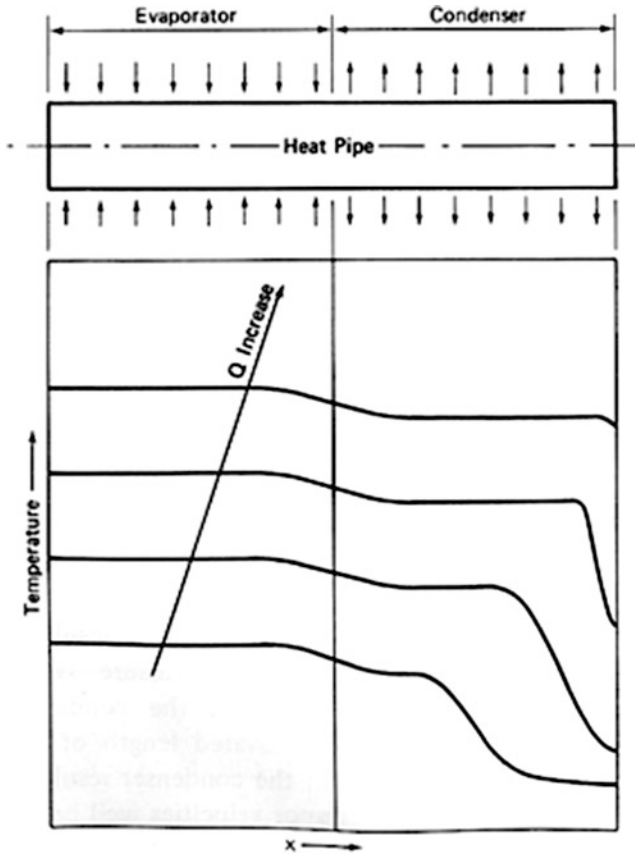


Fig. 2.56 Frontal startup with a non-condensable gas in the pipe [18]

In conclusion, the startup of a heat pipe from high vapor pressure does not present a special problem. However, the startup of a heat pipe with an initial low vapor pressure generally involves high vapor velocities, and in many cases, the velocity can be sonic or supersonic. This results in choked flow and a large temperature gradient along the heat pipe. The sonic limit in itself does not inhibit the startup. Under certain conditions, however, high vapor velocity sweeps liquid out of the wick and disrupts fluid circulation, and startup becomes impossible. Even though a pipe could perform properly at design condition, it may not be possible to reach the design level. A common cause for the failure of a heat pipe to startup is due to an initial low vapor pressure at startup accompanied by low interface thermal resistance at the condenser. One method to aid in the startup is to add a small amount of inert non-condensable gas to the pipe. The gas has the effect of increasing the interface thermal resistance at the condenser during startup [18].

2.19.2 Normal Startup Characteristic

Early analytical papers written around heat pipes and their transient characteristic (thermosyphon), by Cotter [26] and others, identified three fundamental startup modes, and they were described in previous section. These three fundamental startup modes are known as uniform startup, frontal startup, and frontal startup with a non-condensable gas (NCGs), and they schematically were shown in Figs. 2.52, 2.53, and 2.54, where the numbers indicate increasing time from startup.

Uniform startup occurs when the vapor density is high at ambient temperature. In this case, the initial vapor density is high enough that a uniform or nearly uniform temperature exists prior to and throughout the start period (see Fig. 2.52). This condition typically occurs during startup of heat pipes with cryogenic working fluids.

Frontal startup occurs where the initial vapor density is low, as represented by Fig. 2.53. In this mode compressible flow effects may be important, and sonic velocities are likely to occur during the initial phase due to large axial temperature variations in the vapor.

Frontal startup with NCGs characteristic startup curves are illustrated in Fig. 2.54 where a non-condensable gas has a presence. As it is shown, the movement of the vapor results in the NCG being swept toward the condenser. As the average operating temperature (adiabatic vapor temperature) increases, the NCG front is slowly compressed, blocking a smaller and smaller portion of the condenser [17].

2.19.3 Frozen and Startup Characteristic

Generally speaking, the fundamental principles involved in the steady-state and transient operation of heat pipes are relatively well understood by different authors and researchers in field of heat pipes. However, several phenomena commonly found in heat pipe operations have not been fully investigated, including transient processes of freezing and restart from the frozen state. Experimental data exist primarily from investigations conducted on liquid–metal heat pipes, as these designs must at one point always start from working fluid configuration on restart [17]. Although heat pipes that utilize working fluids such as water and ammonia would normally not freeze during standard operation or manufacturing, several situations arise where the freeze–thaw behavior is important [80].

Three types of freezing startup within a heat pipe have been introduced by Antoniuk and Edwards [81], which are defined below:

- Suction freeze-out
- Freezing blow-by
- Diffusion freeze-out

Each of these phenomena in summary is described below:

Suction freeze-out: Is the freezing of the fluid and corresponding depletion of the available liquid inventory in the active region of the heat pipe.

Freezing blow-by: Corresponds to a phenomenon occurring when a complete solid blockage of the vapor and liquid passages is thawed. During melting of the blockage and a low pressure region (evaporator) exists on one side of the blockage and a low pressure region (condenser) exists on the other. When breakthrough of the blockage occurs, liquid is rapidly driven from the higher pressure evaporator into the lower pressure condenser region and may result in rapid dryout of the evaporator wicking structure.

Diffusion freeze-out: Is the freezing of the working fluid that diffuses from the vapor located in the condenser region into the portion of the condenser blocked by non-condenser gas (NDGs) and also presented by Edwards and Marcus [82].

The ability to restart a frozen heat pipe has been discussed by Chi [18] and Ivanovskii et al. [31] as being a direct function of the condenser heat removal rate, heat pipe geometry, working fluid, and condenser-to-evaporator-length ratio. In summary, both sources also noted that the addition of NCGs would aid in the startup due to a progression of the melt front along the length of the heat pipe. Neither source, however, discuss the process of the working fluid freezing, and both assume an essentially uniformly distributed working fluid in the discussions of frozen startup.

Experimental investigation of frozen startup of liquid–metal heat pipes has been conducted by several investigators, including Maerrigan et al. [83], for a molybdenum–lithium heat pipe with varying radiation heat rejection rates during freezing of the working fluid.

With regard to room temperature working fluids of the type more commonly encountered in electronics applications, several investigations have been conducted. Deverall et al. [14] conducted an experimental investigation of frozen startup with a water heat pipe.

Abramenko et al. [84] performed an experimental investigation using an aluminum–ammonia heat pipe with radiation heat rejection, thus resulting in conditions similar to those found in spacecraft thermal control systems. Startup from the frozen state was obtained only after the radiative sink temperature was increased, thus reducing the heat rejection rate at the condenser.

Two recent numerical investigations have been presented that examine the startup of frozen heat pipe. The numerical model of Bowman [85] was compared with experimental data obtained for a copper–water heat pipe and a molybdenum–lithium heat pipe. A more extensive finite element numerical model has been presented by Jang et al. [86] in which both the free molecular flow and continuum flow regimes were examined. This model was used to simulate the startup of a frozen stainless steel–sodium heat pipe, but was not compared with any experimental data.

Startup is best accomplished by using a working fluid which is initially saturated. When this is not possible, as in the case of many cryogenic or liquid–metal heat pipes, the wick should be designed to give good transport during the priming operation. When a variable conductance heat pipe is required, the transient behavior will depend to a large extent on the type of VCHP employed and the choice of the working fluid.

2.20 Summary

In summary for any heat pipe design and its application, certain criteria have to be met, and heat transfer limitations should be considered to make sure the heat pipe works within its design specification and follows its normal operation. Faghri [9] has done an excellent job to summarize these limits and they are reflected here as well. Although heat pipes are very efficient heat transfer devices, they are subject to a number of heat transfer limitations as they were described in various sections of this chapter. These limitations determine the maximum heat transfer rate a particular heat pipe can achieve under certain working conditions. The type of limitation that restricts the operation of the heat pipe is determined by which limitation has the lowest value at a specific heat pipe working temperature. The possible limitation on maximum axial heat transfer rate is shown schematically in Fig. 2.57 below as a function of heat pipe working temperature and are briefly described [9]:

1. **Continuum flow limits:** For small heat pipe, such as micro-heat pipes that are used in electronic application and for cryogenic (operating at very low temperature) heat pipes, the vapor flow in the heat pipe may be in the free molecular or

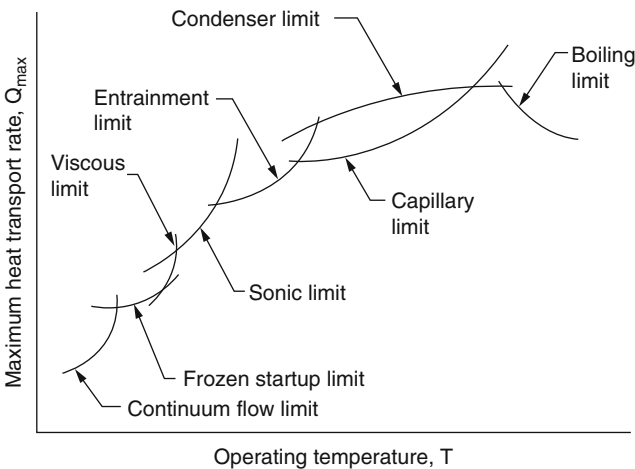


Fig. 2.57 Maximum heat transfer limitation for a heat pipe as a function of operating temperature [9]

rarefied condition. The heat pipe transport capability under this condition is limited because the continuum vapor state has not been reached.

2. **Frozen startup limit:** During any startup process from the frozen state, vapor from the evaporation zone may be frozen in the adiabatic or condensation zones. This may deplete the working fluid from the evaporation zone and cause dryout of the evaporator.
3. **Viscous limit:** When the viscous forces dominate the vapor flow, as for a liquid–metal heat pipe, the vapor pressure at the condenser end may reduce to zero. Under this condition, the heat transport of the heat pipe may be limited. A heat pipe operating at temperature below its normal operating range can encounter this limit, which is also known as the vapor pressure limit.
4. **Sonic limit:** This limit is also known as choking limit, and for some heat pipes, especially those operating with liquid–metal working fluids, the vapor velocity may reach sonic or supersonic values during the startup or steady-state operation. This choked working condition is called the sonic limit.
5. **Entrainment limit:** When the vapor velocity in the heat pipe is sufficiently high, the shear force existing at the liquid–vapor interface may tear the liquid from the wick surface and entrain it into the vapor flow stream. This phenomenon reduces the condensate return to the evaporator and limits the heat transport capability.
6. **Capillary limit:** For a given capillary wick structure and working fluid combination, the pumping ability of the capillary structure to provide the circulation for a given working medium is limited. This limit is usually called the capillary or hydrodynamic limit.
7. **Condenser limit:** The maximum heat rate capable of being transported by a heat pipe may be limited by the cooling ability of the condenser. The presence of non-condensable gases can reduce the effectiveness of the condenser (i.e., variable heat pipes).
8. **Boiling limit:** If the radial heat flux or the heat pipe wall temperature becomes excessively high, boiling of the working fluid in the wick may severely affect the circulation of the working fluid and lead to the boiling limit.

Limitations to heat transport arise mainly from the ability of the wick to return condensate to the evaporator and from thermodynamic barriers encountered in the flow of the vapor. A schematic of the limitations to heat transport in a heat pipe is also shown in Fig. 2.56, which is a graph of the axial heat flux versus the overall temperature drop rather than the operating temperature as shown in Fig. 2.58.

Per Faghri [9], when both ends of the heat pipe are at the same temperature, $T_0 = T_L$, where T_0 and T_L are the evaporator and condenser end cap temperatures, no heat is transported. As the temperature drop is increased, the heat transport quickly increases, since the effective thermal conductivity of heat pipes is very high. At point 1, the heat transport can drop suddenly to the value which is transferred by axial conduction in the pipe wall. Point 1 is either the capillary limit, where the wick structure fails to maintain a sufficient amount of condensate return to the evaporator, or the boiling limit, where the pipe wall overheats due to the formation of vapor bubbles in the wick structure. Assuming that the wick does

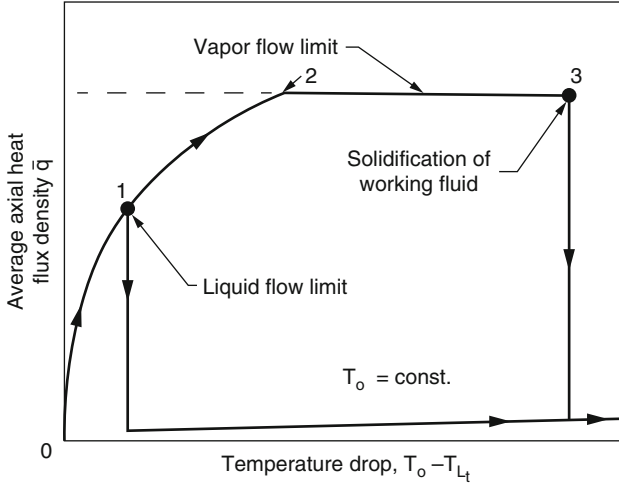


Fig. 2.58 Schematic of the heat transport limitation of a heat pipe [76]

not reach the capillary or boiling limits, the heat transport continues to increase until it levels off at point 2. At point 3, the temperature drop is large enough that the working fluid in the condenser section becomes frozen, and the heat pipe evaporator dries out. This again results in a sudden drop in the heat transport to the level of axial conduction in the wick structure and the pipe wall.

The level portion of the curve between points 2 and 3 is called the vapor flow limit. The vapor flow limit is characterized by the relative magnitude of the viscous and inertia forces on the vapor flow. In the limiting case of negligible viscous forces (inertia flow regime), the vapor flow is limited by the choking phenomenon, where the vapor pressure at the end of the evaporator section is approximately half of that at the upstream end of the evaporator. The vapor flow rate (axial heat flux) can only be increased by increasing the pressure (and therefore temperature) in the evaporator section. This situation is referred to as the sonic limit, since the vapor reaches the local speed of sound at the end of the evaporator.

The other limiting case is when inertia forces are negligible (viscous flow regime). In this situation, the axial heat flux increases with increasing overall pressure drop until the pressure at the condenser end cap reaches essentially zero. At this point, the axial heat flux cannot be increased further, which is called the viscous limit. When both inertia and viscous forces are presented but the inertia forces are dominant, choking again occurs in the heat pipe, but it occurs at the beginning of the condenser section in this case. This is due to the fact that the viscous forces increase the vapor velocity from subsonic at the end of the evaporator to the sonic velocity at the beginning of the condenser (Levy) [87].

Among the heat pipe limitations mentioned above, the capillary, sonic, and boiling limits are most commonly encountered during normal heat pipe operation, and they play major roles in their designs.

References

1. Dhananjay Dilip Odhekar Master of Science, August 8, 2005 (B.E. Mech, K.K.W.C.O.E., University of Pune, 1999).
2. Kishimoto, T. (1994). Flexible-heat-pipe cooling for high-power devices. *The International Journal of Microcircuits and Electronic Packaging*, 17(2), 98–107.
3. Lu, S., & Li, H.-S. (1999). *Oscillatory mode with extremely high heat transfer rate in a flexible heat pipe*. Inter PACK '99: Pacific RIM/A SME International Intersociety Electronics Photonic Packaging Conference 'Advances in Electronic Packaging 1999', Maui.
4. Bliss Jr., F. E., Clark Jr., E. G., & Stein, B. (1970). *Construction and test of a flexible heat pipe*. ASME Conference Paper.
5. Dunn, P. D., & Reay, D. A. (1994). *Heat pipes* (4th ed.). New York: Pergamon.
6. Marcus, B. D. *Theory and design of variable conductance heat pipes: Control techniques*. Research Report 2, Ames Research Center, National Aeronautics and Space Administration. 13111-6027-R0-00.
7. Marcus, B. D. (1971). *Heat pipes: Control techniques*. Report 2, NASA Contract No. NAS2-5503.
8. Bienert, W. (1969). Heat pipes for temperature control. In *Proceedings of the Fourth Intersociety Energy Conversion Conference, Washington, DC* (pp. 1033–1041).
9. Faghri, A. (1995). *Heat pipe science and technology*. Washington, DC: Taylor & Francis.
10. Busse, C. A. (1969). *Heat pipe thermionic converter research in Europe*. Paper #699105, Proc. Fourth Intersociety Energy Conversion Engineering Conf., Washington, DC.
11. Levy, E. K. (1968). Theoretical investigation of heat pipes operating at low vapor pressure. *Journal of Engineering*, 90, 547–552.
12. Wayner Jr., P. C. (1999). *Long range intermolecular forces in change-of-phase heat transfer*. Proc. 33rd National Heat Transfer Conference, Albuquerque, NM, August 15–17, 1999.
13. Kemme, J. E. (1978). Ultimate heat-pipe performance. *IEEE Transaction on Electron Devices*, ED-16, 717–723.
14. Deverall, J. E., Kemme, J. E., & Florschuetz, L. W. (1970, September). *Sonic limitations and startup problems of heat pipes*. Los Alamos Scientific Laboratory Report No. LA-4578.
15. Carey, V. P. (1992). *Liquid-vapor phase-change phenomena*. Washington, DC: Taylor and Francis.
16. Spivak, M. (1999). A comprehensive introduction to differential geometry (3rd ed., Vols. 3–4). Publish or Perish Press, ISBN 0-914098-72-1 (Vol. 3), ISBN 0-914098-73-X (Vol. 4).
17. Peterson, G. P. (1994). *An introduction to heat pipes—Modeling, testing and applications*. New York: John Wiley & Sons.
18. Chi, S. W. (1976). *Heat pipe theory and practice*. New York: McGraw-Hill.
19. Ferrell, K. J., & Alleavitch, J. (1969). *Vaporization heat transfer in capillary wick structures*. Preprint No. 6, ASME-AIChE Heat Transfer Conf., Minneapolis, MN.
20. Eninger, J. E. (1975). *Capillary flow through heat pipe wicks*. Paper No. 75-661. Washington, DC: AIAA. American Institute of Aeronautics and Astronautics.
21. Colwell, G. T., & Chang, W. S. (1984). Measurements of the transient behavior of a capillary structure under heavy thermal loading. *International Journal of Heat and Mass Transfer*, 27 (4), 541–551.
22. Silverstein, C. C. (1992). *Design and technology of heat pipes for cooling and heat exchange*. Washington, DC: Taylor and Francis.
23. Busse, C. A. (1973). Theory of the ultimate heat transfer of cylindrical heat pipes. *International Journal of Heat and Mass Transfer*, 16, 169–186.
24. Wageman, W. E., & Guevara, F. A. (1960). Fluid flow through a porous channel. *Physics of Fluids*, 3(6), 878–881.
25. Mehta, R. C., & Jayachandran, T. (1996). Numerical analysis of transient two phase flow in heat pipe. *Heat and Mass Transfer*, 31, 383–386.

26. Cotter, T. P. (1967). *Heat pipe startup dynamic*. Proc. SAE Thermionic Conversion Specialist Conference, Palo Alto, California.
27. Dunn, P. D., & Reay, D. A. (1982). *Heat pipes* (3rd ed.). New York: Pergamon.
28. Kemme, J. E. (1967). *High performance heat pipe*. Proc. 1967 Thermionic Conversion Specialist Conference, Palo Alto, California, October 1967.
29. Bankston, C. A., & Smith, J. H. (1971). *Incompressible laminar vapor flow in cylindrical heat pipes*. ASME-71-WA/HT-15. New York: ASME.
30. Rohani, A. R., & Tien, C. L. (1974). Analysis of the effects of vapor pressure drop on heat pipe performance. *International Journal of Heat and Mass Transfer*, 17, 61–67.
31. Ivanovskii, M. N., Sorokin, V. P., & Yagodka, I. V. (1982). *The physical properties of heat pipes*. Oxford: Clarendon.
32. Vinz, P., & Busse, C. A. *Axial heat transfer limits of cylindrical sodium heat pipes between 25 W-cm⁻² and 15.5 kW-cm⁻²*. Proc. 1st International Heat Pipe Conference, Stuttgart, Germany, Paper 2-1.
33. Kroliczek, E. J., & Brennan, P. J. (1983). *Axial grooved heat pipes—Cryogenic through ambient*. ASME Paper 73-ENAc-48. Presented at the Intersociety Conference on Environmental System, San Diego, California 1983.
34. Alario, J., Brown, R., & Kosson, R. (1983). *Monogroove heat pipe development for the space constructible radiator system*. AIAA-83-1431. Presented at the AAIA 18th Thermophysics Conference, Montreal, Canada, June 1983.
35. ICICLE Feasibility Study, Final Report, NASA Contract NAS 5-21039, RCA-Defense Electronic Product, Camden, New Jersey, NASA-CR-112308.
36. Shah, R. K., & Giovannelli, A. D. (1988). Heat pipe heat exchanger design theory. In R. K. Shah, E. C. Subbarao, & R. A. Mashelkar (Eds.), *Heat transfer equipment design*. Washington, DC: Hemisphere Publishing.
37. Hendrix, W. A. (1989). *An analysis of body force effects on transient and steady-state performance of heat pipes*. Ph.D. Dissertation, Georgia Institute of Technology.
38. Cassel, S. D. (1991). *The effect of increasing length on the overall conductance and capacitance of long heat pipes*. Ph.D. Dissertation, Georgia Institute of Technology.
39. Wells, K. J., Colwell, G. T., & Berry, J. T. (1985). Two-dimensional numerical simulation of casting solidification with heat pipe controlled boundary conditions. *America Foundryman's Society Transactions*, 1, 84–95.
40. Modlin, J. M., & Colwell, G. T. (1992). Surface cooling of scramjet engine inlets using heat pipe, transpiration, and film cooling. *AIAA Journal of Thermophysics and Heat Transfer*, 6(2), 500–504.
41. Ingram, T. J., Haman, L. L., Andes, G. M., Colwell, G. T., & Wepfer, W. J. (1984). *Non-metallic heat pipes for flue gas reheat*. Report No. 84-JPGC-APC-7. New York: American Society of Mechanical Engineers.
42. Kays, M. W. (1966). *Convective heat and mass transfer*. New York: McGraw-Hill.
43. Marcus, B. D. (1972, April). *Theory and design of variable conductance heat pipes*. NASA CR-2018.
44. Brennan, P. J., & Kroliczek, E. J. (1979). *Heat pipe design handbook* (Vols. I and II). Contract Report No NAS5-23406. Washington, DC: National Aeronautics and Space Administration.
45. Luikov, A. V. (1972). *Heat and mass transfer in capillary-porous bodies*. London: Pergamon Press.
46. Bird, R., Stewart, W., & Lightfoot, E. (1960). *Transport phenomena*. New York: John Wiley & Sons.
47. Von Karman, T. (1935). The problem of resistance in compressible fluids. In *Proc. 5th Volta Congr., Rome*, November 1935 (pp. 255–264).
48. Busse, C. A. (1967). Pressure drop in the vapor phase of long heat pipes. In *Proceedings of the IEEE International Thermionic Conversion Specialist Conferences*. New York: IEEE.
49. Cotter, T., Grover, G., & Erickson, G. (1964). Structures of very high thermal conductance. *Journal of Applied Physics*, 35(6), 1990–1991.

50. Hwang, G. S., Kaviany, M., Anderson, W. G., & Zuo, J. (2007). Modulated wick heat pipe. *International Journal of Heat and Mass Transfer*, 50, 1420–1434.
51. Anderson, W. G., Sarraf, D., & Dussinger, P. M. (2005). Development of a high temperature water heat pipe radiator. In *Proceedings of the International Energy Conversion Engineering Conference (IECEC), San Francisco*, ISBN 1563477696.
52. Anderson, W. G., Bonner, R., Hartenstine, J., & Barth, J. (2006). High temperature titanium–water heat pipe radiator. In *Space Technology & Applications International Forum (STAIF) Conference* (Vol. 813, pp. 91–99). New York: American Institute of Physics.
53. Alario, J., Haslett, R., & Kosson, R. (1981). *The monogroove high performance heat pipe*. AIAA-81-1156. New York: American Institute of Aeronautics and Astronautics.
54. Alario, J., Brown, R., & Kosson, R. (1983). *Monogroove heat pipe development for the space constructible radiator system*. AIAA-83-1431. Presented at the AIAA 18th Thermophysics Conference, Montreal, Canada, June 1983.
55. Mai, T. D., Chen, A. L., Sifuentes, R. T., & Cornwell, J. D. (1994, June). *Space constructible radiator (Scr) life test heat pipe performance testing and evaluation*. Document Number: 941437.
56. Alario, J., Haslett, R., & Kossor, R. (1981). *The monogroove high performance heat pipe*. AIAA-81-1156. New York: American Institute of Aeronautics and Astronautics.
57. Loh, C. K., Harris, E., & Chou, D. J. (2005). Comparative study of heat pipes performances in different orientations. In *Semiconductor Thermal Measurement and Management Symposium, 2005 I.E. Twenty First Annual IEEE*, 15–17 March 2005 (pp. 191–195).
58. Riehl, R. R., & dos Santos, N. *Loop heat pipe performance enhancement using primary wick with circumferential grooves*. National Institute for Space Research, Space Mechanics and Control Division, DMC/Satélite, Av. dos Astronautas 1758, 12227-010 São Jose dos Campos, SP, Brazil.
59. Hsu, H.-C. (2005, November 10). *Wick structure of heat pipe*. United States Patent number US 2005/0247436 A1.
60. Sarraf, D. B., & Anderson, W. G. *High-temperature water heat pipes*. Advanced Cooling Technologies, Inc. 1046 New Holland Ave. Lancaster, PA 17601.
61. Goring, R. L., & Churchill, S. W. (1961). Thermal conductivity of heterogeneous materials. *Chemical Engineering Progress*, 57(7), 53–59.
62. Chi, S. W. (1971). *Mathematical modeling of high and low temperature heat pipes*. George Washington University Report to NASA, Grant No. NGR bzohu00 09-010-070, December 1971.
63. Marcus, B. D. (1972, April). *Theory and design of variable conductance heat pipes*. Report No. NASA CR, 2018, National Aeronautics and Space Administration, Washington, DC.
64. Wallis, G. B. (1969). *One-dimensional two-phase flow*. New York: McGraw-Hill.
65. Griffith, P., & Wallis, J. D. (1960). *The role of surface conditions in nucleate boiling*. ASME-AIChE Heat Transfer Conference, August 1959. Published in Chemical Engineering Progress Symposium Series (Vol. 56). AIChE.
66. Rohsenow, W. M., & Choi, M. (1961). *Heat, mass, and momentum transfer*. Englewood Cliffs, NJ: Prentice-Hall.
67. Busse, C. A. (1967). *Pressure drop in the vapor phase of long heat pipes*. Palo Alto, CA: Thermionic Conversion Specialists.
68. Bystrov, P. I., & Popov, A. N. (1978). *International Heat Pipe Conference, 3rd, Palo Alto, Calif., May 22–24, 1978*. Technical Papers. (A78-35576 14-34) (pp. 21–26). New York: American Institute of Aeronautics and Astronautics.
69. Ochterbeck, J. M. (2003). Heat pipes, Chapter 16. In A. Bejan & A. D. Kraus (Eds.), *Heat transfer handbook*. Hoboken, NJ: John Wiley & Sons.
70. Phillips, E. C. *Low-temperature heat pipe research program*. NASA Report No. NASA CR-66792.
71. Gerrels, E. E., & Larson, J. W. (1971). *Brayton cycle vapor chamber (heat pipe) radiator study*. NASA CR-1677.

72. Joy, P. (1970). *Optimum cryogenic heat pipe design*. ASME Paper 70-HT/SpT-7. New York: American Society of Mechanical Engineers.
73. Bergles, A. E., & Rohsenow, W. M. (1954). A.S.M.E. Transaction, Journal of Heat Transfer. *Transactions of ASME* 76, 553–562.
74. Kemme, J. E. (1966, August). *Heat pipe capability experiments*. Los Alamos Scientific Laboratory, Report LA-3585.
75. Van Andel, E. (1969). *Heat pipe design theory*. Euratom Center for Information and Documentation. Report EUR No. 4210 e, f.
76. Busse, C. A. (1973). Theory of the ultimate heat transfer limit of cylindrical heat pipes. *International Journal of Heat and Mass Transfer*, 16, 169–186.
77. Anon. (1980). *Heat pipes—General information on their use, operation and design*. Data Item No. 80013, Engineering Sciences Data Unit, London.
78. Faghri, A. (1974). *Continuum transient and frozen funding numbers startup behavior of conventional and gas-loaded heat pipes*. Final Report, Department of Mechanical and Materials Engineering Wright State University, Dayton OH, February 1974.
79. Sockol, P. M., & Forman, R. *Re-examination of heat pipe startup*. NASA Lewis Research Center, Cleveland, Ohio, Technical Paper, NASA TMX-52924.
80. Ochterbeck, J. M., & Peterson, G. P. (1993). Freeze/thaw characteristic of a copper-water heat pipe: Effects of non-condensable gas charge. *AIAA Journal of Thermophysics and Heat Transfer*, 7(1), 127–132.
81. Antoniuk, D., & Edwards, D. K. (1990). *Depriming of arterial gas-controlled heat pipes*. Proc. 7th Int'l Heat Pipe Conf., Minsk, USSR, May 1990.
82. Edwards, D. K., & Marcus, B. D. (1972). Heat and mass transfer in the vicinity of the vapor-gas front in a gas-loaded heat pipe. *ASME Journal of Heat Transfer*, 94, 155–162.
83. Merrigan, M. A., Keddy, S. E., & Sena, J. T. (1985). *Transient heat pipe investigation for space power systems*. Report No. LA-UR-85-3341. Los Alamos, NM: Los Alamos National Laboratory.
84. Abramenko, A. N., Kanonchik, L. E., & Prokhorov, Y. M. (1986). Startup dynamics of an arterial heat pipe from the frozen or chilled state. *Journal Engineering Physics*, 51(5), 1283–1288.
85. Bowman, W. (1990, June). *Transient heat-pipe modeling. The frozen start-up problem*. Paper No. 90-1773, AIAA/ASME 5th Joint Thermophysics and Heat Transfer Conference, Seattle, WA. Washington, DC: American Institute of Aeronautics and Astronautics.
86. Jang, J. H., Faghri, A., Chang, W. S., & Mahefkey, E. T. (1990). Mathematical modeling and analysis of heat pipe start-up from frozen sate. *ASME Journal of Heat Transfer*, 112, 586–594.
87. Levy, E. K. (1971). *Effects of friction on the sonic velocity limit in sodium heat pipes*. Proc. 6th AIAA Thermophysics Conf.

Chapter 3

Mathematical Modeling and Available Computer Codes

Heat pipes and its closed two-phase thermosyphons are highly efficient heat transfer devices utilizing the continuous evaporation–condensation of suitable working fluid for two-phase heat transport in a closed system. Due to a variety of advantageous features, these devices have found a number of applications both in space, terrestrial, nuclear power plant, and electronics technology. The operational principles and the performance characteristics of the different types of heat pipes are described. For the heat pipes designs, which have found the widest application, versus the classical capillary-wick heat pipes and the wickless heat pipes or closed two-phase thermosyphons, mathematical schemes are given to calculate the performance and performance limits in Chap. 2. Here in this chapter, we will discuss the design criteria and steps for a heat pipe depending on its application. This chapter also provides few computer code descriptions that are available from both Galaxy Advanced Engineering and other commercial companies and open source, and the author has identified those codes wherever are appropriate. In this chapter, also few design examples are gathered from different authors or researchers in this field to provide a better guideline and procedures to the readers.

Most of the mathematical modeling, analysis, mechanical, and thermodynamic of design theory of heat pipe can be found in various references and few books that are available in the market as well as Chap. 2. Provided computer code names that are available commercially from various companies and manufactures as well as what are mentioned in this book are subjects of this chapter. Few examples of steps and procedures are also provided in this chapter which are needed to design a conventional heat pipe. The problem statement or specification may indicate the heat source and sink conditions and their physical dimensions and locations. Several combinations of pipe working fluids, wick structure, and container materials are discussed and can often be selected to satisfy the required specifications and operating conditions of the heat pipe. Design theory developed in this chapter will be used to determine the container and wick details so that the heat pipe will operate as specified.

The final results are an output to manufacture and select an optimum design or possibly several suggested designs, which can be presented to the clientele of your operations. These optional solutions combined with computer analysis and results are evaluation criteria that serve as the input to the procedures and support your suggested choice of heat pipe for a given specification and usage of that pipe within the given environment.

3.1 One-Dimensional Models

A heat pipe is a simple device that can quickly transfer heat from one point to another, which is usually used for cooling an electronic component in airconditioners, refrigerators, heat exchangers, transistors, capacitors, etc. Heat pipes are also used in laptops to reduce the working temperature for better efficiency. The design of a heat pipe or the thermosyphon to fulfill a particular duty involved four broad processes:

1. Selection of appropriate type and geometry. Heat pipe geometry such as diameter will be first identified so that the vapor is not excessive.
2. Selection of candidate materials. As a result, the mechanical design should be examined to determine container details.
3. Wick details should be designed considering the capillary limit.
4. Evaluation of performance limits.
5. Other heat transport limits, i.e., entrainment and boiling limits, have to be checked out to ensure that the heat pipe operated within the limits of its specification.
6. Evaluation of the actual performance.

Most of these stages are defined and explained in previous chapters and here we provide computer codes and as well as the practical aspect of the design along with few examples (Fig. 3.1).

Computer programs have been written by various authors or researchers for the design of heat pipe that are described in this chapter. Chi [1, 2] has few computer programs that are very basic but useful. Bienert and Skrabek provided other useful computer codes that should be consulted [3]. At the time of publishing this book, effort was taken by this author in typing the FORTRAN codes from Refs. [1, 2], but

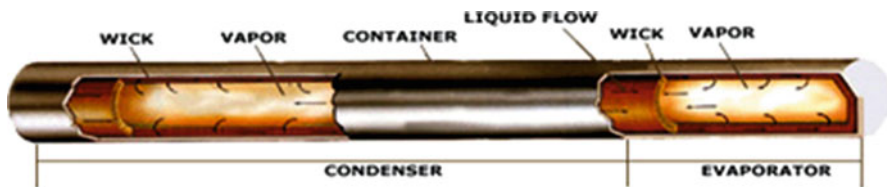


Fig. 3.1 Heat pipe structures (Dynatron Corporation)

the integrity of these codes cannot be guaranteed due to poor quality of the documents which are not clear to read. Whoever is interested to obtain what I have about these codes so far, please reach out to me or consult the web site that is provided by the publisher for this book. I will also be interested in receiving any of these codes, if someone out there has a better version of them, and share it with rest of readers.

3.2 Overview of Heat Pipes

Heat pipes are classified into two general types: “conventional” and “variable conductance.” The conventional heat pipe is a completely passive device. It is not restricted to a fixed operating temperature but adjusts its temperature according to the heat load and the sink condition. Its thermal conductance is very high but, nevertheless, a nearly constant parameter. With minor modifications, the heat pipe can be made a device of variable thermal conductance. There are some means of achieving variable conductance, but they are not discussed in this material. The theory of variable conductance heat pipes is outlined in Chap. 1.

A heat pipe structure is consisting of the following three basic components:

1. Selection of the working fluid
2. Selection of the wick or capillary structure
3. Selection of the container

These three components are the starting point for any designer of a heat pipe and their applications in industry. Choosing the right fluid for a normal operating temperature of a heat pipe combined with right wick materials and structure will allow the designers to start their process of the right selection for the heat pipe.

Operating ranges of heat pipe are shown in Fig. 3.2, and in this content, the operating temperature ranges of heat pipes are referred to as “cryogenic” (0–150 K), “low temperature” (150–750 K) and “high temperature” (750–3000 K).

These ranges have been defined somewhat arbitrarily such that the currently known working fluids are generally the same type within each range, and each range is roughly four times as large as the preceding one.

Working fluids are usually elemental or simple organic gases in the cryogenic range, mainly polar molecules or halocarbons in the low-temperature range and liquid metals in the high-temperature range. The approximate useful range of some working fluids is indicated in Fig. 3.2. The limits of the three regimes as defined above are also indicated. The limits of the ranges should only be considered as approximate since some of the fluids overlap into the next temperature range.

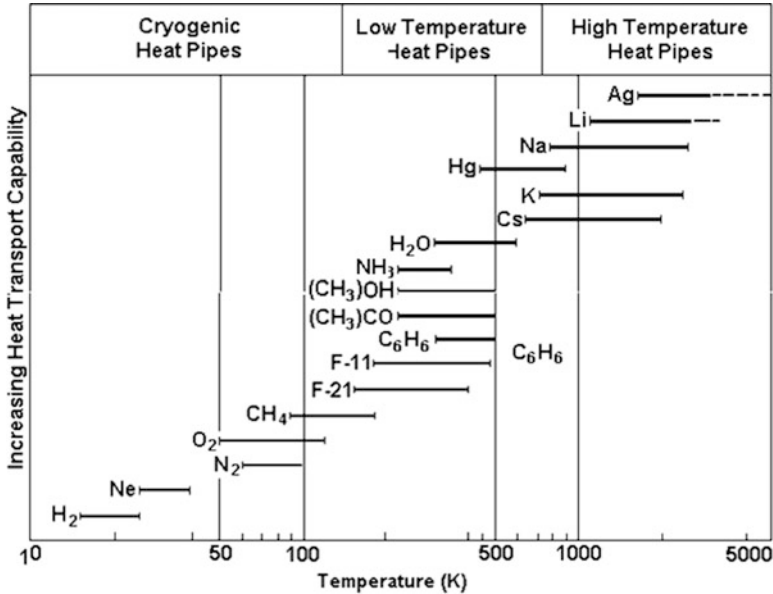


Fig. 3.2 Operating ranges of heat pipe

3.2.1 Selection of the Working Fluid

A first consideration in the identification of a suitable working fluid is the operating vapor temperature range and a selection of fluids is shown in Table 3.1. Within the approximate temperature band several possible working fluids may exist, and a variety of characteristics must be examined in order to determine the most acceptable of these fluids for the application being considered. The prime requirements are as follows:

- Compatibility with wick and wall materials
- Good thermal stability
- Wettability of wick and wall materials
- Vapor pressures not too high or low over the operating temperature range
- High latent heat
- High thermal conductivity
- Low liquid and vapor viscosities
- High surface tension
- Acceptable freezing or pour point.

The selection of the working fluid must also be based on thermodynamic considerations which are concerned with the various limitations to heat flow occurring within the heat pipe.

Note that heat pipes are not functional when the temperature of the pipe is lower than the freezing point of the working fluid. Freezing and thawing is a design issue, which may destroy the sealed joint of a heat pipe when placed vertically. Proper engineering and design can overcome this limitation. Many of the problems

Table 3.1 Heat pipe working fluids [4]

Medium	Melting point (°C)	Boiling point at atmos. press. (°C)	Useful range (°C)
Helium	-271	-261	-271 to -269
Nitrogen	-210	-196	-203 to -160
Ammonia	-78	-33	-60 to 100
Pentane	-130	28	-20 to 120
Acetone	-95	57	0 to 120
Methanol	-98	64	10 to 130
Flutec PP2 ^a	-50	76	10 to 160
Ethanol	-112	78	0 to 130
Heptane	-90	98	0 to 150
Water	0	100	30 to 200
Toluene	-95	110	50 to 200
Flutec PP9 ^b	-70	160	0 to 225
Thermex ^b	12	257	150 to 350
Mercury	-39	361	250 to 650
Cesium	29	670	450 to 900
Potassium	62	774	500 to 1000
Sodium	98	892	600 to 1200
Lithium	179	1340	1000 to 1800
Silver	960	2212	1800 to 2300

^aIncluded for cases where electrical insulation is a requirement

^bAlso known as Dowtherm A, an eutectic mixture of diphenyl ether and diphenyl

associated with long-life heat pipe operation are a direct consequence of material incompatibility as well. For more detailed information, refer to Reay and Kew [4].

3.2.2 Selection of the Wick or Capillary Structure

One of the several factors that influence the selection of heat is a close link between the properties of the working fluid and wick of choice. Based on the discussion and analysis in Chap. 2, the main function of the wick is to generate capillary pressure to transport the working fluid from the condenser to the evaporator. It should be able to handle the distribution of the liquid around the evaporator section to any areas where heat is likely to be received by the heat pipe. Depending on the heat pipe operational environment where there is gravity or not, the two above functions for wick influence the selection of wick type and its structure.

Another feature of the wick which should be considered is its thickness in order to optimize the heat transport capability of heat pipe that is raised by increasing the wick thickness. However, the increased radial thermal resistance of the wick created by this step would work against increased capability and would lower the allowable maximum evaporator heat flux. The overall thermal resistance at the evaporator also depends on the conductivity of the working fluid in the wick. In summary the wick selection is threefold:

1. To provide the necessary flow passage for the return of liquid from the condenser to the evaporator of the heat pipe
2. To provide surface pores at the liquid–vapor interface for the development of capillary pumping pressure
3. To provide a heat flow path from the inner wall of the container to the liquid–vapor interface

In reference to Eq. (3.1) and Fig. 3.6, it can be seen that for a large heat transport capability, the wick structure must have large permeability K and small capillary pore radius r_c . Additionally from Eq. (2.48), it can be seen that the wick permeability, K , is proportional to the product of the porosity ε and the square of the hydraulic radius r_{hi}^2 . Numerous wick structures, both homogeneous and composite, are shown in Fig. 3.3.

The details of different wick descriptions and their structure are given in Chap. 2 and can be found in different references that are provided as well.

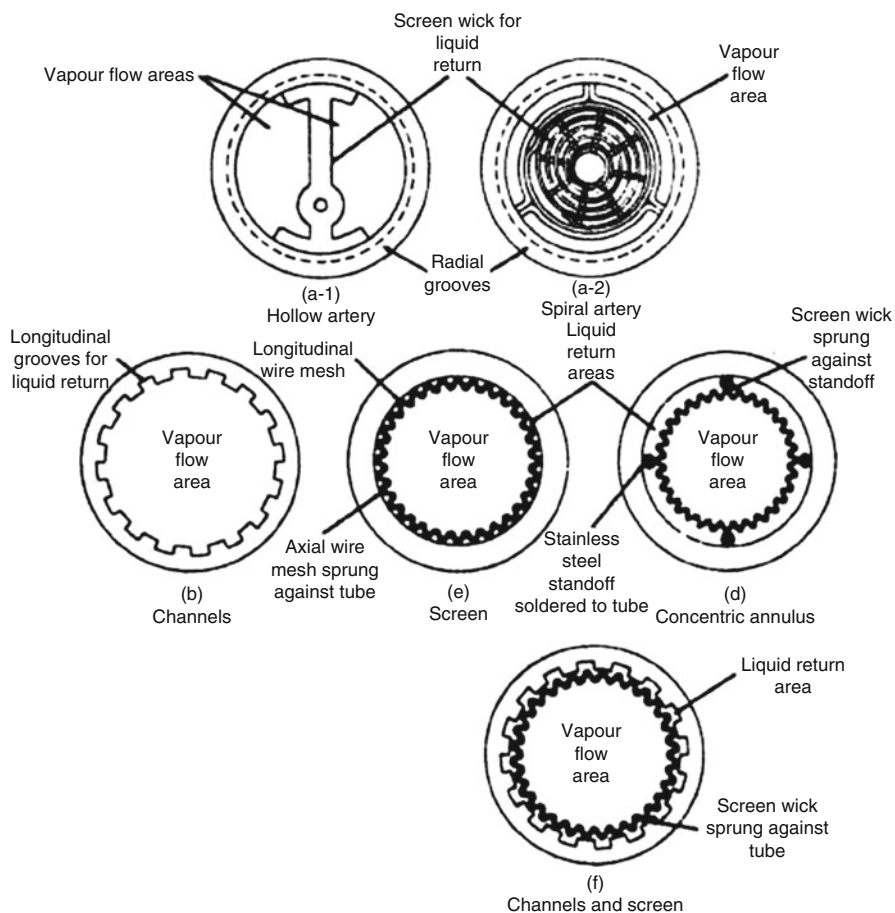


Fig. 3.3 Forms of wick used in heat pipes (Courtesy of NASA)

Table 3.2 Thermal conductivity of heat pipe container and wick materials [4]

Material	Thermal conductivity (W/m °C)
Aluminum	205
Brass	113
Copper (0–100 °C)	394
Glass	0.75
Nickel (0–100 °C)	88
Mild steel	45
Stainless steel (type 304)	17.3
Teflon	0.17

3.2.3 Selection of the Container

The function of the container is to isolate the working fluid from the outside environment. It has, therefore, to be leakproof, to maintain the differential pressure across its walls, and to enable the transfer of heat into and from the working fluid. Selection of the container material depends on several factors [4].

These are as follows:

1. Compatibility (both with working fluid and the external environment)
2. Strength-to-weight ratio
3. Thermal conductivity
4. Ease of fabrication, including weldability, machinability, and ductility
5. Porosity
6. Wettability

Most of these are self-explanatory. A high strength-to-weight ratio is more important in spacecraft applications, and the material should be nonporous to prevent the diffusion of gas into the heat pipe. A high thermal conductivity ensures minimum temperature drop between the heat source and the wick. The thermal conductivity of some wall materials is given in Table 3.2.

3.3 Design Guide and Heat Pipe Selection Criteria

Heat pipes are being used very often in particular applications when conventional cooling methods are not suitable. Once the need for heat pipe arises, the most appropriate heat pipe needs to be selected. Often this is not an easy task, and the following needs to be considered.

It was recognized rather early in the history of the heat pipe research [6] that techniques could be developed which would provide for control of the effective thermal conductance of the heat pipe. This was first envisioned as blocking a portion of the condenser by a non-condensable gas. More recently several other types of control have been developed including liquid blockage and liquid and

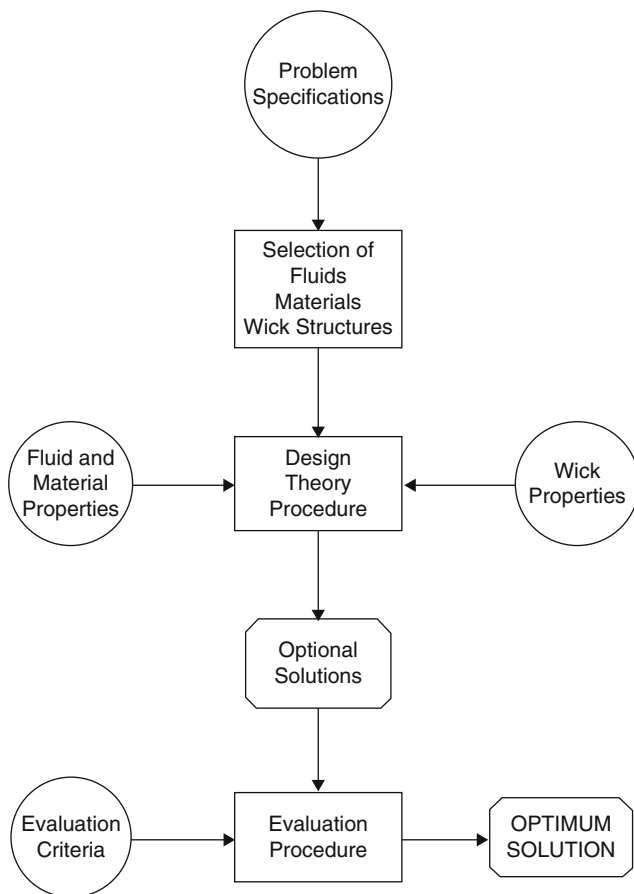


Fig. 3.4 Schematic of a heat pipe design procedure [5]

vapor modulation. Such techniques enable the device to be operated at a fixed temperature independent of source and sink conditions.

The methodology of arriving at the optimum heat pipe design is a complex one, not only because of the mathematical analysis involved but more particularly the many qualitative judgments that must be considered and introduced. Figure 3.4, an illustration by Chi [5], schematically provides a high-level approach and design procedure. Physical properties of several metals and fluids are given in Appendices B and C.

Figure 3.5 shows temperature ranges for several fluids from the melting point to critical temperatures. Because of overlapping of these temperature ranges for different fluids, several fluids can often be used for a given operating temperature. Heat pipe design guidelines in this chapter will provide information on the selection of the pipe working fluids, wick structures, and container materials along with some data that are gathered from various references and researchers reports in this field.

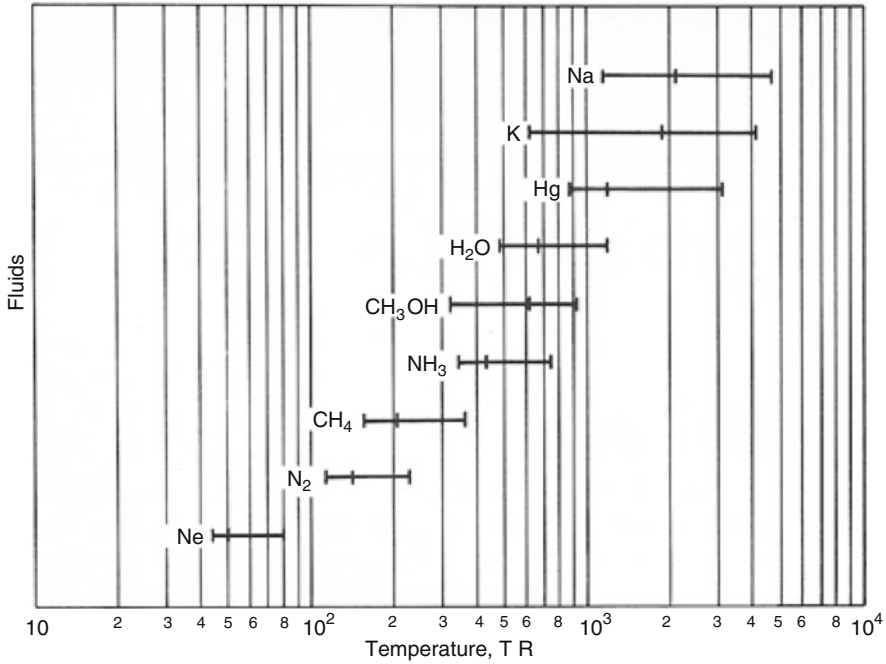


Fig. 3.5 Normal melting point, boiling point, and critical point temperatures for several heat pipe working fluids ($1 R = 0.5556 K$) [5]

A simple approximation theory is developed around a simple cylindrical shape heat pipe operation in a zero-gravity field. The following simplified assumptions also are made [5]:

1. The pipe is capillary limited.
2. Vapor pressure losses are negligible.
3. Wick thickness of t_w is much smaller than the vapor core radius.
4. Heat flux density is uniform at the evaporator or condenser surface.
5. Thermal conductivity of the liquid-saturated wick is proportional to that of the liquid.

The heat transport factor $(QL)_{\text{capillary}_{\text{max}}}$ under the above assumptions can then be written as follows using Eq. (2.81):

$$(QL)_{\text{capillary}_{\text{max}}} = 2 \left(\frac{\sigma \rho_1 \lambda}{\mu_1} \right) \left(\frac{K}{r_c} \right) (2\pi r_w t_w) \tag{Eq.3.1}$$

where

- Q = Heat flow rate
- L = Heat pipe length
- σ = Surface tension coefficient
- ρ_1 = Liquid density
- λ = Latent heat of vaporization

- μ_l = Liquid dynamic viscosity
- K = Wick permeability
- r_c = Effective capability radius
- r_v = Vapor core radius
- t_w = Wick thickness

The first term in bracket represents the liquid property, the second one is the wick property, and the third is the wick cross-sectional area.

Equation (3.1) indicates that for a pipe of fixed wick structure and dimensions, its heat transport factor $(QL)_{\text{capillary max}}$ is proportional to the liquid transport factor N_l , which is defined as $\left(\frac{\sigma \rho_l \lambda}{\mu_l}\right)$. Figure 3.6 shows the values of the liquid transport factor N_l for several fluids. For a maximum temperature gradient of a heat pipe, the temperature drop across the liquid-saturated wick must be minimum. If we further simplify assumptions (3) and (4) that are described above, the temperature drop across the wick is proportional to Qt_w/k_l and can be written as follows [5]:

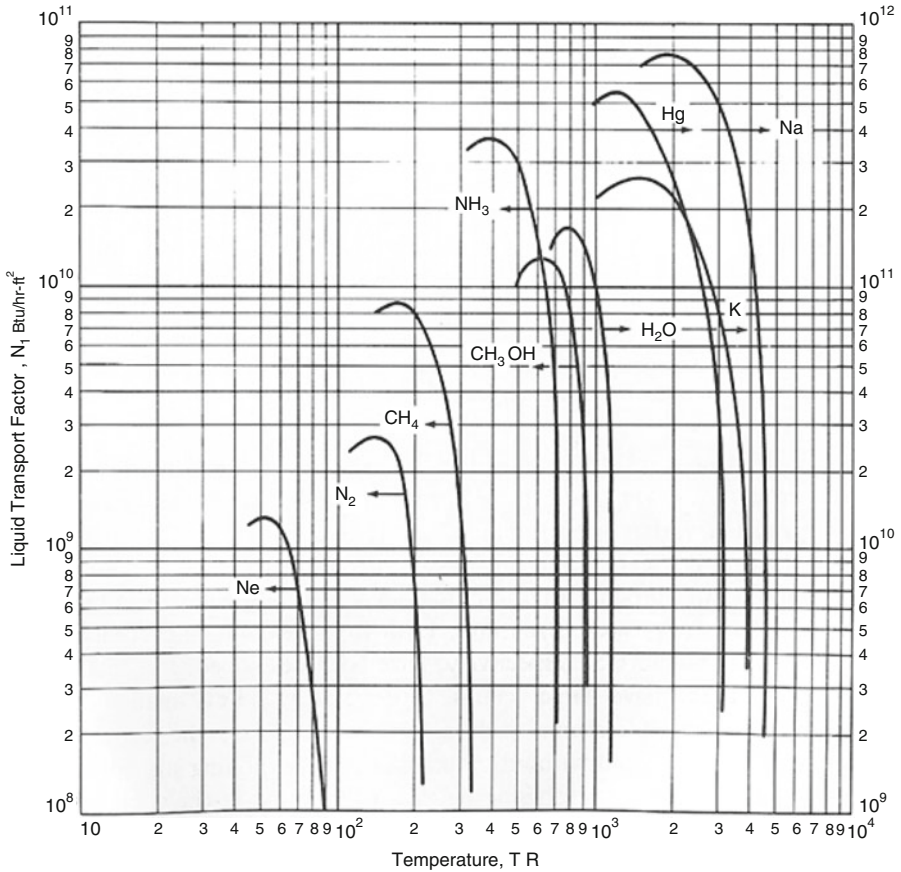


Fig. 3.6 Liquid transport factor versus temperature for several heat pipe working fluids (1 Btu/h ft² = 3.153 W/m²; 1 R = 0.5556 K) [5]

$$\Delta T \propto \frac{Qt_w}{k_1} \tag{Eq.3.2}$$

where k_1 is thermal conductivity of liquid.

Also from Eq. (3.1), we can deduce that the required wick thickness t_w for the same heat transport is inversely proportional to the liquid transport factor N_1 , so the Eq. (3.2) can be written as

$$\Delta T \propto \frac{Q}{k_1 N_1} \tag{Eq.3.3}$$

From this equation, one can induce that the temperature drop across a wick is inversely proportional to the liquid property ($k_1 N_1$), which has been called the liquid conductance factor. The values of the liquid conductance factor ($k_1 N_1$) for several fluids are shown in Fig. 3.7.

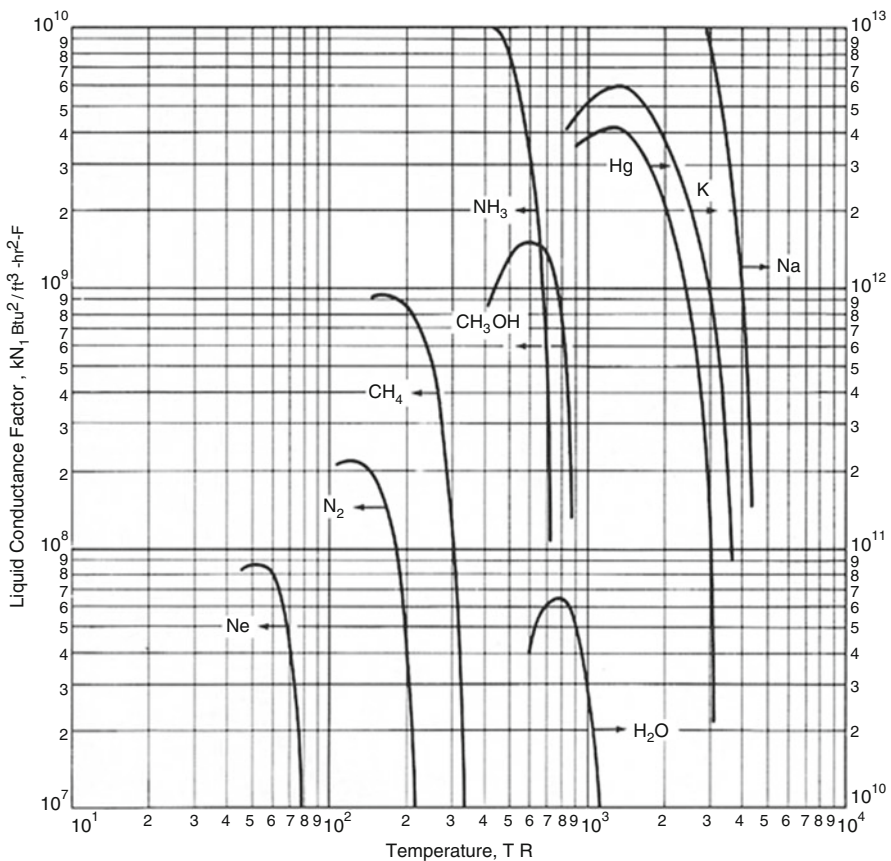


Fig. 3.7 Liquid conductance factor versus temperature for several heat pipe working fluids ($1 \text{ Btu}^2/\text{ft}^3 \text{ h}^2 \text{ F} = 5.455 \text{ W}^2/\text{m}^3 \text{ K}$; $1 \text{ R} = 0.5556 \text{ K}$) [5]

Per Dunn and Kew [4], the design of a heat pipe or thermosyphon to fulfill a particular duty involves four broad processes:

1. Selection of appropriate type and geometry
2. Selection of candidate materials
3. Evaluation of performance limits
4. Evaluation of the actual performance

The background to each of these stages is covered in Chap. 2. In this chapter, the theoretical and practical aspects are discussed with reference to sample design calculations.

Per same reference [4] the design procedure for a heat pipe is outlined in Fig. 3.8. As with any design process, many of the decisions that must be taken are interrelated and the process is iterative. For example, choice of wick and case material eliminates many candidate working fluids (often including water) due to compatibility constraints. If the design then proves inadequate with the available fluids, it is necessary to reconsider the choice of construction materials.

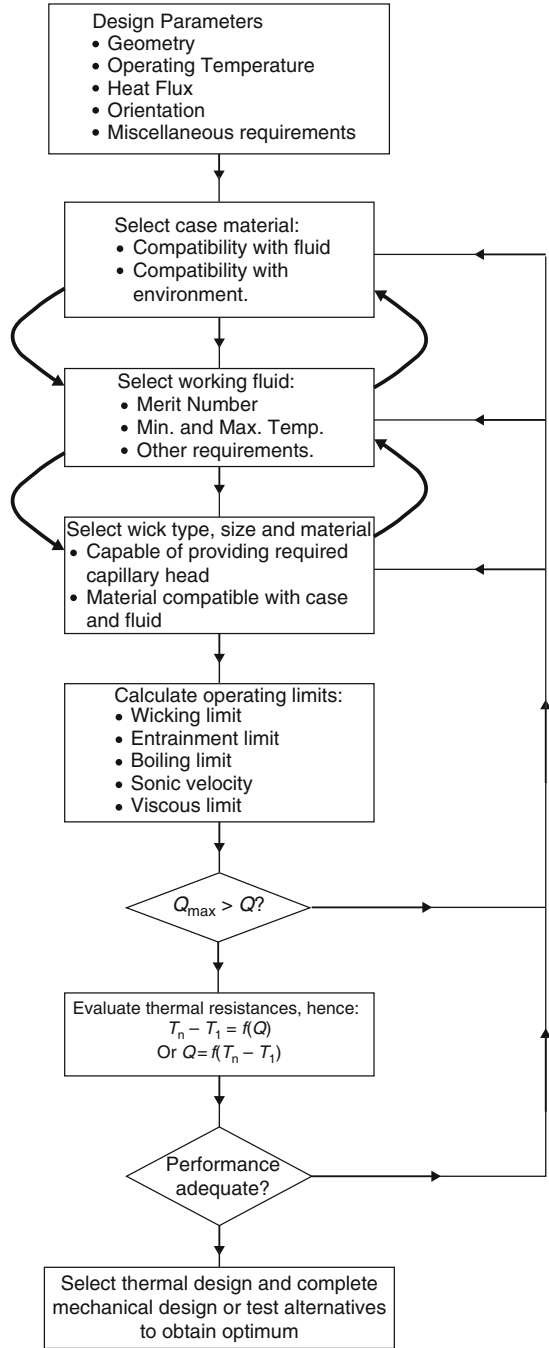
Two aspects of practical design, which must also be taken into consideration, are the fluid inventory and startup of the heat pipe.

3.3.1 *Fluid Inventory*

A feature of heat pipe design, which is important when considering small heat pipes and units for space use, is the working fluid inventory. It is a common practice to include a slight excess of working fluid over and above the required saturating the wick, but when the vapor space is of small volume a noticeable temperature gradient can exist at the condenser, similar to that indicating the presence of non-condensable gas. This reduces the effective length of the condenser, hence impairing heat pipe performance. Another drawback of excess fluid is peculiar to heat pipes in space, where in zero gravity the fluid can move about the vapor space, affecting the dynamics of the spacecraft. If there is a deficiency of working fluid, the heat pipe may fail because of the inability of any artery to fill. This is not as critical with homogeneous wicks as some of the pores will still be able to generate capillary action. Marcus [7] discusses in detail these effects and the difficulties encountered in ensuring whether the correct amount of working fluid is injected into the heat pipe. One way of overcoming the problem is to provide an excess fluid reservoir, which behaves as a sponge, absorbing working fluid that is not required by the primary wick structure.

For the successful operation of heat pipe, its working fluid must be in liquid state and selected fluid for the heat pipe must have a melting or evaporation point temperature *below* and its critical point temperature *above* the heat pipe operating temperature.

Fig. 3.8 Flow sheet for heat pipe design



3.3.2 *Priming Heat Pipe*

The artery of a heat pipe includes a closed tube mounted at the evaporator end of the artery and having one or more venting pores located in a thin-walled section of the tube. The wall section containing the venting pore is so thin as to cause meniscus coalescence of liquid tending to fill the pore when it borders a gas bubble. By the action of meniscus coalescence, the pore remains open to vent any gas bubbles that are present within the artery during priming thereof. The wick must satisfy two main requirements.

First, it must be capable of generating a high capillary pressure. The capillary pressure of a wick is a term that is used to define the ability of the pore structure of the wick to tolerate the pressure difference between the vapor and the liquid in the wick that it can withstand without causing the liquid menisci in the pores to collapse.

Secondly the wick must have a low liquid flow resistance. The liquid flow resistance is a measure of the pressure drop that the liquid experiences when flowing at a given flow rate from the condenser to the evaporator. With increasing heat input, the liquid flow rate increases so as to increase the pressure drop in the liquid. The thermal capacity of the heat pipe is reached when the pressure drop is so great that the maximum capillary pressure of the wick pores in the evaporator region is exceeded and the wick ultimately dries out. The wick can be designed and fabricated in a tight structure with small pore size to achieve a high capillary pressure. However, the smaller the pore size of the wick, the greater will be its flow resistance. To overcome the above conflicting wick requirements of high capillary pressure and low liquid flow resistance, designers of heat pipes have restored the use of arteries to handle very high heat loads. Generally, an artery is a closed tube filled with liquid and having at least a portion of its wall structure porous and in communication with the wick. In the artery, the maximum capillary pressure is determined by the pore size of the wall, whereas the flow resistance is determined by the diameter of the tube. Thus, these two parameters can be adjusted independently.

Although arteries can provide an order of magnitude increase in heat pipe capacity, they suffer a serious disadvantage in that they are extremely difficult to *prime* and *re-prime* reliably without entrapment of a bubble. An arterial bubble is intolerable because far before maximum capacity is reached, the bubble grows and the artery empties of liquid.

Bubbles present problems only if the heat pipe contains non-condensable gas as well as the heat-pipe working fluid, since a pure vapor bubble will spontaneously collapse. It is unlikely, however, that heat pipe fluid can be maintained so free of non-condensable gas that bubbles will not be a problem. Also, there is an important class of heat pipes that are intentionally filled with some non-condensable gas for the purpose of heat pipe control. The reason an arterial bubble is formed is that a liquid sheath on the artery wall prevents gas from venting during the priming process which usually proceeds from the condenser to the evaporator. An artery

can deprime when vapor bubbles become trapped in it. It may be necessary to reduce the heat load in such circumstances, to enable the artery to re-prime.

If some form of arterial wick is built into a heat pipe, it is necessary to ensure that an artery become depleted of working fluid; it should be able to refill automatically. It is possible to calculate the maximum diameter of an artery to ensure that it will be able to *re-prime*. The maximum priming height that can be achieved by a capillary is given by the equation [4]:

$$h + h_c = \frac{\sigma_1 \cos \theta}{(\rho_l - \rho_v)} \times \left(\frac{1}{r_{p1}} + \frac{1}{r_{p2}} \right) \quad (\text{Eq.3.4})$$

where

h = The vertical height to the base of the artery

h_c = The vertical height to the top of the artery

ρ_l = Density of liquid

ρ_v = Density of vapor

σ_1 = Liquid surface tension

r_{p1} = The first principal radius of curvature of the priming meniscus

r_{p2} = The second principal radius of curvature of the priming meniscus

θ = Contact angle.

Per Reay and Kew [4], for the purpose of priming, the second principal radius of curvature of the meniscus is extremely large ($\approx 1 \sin \phi$). For a cylindrical artery

$$h_c = d_a$$

and

$$r_{p1} = \frac{d_a}{2}$$

where d_a is the artery diameter.

Hence Eq. (3.4) can be rearranged and becomes as follow:

$$h + d_a = \frac{2\sigma_1 \cos \theta}{(\rho_l - \rho_v)g \times d_a} \quad (\text{Eq.3.5})$$

which produces a quadratic in d_a that may be solved, and Eq. (3.6) can be obtained by

$$d_a = \frac{1}{2} \left[\left(\sqrt{h^2 + \frac{8\sigma_1 \cos \theta}{(\rho_l - \rho_v)}} \right) - h \right] \quad (\text{Eq.3.6})$$

Several patents have been filed by various designers in regard to assembly and structure of different artery wicks such as helically grooved, trapezoidal grooves, sinusoidal grooves, or an artery, disposed within the tube, conducts condensed liquid by capillary action from the condenser to the evaporator and is provided with a channel formed on its upper surface. See the picture below (Fig. 3.9).

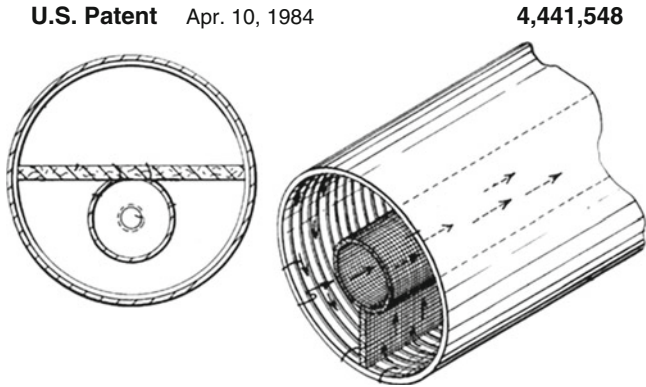


Fig. 3.9 Partial perspective schematic view of a conventional heat pipe having an arterial US Patent 4,441,548 by Franklin et al. [8]

3.4 How to Select a Heat Pipe

As part of heat pipe selection process, we need to follow the steps below:

1. Investigate and determine the following operational parameters:
 - (a) Heat load and geometry of the heat source
 - (b) Possible heat sink location, the distance and orientation relative to the heat source
 - (c) Temperature profile of heat source, heat sink and ambient
 - (d) Environmental condition (such as existence of corrosive gas)
2. Select the pipe material, wick structure, and working fluid. (Consult with an expert engineer or original heat pipe manufacturer to select the most appropriate heat pipe designed by them. The list of these manufactures are provided in Chapter 1:
 - (a) Determine the working fluid appropriate for your application.
 - (b) Select the pipe material compatible to the working fluid.
 - (c) Select the wick structure for the operating orientation.
 - (d) Decide on the protective coating.
 - (e) Determine the length, size, and shape of the heat pipe.

Figure 3.10 gives the performance of heat pipes with a diameter from 3 to 22.23 mm. In this case, the selection should be within this given range for diameter of chosen heat pipe. Note that the constraint in this selection is based on the vertical orientation of operation environment for the heat pipe, and plots are depicted for a copper–water artery-grooved wick heat pipe. Similar plots can be obtained for different types of working fluid and wick selections.

The rate of vapor traveling from the evaporator to the condenser is governed by the difference in vapor pressure between them. It is also affected by the diameter

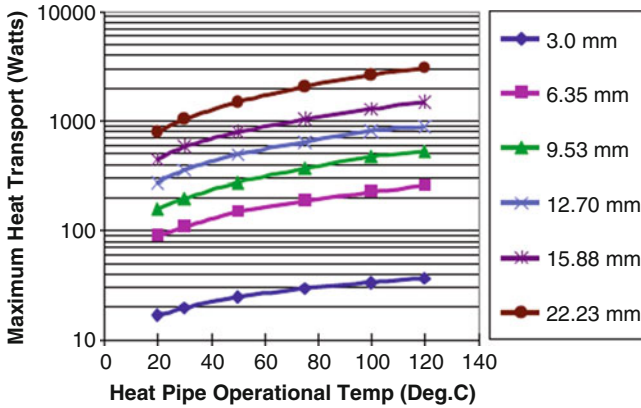
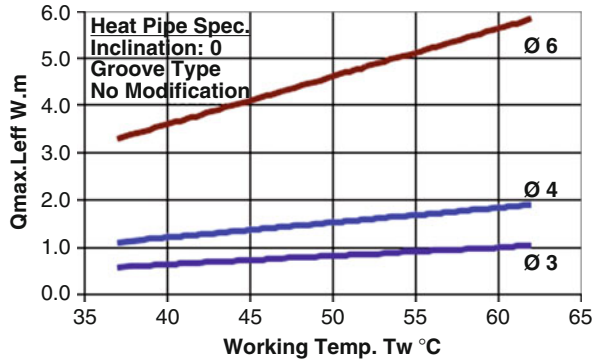


Fig. 3.10 Performance of copper–water groove heat pipe at vertical orientation (gravity assist). Courtesy of Enertron Corporation

Fig. 3.11 The performance of various groove wick copper–water heat pipes



and the length of the heat pipe. In the large-diameter heat pipe, the cross-sectional area will allow higher vapor volume to be transported from the evaporator to the condenser than in a small-diameter pipe. The cross-sectional area of a heat pipe is the direct function for both the sonic limit and entrainment limit. Figure 3.11 compares the heat transport of heat pipes with different diameters. Also, the operational temperature of a heat pipe affects the sonic limit. We can see, in Fig. 3.11, that heat pipes transport more heat at higher operational temperatures.

The rate of working fluid return from the condenser to the evaporator is governed by capillary limit and is the reciprocal function of the heat pipe length. A longer heat pipe transports less heat versus the same heat pipe with a shorter length. In Fig. 3.11, the unit of the Y-axis is $Q_{max}L_{effective}$ (W m) representing the amount of heat a pipe can carry per meter length. If the pipe is half a meter, it can carry twice the wattage.

As it can be seen, the selection of an appropriate heat pipe can be a complicated process.

3.5 What Materials Can Be Used to Construct a Heat Pipe

A particular working fluid can only be functional at certain temperature ranges. Also, the particular working fluid needs a compatible vessel material to prevent corrosion or chemical reaction between the fluid and the vessel. Corrosion will damage the vessel, and chemical reaction can produce a non-condensable gas. Refer to Table 3.3. For example, the liquid ammonia heat pipe has a temperature range from -70 to $+60$ °C and is compatible with aluminum, nickel, and stainless steel.

The liquid ammonia heat pipe has been widely used in space, and only aluminum vessels are used due to lightweight. Water heat pipes, with a temperature range from 5 to 230 °C, are most effective for electronics cooling applications, and copper vessels are compatible with water.

Heat pipes are not functional when the temperature of the pipe is lower than the freezing point of the working fluid. Freezing and thawing is a design issue, which may destroy the sealed joint of a heat pipe when placed vertically. Proper engineering and design can overcome this limitation.

Table 3.3 Typical operating characteristics of heat pipes

Temperature range (°C)	Working fluid	Vessel material	Measured axial ^a heat flux (kW/cm ²)	Measured surface ^a heat flux (W/cm ²)
-200 to -80	Liquid nitrogen	Stainless steel	0.067 @ -163 °C	1.01 @ -163 °C
-70 to $+60$	Liquid ammonia	Nickel, aluminum, stainless steel	0.295	2.95
-45 to $+120$	Methanol	Copper, nickel, stainless steel	0.45 @ 100 °C ^b	75.5 @ 100 °C
$+5$ to $+230$	Water	Copper, nickel	0.67 @ 200 °C	146 @ 170 °C
$+190$ to $+550$	Mercury ^c +0.02 % Magnesium +0.001 %	Stainless steel	25.1 @ 360 °C ^d	181 @ 750 °C
$+400$ to $+800$	Potassium ^c	Nickel, stainless steel	5.6 @ 750 °C	181 @ 750 °C
$+500$ to $+900$	Sodium ^c	Nickel, stainless steel	9.3 @ 850 °C	224 @ 760 °C
$+900$ to $+1500$	Lithium ^c	Niobium + 1 % zirconium	2.0 @ 1250 °C	207 @ 1250 °C
1500 + 2000	Silver ^c	Tantalum + 5 % tungsten	4.1	413

^aVaries with temperature

^bUsing threaded artery wick

^cTested at Los Alamos Scientific Laboratory

^dMeasured value based on reaching the sonic limit of mercury in the heat pipe reference of "Heat Transfer," 5th Edition, JP Holman, McGraw-Hill

3.6 When to Consider a Heat Pipe

Heat pipes are classified into two general types—“fixed conductance” and “variable conductance.” A fixed conductance heat pipe is a device of very high thermal conductance with no fixed operating temperature. Its temperature rises or falls according to variations in the heat source or heat sink.

3.7 Things to Consider, When Designing a Heat Pipe

As an effective heat conductor, heat pipe can be used in situations when a heat source and a heat sink need to be placed apart, to aid heat conduction of a solid or to aid heat spreading of a plane. However, not every heat pipe is suitable for all applications. For that reason, the following need to be considered when designing heat pipes:

1. Heat transport limitation of the heat pipe
2. Wick structure of the heat pipe
3. Length and diameter of the heat pipe
4. Heat pipe orientation
5. Effect of bending and flattening of the heat pipe
6. Heat pipe reliability

3.7.1 *What the Four Heat Transport Limitations of a Heat Pipe Are*

A heat pipe is a hermetically sealed evacuated tube normally containing a mesh or sintered powder wick and a working fluid in both the liquid and vapor phase. When one end of the tube is heated, the liquid turns to vapor absorbing the latent heat of vaporization. The hot vapor flows to the colder end of the tube where it condenses and gives out the latent heat. The recondensed liquid then flows back through the wick to the hot end of the tube. Since the latent heat of evaporation is usually very large, considerable quantities of heat can be transported with a very small temperature difference from one end to the other.

The vapor pressure drop between the evaporator and the condenser is very small, and, therefore, the boiling–condensing cycle is essentially an isothermal process. Furthermore, the temperature losses between the heat source and the vapor and between the vapor and the heat sink can be made small by proper design. Therefore, one feature of the heat pipe is that it can be designed to transport heat between the heat source and the heat sink with very small temperature losses.

The amount of heat that can be transported as latent heat of vaporization is usually several orders of magnitude larger than can be transported as sensible heat in a conventional convective system with an equivalent temperature difference. Therefore, a second feature of the heat pipe is that relatively large amounts of heat can be transported with small lightweight structures. The performance of a heat pipe is often expressed in terms of equivalent thermal conductivity. The huge effective thermal conductivity of the heat pipes can be illustrated by the following examples. A tubular heat pipe using water as the working fluid and operated at 150 °C would have a thermal conductivity several hundred times that of a copper bar of the same dimensions.

A heat pipe using lithium as the working fluid at a temperature of 1500 °C will carry an axial heat flux of 10–20 kW/cm². By suitable choice of working fluid and container materials, it is possible to manufacture heat pipes for use at temperatures ranging from –269 °C to in excess of 2300 °C.

The four heat transport limitations can be simplified as follows:

- (a) **Sonic limit**—The rate that vapor travels from evaporator to condenser
- (b) **Entrainment limit**—The friction between working fluid and vapor that travel in opposite directions
- (c) **Capillary limit**—The rate at which the working fluid travels from condenser to evaporator through the wick
- (d) **Boiling limit**—The rate at which the working fluid vaporizes from the added heat to condenser side

3.7.2 Heat Pipe Diameter

For this purpose, the round tubes and pipes of different materials are readily available, and they are the most efficient configuration from the stress point of view. The size of the pipe diameter necessary for a given application requirement should be analyzed so that vapor velocity is not excessive. Control of vapor velocity is required since at high *Mach* numbers the flow compressibility of vapor contributes to a large axial temperature gradient. For that matter, the heat pipe can be designed so that its maximum *Mach* number in the vapor flow passage does not exceed value the of 0.2. Given that value for consideration of first step of the design, the vapor can be considered incompressible which is the common theory approaches and heat pipe operating condition and available computer codes. Under this condition, the axial temperature gradient is negligibly small as well (Figs. 3.12, 3.13, 3.14, and 3.15).

For a heat pipe operation under this constraint, whose heat transport mode requirements and consequently maximum axial heat flux Q_{Max} are known, the required vapor core diameter d_v at vapor Mach number M_v equal to 0.2 can be determined by utilizing Eq. (2.62), and as a result, we get the following relationship:

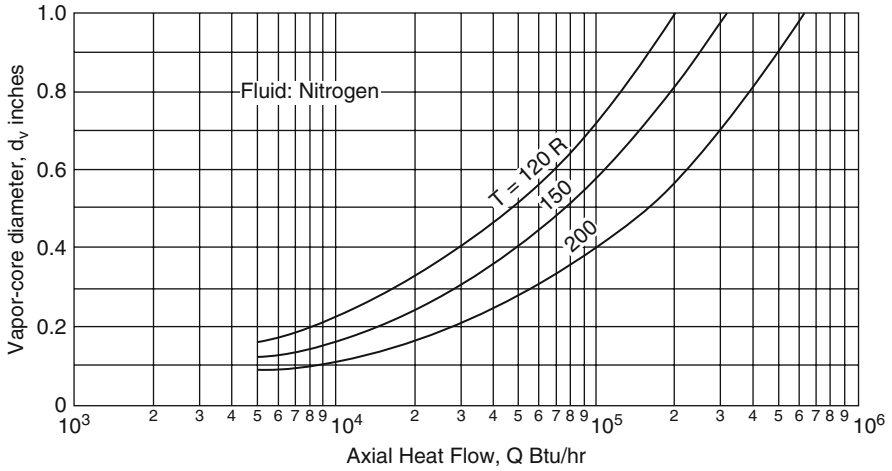


Fig. 3.12 Vapor core diameter versus heat transfer rate for vapor Mach Number of 0.2 for nitrogen [5] (Inch = 0.0254 m, 1 Btu/h = 0.2929 W, 1 R = 0.5556 K)

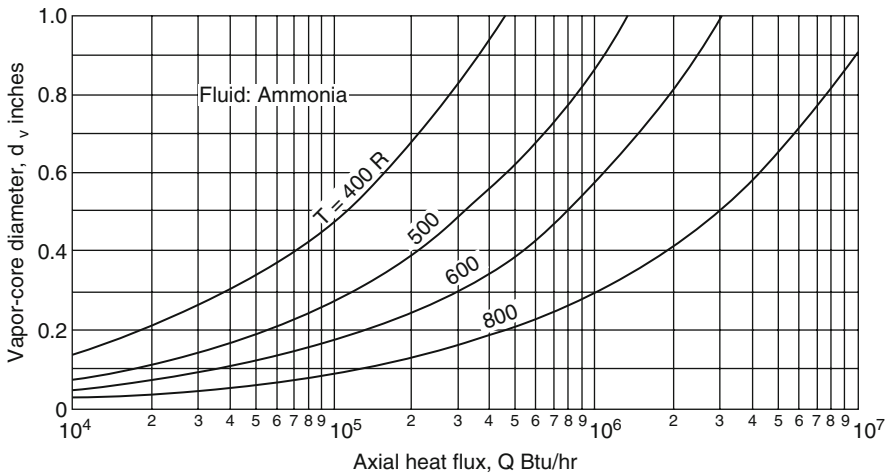


Fig. 3.13 Vapor core diameter versus heat transfer rate for vapor Mach Number of 0.2 for ammonia [5]

$$d_v = \left(\frac{20Q_{Max}}{\pi\rho_v\lambda\sqrt{\gamma_v}R_vT_v} \right)^{1/2} \tag{Eq.3.7}$$

where

- d_v = Vapor core diameter
- Q_{Max} = Maximum axial heat flux

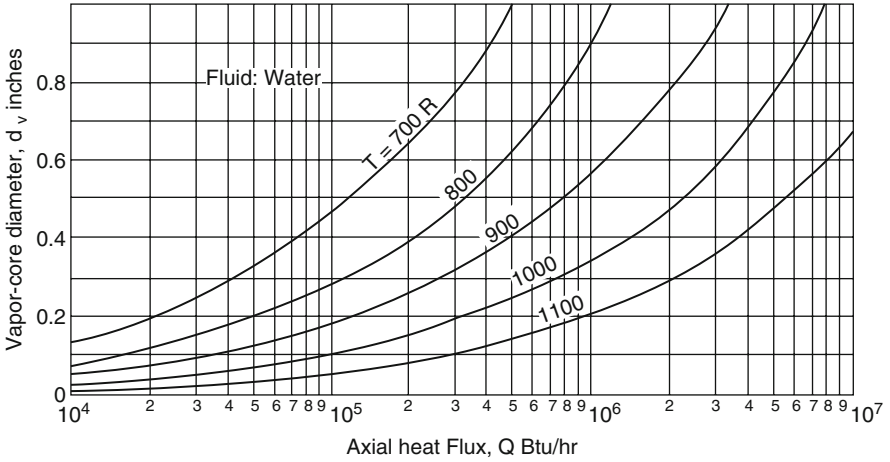


Fig. 3.14 Vapor core diameter versus heat transfer rate for vapor Mach number of 0.2 for water [5]

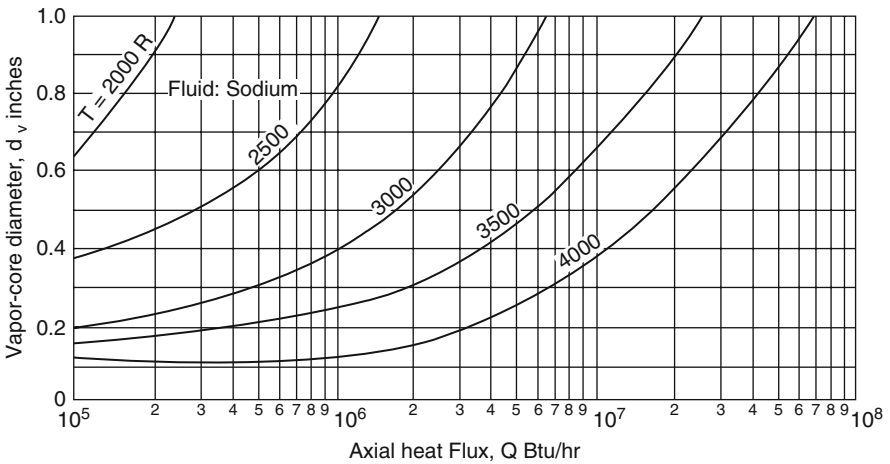


Fig. 3.15 Vapor core diameter versus heat transfer rate for vapor Mach number of 0.2 for sodium [5] (Inch = 0.0254 m, 1 Btu/h = 0.2929 W, 1 R = 0.5556 K)

- ρ_v = Vapor density
- λ = Latent heat of vaporization
- γ_v = Vapor-specific heat ratio
- R_v = Gas constant for the vapor
- T_v = Vapor temperature

3.7.3 Heat Pipe Containers Design

The American Society of Mechanical Engineering (AMSE) standard for unfired pressure vessels [9] specifies that the maximum allowable stress at any temperature be one-quarter of the material's ultimate strength f_{tu} at that temperature. Metal properties including ultimate tensile strength for several metals can be found in Appendix B.

Per Chi [5], for round tubes in which the wall thickness is less than 10 % of the diameter, the maximum pressure stress is closely approximated by the simple expression

$$f_{\max} = \frac{Pd_o}{2t} \quad (\text{Eq.3.8})$$

where

- f_{\max} = Maximum hoop stress in the wall
- P = Pressure differential across the wall
- d_o = Tube outside diameter
- t = Tube wall thickness

The maximum hoop stress in a thick-walled cylinder, subject to internal pressure, is given by the expression

$$f_{\max} = \frac{P(d_o^2 + d_i^2)}{d_o^2 - d_i^2} \quad (\text{Eq.3.9})$$

where

- f_{\max} = Maximum hoop stress in the wall
- P = Pressure differential across the wall
- d_o = Tube outside diameter
- d_i = Tube inside diameter

Ends of the heat pipe container can be capped off either with hemispherical, conical, or flat end caps. The maximum stress in a thick-walled hemispherical end cap is;

$$f_{\max} = \frac{P(d_o^3 + 2d_i^3)}{2(d_o^3 - d_i^3)} \quad (\text{Eq.3.10})$$

If the wall thickness of the hemispherical end cap is less than 10 % of its diameter, Eq. (3.10) can be approximated by

$$f_{\max} = \frac{Pd_o}{4t} \quad (\text{Eq.3.11})$$

The maximum stress in a flat circular end cap can be calculated by the

$$f_{\max} = \frac{Pd_o^2}{8t^2} \tag{Eq.3.12}$$

where

- f_{\max} = Maximum stress
- P = Pressure differential across the cap
- d_o = End cap diameter
- t = End cap thickness

For design calculation, the internal pressure of the pipe is equal to the saturation vapor pressure of the pipe working fluid at its operating temperature or its maximum cycle pressure whichever is larger. The pressure differential is equal to the vapor pressure minus the ambient pressure. As the vapor pressure is usually much larger than the ambient pressure, the vapor pressure is, therefore, approximately equal to the pressure differential. Figure 3.16 contains vapor pressure versus

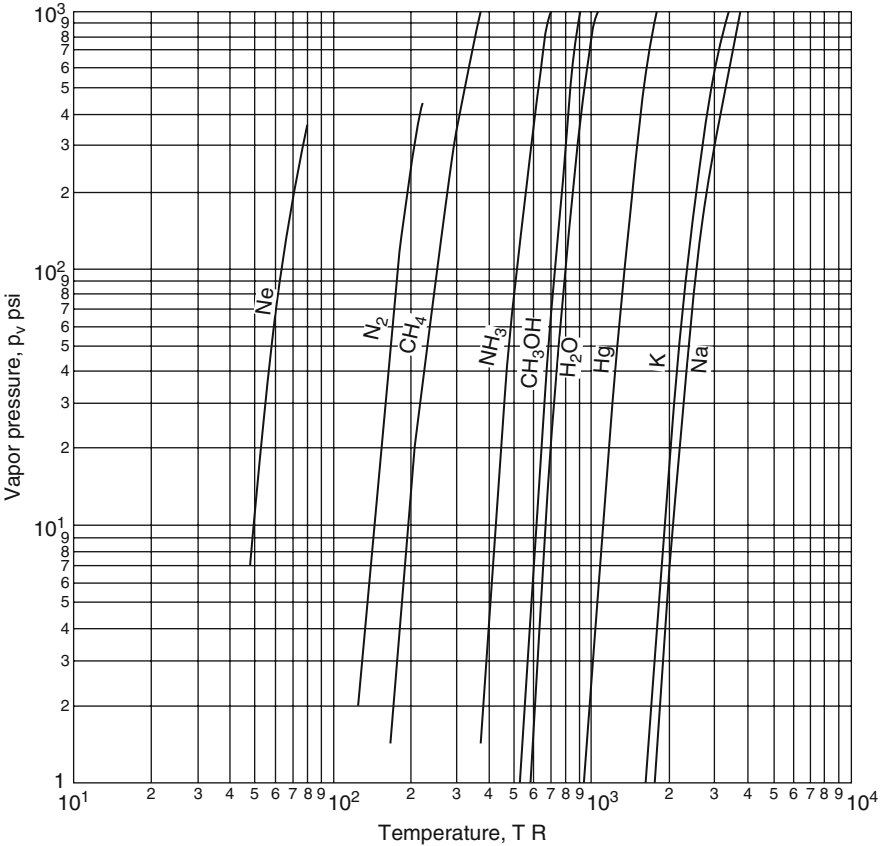


Fig. 3.16 Vapor pressure versus temperature for several heat pipe working fluids. (1 psi = 6.895 $\times 10^3$ N/m², 1 R = 0.5556 K) [5]

temperature information for several fluids. The maximum allowable stress is equal to one-quarter of the ultimate tensile stress (UTS).

Appendix B is providing UTS for different materials. Having the knowledge and information about heat pipe outside diameter of tube, which will be equal to the vapor diameter plus allowances for the wick and wall thickness, one can use Eqs. (3.8–3.12) to calculate the wall thickness for the pipe container and both end caps.

Figure 3.17 represents design curves, which can be utilized to determine the required tube size very quickly when the heat pipe operation pressure and the material UTS are known. Figure 3.18 also represents similar design curves for analyzing the required thickness of the flat end caps.

Additionally, Table 3.4 contains the dimensional data for commercial tubes ranging from 1/4 to 1 in. outside diameter.

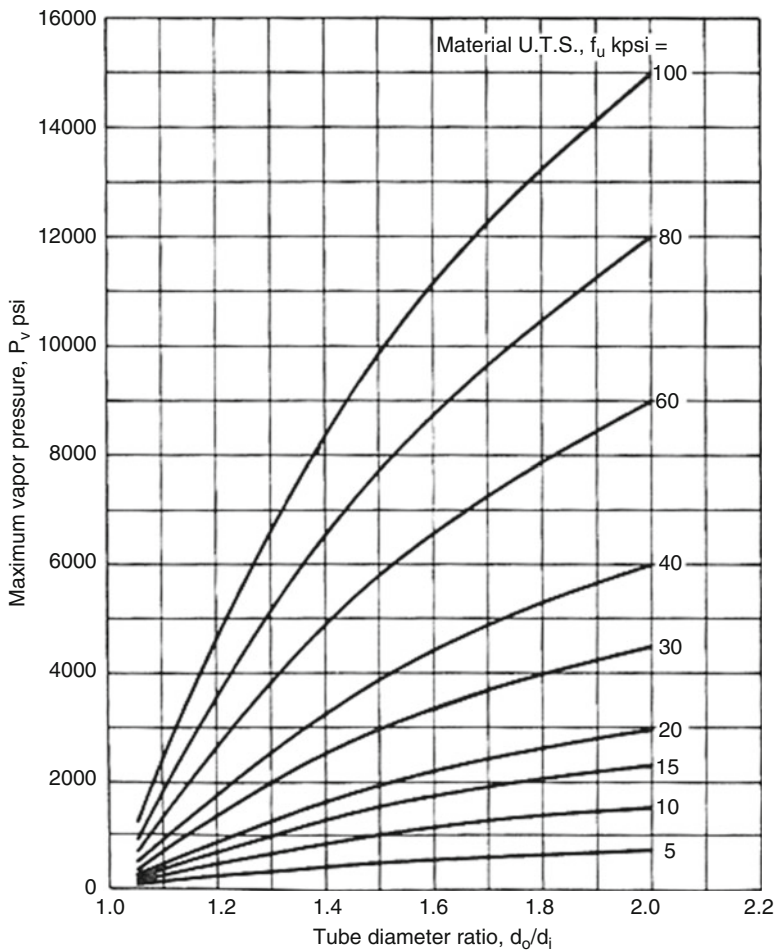


Fig. 3.17 Design chart for heat pipe container tubes (1 psi = 6.895 × 10³ N/m², 1 kpsi = 6.895 × 10⁶ N/m²) [5]

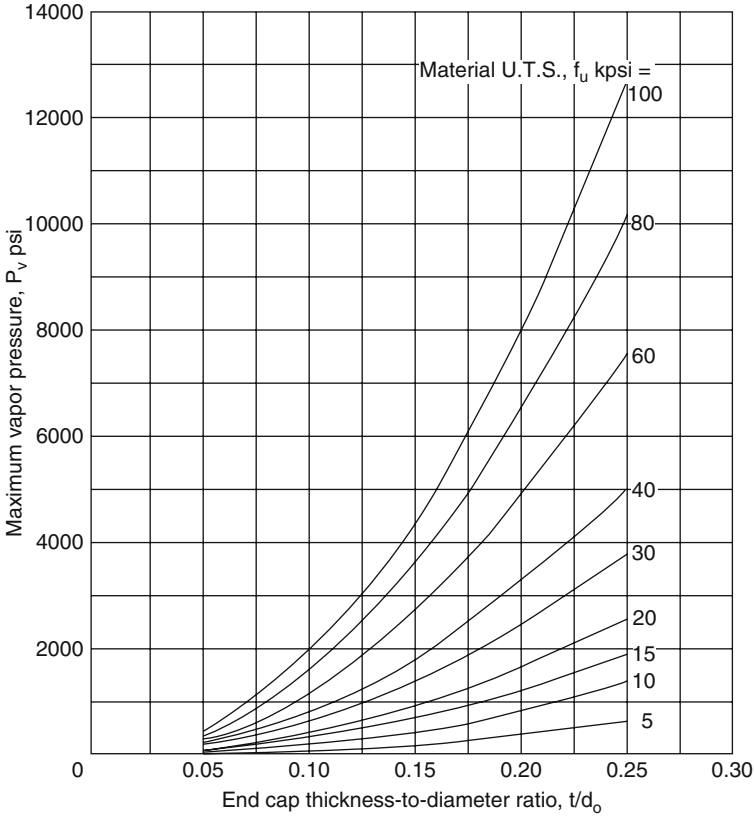


Fig. 3.18 End cap thickness-to-diameter ratio t/d_o

3.7.4 Heat Pipe Material Selection

The important consideration for material selection of heat pipe is its wick and container compatibility with working fluids since the heat pipes are subject to continuous performance degradation as a result of chemical reaction or decomposition of the working fluid and corrosion or erosion of the container or wick. Chemical reaction or decomposition of the working fluid may give rise to non-condensable gas evolution. A specific example of this is the hydrolysis of water-yielding hydrogen gas in a water-aluminum heat pipe. In a conventional heat pipe, all non-condensable gas is swept to the condenser end, thus, inactivating a portion of the condenser [5].

Corrosion and erosion of the container and wick may result in a change of the fluid wetting angle and the permeability or capillary pore size of the wick. As a result solid, particles resulting from corrosion and erosion are transported by the flowing liquid to the evaporator region and deposited there. Table 3.5 is a

Table 3.4 Data for sample commercial tubes (1 in. = 0.0245 m) [5]

Tube o.d. (in.)	o.d./i.d.	Bwg ^a	Thickness (in.)	i.d. (in.)
1/4	1.289	22	0.028	0.194
	1.214	24	0.022	0.206
	1.168	26	0.018	0.214
3/8	1.354	18	0.049	0.277
	1.233	20	0.035	0.305
	1.176	22	0.028	0.319
	1.133	24	0.022	0.331
1/2	1.351	16	0.065	0.370
	1.244	18	0.049	0.402
	1.163	20	0.035	0.430
	1.126	22	0.028	0.444
5/8	1.536	12	0.109	0.407
	1.362	14	0.083	0.459
	1.263	16	0.065	0.495
	1.186	18	0.049	0.527
	1.126	20	0.035	0.555
3/4	1.556	10	0.134	0.482
	1.410	12	0.109	0.532
	1.284	14	0.083	0.584
	1.210	16	0.065	0.620
	1.150	18	0.049	0.652
	1.103	20	0.035	0.680
7/8	1.441	10	0.134	0.607
	1.332	12	0.109	0.657
	1.234	14	0.083	0.709
	1.174	16	0.065	0.745
	1.126	18	0.049	0.777
	1.087	20	0.035	0.805
1	1.493	8	0.165	0.670
	1.366	10	0.134	0.732
	1.279	12	0.109	0.782
	1.199	14	0.083	0.834
	1.149	16	0.065	0.870
	1.109	18	0.049	0.902
	1.075	20	0.035	0.930

^aBirmingham wire gauge

compatibility compilation for fluid–metal combinations. It can be used for selection of wick and container materials.

Besides material compatibility, other factors, such as weight, temperature characteristic, and material fabrication costs, may also be of importance.

Figure 3.19 shows the values of density divided by ultimate tensile stress versus temperature for several materials. For a minimum weight, the material with the

Table 3.5 Fluid–solid compatibility

Fluids	Solids					
	Al	Cu	Fe	Ni	SS ^a 304	Ti
Nitrogen	C ^b	C	C	C	C	
Methane	C	C			C	
Ammonia	C		C	C	C	
Methanol	I	C	C	C	C	
Water	I	C		C	C ^c	C
Potassium				C		I
Sodium				C	C	I

^aSS = stainless steel

^bC compatible, I incompatible, blank data not available

^cPossible hydrogen generation

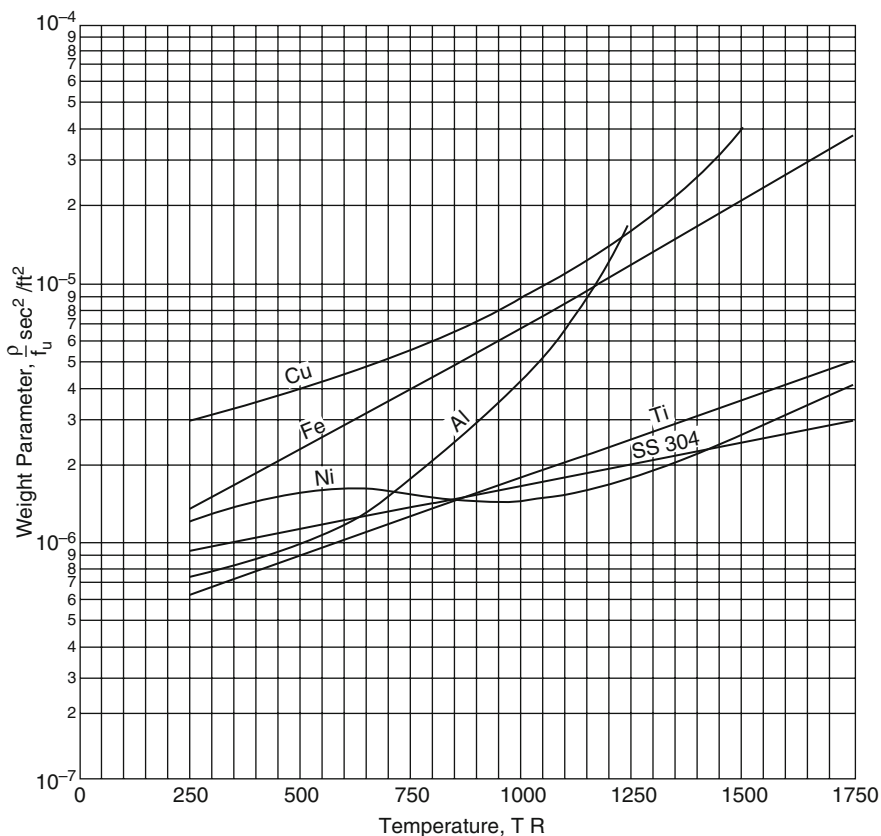


Fig. 3.19 Material weight parameter versus temperature for several heat pipe materials [5] ($1 s^2/ft^2 = 10.76 s^2/m^2$; $1 R = 0.5556 K$)

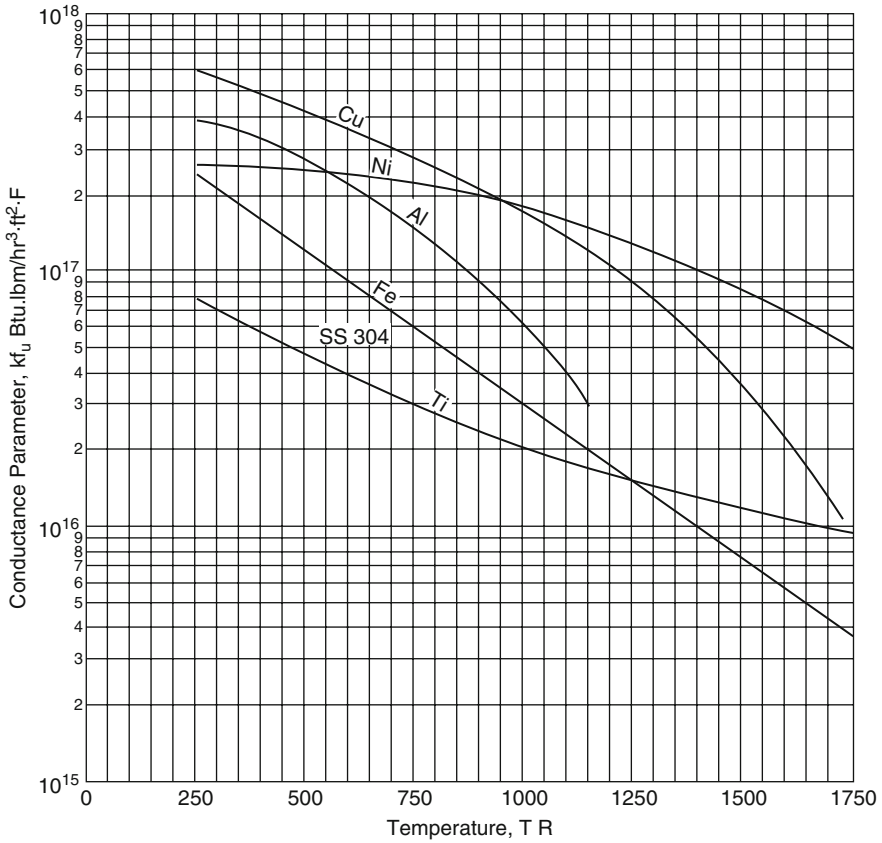


Fig. 3.20 Material conductance parameter versus temperature for several heat pipe materials [5] (1 Btu lbm/h³ ft² F = 1.986 × 10⁻⁷ W kg/s² m² K; 1 R = 0.5556 K)

smallest value of (ρ/f_u) should be chosen, where ρ is material density and f_u is ultimate tensile stress.

The temperature drop across the container wall is directly proportional to the wall thickness and inversely proportional to the thermal conductivity of the material. Hence, for small temperature drop, the materials chosen must have a large product for thermal conductivity times the ultimate tensile strength (kf_u). Values of (kf_u) for several materials are plotted in Fig. 3.20.

3.8 Entrainment and Boiling Limitations

Equation (2.34) was developed by Chi [5] to show the entrainment limit on the axial heat flux and can be shown as follows:

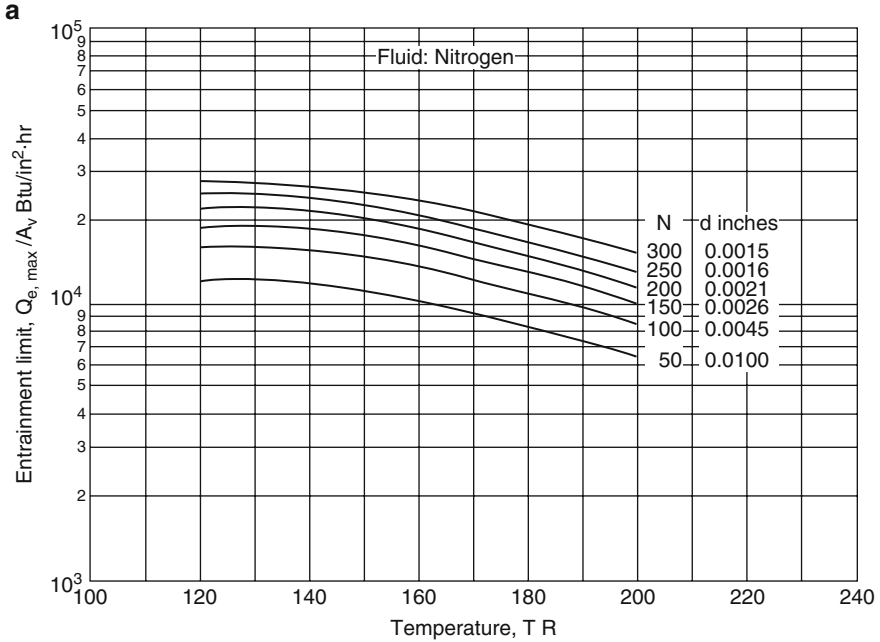


Fig. 3.21 Entrainment limit on axial heat flux density for heat pipe with screen wicks for nitrogen as working fluid [1] (1 Btu/in.² h = 454 W/m², 1 R = 0.5556 K, 1 in. = 0.0254 m)

$$\frac{Q_{e_{\max}}}{A_v} = \lambda \sqrt{\frac{\sigma \rho_v}{2r_{h,s}}} \tag{Eq.3.13}$$

where

$Q_{e_{\max}}$ = Entrainment limit

λ = Latent heat of vaporization

ρ_v = Vapor density

$r_{h,s}$ = Hydraulic radius of the surface pores of the wick

The value of $r_{h,s}$ is equal to half of the wire screen for any kind of wrapped-screen wick. Figures 3.21, 3.22, 3.23, and 3.24 from Chi show values for entrainment limit on the heat flux density, which is in alignment with Eq. (3.13) with the pipe fluid, screen mesh, and operating temperature of heat pipe as parameters. One can use this figure to easily read the value of $\frac{Q_{e_{\max}}}{A_v}$ for the design of a heat pipe. This value should be larger than the actual value of Q/A_v at which the heat pipe is going to operate.

The boiling limits and its theory have been discussed in Sect. 2.8, and Eq. (2.94) has been developed, and another version of it is written as follows:

$$\frac{Q_{\text{BoilingMaximum}}}{L_e} = \frac{2\pi k_e T_v}{\lambda \rho_v \ln\left(\frac{r_i}{r_v}\right)} \left(\frac{2\sigma}{r_n} - P_c \right) \tag{Eq.3.14}$$

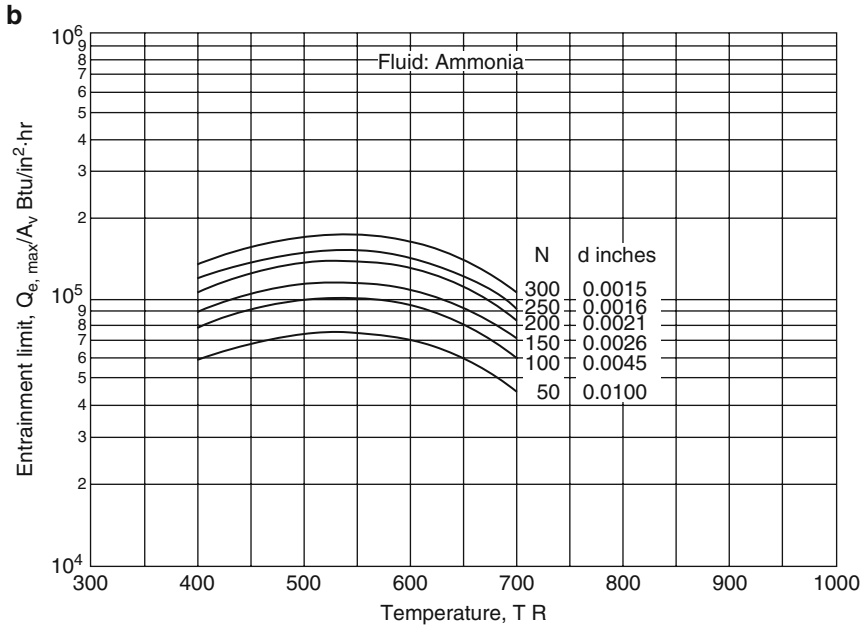


Fig. 3.22 Entrainment limit on axial heat flux density for heat pipe with screen wicks for ammonia as working fluid [1] (1 Btu/in.²h = 454 W/m², 1 R = 0.5556K, 1 in. = 0.0254m)

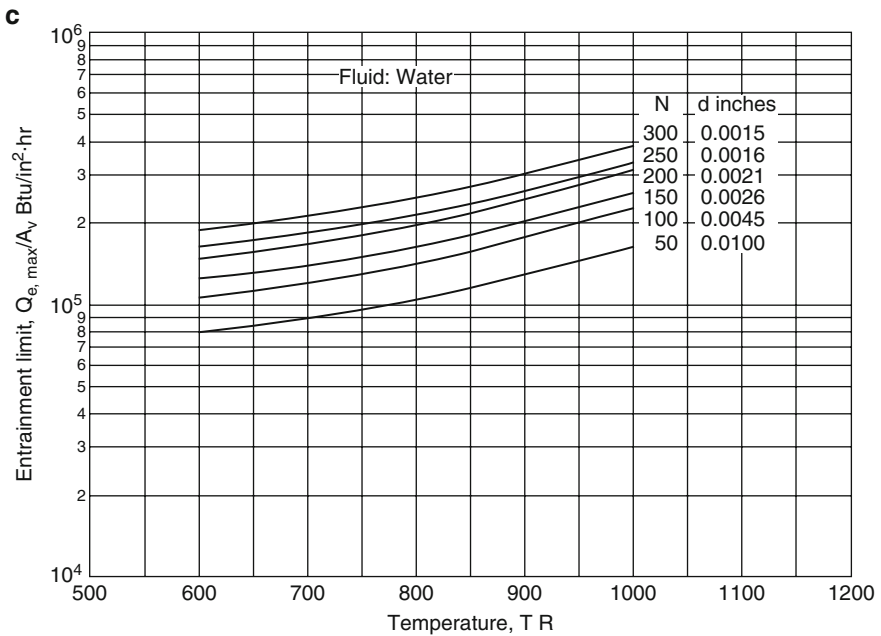


Fig. 3.23 Entrainment limit on axial heat flux density for heat pipe with screen wicks for water as working fluid [1] (1 Btu/in.²h = 454 W/m², 1 R = 0.5556K, 1 in. = 0.0254m)

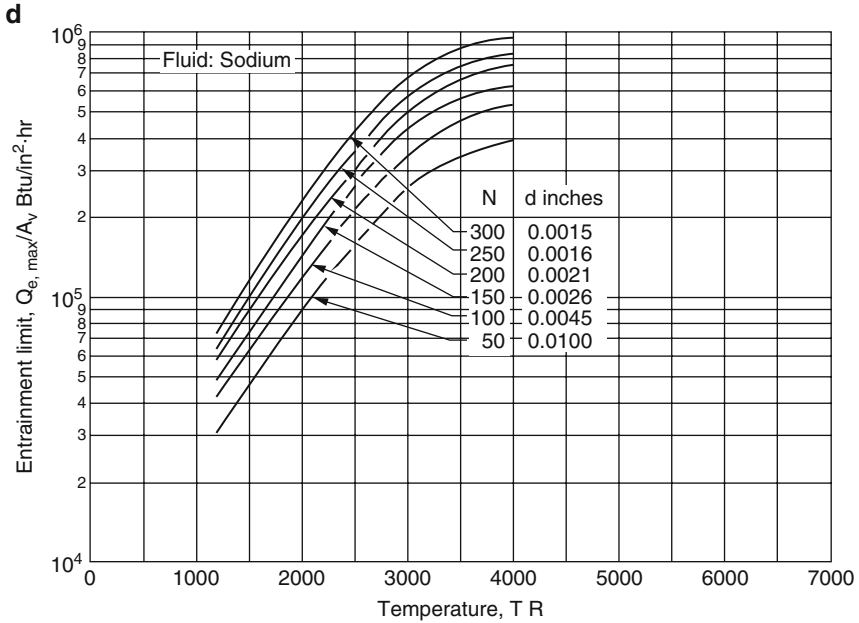


Fig. 3.24 Entrainment limit on axial heat flux density for heat pipe with screen wicks for sodium as working fluid [1] (1 Btu/in.² h = 454 W/m², 1 R = 0.5556 K, 1 in. = 0.0254 m)

where

$\frac{Q_{BoilingMaximum}}{L_e}$ = Boiling heat transfer limit per unit length of the evaporator

L_e = Effective thermal conductivity of the liquid-saturated wick

T_v = Vapor temperature

λ = Latent heat of vaporization

ρ_v = Vapor density

σ = Surface tension coefficient

P_c = Capillary pressure

r_i = Inside radius of pipe container

r_v = Vapor core radius of the pipe

r_n = Critical radius for nucleate boiling

For the wick structure of wrapped screen, the value of k_e can be calculated by Eq. (3.15), namely,

$$k_e = \frac{k_1[(k_1 + k_w) - (1 - \varepsilon)(k_1 - k_w)]}{[(k_1 + k_w) + (1 - \varepsilon)(k_1 - k_w)]} \tag{Eq.3.15}$$

where

k_e = Effective thermal conductivity

k_w = Thermal conductivity of wick material

k_1 = Liquid thermal conductivity

ε = Screen porosity = $1 - 1.05\pi Nd/4$

N = Wire cloth number

d = Wire diameter

Referring to Sect. 2.8, a conservative value for r_n for the conventional heat pipe is 10^{-5} in.

Equation (3.14) can be approximated if the value of $2\sigma/r_n$, in general, is much larger than P_c and can be shown as follows [5]:

$$\frac{Q_{\text{BoilingMax}}}{L_e} = \frac{4\pi k_e T_v \sigma}{\lambda \rho_v r_n \ln\left(\frac{r_i}{r_v}\right)} \tag{Eq.3.16}$$

Figures 3.25, 3.26, 3.27, and 3.28 [5] demonstrate values calculated by the right-hand side of Eq. (3.16) with the pipe fluid, mesh screen, diameter ratio (d_i/d_v), and

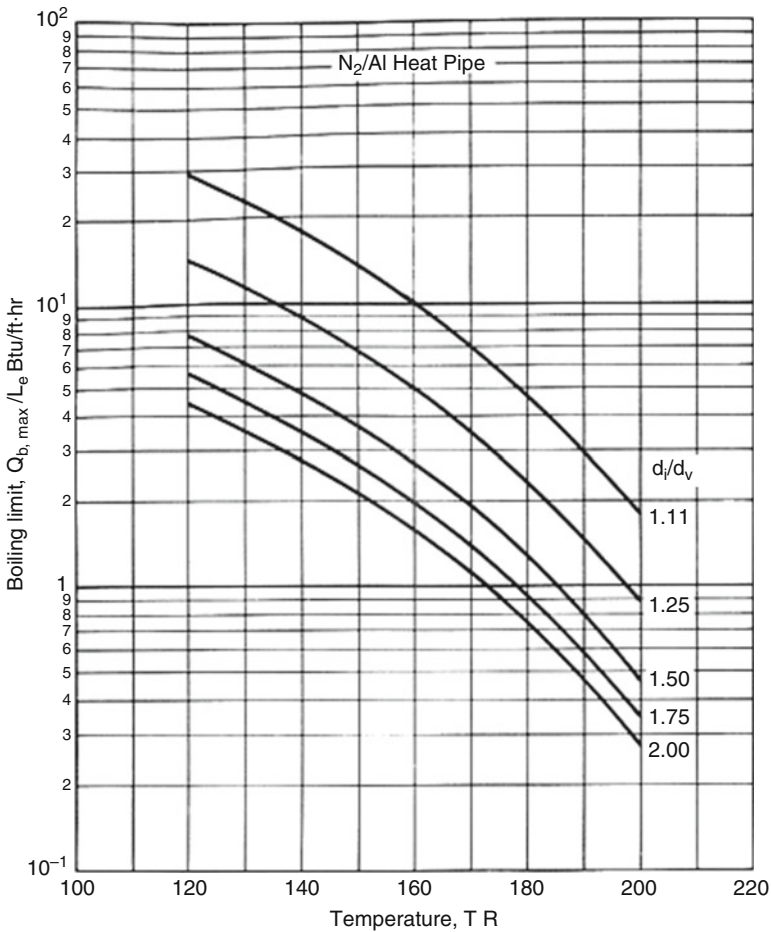


Fig. 3.25 Boiling limit on heat flux per unit length of evaporator [5] (1 Btu/ft-h = 0.961 W/m, 1 R = 0.5556K); nitrogen

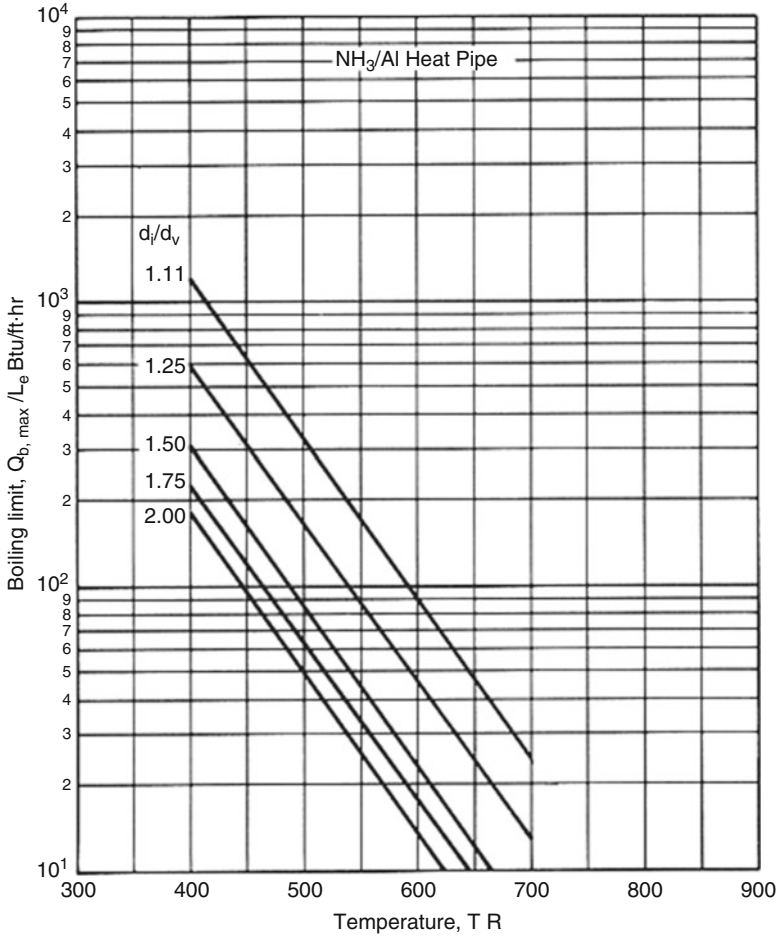


Fig. 3.26 Boiling limit on heat flux per unit length of evaporator [5] (1 Btu/ft·hr = 0.961 W/m, 1 R = 0.5556K); ammonia

operating temperature as parameters. Per Chi [5], these values calculated with the diameter of the screen wire equal to two-thirds of the wire spacing are very conservative values for the commonly designed commercial wire screens for wick, and normally for a conservative pipe design approximation, we should consider the value of $Q_{BoilingMax}/L_e$ to be larger than the actual value of Q/L_e at which the pipes are to operate.

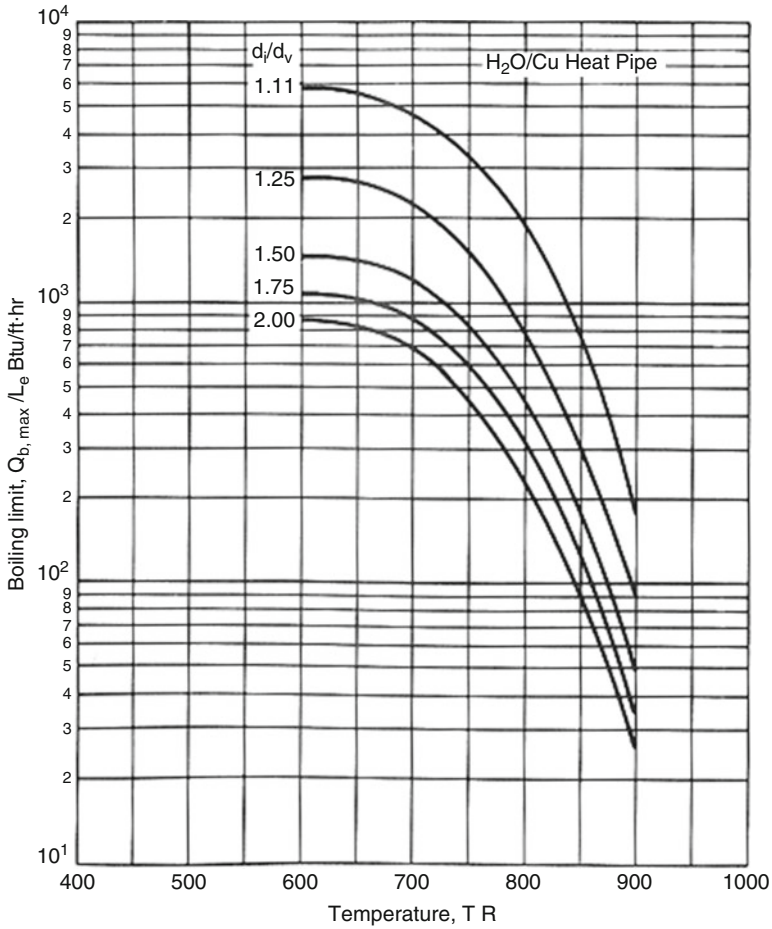


Fig. 3.27 Boiling limit on heat flux per unit length of evaporator [5] (1 Btu/ft·h = 0.961 W/m, 1 R = 0.5556K); water

3.9 What the Common Heat Pipe Wick Structure Is

There are four common wick structures used in commercially produced heat pipes: groove, wire mesh, powder metal, and fiber/spring. Each wick structure has its advantages and disadvantages. There is no perfect wick. Refer to Fig. 3.29 for a brief glance of the actual test performance of the four commercially produced wicks. Every wick structure has its own capillary limit. The groove heat pipe has the lowest capillary limit among the four but works best under gravity-assisted conditions where the condenser is located above the evaporator.

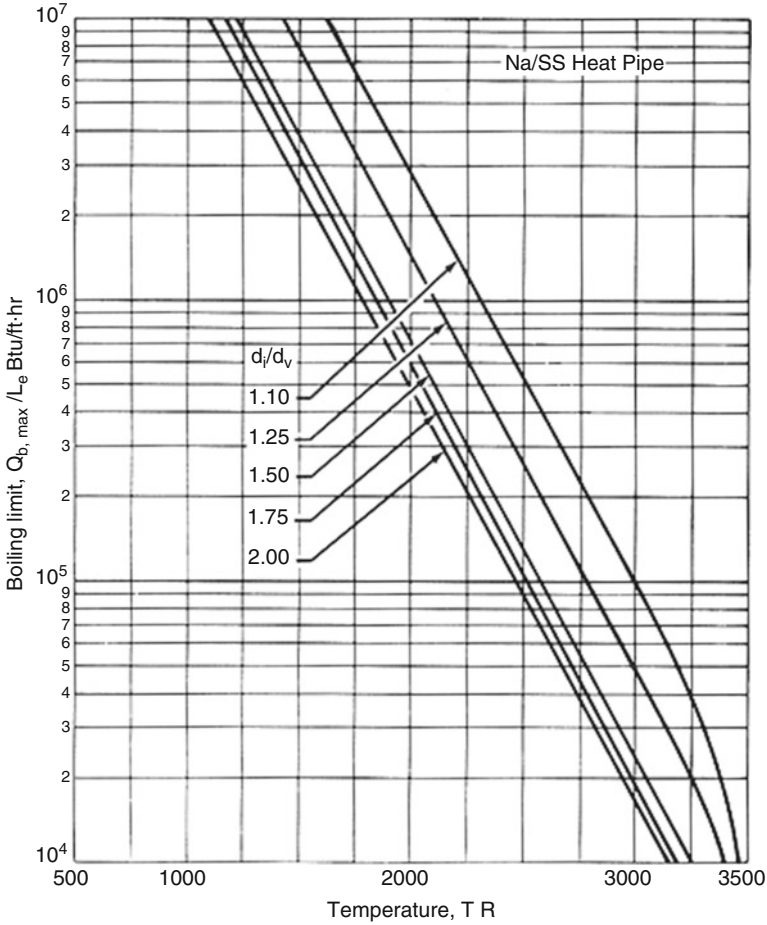


Fig. 3.28 Boiling limit on heat flux per unit length of evaporator [5] (1 Btu/ft-h = 0.961 W/m, 1 R = 0.5556K); sodium

3.9.1 Wick Design

The general procedure for the design of the wrapped-screen wick for a heat pipe operating in the normal and steady-state heat pipe mode one can use is shown in Figs. 3.30, 3.31, 3.32, 3.33, 3.34, 3.35, 3.36, 3.37, 3.38, 3.39, 3.40, 3.41, and 3.42 in order to quickly determine the wick dimensions using the following rule of thumbs.

1. Given the knowledge of the inside pipe diameter d_i and total length L_t as well as the tilting angle of ψ , the gravitational hydrostatic pressure can be calculated using the following equation, where ρ_l is the liquid density and g is the gravitation, force and the value of $\rho_l g$ can be read from Fig. 3.29:

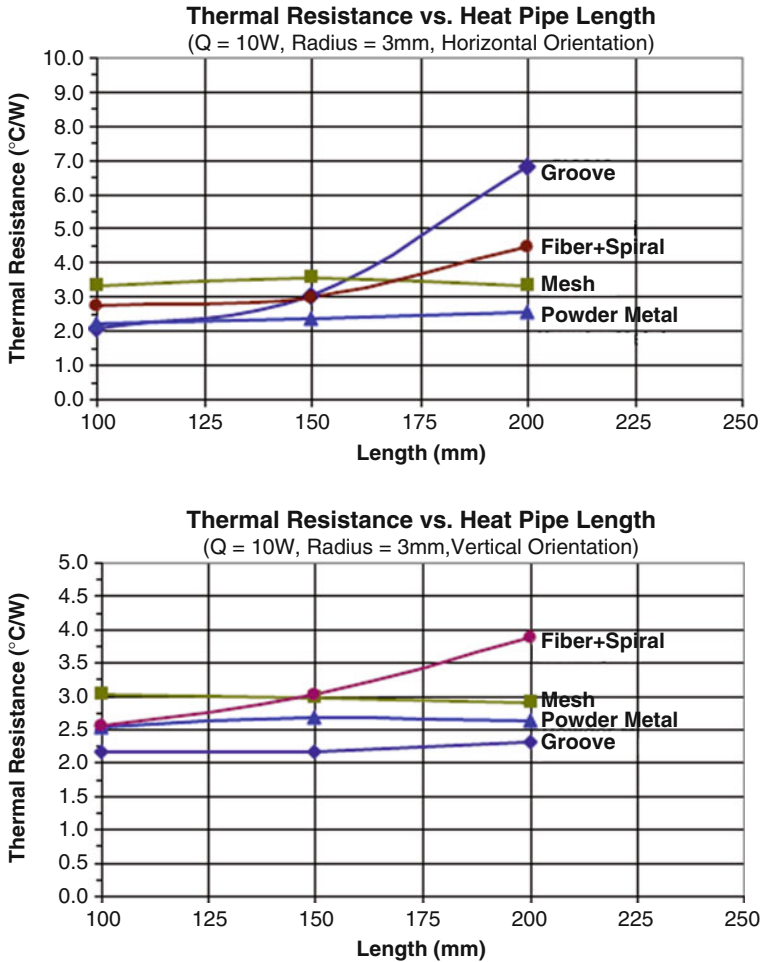


Fig. 3.29 The actual test results of heat pipe with different wick structure at horizontal and vertical (gravity assist) orientations. Courtesy of Enertron Corporation

$$P_g = \rho_l g (d_t \cos \psi + L_t \sin \psi) \tag{Eq.3.17}$$

2. The required mesh number for the wick can be selected using Figs. 3.21, 3.22, 3.23, and 3.24 considering that P_c should not be much smaller than twice the value of P_g that is calculated in step 1 in above.
3. Now we can assume that t_w is required wick thickness for the pipe and a vapor core diameter of d_v equal to $(d_v - 2t_w)$. In that case, from Eqs. (2.44) and (2.59) liquid and vapor frictional coefficients F_l and F_v can then be read from Figs. 3.30, 3.31, 3.32, 3.33, 3.35, 3.36, 3.37, and 3.38, respectively.

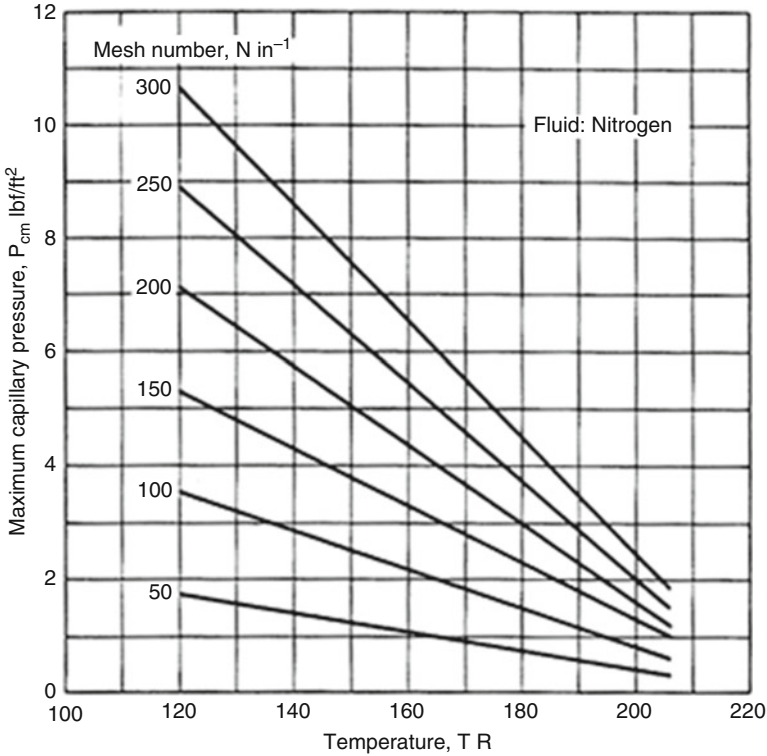


Fig. 3.30 Maximum capillary pressure for screen wicks [5] (1lbf/ft² = 47.88N/m², 1R = 0.5556K, 1in.⁻¹ = 39.37m⁻¹) nitrogen

- Using the assumed wick thickness as mentioned above, the heat transport limit for the pipe that is defined by Eq. (2.81) can be calculated as follows:

$$(QL)_{\text{CapillaryMax}} = \frac{P_c - P_g}{F_1 + F_v} \tag{Eq.3.18}$$

- Check to see if $(QL)_{\text{CapillaryMax}}$ that is calculated by Eq. (3.17) has a value greater than the required (QL) for the problem under consideration. If so, then the assumed wick thickness is satisfactory. If that is not the case, a larger wick thickness is needed to be used, and steps 3 through 5 are repeated until a satisfactory wick thickness is chosen.

It can be seen that the above design procedure may be completed quickly with the aid of design charts. These procedures are offered specifically with reference to the conventional heat pipe operating in a heat pipe mode, and the values for P_c , $\rho_l g$, F_1 and F_v that are presented in Figs. 3.21, 3.22, 3.23, 3.24, 3.25, 3.26, 3.27, 3.28, 3.29, 3.30, 3.31, 3.32, and 3.33 can also be used for the heat pipe operating in other modes.

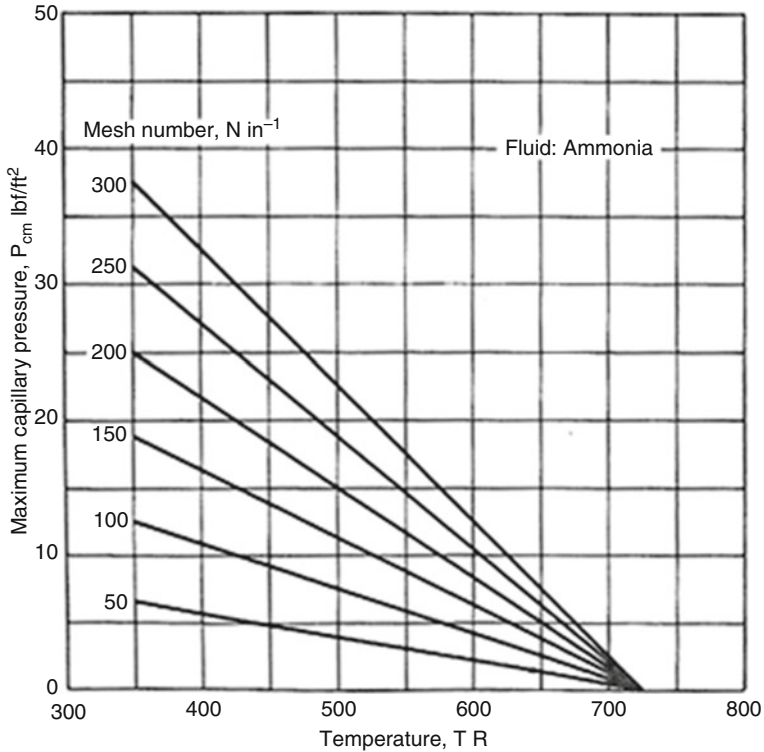


Fig. 3.31 Maximum capillary pressure for screen wicks [5] ($1 \text{ lbf/ft}^2 = 47.88 \text{ N/m}^2$, $1 \text{ R} = 0.5556 \text{ K}$, $1 \text{ in.}^{-1} = 39.37 \text{ m}^{-1}$) ammonia

Note that preliminary consideration for these arguments is based on the wick design of wire cloth element with the wrapped-screen in this section. The principal properties of the wire cloth important for heat pipe applications are first considered from a practical point of view. The wire cloth that is commonly used for heat pipe wicks has square meshes, and the mesh size is usually specified in mesh number, which is defined as the number of mesh per linear inch measured in a direction perpendicular to the wire. Although different wire sizes can be used for the woven wire cloth, in many cases, the wire size is approximately equal to the wire spacing. Approximate characteristic of wick structures, as we discussed before, indicate that the liquid flow resistance in wick structures is inversely proportional to the square of the mesh size and the capillary pumping pressure is inversely proportional to the mesh size. However, wire cloth with mesh numbers from 50 to 300 are the most commonly used wicks in practice. Practical experience indicates that for successful operation of heat pipes in a gravitational field, the maximum capillary pressure must at least be about twice that of the liquid hydrostatic pressure. Figures 3.30, 3.31, 3.32, and 3.33 contain data on maximum capillary pressure as calculated by

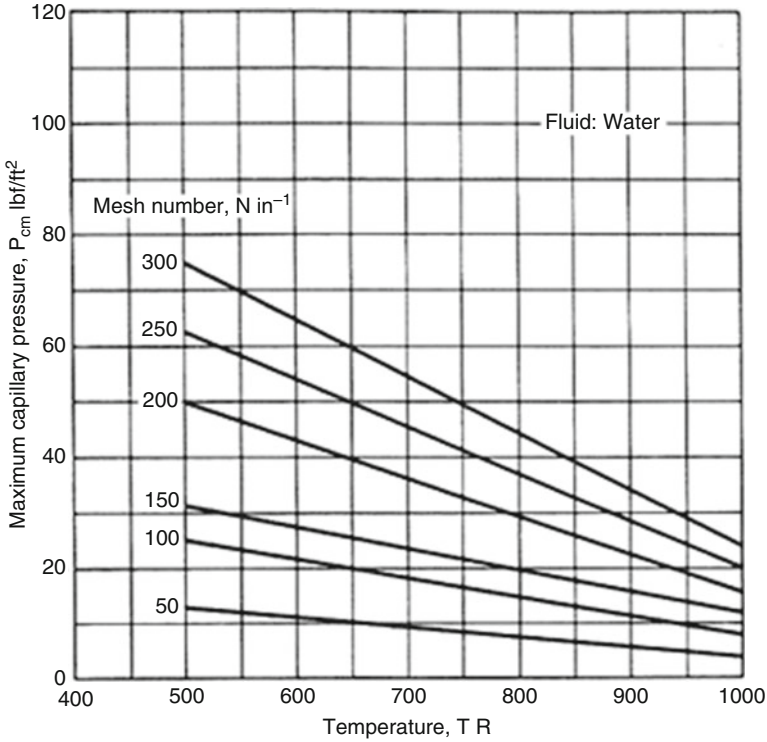


Fig. 3.32 Maximum capillary pressure for screen wicks [5] ($1 \text{ lbf/ft}^2 = 47.88 \text{ N/m}^2$, $1 \text{ R} = 0.5556 \text{ K}$, $1 \text{ in.}^{-1} = 39.37 \text{ m}^{-1}$) water

Eq. (2.7) and as shown in Table 2.1 for wire screen. Figure 3.34 contains data on the hydrostatic pressure per unit vertical elevation of various liquids under a standard gravitational field of $32.2 \text{ ft/s}^2 (9.81 \text{ m/s}^2)$. As shown in Table 2.1, in case of parallel wire wick, the effective capillary radius r_c for screen wicks is expected to be equal to half of the spacing between the wires. However, due to staggering of the wires and the interference among adjacent layers of the screen, it has not so far been possible to determine the effective radius for screen wicks by a means of theory, but experimental data [10] from tests on single-layer screens seem to suggest that r_c is equal to half of the sum of the wire diameter d and the spacing w instead of being equal to only half of the spacing. For multilayer screens, no generalized data are yet available. It also appears that the effective radius for screen wicks can be calculated in a very conservative approach by following equation:

$$r_c = \frac{d + w}{2} = \frac{1}{2N} \tag{Eq.3.19}$$

where N is the mesh number defined as number of wires per unit length [5].

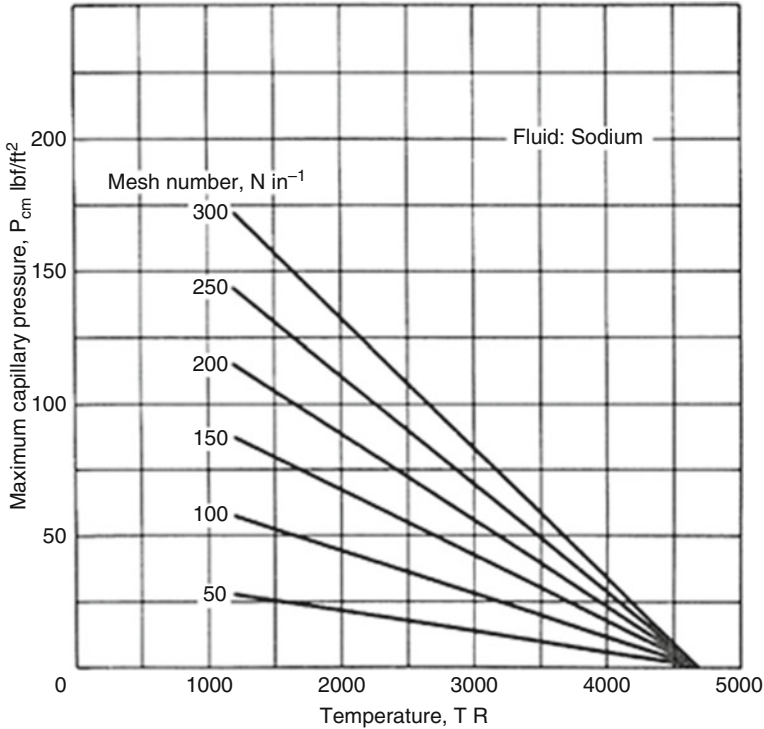


Fig. 3.33 Maximum capillary pressure for screen wicks [5] ($1 \text{ lb/ft}^2 = 47.88 \text{ N/m}^2$, $1 \text{ R} = 0.5556 \text{ K}$, $1 \text{ in.}^{-1} = 39.37 \text{ m}^{-1}$) water

3.10 Steady-State and Transient Regime

According to the definition from thermodynamics, steady state is a process which does not alter the state of a system but does change the surroundings. However, under steady-state conditions inputs and outputs of the system remain in balance so that the properties of the system are not altered, but changes do occur in the surroundings as a result of such processes. Under the prevailing steady-state or equilibrium conditions, the system remains essentially unaltered in the virtual displacements and is a more general situation than dynamic equilibrium. If a system is in steady state, then the recently observed behavior of the system will continue into the future. In stochastic systems, the probabilities that various different states will be repeated will remain constant.

A system in a steady state has numerous properties that are unchanging in time. This implies that for any property p of the system, the partial derivative with respect to time is zero.

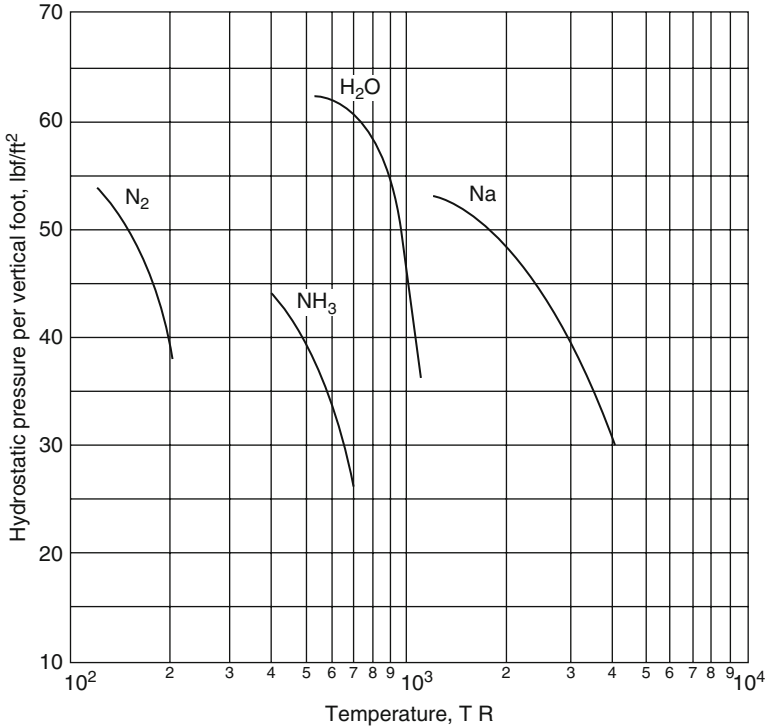


Fig. 3.34 Liquid gravitational hydrostatic pressure per unit vertical elevation versus temperature in a standard gravitational field [5] (1 lbf/ft³ = 1.57 N/m³, 1 R = 0.5556 K)

$$\frac{\partial p}{\partial t} = 0 \tag{Eq.3.20}$$

In many systems, steady state is not achieved until some time has elapsed after the system is started or initiated. This initial situation is often identified as a transient state, startup or warm-up period.

Yet the transient state is a process which is dependent on time, in other words, **transience** means passing with time or is the state of being brief and short-lived. Something which has the property of transience is said to be **transient** or often simply a *transient* or *transient state*.

Summary

1. Steady state

Many engineering systems can be idealized as being at **steady state**, meaning that *all* properties are unchanging in time.

2. Transient state

Many engineering systems undergo periods of transient operation where the state changes with time and this operation is known as the **transient state**. This is observed during startup and shutdown periods.

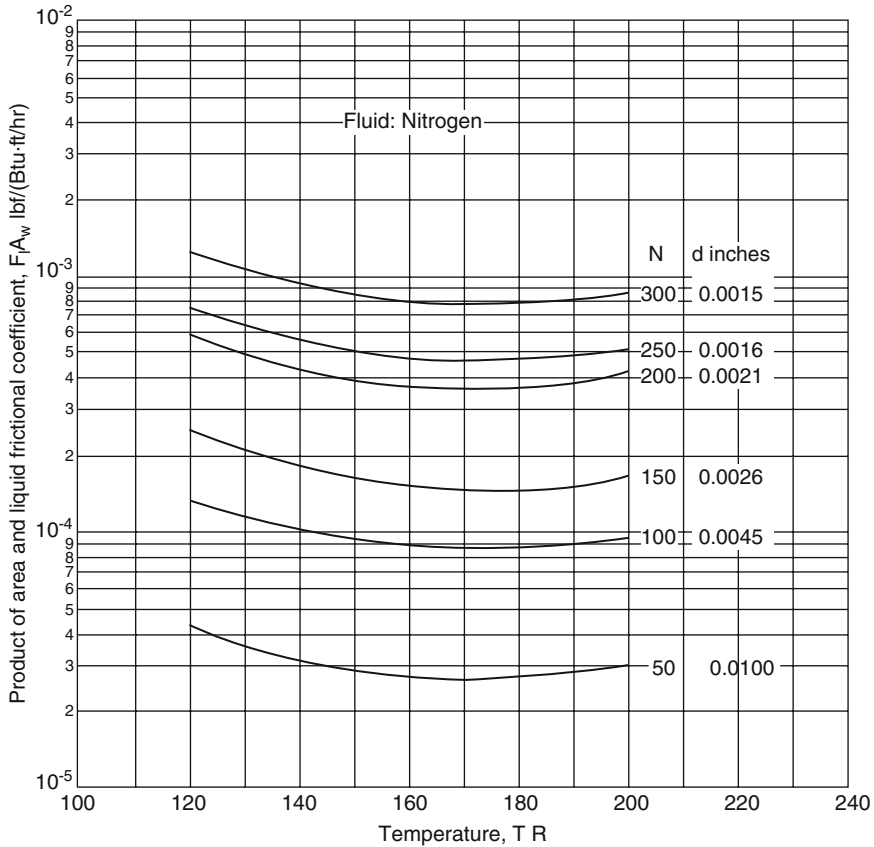


Fig. 3.35 Liquid frictional coefficient versus temperature for liquid flow in wrapped-screen wicks [5] [1 lbf/(Btu ft/h) = 49.82 N/W m, 1 R = 0.5556 K, 1 in. = 0.0254 m] nitrogen

3.11 Heat Pipe Steady-State and Transient Analysis

Operation status of a heat pipe may either take place under steady-state or transient conditions. In a steady-state mode, heat is removed from the heat pipe condenser (heat source) at the same rate as heat is added to evaporator (heat sink), and heat pipe temperature remains constant.

In transient state, there is an imbalance between the added heat rate to evaporator versus heat rejected from the condenser side of the heat pipe, and heat pipe temperature varies with time. This condition always takes place during heat pipe startup from ambient (frozen-state) temperature.

If the heat input rate is smaller than the heat absorption capability of the heat pipe, the startup process will be slow and gradual. Under this condition, overheating and/or operational difficulty will not likely take place. On the other hand, the startup

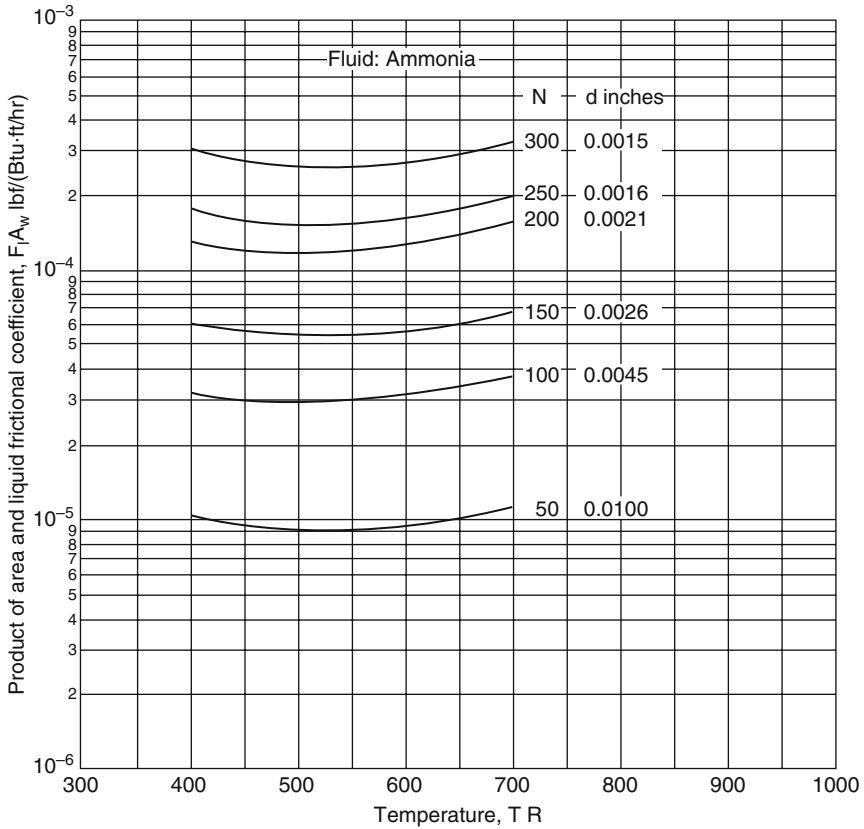


Fig. 3.36 Liquid frictional coefficient versus temperature for liquid flow in wrapped-screen wicks [5] [1 lbf/(Btu ft/h) = 49.82 N/Wm, 1 R = 0.5556 K, 1 in. = 0.0254 m] ammonia

within heat pipe might be quite rapid if the input rate of heat is significant or much larger than the heat absorption capability. Potential startup problems within heat pipe become a concern if the ambient temperature is below the freezing point of the heat pipe working liquid. Under this condition, the heat pipe does not become operational until the temperature of the evaporator section significantly rises above this freezing point and consequently the vapor pressure inside the heat pipe is then extremely low.

When the heat pipe reaches its operational stage, its heat transport capability could initially be insufficient to prevent freeze out of condensate if there is good thermal coupling between the heat pipe condenser and the heat sink. Dryout of the evaporator wick, overheating, and possible destruction of the heat pipe could soon follow [11]. The heat pipe may fail to become in full operation even if freeze out of condensate did not occur when only a portion of condenser length is in the thermal coupling for dissipating the incident heat load.

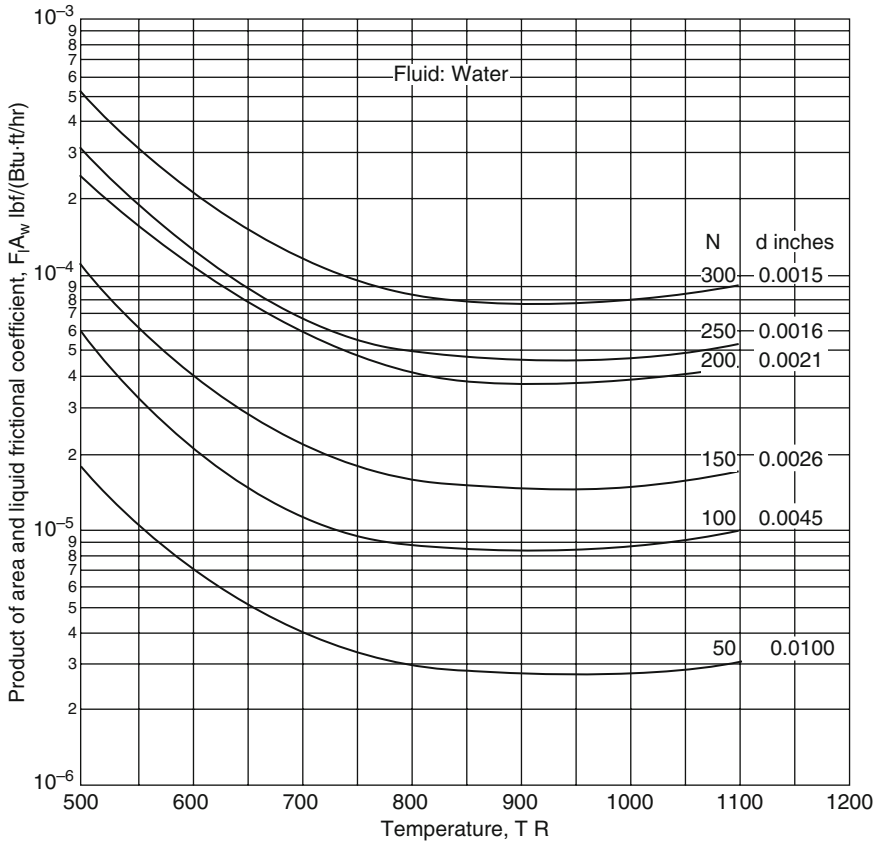


Fig. 3.37 Liquid frictional coefficient versus temperature for liquid flow in wrapped-screen wicks [5] [1 lbf/(Btu ft/h) = 49.82 N/Wm, 1 R = 0.5556 K, 1 in. = 0.0254 m] water

The heat pipe would then not necessarily overheat but could remain in a high non-isothermal state throughout startup and into the steady-state operational phase. Under such circumstance, a *transient analysis* of the heat pipe startup is advisable. The purpose of the transient analysis is threefold [11]:

1. To determine whether overheating or excessive thermal stress develops in the heat pipe wall
2. To determine whether heat pipe transport limits are exceeded
3. To determine whether startup difficulty is encountered because of excessive thermal coupling between the heat pipe condenser and the heat sink

The above three objectives are achievable by calculating the time dependency of the temperature at key heat pipe locations and the actual heat transport rate, and the position of the continuum front heat separates heated vapor from the condenser. The adequacy of the heat pipe design during startup can then be established by

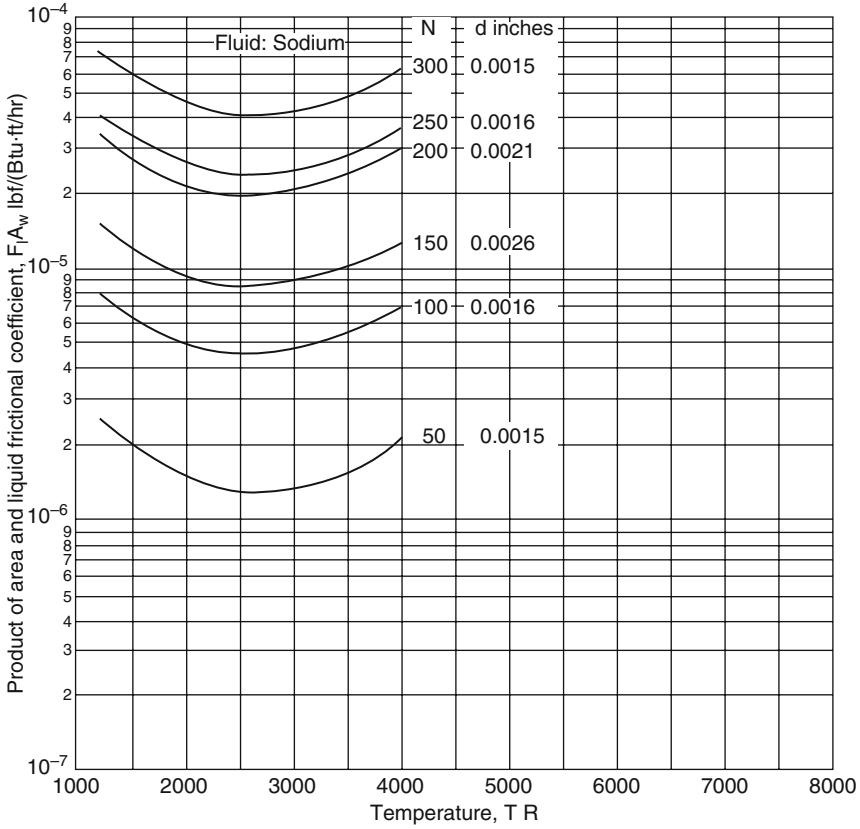


Fig. 3.38 Liquid frictional coefficient versus temperature for liquid flow in wrapped-screen wicks [5] [$1 \text{ lbf}/(\text{Btu}\cdot\text{ft}/\text{h}) = 49.82 \text{ N}/\text{W}\cdot\text{m}$, $1 \text{ R} = 0.5556 \text{ K}$, $1 \text{ in.} = 0.0254 \text{ m}$] sodium

comparing the temperatures and heat transport rate with temperature and heat transport limitations and by observing whether the continuum front has reached the rear of the condenser.

One should consider that the steady-state design is the starting point for the transient analysis. The steady-state design may be based on the heat load at the steady-state operating condition (if there exist one) or on the maximum expected heat load during the transient. If the maximum heat load occurs after the entire heat pipe has become functional, peak transient heat pipe temperature will probably not differ appreciably from steady-state temperatures based on the maximum heat load. If the peak heat load occurs before the entire heat pipe has become functional, predicted heat pipe temperatures based on the maximum heat load at steady-state conditions could be substantially overstated [11].

Generally speaking the heat pipe startup process is very complex, which involves temperature variations in two- and three-dimensional space as well as

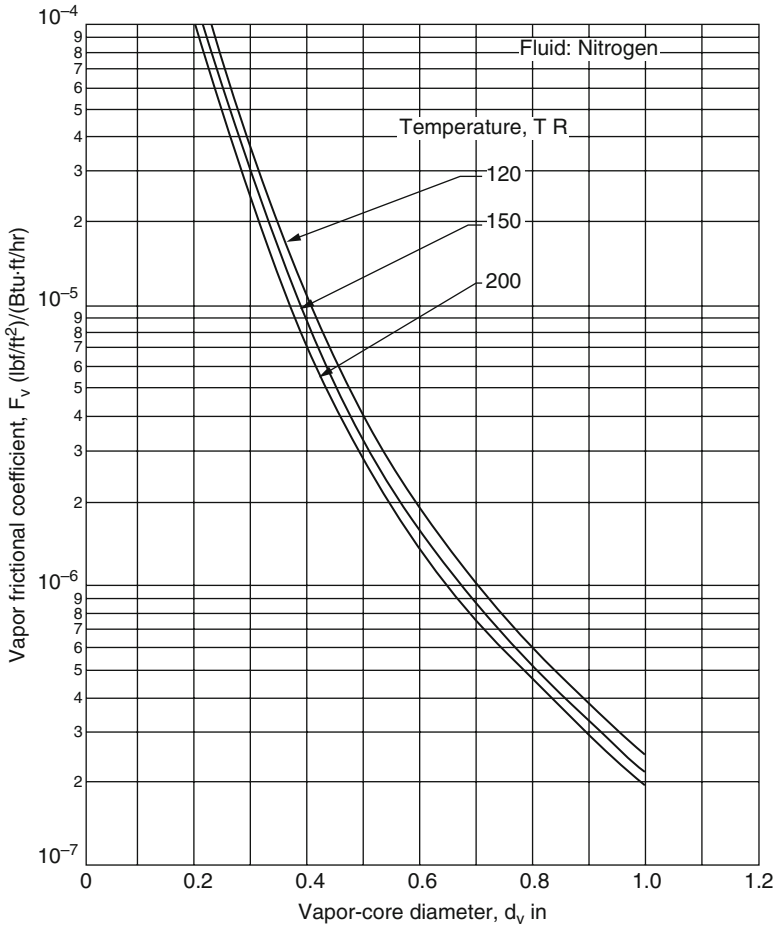


Fig. 3.39 Vapor friction coefficient for vapor flow in round tubes [5] [$1 (\text{lb}/\text{ft}^2)/(\text{Btu}\cdot\text{ft}/\text{h}) = 536.3 (\text{N}/\text{m}^2)/\text{W}\cdot\text{m}$, $1 \text{ in.} = 0.0254 \text{ m}$, $1 \text{ R} = 0.5556 \text{ K}$] nitrogen

over time, vapor heat transport in the free molecular and continuum flow regimes, expansion of the heat pipe vapor into a hard vacuum accompanied by condensation, nonequilibrium expansion effects in a nominally saturated vapor, and solid–liquid as well as liquid–vapor phase changes. One approach to this problem is analyzed by Colwell, et al. [12].

Startup is best accomplished by using a working fluid which is initially saturated. When this is not possible, in the case of many cryogenic or liquid-metal heat pipes, the wick should be designed to give good transport during the priming operation. When a variable conductance heat pipe is required, the transient behavior will depend to a large extent on the type of variable cryogenic heat pipe (VCHP) employed and the choice of the working fluid.

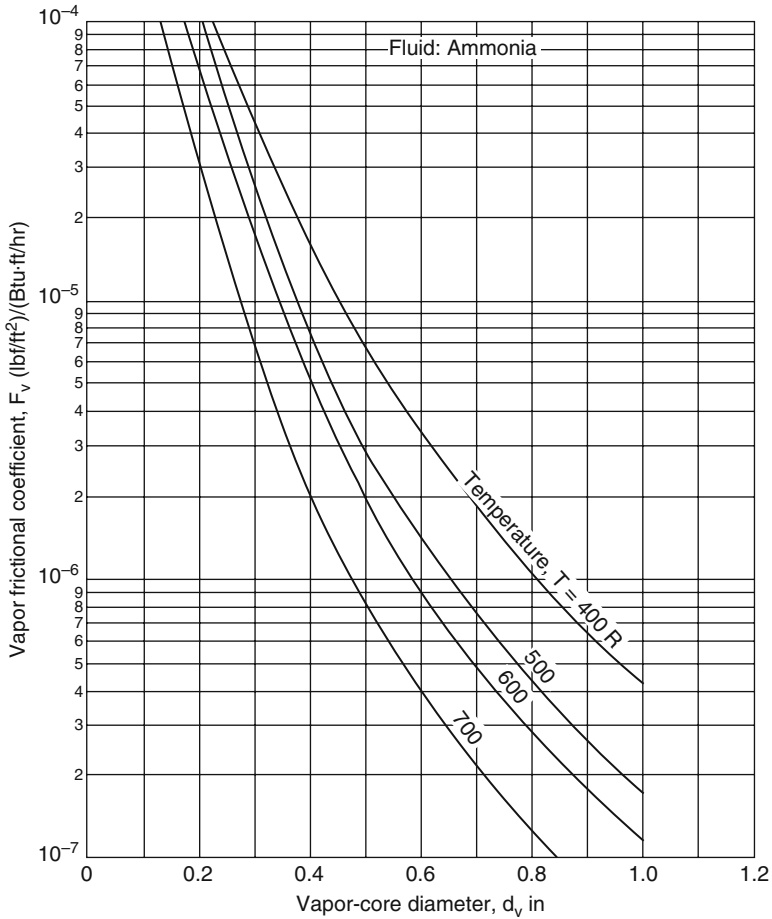


Fig. 3.40 Vapor friction coefficient for vapor flow in round tubes [5] [$1 (\text{lb/ft}^2)/(\text{Btu}\cdot\text{ft}/\text{h}) = 536.3 (\text{N/m}^2)/\text{W}\cdot\text{m}$, $1 \text{ in.} = 0.0254 \text{ m}$, $1 \text{ R} = 0.5556 \text{ K}$] ammonia

Faghri [13] has provided a good mathematical modeling around the transient response to a sudden change in heat input or temperature. He presents the cases that, after a heat pipe reached a fully steady state, it is often desirable particularly in case of variable heat pipe (VHP) to determine the period of time required to reach another steady state for a given increase in the heat increase at sink point or evaporator side of heat pipe. He describes three separate analysis and model which shows the solutions for 1-D and 2-D heat equation in transient continuum model in cylindrical coordinate, and they are summarized as follows:

1. Transient lumped model
2. One-dimensional transient continuum model
3. Two-dimensional transient continuum model

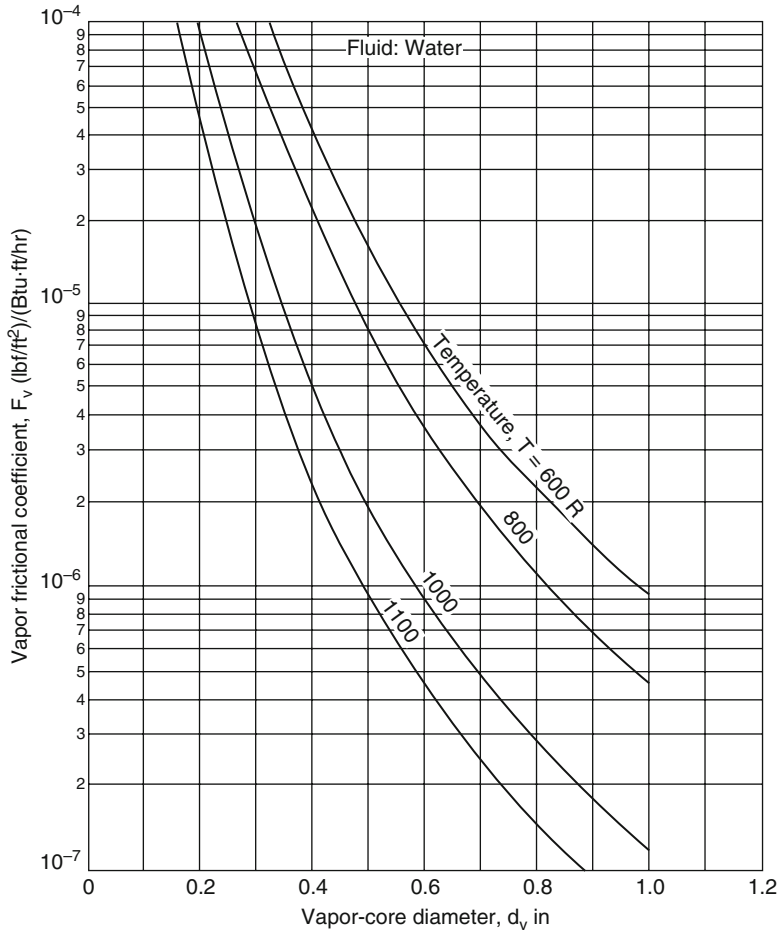


Fig. 3.41 Vapor friction coefficient for vapor flow in round tubes [5] [$1 \text{ (lb/ft}^2\text{)}/(\text{Btu ft/h}) = 536.3 \text{ (N/m}^2\text{)}/\text{W m}$, $1 \text{ in.} = 0.0254 \text{ m}$, $1 \text{ R} = 0.5556 \text{ K}$] water

Although 1-D and 2-D numerical models are generally more comprehensive and accurate, it requires considerable cup time and effort by the computer coding. The lumped analytical model, on the other hand, provides a quick and convenient approach for the heat pipe designers.

1. Transient lumped model

Present by Faghri and Harley [14], a transient lumped heat pipe model determines the average temperature as a function of time where they formulate a derivation from the general lumped capacitance analysis, which is an application of an energy balance over a control volume as shown in Fig. 3.43. The resulting energy equation

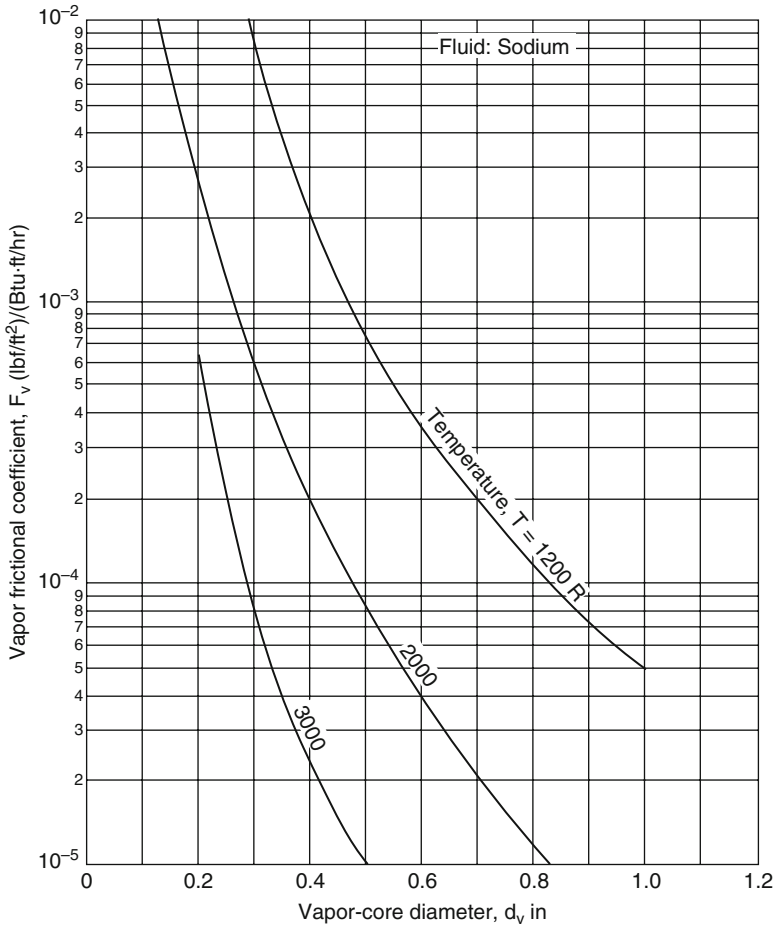


Fig. 3.42 Vapor friction coefficient for vapor flow in round tubes [5] [1 (lb/ft²)/(Btu ft/h) = 536.3 (N/m²)/W m, 1 in. = 0.0254 m, 1 R = 0.5556 K] sodium

in the case of both radiative and convective heat transfer from the condenser surface and an imposed heat input to the evaporator is shown below:

$$Q_e - (q_{convective} + q_{radiative})S_c = C_t \frac{dT}{dt} \tag{Eq.3.21}$$

where

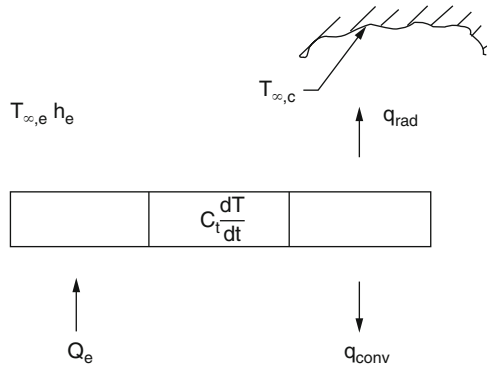
Q_e = The heat input

$q_{convective}$ = The output heat flux by convection

$q_{radiative}$ = The radiation heat flux

S_c = The surface area around the circumference of the cooled section

Fig. 3.43 Control volume for general lumped capacitance analysis [13]



C_t = The total thermal capacity of the system

T = Uniformed temperature of the heat pipe

t = Time period

The total thermal capacity of the system defined as follows:

$$C_t = \rho V_t c_p \tag{Eq.3.22}$$

where

ρ = Density

V_t = Total volume

c_p = Specific heat of the system

In heat pipe applications, the total thermal capacity is defined as the sum of the heat capacities of the solid and liquid components of the heat pipe, and the heat capacity of the liquid-saturated wick is modeled accounting for both the liquid in the wick and the wick structure itself and is represented by Eq. (3.23) as follows:

$$(\rho c_p)_{\text{effective}} = \varphi (\rho c_p)_\ell + (1 - \varphi) (\rho c_p)_s \tag{Eq.3.23}$$

where φ is the porosity of the wick. For more details on this approach, the reader should go through Faghri’s book [13]

In this figure, $T_{\infty, c}$ is the ambient temperature surrounding the condenser, $T_{\infty, e}$ is the ambient temperature surrounding the evaporator side of the heat pipe, h_c is the external convective coefficient for condenser, and h_e is representing same value for evaporator side of the system (i.e., heat pipe).

2. One-dimensional transient continuum model

From a mathematical analysis point of view, naturally, any one-dimensional modeling is an easier process that a two-dimensional to solve. Therefore, in the relative case of any one-dimensional heat pipe modeling over the more complex two-dimensional models, it is important that we take this approach first. Although either of these approaches (1-D or 2-D) is more involved than the lumped analysis

method, it provides better understanding of axial variation of temperature along the heat pipe with time. The first presentation of a one-dimensional simulation of the transient vapor flow was performed by Jang et al. [15] to reduce the CPU time of computer required as compared to a two-dimensional vapor flow model, but it did not include the thermal effects of wick and wall of heat pipe on its transient operation. Faghri [13] uses the conservation equations for vapor flow with negligible body forces formulated using the principles of conservation of mass and momentum in a control volume and presents the following equation applying the law of mass conservation over an elementary vapor control volume:

$$\frac{\partial \rho}{\partial t} A_v \Delta z + \frac{\partial}{\partial z} (\rho \bar{w}) \Delta z A_v - \rho_\delta v_\delta dS = 0 \quad (\text{Eq.3.24})$$

where

\bar{w} = Average axial vapor velocity

$$A_v = \pi R_v^2$$

$$dS = 2\pi R_v \Delta z$$

Using the above definitions and dividing by $A_v \Delta z$, the conservation of mass equation is

$$\frac{\partial \rho}{\partial t} + \frac{\partial}{\partial z} (\rho \bar{w}) = \frac{2\rho_\delta v_\delta}{R_v} \quad (\text{Eq.3.25})$$

Faghri [13] analysis also continues to show that applying the law of conservation of momentum to the same control volume gives

$$\frac{\partial}{\partial t} (\rho \bar{w}) A_v \Delta z + \frac{\partial}{\partial z} (\rho \bar{w}^2) A_v \Delta z = \frac{\partial \sigma_z}{\partial z} - \tau_w dS \quad (\text{Eq.3.26})$$

where the normal stress function is

$$\sigma_z = -p + \frac{4}{3} \mu \frac{\partial \bar{w}}{\partial z} \quad (\text{Eq.3.27})$$

Using the above definition for the normal stress function, A_v , dS and the friction coefficient, and dividing by $A_v \Delta z$ gives the conservation of axial momentum equation:

$$\frac{\partial}{\partial t} (\rho \bar{w}) A_v \Delta z + \frac{\partial}{\partial z} (\rho \bar{w}^2) A_v \Delta z = -\frac{\partial}{\partial z} \left(p + \frac{4}{3} \mu \frac{\partial \bar{w}}{\partial z} \right) - \frac{f \rho \bar{w}^2}{R_v} \quad (\text{Eq.3.28})$$

The friction coefficient f is a function of the axial Reynolds number of the vapor flow. Since the vapor flow remains laminar in evaporator, it allows the conventional pipe flow correlations to be used:

$$f = \frac{16}{\text{Re}} \quad \text{for } \text{Re} < 2000 \quad (\text{Eq.3.29})$$

If it turns out that the axial Reynolds number was greater than 2000, the flow at the condenser may be turbulent. The friction coefficient in this case can be induced from the following equation:

$$f = \frac{0.079}{\text{Re}_{0.25}} \quad \text{for } \text{Re} \geq 2000 \quad (\text{Eq.3.30})$$

One can use the ideal gas law below account for the compressibility status.

$$p = \rho R_g T \quad (\text{Eq.3.31})$$

The conservation of energy equation in the vapor space is derived by assumption of a uniform temperature in the radial direction and negligible energy transfer from tangential and normal stresses (viscous shear and static pressure) [13]:

$$\frac{\partial T}{\partial t} = -\frac{\partial}{\partial z}(\bar{w}T) + \alpha \frac{\partial^2 T}{\partial z^2} + \frac{2v_\delta T_\delta}{R_v} \quad (\text{Eq.3.32})$$

If the temperature is assumed to be uniform in the radial direction, then $T_\delta = T = T_v$. Therefore, the energy equation is given as follows:

$$\frac{\partial T_v}{\partial t} + \bar{w} \frac{\partial T_v}{\partial z} = +\alpha \frac{\partial^2 T_v}{\partial z^2} + \frac{2v_\delta T_v}{R_v} \quad (\text{Eq.3.33})$$

In the evaporator, $v_\delta < 0$ implies that heat is added to the vapor and conversely, in the condenser, $v_\delta > 0$ then heat is removed.

It is this interfacial velocity term which couples the solutions of the energy equation in the wall-wick region and vapor space regions since the blowing/suction rate is determined from an energy balance at the liquid-vapor interface [13].

The boundary condition at the liquid-vapor interface is more complex since it couples the wick and vapor flow. The blowing or suction velocity $v_\delta \rho_\delta$ can be found from an energy balance at the interface:

$$v_\delta \rho_\delta = \frac{k_{\text{eff}}}{hf_g} \frac{\partial T_\ell}{\partial r} \begin{cases} > 0 \text{ (blowing)} \\ < 0 \text{ (suction)} \end{cases} \quad (\text{Eq.3.34})$$

For more details of these analyses, the reader should refer to Faghri's book [13].

3. Two-dimensional transient continuum model

Any operational process of heat pipe such as startup, shutdown, and operational transients such as pulsed heat inputs is very important and requires detailed study of

heat pipe transient analysis. At some time during transient operation, heat pipes have a two-dimensional behavior which cannot be accounted for by a one-dimensional model. Additionally a two-dimensional formulation and analyses do not require any empirical relations for frictional specification and result in a more accurate solution than one-dimensional models. Furthermore, a two-dimensional model is required to simulate certain important phenomena such as nonuniform input heat fluxes and multiple heat sources or sinks [13]. Extensive formulation and details including mathematical analyses are provided by Faghri [13], and reader should refer to his book.

3.11.1 Solution of the Steady-State Equation

Many of the problems of mathematical physics involve the solution of partial differential equations (PDEs) and may apply to a variety of physical problem including heat transfer both in steady and transient state. In general the diffusion or heat flow equation may be represented by the following equation:

$$\nabla^2 u = \frac{1}{\alpha^2} \frac{\partial u}{\partial t} \quad (\text{Eq.3.35})$$

Here T may be the non-steady-state temperature where temperature varies with time t in a region with no heat source, or it may be the concentration of a diffusing substrate. The quantity α^2 is a constant known as the diffusivity in a simple case conduction of heat in solid problem. In a simple form of steady-state where the temperature is not changing with time in a region containing no source of heat, the above Eq. (3.35) reduces to Laplace's equation form as below:

$$\nabla^2 T(x, y, z, t) = 0 \quad (\text{Eq.3.36})$$

The function u may represent the same physical quantities listed for Laplace's equation but in a region containing sources of heat or fluid, respectively, for the various cases. In this case, Laplace's equation take a new form known as Poisson's equation as below when the flow is steady:

$$\nabla^2 T(x, y, z, t) = f(x, y, z) \quad (\text{Eq.3.37})$$

In general if heat is produced in the solid, so that at the point $P(x, y, z)$ heat is supplied at the rate $A(x, y, z, t)$ per unit time per unit volume, a term has to be added, and the following equation is defined:

$$\nabla^2 T(x, y, z, t) - \frac{1}{\alpha^2} \frac{\partial T(x, y, z, t)}{\partial t} = -\frac{A(x, y, z, t)}{K} \quad (\text{Eq.3.38})$$

where K is a constant, and in case of steady flow where $\frac{\partial T(x,y,z,t)}{\partial t} = 0$, then Eq. (3.38) reduces to Eq. (3.37). In the theory of heat conduction, an assumption is made that heat flows in the direction of decreasing temperature. Another assumption is that the time rate at which heat flows across a surface area is proportional to the component of the temperature gradient in the direction perpendicular to the surface area. If the temperature $T(x, y, z, t)$ does not depend on time, then the heat flow at the point (x, y, z, t) is given by the vector version of Eq. (3.38). For more details reader should refer to Carslaw and Jaeger [16] where solution of Laplace or Poisson's equations is solved for various cases and different coordinates (i.e., Cartesian, cylindrical, and spherical).

A wide variety of problems in engineering and physics involve harmonic functions, which are the real or imaginary part of an analytic function. The standard applications are two-dimensional steady-state temperatures, electrostatics, fluid flow, and complex potentials. The techniques of conformal mapping and integral representation can be used to construct a harmonic function with prescribed boundary values. Noteworthy methods include Poisson's integral formulae, the Joukowski transformation, and Schwarz–Christoffel transformation. Modern computer software is capable of implementing these complex analysis methods.

In most applications involving harmonic functions, a *harmonic function* that takes on prescribed values along certain contours must be found.

Harmonic Function

Any *real function* $T(x, y)$ with continuous second *partial derivative* which satisfies Laplace's equation of

$$\nabla^2 T(x, y) = 0 \quad (\text{Eq.1})$$

is called a harmonic function. Harmonic functions are called *potential functions* in physics and engineering. Potential functions are extremely useful, for example, in electromagnetism, where they reduce the study of a three-component *vector field* to a one-component *scalar function*. A scalar harmonic function is called a *scalar potential*, and a vector harmonic function is called a *vector potential*.

To find a class of such functions in the *plane*, write the Laplace's equation in polar coordinates

$$T_{rr} + \frac{1}{r}T_r + \frac{1}{r^2}T_{\theta\theta} = 0 \quad (\text{Eq.2})$$

and consider only radial solutions

$$T_{rr} + \frac{1}{r}T_r = 0 \quad (\text{Eq.3})$$

(continued)

This is integrable by quadrature, so define $V = \frac{dT}{dr}$, then we have

$$\frac{dV}{dr} + \frac{1}{r}V = 0 \quad (\text{Eq.4})$$

$$\frac{dV}{dr} = -\frac{dr}{r} \quad (\text{Eq.5})$$

Integrating Eq. (5) with respect to r we have the following:

$$\ln\left(\frac{V}{A}\right) = -\ln r \quad (\text{Eq.6})$$

$$\frac{V}{A} = \frac{1}{r} \quad (\text{Eq.7})$$

$$V = \frac{dT}{dr} = \frac{A}{r} \quad (\text{Eq.8})$$

$$dT = A \frac{dr}{r} \quad (\text{Eq.9})$$

So the solution is

$$u = A \ln r \quad (\text{Eq.10})$$

Ignoring the trivial additive and multiplicative constants, the general pure radial solution then becomes

$$\begin{aligned} T &= \ln \left[(x-a)^2 + (y-b)^2 \right]^{1/2} \\ &= \frac{1}{2} \left[(x-a)^2 + (y-b)^2 \right]^{1/2} \end{aligned} \quad (\text{Eq.11})$$

Other solutions may be obtained by differentiation, such as

$$T = \frac{x-a}{(x-a)^2 + (y-b)^2} \quad (\text{Eq.12})$$

$$Q = \frac{y-a}{(x-a)^2 + (y-b)^2} \quad (\text{Eq.13})$$

$$T = e^x \sin y \quad (\text{Eq.14})$$

$$Q = e^x \cos y \quad (\text{Eq.15})$$

(continued)

and

$$\tan^{-1}\left(\frac{y-b}{x-a}\right) \tag{Eq.16}$$

Harmonic functions containing azimuthal dependence include

$$T = r^n \cos(n\theta) \tag{Eq.17}$$

$$Q = r^n \sin(n\theta) \tag{Eq.18}$$

The *Poisson Kernel* is

$$T(r, R, \theta, \phi) = \frac{R^2 - r^2}{R - 2rR \cos(\theta - \phi) + r^2} \tag{Eq.19}$$

is another harmonic function.

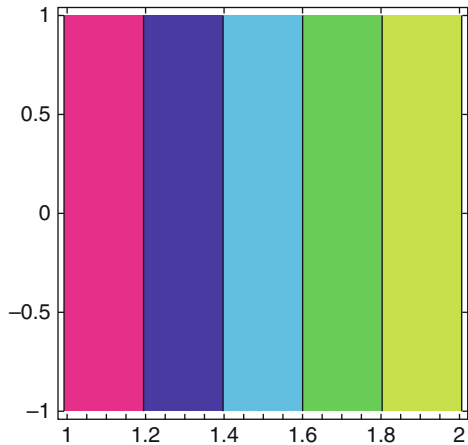
Example 3.1 Find the function $T(x, y)$ that is harmonic in the vertical strip $a < \text{Re}(z) < b$ and takes on the boundary values

$$T(a, y) = T_1 \quad \text{for all } y$$

$$T(b, y) = T_2 \quad \text{for all } y$$

Along the vertical line $x = a$ and $x = b$, respectively (Fig. 3.44).

Fig. 3.44 Application preliminary mod



Solution Intuition suggests that we should seek a solution that takes on constant values along the vertical lines of the form $x = x_0$ and that $T(x, y)$ be a function of x alone, that is,

$$T(x, y) = P(x) \text{ for } a \leq x \leq b \text{ and for all } y$$

Laplace's equation, $T_{xx}(x, y) + T_{yy}(x, y) = 0$, implies that $P''(x) = 0$, which implies $P(x) = mx + c$, where m and c are constants. The boundary conditions $T(a, y) = P(a) = T_1$ and $T(b, y) = P(b) = T_2$ lead to the solution

$$T(x, y) = T_1 + \frac{T_2 - T_1}{b - a}(x - a)$$

The level curves $T(x, y) = \text{constant}$ are vertical lines as indicated in Fig. 3.45.

Example 3.2 Suppose that two parallel planes are perpendicular to the z plane and pass through the horizontal lines $y = a$ and $y = b$ and that the temperature is held constant at the values $T(x, a) = T_1$ and $T(x, b) = T_2$, respectively, on these planes. Then $T(x, y)$ is given by (Fig. 3.46)

$$T(x, y) = T_1 + \frac{T_2 - T_1}{b - a}(y - a)$$

Solution The two-dimensional solution is constructed at points in the horizontal strip $a < \text{Im}(z) < b$ in the complex plane. A reasonable assumption is that the temperature at all points on the plane passing through the line $y = y_0$ is constant.

Fig. 3.45 Level curves of the harmonic function
 $T(x, y) = T_1 + \frac{T_2 - T_1}{b - a}(x - a)$

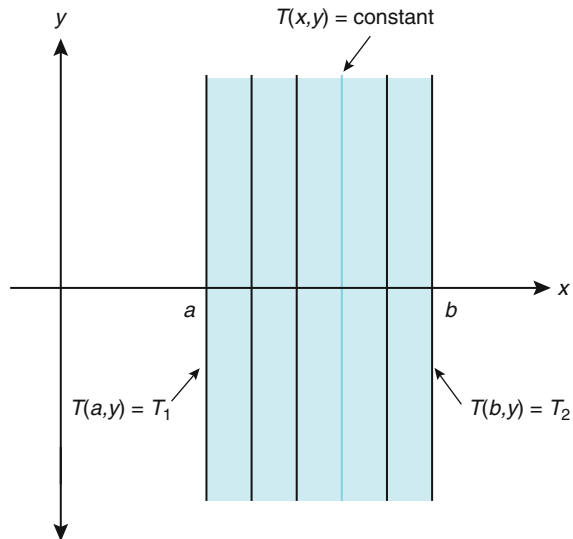


Fig. 3.46 Temperatures mod

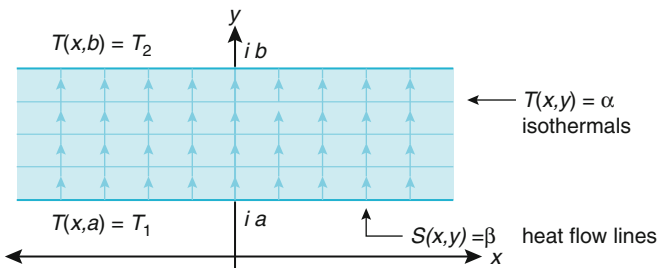
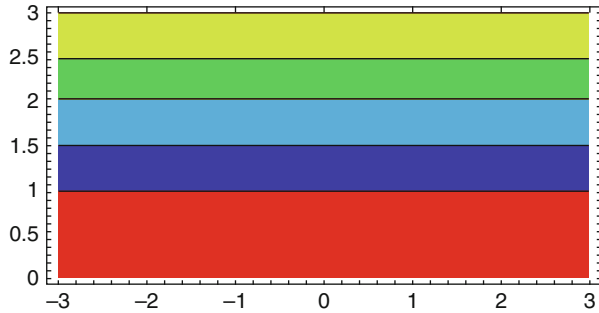


Fig. 3.47 The temperature between parallel planes where $T_1 > T_2$

Hence $T(x, y) = t(y)$, where $t(y)$ is a function of y alone. Laplace’s equation implies that $t''(y) = 0$ and an argument, similar to that in Example 3.1, will show that the solution $T(x, y)$ has the form given in the preceding equation.

The isotherms $T(x, y) = \alpha$ are easily seen to be horizontal lines. The conjugate harmonic function is

$$S(x, y) = \frac{T_1 - T_2}{b - a} x$$

and the heat flow lines $S(x, y) = \beta$ are vertical segments between the horizontal lines. If $T_1 > T_2$, then the heat flows along these segments from the plane through $y = a$. As illustrated in Fig. 3.47.

3.11.2 Solution of the Transient Equation

The heat pipe is a highly effective device for transporting heat between a source and a sink. Since the heat pipe concept was first introduced most theoretical studies concern certain portions of the heat pipe, such as the evaporator, condenser,

capillary structure, and vapor flow region. The overall performance of the entire heat pipe, including the thermal behavior along the heat pipe wall and capillary structure, the vapor flow dynamics, and the various types of boundary conditions on the evaporator and condenser surfaces, has received less attention. However, the steady-state characteristics of heat pipe performance at low temperatures and under normal operating conditions are relatively well understood, and heat pipes have been successfully applied in various fields. Little research has been done on the transient case. The transient behavior of heat pipes has been experimentally and numerically studied for low temperatures and working fluids with high vapor density by Chang and Colwell [17–19].

In certain applications such as leading edges of reentry vehicles and hypersonic aircraft as well as nuclear reactors where heat pipe has been considered as a means of reducing the peak temperature and alleviating the thermal gradients, liquid-metal heat pipe is used. In such applications, since the rate of heat transfer may be large, and the range of operating temperatures expanded, from ambient to high temperature, so that liquid metal, which is in the solid state at ambient temperature, may be used as the working fluid. Under these conditions, the working fluid in the capillary structure may be in the solid or liquid state, or may be freezing or thawing, with some liquid and some solid present. The vapor flow may be free molecular, continuum, choked, or some combination of these. No complete research has been reported on this subject. Colwell [20] has investigated an analytical way of the performance of an entire heat pipe with metallic working fluid during startup from a frozen state. To accomplish this goal, a mathematical model has been developed and a numerical solution technique tested to predict the transient temperature distributions along the heat pipe and the optimal heat transfer rate.

In addition to heat pipe limitations that were discussed in Chap. 2, when liquid metal is used as the working fluid, startup difficulty may take place due to the possible solid state of the working fluid and extremely low vapor density. Since the working fluid of the heat pipe is initially in the solid state and the wick structure is saturated, the transient conduction equation may be applied to the heat pipe shell and wick structure [20]. The variable heat flux and radiation boundary condition may be considered on the outside surface of the heat pipe. The adiabatic boundary condition also may be used at the liquid–vapor interface, due to the vacuum in the vapor space.

Colwell [20] analyses show that when energy is continuously added to the evaporator, the frozen working fluid in the evaporator is melted, so that evaporation can take place at the liquid–vapor interface and vapor flows into the condenser section due to the large pressure gradient. Vapor therefore freezes on the inner surface of the frozen working fluid in the cold zone and the vapor–solid interface temperature increases until the melting temperature is reached. During this stage, energy is mainly transferred as latent heat owing to vaporization in the heated zone and condensation and freezing in the cooled zone. The vapor flow may be choked at the exit of the evaporator because of very low pressure in the cold zone.

This process continues until the frozen working fluid is completely melted and the continuum flow regime reaches the end of the heat pipe, at which time the liquid

which returned to the evaporator is sufficient for normal transient operation. Eventually the heat pipe may reach a steady-state condition. As suggested, during the startup of the heat pipe from a frozen state, the behavior of vapor flow may be divided into three distinct phases for convenience of analysis:

Phase I: Vapor flow in the heat pipe is in free molecular condition through the vapor space.

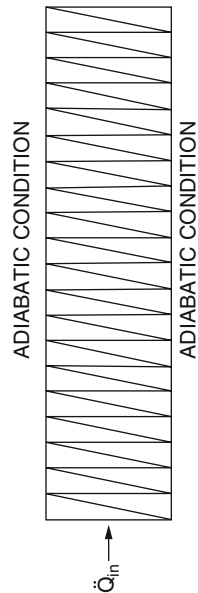
Phase II: In the vapor space, a region of continuum flow is established in the heated zone and a continuum flow front moves toward the heat pipe-cooled end. Vapor flow may be choked at the end of the evaporator.

Phase III: Continuum flow exists over the entire heat pipe length in the vapor region and the sonic limit is not encountered.

Cotter [21] described three basic transient modes for heat pipe startup. A frontal startup mode was observed when the vapor density is so low that the molecular mean free path exceeds the diameter of the vapor passage. In this mode of startup, the vapor in the hot zone is in continuum flow and that in the cold zone is in free molecule flow. A large-temperature gradient is developed and decreases with time. Eventually, an isothermal steady state could be reached.

To verify the validity of transient conduction and phase changes, one employee can help from finite element formulation and algorithm to compute numerical solutions and compare that with available solutions, such as analytical and other approximation solutions. The case of temperature of a semi-infinite body that involves pure conduction of heat without any phase change over a semi-infinite body is a good example. This problem is solved as a two-dimensional problem, as shown in Fig. 3.48.

Fig. 3.48 Finite element mesh for the transient conduction heat transfer problem [20]



The exact solution to this problem is give by Luikov [22] as the following equation:

$$T(x, t) = \frac{2\ddot{Q}}{K} \sqrt{\alpha t} \left[\frac{1}{\sqrt{\pi}} \exp\left(\frac{-x^2}{4\alpha t}\right) - \frac{x}{2\sqrt{\alpha t}} \operatorname{erfc}\left(\frac{x}{2\sqrt{\alpha t}}\right) \right] + T_0 \quad (\text{Eq.3.39})$$

where $\alpha = \frac{K}{\rho c_p}$

For more details of this analysis, reader should refer to Colwell's paper [20]. The computer code that is developed by Colwell et al. [11] for this purpose is the only available good in the open domain, and the list of his code is provided in his paper [20].

3.12 Design Criteria and Constraints

In order for a heat pipe to perform and operate properly within its conditions and requirements, a design criteria has to be imposed to which the heat pipe design must conform. Qualitative restrictions around design criteria are to be taken into account in the heat pipe design in order to maximize its practical extent. An example of these design criteria is to cool down a component and remove the heat from a component by a heat pipe at its upper temperature, or to hold the weight of heat pipe cooling system to its bear minimum is another example of these criteria. Constraints and considerations that are adhering to a heat pipe design will be are as follows:

- Characteristics of the heat source
- Characteristics of the heat sink
- Heat pipe operating environment
- Size and weight constraints
- Temperature constraints
- Fabrication constraints
- Cost constraint

3.12.1 Heat Source Characteristics

The heat source design criteria is dealt in a way in which the heat source is thermally coupling with the heat pipe over the surface area or evaporator where the heat is to be added, the rate of heat transfer, and the heat source temperature. The heat source may be a solid or fluid. Thermal coupling may be direct solid-to-solid (conduction) contact, via fluid-to-solid (convection) contact, by radiation, or by electrical induction heating [23]. As part of design requirements, the heat transfer and/or the heat source temperature may be provided, or alternatively the information may be given as part of the operational condition of heat pipe under

which such heat transfer from source is taking place. The heat transfer rate or heat source temperature would then have to be calculated as part of design process. Computer codes are developed around such analyses that are described in Sect. 3.16.

3.12.2 Heat Sink Characteristics

Heat sinks work very well in transporting heat, but their capabilities have limits. If temperatures are too extreme, the heat sinks themselves will not be able to dissipate enough heat in time and become a heat source themselves. Most heat sinks are also known to be fragile. If some heat fins on a heat sink are damaged, the functionality of the heat sink will be compromised. Heat sinks work well only when there is optimal contact with the heat source, if not the heat sink will not absorb enough heat.

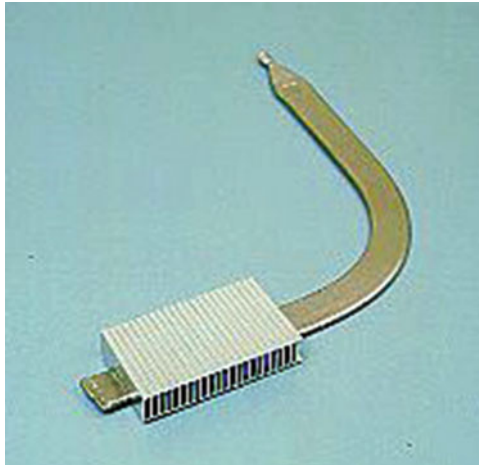
The heat sink may also be coupled to the heat pipe (condenser section) by conduction, convection, radiation or some combination of these very similar to heat source characteristics. The heat sink temperature would be specified as part of design criteria, along with information needed to calculate the heat transfer rate between the heat pipe and the heat sink. For convective heat sink, the heat transfer coefficient might be known or would have to be calculated from fluid thermophysical and flow properties. For a radiative heat sink, the heat pipe and heat sink emissivities would be established, along with view factors for radiative heat transfer between the heat and heat sink [23]. Computer codes are developed around such analyses that are described in Sect. 3.17.

3.12.2.1 Fins as Heat Sink

Recent years have seen drastic increases in the heat density of electronic equipment due to rapid improvement in the speed and the size, making efficient means of heat dissipation an important issue toward practical applications. Even though this issue can generally be settled using a large heat radiator with a large fan, better means have to be sought if the equipment is required to be compact and light. Thus, various heat sinks are finding practical applications for electronic equipment, such as a heat sink incorporating micro-heat pipes together with radiating plates and fins and a high-performance heat sink of low profile, which incorporates die-cast radiator combined with micro-heat pipes and specialty fans. Even with these devices, however, it is becoming difficult to cope with the drastic increases in the heat density, and thus it is an urgent need to develop new heat sinks that show lower heat resistances.

After extensive investigations by companies such as Furukawa Electric, a heat sink using micro-heat pipes has been developed and brought to the market. The new device can deal with high heat densities of electronic equipment and is available at low price. They have developed an extra-high-performance device that cuts more than 30% of both the weight and the volume of conventional products with

equivalent performance. The standard type of this heat sink comprises a heat-receiving block, a micro-heat pipe, a plurality of fins with a thickness of 0.3 mm which serve as a duct for airflow, and a fan. Conventionally, it was impossible to attach with a small heat resistance a number of fins of extremely small thickness onto a heat pipe, since the latter is soft annealed to permit easy thermal wiring. We have developed a new technique to carry out this fin attachment at low cost. Since the fins are arranged to form a duct for airflow, the heat sink makes an efficient use of the airflow from the fan, thereby contributing substantially to lower the heat resistance. While the standard heat block uses an ordinary die-cast material, a special material with a heat conductivity that is twice as large is also available to lower the heat resistance further. This special die-cast material enables replacing the specialty fan with a standard fan of low price, so that the total cost of heat dissipation can be reduced [6].



It is possible to realize a heat resistance of $2\text{ }^{\circ}\text{C}/\text{W}$ or less using this new heat sink, which was impossible conventionally. The new heat sink is finding practical applications where such advantages of small size, lightweight, and low price in addition to low heat resistance are highly appreciated. Meanwhile, several applications for relating patents have been filed.

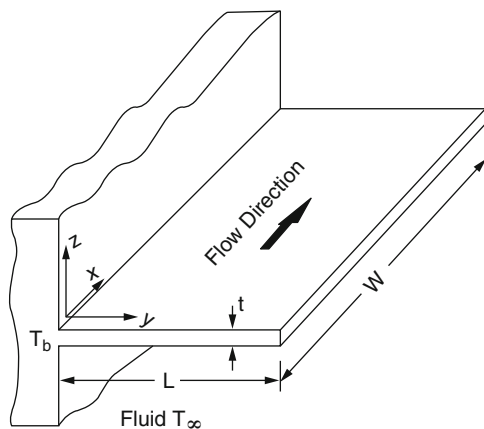
When heat pipe designs have size, weight, and variation of heat source and sink temperature constraints in cases of both fixed and variable heat pipes, the usage of the fin as an extended surface for conduction and convection of heat on the condenser side of the pipe plays an important role. In this section, readers will get some simple exposure to a very basic approach for a heat pipe design when the real estate of the condenser area and variation of temperature as well as size of the design is an issue. This approach utilizes both passive and forced convection and conduction for the purpose of heat transfer in heat pipe design. For further information, readers should refer to the various literature and textbooks on fin design analysis.

For a given log mean temperature difference, also known as **LMTD**, the only way of increasing heat transfer rates in a heat exchanger is to increase the surface area. One way of achieving this is through the use of extended or finned surfaces. With liquid/gas heat exchanger such as heat pipe, very often, the heat transfer coefficient on the liquid side is much greater than that on the gas side. Fins would then be used on the gas side so that the resistance to heat transfer was approximately the same on both sides. Fins come in many shapes and sizes, and they can be broadly classified into two types of fins as follows:

- Fins of a constant cross section:
 - Rectangular or pin (spike) fins.
- Fins of varying cross sections:
 - Tapered fins.

Fins are used to enhance the convective heat transfer in a wide range of engineering applications. A finite element numerical study has been conducted of two-dimensional heat conduction in a rectangular fin with a variable heat transfer coefficient (h) in the flow direction. A power function variation of the local Nusselt number corresponding to forced convection was assumed. The results show that fin efficiency with variable heat transfer coefficient can be significantly lower than when a uniform h value is assumed, because of the spreading resistance associated with the lateral flow of heat toward the leading edge. The effect of variable h was found to increase as the fin length-to-width ratio (L/W) decreased. For laminar boundary layer flow at $L/W = 0.1$, the fin efficiency with variable h was as much as 8.7% lower than with a uniform heat transfer coefficient. For a turbulent flow conditions, the effect of variable h was found to be much less significant. The results presented in this study can be used (in conjunction with traditional one-dimensional fin analysis) to correct for the effect of variable local heat transfer coefficient (Fig. 3.49).

Fig. 3.49 Problem geometry and effect of lateral conduction on the efficiency of rectangular fins with variable heat transfer coefficient



Heat transfer through extended surfaces has been studied extensively in the literature. Constant thermophysical properties and uniform heat transfer coefficient is often assumed in the determination of the temperature distribution along an extended surface. The mathematical complexity of the conservation energy equation is then reduced by this assumption, and therefore well-established closed-form analytical solution can be obtained for a number of cases. However, this assumption will lead to a poor prediction of the thermal performance of the extended surface especially for certain fin geometries [24].

The function of fins could be analyzed starting with Newton's law of cooling for surface heat transfer by convection:

$$q_s = hA_s(T_s - T_\infty) \quad (\text{Eq.3.40a})$$

Equation (3.40a) provides an insight as to the options available for increasing surface heat transfer rate q_s . One option is to increase the heat transfer coefficient h by changing the fluid and/or manipulating its motion. A second option will be to lower the ambient temperature T_∞ . There will be a third option which is increasing the surface area A_s . This option is exercised in many cases of engineering application and will work in case of heat pipe miniaturization design infrastructure in particular if designer deals with small real estate on condenser side of the pipe and requires a variation on of temperature at the source side (evaporator section). In this case, the heat transfer surface is "extended" by adding fins to the condenser side providing that other design limitations carefully are analyzed and are under envelope of the design requirements and application of that particular heat pipe.

There are different types and various fin geometries, and configurations are used to construct fins. Some samples of these fins are depicted in Fig. 3.50 below. Each

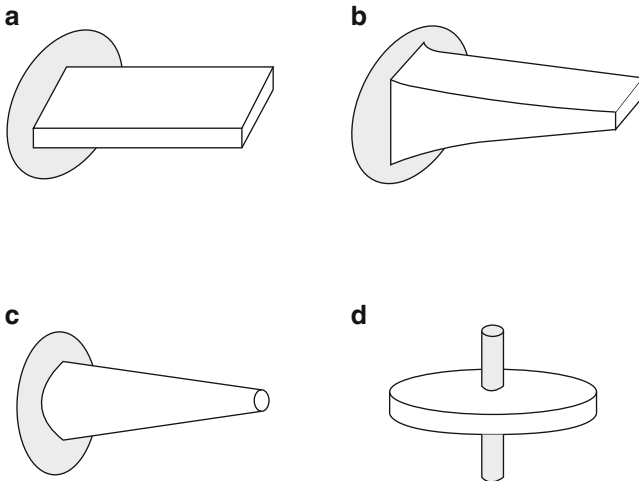


Fig. 3.50 Illustration of different fin types [25]. (a) Constant area straight fin, (b) variable area fin straight fin, (c) pin fin, (d) annular fin

fin shown is attached to a wall or surface. The end of the fin which is in contact with the surface is called the *base*, while the free end is called the *tip*. The term *straight* is used to indicate that the base extends along the wall in a straight fashion as shown in Fig. 3.50a, b.

If the cross-sectional area of the fin changes as one move from the base toward the tip, the fin is characterized as having a variable cross-sectional area. Examples are the fins shown in Fig. 3.50b–d. A spine or a pin fin is distinguished by a circular cross section as in Fig. 3.50c. A variation of the pin fin is a bar with a square or other cross-sectional geometries. An annular or cylindrical fin is a disk which is mounted on a tube as shown in Fig. 3.50d. Such a disk can be either of uniform or variable thickness. A great deal of fin analysis is presented by Jiji [25].

One- and two-dimensional analyses can be found in different literatures and heat transfer textbooks around developing a generalized analytical solution for the computation of heat loss from an extended surface based on variable heat transfer coefficient [26]. Also reader can find references to application of hybrid numerical method of Laplace transformation and finite difference method to solve the transient thermoelastic problem of an annular fin assuming the heat transfer coefficient is a function of the radius of the fin [27].

Plate-fin heat exchangers are being considered for many condenser applications. They are commonly used for the gas-separation process because they can provide a high thermal performance to obtain a low mean temperature difference, essential for the gas-separation process. Plate-fin heat exchangers are also considered for the heat pump system using nonazeotropic refrigerant mixtures. The brazed plate-fin condenser was considered to be a leading candidate for the ocean thermal energy conversion (OTEC) system, where high-performance heat exchangers are essential for maintaining a low mean temperature difference. Calculation of the fin efficiency is difficult for condensation in the presence of non-condensable gases due to the spatial variation of the interfacial temperature. An analysis was carried out to develop a simplified method to calculate the fin efficiency for condensation of a vapor in the presence of non-condensable gases. The analysis includes the variation in the interfacial temperature along the fin surface. Appropriate assumptions are made to simplify the coupled heat conduction equation in the fin and the heat/mass fluxes at the interface. The resulting expression for the fin efficiency includes mass flux parameters, and it is similar to the common expression used for single-phase flow.

To model the behavior of the fins, one should know that the law for convective cooling is given as

$$q'' = h(T - T_\infty) \quad (\text{Eq.3.40b})$$

where q'' is the heat flux in W/m^2 , h is the convection coefficient, T is the local fin temperature, and T_∞ is the temperature of the surrounding air. Predicting h mathematically is very complicated, and most information on its value comes from experiment. For natural convection in air in your fin geometry, $h \approx 10 \text{ W/m}^2 \text{ K}$. This estimate is only an order of magnitude approximation, but will suffice for now.

For the simplicity of our analysis, we will assume that the temperature of the fin is a function of x only, the fin is at steady state. We will assume that the fin is thin compared to its length and therefore will treat the conduction as one dimensional. Consider a differential element of fin Δx in length. At steady state, energy flows in and out of the sides of the element by conduction (the axial direction) and leaves from the surface by convection. We can easily show that

$$kA \frac{dT}{dx} \Big|_{X=x+\Delta x} - kA \frac{dT}{dx} \Big|_{X=x} = hP\Delta x(T(x + \Delta x/2) - T_\infty) \quad (\text{Eq.3.41})$$

where A is the cross-sectional area of the fin, k is the thermal conductivity of the fin material, and P is the perimeter of the fin cross section. Rearranging yields,

$$\frac{kA \frac{dT}{dx} \Big|_{X=x+\Delta x} - kA \frac{dT}{dx} \Big|_{X=x}}{\Delta x} = \frac{hP}{kA} (T(x + \Delta x/2) - T_\infty) \quad (\text{Eq.3.42})$$

Taking the limit as Δx goes to zero yields the expression

$$\frac{d^2T}{dx^2} = \frac{hP}{kA} (T(x) - T_\infty) \quad (\text{Eq.3.43})$$

Defining the temperature difference as $\Theta = (T(x) - T_\infty)$ yields

$$\frac{d^2\Theta}{dx^2} = \frac{hP}{kA} \Theta \quad (\text{Eq.3.44})$$

The above equation will describe the temperature profile of the fin at steady state. To solve the equation, one needs two boundary conditions, one at each end of the fin.

3.12.2.1.1 Modeling of the Fin Analysis

In order to model and design a fin, one should compare the temperature data that is obtained experimentally to a solution of the model. To solve the model, you need two boundary conditions. You can take the boundary conditions at $x = 0$ to be fixed temperature; in this case, the temperature measured by a possible sensor mounted near the heater. The boundary condition at the other end $x = L$ should be $-k \frac{dT}{dx} = h(T(x) - T_\infty)$. This condition states that the energy transfer to the end of the fin by conduction must be lost by convection.

3.12.2.1.2 Fin Experiment and Collecting Data

One suggestion to collect some sort of experimental data in order to compare with numerical solution of Eq. (3.44) is to take a fin of about 1 ft long and have different

thickness, width, and material. One end heated with a power resistor, the rest hangs free in the air. The fins will be at steady state. Using temperature sensors and liquid crystal film, we will measure and visualize the behavior of the temperature as a function of space. Data for all the fins will be recorded for the comparing purpose with numerical solution of the Eq. (3.44).

3.12.2.1.3 Numerical Model

To do the numerical modeling, one should solve a simple one-dimensional *transient diffusion* equation and then consider the steady-state behavior and count for the heat loss along the length of the fin.

Integrate forward in time until the simulation reaches steady state. Compare the steady state solution to a few fins. If needed, do adjust for convection coefficient value of the h and if that accounts for any differences and provide a better fit. Your value of h should be the same for all fins under experiment.

3.12.2.1.4 Analytical Model

We can see that Eq. (3.44) is an ordinary differential equation, and if one needs to use a numerical method to solve this equation, it may require some sort of initial condition (time depended condition), not boundary condition (which are spatial). But one can solve this equation numerically with a Simulink model (two integrators with feedback) and simply guessing and iterating the initial condition at $x = 0$ such that you get the answer you require at $x = L$.

However, it is easy to solve this equation analytically, so let us walk through the solution. You can complete this solution and compare it to all the experimental data. A general solution to Eq. (3.44) is $\Theta = Ae^{mx} + Be^{-mx}$ where A and B are constants determined from the boundary conditions and $m^2 = \frac{hP}{kA}$. Substituting the above expression into Eq. (3.44) shows that the equation is satisfied for any value of A or B . By assuming the above form of the solution, you can put the assumed form into the governing equation and solve for the constants A and B using the boundary conditions:

1. Plot the solutions of the fin equation and compare these closed-form solutions to your experimental data.
2. Find h such that it seems you have a reasonable fit. You should find that $h = 10 \text{ W/m}^2$; note that this is an order of magnitude estimate and, your value may be somewhat higher or lower. h should be the same in all your data sets.
3. Calculate how much heat each fin is dissipating. Explain why the different metals give different results.
4. Use your mathematical model to examine some possible engineering trade-offs. Is it better to be thick or thin, wide or narrow fins. Compare the performance of different materials.

5. See if you can develop a simple plot or equation that would easily allow a designer to trade-off cost versus “size” for a given material. Note: there is not a “right” answer here. You may need to try some different ideas and see how they would work. You should assume that cost is proportional to total mass. There is clearly an “optimum,” though what this optimum depends on the designer and the application. It is easy to see that a fin of zero size has zero cost. However, in some applications, no fin will cause your system to reach an unacceptable temperature. A fin of infinite length and width could dissipate the most heat; however, at some point, making the fin bigger has diminishing returns.

Very limited amount of work can be found on the similarity solution to heat transfer problems through extended surfaces especially with variable thermal properties. Campo and Salazar [28] studied the analogy between unsteady-state conduction in a planar slab for short times and steady-state conduction in a straight fin of uniform cross section. They also presented approximate analytical solutions of the transient heat conduction equation for short times in a plane having a uniform initial temperature and subjected to a uniform surface temperature. Kuehn et al. [29] studied the similarity solution or conjugate natural convection heat transfer from a long vertical plate fin. They presented complete result for a uniform conductivity plate fin as a function of the fluid Prandtl number.

In the presentation by Pakdemirli and Sahin [24], a similar solution is attempted to the nonlinear fin equation in which the thermal conductivity is an arbitrary function of temperature and heat transfer coefficient is an arbitrary function of spatial variable. The types of functions for the thermal conductivity and the heat transfer coefficient for which similarity solutions could be obtained were investigated.

Some simple finite difference method is presented by Rozza and Patera [30] to solve the thermal fin problem as an engineering motivation. They show this problem as a consideration of the performance of a heat sink designed for the thermal management of high-density electronic components. The heat sink, shown in Fig. 3.51, is comprised of a base/spreader which in turn supports a number of plate fins exposed to flowing air. We model the flowing air through a simple convection heat transfer coefficient. Our interest is in the conduction temperature distribution at the base of the spreader. From the engineering point of view, this problem illustrates the application of conduction analysis to an important class of cooling problems: electronic components and systems.

Fig. 3.51 Heat sink [30]

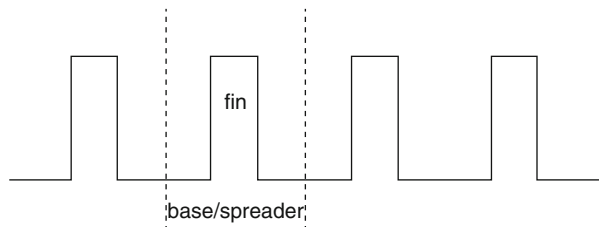
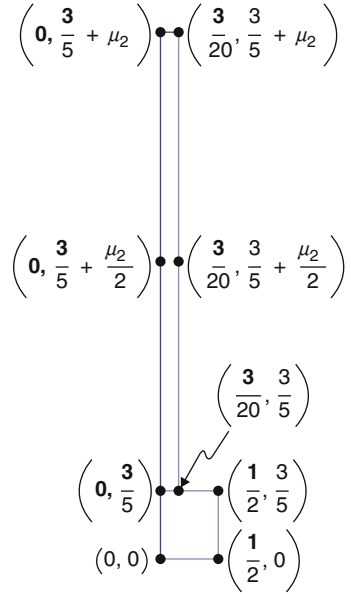


Fig. 3.52 Parameterized geometry



1. Physical principles:

From the physical point of view, this worked problem illustrates many aspects of steady conduction heat transfer: (1) the basic elements of thermal resistance, (2) the notion of a constriction resistance, and most importantly (3) the utility of the “thermal fin” concept and (4) the relevance of the classical “1-D thermal fin” idealization.

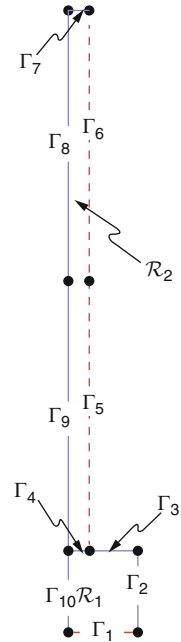
2. Problem description:

Consider the physical domain $\Omega(\mu)$ shown in Figs. 3.52 and 3.53, representing only one half cell of the heat sink single thermal fin with its spreader at the basis. Bear in mind that this element is a part of repetitive geometrical configuration. Here $x = (x_1, x_2)$ denotes a point in $\Omega(\mu)$, non-dimensionalized with respect to the unity length representing the distance between fins, \tilde{d}_{per} . Note that a tilde \sim denotes dimensional quantities, and the absence of a tilde signals a non-dimensional quantity. We identify in Fig. 3.51 the regions $R_\ell \leq \ell \leq 2$, which will serve to define the geometry or introduce inhomogeneous physical properties.

We assume that the spreader has thermal conductivity \tilde{d}_{sp} and that the plate fin has thermal conductivity \tilde{d}_{fin} ; we denote the ratio of these conductivities as $\kappa \equiv \tilde{d}_{sp}/\tilde{d}_{fin}$. We characterize the heat transfer from the fin to the air by a heat transfer coefficient \tilde{h}_c and the corresponding non-dimensional Biot number, $Bi \equiv \tilde{h}_c \tilde{d}_{per}/\tilde{d}_{fin}$.

The steady-state (non-dimensional) temperature distribution $u(\mu)$ is governed by the equations of heat conduction. In the domain, the temperature satisfies the

Fig. 3.53 Domain boundaries



Laplacian. We impose uniform heat flux at the base of the spreader (as a model of the Joule heating from the electronic component); continuity of temperature and heat flux at the spreader-fin interface; zero heat flux (conservatively) on the horizontal exposed surfaces of the spreader and fin; and heat-transfer coefficient/convection (Robin) boundary conditions on the vertical face of the fin, the surface exposed to the flowing air; and symmetry condition on the other vertical cut. Note that the temperature is measured relative to the temperature of the air “at infinity” and non-dimensionalized with respect to $(\tilde{q} \tilde{d}_{\text{per}} / \tilde{d}_{\text{fin}})$, where \tilde{q} is the dimensional heat flux into the spreader base.

We consider here $P = 3$ parameters. Here μ_2 is the geometry parameter defined in Fig. 3.50 as the length of the thermal fin (scaled by \tilde{d}_{per}), L . The remaining (always non-dimensional) parameters are given by μ_1 as the Biot (Bi) number and μ_3 as the spreader-to-fin conductivity ratio, κ . The parameter domain is given by $D = [0.01, 0.5] \times [2, 8] \times [1, 10]$.

The governing equation for $u(\mu)$ is a generalized Laplacian in each region which is given by Eq. (3.45) below with imposing boundary conditions. On all internal interfaces (interior boundaries of regions), we impose continuity of temperature $u(\mu)$ and heat flux $n_i \kappa_{ij} \frac{\partial}{\partial x_j} u(\mu)$, where n_i and e_i denote normal and tangential unit vectors. Figure 3.52 shows the boundaries of the domain.

$$-\frac{\partial}{\partial x_i} \left(\underbrace{\begin{bmatrix} \mu_3 & 0 \\ 0 & \mu_3 \end{bmatrix}}_{k_{ij}^1} \frac{\partial}{\partial x_j} u(\mu) \right) = 0 \text{ in } \mathfrak{R}_1 \tag{Eq.3.45}$$

$$-\frac{\partial}{\partial x_i} \left(\underbrace{\begin{bmatrix} \mu_3 & 0 \\ 0 & \mu_3 \end{bmatrix}}_{k_{ij}^1} \frac{\partial}{\partial x_j} u(\mu) \right) = 0 \text{ in } \mathfrak{R}_2$$

with summation $(i, j = 1, 2)$ over repeated indices.

On boundaries $\Gamma_2, \Gamma_3, \Gamma_7, \Gamma_8, \Gamma_9$ and Γ_{10} we impose homogeneous Neumann conditions $n_i \kappa_{ij} \frac{\partial}{\partial x_j} u(\mu) = 0$. In addition we impose nonhomogeneous Neumann condition,

$$n_i \kappa_{ij}^1 \frac{\partial u}{\partial x_j}(\mu) = 1 \quad \text{on } \Gamma_1 \tag{Eq.3.46}$$

Corresponding to unit flux, and Robin conditions,

$$n_i \kappa_{ij}^2 \frac{\partial u}{\partial x_j}(\mu) + (\mu_1)\mu = 0 \quad \text{on } \Gamma_5 \tag{Eq.3.47}$$

$$n_i \kappa_{ij}^2 \frac{\partial u}{\partial x_j}(\mu) + (\mu_1)\mu = 0 \quad \text{on } \Gamma_6 \tag{Eq.3.48}$$

corresponding to heat transfer coefficient/convection on the vertical faces of the fin.

The output for this problem is the average temperature over the base of the spreader which corresponds not only to the point of interest (the electronic component to be cooled) but also to the hottest location in the system. We denote this output by

$$T_{av}(\mu) = \int_{\Gamma_1} 2u(\mu) \tag{Eq.3.49}$$

Note that the output will depend on our three parameters, $\mu \equiv (\text{Bi}, L, \kappa)$. (Recall that this output is non-dimensionalized: to translate $T_{av}(\mu)$ into the actual dimensional temperature we must multiply by $\tilde{q} \tilde{d}_{per} / \tilde{k}_{fin}$ and then add the ambient temperature level.) Other outputs of interest may include the average temperature at the root of the fin (i.e., at the spreader-fin interface), and the average temperature at the tip of the fin.

Fig. 3.54 Finite element mesh



This problem is then modeled by the P_1 **finite element** (FE) discretization over the triangulation shown in Fig. 3.54; the FE space contains $N_t = 1116$ degrees of freedom. This FE approximation is typically too slow for many applications, and we hence approximate the FE prediction for the output and field variable by the reduced basis (RB) method.

The user can obtain the RB prediction for the output and field variable (visualization) as well as a rigorous error bound for the difference between the RB and FE predictions through website <http://augustine.mit.edu/index.htm> webserver. (Users who wish to run on their own computers and who have already downloaded our rbMIT software package can also create the RB approximation on their own computer from the rbU file.)

3.12.2.2 Fins Analysis

The normal textbook treatment of heat transfer from fins involves the solution by analytical means of an ordinary differential equation describing transport by conduction along the fin and convection from its surface. Even with a straight, rectangular fin, there is the quandary about what boundary condition to apply at the tip (which is usually resolved using an extended length), and the solution is expressed in terms of hyperbolic functions. In the case of straight fins of triangular cross section and annular fins of constant thickness, the solutions are given in terms of Bessel functions, which the student may or may not have studied. Also in the

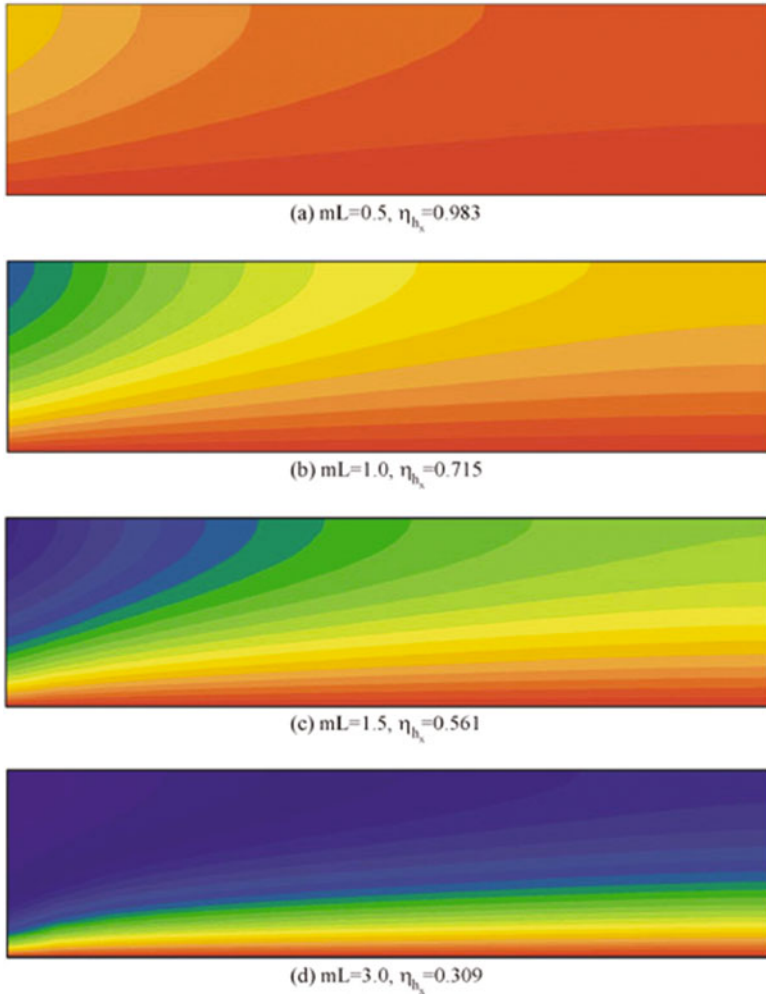


Fig. 3.55 Sample results

latter cases, he or she never sees the temperature distribution along the fin; only an overall parameter, the fin efficiency, is usually graphed.

Figure 3.55 shows the temperature field a fin with an aspect ratio of $L/W = 0.25$ for various values of mL with variable heat transfer coefficient (laminar boundary layer flow). It can be seen that for $mL = 0.5, 1.0,$ and $1.5,$ the temperature field near the leading edge of the fin is strongly two-dimensional, especially near the fin tip. However, for $mL = 3.0,$ the temperature field appears to be more one-dimensional than these other cases. The reason for the more one-dimensional behavior is low fin efficiency. As efficiency drops, the region of the fin far from the base plays less of a role in total heat transfer rate and the region closest to fin base dominates. The heat

flow close to the fin base is almost one-dimensional, in the y -direction. So for low fin aspect ratios, the effect of variable h diminishes when the fin efficiency decreases below about 60 %.

3.12.2.3 Radiation View Factors

The View Factor from one surface to another (also known as the Shape Factor and the Configuration Factor) is the fraction of radiation leaving the first surface that is intercepted by the second. For some very simple geometry this quantity can be determined by geometric arguments. The reciprocity theorem and shape factor algebra may be useful for other arrangements. For a very few geometries, e.g., perpendicular rectangles with a common edge, coaxial parallel disks, coaxial cylinders and aligned parallel rectangles, the very complicated quadruple integral defining the view factor between two surfaces may be integrated analytically. The resulting values are given in the form of charts in virtually every heat transfer book. An Excel spreadsheet that evaluates these analytical solutions for any of the four geometries listed above may be downloaded by clicking on any of the links above. View factors for still other geometries are tabulated in many sources. Several modern applications of radiation heat transfer, including the thermal analysis of large space structures and the rendering of complex three-dimensional scenes on computers using the radiosity method, require the computation of the view factors between thousands of pairs of surfaces. The numerical scheme used in this module by Professor Robert J. Ribando at the University of Virginia, Charlottesville, Virginia, is typical of modern means developed for such applications. This module computes the view factor between two parallelograms arbitrarily positioned in three-dimensional space using numerical implementation of the Nusselt unit sphere method based on the NASA TRASYS code that is described in Sect. 3.16.10. For further information on the analysis and calculation of view factor and possible free download of this module, reader should refer to the following web site: <http://faculty.virginia.edu/ribando> (Figs. 3.56, 3.57, 3.58, and 3.59).

The above equations for blackbodies and graybodies assumed that the small body could see only the large enclosing bodies and nothing else. Hence, all radiation leaving the small body would reach the large body. For the case where two objects can see more than just each other, then one must introduce a view factor F and the heat transfer calculations become significantly more involved.

The view factor F_{12} is used to parameterize the fraction of thermal power leaving object 1 and reaching object 2. Specifically, this quantity is equal to

$$\dot{Q} = A_1 F_{12} \varepsilon_1 \sigma T_1^4 \quad (\text{Eq. 3.50})$$

Likewise, the fraction of thermal power leaving object 2 and reaching object 1 is given by

Fig. 3.56 View factor for perpendicular rectangles with a common edge. Copyright 1999–2009, Robert J. Ribando [8]

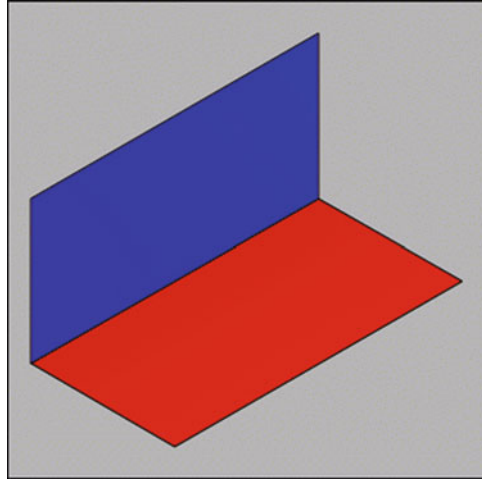
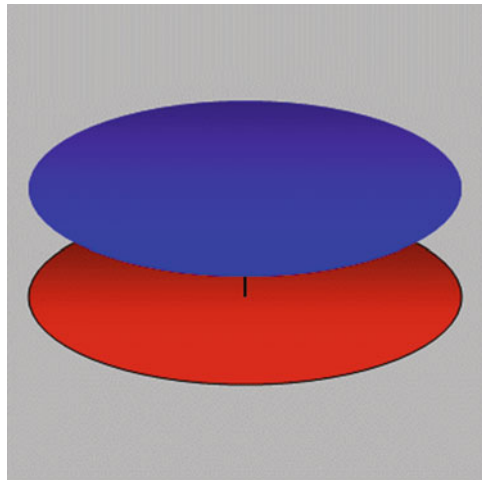


Fig. 3.57 View factor for coaxial, parallel disks. Copyright 1999–2009, Sean R. Travis



$$\dot{Q} = A_2 F_{21} \epsilon_2 \sigma T_2^4 \tag{Eq.3.51}$$

The case of two blackbodies in thermal equilibrium can be used to derive the following **reciprocity** relationship for view factors:

$$A_1 F_{12} = A_2 F_{21} \tag{Eq.3.52}$$

Thus, once one knows that F_{12} and F_{21} can be calculated immediately.

Radiation view factors can be analytically derived for simple geometries and are tabulated in several references on heat transfer (e.g., Holman) [31]. They range from zero (e.g., two small bodies spaced very far apart) to one (e.g., one body is

Fig. 3.58 View factor for coaxial, finite cylinders.
Copyright 1999–2009, John K. Koehler

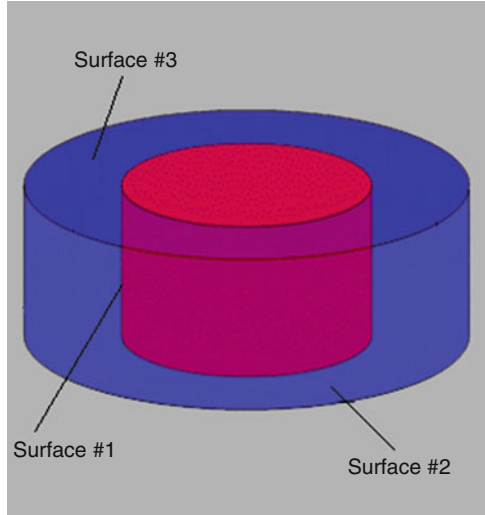
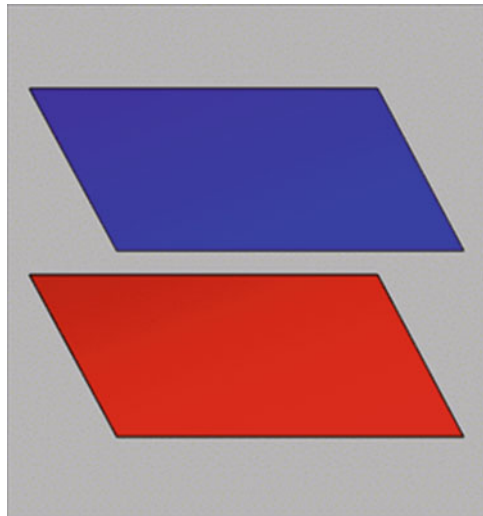


Fig. 3.59 View factor for aligned parallel rectangles.
Copyright 2000–2009, Robert J. Ribando [8]



enclosed by the other). The computer code FACET and its pre- and post-processors of this code, namely, MAZE and TAURUS, are the best publicly available code, and more information about these codes is provided Sect. 3.16.4. There are other codes such as MONTE2D and MONTE3D that are developed in the Department of Mechanical Engineering at Colorado State University (CSU). These two codes are used to calculate radiative exchange factors for enclosures with a nonparticipating medium. For details about these two codes, refer to Sect. 3.16.5 or the site of the code by CSU at the following URL <http://www.colostate.edu/~pburns/monte/code.html>.

3.12.2.4 Heat Transfer Between Two Finite Graybodies

The heat flow transferred from object 1 to object 2 where the two objects see only a fraction of each other and nothing else is given by

$$\dot{Q} = \left(\frac{1 - \epsilon_1}{\epsilon_1} + \frac{1}{F_{12}} + \left(\frac{1 - \epsilon_2}{\epsilon_2} \right) \frac{A_1}{A_2} \right)^{-1} A_1 \sigma (T_1^4 - T_2^2) \quad (\text{Eq.3.53})$$

This equation demonstrates the usage of F_{12} , but it represents a nonphysical case since it would be impossible to position two finite objects such that they can see only a portion of each other and “nothing” else. On the contrary, the complementary view factor $(1 - F_{12})$ cannot be neglected as radiation energy sent in those directions must be accounted for in the thermal bottom line.

A more realistic problem would consider the same two objects surrounded by a third surface that can absorb and readmit thermal radiation yet is nonconducting. In this manner, all thermal energy that is absorbed by this third surface will be readmitted; no energy can be removed from the system through this surface. The equation describing the heat flow from object 1 to object 2 for this arrangement is

$$\dot{Q} = \left(\frac{1 - \epsilon_1}{\epsilon_1} + \frac{A_1 + A_2 - 2AF}{A_2 - A_1(F_{12})^2} + \left(\frac{1 - \epsilon_2}{\epsilon_2} \right) \frac{A_1}{A_2} \right)^{-1} A_1 \sigma (T_1^4 - T_2^2) \quad (\text{Eq.3.54})$$

This equation is subject to the reciprocity condition for the three-body problem

Note: Radiation view factor, F12

The fraction of thermal energy is leaving the surface of object 1 and reaching the surface of object 2, determined entirely from geometrical considerations. Stated in other words, F_{12} is the fraction of object 2 visible from the surface of object 1 and ranges from zero to one. This quantity is also known as the radiation shape factor. Its units are dimensionless.

Below are some of the definitions of different thermal parameters.

Blackbody	A body with a surface emissivity of one. Such a body will emit all of the thermal radiation it can (as described by theory) and will absorb 100 % of the thermal radiation striking it. Most physical objects have surface emissivities less than one and hence do not have blackbody surface properties
Density, ρ	The amount of mass per unit volume. In heat transfer problems, the density works with the specific heat to determine how much energy a body can store per unit increase in temperature. Its units are kg/m^3
Emissive power	The heat per unit time (and per unit area) emitted by an object. For a blackbody, this is given by the Stefan–Boltzmann relation σT^4
Graybodies	A body that emits only a fraction of the thermal energy emitted by an equivalent blackbody. By definition, a graybodies has a surface emissivity less than one, and a surface reflectivity greater than zero
Heat flux, q	The rate of heat flowing past a reference datum. Its units are W/m^2

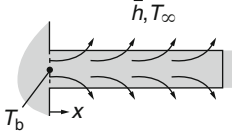
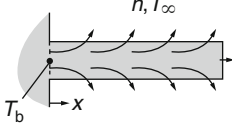
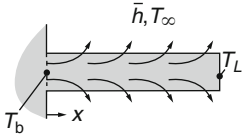
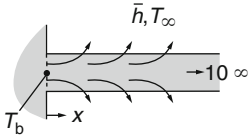
(continued)

Internal energy, e	A measure of the internal energy stored within a material per unit volume. For most heat transfer problems, this energy consists just of thermal energy. The amount of thermal energy stored in a body is manifested by its temperature
Radiation view factor, F_{12}	The fraction of thermal energy leaving the surface of object 1 and reaching the surface of object 2, determined entirely from geometrical considerations. Stated in other words, F_{12} is the fraction of object 2 visible from the surface of object 1, and ranges from zero to one. This quantity is also known as the radiation shape factor. Its units are dimensionless.
Rate of heat generation, q_{gen}	A function of position that describes the rate of heat generation within a body. Typically, this new heat must be conducted to the body boundaries and removed via convection and/or radiation heat transfer. Its units are W/m^3
Specific heat, c	A material property that indicates the amount of energy a body stores for each degree increase in temperature, on a per unit mass basis. Its units are $\text{J}/\text{kg K}$
Stefan–Boltzmann constant, σ	Constant of proportionality used in radiation heat transfer, whose value is $5.669 \times 10^{-8} \text{W}/\text{m}^2 \text{K}^4$. For a blackbody, the heat flux emitted is given by the product of σ and the absolute temperature to the fourth power
Surface emissivity, ϵ	The relative emissive power of a body compared to that of an ideal blackbody. In other words, the fraction of thermal radiation emitted compared to the amount emitted if the body were a blackbody. By definition, a blackbody has a surface emissivity of one. The emissivity is also equal to the absorption coefficient or the fraction of any thermal energy incident on a body that is absorbed
Thermal conductivity, k	A material property that describes the rate at which heat flows within a body for a given temperature difference. Its units are $\text{W}/\text{m K}$
Thermal diffusivity, α	A material property that describes the rate at which heat diffuses through a body. It is a function of the body's thermal conductivity and its specific heat. A high thermal conductivity will increase the body's thermal diffusivity, as heat will be able to conduct across the body quickly. Conversely, a high specific heat will lower the body's thermal diffusivity, since heat is preferentially stored as internal energy within the body instead of being conducted through it. Its units are m^2/s
Emissivity, ϵ	The relative emissive power of a body compared to that of an ideal blackbody. In other words, the fraction of thermal radiation emitted compared to the amount emitted if the body were a blackbody. By definition, a blackbody has a surface emissivity of one. The emissivity is also equal to the absorption coefficient or the fraction of any thermal energy incident on a body that is absorbed

3.12.2.5 Fin Optimization Analysis

It is useful to go through the exercise of optimizing a fin in order achieve the highest rate of heat transfer per volume of fin material; the result of this optimization provides general guidelines relative to the dimensionless characteristics of a well-designed fin [32]. The rate of heat transfer to a constant cross-section fin with an adiabatic tip from Table 3.6 is given by G. Nellis [33]:

Table 3.6 Solutions for constant area extended surfaces with different end conditions [33]

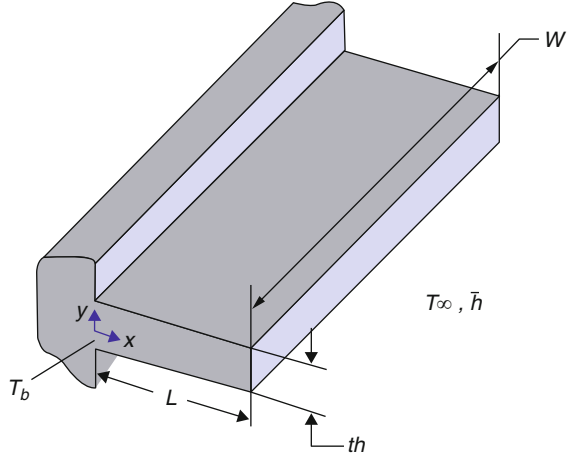
End condition	Temperature distribution
Adiabatic tip 	$\frac{T - T_\infty}{T_b - T_\infty} = \frac{\cosh(m(L - x))}{\cosh(mL)}$ $\dot{q}_{\text{fin}} = (T_b - T_\infty) \sqrt{\bar{h} \text{ per } k A_c} \tanh(mL)$ $\eta_{\text{fin}} = \tanh(mL) / (mL)$
Convection from tip 	$\frac{T - T_\infty}{T_b - T_\infty} = \frac{\cosh(m(L - x)) + \frac{\bar{h}}{mk} \sinh(m(L - x))}{\cosh(mL) + \frac{\bar{h}}{mk} \sinh(mL)}$ $\dot{q}_{\text{fin}} = (T_b - T_\infty) \sqrt{\bar{h} \text{ per } k A_c} \frac{\sinh(mL) + \frac{\bar{h}}{mk} \cosh(mL)}{\cosh(mL) + \frac{\bar{h}}{mk} \sinh(mL)}$ $\eta_{\text{fin}} = \frac{[\tanh(mL) + mL \text{AR}_{\text{tip}}]}{mL [1 + mL \text{AR}_{\text{tip}} \tanh(mL)] (1 + \text{AR}_{\text{tip}})}$
Specified tip temperature 	$\frac{T - T_\infty}{T_b - T_\infty} = \frac{\left[\frac{T_t - T_\infty}{T_b - T_\infty} \right] \sinh(mx) + \sinh(m(L - x))}{\sinh(mL)}$ $\dot{q}_{\text{fin}} = (T_b - T_\infty) \sqrt{\bar{h} \text{ per } k A_c} \frac{\left(\cosh(mL) - \left[\frac{T_t - T_\infty}{T_b - T_\infty} \right] \right)}{\sinh(mL)}$
Infinitely long 	$\frac{T - T_\infty}{T_b - T_\infty} = \exp(-mx)$ $\dot{q}_{\text{fin}} = (T_b - T_\infty) \sqrt{\bar{h} \text{ per } k A_c}$
where	
T_b = base temperature	\bar{h} = heat transfer coefficient
T_∞ = fluid temperature	A_c = cross-sectional area
per = perimeter	k = thermal conductivity
L = length	\dot{q}_{fin} = fin heat transfer rate
T = temperature	x = position (relative to base of fin)
$mL = \sqrt{\frac{\text{per } \bar{h}}{k A_c}} L = \text{fin constant}$	$\text{AR}_{\text{tip}} = \frac{A_c}{\text{per } L} = \text{tip area ratio}$

$$\dot{q}_{\text{fin}} = \sqrt{k A_c \bar{h} \text{ per}} (T_b - T_\infty) \tanh(mL) \tag{Eq.3.55}$$

where mL is given by

$$mL = \sqrt{\frac{\text{per } \bar{h}}{k A_c}} \tag{Eq.3.56}$$

Fig. 3.60 A constant cross-sectional fin [33]



For a given rectangular-shaped fin with width of W and thickness th shown in Fig. 3.60 down below, the cross-sectional area is defined by $th \cdot W$, and the perimeter is calculated by $2W$, considering that the fin thickness is small compared to its width ($th \ll W$); therefore, Eq. (3.55) can be presented as follows:

$$\begin{aligned} \dot{q}_{\text{fin}} &= \sqrt{kthW \bar{h} 2W} (T_b - T_\infty) \tanh \left(\sqrt{\frac{2W \bar{h}}{kWh}} L \right) \\ &= W \sqrt{kth \bar{h} 2} (T_b - T_\infty) \tanh(mL) \end{aligned} \quad (\text{Eq.3.57})$$

where

$$mL = \sqrt{\frac{2\bar{h}}{kth}} L \quad (\text{Eq.3.58})$$

The rate of heat transfer per width of surface is then given by

$$\frac{\dot{q}_{\text{fin}}}{W} = \sqrt{kth \bar{h} 2} (T_b - T_\infty) \tanh(mL) \quad (\text{Eq.3.59})$$

The volume of the fin is then

$$V = WthL \quad (\text{Eq.3.60})$$

For this optimization, the volume of the fin materials per width of surface (V/W) will be held constant:

$$\frac{V}{W} = thL \quad (\text{Eq.3.61})$$

Therefore, the fin parameter, mL , can be presented as

$$mL = \sqrt{\frac{2W\bar{h}}{kV}} L^{3/2} \quad (\text{Eq.3.62})$$

and heat transfer per width can be written as

$$\frac{\dot{q}_{\text{fin}}}{W} = \sqrt{\frac{kV\bar{h}2}{WL}} (T_b - T_\infty) \tanh(mL) \quad (\text{Eq.3.63})$$

Calculating length L by solving Eq. (3.62) and allowing the length to be expressed in terms of the fin parameter (mL)

$$L = \frac{(mL)^{2/3}}{\left(\frac{2W\bar{h}}{kV}\right)^{1/3}} \quad (\text{Eq.3.64})$$

Substituting Eq. (3.64) into Eq. (3.63) and manipulating around it will result in heat transfer per width to be presented in terms of the volume per width and the fin constant:

$$\frac{\dot{q}_{\text{fin}}}{W} = \sqrt{\frac{kV\bar{h}2}{W}} \frac{\left(\frac{2W\bar{h}}{kV}\right)^{1/6}}{(mL)^{1/3}} (T_b - T_\infty) \tanh(mL) \quad (\text{Eq.3.65})$$

which can be simplified as the following equation:

$$\frac{\dot{q}_{\text{fin}}}{W} = \left(\frac{V}{W}\right)^{1/3} k^{1/3} \bar{h}^{2/3} (T_b - T_\infty) 2^{2/3} \frac{\tanh(mL)}{(mL)^{1/3}} \quad (\text{Eq.3.66})$$

Equation (3.66) provides [33] a useful result; in a typical design, the objective will be to maximize the rate of heat transfer per unit width (\dot{q}_{fin}/W) that can be obtained for a given volume per unit width (V/W) given constraints related to the conductivity, heat transfer coefficient, and driving temperature difference.

Equation (3.66) shows that the performance of the fin will become larger as any of these parameters (k, \bar{h} ,) or $(T_b - T_\infty)$ are increased; however, the only free parameter on the right-hand side is then fin parameter, mL . The dimensionless fin performance (\tilde{q}_{fin}) can be defined as

$$\tilde{q}_{\text{fin}} = \frac{\left(\frac{\dot{q}_{\text{fin}}}{W}\right)}{\left(\frac{V}{W}\right)^{1/3} k^{1/3} \bar{h}^{2/3} (T_b - T_\infty) 2^{2/3}} = 2^{2/3} \frac{\tanh(mL)}{(mL)^{1/3}} \quad (\text{Eq.3.67})$$

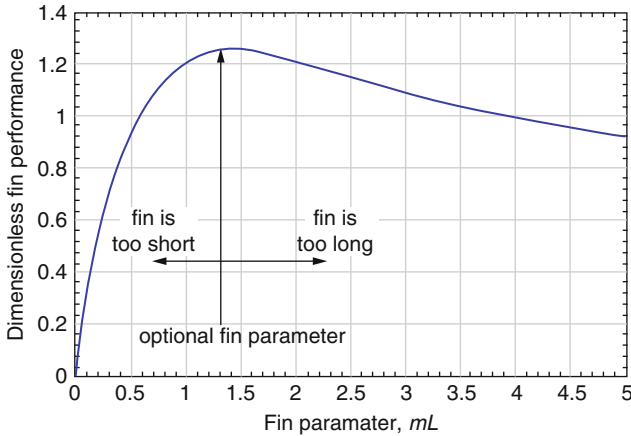


Fig. 3.61 Dimensionless fin performance as a function of the fin parameter [33]

G. Nellis [33] goes on to show that the denominator of the dimensionless fin performance definition has units of heat transfer rate per unit width and represents, approximately, the highest performance that is possible for a well-designed fin. The dimensionless fin performance is a function only of the fin parameter, as shown in Fig. 3.61. This figure shows that the optimal value of mL is approximately 1.4.

For more details of these analyses, please refer to the *Heat Transfer* book by G. Nellis [33].

3.12.3 Heat Pipe Thermal Resistance

The overall temperature difference between the heat sink and the heat source is an important characteristic for thermal control systems utilizing heat pipes. As the heat pipe is typically referred to as an overall structure of very high effective thermal conductivity, an electrical resistance analogy similar to that found in conduction heat transfer analysis is used. As the heat transfer occurs from the heat source to the heat sink, each part of the heat pipe can be separated into an individual thermal resistance.

The combined resistances provide a mechanism to model the overall thermal resistance and the temperature drop from heat sink to heat source associated with the given heat input. In addition, the resistance analogy provides a means to estimate the mean operating temperature (adiabatic vapor temperature) that is typically needed in determining the transport limit at a given operating condition. The temperature gradient is found utilizing a thermal resistance network, where Fig. 3.62 illustrates the analogy for a simple cylindrical heat pipe. The overall thermal resistance of the heat pipe only is comprised typically of nine resistances arranged in a series-parallel combination.

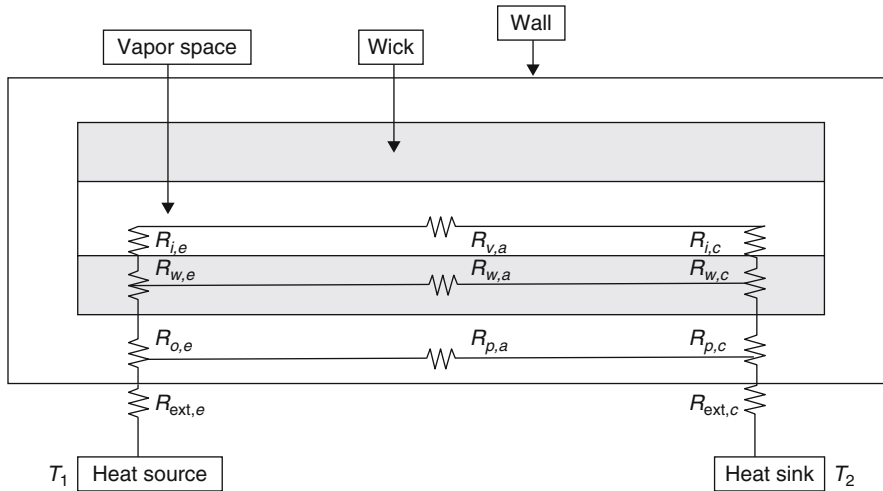


Fig. 3.62 Equivalent thermal resistance of a heat pipe [34]

The resistances can be summarized along with estimates of typical magnitudes as follows:

1. $R_{p,e}$: pipe wall radial resistance, evaporator ($\sim 10^{-1} \text{ }^\circ\text{C/W}$)
2. $R_{w,e}$: saturated liquid–wick radial resistance, evaporator ($\sim 10^{+1} \text{ }^\circ\text{C/W}$)
3. $R_{i,e}$: liquid–vapor interface resistance, evaporator ($\sim 10^{-5} \text{ }^\circ\text{C/W}$)
4. $R_{v,a}$: adiabatic vapor section resistance ($\sim 10^{-8} \text{ }^\circ\text{C/W}$)
5. $R_{p,a}$: pipe wall axial resistance ($\sim 10^{+2} \text{ }^\circ\text{C/W}$)
6. $R_{w,a}$: saturated liquid–wick axial resistance ($\sim 10^{+4} \text{ }^\circ\text{C/W}$)
7. $R_{i,c}$: liquid–vapor interface resistance, condenser ($\sim 10^{-5} \text{ }^\circ\text{C/W}$)
8. $R_{w,c}$: saturated liquid–wick radial resistance, condenser ($\sim 10^{+1} \text{ }^\circ\text{C/W}$)
9. $R_{p,c}$: pipe wall radial resistance, condenser ($\sim 10^{-1} \text{ }^\circ\text{C/W}$)

By examination of the typical range of resistance values, several simplifications are possible. First, due to comparative magnitudes of the resistance of the vapor space and the axial resistances of the pipe wall and liquid–wick combinations, the axial resistance of the pipe wall, $R_{p,a}$, and the liquid–wick combination, $R_{w,a}$, may be treated as open circuits and neglected. Second, the liquid–vapor interface resistances and the axial vapor resistance (in most situations) can be assumed negligible. Thus, the primary resistances of the heat pipe are the pipe wall radial resistances and the liquid–wick resistances in the evaporator and condenser.

Asselman and Green [35] give estimate of the order of magnitude for each of these resistances (Table 3.7) for a typical application. For more details, reader should refer to Peterson [12].

The radial heat pipe wall resistances that can be computed are found using Fourier law for flat plates as

Table 3.7 Comparative values for heat pipe [35]

Resistance	°C/W
$R_{p,e}$ and $R_{p,c}$	10^{-1}
$R_{w,e}$ and $R_{w,c}$	10^{+1}
$R_{i,e}$ and $R_{i,c}$	10^{-5}
$R_{v,a}$	10^{-8}
$R_{p,a}$	10^{+2}
$R_{w,a}$	10^{+4}

$$R_{p,e} = \frac{\delta}{k_p A_e} \quad (\text{Eq.3.68})$$

where δ is the plate thickness and A_e is the evaporator surface area, and for cylindrical pipes as

$$R_{p,e} = \frac{\ln(d_o/d_i)}{2\pi L_e k_p} \quad (\text{Eq.3.69a})$$

where L_e is the evaporator length (or is replaced by the condenser length when evaluating $R_{p,c}$). The resistance of the liquid–wick combination is also found from Eqs. (3.69a and 3.69b), where the effective conductivity K_{eff} is used instead of the pipe wall value K_p . When it is dealt with the resistance of the liquid–wick combination, an equivalent thermal resistance of Eq. (3.69b) in the evaporator of a circular pipe is given in terms of Eq. (3.69a):

$$R_{w,e} = \frac{\ln(d_o/d_i)}{2\pi L_e k_{\text{eff}}} \quad (\text{Eq.3.69b})$$

where values for the effective conductivity k_{eff} can be found in Table 2.1. In the above equation, d_o and d_i are outer and inner diameter of heat pipe in meters, respectively, and L_e is the length of entrainment.

Relationships for calculating K_{eff} are given in Table 3.8.

Two other resistances shown in Fig. 3.54 have a significant role in the design of heat pipe thermal control systems. These are the external resistances occurring between the heat source and heat pipe evaporator and the heat pipe sink and heat pipe condenser, $R_{\text{ext},e}$ and $R_{\text{ext},c}$, respectively. The external resistances are found by using information related to contact resistances and convective resistance where information on these can be found in most heat transfer textbooks. In many applications, these two resistances combined are greater than the overall heat pipe resistance; thus, these are typically the controlling resistances in applications.

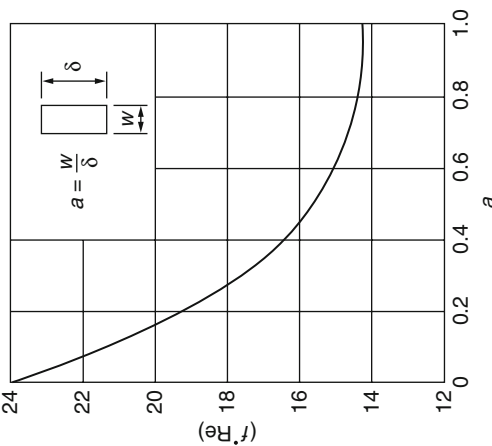
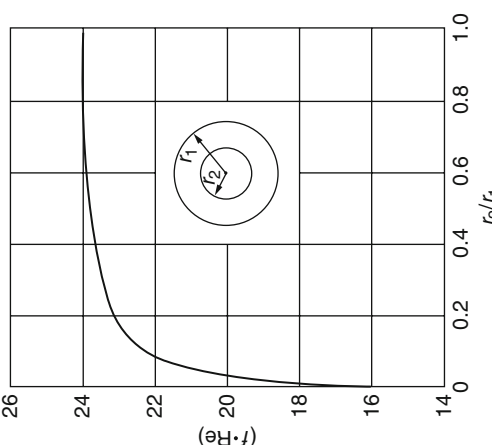
One additional important observation from the resistance analogy can be made. This is the case where the heat pipe reaches a dryout condition, such as exceeding the capillary limit. In the case of dryout, the vapor flow from the evaporator to the condenser will be discontinued, and the resistance $R_{v,a}$ will increase significantly, such that this circuit now may be considered as an open circuit. Thus, any heat input

Table 3.8 Expressions of wick permeability K for several wick structures [5]

Wick structure	K Expression
Circular artery	$K = \frac{r^2}{8}$
Open rectangular grooves	$K = \frac{2\epsilon r_{h,1}^2}{f_1 \cdot \text{Re}_1}$
	$\epsilon = \text{porosity} = \frac{w}{s}$
	$s = \text{groove pitch}$
	$r_{h,1} = \frac{2w\delta}{w+2\delta}$
	$w = \text{groove width}$
	$\delta = \text{groove depth}$
Circular annular wick	$(f_1 \cdot \text{Re}_1)$ from (a) below
	$r_{h,1} = r_1 - r_2$
Wrapped screen wick	$(f_1 \cdot \text{Re}_1)$ from (b) below
	$d = \text{wire diameter}$
	$\epsilon = 1 - \frac{1.05\pi Nd}{4}$
	$N = \text{mesh number}$

(continued)

Table 3.8 (continued)

Wick structure		K Expression
<p>Packed sphere</p> 	$K = \frac{r_s^3 \epsilon^3}{37.5(1 - \epsilon)^2}$ 	r_s = sphere radius ϵ = porosity (value depends on packing mode)

to the system must be transported along the heat pipe wall $R_{p,a}$, and the wick structure combination, $R_{w,a}$. As the difference between the axial resistances is several orders of magnitude, the temperature drop along the heat pipe will correspond to an increase of several orders of magnitude. This is as expected since the heat must now be transferred by conduction instead of using the latent heat of vaporization of the working fluid.

3.12.4 *Effective Thermal Conductivity and Heat Pipe Temperature Difference*

One important aspect of heat pipe feature is that it can transfer a large amount of heat while maintaining nearly isothermal conditions. The temperature difference between the external surfaces of the evaporator and the condenser can be determined from the following expression:

$$\Delta T = R_t Q \quad (\text{Eq.3.70})$$

where R_t is the total thermal resistance ($^{\circ}\text{C}/\text{W}$) and Q is the heat transfer rate (W). Figure 3.63 shows the thermal resistance network for a typical heat pipe and the associated thermal resistances. In most cases, the total resistance can be approximated by

$$R_t = R_1 + R_2 + R_3 + R_4 + R_5 + R_6 + R_7 + R_8 + R_9 \quad (\text{Eq.3.71})$$

The reader is referred to Peterson [12] for the specific mathematical relationships used to calculate each thermal resistance. The effective thermal conductivity of the heat pipe is defined as the heat transfer rate divided by the temperature difference between the heat source and heat sink as follows:

$$k_{\text{eff}} = \frac{L_t}{R_t A_t} \quad (\text{Eq.3.72})$$

where

k_{eff} : Effective thermal conductivity of the heat pipe ($^{\circ}\text{C W}/\text{m}$)

L_t : Total length of the heat pipe (m)

A_t : The overall cross-sectional area of the heat pipe (m^2)

R_t : The total thermal resistance ($^{\circ}\text{C}/\text{W}$)

The values for the effective thermal conductivity k_{eff} for liquid-saturated wick can be found in Table 2.4. Under normal operating conditions, the total thermal resistance is relatively small, making the external surface temperature in the evaporator approximately equal to that in the condenser. Thus, the effective thermal conductivity in a heat pipe can be very large (at least an order of magnitude larger than that of aluminum).

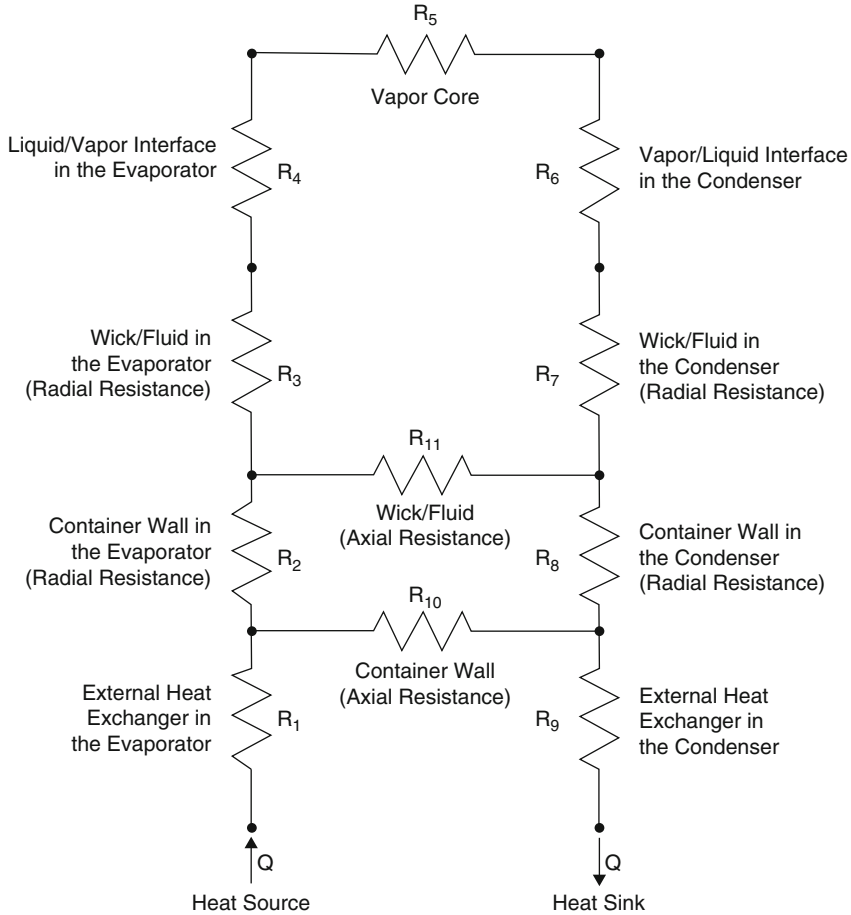


Fig. 3.63 Thermal resistance network in heat pipe

Example 3.3 [12] Assume a round copper–water heat pipe with an overall length of 25.4 mm; a finned condenser section of 9.39 mm long; an evaporator section 11.81 mm long, constructed from 3.2 mm-diameter copper tubing with a wall thickness of 0.9 mm; a wicking structure constructed from phosphor bronze wire mesh (No. 325) with a wire diameter of 0.0355 mm; and a condenser section with a series of ten fines approximately 6 mm square, 0.2 mm thick, at a spacing of 1 mm. Determine the overall thermal resistance of the heat pipe. Neglect the convective heat transfer at the finned condenser end and the contact resistance external to the case in the evaporator.

Solution The overall heat transfer coefficient is comprised of the resistance of the pipe wall at the evaporator, the resistance of the liquid–wick combination in the evaporator, the resistance of the vapor in the adiabatic section, the resistance

of the liquid–wick combination in the condenser, and the resistance of the pipe wall at the condenser. This combination of resistance can be expressed as

$$U_p = \frac{1}{R_{p,e} + R_{w,e} + R_v + R_{w,c} + R_{p,c}}$$

Assuming a temperature of 373 K, the individual resistance can be found as follows:

The thermal resistance due to the pipe wall in the evaporator $R_{p,e}$

$$R_{p,e} = \frac{r_o \delta_p}{2L_e k_p} = \frac{(1.6 \times 10^{-3} \text{ m})(8.89 \times 10^{-4})}{2(0.01181)(379)} = 1.59 \times 10^{-7} \text{ m}^2 \text{ K/W}$$

The thermal resistance due to the liquid–wick combination in the evaporator $R_{w,e}$

$$R_{w,e} = r_o^2 \frac{\delta_w}{2} L_e r_i k_{\text{eff}} = \frac{(1.6 \times 10^{-3} \text{ m})(7.10 \times 10^{-5})}{2(0.01181)(0.000695)(1.491)} = 7.43 \times 10^{-6} \text{ m}^2 \text{ K/W}$$

The thermal resistance of the vapor flow R_v

$$R_v = \frac{\pi r_o^2 T_v F_v \left(\frac{1}{6} L_e + L_a + \frac{1}{6} L_c\right)}{P_v \lambda} \\ = \frac{(3.14)(1.6 \times 10^{-3} \text{ m})^2 (373.15)(168.66)(0.0077)}{(0.580)(2.184 \times 10^6)(1)} = 3.08 \times 10^{-9} \text{ m}^2 \text{ K/W}$$

The thermal resistance due to the liquid–wick combination in the condenser $R_{w,c}$

$$R_{w,c} = \frac{r_o \varepsilon_p}{2L_c r_i k_{\text{eff}}} = \frac{(1.6 \times 10^{-3} \text{ m})^2 (7.10 \times 10^{-5})}{2(0.00939)(0.000695)(1.491)} = 9.34 \times 10^{-6} \text{ m}^2 \text{ K/W}$$

The thermal resistance due to the pipe wall in the condenser

$$R_{p,c} = \frac{r_o \varepsilon_p}{2L_c k_p} = \frac{(1.6 \times 10^{-3} \text{ m})^2 (8.89 \times 10^{-4})}{2(0.00939)(379)} = 1.99 \times 10^{-7} \text{ m}^2 \text{ K/W}$$

These values can be summarized as follows:

$$R_{p,e} = 1.59 \times 10^{-7} \text{ m}^2 \text{ K/W}$$

$$R_{w,e} = 7.43 \times 10^{-6} \text{ m}^2 \text{ K/W}$$

$$R_v = 3.08 \times 10^{-9} \text{ m}^2 \text{ K/W}$$

$$R_{w,c} = 9.34 \times 10^{-6} \text{ m}^2 \text{ K/W}$$

$$R_{p,c} = 1.99 \times 10^{-7} \text{ m}^2 \text{ K/W}$$

Substituting for these values in U_p fraction results in overall heat transfer coefficient of

$$U_p = 5.84 \times 10^{-5} \text{ W/m}^2 \text{ K}$$

3.12.5 *Heat Pipe Operating Environments*

In any heat pipe applications, the conditions for the heat source and heat sink are usually specified. This will determine the operating conditions and the suitability and effectiveness of a given heat pipe for the specified application. The calculation method is essentially a step-by-step iteration process and can be best determined with the aid of a good computer program and numerical examples inputs. Operating and nonoperating thermal environment of heat pipe requirement represents the primary constraint on the selection of the working fluid of that particular heat pipe. Naturally based freezing point and critical temperature will also determine the operating limits of a fluid. However, to play the design in a very safe and optimal mode of heat pipe operating limits (i.e., viscous, sonic, entrainment, capillary, wicking, and Boiling), the useful temperature range must be well under envelope of these limits. Clearly defined upper and lower operating temperature bounds are therefore required for proper selection of the working fluid. By the same arguments, it is often necessary to define maximum and minimum nonoperating temperature conditions. Upper temperature limits can affect the pressure containment design and may impact working fluid degrading and materials compatibility. The minimum nonoperating temperature on the other hand can affect the heat pipe's startup behavior especially if operation is to be initiated from a frozen or low vapor temperature state at which point the pipe has negligible heat transport capacity [36].

Sink temperature variations and temperature control requirements are the most significant design constraints associated with thermal control heat pipes. They can affect the selection of in particular variable conductance heat pipe design working fluids and reservoir size. For diode designs, the variation in sink temperature determines the degree of shutdown required and the maximum permissible reverse conductance. In addition any extra conductance surface around condenser area such as adding fins will play important rule into analysis and design of fixed heat pipe rather than variable one. As we discussed before, the wick is saturated with the liquid phase of working fluid, and the remaining volume of the heat pipe tube contains the vapor phase. Heat incident at evaporator by an external source vaporizes the working fluid in that section. As a result of pressure difference, vapor drives from evaporator to the condenser section of heat pipe where it condenses releasing the latent heat of vaporization to the heat sink in that section of the heat pipe. Depletion of the liquid by evaporation causes the liquid-vapor interface in the evaporator to enter into the wick surface (see Figs. 3.64 and 3.65), and a capillary pressure is developed there. The amount of heat that can be transported as latent heat of vaporization is usually several orders of magnitude larger than that which

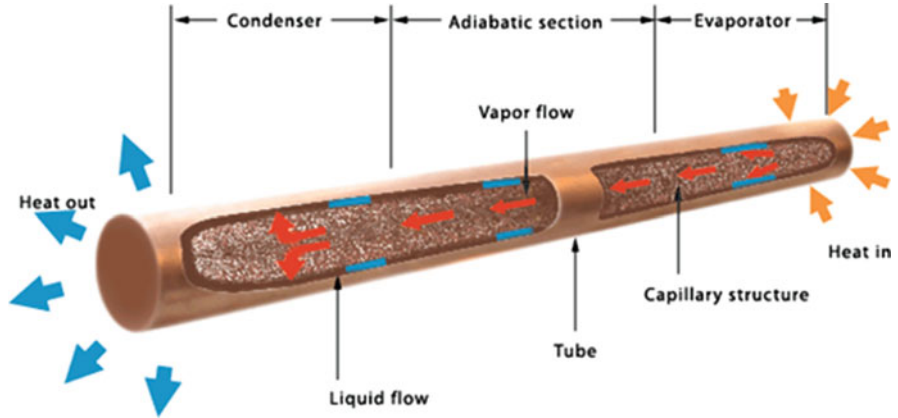


Fig. 3.64 Components and principle heat of operation of a conventional (fixed) heat pipe

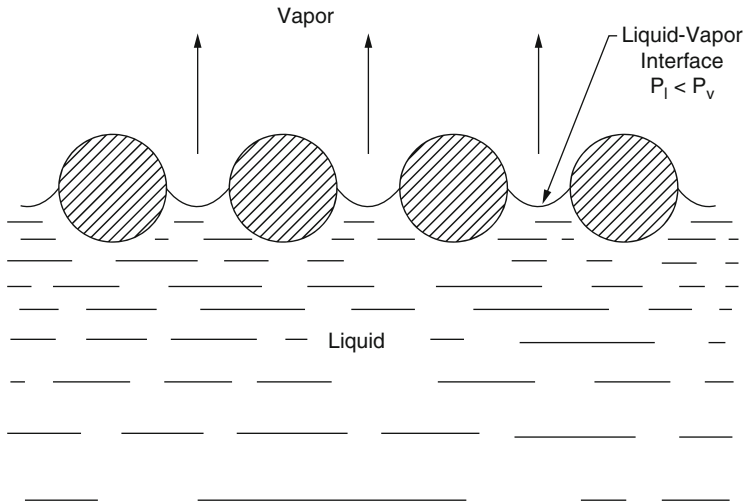


Fig. 3.65 Development of capillary pressure at liquid–vapor interface [5]

can be transported as sensible heat in a conventional convective system. As a result, the heat pipe can transport a large amount of heat with a small unit size.

Heat pipes having thermal characteristic order of magnitude better than any heat known so far have been developed because of their thin wick structure and the small temperature drop for their vapor flow. Unlike solid conductors, heat pipe characteristics are dependent not only upon size, shape, and material but also upon construction, working fluid, and heat transfer rate. Considerably heat transfer within heat pipe possesses limitation and in some cases to startup dynamically. There are methods that have been developed and discussed before to control and modify such characteristics in particular in a conventional heat pipe such as in Fig. 3.66.

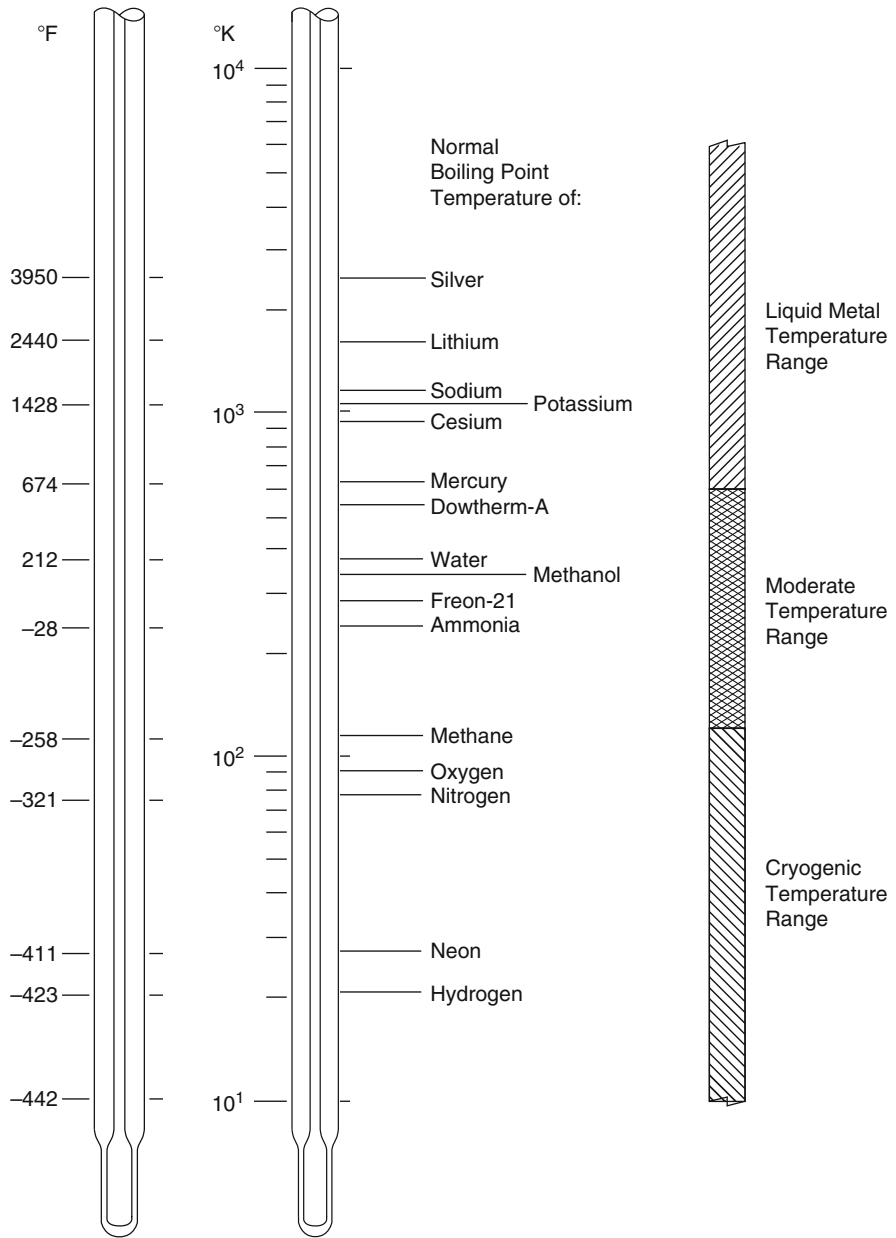


Fig. 3.66 Logarithmic thermometers with sample working fluids for cryogenic, moderate-temperature, and liquid-metal heat pipes indicated [5]

3.12.6 Wick Structures

Wick is one of the most important aspects and infrastructures of heat pipe. Its purpose is to provide the following [5]:

1. The necessary flow passages for the return of the condensed liquid
2. Surface pores at the liquid–vapor interface for the development of the required capillary pumping pressure
3. A heat flow path between the inner wall of the container and the liquid–vapor interface

Generally speaking, an effective wick structure requires small surface pores for large capillary pressure, large internal pores (in the direction normal to the liquid flow) for minimal liquid flow resistance, and an uninterrupted highly conductive heat flow path across the wick thickness for a small temperature drop. Due to the above reasoning and requirements, many types of wick structure have been developed, and they all were described in Sect. 2.7.4. Mesh screen, fiberglass, sintered porous metal, and narrow grooves cut in the inner surface of the container wall have been used as wick materials.

Computer programs have been developed around the wick structure analysis, and they are described in Sect. 3.15 such as the computer program GRADE for Design and Analysis of Graded-Porosity Heat Pipe Wicks (TRW Systems Group) [36] and computer program GRADE II for the Designed Analysis of Heat-Pipe Wicks (TRW Systems Group) [37]. These computer programs are designed to numerically solve the differential equations that describe heat pipes with graded-porosity fibrous wicks. Such wicks have an axial variation in porosity so that, at the maximum heat transfer rate, the porosity is just low enough for the wick to support the local liquid flow pressure drop plus any hydrostatic head.

In GRADE, calculating the highest possible permeability is obtained along the wick. For comparison of graded-to-uniform-porosity wicks, GRADE can also compute the performance of the latter. In fact, the user can have GRADE calculate the porosity for a given fiber diameter, or both the porosity and fiber diameter, that gives the highest heat transfer capacity for a uniform-porosity wick.

The revision version GRADE II is incorporating the mathematical model more completely that describes an actual graded-porosity wick heat pipe. In particular, it includes:

- Automatic calculation of the minimum condenser end stress that will not result in an excess liquid puddle or a liquid slug in the vapor space
- Numerical solution of the equations describing flow in the circumferential grooves to assess the burnout criterion
- Calculation of the contribution of excess liquid in fillets and puddles to the heat transport
- Calculation of the effect of partial saturation on the wick performance
- Calculation of the effect of vapor flow, which includes viscous–inertial interactions

The wicks are generally classified into two general classes:

1. Homogeneous wicks
2. Composite wicks

Homogeneous wicks are made of a single material, while composite wicks consist of two or more materials. Several examples of both homogeneous and composite wicks are demonstrated in Chap. 2 under different types of wicks section. Wick selection is adequately described in Sect. 3.2.2.

3.12.7 *Multicomponent Fluids*

For a heat pipe to operate, its wick structure must remain saturated with the liquid phase of a working fluid. Heat pipes have been developed with working fluids ranging from cryogenic liquids to liquid metals. Accordingly, heat pipes can be categorized into cryogenic, moderate-temperature, and liquid-metal types. The dividing line between cryogenic and moderate and liquid-metal temperature is set at -240 F (122 K), and the dividing line between moderate and liquid-metal temperature is at 670 F (628 K). These are logical lines since [5]:

1. The normal boiling points of so-called permanent gases such as hydrogen, neon, nitrogen, oxygen, and methane lie below -240 F (122 K).
2. Those of metals such as mercury, cesium, potassium, lithium, and silver lie above 670 F (628 K).
3. Common refrigerants and liquids such as Freon, methanol, ammonia, and water all boil under one standard atmospheric pressure at temperatures between -24 F (122 K) and 670 F (628 K).

Moreover, it has been observed for most fluids that properties relevant to heat pipe performance are going to be maximum in the vicinity of the fluid's normal boiling points. The normal boiling points of several fluids and the useful temperature ranges of individual classes of the heat pipes are illustrated on a logarithmic thermometer in Fig. 3.66 [5].

The most important differences among these three classes of heat pipes, besides their respective useful temperature ranges, are their maximum heat transport capabilities and temperature drops at the same heat transport rate in a heat pipe similar geometry. Comparison of properties of sample fluids for cryogenic, moderate-temperature, and liquid-metal heat pipes at normal boiling point temperature is presented in Table 3.9 [5]. These variations are due to mainly to the normally large values of the surface tension coefficient, the latent heat of vaporization, and the thermal conductivity for liquid metals in comparison with those values of these properties for the moderate-temperature and cryogenic liquids [5].

For selection of a working fluid, a variety of physical, chemical, and thermodynamic properties of a particular working fluid must be evaluated to determine

Table 3.9 Comparison with those values of these properties for the moderate-temperature and cryogenic liquids [5]

Properties	Fluids		
	Nitrogen	Ammonia	Sodium
Normal boiling point temperature, F (K)	-321 (77)	-28 (240)	1621 (1156)
Liquid density, lbm/ft ³ (kg/m ³)	50.6 (811)	42.5 (681)	46.1 (739)
Liquid surface tension, lbf/ft (N/m)	6.1×10^{-4} (8.9 $\times 10^{-3}$)	2.3×10^{-3} (3.36 $\times 10^{-2}$)	7.9×10^{-3} (1.15 $\times 10^{-1}$)
Liquid viscosity, lbm/ft h (kg/m s)	0.38 (1.57 $\times 10^{-4}$)	0.65 (2.69 $\times 10^{-4}$)	0.42 (1.74 $\times 10^{-4}$)
Liquid thermal conductivity, Btu/ft h F (W/m K)	0.080 (0.138)	0.32 (0.554)	31.8 (55)
Latent heat of vaporization, Btu/lbm (J/kg)	85.3 (1.98 $\times 10^5$)	601 (1.40 $\times 10^6$)	1700 (3.95 $\times 10^6$)
Vapor viscosity, lbm/ft h (kg/m s)	0.013 (5.39 $\times 10^{-6}$)	0.020 (8.27 $\times 10^{-6}$)	0.056 (2.32 $\times 10^{-5}$)
Vapor density, lbm/ft ³ (kg/m ³)	0.288 (4.61)	0.056 (0.90)	0.017 (0.27)

whether or not that fluid is suitable for the specific heat pipe application. The general considerations which apply to candidate fluids are [38]:

1. Operating temperature range
2. Liquid transport factor
3. Vapor phase properties
4. Wicking capability in body-force field
5. Thermal conductivity
6. Fluid operating pressure
7. Fluid compatibility and stability

A number of heat pipe fluids and their operating temperature range are summarized in Table 3.6 [38]. These are categorized into three operating temperature ranges: cryogenic (Group 1), intermediate (Group 2), and high temperature (Group 3). Properties which directly affect heat pipe design and performance are given in Figs. 4.2–4.13 in Volume I of Brennan and Krociczek [38]. A detailed listing of the fluid properties together with a computer program for tabulating fluid properties (heat pipe fluid, HPF) is presented in Volume II of this manual as well described in Sect. 3.15.6.

The effects of these various parameters on the selection of a working fluid are discussed below (Table 3.10).

Table 3.10 Selected properties of heat pipe working fluids [38]

Fluid	Formula	Group	Molecular weight	Melting point		Normal boiling point		Critical temperature		Critical pressure 10^5 N/m^2	Critical pressure P _{sia}	Temperature range of tabulated data (K)	References
				K	°F	K	°F	K	°F				
1. Helium	He	1	4.0	1.3	-457.3	4.2	-452.1	5.2	-450.3	2.3	33.4	2.4-4.0	[6]
2. Hydrogen	H ₂	1	2.0	14.0	-434.4	20.4	-423.0	33.0	-400.3	12.9	187.2	14-33	[5, 6, 39]
3. Neon	Ne	1	20.2	24.5	-415.6	27.1	-410.9	44.4	-379.8	26.5	384.5	27-44	[4, 6, 39]
4. Oxygen	O ₂	1	32.0	54.3	-361.8	90.2	-297.3	154.8	-181.1	50.9	738.6	55-154	[4-6, 39]
5. Nitrogen	N ₂	1	28.0	63.1	-346.0	77.3	-320.4	126.2	-232.4	34.0	493.3	65-125	[4-6, 40]
6. Argon	A	1	39.9	83.8	-308.8	87.3	-302.5	150.9	-188.1	50.0	725.5	85-150	[4, 6, 7]
7. Propane	C ₃ H ₈	1	44.1	85.5	-305.8	231.1	43.7	370.0	206.3	42.6	618.1	190-367	[1, 6, 41]
8. Freon-14	CF ₄	1	88.0	89.4	-298.7	145.5	-197.8	227.7	-49.8	37.4	542.7	130-222	[10]
9. Ethane	C ₂ H ₆	1	30.1	89.9	-297.8	184.5	-127.6	305.5	90.2	49.1	712.4	100-305	[1, 4, 6, 41]
10. Methane	CH ₄	1	16.0	90.7	-296.4	111.4	-259.2	190.5	-116.8	46.4	673.3	91-190	[4, 6, 40, 41]
11. Freon-13	CClF ₃	1	104.5	93.2	-291.9	191.7	-114.6	302.3	84.5	39.0	565.9	163-293	[4, 6]
12. Butane	C ₄ H ₁₀	1	58.1	134.8	-217.0	272.7	31.2	425.0	305.3	38.0	550.7	260-350	[1, 4, 6, 40, 41]
13. Freon-21	CHCl ₂ F	1	102.9	138.2	-210.9	282.1	48.1	451.4	352.8	51.8	751.8	213-450	[4, 6, 40]
14. Freon-11	CCl ₃ F	1.2	137.4	162.2	-167.8	296.9	74.7	471.2	388.5	44.1	639.9	293-413	[4, 6, 40]
15. Methanol	CH ₃ OH	2	32.0	175.2	-144.3	337.9	148.5	513.2	464.1	79.5	1153.0	273-503	[6]
16. Toluene	C ₇ H ₈	2	92.1	178.1	-139.1	383.7	231.0	593.9	609.3	41.6	603.6	275-473	[6, 40, 41]
17. Acetone	(CH ₃) ₂ CO	2	59.1	180.0	-135.7	329.4	133.2	508.2	455.1	47.6	690.0	250-475	[40, 41]
18. <i>N</i> -Heptane	C ₇ H ₁₆	2	100.2	182.6	-131.0	371.6	209.2	540.2	512.7	27.4	397.6	273-473	[6, 40, 41]
19. Ammonia	NH ₃	1.2	17.0	195.5	-107.8	239.8	-28.0	405.6	270.4	112.9	1638.0	200-405	[4-6, 40]
20. <i>M</i> -Xylene	C ₈ H ₁₀	2	106.2	225.3	-54.1	412.3	282.5	619.2	654.9	36.5	529.6	275-473	[6, 41]

21. Mercury	Hg	2, 3	200.6	234.3	-37.9	630.1	674.5	1763	2714	1510	21,910	280-1070	[6, 39, 42]
22. Dowtherm E		2	147.0			453.4	356.4	690.2	785.0	40.3	584.7	283-610	[43]
23. Water	H ₂ O	2	18.0	273.2	32.0	373.2	212.0	647.3	705.4	221.2	3210	273-643	[6]
24. Benzene	C ₆ H ₆	2	78.1	278.7	42.0	353.3	176.2	562.6	553.0	49.2	713.9	280-560	[6, 40]
25. Dowtherm A		2	166.0	285.2	53.6	531.1	496.4	801.2	982.4	40.2	583.3	373-670	[6]
26. Cesium	Cs	3	132.9	301.6	83.2	943.0	1237.8	2050	3230	117.0	1698.9	400-1500	[6, 39]
27. Potassium	K	3	39.1	336.4	145.8	1032.2	1398.3	2250	3590	160.0	2322	400-1800	[6, 39]
28. Sodium	Na	3	23.0	371.0	208.1	1152.2	1614.3	2500	4040	370.0	5369	400-1500	[6, 39]
29. Lithium	Li	3	6.9	453.7	357.0	1615.0	2447.0	3800	6380	970.0	14,074	500-2100	[6, 39]
30. Silver	Ag	3	107.9	1234	1761	2450.0	3950.3	7500	13,040	336.0	4875	1600-2400	[9, 39, 42]

3.12.8 Maximum Heat Flux

Heat flux or **thermal flux**, sometimes also referred to as **heat flux density** or **heat flow rate intensity**, is a flow of energy per unit of area per unit of time. In SI units, it is measured in $[\text{W}/\text{m}^2]$. It has both a direction and a magnitude, so it is a vectorial quantity. To define the heat flux at a certain point in space, one takes the limiting case where the size of the surface becomes infinitesimally small.

Heat flux is often denoted, $\vec{\phi}_q$ the subscript q specifying *heat flux*, as opposed to *mass* or *momentum* flux. The most important appearance of heat flux in physics is in Fourier's law describing heat conduction (Fig. 3.67).

Generally speaking, the rate at which heat is transferred is represented by the symbol Q . A common unit for heat Q transfer rate is Btu/h in British system or W/h in SI unit system. Sometimes it is important to determine the heat transfer rate per unit area, or *heat flux*, which has the symbol Q'' . Units for heat flux are Btu/h ft² in British system or W/h m². The heat flux can be determined by dividing the heat transfer rate by the area through which the heat is being

$$Q'' = \frac{Q}{A} \quad (\text{Eq.3.73})$$

where

Q'' = Heat flux (Btu/h ft²) or (W/h m²)

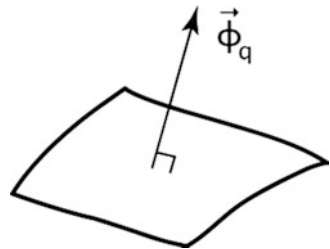
Q = Heat transfer rate (Btu/h) or (W/h)

A = Area (ft²) or (m²)

Also we should know that *thermal conductivity* is the heat characteristics of a solid material measured by a property called the thermal conductivity (k) measured in Btu/h ft °F or W/h m °C. It is a measure of a substance's ability to transfer heat through a solid by conduction. The thermal conductivity of most liquids and solids varies with temperature. For vapors, it depends upon pressure.

In addition to the capillary, the sonic, and the entrainment limits, the heat pipe performance is also limited by the evaporator heat flux. Heat is transferred into and out of the heat pipe through the pipe wall and through at least part of the wick. If the radial heat flux becomes excessive, the circulation of the working fluid can be severely affected, and the heat transport capability may be controlled by the radial heat flux rather than by the axial heat transport.

Fig. 3.67 Heat flux $\vec{\phi}_q$ through a surface



The limitation of the axial heat flux is not nearly as well understood as the condenser, flooding hydrodynamic climates. There appears to be no limit to the heat flux at the condenser. High condenser heat fluxes contribute, of course, directly to the heat pipe conductance, but they do not affect circulation of the working fluid. The evaporator heat flux, on the other hand, has definite upper bounds which limit the axial heat transport.

Unlike the previously described limits, which specify a maximum axial heat transport Q_t'' , the heat flux limit specifies the maximum radial evaporator heat flux q_e'' . The two quantities are related through the evaporator area A_e as follows:

$$Q_t'' = q_e'' A_e \quad (\text{Eq.3.74})$$

Thus, for a given evaporator geometry, the heat flux limit also specifies the maximum axial heat transport. The heat flux limit is generally considered to coincide with the onset of nucleate boiling in the wick. Heat is conducted from the heat pipe wall through the wick, and evaporation is assumed to occur at the liquid–vapor interface. This model has been substantiated by extensive experimental evidence [44–46]. When boiling occurs within the wick, the presence of the vapor bubbles that are generated reduce the liquid flow area and consequently decrease the transport capability [3].

With the onset of nucleate boiling, the hydrodynamic equations previously developed are no longer applicable since they were based on one-dimensional, laminar, liquid flow in a fully saturated wick. Breakdown of the mathematical model does not necessarily indicate a heat transfer limit. Since the hydrodynamic theory does not account for boiling in the wick, it is a good design practice to define the heat flux limit as the onset of nucleate boiling [3]. The boiling heat flux limit corresponds to the conduction heat flux which yields a “critical” superheat $\Delta T_{\text{critical}}$ in the liquid. The boiling heat flux limit is therefore

$$q_{\text{max}} = \frac{K_{\text{eff}}}{t_w} \Delta T_{\text{critical}} \quad (\text{Eq.3.75})$$

where K_{eff} is the effective thermal conductivity of the wick–liquid matrix. A model for the effective conductivity was discussed in Sect. 2.7.7. Marcus [33] has derived an expression for the critical superheat which is based on criteria similar to those which apply to nucleate boiling from planar surfaces:

$$\Delta T_{\text{critical}} = \frac{T_{\text{sat}}}{\lambda \rho_v} \left(\frac{2\sigma}{r_n} - (\Delta P_i)_{\text{max}} \right) \quad (\text{Eq.3.76})$$

where T_{sat} is the saturation temperature of the fluid and r_n is the effective radius of the critical nucleation cavity. This equation is based on the assumption that a bubble of a certain size will grow if its internal vapor pressure associated with the local superheat exceeds the restraining forces of saturation and capillary pressure.

The radius of nucleation cavities, r_n , is a function of the boiling surface. Typical values for smooth surfaces are between 10^{-4} and 10^{-3} cm. For wicked surfaces, little is known about the critical radii of nucleation cavities, but an upper bound is certainly the pore size of the wick.

The model predicts very conservative superheat tolerances. Even if the lower bound for the critical radius is used, the calculated critical superheat is sometimes one order of magnitude lower than that actually measured. Marcus [44] attributes this to the absence of a gaseous phase at the nucleation sites because heat pipes contain a highly degassed working fluid. However, incipient boiling is difficult to detect through temperature measurements alone, and many wicks which provide for adequate venting of internally generated vapor can tolerate some nucleate boiling without affecting the hydrodynamic limit.

A definite upper heat flux limit exists for every wick, and it is reached when the vapor generated within the wick is at such a high rate that it cannot escape fast enough from the heated surface. This is equivalent to the inability of the capillary forces to replenish liquid at a sufficient rate. Boiling in the wick and the associated heat flux has been the subject of many investigations [3].

3.12.9 Size and Weight Constraints

Imposed gravitation force or an external acceleration may produce some kind of static pressure drop within heat pipe that may put a limitation on the heat pipe length for a particular application. Also any constraints on heat pipe size and weight may be imposed by volume restrictions of the application and the requirement for minimal system weight. Any application for heat pipe use will also define the area covered by the heat source and that result in defining the evaporator surface area for the heat pipe as well.

Depending on the application of the heat pipe and designer's goal for that application in order to cool down the heated components, the size and weight of the heat pipe cooling system will be minimized by maintaining the temperature of the heated component as close as possible to the source temperature. Particularly this is a very important step and consideration that a designer of the pipe should bear in mind in case the application for cooling and temperature of the source is steady or transient. In this manner, the heat load to be transferred to the heat pipe cooling system is minimized. However, the type of materials that will be used for a given application and its strength and environment of operation and its compatibility considerations could limit the temperature of the component being cooled to a level well below that of the heat source [23]. There are computer programs that are offering material strength analysis for exactly very similar to heat pipe design, and operational requirements that are also mentioned in Sect. 3.17.1.

On the other hand, size optimization becomes more complex and involved, if the goal of heat transfer is at a specified rate from a hotter heat source to a cooler heat

sink in particular in a mode such as heat exchanger that a fluid is involved. A heat exchanger will be composed of a relatively large number of individual heat pipes. The total cumulative area of the heat pipes will be determined by fluid properties and flow rates on the hot and cold sides of the heat exchanger and by the flow passage and heat pipe dimensions [23]. One of the most important considerations or constraints of minimizing system size is depending on adjusting system variables to its maximum hot and cold side of heat transfer coefficients. However, a reduction in overall system size is usually in alignment with an increase in pressure drop of the heat exchanger fluids to the extent that system size can be reduced. In that case, it is determined by allowing the proper pressure for the application in the hand.

3.12.10 Temperature Constraints

If the design of the heat pipe is a not function of the heat source or other temperature variations or limitations, then an upper limit on heat pipe temperature may be imposed by the strength of the heat pipe-fabricated materials, which generally decreases with an increase in temperature. The decreasing effectiveness of oxidation or corrosion-resistant coating may cause a constraint on temperature limitation that one should be concern about. Another upper limit temperature constraint of heat pipe operation will come from the boiling limit of design. If this occurs, substitution of another heat pipe fluid as working fluid should be considered, and a lot of different computer coding capabilities are offered in this chapter to overcome this problem (both steady-state and transient conditions). In case of a sodium heat pipe (i.e., a high-temperature environment such as nuclear reactor core cooling system) if the boiling limit is encountered, replacement of such working fluid for the heat pipe with another fluid such as lithium is highly recommended. However, it might be necessary to operate the lithium heat pipe at higher temperature to ensure that the vapor pressure is high enough to avoid capillary pumping, sonic, or entrainment limits.

3.12.11 Fabrication and Cost Constraints

The more difficult a heat pipe is to fabricate, the more costly it is likely to be. Some aspects of fabrication are under the control of the designer, whereas others may be inherent in the application. An example of the latter would be a heat pipe system that transports heat generated in a nuclear reactor to an associated energy-conversion plant. The need to avoid direct nuclear radiation leakage paths may dictate that the heat pipe elements follow a tortuous path while passing through the radiation shield. Similarly, the very high incident heat flux in the stagnation regions of high-speed aircraft may dictate a very thin wick in the evaporator region of a heat pipe cooling system to avoid boiling [23].

Heat pipe fabrication will be simpler and less costly if readily available, easily machinable materials can be used. Thus, if the operating temperature of a sodium heat pipe can be held to 1700 °F (927 °C) or less, super alloy construction from an alloy such as Hastelloy X or Haynes 188 may be feasible. A more difficult to machine refractory alloys such as TZM molybdenum might be required at higher temperatures, with the additional requirement of an oxidation-resistant coating [23].

A single-layer wick, relatively thick with a relatively coarse pore structure, may be fabricated more easily and cheaply than a thin, two-layer wick of more complex design with a finer pored wick structure.

Within constraints that may be imposed by the application, there may be a considerable room for design trade-offs, and as a result of it, the desire for heat pipe system of minimal size and weight would be balanced against factors such as material strength and corrosion characteristic, fabricability, and cost. Final design decisions may be well based on the experience and judgment of the designer [23].

3.12.12 Heat Pipe Area–Temperature Relations

Procedures and designing steps for establishing the heat pipe size and operating temperature will be a function of the way the heat pipe is thermally coupled to the heat source and sink. These are schematically represented by Silverstein [23] and are reproduced here again in Fig. 3.38. The rule of thumb and what they have in common between case Fig. 3.68a–c is that to equate the heat transfer rate between the heat source and the heat pipe to that between the heat pipe and the heat sink and one can establish the area–temperature relationships that need to be considered for all the cases in Fig. 3.68.

3.12.12.1 Convective Heat Source and Heat Sink

Taking into consideration, a heat pipe is used to transfer heat from a hot gas at temperature T_h to a cooler gas at temperature, T_c , as indicated in Fig. 3.68a. This situation is representative of heat transfer in a single stage of a heat pipe heat exchanger. The heat transfer coefficient is h_h on the hot (evaporator) side and h_c on the cold (condenser) side [23]. The surface area of the heat pipe is A_c on the hot side and A_e on the cold side. The heat transfer rate between the gases and the heat pipe is assumed to be small compared to their heat content, so that T_h and T_c remain approximately constant.

The heat pipe temperature T_p is assumed to be constant (wall and wick ΔT s and the ΔT along the heat pipe length are assumed to be negligible) [23].

A heat balance between the two gases yields the equation

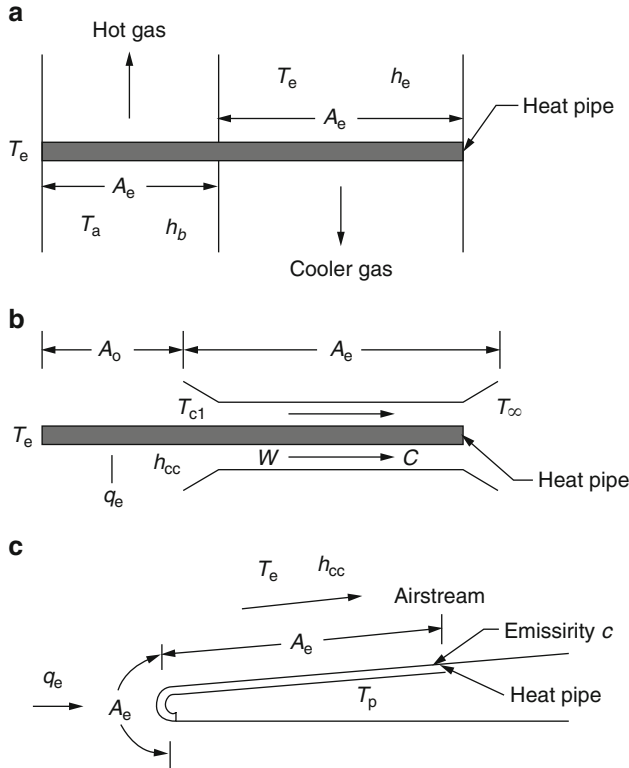


Fig. 3.68 Heat source, heat sink configurations for heat pipe [23]. (a) Convective heat source and heat sink. (b) Constant heat source and convective heat sink. (c) Heat pipe-cooled leading edge

$$h_h A_e (T_h - T_p) = h_c A_c (T_p - T_c) \quad (\text{Eq.3.77})$$

From this equation, the ratio of cold and hot side areas can be presented in the form

$$\frac{A_c}{A_e} = \frac{h_h}{h_c} \left[\frac{(T_h/T_c) - (T_p/T_c)}{(T_p/T_c) - 1} \right] \quad (\text{Eq.3.78})$$

In case A of Fig. 3.61, A_c/A_e is plotted as a function of T_p/T_c with $T_h/T_c = 2$ and $h_h/h_c = 1$.

Note: The required cold side area varies inversely with the heat pipe temperature, varying from zero at $T_p = T_h$ to infinity at $T_p = T_c$

3.12.12.2 Constant Heat Source and Convective Heat Sink

In another example (Fig. 3.68b), heat is added at a constant mean heat flux q_e over an area A_e to a heat pipe at T_p . The heat is rejected by convective heat transfer from

area A_c to a surrounding liquid flow stream with inlet temperature T_{ci} and outlet temperature T_{co} . The specific heat of the liquid is c , its mass flow rate is W , and the convective heat transfer coefficient is h_{cc} . This situation is representative of a laboratory setup to measure heat pipe performance. The constant rate heat source might be an induction coil surrounding the evaporator section of the heat pipe [23].

The energy balance in this case is

$$q_e A_e = Wc(T_{co} - T_{ci}) \quad (\text{Eq.3.79})$$

Upon introducing the concepts of heat exchange, effective ε and number of heat transfer unit NTU [23] for heat transfer between a condensing vapor (the heat pipe fluid) and a second fluid, where

$$\varepsilon = \frac{T_{co} - T_{ci}}{T_p - T_{ci}} \quad (\text{Eq.3.80})$$

and

$$\text{NTU} = \frac{h_{cc} A_c}{Wc} = \ln \frac{1}{1 - \varepsilon} \quad (\text{Eq.3.81})$$

the energy balance may be written (with some manipulation) [23] as

$$\frac{A_c}{A_e} = \frac{q_e}{h_{cc}(T_{co} - T_{ci})} \ln \left[\frac{(T_p/T_{ci}) - 1}{(T_p/T_{ci}) - (T_{co}/T_{ci})} \right] \quad (\text{Eq.3.82})$$

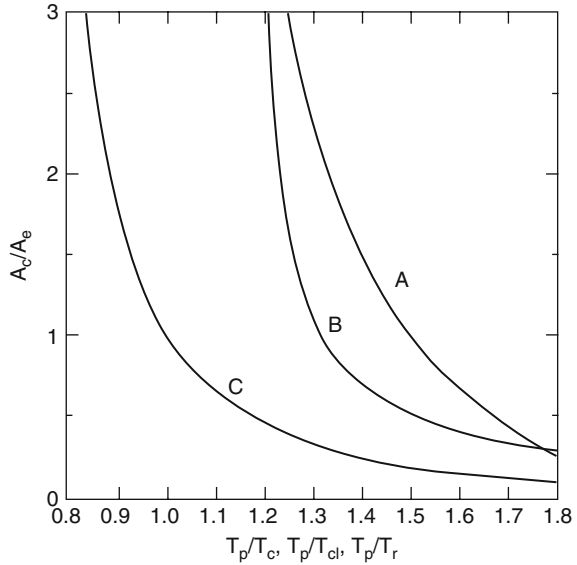
The minimum heat pipe temperature in this case is T_{co} , when the denominator in the log term of the above equation is equal to zero and the condenser area is infinite [23]. The ratio of condenser and evaporator areas is plotted against T_p/T_{ci} as in case B of Fig. 3.69, with $q_e/[h_{cc}(T_{co} - T_{ci})] = 1$ and $T_{co}/T_{ci} = 1.2$.

3.12.12.3 Heat Pipe-Cooled Leading Edge

Finally in the example that is depicted in Fig. 3.68c, the outer surface on the forward section of an aircraft wing is fabricated as a heat pipe structure. Aerodynamic heat incident on the area A_e of the leading edge at a constant mean heat flux q_e is to be dissipated over area A_c of the lateral surfaces by radiation. Variation of the aerodynamic heat flux with the leading edge temperature is neglected here. The lateral surfaces are also subjected to aerodynamic heating at a heat flux q_{ah} give by the following equation [23]:

$$q_{ah} = h_{aa}(T_r - T_p) \quad (\text{Eq.3.83})$$

Fig. 3.69 Variation of condenser heat transfer area with temperature. (a) Convective heat source, convective heat sink. (b) Constant heat source and convective heat sink. (c) Heat pipe-cooled leading edge



where

h_{aa} = The convective heat transfer coefficient of the flowing air stream

T_r = The recovery temperature (temperature elevation due to deceleration of the air stream in the boundary layer)

T_p = The heat pipe temperature

Again, temperature drops through the heat pipe walls and along its length are neglected. A heat balance equating heat incident on the leading edge and lateral surfaces to heat radiated to the environment from the lateral surfaces (radiation from the leading edge is neglected) has the form [23]

$$q_c A_c + h_{cc} A_c (T_r - T_p) = \epsilon_s \sigma_r T_p^4 A_c \tag{Eq.3.84}$$

where

ϵ_s = The surface emissivity

σ_r = The Stefan–Boltzmann radiation constant

With some manipulation, this equation may be recast into the form [23]

$$\frac{A_c}{A_e} = \frac{q_c / (\epsilon_s \sigma_r T_r^4)}{\left(\frac{T_p}{T_r}\right)^4 - \left(\frac{h_{cc}}{\epsilon_s \sigma_r T_r^3}\right) \left(1 - \frac{T_p}{T_r}\right)} \tag{Eq.3.85}$$

When the denominator of the above equation is equal to zero, the lateral area needed to dissipate the heat incident on the leading edge becomes infinite. The temperature at which this occurs is called the radiation equilibrium temperature T_c , and it represents the minimum possible heat pipe temperature. At T_c , only the

aerodynamic heat incident on the lateral surfaces can be radiated away. When T_p is higher than T_e , both the leading edge heat load and that on the lateral surfaces can be dissipated radiatively [23].

The required radiator area decreases as T_p increases. When T_p exceeds the recovery temperature T_r , the lateral surfaces are subjected to aerodynamic cooling instead of aerodynamic heating.

The variation of A_c/A_e with T_p/T_r is shown as case c in Fig. 3.68, with $q_e/(\epsilon_s \sigma_r T_r^4) = 1$ and $h_{cc}/\epsilon_s \sigma_r T_r^3 = 1$.

As is evident from Fig. 3.68, substantial reductions in heat rejection area, and hence overall size, are associated with operation at the highest feasible heat pipe temperature [23].

Heat pipes provide cooling of stagnation regions by transferring heat nearly isothermally to locations aft of the stagnation region, thus raising the temperature aft of the stagnation region above the expected radiation equilibrium temperature. When applied to leading edge cooling, heat pipes operate by accepting heat at a high rate over a small area near the stagnation region and radiating it at a lower rate over a larger surface area, as shown in Fig. 3.70. The use of heat pipes results in a nearly isothermal leading edge.

The design of a heat pipe-cooled leading edge is very complex due to the numerous variables involved. However, a simple set of closed-form equations is presented here that can be used to determine if a heat pipe-cooled leading edge is feasible with various material combinations (Fig. 3.71).

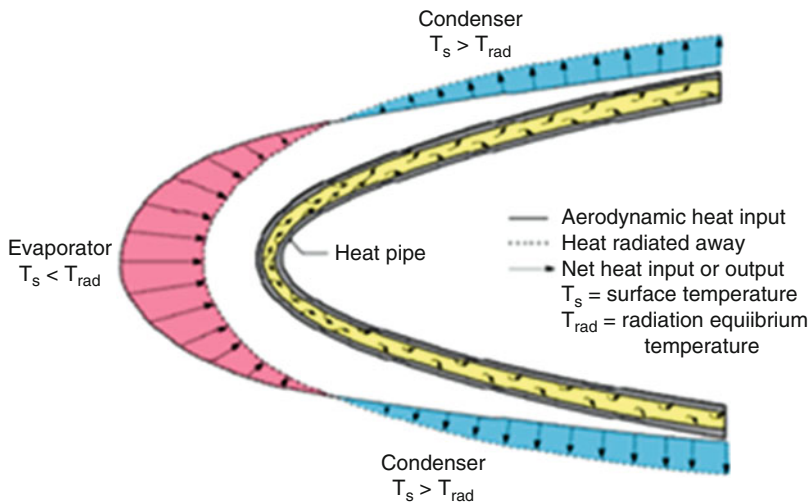


Fig. 3.70 Schematic diagram of a heat pipe-cooled leading edge showing regions of net heat input (evaporator) and net heat output (condenser) [47]

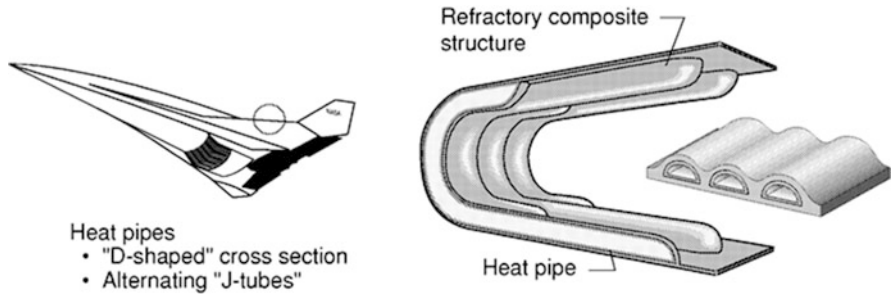


Fig. 3.71 Schematic drawing of a hypersonic vehicle with a diagram of a heat pipe-cooled wing leading edge [47]

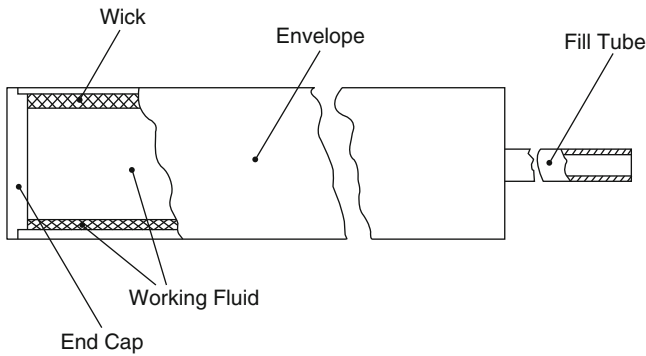


Fig. 3.72 Typical components of a heat pipe [2]

3.12.13 Heat Pipe Manufacturing

Heat pipe manufacturing methods either they are **fixed conductance heat pipes** (FCHP) or **variable conductance heat pipe** (VCHP) structures are very important and require careful examination with the goal of establishing cost-effective procedures that will ultimately result in cheaper and more reliable heat pipes. Those methods which are commonly used by all heat pipe manufacturers have been considered, including envelope and wick cleaning, end closure and welding, mechanical verification, evacuation and charging, working fluid purity, and charge tube pinch-off. Here we present the study that was done by Edelstein and Haslett [48] as part of the final report that was prepared by Grumman Aerospace Corporation for NASA, and it is limited to moderate-temperature aluminum and stainless steel heat pipes with ammonia, Freon-21, and methanol working fluids. Review and evaluation of available manufacturer's techniques and procedures together with the results of specific manufacturing oriented tests have yielded a set of recommended cost-effective specifications which can be used by all manufacturers.

A heat pipe is essentially composed of five components as shown in Fig. 3.72, namely, the envelope (or container), wick, end cap, fill tube, and working fluid.

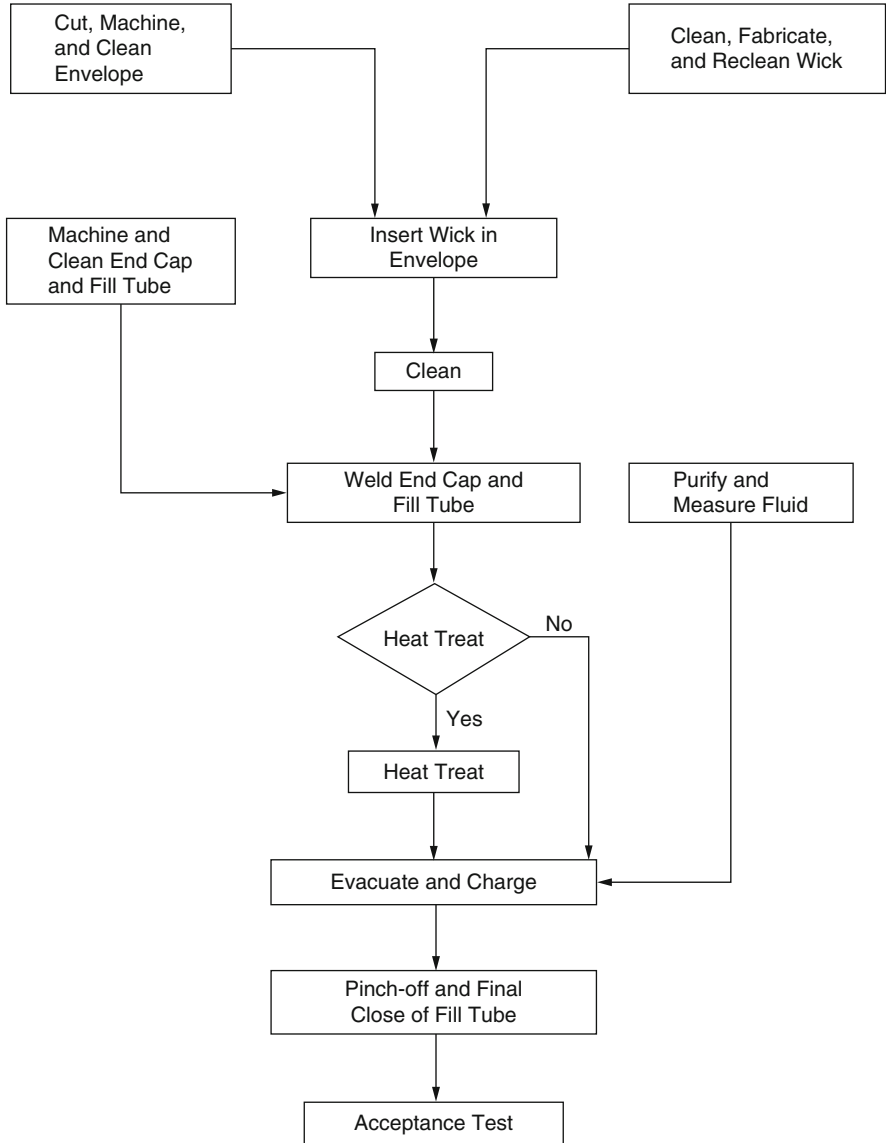


Fig. 3.73 Typical flowchart for heat pipe manufacturing [2]

The selection of pipe working fluid and material and sizing of pipe components have been discussed in some detail in the above sections. In this section, techniques for the manufacture of heat pipes are described. Figure 3.73 illustrates schematically a flowchart of the basic operations involved in manufacturing a heat pipe as modified from material presented by Edelstein and Haslett [48]. The basic elements of manufacture, as can be seen from this figure, are parts manufacturing, cleaning,

assembly and welding, evacuation and charging, closure of the fill tube, and acceptance tests; they form the topics for this section.

As the title of this section implies, this effort is concerned with lowering the costs of producing heat pipes to be competitive with existing thermal control devices such as heaters, coatings, louvers, etc. A key goal of the section is to develop standardized manufacturing procedures which would assure the reliability of the final product. By evaluating and defining acceptable cleaning procedures, for example, the reliability of a properly fabricated heat pipe will be increased. Moreover, since each manufacturer is currently using essentially independent procedures, heat pipes supplied to users are built to different specifications and quality. There is a good deal of duplication of effort in the field; many individual company's procedures have been established iteratively, which is a costly and time-consuming way to develop a technology.

This effort, therefore, is only the forerunner of others which will ultimately develop basic heat pipe manufacturing specifications and details for all manufacturers. Because there are so many different types and styles of heat pipes covering a wide range of applications and temperatures, it was decided to limit this study to those commonly used today. Thus, single fluid devices operating in the moderate or room temperature range were selected (Edelstein and Haslett [48]). Construction materials were aluminum and stainless steel envelopes and wicks; working fluids were ammonia, Freon-21, and methanol; for more details of this study, please refer to their report.

A flowchart of the basic operations involved in manufacturing a heat pipe is presented in Fig. 3.73. A brief summary of the major elements of the manufacturing cycle discussed is as follows:

1. Envelope and wick cleaning

Probably the most significant manufacturing problem existing today is the lack of a simple reliable, effective cleaning procedure for heat pipe envelopes and wicks. For example, the incomplete removal of water from aluminum heat pipes has proven to be an expensive oversight for many heat pipe programs. A variety of techniques are currently being used by manufacturers, with varying degrees of success. In Sect. 3 of the report by Edelstein and Haslett [48], the experiences encountered with these techniques are presented along with recommended detailed cleaning procedures for both aluminum and stainless steel. These involve solvent, acid, and alkaline cleaning for aluminum, and passivation for stainless steel.

2. End closure and welding

An improperly designed end cap or poor welding technique can lead to questionable joints which may fail to pass X-ray examination or, worse, fail in service. Weld defects may be present which cannot be detected by X-rays. These minute defects may open up during service causing leaks, cracks, or even catastrophic mechanical failure. Various forces (such as fatigue cycling, the release of internal weld stresses, or a stress riser) may be the triggering action. A number of joint designs used in the past are evaluated in Sect. 4 of the

report by Edelstein and Haslett [48]. Square butt joint and lipped butt joint end cap designs are recommended for aluminum and stainless steel, respectively. In addition, gas tungsten arc welding is recommended as the most cost-effective welding technique.

3. **Mechanical verification**

A sound structural design that has been properly verified by nondestructive tests is paramount to reliable, long-term heat pipe operation. The ASME pressure vessel code is recommended when specifying allowable design stresses, proof pressure, and burst pressure. Simplified methods are also presented in Sect. 5 of the report by Edelstein and Haslett [48] for including the stress effects due to internal pressure, end caps, thermal expansion, saddle attachments, pipe bends, and dynamic loading. Cost-effective methods of leak detection for ammonia, Freon, and methanol used during pre-charging and postcharging operations include X-ray examination, pressurization under water, helium detection, and copper sulfate/ethylene glycol (for ammonia).

4. **Evacuation and charging**

Evacuation of foreign gaseous material from a heat pipe prior to charging must be effective to prevent non-condensable gases from subsequently appearing. The amount of material removed during evacuation is a function of many variables: charge tube geometry, temperature of pipe during evacuation, evacuation time, history of surface from prior cleaning operation, etc. In Sect. 6 of the report by Edelstein and Haslett [48], an attempt is made to experimentally correlate some of these variables. This correlation forms the basis for recommending effective evacuation parameters. Charging techniques for high- and low-pressure fluids used by various manufacturers are presented along with methods of charge bottle preparation. Based on test data and manufacturers' experience, techniques are outlined which minimize the introduction of detrimental impurities.

5. **Fluid parity**

Working fluids available from manufacturers come in different grades, with different purity levels. It is important to know, through a certified analysis, which impurities are present and to what extent to decide if additional purification is required. Considering only the impurities in the pipe prior to charging, it is shown in Sect. 7 of the report by Edelstein and Haslett [48] that the material absorbed on the pipe wall can be significant compared to the residual gas remaining after evacuation. Techniques are presented which permit the designer to quickly estimate condenser blockage as a function of impurity level, pipe design, and operating conditions, thereby allowing him to estimate the maximum quantity of impurities for his particular application.

6. **Charge tube pinch-off**

The final mechanical operation performed on the heat pipe is to permanently seal in the working fluid. If not properly done, in-leakage of non-condensable gas can occur during the processes which can result in either scrapping the pipe or placing it through an expensive refurbishment cycle. Except for differences in technique, most manufacturers employ the same procedure involving sequentially: crimping the fill tube to form a temporary leak-tight closure, severing the

charge valve from the fill tube, and finally welding shut the cut end (Sect. 8 of the report by Edelstein and Haslett [48]). Other less common techniques having the potential of making the pinch-off operation less operator dependent are also presented.

In this report, each of the foregoing areas is discussed in greater depth. Finally, based on these evaluations, a preliminary baseline manufacturing specification is presented in Sect. 9 of report by Edelstein and Haslett [48]. It represents an initial attempt at establishing a standardized manufacturing procedure.

For more details, a study of the report by Edelstein and Haslett [48] is highly recommended.

3.13 Optimal Heat Pipes

Optimal heat pipes are the pipes that are following an optimal design and manufacturing guideline. In general criteria for the selection of heat pipe components such as the fluid, wick, and container are few that can be discussed. Specific quantitative design procedure for the heat pipe briefly is described here for overall review by the readers of this book.

The selection of most suitable working fluid is an important step, and it should be selected in ways that the working fluid should not freeze in required operating temperature range of the heat pipe. Table 3.11 is a summary presentation of useful operating temperature ranges and melting and boiling temperature for several heat pipe fluids.

With heat source and sink conditions of the heat pipe usually specified for a given design problem, the operating temperature of the heat pipe can usually be calculated as the average of the condenser and evaporator pipe wall temperatures. With the approximate temperature band, several fluids may exist, and a variety of characteristics must be examined in order to determine the most acceptable working fluid for a given application. The prime requirements of the working fluid are:

1. High latent heat of vaporization to enable a large quantity of heat to be transferred axially with a low liquid mass flow rate, hence maintaining low pressure drops within the heat pipe.
2. High liquid and vapor densities to allow for small cross-sectional wick and vapor core areas for a given mass flow rate and Reynolds number.
3. High liquid surface tension to enable the heat pipe to operate against gravity by producing a high capillary driving force.
4. Low liquid and vapor viscosities to minimize the resistance to fluid flow.
5. High thermal conductivity of the working fluid in order to minimize the temperature gradient in the radial direction and to reduce the possibility of nucleate boiling at the wick wall interface.

Table 3.11 Operating temperature ranges of heat pipe working fluid [4]

Medium	Melting point (°C)	Boiling point at atmos. press. (°C)	Useful range (°C)
Helium	-271	-261	-271 to -269
Nitrogen	-210	-196	-203 to -160
Ammonia	-78	-33	-60 to 100
Pentane	-130	28	-20 to 120
Acetone	-95	57	0 to 120
Methanol	-98	64	10 to 130
Flutec PP2 ^a	-50	76	10 to 160
Ethanol	-112	78	0 to 130
Heptane	-90	98	0 to 150
Water	0	100	30 to 200
Toluene	-95	110	50 to 200
Flutec PP9 ^a	-70	160	0 to 225
Thermex ^b	12	257	150 to 350
Mercury	-39	361	250 to 650
Cesium	29	670	450 to 900
Potassium	62	774	500 to 1000
Sodium	98	892	600 to 1200
Lithium	179	1340	1000 to 1800
Silver	960	2212	1800 to 2300

Note: (The useful operating temperature range is indicative only.) Full properties of most of the above are given in Appendix A

^aIncluded for cases where electrical insulation is a requirement

^bAlso known as Dowtherm A, an eutectic mixture of diphenyl ether and diphenyl

6. Compatibility between the working fluid, container, and wick material mandatory.
7. Good thermal stability within its operating temperature range thus avoiding chemical decomposition upon temperature fluctuations.
8. Acceptable freezing or poor point to ensure a low viscosity especially upon startup.
9. Good wettability of wick and wall materials.
10. Vapor pressures not too high or low over the operating temperature range. The vapor pressure of the fluid should not be excessive to warrant a very thick-walled container, nor should the vapor pressure be so low resulting in low vapor densities and high pressure drops in the vapor flow.
11. Toxicity and flammability of the fluid may have to be considered in some applications.

Applications are related to five principal functions of the heat pipe: separation of heat source and sink, temperature flattening, heat flux transformation, temperature control, and action as a thermal diode or switch. The two major applications, cooling of electronic components and heat exchange, can involve all of these features. In the case of electronic cooling and temperature control, all features

can be important. In heat exchangers employing heat pipes, the separation of heat source and sink and the action as a thermal diode or switch are most significant.

Optimal heat pipes are the ones that are briefly designed based on the following guideline

Heat Pipe Assembly Design Guidelines

Orientation with Respect to Gravity

For the best performance, the application should have gravity working with the system, that is, the evaporator section (heated) should be lower, with respect to gravity, than the condenser (cooling) section. In other orientations where gravity is not aiding the condensed liquid return, the overall performance will be degraded. Performance degradation depends on a number of factors including wick structure, length, and working fluid of the heat pipe along with heat flux of the application. Careful design can minimize the performance loss and allows an accurate prediction of performance.

Temperature Limits

Most pipes use water and methanol/alcohol as the working fluids. Depending on the wick structure, pipes will operate in environments with temperatures as low as -40°C . Upper temperature limits depend on the fluid, but $60\text{--}80^{\circ}\text{C}$ is the average limit.

Heat Removal

Heat can be removed from the condenser using air cooling in combination with conventional extrusion, bonded-fin heat sinks, or flat-fin stock. Enclosing the condenser in a cooling jacket allows liquid cooling.

Reliability

Heat pipes has no moving parts and has demonstrated life of over 20 years. The largest contributor to heat pipe reliability comes from the control of the manufacturing process. The seal of the pipe, purity of the materials used in the wick structure, and cleanliness of the internal chamber have measurable effect on the long-term performance of a heat pipe. Any leakage will eventually render the pipe inoperable. Contamination of the internal chamber and wick structure will contribute to the formation of non-condensable gas (NCG) that will degrade performance over time. Well-developed processes and rigorous testing are required to ensure reliable heat pipes.

Forming or Shaping

Heat pipes are easily bent or flattened to accommodate the needs of the heat sink design. Forming heat pipes may affect the power handling capability as the bends and flattening will cause a change in fluid movement inside the pipe. Therefore design rules that take into consideration heat pipe configurations and the effect on thermal performance ensure the desired solution performance.

(continued)

Effects of Length and Pipe Diameter

The vapor pressure differential between the condenser end and the evaporator end controls the rate at which the vapor travels from one end to the other. The diameter and length of the heat pipe also affect the speed at which the vapor moves and must be considered when designing with heat pipes. The larger the diameter, the more cross-sectional area available to allow vapor to move from the evaporator to the condenser. This allows for greater power carrying capacity. Conversely, the length when in opposition to gravity has a negative effect on heat transport as the rate at which the working fluid returns from the condenser end to the evaporator end is controlled by the capillary limit of the wick which is an inverse function of the length of the pipe. Therefore, shorter heat pipes carry more power than longer pipes when used in application not assisted by gravity.

Wick Structures

Heat pipe inner walls can be lined with a variety of wick structures. The four most common wicks are:

- (a) Groove
- (b) Wire mesh
- (c) Sintered powder metal
- (d) Fiber/spring

The wick structure provides a path for the liquid to travel from the condenser to the evaporator using capillary action. Wick structures have performance advantages and disadvantages depending on the desired characteristics of the heat sink design. Some structures have low capillary limits making them unsuitable for applications where they must work without gravity assist.

3.14 Design Examples

This example is directly reflected from Chi's book [5], and this author has decided to repeat this with permission to demonstrate the application of the above sections and some of the computer codes that are presented in this section is based on theories developed by Chi [5]. A numerical example is now given as follows.

Problem and Examples Design a $\frac{3}{4}$ -in. (0.0191 m) o.d. heat pipe with a wrapped-screen wick for transferring 100 Btu/h (29.3 W) of the heat at 400 °F (478 K). Space requires the heat pipe be 4 ft (1.22 m); log-half of it being the evaporator and the other half the condenser. Note that the heat pipe does not call for any adiabatic section at this point. In addition, the evaporator is required to be 3 in. (0.0762 m) above the condenser.

Solution We begin our design by selecting a fluid and a material. For a pipe operating at 400 °F (478 K), i.e., 860 R, water or methanol is a suitable working fluid (Fig. 3.5). Figures 3.6 and 3.7 indicate, however, that water has better liquid transport and conductance properties than methanol. Hence, water is chosen as the working fluid. Table 3.5 indicates that copper, nickel, and titanium are compatible materials for a water pipe, but Fig. 3.19 shows that copper has superior conductance characteristic at 860 R (478 K). In addition, there is a cost advantage in using copper. Copper is therefore selected as the material for the heat pipe container and wick.

From the above preliminary consideration, we have determined the use of a H₂O/Cu heat pipe. Figure 3.14 indicates that at Mach number equal to 0.2, the axial heat flux for a 3/4-in. (0.0191 m) water pipe is of the order of 10⁶ Btu/h (29.3 W), i.e., compressibility is no problem for this design at 100 Btu/h (29.3 W). The container tube dimension can now be determined in the following manner. At 860 R (478 K), the water vapor pressure is 250 psi (1.72 × 10⁶ N/m²) (see Figs. 3.12, 3.13, 3.14, and 3.15) and the copper ultimate tensile stress (UTS) is 18 kpsi (1.24 × 10⁸ N/m²) (see Appendix B). Figure 3.16 indicates that the required tube diameter ratio d_o/d_i may conservatively be 1.15. Table 3.4 indicates that a 3/4-in. (0.0191 m) o.d. tube with a wall thickness of 0.049 in. (1.2 × 10⁻³ m) (i.e., 18 Bwg) has a d_o/d_i ratio equal to 1.15 and a d_i equal to 0.652 in. (0.0166 m). This tube is then chosen as the heat pipe container. With P_v equal to 250 psi (1.72 × 10⁶ N/m²) and UTS equal to 18 kpsi (1.24 × 10⁸ N/m²), that end cap thickness-to-diameter ratio t/d_o , from Fig. 3.17, is equal to 0.08. Hence, the required end cap thickness is 0.06 in. (1.52 × 10⁻³ m). With the above-determined heat pipe container dimensions, the wick design can now proceed. The pipe has an elevation of inch (7.62 × 10⁻² m) (evaporator above), t its total length is 4 ft (1.22 m), and its d_i is 0.652 in. (1.66 × 10⁻² m). It is therefore required to overcome a hydrostatic height h_s of 0.304 ft (9.3 × 10⁻² m) as calculated by

$$h_s = 3 + 0.652 \left[\frac{48^2 - 3^2}{48^2} \right]^{1/2} = 3.647 \text{ in.} = 0.304 \text{ ft} (9.3 \times 10^{-2} \text{ m})$$

Since the hydrostatic pressure per foot of water at 860 R (478 K) is 56 lbf/ft² (2.68 × 10³ N/m²) (see Fig. 3.22), the pipe is required to overcome a hydrostatic pressure of 17 lbf/ft² (8.14 × 10² N/m²). Wire screen can now be chosen with the aid of Fig. 3.23c so that maximum capillary pressure will be about twice 17 lbf/ft² (8.14 × 10² N/m²). That is, a wire screen of 250 mesh (9.84 × 10³ m⁻¹) with P_{cm} equal to 32 lbf/ft² (1.53 × 10³ N/m²) is chosen. The required wick thickness can now be determined by Eqs. (2.7c) and (2.76), i.e.,

$$(QL)_{\text{Capillary}_{\text{max}}} = \frac{P_{\text{cm}} - \Delta P_{\perp} - \rho_1 g L_t \sin \psi}{F_1 + F_v}$$

The value of $(P_{cm} - \Delta P_{\perp} - \rho_1 g L_t \sin \psi)$ for the present case is 15 lbf/ft² ($7.18 \times 10^2 \text{ N/m}^2$), i.e., 32 lbf/ft² ($1.53 \times 10^3 \text{ N/m}^2$) minus 17 lbf/ft² ($8.14 \times 10^2 \text{ N/m}^2$). The value of F_v for water at $d_v = 0.5 \text{ in.}$ ($1.27 \times 10^{-2} \text{ m}$) and $T_v = 860\text{R}$ (478 K) is equal to $4 \times 10^{-6} (\text{lbf/ft}^2)/(\text{Btu/h}) [2.2 \times 10^{-3} (\text{N/m}^2)/\text{W m}]$ from Fig. 3.41. The value of $F_1 A_w$ at $N = 250 \text{ in.}^{-1}$ ($9.84 \times 10^3 \text{ m}^{-1}$) and $T_v = 860\text{R}$ (478 K) is equal to $4.6 \times 10^{-5} \text{ lbf}/(\text{Btu ft/h})$ ($2.29 \times 10^{-3} \text{ N/W m}$). Assuming d_v is equal to 0.5 in. ($1.27 \times 10^{-2} \text{ m}$), we obtain A_w equal to $9.55 \times 10^{-4} \text{ ft}$ ($8.87 \times 10^{-5} \text{ m}^2$). Then $F_1 = F_1 A_w / A_w$ is equal to 0.0482 (lbf/ft²)/ (Btu ft/h) [$25.9 (\text{N/m}^2)/\text{W m}$]. Substituting the above values of $(P_{cm} - \Delta P_{\perp} - \rho_1 g L_t \sin \psi)$, F_v and F_1 into the above mentioned equation yields $(QL)_{\text{Capillary,max}}$ equal to 311 Btu ft/h (27.8 W m). The required (QL) for the design under consideration is equal to 200 Btu ft/h (17.9 W m), i.e.

$$(QL) = 0.5(L_e + L_c)Q = 200 \text{ Btu ft/h} (17.9 \text{ W m})$$

Hence, the assumed d_v of 0.5 in. ($1.27 \times 10^{-2} \text{ m}$) is appropriate for the design under consideration. In summary, we have designed a heat pipe with the following specification:

Work fluid	H ₂ O
Container material	Copper
Wick material	Copper
Container o.d.	0.75 in. ($1.91 \times 10^{-2} \text{ m}$)
Container i.d.	0.652 in. ($1.66 \times 10^{-2} \text{ m}$)
Vapor core diameter	0.5 in. ($1.27 \times 10^{-2} \text{ m}$)
End cap thickness	0.060 in. ($1.52 \times 10^{-3} \text{ m}$)
Wire-screen mesh number	250 in ⁻¹ ($9.84 \times 10^3 \text{ m}^{-1}$)
Wire-screen wire diameter	0.0016 in. ($4.06 \times 10^{-5} \text{ m}$)
Screen wick thickness	0.076 in. ($1.93 \times 10^{-3} \text{ m}$) (24 layers)

In order to check the entrainment and boiling limits of the pipe, we read from Figs. 3.23 and 3.27 that the limits are equal to $2.5 \times 10^5 \text{ Btu/h}$ ($1.13 \times 10^8 \text{ W}$) per in.² (m²) of vapor core cross-sectional area and 210 Btu/h (202 W) per ft (m) of evaporator length, respectively. That is $Q_{e,\text{max}}$ and $Q_{b,\text{max}}$ for the specified pipe are $4.91 \times 10^4 \text{ Btu/h}$ ($1.44 \times 10^4 \text{ W}$) and 420 Btu/h (123 W), respectively. Both of these limits exceed the required heat transport of 100 Btu/h (29.3 W). Hence, the above designed pipe will operate satisfactory at 100 Btu/h (29.3 W) at 400 F (478 K).

3.15 Computer Codes for Designing Heat Pipes

A number of heat pipe computer programs have been written over the past 20 years. These codes are listed below in Table 3.6 along with investigator and other relevant information and availability of each code in the market. Also each code has been defined in different sections of this chapter under their own name to describe its capability and functionality. Most of these codes that are available are used to predict the hydrodynamic behavior or maximum transport capability as function of the specified wick and fluid properties. In most cases, the code is limited to a specific wick type such as GAP (Groove Analysis Program) [49, 50] computer code which was developed for axially grooved geometries.

HPAD [51] and MULTIWICK [52] are relatively versatile in that they consider a number of different wick designs. None of these codes as presently developed are able to predict heat pipe performance with a gravity assist as would be the case in many commercial applications.

GASPIPE 2 [53] and VCHPA are both applicable to the design and analysis of gas-controlled variable conductance heat pipes. GASPIPE 2 is more extensive and incorporates both axial conduction and mass diffusion. Either active or passive control with hot or cold reservoir can be handled with GASPIPE 2. In addition to these codes, a number of subroutines have been developed for use in conjunction with existing thermal programs to define steady-state and in some cases transient heat pipe behavior.

ANLHTP [43] is a computer code for the simulation of heat pipe operation which is developed by Argonne National Laboratory. The code predicts heat pipe performance and temperature distribution during steady-state operation of heat pipe but not the transient aspect of it.

The NASA Lewis Steady State Heat Pipe Code [39] has been developed by the Lewis Research Center to predict the performance of heat pipes in the steady state for a variety of wick structures, including a user input option, which can be used.

Chi [2] has also developed few codes around cryogenic, low- and high-temperature heat pipe under normal heat pipe operation. The first code under *Mathematical Modeling of Cryogenic Heat Pipes* [2] for NASA which is investigating performance of heat pipes using different working fluids where he observed significance of liquid property variation on the performance of cryogenic heat pipe.

Under *Mathematical Modeling of High and Low Temperature Heat Pipe* [1] of Chi report, he analyzed a heat and mass transfer theory relevant to heat pipe performance; then he wrote two codes for mathematic models for calculating heat transfer limitations of high-temperature heat pipes and heat transfer limitations and temperature gradient of low-temperature heat pipes.

HTPIPE, a steady-state heat pipe analysis program [54], operational on CRAY computers, is originally documented by Keith A. Woloshun, Michael A. Merrigan, and Elaine D. Best. The manual and code recently were modified by Galaxy Advanced Engineering adding UGL graphic capabilities to produce plots needed to depict the result of the analysis. HTPIPE has two input/output (I/O) options:

(1) pressure and temperature profiles along the heat pipe and (2) calculation of performance limits. Pressure and temperature profiles are calculated based on user-specified boundary conditions, which may be any two of the following: (1) power throughput, (2) evaporator exit temperature, (3) source temperature, and (4) sink temperature. The performance limits represent the maximum heat transport limits at a specified evaporator exit temperature. The calculated performance limits are the capillary, viscous, sonic, entrainment, and boiling limits.

User input is interactive, with the available option of parametric variation during a single program execution to facilitate heat pipe design optimization. The hydrodynamic model is described. Program I/O is detailed and supplemented with examples. A program listing and a flowchart are included in this manual. HTPPIPE is consistent with the theories and correlations used for heat pipe design originally at Los Alamos National Laboratory to date.

Recently, Kamotani [55] completed a thermal analysis program for axially grooved heat pipes (HTGAP). This program can be used to predict both evaporator and condenser film coefficients for a specified groove geometry and heat pipe operating condition.

This is the first code to consider in detail two-phase heat transfer coefficients for a given heat pipe wick geometry. In addition, the program predicts various heat transfer aspects of axially grooved heat pipes

3.15.1 SINDA/FLUINT Computer Codes for Loop Heat Pipe Analysis

Under a NASA contract, Martin Marietta Corporation developed an advanced SINDA thermal analysis computer program in 1983. The final version of the code was SINDA 85. This version of SINDA has been improved by a series of enhancements that included the fluid flow network capability known as the fluid integrator (FLUINT). The combined new computer code SINDA/FLUINT has both thermal and fluid network capabilities. It can perform the pressure/flow analysis of a system containing an arbitrary tube network simultaneously with the thermal analysis of the entire system size being cooled, permitting the mutual influences of thermal and fluid problems to be included in the analysis. Companion codes Thermal Desktop and FloCAD provide a graphical user interface for building one-dimensional flow models within a 3-D thermal model.

FLUINT is intended to provide a general analysis framework for internal one-dimensional fluid systems. The computer code can be applied to any arbitrary fluid system; it is not restricted to specific geometries or configurations. Users can select from 20 refrigerants that are immediately available as working fluids, or they can specify their own fluid properties for any specific applications. The code can handle both single- and two-phase flow as well as transitions between these states. FLUINT also includes some common fluid system components (pumps, valves, and

ducts). Inputs are parameterized within spreadsheet-like variables, allowing complex models to be rapidly manipulated, and routines are available for automated model correlation to test data.

Systems Improved Numerical Differencing Analyzer/Fluid Integrator, formerly SINDA '85, (SINDA/FLUINT) is a computer code used to analyze thermal/fluid systems that can be represented in finite difference or lumped parameter form. In addition to conduction and radiation heat transfer, the code is capable of modeling steady or unsteady single- and two-phase flow networks, their associated hardware, and their heat transfer processes. Because it is generalized, versatile, and user extensible, SINDA/FLUINT is a standard in the aerospace industry for modeling thermal control systems. It is also used in the automotive, commercial aircraft, electronic packaging, petrochemical, and process industries.

SINAPS (SINDA Application Programming System) is a complete graphical user interface to SINDA/FLUINT. SINAPS is a schematic-oriented pre- and postprocessor that brings modern visualization methods to a simulation code that lacks geometric constraints. Together, these unique tools are able to accommodate higher-order (perhaps vehicle-level) modeling, indefinite or parametric geometries, and other problems inappropriate for geometry-based CAD (computer-aided design), FEM (finite element method), and CFD (computational fluid dynamics) codes.

Solving Problems with SINDA/FLUINT

A software system utilized by NASA generated a wealth of commercialization and expansion opportunities for Cullimore & Ring Technologies (C&R), Inc., of Littleton, Colorado. SINDA/FLUINT, the NASA standard software system for thermo-hydraulic analysis, provides computational simulation of interacting thermal and fluid effects in designs modeled as heat transfer and fluid flow networks. It is used to design and analyze aerospace systems, such as thermal control and propulsion.

SINDA/FLUINT is an integral combination of two subprograms. The Systems Improved Numerical Differencing Analyzer (SINDA) program is a software system for solving lumped parameter, finite difference, and finite element representations of physical problems governed by diffusion-type equations. The Fluid Integrator (FLUINT) program is an advanced, one-dimensional fluid analysis program that solves equations of arbitrary fluid flow networks. Working fluids that can be modeled in SINDA/FLUINT include single-phase gases and liquids, two-phase fluids, and mixtures of substances.

The system's code was written for NASA's Johnson Space Center by the founders of C&R while they worked at Martin Marietta (now Lockheed Martin Corporation). The technology won the NASA Space Act Award in 1991. Since Johnson could not indefinitely support the code by making necessary upgrades and software expansions, C&R was formed to take over SINDA/FLUINT, supporting NASA's use of the software. After obtaining a license from NASA and receiving Martin Marietta's consent, C&R began marketing SINDA/FLUINT as a commercial product applicable to diverse industries (Fig. 3.74).

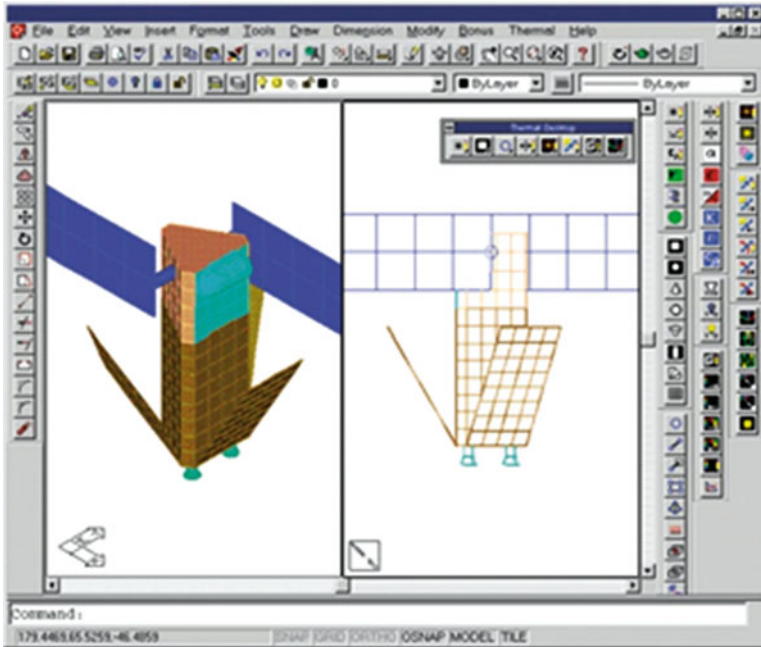


Fig. 3.74 This Thermal Desktop[®] sample screen shows a satellite model in two independent viewports. The *right side* of the picture contains icons of the commonly used thermal desktop commands

The program saves time and money by making the user's design process faster and easier and allowing the user to gain a better understanding of complex systems. The code is completely extensible, allowing the user to choose the features, accuracy and approximation levels, and outputs. Users can also add their own customizations as needed to handle unique design tasks or to automate repetitive tasks. C&R received multiple **Small Business Innovation Research (SBIR)** awards from Johnson to expand the system, which helped to make it the most flexible and powerful thermo-hydraulic analyzer currently available. To further enhance SINDA/FLUINT, C&R completed the development of SinapsPlus[®], which also originated from the founders of C&R while at Martin Marietta. SinapsPlus, a sketchpad graphical user interface (GUI), provides a visual means of accessing the solution power of SINDA/FLUINT, making the system more approachable.

C&R also created a geometric graphical user interface (GUI) to work with SINDA/FLUINT, known as Thermal Desktop[®]. An optional computer-aided design (CAD) module of Thermal Desktop, RadCAD[®], calculates radiation exchange factors for input to SINDA/FLUINT. Together, these two codes, which began as SBIR projects at NASA's Marshall Space Flight Center, solved a long-standing concurrent engineering problem. Thermal Desktop is the first tool that enables concurrent engineering for thermal analysts by providing full access to

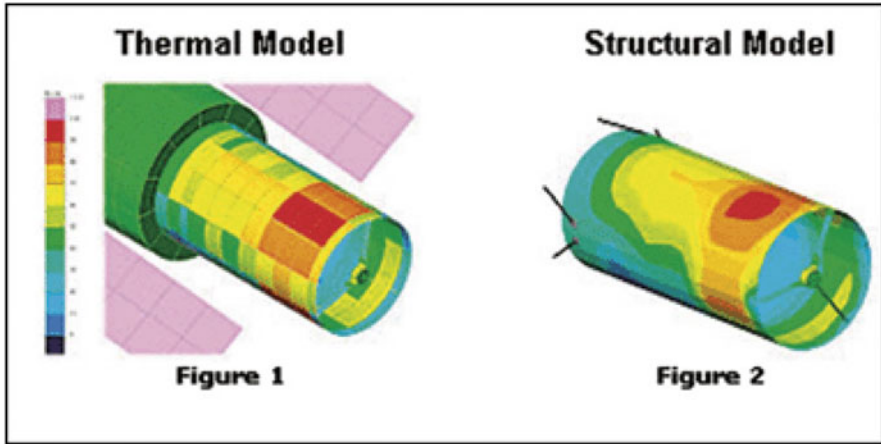


Fig. 3.75 A long-standing concurrent engineering problem was solved by the integration of SINDA/FLUINT within C&R's Thermal Desktop[®]. Thermal engineers can work side by side with structural engineers and CAD designers for the first time, greatly enhancing both productivity and analysis accuracy

CAD-based geometry, as well as data exchange to and from structural codes without compromising traditional thermal modeling practices. Eliminating productivity bottlenecks, these two products benefit the aerospace and electronic packaging communities.

According to C&R, the funds generated from the success of the NASA-initiated products supported the development of the company's FloCAD[®] product, a geometric GUI for fluid network modeling (the FLUINT side of SINDA/FLUINT). This GUI provides fast, inexpensive, parametric modeling capabilities for air-, liquid-, or two-phase-cooled electronics. It also facilitates the analysis of heat pipes.

With over 4000 users in 30 countries, applications for SINDA/FLUINT include the pharmaceutical, petrochemical, biomedical, electronics, and energy industries. The system has simulated nuclear reactors, windshield wipers, and human windpipes. SINDA/FLUINT simulates the transient liquid-vapor flows within air-conditioning systems, helping the automotive industry to meet standards for fuel efficient, low-emission cars. The system was the basis of General Motor's E-Thermal vehicle-level thermal management software, which is being deployed globally (Fig. 3.75).

3.15.1.1 Heat Pipe Modeling and Two-Phase Loops Using SINDA/FLUINT

C&R Corporation has provided certain processes along with their suggested computer code SINDA/FLUINT for designing the loop heat pipe (LHP), capillary pumped loop (CPL) as well as loop thermosyphons (LTSs). C&R tools are routinely

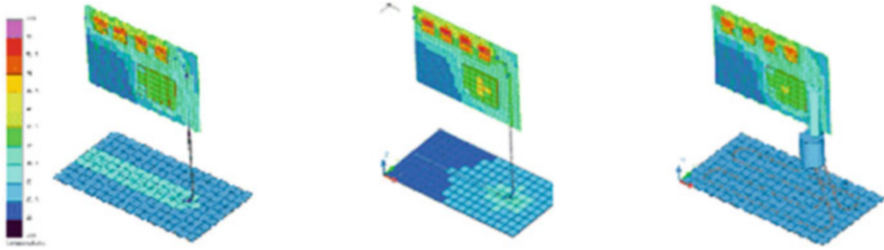


Fig. 3.76 SINDA/FLUINT computer run (Courtesy of C&R Corporation). (a) Constant conductance heat pipe. (b) Gas blocked heat pipe. (c) Loop heat pipe

used to model the complexities of two-phase transport devices such as loop heat pipes (LHPs), capillary pumped loops (CPLs), heat pipes, vapor chamber fins, thermosyphons, and loop thermosyphons (LTSs). **SINDA/FLUINT** has been enhanced over the past 15 years specifically to handle the modeling of these complex devices. The code has been used for a variety of modeling tasks from capturing steady-state system level effects of two-phase devices to simulating detailed startup transients for component design and sizing. **SINDA/FLUINT** is unique in its ability to co-solve integrated thermal and fluid systems while providing the complete thermodynamics of two-phase flow necessary to model these devices accurately.

The early version of the code was developed by NASA, Johnson Space Center, and version of 2.6 is available for a run on **SINDA/FLUINT/Windows/PC** machine from Galaxy Advanced Engineering, Inc., which is a direct port of NASA version to Window operating system (Fig. 3.76).

3.15.1.2 Two-Phase Capabilities

The two-phase flow capability built into the code in **FLUINT** aspect of the code as the flow analyzer in **SINDA/FLUINT**, was designed right from the start to handle the peculiarities of two-phase flows. In fact, its development was initiated specifically to avoid the shortcomings of single-phase analyzers that had been retrofitted to adapt to two-phase problems.

Combined with the heat transfer capabilities of **SINDA**, the sketchpad interface of **Sinaps**[®], the CAD-based interface of **FloCAD**[®] (a module of **Thermal Desktop**[®]), and the unique capabilities such as parametric analyses, optimization, calibration, and statistical design, **SINDA/FLUINT** is truly in a class by itself.

The most comprehensive two-phase thermo-hydraulic analyzer available from C&R Corporation based on their version of **SINDA/FLUINT** computer code with its following capabilities:

Fig. 3.77 Flow regime mapping (Courtesy of C&R Corporation)

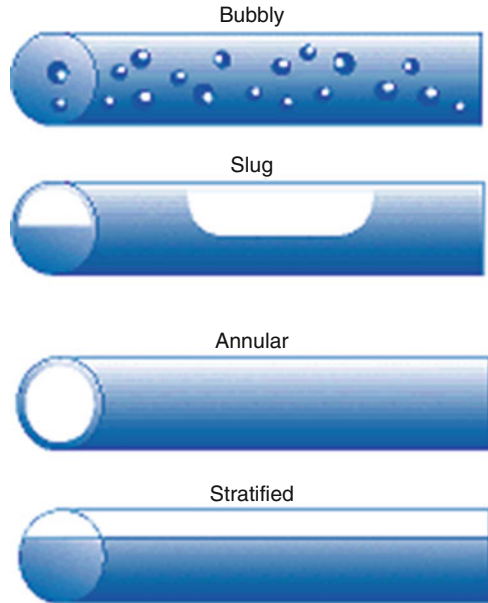
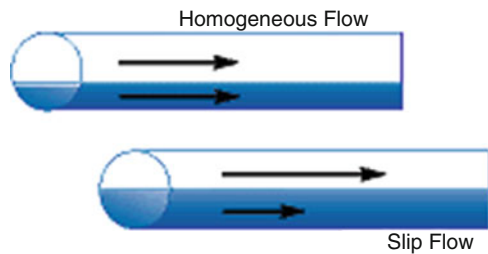


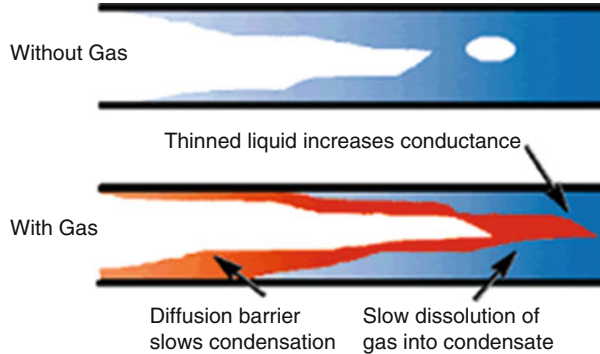
Fig. 3.78 Slip flow, nonequilibrium flow, mixtures, dissolution. (Courtesy of C&R Corporation)



Two-Phase Mixture Capabilities

- Complete thermodynamics: phases appear and disappear as conditions warrant.
- Two-phase heat transfer correlations built-in or user defined
- Two-phase pressure drop correlations built-in or user defined (Fig. 3.77).
- From quasi-steady homogeneous equilibrium to fully transient two-fluid modeling.
- Optional slip flow modeling (separate phasic momentum equations) (Fig. 3.78).
- Optional non-equilibrium transients (separate phasic energy and mass equations).
- Capillary modeling tools for static or vaporizing wicks.
- Optional tracking of liquid–vapor interfaces.
- Mixtures of up to 26 liquids and/or gases.
- Optional condensable/volatile component in mixture, including effects such as diffusion-limited condensation
- Optional dissolution of any number of gaseous solutes into any number of liquid solvents, including homogeneous nucleation models (Fig. 3.79)

Fig. 3.79 Complex phenomena example: condensing in the presence of non-condensable gases (Courtesy of C&R Corporation)



3.15.1.3 How Not to Model a Heat Pipe

Heat pipe routines built into SINDA/FLUINT provide fast system level solutions to modeling heat pipes when a full two-phase solution is not required. Both constant conductance (CCHP, also called FCHP), with or without non-condensable gas (NCG), and variable conductance (VCHP) pipes can easily be simulated. Unlike other non-C&R heat pipe routines, this routine was written specifically to co-solve wall temperatures and gas front locations, resulting in a more robust tool.

3.15.1.4 How to Model a Heat Pipe

A common “trick” is to model a heat pipe as a bar of highly conductive material. However, that method does not simulate a heat pipe’s length-independent resistance, cannot account for differences in film coefficients between vaporization and condensation, and cannot be extended to include NCG effects. Another misconception is that heat pipes, being two-phase capillary devices, require detailed two-phase thermo-hydraulic solutions. While codes capable of such details exist, such as C&R’s SINDA/FLUINT, such an approach would represent computational overkill in almost all cases: even heat pipe vendors use simpler calculations when designing heat pipes.

FloCAD[®], a Thermal Desktop[®] module, provides a unique tool for modeling heat pipes within a CAD-based environment. Complex geometries, such as serpentine condensers or large networks of heat pipes, can easily be generated (Fig. 3.80).

3.15.1.5 SINDA/FLUINT Code Availability

SINDA/FLUINT—This is a finite-differencing thermal and fluid network analyzer. Originating in the 1960s as CINDA (Chrysler Improved Numerical Differencing Analyzer), subsequently improved and released as SINDA/SINFLO in the 1970s, and then transformed into SINDA/FLUINT in the mid 1980s, this

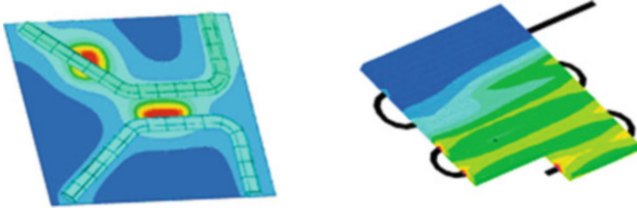


Fig. 3.80 A computer run result of SINDA/FLUINT. (Courtesy of C&R Corporation). (a) Flat heat pipe for electronics cooling. (b) Two-phase condenser

workhorse code has been evolving for more than 30 years. The current version includes a complete library of fluid flow routines. It is used at GSFC for modeling complex spacecraft thermal control systems, including those which incorporate single- and two-phase fluid loops and capillary devices. Johnson Space Center (JSC) funded the development of SINDA/FLUINT and has made it available to private industry through the National Technology Transfer Center. This code has been ported to the thermal engineering branch's computer platforms (HP-UX and MS Windows 95/98/NT). An enhanced version of SINDA/FLUINT is also available as a commercial product from C&R Technologies

The SINDA/FLUINT 85 source code and executable version of this code is available from NASA Johnson Space Center in Houston Texas as well as version 4.1 that requires a NASA contract for the users to obtain the code. The 85 version of the code also is available from Galaxy Advanced Engineering, Inc through www.GAEINC.COM web site.

3.15.2 LERCHP NASA Glenn Steady-State Heat Pipe Code

The NASA Lewis Research Center Heat Pipe (**LERCHP**) [41] code was developed by Tower et al. [39] to predict the performance of heat pipes in the steady state. Version 1 was released in 1992 and with a revision as Version 2 in 2000. A further extension of Version 2, not reported [42], available as code, is discussed below. LERCHP can be used as a design tool on a personal computer or, with a suitable calling routine, as a subroutine for a mainframe radiator code. Both versions and updates have the following features.

3.15.2.1 Features Common to All Code Versions

A large selection of working fluids is available, spanning the temperature range from ammonia at the bottom to alkali metals including potassium, sodium, and lithium, for which the monomer-dimer equilibrium is considered. Many materials

of construction, among which several are commercially available as tubing, are also included. Heat pipes can be in gravitational fields with inclination with respect to the field given, but refluxing pipes (thermosyphons) are not considered.

A vapor flow algorithm is employed that considers compressibility and axially varying heat input. This was derived by Tower and Hailey [41] from expressions presented by Busse [40] for incompressible flow. The possible sub-cooling of the expanding vapor core relative to the vapor saturation condition at the evaporator liquid–vapor interface is considered. Laminar vapor flow is assumed for the evaporator and adiabatic sections, with transition to turbulence in the condenser as a preferred option.

Heat pipes with multiple evaporators, condensers, and adiabatic sections in series and with wick structures that differ among sections can be modeled by **LERCHP**. The heat pipe can be subdivided into as many as 20 sections, far more than will normally be required. These sections can be heat input or evaporator sections, adiabatic sections, and heat removal or condenser sections, mixed in any manner provided that the first section is a heat input section. The nature of any section is indicated by the type of boundary condition data that is entered for that section. A variety of wick structures are available to the user, including a user wick input option. **LERCHP** facilitates the determination of heat pipe operating temperatures and heat pipe limits that may be encountered at the specified heat input and environment temperature.

Data input is by means of an interactive subroutine that queries the user concerning the options to be employed in the case to be run. For each section, the required data can be entered as single values pertaining to the entire section. Values of the input parameters can also be entered at as many as 20 points spaced along the section, with a different magnitude at each point, interpolated by spline fit. Computations along the pipe are made by a Runge–Kutta routine for which the initial step size is chosen, with automatic reduction or increase as the slope of the principal dependent variable, pressure, exceeds or falls below certain bounds.

Output of principal variables such as liquid and vapor pressures and temperatures can be printed at equally spaced axial positions along the pipe as determined by the user. **LERCHP** allows the user to select the number of uniformly spaced points along the pipe axis at which the principal variables will be printed out. The spacing of these points need not correspond with the step size chosen for the Runge–Kutta solution. A printout is furnished after thermal convergence of the solution has been obtained. When a heat pipe limit is encountered during calculation of the solution but does not cause the calculation to halt, the type of limit is printed out with the solution. Output can be directed to a plotting device if a suitable plotting utility is available and the necessary changes are made in the source code.

3.15.2.2 Thermal Boundary Condition Specifications

The thermal boundary condition specifications available are as follows:

1. Specified heat input or removal rate at the pipe exterior surface (Versions 1 and 2).
2. Specified environment temperature external to the pipe sections, including radiation or convection to the evaporator, with heat transfer properties of the pipe surface to the environment provided by the user (Versions 1 and 2).
3. Uniform and fixed evaporator surface temperature, as from a clamped block (Version 2).

3.15.2.3 Individual Features of Versions

Version 1 pipes are assumed to be cylindrical and to have cylindrical vapor space. Pipes are straight.

Version 2 pipes can be straight or have gentle bends specified within gravitational or “g” fields.

In code extending Version 2, some further features are added. In particular, noncircular cross sections can be handled by using the hydraulic radius approach. In pipe sections containing arteries, the artery presence is indicated by specifying the extent of lost vapor area and additional wetted perimeter. The code has been modified to enable the proper input for these features.

Heat pipes with multiple evaporators, condensers, and adiabatic sections in series and with wick structures that differ among sections can be modeled by **LERCHP**. The heat pipe can be subdivided into as many as 20 sections, far more than will normally be required. These sections can be heat input or evaporator sections, adiabatic sections, and heat removal or condenser sections, mixed in any manner provided that the first section is a heat input section.

3.15.2.4 LERCHP Computer Code Availability

Version 1.0 of this code is available from two sources that are identified below:

1. Open Channel Foundation or <http://www.openchannelsoftware.com> where one can purchase the source code without any manual available at their site to request. In this case, the user needs to compile their source for their desired operation system and computing platform.
2. Galaxy Advanced Engineering or <http://www.gaeinc.com> where one can purchase the source code as well as the manual written for the code. The version from this company will run on Windows/PC.

Version 2.0 of this code is available from

1. Galaxy Advanced Engineering or <http://www.gaeinc.com> where one can purchase the source code as well as the manual written for the code. The version from this company will run on Windows/PC.

Version 3.0 of this code and extended version of 2.0 both are available from

1. Galaxy Advanced Engineering or <http://www.gaeinc.com> where one can purchase the source code as well as the manual written for the code. The version from this company will run on Windows/PC

Note: Both versions of user's manuals might be available from NASA TECHNICAL REPORTS SERVER (NTRS) or <http://naca.larc.nasa.gov/search.jsp> which is downloadable in PDF format.

3.15.3 Los Alamos (HTPIP) Steady-State Heat Pipe Analysis Program Codes

A steady-state heat pipe analysis program, HTPIPE [54], written at Los Alamos National Laboratory around November 1988, operational originally on CRAY and now presently on Windows/PC computers, is documented. HTPIPE has two Input/Output (I/O) options:

1. Pressure and temperature profiles along the heat pipe
2. Calculation of performance limits

Pressure and temperature profiles are calculated based on user-specified boundary conditions, which may be any two of the following:

1. Power throughput
2. Evaporator exit temperature
3. Source temperature
4. Sink temperature

The performance limits represent the maximum heat transport limits at a specified evaporator exit temperature. The calculated performance limits are the capillary, viscous, sonic, entrainment, and boiling limits. User input is interactive, with the available option of parametric variation during a single program execution to facilitate heat pipe design optimization. The hydrodynamic model is described. Program I/O is detailed and supplemented with examples.

A program listing and a flowchart are included in this manual. HTPIPE is consistent with the theories and correlations used for heat pipe design at Los Alamos National Laboratory to date.

3.15.3.1 HTPIPE Computer Code Availability

The original version of computer code utilizing a graphics library known as CA-DISSPLA is no longer available in the market, and without it the graphics output capability of the code is not going to function. There are two versions of the code that are available on Windows/PC. One is from the Galaxy Advanced

Engineering that has ported the CRAY version of the code to Windows/PC and has developed CA-DISSPLA functionality known as Universal Graphics Library (UGL) to make the code to run like its original version written at Los Alamos.

To obtain this code for Windows/PC with its graphics capabilities, go to the following site:

1. Galaxy Advanced Engineering or <http://www.gaeinc.com> where one can purchase the source code as well as the manual written for the code. The version from this company will run on Windows/PC plus UGL functionality.

Note: User's manuals might be available from NTIS National Technical Information Service or <http://www.ntis.gov> to purchase. The manual has the list of computer codes for CRAY, and one can use the manual labor and time to type the code from it. The listing of the code is of very poor quality, and it is labor-intensive to write the entire code into a source that is compilable without any mistake.

3.15.4 ANLHTP: A Computer Code for the Simulation of Heat Pipe Operation

ANLHTP [43] is a computer code for the simulation of heat pipe operation and transport system that has been developed at Argonne National Laboratory around 1983 by McLennan [43]. Argonne National Laboratory Heat Pipe (**ANLHTP**) is designed to predict heat pipe performance and temperature distributions during steady-state operation. Source and sink temperatures and heat transfer coefficients can be set as input boundary conditions and varied for parametric studies. Five code options are included to calculate performance for fixed operating conditions or to vary any one of the four boundary conditions to determine the heat pipe limited performance. The performance limits included are viscous, sonic, entrainment, capillary and boiling, using the best available theories to model these effects.

The code has built-in models for a number of wick configurations—open grooves, screen-covered grooves, screen-wrap, and arteries, with provision for expansion. The current version of the code includes the thermophysical properties of sodium as the working fluid in an expandable subroutine. The code-calculated performance agrees quite well with measured experiment data. Of particular interest are the effects of the heat transfer coefficients coupling the heat pipe to the source and power system, as well as the ability of a given heat pipe to operate under different load conditions and to move from one load state to another. The code was developed based on theory, analysis, and experimental data obtained from a review of the available literatures. The models used for the heat pipe are those generally accepted by other researchers and follow very closely those presented by Chi [5] and Dunn and Reay [4]. Where different theoretical models were available, the selection was based on consistency with other aspects of the code. The code was developed to be general, as opposed to specific for a particular heat pipe design.

All the thermophysical properties of the working fluid are provided in a separate subroutine, which can be expanded easily to add additional fluids.

A new version of code internally was developed at Galaxy Advanced Engineering now known as ANLYZIP which analyzes heat pipe new functionalities that are implemented into the new version. The ANLYZHP code is an upgraded version of the Argonne Code ANL/HTP written by G. A. McLennan [43]. The code has been expanded to consider many more fluids including several cryogenic materials and additional heat pipe materials. It analyzes a given heat pipe design and computes the heat transfer boundaries for the various limiting modes of operation. All input is controlled through a NAMELIST block so that multiple variations of a design can be analyzed very efficiently. It also writes a graphics file that can be plotted with the UGLI[®] package to give a graphical interpretation of the various operating regimes

Note: UGLI[®] is Galaxy Advanced Engineering, Inc. product that can run on any computing platform independent of its Operating System.

3.15.4.1 ANLHP Computer Code Availability

The code is not very friendly using it on Windows/PC and requires major modification to be able to make it to run on Linux or Windows/PC. Code is using the old fashion way of reading the input deck utilizing NAMELIST functionality of FORTRAN IV and requires careful handling by someone who wants to make it to work on Linux or PC. The input deck which is provided in the user's manual is not very clear and complete what the author of the code had in his mind and causes the code not execute properly unless certain care has been taken by users who want to type the code from the listing which is provided in the user's manual. A modified version of the code is available from the following source that works properly after many hours of effort that was put into its modified version to make it to run properly;

1. Galaxy Advanced Engineering or <http://www.gaeinc.com> where one can purchase the source code as well as the manual written for the code. The version from this company will run on Windows/PC plus UGL functionality.

Note: User's manuals might be available from NTIS National Technical Information Service to purchase. The manual has the list of original computer code for IBM 360, and one can use the manual labor and time to type the code from it. The listing of the code is of very poor quality, and it is labor-intensive to write the entire code into a source that is compilable without any mistake. There is no guarantee that if one uses the listing from the manual, the code will run on first attempt unless some modification can be done to the original list of source from the user's manual.

3.15.5 *Heat Pipe Fluid (HPF) Properties Program*

The HPF [51] code is used to generate the fluid property data and derives parameter for working fluids which have used extensively in both aerospace and terrestrial applications. The code was written by Brennan and Kroliczek [38] from B & K Engineering, Incorporation under NASA contract. In the report that is produced for this code as user's manual part II, the data for a total of 30 fluids is tabulated. The following invariable properties are listed for each of these fluids in both International System (SI) and in British Engineering (BE) Units . The fluids are listed in the order of their ascending melting points and are divided into three groups on their operating temperature range.

The three groups have been defined as follows and Table 6.3 also presented from same Ref. [38].

Group 1—Cryogenic and low-temperature range, 0–350 K

Group 2—Ambient and intermediate temperature range, 200–600 K

GROUP 3—High-temperature range, 600–3000 K

Most aerospace applications to date have required the use of cryogenic, low-temperature, and ambient working fluids with ammonia being used most extensively.

The heat pipe fluid (HPF) property program which is used to tabulate the thermodynamical properties of various heat pipe working fluids at saturation conditions, derives properties such as the liquid transport factor, wicking height factor, etc. which are also calculated and tabulated by the program. The code is using a least square curve fit to determine the coefficients of the polynomial which best fits the specified physical properties. The polynomials are then used to generate fluid property data versus temperature. The coefficients of the least square polynomial for each set of physical properties are also generated as well as the standard deviation and the percentage of error between the input values and the calculated values. This error analysis is performed for both physical and derived properties.

3.15.5.1 *Heat Pipe Fluid (HPF) Properties Program Availability*

The user's manual of this code both part I and II are available from the following site:

1. User's manuals might be available from <http://www.ntis.gov> to purchase or possibly download the PDF version of it for free.

PART II has the listing of the code which is again labor-intensive to type the list of FORTRAN code for your own compiler to compile and make an executable code out of the source.

The proven and quality-assured version of this is available from the following site:

2. Galaxy Advanced Engineering or <http://www.gaeinc.com> where one can purchase the source code as well as the manual written for the code.

3.15.6 Groove Analysis Program (GAP) Computer Program

Groove Analysis Program (GAP) [50] computer program describes the utilization of the IBM Personal Computer (PC) version of the Groove Analysis Program (GAP) computer program, Version 1.0. This version is an upgrade of the model described in Ref. [6]. In the old code, the liquid friction pressure drop was slightly underestimated and is corrected in this PC version. The present PC code has been intended to be interactive and user friendly and can be run with most of today's IBM PC or compatible models. Other special features of the code include:

- Multiple runs for various heat pipe elevations and over a wide range of temperature values are readily achieved.
- Fluid properties are determined directly by the code. A comprehensive database that contains the properties of 24 heat pipe working fluids is included with the code.
- For pressure containment, the minimum required heat pipe wall thickness can be determined for specified factors of safety.
- At the user's discretion, the desired output data is written to a plot file which can be imported to most spreadsheet or graphic software programs for fast quality plotting.

The code is designed to predict the steady-state heat transport capability of an axially grooved heat pipe for a specified groove geometry and working fluid. The "capillary limit" is determined by the numerical solution of the differential equation for momentum conservation with the appropriate boundary conditions.

This governing equation accounts for the hydrodynamic losses due to friction in liquid and vapor flows and due to liquid-vapor shear interaction. Back-pumping in both 0 g and 1 g is accounted for the boundary condition at the condenser end. Slug formations in 0 g and puddle flow in 1 g are also considered in the model. At the user's option, the code will perform the analysis for various fluid inventories (undercharge, nominal charge, overcharge, or a fixed fluid charge) and heat pipe elevations. GAP 1.0 will also calculate the minimum required heat pipe wall thickness for pressure containment at design temperatures that are greater than or lower than the critical temperature of the working fluid.

3.15.6.1 Groove Analysis Program (GAP) Computer Program Availability

Unfortunately the source code is not available for this program neither from NASA or OAO Corporation that originally was responsible to develop this code. There is an executable version of this code available from the following sites to purchase:

1. <http://www.openchannelsoftware.com/projects/GAP/> where one can purchase the executable version of the code that runs under DOS or any Windows/PC except window 7 that will run under DOS mode.
2. Galaxy Advanced Engineering or <http://www.gaeinc.com> where one can purchase the executable version of the code that runs under DOS or any Windows/PC except window 7 that will run under DOS mode.

3.15.7 GASPIPE 2 Computer

The GASPIPE 2 [53] is for a vapor–gas front analysis program for heat pipe containing non-condensable gas and is developed by TRW under a NASA contract NAS2-5503 by Edwards, Fleischman, and Marcus. This computer program is useful in the design and analysis of heat pipes which contain non-condensable gases, either for temperature control or to aid in start-up from the frozen state. Because the program includes the effects of axial conduction and mass diffusion on the performance of such heat pipes, represents a significant advance in steady-state design technology over the “flat front” theory previously found in the Refs. [56, 57]. It allows one to:

- Calculate the wall temperature profile along a gas-loaded heat pipe.
- Calculate the amount of gas loading necessary to obtain a desired evaporator temperature at a desired heat load.
- Calculate the heat load versus the evaporator temperature for a fixed amount of gas in the pipe.
- Calculate the heat and mass transfer along the pipe, including the vapor–gas front region.
- Calculate the heat leak when the condenser is filled with gas.
- Calculate whether or not freezing occurs in the condenser and, if so, at what rate.
- Determine the information required to size the gas reservoir of gas-controlled heat pipes.

The program contains numerous reservoir options which allow it to be used for hot or cold reservoir passive control as well as heated reservoir active control heat pipes. Additional input options permit its use for parametric studies and off-design performance predictions as well as heat pipe design.

Provision is also made in the program for two condenser sections and an adiabatic section. Basically, a one-dimensional steady-state analysis has been used, and the equations written assuming small wick resistance and negligible vapor pressure drop along the pipe.

3.15.7.1 GASPIPE 2 Computer Program Availability

This code is not available anywhere in open and public domain. The only way user can get their hand on it by downloading the PDF file that is available from <http://ntrs.nasa.gov> and look for NASA-CR-114672. At the end of this manual the source code has been listed but has very poor quality to read. It is very labor-intensive to type the source code into some compiler of a user’s choice without any error. On the other hand, you may also reach out to the following resources for updated version of it that runs under Windows/PC:

1. Galaxy Advanced Engineering or <http://www.gaeinc.com> where one can purchase the update version of the code that runs under Windows/PC.

3.15.8 *Computer Program GRADE*

TRW computer program grade for design and analysis of graded porosity heat pipe wicks [58] under NASA report CR-137618 is developed to numerically solve the differential equations that describe heat pipes with graded-porosity fibrous wicks. Such wicks have an axial variation in porosity so that, at the maximum heat transfer rate, the porosity is just low enough for the wick to support the local liquid flow pressure drop plus any hydrostatic head. Thus, the highest possible permeability is obtained along the wick. For comparison of graded-to-uniform-porosity wicks, GRADE can also compute the performance of the latter. In fact, the user can have GRADE calculate the porosity for a give fiber diameter, or both the porosity and fiber diameter, that gives the highest heat-transfer capability for a uniform-porosity wick.

In the graded-porosity case, the user specifies an initial porosity (if the user wishes, he can have GRADE compute the initial porosity as the highest for which the wick's condenser end will self-prime in a gravitational field) at the condenser end and either a final porosity or maximum liquid stress (we define stress as the local vapor-liquid pressure difference) at the evaporator end. GRADE then calculates the optimum porosity variation along the wick and the maximum heat transfer rate. A summary of GRADE's capabilities follows:

- Calculation of optimum porosity variation and corresponding maximum heat transfer rate
- Calculation of maximum heat-transfer rate at other than the wick's design condition
- Both earth-gravity and zero-gravity computations
- Heat pipes having multiple sections each having different tilts
- Multiple heat input and output zones
- Calculation of the amount of liquid contained in the wick
- Calculation of the performance of uniform-porosity wicks with a specified constant porosity
- Calculation of optimum uniform-porosity wicks

3.15.8.1 **GRADE Computer Program Availability**

This code is not available anywhere in open and public domain. The only way the user can get their hand on it is by downloading the PDF file that is available from <http://ntrs.nasa.gov> and look for NASA-CR-137618. At the end of this, manual the source code has been listed but has very poor quality to read. It is very labor-intensive to type the source code into some compiler of user choice without any error. On the other hand, you may also reach out to the following resource for updated version of it that runs under Windows/PC:

1. Galaxy Advanced Engineering or <http://www.gaeinc.com> where one can purchase the update version of the code that runs under Windows/PC.

3.15.9 Extended Development of Variable Conductance Heat Pipes

The vapor-modulated heat pipe program was developed by TRW [59] and TRW has been actively involved during the last few years in the development of variable conductance heat pipes for application in advanced space thermal control systems. In 1975, under Contract NAS2-8310 to Ames Research Center, TRW fabricated and tested two prototype vapor-modulated heat pipes which achieved variable conductance by induced wick/groove dryout. The first prototype was designed for moderate capacity in a double heat pipe configuration.

Tests of this prototype showed the roundness of the new induced dryout mechanism and uncovered some secondary elements that adversely affected performance. Recommendations for an improved design were subsequently incorporated in the fabrication of a second high-capacity vapor-modulated prototype. The new design, which uses a short vapor-modulated heat pipe to couple two conventional heat pipes, was tested successfully. The heat pipe operated at twice the 100-W design heat load, and the source temperature was practically independent of sink conditions and increased with heat load at a rate of only 0.03 °C/W. The results of the preliminary tests, as well as details of the configuration of the heat pipe, are presented in a research report, CR-137782, prepared for Ames Research Center. The details of the vapor-modulated heat pipe (VMHP) are presented in Research Report CR-137782

3.15.10 SODART Program

This code is about Studies on the Startup Transients and Performance of a Gas-Loaded Sodium Heat Pipe [23]. High-temperature metal heat pipes have exhibited difficulties startup from frozen state due to inherent low near-room temperature vapor pressures associated with working fluids. Inert gas loading is a possible solution to the frozen-state startup problem. This code was developed around this problem under three-stage contracts by the Universal Energy Systems, Incorporation, for Wright-Patterson Air Force Base, Ohio, in June of 1987. A few research papers give results of this technique. The applicability of the method to heat pipes with arterial grooves and long adiabatic length is unknown. The study in this code deals with the design, fabrication and startup testing of gas-loaded sodium heat pipe of the double walled type with grooved artery channel and long adiabatic section. A two-dimensional, quasi-steady-state, binary vapor-gas diffusion model determined energy transport rate of vapor at the diffusion front. The hot vapor front based on the study in this reference seems that it did not move at all until the vapor pressure became equal to the initial gas charge pressure. At the beginning of startup, the diffusion rate was high and decreased exponentially to a very low value as

steady state was approached. A one-dimensional transient thermal model of the startup process considered energy balance on hot and cold zones individually with the vapor diffusion process as the heat transfer coupling between the two zones. The diffusion model was solved analytically to give the vapor flux which in turn was used in the thermal model to predict the time rate of change of temperature and position of the hot front. The computer code SODART was developed to solve the transient problem calculated fluid depletion in the evaporator during startup which dictated the maximum limit on gas pressure. Start temperature and time were also determined. It seems from this study that a gas-loaded liquid-metal heat pipe could be easily started from the frozen state without adverse effects even if the heat pipe had a long adiabatic artery channel. This code also deals with solving the first order, nonlinear, ordinary differential equations with a set of known initial and boundary conditions. The code determines the time rate of change of hot front lengths and temperature of the hot front. The mass depletion of sodium from the evaporator by evaporation during following major conclusions where startup also is computed in the code in order to limit the evaporator heat from causing a dryout. The report also goes on to report additional experiment on a heat pipe capable of transporting 1800 W at 1000 K and capillary limited at high temperature and sonic limited at low temperature. So in the summary, the report deals with the following major conclusions that were reached from this study:

1. Non-condensable gas loading of the liquid-metal heat pipe helped the pipe to start easily even from frozen state. Target power inputs (>600 WA), if suddenly applied, caused evaporator dryout. The gas charge pressure could be predetermined to minimize the inactive condenser length.
2. The long adiabatic artery without a fine capillary surface did not pose any priming problem in the presence of non-condensable gas.
3. In gas-loaded mode, the heat front propagation during startup was found to be solely diffusion controlled, while in the steady state, axial conduction determined the temperature profile of the front. The axial conduction rate accounted for approximately 15 W which was only 2–10% of the condenser radiated power.
4. The variable conductance feature would be an added benefit of the startup solution.
5. The theoretical predictions of the rise time, rise temperature, startup time, startup temperature, heat front versus time plot, and hot zone temperature versus time plot and the experimental verification were in good agreement.
6. The computational time required for the transient prediction was small.
7. The unheated lengths and the reservoir wick kept the evaporator end relatively cooler than evaporator exit.
8. The temperature of the hot zone remained more isothermal in the gas-loaded mode than in the vacuum mode. As expected, the startup from the liquid state of the working fluid was smoother compared to that from the frozen state.
9. The steady-state transport performance data followed very closely with the predicted sonic limit curve.

10. A completely gas-free mode (perfect vacuum mode) of the present heat pipe could not be achieved due to experimental setup limitations. Hence, the difficulty of frozen-state startup in the vacuum mode was not demonstrated to contrast the easy gas-loaded mode startup. The nicrome resistance heating was another drawback which restricted the heater temperature to less than 1000 °C.

3.15.10.1 SODART Program Availability

This code is not available anywhere in open and public domain. The only way user can get their hand on it by downloading the PDF file that might be available from <http://www.dtic.mil> and look for AD-A211880. At the end of this manual, the source code has been listed but has a very poor quality to read. It is very labor-intensive to type the source code into some compiler of a user's choice without any error. On the other hand, you may also reach out to the following resource for updated version of it that runs under Windows/PC:

1. Galaxy Advanced Engineering or <http://www.gaenc.com> where one can purchase the update version of the code that runs under Windows/PC.

3.16 Computer Codes for Heat Transfer and Fin Designs and Materials Composite

There are so many heat transfer compute codes that are developed by many authors, nationwide and worldwide, and each readers or users of this book may have their own flavor of the software. The author has come across of few codes that are mentioned in the following sections and they are either available from national laboratories or universities around the nation that developed these codes or Galaxy Advanced Engineering, Incorporation where the author works. Some are subroutines that are dealing with finite elements or finite difference solution and analysis of heat conductions which can be found in any heat transfer or heat conduction books. For example, the book written by Myers [60] provides such subroutines that are written in FORTRAN, and the user can modify the codes and use them as desired. There are also some known codes that analyze fin designs based on their efficiencies and composite materials both used in fin or heat pipe container. If fins are used on the outside of a heat pipe heat exchanger, the fin efficiency η_f needs to be evaluated. Subsequently, the extended surface efficiency η_o is determined [32].

3.16.1 Existing Computer Codes

The following codes discussed in the following sections are the ones that this author has been exposed to and either modified them so they can work on Windows/PC or it is a direct migration of the code from main or miniframe to a macroframe computing platforms such as Windows/PC. As it is mentioned, these codes can be obtained from the resource that are identified in each code section below, and it is the responsibility of the reader or user of this book to obtain from the resource of their own choice. The codes that are obtained from Galaxy Advanced Engineering, Incorporation are fully tested and validated to run on the platforms that are advertised.

3.16.2 TOPAZ2D Finite Element Computer Codes and Its Pre- and Post-processors

TOPAZ2D/PC is a two-dimensional implicit finite element computer code for heat transfer analysis, electrostatics, and magnetostatics problems. The code can be used to solve for the steady or transient temperature field on two-dimensional planar or axisymmetric geometries. Material properties may be temperature dependent and either isotropic or orthotropic. A variety of time- and temperature-dependent boundary conditions can be specified including temperature, flux, convection, and radiation. By implementing the user subroutine feature, users can model chemical reaction kinetics and allow for any type of functional representation of boundary conditions and internal heat generation.

TOPAZ2D/PC can solve problems of diffuse and specular band radiation in an enclosure coupled with conduction in the material surrounding the enclosure. Additional features include thermal contact resistance across an interface, bulk fluids, phase change, and energy balances. Thermal stresses can be calculated using the solid mechanics code NIKÉ2D (available on PC for Windows as well as Linux Operating System from Galaxy Advanced Engineering also), which reads the temperature-state data calculated by TOPAZ2D.

Although originally intended for heat transfer analysis, TOPAZ2D has been used to solve problems in electrostatics and magnetostatics. TOPAZ2D offers an effective alternative for these problems. A simplified input data for E&M problems is included in the package. This code has its own pre- and post-processor, namely, MAZE and ORION, that are both available to prepare input and plot output for the code.

3.16.2.1 TOPAZ2D Program Availability

1. PC version of this code accompanied by its pre- and post-processor is available from the following site Galaxy Advanced Engineering or <http://www.gaeinc.com> where one can purchase the updated version of the code that runs under Windows/PC with all the bugs fixed and modified from its original version that was developed at Lawrence Livermore Laboratory by Art Shapiro.
2. The old version of these codes (i.e., TOPAZ2D, MAZE, and ORION) for VAX is possibly available from the Department of Energy and Oak Ridge National Laboratory which is repository of most computer codes funded by DOE. But based on the author's experiences with these codes, the users are required to have a good understanding of FORTRAN coding as well as understanding of the computer-designed graphics to deal with these codes to be able to make them run on any other computing platforms than VAX, CDC, or CRY where these codes were originally developed and neither DOE of Oak Ridge will take any responsibility for porting these codes.

3.16.3 *TOPAZ3D Finite Element Computer Codes and Its Pre- and Post-processors*

TOPAZ3D/PC is a three-dimensional implicit finite element computer code for heat transfer analysis. This code originally was implemented on the CRAY and VAX computers by Lawrence Livermore National Laboratory by Art Shapiro, and **Galaxy Advanced Engineering, Inc.** took the initiative of porting same functionality and capability into Windows/PC and Linux platforms. TOPAZ3D/PC can be used to solve for the steady-state or transient temperature field on three-dimensional geometries. Material properties may be temperature dependent and either isotropic or orthotropic. A variety of time- and temperature-dependent boundary conditions can be specified including temperature, flux, convection, and radiation. By implementing the user subroutine feature, users can model chemical reaction kinetics and allow for any type of functional representation of boundary conditions and internal heat generation. TOPAZ3D can solve problems of diffuse and specular band radiation in an enclosure coupled with conduction in the material surrounding the enclosure. Additional features include thermal contact resistance across an interface, bulk fluids, phase change, and energy balances. Thermal stresses can be calculated using the solid mechanics code **NIKE3D/PC** (also available from Galaxy Advanced Engineering, Inc.) which reads the temperature-state data calculated by TOPAZ3D.

TOPAZ3D has no general mesh generation capability. Rows of evenly spaced nodes and rows of sequential elements may be generated. For complex zoning, the mesh generation code and preprocessor **INGRID/PC** (also available from Galaxy Advanced Engineering, Inc.) should be used. The **TAURUS/PC** (also available

from Galaxy Advanced Engineering, Inc.) interactive post-processor can be used to provide temperature contour, temperature-time history and various geometry plots.

TOPAZ3D is an extension of the two-dimensional heat transfer code TOPAZ2D to three dimensions. This code is based to some extent on work by W.E. Mason and P.J. Burns in developing TACO3D. (TACO3D/PC is also available from Galaxy Advanced Engineering, Inc.) S.J. Sackett has been influential in the development of TOPAZ3D by writing the bandwidth and profile minimization routines, the equation solver FISSLE, and many utility routines.

3.16.3.1 TOPAZ3D Program Availability

1. PC version of this code accompanied by its pre- and post-processor is available from the following site Galaxy Advanced Engineering or <http://www.gaeinc.com> where one can purchase the updated version of the code that runs under Windows/PC with all the bugs fixed and modified from its original version that was developed at Lawrence Livermore Laboratory by Art Shapiro.
2. The old version of these codes (i.e., TOPAZ3D, TAURUS, and INGRID) for VAX is possibly available from the Department of Energy and Oak Ridge National Laboratory which is repository of most computer codes funded by DOE. But based on the author's experiences with these codes, the users are required to have a good understanding of FORTRAN coding as well as understanding of the computer-designed graphics to deal with these codes to be able to make them run on any other computing platforms than VAX, CDC, or CRY where these codes were originally developed and neither DOE of Oak Ridge will take any responsibility for porting these codes.

3.16.4 FACET Computer Code

The computer code FACET calculates the radiation geometric view factor (alternatively called shape factor, angle factor, or configuration factor) between surfaces for axisymmetric, two-dimensional planar, and three-dimensional geometries with interposed third surface obstructions. FACET was developed to calculate view factors for input to finite element heat transfer analysis codes.

The finite difference computer code TRUMP was used for heat transfer analysis at LLNL during the 1970s. Geometric black body radiation node-to-node view factors were calculated using CNVUFAC. CNVUFAC was originally developed by General Dynamics and subsequently modified by J.C. Oglebay from NASA—Lewis and finally by R.W. Wong at Lawrence Livermore National Laboratory (LLNL). The computer code GRAY was used to calculate graybodies exchange factors using as input the black body view factors calculated by CNVUFAC.

From 1979, the finite element computer code TACO has been used for heat transfer analysis at LLNL. There are several computer codes available to calculate

view factors for finite element models. The code VIEW a modified version of RAVFAC, was developed to support the NASTRAN thermal analysis program. This code is presently being used at ORNL. Generation of an input deck for VIEW is very cumbersome. The code SHAPEFACTOR uses the contour integration technique originally developed by Mitalas and Stephenson to calculate view factors for a 3-D finite element mesh. SHAPEFACTOR is very inefficiently coded and does not use dynamic storage allocations. The code GLAM is adaptable to a finite element grid to calculate view factors for axisymmetric geometries with shadowing surfaces. Generation of an input deck for GLAM is very straightforward; the code calculates accurate view factors, and is presently being supported. The code MONTE, using a Monte Carlo method, can be used to calculate exchange factors (i.e., script f) for specular emitting and reflecting surfaces for 2-D planar geometries. There might be other codes available and would appreciate being informed of their existence.

3.16.4.1 FACET Program Availability

1. PC version of this code accompanied by its pre- and post-processor is available from the following site Galaxy Advanced Engineering or <http://www.gaeinc.com> where one can purchase the updated version of the code that runs under Windows/PC with all the bugs fixed and modified from its original version that was developed at Lawrence Livermore National Laboratory by Art Shapiro.
2. The old version of these codes (i.e. FACET, MAZE and ORION) for VAX is possibly available from Department of Energy and Oak Ridge National Laboratory which is repository of most computer codes funded by DOE. But based on this author experiences with these codes, the users are required to have a good understanding of FORTRAN coding as well as understanding of the computer-designed graphics to deal with these codes to be able to make them to run on any other computing platforms than VAX, CDC, or CRY where these codes were originally developed and neither DOE of Oak Ridge will take any responsibility for porting these codes

3.16.5 MONTE2D Computer Code

MONTE2D was in the Department of Mechanical Engineering at Colorado State University (CSU) beginning with the work of Scott Statton in 1983 [61] and continuing with the work of James D. Maltby [62, 63]. The code encompasses a 2-D Monte Carlo radiative factor computer code known as MONTE2D. The code is used to calculate radiative exchange factors for enclosures with a nonparticipating medium. The focus is complex geometries rather than sophisticated physics. The types of geometries which can be simulated are shown in Fig. 3.81. Note that the 2-D code is capable of simulating both axisymmetric and prismatic geometries, as

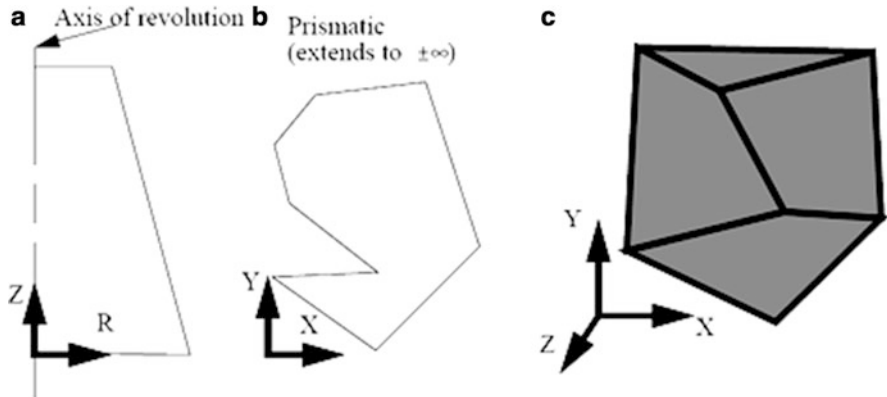


Fig. 3.81 Types of geometries which can be simulated. (a) 2-D Axisymmetric frustum. (b) 2-D Cartesian, cross section of prismatic geometry. (c) 3-D Cartesian

shown in views Fig. 3.81a, b, respectively. The 3-D code is capable of simulating geometries modeled as assemblages of generalized quadrilaterals, which are constrained to be flat. Curved surfaces must be approximated by a sufficient number of flat surfaces to “capture” the curvature. Surfaces may absorb photons, or they may reflect or transmit them specularly and/or diffusely. All exterior surfaces must be non-transmissive (it is left to the user to ensure this). All material radiative properties may be explicit functions of the incident photon angle and be dependent upon energy through the band wavelength formulation. Mark Havstad and Charlie Landram at the Lawrence Livermore National Laboratory (LLNL) have exhaustively exercised the 2-D code, checking it for validity. Similar exercises have been conducted by Donald L. Brown of LLNL and Katherine Bryan of Oak Ridge National Laboratory with the 3-D code.

A number of related publications exist wherein the code has been applied to various problems, including a detailed test of the Separator Development Facility (SDF) [62], the calculation of radiative exchange in passive solar enclosures [63] and the application to the Laser Isotope Separation (LIS) process [64]. Two recent publications of interest are [65, 66]. Finally, an alternative approach for diffuse view factors is the FACET code of Shapiro [67].

3.16.5.1 MONTE2D Program Availability

1. In order to serve users better, a World Wide Web site for the code exists at <http://www.colostate.edu/~pburns/monte.html>.

The WWW site will include general information about the code, contact information for the authors, the current version of the manual, and other documents of interest.

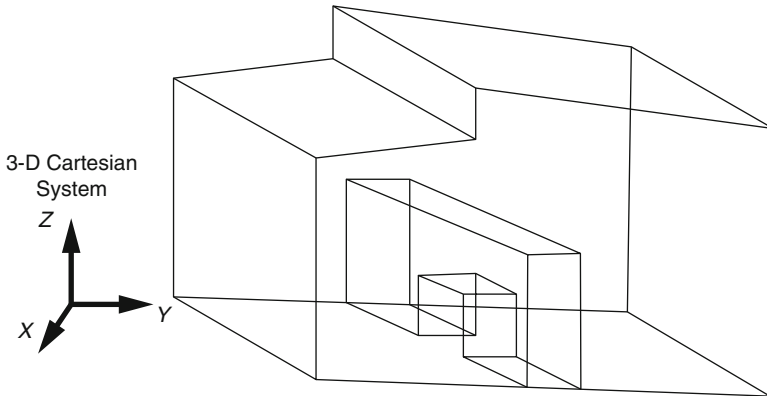


Fig. 3.82 Example geometry which can be simulated

3.16.6 MONTE3D Computer Code

MONT3D was developed in the Department of Mechanical Engineering at Colorado State University (CSU) beginning with the work of Scott Statton in 1983 and continuing with the work of James D. Maltby [62, 68], Charles N. Zeeb (Zeeb 1997; Zeeb and Burns 1999), and Klemens Branner (Branner 1999). The code is used to calculate radiative exchange factors for enclosures with a nonparticipating medium. The focus is complex geometries rather than sophisticated physics. A simple geometry which may be simulated is shown in Fig. 3.82. The 3-D code is capable of simulating geometries modeled as assemblages of generalized quadrilaterals (and triangles), which are constrained to be flat but may otherwise be in any orientation. Curved surfaces must be approximated by a sufficient number of flat surfaces, sometimes termed “faceting,” to “capture” the curvature. Surfaces may absorb photons, or they may reflect and/or transmit them specularly, semi-specularly and/or diffusely. All exterior surfaces must be non-transmissive (it is left to the user to ensure this). All material incident radiative properties may be explicit functions of the incident photon angle and be dependent upon energy through the band wavelength formulation. Donald L. Brown of Lawrence Livermore National Laboratory (LLNL) and Katherine Bryan of Oak Ridge National Laboratory have exhaustively exercised the 3-D code, checking it for validity.

The code has recently been updated extensively. The core of the code has been recoded, improving the efficiency of the code by around 44% in test cases (Zeeb 1997; Zeeb and Burns 1999). Also, the 3-D code has been parallelized to run under the PVM (Geist et al. 1994) environment, with very good success. Furthermore, a new material model, which includes semi-specular components of reflectance and transmittance, has been implemented in the 3-D code. In order to use these enhanced capabilities to the greatest effectiveness, additional detail is required in the input file, which has been changed from the older format to the one described herein. However, input files in the “old” format will still work, as the changes are backward compatible.

3.16.6.1 MONTE3D Program Availability

1. In order to serve users better, a World Wide Web site for the code exists at <http://www.colostate.edu/~pburns/monte.html>.

The WWW site will include general information about the code, contact information for the authors, the current version of the manual and other documents of interest.

3.16.7 VIEW Radiation View Factor Computer Code

The calculation of the radiation exchange between two gray, diffuse surfaces by the usual engineering method presents difficulties since it requires a full and precise description of both surfaces. Often the major difficulty in calculating the heat transfer rests with the accurate determination of the surface conditions. For multi-surface enclosure problems, or for radiation between surfaces whose mutual views are obstructed, the evaluation of the view factor is a major effort. For many situations, as in spacecraft or space structures, solar receivers, or industrial furnaces, estimates using graphical and numerical techniques are not adequate. Furthermore, in structures for which the changing position of the sun leads to different surfaces becoming radiantly important at different times, accurate determination of the view factor for all surfaces is particularly important.

The family of computer codes, **VIEW**, has been created to accomplish this task. VIEW is an interactive program that determines the view factors, graphically displays surfaces, and evaluates the solar irradiation of an assemblage of surfaces.

VIEWC and VIEWH

VIEWC and VIEWH compute the view factors between surfaces. These views may be obstructed either by other surfaces or by themselves. The view factors are generally computed by means of the contour integration technique originally developed by Mittal and Stevenson. When there is the possibility that the radiation between any two surfaces is obstructed, their view factor is calculated either by means of a double area integral technique or by contour integration applied to surface sub-elements (VIEWC) or by a pixel projection method (VIEWH). Structures are defined to VIEWC/VIEWH in terms of a collection of flat surfaces, each of which has three or four edges (i.e. a triangle or a quadrilateral). VIEWC can also compute view factors for 2-D surfaces. There are several ways to enter the data for VIEWC/VIEWH. One way is compatible with the usual finite element surface definitions, allowing the use of finite element mesh generation programs to create input for VIEWC/VIEWH. The VIEWCI program eliminates excess common nodes in free form data input, thus reducing the amount of storage required.

VIEWI

VIEWI is an interactive graphics program for generating the surface information needed for VIEWC. The surfaces may be generated singly or in groups, and the user may manipulate them in a variety of different ways to create the structure desired. VIEWI may also be used to generate finite element 2-D meshes. VIEWCM combines the output from two different VIEWI sessions in order to make a composite body. VIEWG provides interactive graphical display of the surfaces generated by VIEWI, with full hidden line removal and storage of the picture for high-speed processing (e.g., rapid rotation or perspective viewing of the structure).

VIEWO

VIEWO computes the solar radiation falling on an orbiting structure and the solar radiation which is reflected from the Earth. Input is the same as VIEWC/VIEWH, with additional data on the position of the structure with respect to the sun and earth. VIEWO runs in either batch or interactive mode and computes the solar load as a function of orbital position. The output from VIEWO includes solar view factor, earth's long wave view factor, reflected solar view factor, and total solar load.

IEWS

IEWS computes specular reflections from surfaces and can be used in conjunction with VIEWO to track the progress of the sun's rays as they reflect throughout the assemblage of surfaces.

3.16.7.1 VIEW Program Availability

This code is available from the following two sites and sources:

1. <http://www.openchannelsoftware.com/projects/GAP/> where one can purchase different source and executable version of the code that runs on choice of platform and OS that is offered by this resource
2. Galaxy Advanced Engineering or (<http://www.gaeinc.com>) where one can purchase a modified version of the code that runs under Windows/PC mode

3.16.8 *ALE3D (Arbitrary Lagrange/Eulerian Multiphysics 3D) Computer Code*

Composite materials are used in many advanced application systems and structures at Lawrence Livermore National Laboratory (LLNL). We have previously enhanced our ability to simulate structural response and progressive failure of composite systems in ALE3D (an Arbitrary Lagrange/Eulerian multiphysics code developed at LLNL) by porting an existing composite constitutive model (Model 22, the Fiber Composite with Damage Model) from DYNA3D (a nonlinear,

explicit, 3-D FEM code for solid and structural mechanics). This year, a more advanced model (DYNA3D Model 62, the Uni-Directional Elasto-Plastic Composite Model) has been implemented. Experiments were conducted to validate the elastic response of the model and to give insights and data needed for the addition of a failure algorithm into the model.

They implemented the Uni-Directional Elasto-Plastic Composite Model into ALE3D. This included implementing the ability to input orthotropic orientation data into prescribed local volume elements. Another modeling goal was to enhance the model by incorporating a failure algorithm that includes matrix delamination, fiber tensile, and fiber compressive failure. Several experiments were conducted to provide data for the verification and validation of the model's implementation in ALE3D.

The improved fiber composite material models can be used in simulations (to failure) in the many LLNL programs, such as those for composite munitions, armor penetration, pressure vessels, and rocket motors. This project has been beneficial in supporting the composite modeling efforts within the DOD Joint Munitions Program and the Focused Lethality Munitions Program. This study supports LLNL's engineering core competency in high-rate mechanical deformation simulations of large complex structures by providing an enhanced capability to model composite structures with ALE3D.

The implementation of the fiber composite with the damage model into ALE3D, which was completed in the first year of this project, was verified with several code-to-code comparisons. The hoop stresses in pressurized cylinders from simulations run with DYNA3D, with the new fiber composite model in ALE3D, and with an existing anisotropic ALE3D model, all agreed within 1%. This included both explicit and implicit ALE3D runs.

The Uni-Directional Elasto-Plastic Composite model was implemented into ALE3D. An important part of this task was creating an algorithm to initialize and update material directions at the ply and element levels. The model was validated using the same pressurized cylinder simulations described above, and the results were found to closely match the DYNA3D predictions.

Composite failure mechanisms can be divided into two types: intra-ply failure mechanisms, such as fiber breakage, matrix failure (cracking/crushing), and fiber buckling; and inter-ply failure mechanisms involving ply delamination.

Intra-ply failure can be applied at the ply level and so fits well with this model's "unit cell" approach. Inter-ply failure that includes crack opening between plies and plies sliding relative to each other affect all layers simultaneously and so is more difficult to implement. All the relevant mathematical expressions necessary for these functionalities have been derived, and the corresponding changes to the existing code have outlined. Implementation will be undertaken next year.

A series of compression tests to failure were conducted on eight different composite cylinder specimens with different fiber, fiber orientations, and resins. The data collected on the stiffness, Poisson's ratio, and ultimate strength of each specimen provide model validation data for the newly implemented models 22 and 62. The data also provide an expanded source of failure data for upcoming failure model validation in ALE3D.

Fig. 3.83 Fiber composite compression cylinder with 1.0-in. diameter pin

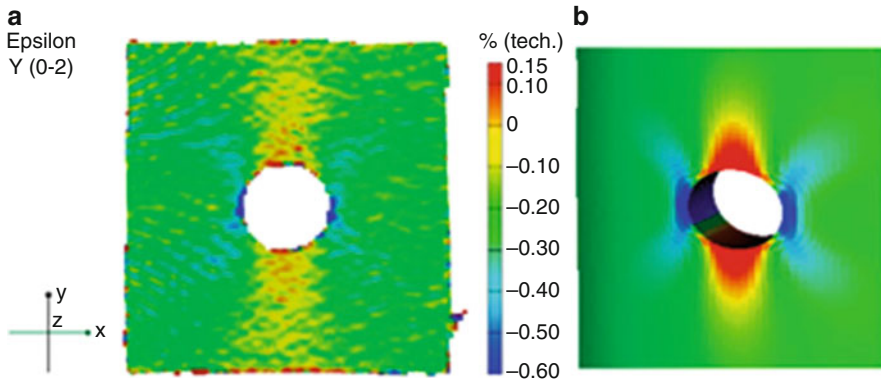


Fig. 3.84 (a) Aramis axial strain results for fiber composite compression cylinder with no pin at 300,000 lb of load. (b) The ALE3D simulation

Strain concentration factors in fiber composite cylinders with holes and bonded pins were measured using the Aramis video strain measurement system. The basic fiber composite cylinder with pin configuration is shown in Fig. 3.83. Figure 3.84 shows a comparison for the case of no pin (open hole) between the measured experimental data and the simulated response from ALE3D. The results appear to be very similar.

Strain concentration factors due to focused shear in composites were measured using the specimen shown in Fig. 3.85. This sample was loaded in compression to produce a concentrated shear band in the composite sample. The Aramis load strain curve is shown in Fig. 3.86.

In a proposed follow-on project, we will continue to improve fiber composite modeling in ALE3D, with an emphasis on local bending response and progressive damage. We plan to implement ply-level capabilities and damage algorithms taken from a specialized LLNL ply-level composite code known as ORTHO3D, and verify their implementation experimentally.

Fig. 3.85 Composite shear specimen from section of a MK82

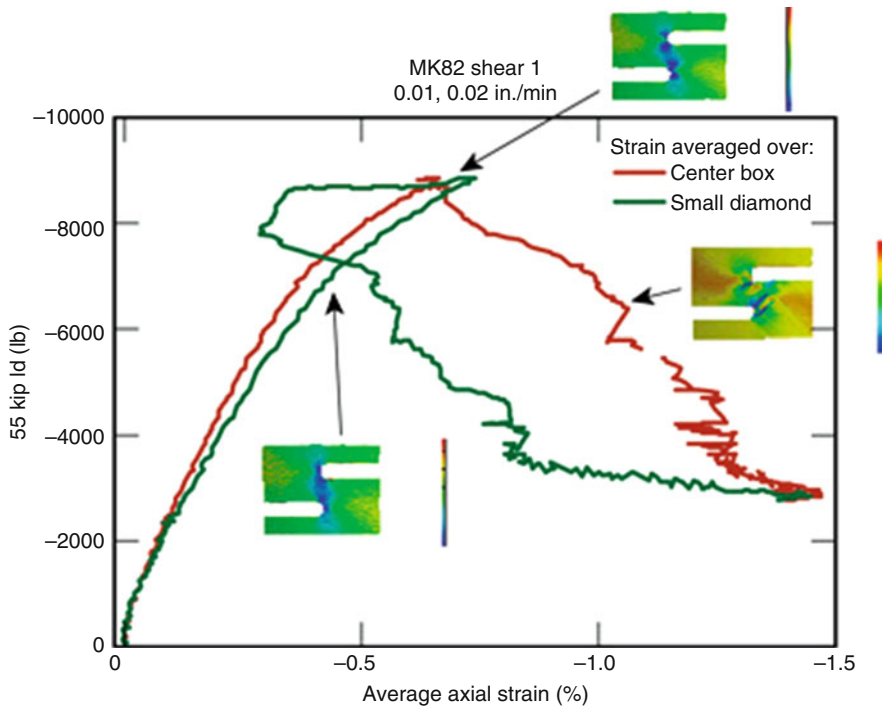


Fig. 3.86 Shear strain concentration in composite Mk82 shear specimen

3.16.8.1 ALE3D Program Availability

This code is available from Lawrence Livermore National Laboratory and users need to obtain their own copy by applying to LLNL technology transfer office or contact the author of the code Andrew Anderson (925) 423-9634 or refer to the site of this code at the following URL:

https://www-eng.llnl.gov/mod_sim/mod_sim_tools.html

3.16.9 NASTRAN Computer Code

NASTRAN, the NASA Structural Analysis System, is a powerful general purpose finite element analysis (FEA) program for use in computer-aided engineering. NASTRAN is a standard in the structural analysis field, providing the engineer with a wide range of modeling and analysis capabilities. Development of NASTRAN was initiated in the mid-1960s by the National Aeronautics and Space Administration to provide an FEA capability for its aerospace research projects. Over the years, NASA has actively maintained and improved NASTRAN such that it remains a state-of-the-art structural analysis system.

NASTRAN applications include almost every kind of structure and construction. Structural and modeling elements are provided for the specific representation of the more common types of structural building blocks including rods, beams, shear panels, plates, and shells of revolution. More general types of building blocks can be treated by combining these simple elements or by using the “general” element capability. The sub-structuring capability allows different sections of a structure to be modeled jointly after having already been modeled separately.

NASTRAN permits the effects of control systems, aerodynamic transfer functions, and other nonstructural features to be incorporated into the solution of the structural problem. Among other analysis capabilities, NASTRAN can handle:

- **Static response** to concentrated and distributed loads, thermal expansion, and enforced deformations
- **Dynamic response** to transient and steady-state sinusoidal loads, and random excitation
- **Complex eigenvalue** determination for vibration analysis, dynamic stability analysis
- **Elastic stability analysis**

NASTRAN also has a limited capability for the solution of nonlinear problems, including piecewise linear analysis of nonlinear static response and transient analysis of nonlinear dynamic response. Users may develop their own analysis capabilities by using the direct matrix abstraction programming (DMAP) language to direct NASTRAN in the solution of general matrix problems.

3.16.9.1 NASTRAN Program Availability

This code the way NASA has released it without any modification is available for open channel software at some nominal fee and two types of NASTRAN licenses are available for some destination platforms. Source code licenses, which are available for all supported platforms, include the source code, executables, demonstration problems and a four-volume set of documentation which includes the programmer's manual. Executable code only licenses are also available. See the abstract for NASTRAN/XE. The individual volumes of the four-volume set of documentation for NASTRAN are also available separately. Users that by this code from open channel software are on their own for the integrity and portability of the code to any computing and operation system of their own choice and should refer to the following site:

1. <http://www.openchannelsoftware.com/projects/GAP/> where one can purchase different source and executable version of the code that runs on choice of platform and OS that is offered by this resource
2. Galaxy Advanced Engineering or (<http://www.gaeinc.com>) where one can purchase a modified version of the code that runs under Windows/PC mode

3.16.10 NASA TRASYS Computer Code

The thermal radiation analyzer system, **TRASYS**, is a computer software system with generalized capability to solve the radiation related aspects of thermal analysis problems. TRASYS computes the total thermal radiation environment for a spacecraft in orbit. The software calculates internodes radiation interchange data as well as incident and absorbed heat rate data originating from environmental radiant heat sources. TRASYS provides data of both types in a format directly usable by other thermal analyzer programs.

One primary feature of TRASYS is that it allows users to write their own driver programs to organize and direct the preprocessor and processor library routines in solving specific thermal radiation problems. The preprocessor first reads and converts the user's geometry input data into the form used by the processor library routines. Then, the preprocessor accepts the user's driving logic, written in the TRASYS modified FORTRAN language. In many cases, the user has a choice of routines to solve a given problem. Users may also provide their own routines where desirable. In particular, the user may write output routines to provide for an interface between TRASYS and any thermal analyzer program using the R-C network concept.

Input to the TRASYS program consists of options and edit data, model data, and logic flow and operations data. Options and edit data provide for basic program control and user editing capability. The model data describe the problem in terms of geometry and other properties. This information includes surface geometry data,

documentation data, nodal data, block coordinate system data, form factor data, and flux data. Logic flow and operations data house the user's driver logic, including the sequence of subroutine calls and the subroutine library.

Output from TRASYS consists of two basic types of data: internodes radiation interchange data and incident and absorbed heat rate data. The flexible structure of TRASYS allows considerable freedom in the definition and choice of solution method for a thermal radiation problem. The program's flexible structure has also allowed TRASYS to retain the same basic input structure as the authors update it in order to keep up with changing requirements.

Among its other important features are the following:

1. Up to 4000 node problem size capability (3200 under VAX/VMS) with shadowing by intervening opaque or semi-transparent surfaces
2. Choice of diffuse, specular, or diffuse/specular radiant interchange solutions
3. A restart capability that minimizes re-computing
4. Macroinstructions that automatically provide the executive logic for orbit generation that optimizes the use of previously completed computations
5. A time variable geometry package that provides automatic pointing of the various parts of an articulated spacecraft and an automatic look-back feature that eliminates redundant form factor calculations
6. Capability to specify sub-model names to identify sets of surfaces or components as an entity
7. Subroutines to perform functions which save and recall the inter-nodal and/or space form factors in subsequent steps for nodes with fixed geometry during a variable geometry run

3.16.10.1 TRASYS Program Availability

This code for time being is available from the following sites as well as by request from NASA Johnson Space Center Innovation Partnership Office/AF2, Houston, Texas:

1. <http://www.openchannelsoftware.com/projects/GAP/> where one can purchase different source and executable version of the code that runs on choice of platform and OS that is offered by this resource
2. Galaxy Advanced Engineering or (<http://www.gaeinc.com>) where one can purchase a modified version of the code that runs under Windows/PC mode

3.17 Piping Stress Analysis Software

The **Piping Stress Analysis Software** calculates the stress, working pressure, or the required pipe wall thickness for a given application in a simple, straightforward manner. Current methods used for piping stress analysis tend to rely on basic

formulas and a hand calculator or on complex software packages that are often difficult to use for even simple cases. The Piping Stress Analysis Software offers individuals and companies an opportunity to use a product that is more powerful and flexible than traditional paper and calculator techniques and easier to use than most of the currently available software packages. It is also more flexible since it can calculate the stress level in a given pipe at a given pressure, the minimum pipe wall thickness, or the maximum allowable pressure.

The Piping Stress Analysis program allows the user to select a specific material from a database of commonly used materials or to create a customized database for an unlisted material. The program analyzes pipes according to several sets of requirements, such as the ASME/ANSI B31.1 and B31.3 piping codes and the JIC hydraulics code. Both standard and SI metric versions are available.

This utility is based on the well-established theory of elasticity, the strength of materials, and the work of the industry piping standard committees. It utilizes the Lamé equation, standard piping code equations, and custom-derived elastic-plastic equations for high pressures.

Advantages

The Piping Stress Analysis Software program is easier to use and more compact than other commercially available packages of its type, thus filling a need for many users. It is also more flexible since it can calculate the stress level in a given pipe at a given pressure, the minimum pipe wall thickness, or the maximum allowable pressure.

3.17.1 Piping Stress Analysis Software Availability

This code is available from the following two sites:

1. <http://www.openchannelsoftware.com/projects/GAP/> where one can purchase different source and executable version of the code that runs on choice of platform and OS that is offered by this resource
2. Galaxy Advanced Engineering or <http://www.gaeinc.com> where one can purchase a modified version of the code that runs under Windows/PC mode

3.18 Other Heat Pipe Analysis Codes

There are other heat pipe design codes in particular considering transient analysis rather than steady-state cases. The following is a list of few programs that are named, and their description and functionality are mentioned.

3.18.1 *VCHPDA: A Computer Program Subroutine Usage Code*

The variable conductance heat pipe system (VCHPS) program solves numerically the analytical VCHP model described in preceding sections of this report. Its solution logic is written in FORTRAN language and has been upgraded by Galaxy Advanced Engineering which is now compatible with current Windows/PC computing platform rather than its original version that was dealing with Control Data Corporation (CDC) compilers. As a program subroutine, VCHPDA is meant to interact with general lumped parameter thermal systems. In its present form, however, VCHPDA is only suitable for usage in conjunction with TRWS System Improved Numerical Differencing Analyzer (SINDA),

Variable conductance heat pipe data analysis) (VCHPDA) is a subroutine that provides accurate mathematical models of transient as well as steady-state performance of variable conductance heat pipes over a wide range of operating conditions. It applies to heat pipes with either cold, wicked, or hot, non-wicked gas reservoirs and uses ideal gas law and “flat front” (negligible vapor diffusion) gas theory. VCHPDA calculates length of gas-blocked region and temperature of vapor in active portion of heat pipe by solving set of nonlinear equations for conservation of energy and mass.

VCHPDA was developed in response to the need to predict accurately and efficiently the performance of variable conductance heat pipes (VCHPs) incorporated in spacecraft thermal control systems. As such, VCHPDA interacts with thermal analyzer programs such as SINDA (Systems Improved Numerical Differencing Analyzer).

VCHPDA provides accurate mathematical models of transient as well as steady-state performance of variable conductance heat pipes over a wide range of operating conditions. This applies to heat pipes with either cold, wicked, or hot, non-wicked gas reservoirs and uses ideal gas law and “flat front” (negligible vapor diffusion) gas theory. It calculates length of gas-blocked region and temperature of vapor in active portion of heat pipe by solving set of nonlinear equations for conservation of energy and mass.

Advantages of VCHPDA over prior programs include improved accuracy, unconditional stability, and increased efficiency of solution resulting from the use of state-of-the-art numerical techniques for solving VCHP mathematical model. The VCHPDA code is a valuable tool in the design and evaluation of advanced thermal-control systems using variable conductance heat pipes.

The subroutine is generally called from VARIABLES:

1. In the process of generating a thermal model which involves a VCHP subsystem, the following convention must be followed:
 - (a) Heat pipe wall nodes are numbered and input sequentially stepping out from the reservoir end.
 - (b) Wall to vapor conductors are numbered and input sequentially as in (a).
 - (c) The vapor temperature of each heat pipe must be declared a boundary node.
 - (d) The arrays A1 through A5 must be input as positive SINDA arrays.

3.18.1.1 VCHPDA: A Computer Program Subroutine Usage Code Availability

This code is available from the following site:

1. Galaxy Advanced Engineering or (<http://www.gaeinc.com>) where one can purchase a modified version of the code that runs under Windows/PC mode.

3.18.2 HPMAIN Computer Code

Program HPMAIN is code as partial fulfillment of the requirements for the degree Doctor of Philosophy in Mechanical Engineering at Georgia Institute of Technology by Jong Hoon Jang around February 1988 and handles an analysis of startup from the frozen-state and transient performance of heat pipes.

Mathematical models and an associated computer program have been developed for heat pipe startup from the frozen state. The models have been checked against previously published analytical and experimental data. Agreement is relatively good for most situations examined. When a liquid-metal heat pipe is started by introducing heat to one end while cooling the other end of it, internal working fluid dynamics may greatly affect temperature distributions and fluid properties within the pipe as well as the overall conductance of the pipe. For example, if the working fluid is initially frozen, during startup, melting will occur in the capillary structure, and the vapor will experience free molecular, choked, and continuum flow at various times. These changing internal conditions generally make the heat pipe relatively slow to transport energy from heated to cooled ends and very large radial and axial temperature gradients may develop.

The work uses finite element formulations of the governing equations written for each heat pipe region for each operating condition experienced during startup from a frozen state. In the shell, energy transport is by conduction only. In the capillary structure, conduction and heat of fusion are considered. In the vapor region, different sets of governing equations are utilized for regions undergoing free molecular, choked, and normal continuum flow. The various models were checked against analytical and experimental data available in the literature for three specific types of operation. For example, the models used to predict melting in the capillary structure were checked against analytical results previously published for melting in a corner region. Computation using the finite elements methods developed in the present work was made for a space shuttle reentry mission where a heat pipe-cooled leading edge was used on the wing. This wing had a sodium heat pipe built into the wing near the leading edge. Charles J. Camarda of NASA Langley Research Center made experimental measurements of startup behavior for such a heat pipe. Results computed in this work compared well with Camarda's data.

This program solves the startup and transient performance of heat pipe with metallic working fluids by using a finite element method. The temperature is

predicted from two-dimensional and transient heat conduction equation, which incorporates the effects of the phase change process in an expression for the volumetric heat capacity by using the enthalpy method. The Galerkin weighted residual method is used to drive finite element formulations. The flow dynamics of the vapor are described by 1-D, compressible, and laminar momentum and energy equations. In one-D model, the variation of velocity at cross section, friction at the liquid–vapor interface, and quality of vapor are considered. Five 1-D governing differential equations for vapor are solved by a subroutine known as DVERK which uses Runge–Kutta method. The specified temperature, heat flux, convective, and radiation boundary conditions are applicable. This program can be used to solve pure conduction or phase change problem alone. Implicit or explicit time stepping schemes are used. Since explicit scheme is not self-starting method, implicit scheme is used for first few time steps. For this purpose, the set proper number for variable NTS. Grid system can be generated by the program HPGRNW or for that matter the grid generator program. The input data file for the program HPMAN consists of the output data file of HPGRNW and general data which specifies some general conditions. The use IMSLIB mathematical library is required by this code, and one has to use a FORTRAN compiler that supports this library and is able to incorporate that as part of program execution.

3.18.2.1 HPMAN Computer Code Availability

This code is available from the following site:

1. [Galaxy Advanced Engineering](http://www.gaeinc.com) or (<http://www.gaeinc.com>) where one can purchase a modified version of the code that runs under Windows/PC mode

3.18.3 SMLBUB Spherical Bubble Model Computer Program

A part of the experimental program at TRW under aspics of NASA was to investigate the potential of various mechanisms to cause artery depriving, a series of the experiments have been conducted to examine bubble nucleation in methanol as working fluid. The experiments were to determine whether gas bubbles could be generated in the bulk of liquid methanol saturated with either helium or nitrogen gas as it undergoes temperature and/or pressure reduction [69]. The SMLBUB code was developed to validate such experimental and related theory behind it.

Prior to the experiments, a theoretical analysis of the potential for bubble formation in Communication Technology Satellite (CTS) heat pipes had shown ~11 that large numbers of bubbles could be generated in methanol due to supersaturation resulting from temperature and pressure reduction under conditions

similar to those prevailing prior to the anomalies. An objective of these experiments was to verify, at least qualitatively, the theoretical results.

In addition the experiments considered the potential of a mesh screen artery to provide bubble nucleating sites.

The experimental setup consisted of a glass flask half filled with 50 cc of spectral grade methanol and instrumented to allow continuous monitoring of temperature and pressure. A sketch of the apparatus is attached. A needle valve located between the flask and a vacuum pump were used to control the pressure level or the rate of pressure reduction of the liquid. Cooling of the liquid was attained by immersion of the test flask in liquid nitrogen. This technique, however, did not allow for arbitrary control of the cooling rate. The liquid was saturated by bubbling either nitrogen or helium gas through the liquid using a frit glass tube. This process was allowed to be continued for at least 2 h.

A typical pressure reduction experimental sequence was as follows:

1. Saturate methanol with either nitrogen or helium at ambient conditions.
2. Reduce temperature at atmospheric pressure. Two temperature levels, 21 and -40°C were used.
3. Drop into the liquid a dry section of mesh screen artery.
4. Reduce pressure from 14.7 to 4 psia. In some cases this pressure drop was accomplished in 10 s and in others in 5 min.

A typical temperature reduction experimental sequence was as follows:

1. Saturate methanol at ambient conditions.
2. Drop into the liquid a dry section of mesh screen artery.
3. Reduce pressure at ambient temperature. Pressure levels of 14.7, 10, and 4 psia were used.
4. Reduce temperature. In some cases the temperature was reduced from 21 to -40°C in approximately 20 min. This was accomplished by placing the flask near the liquid nitrogen surface contained in a Dewar flask where cooling of the methanol occurred by natural convection. In other cases, the liquid was rapidly chilled by immersing the flask in liquid nitrogen for approximately 10 s at which point the liquid on the bottom of the test flask and inside the artery froze (Fig. 3.87).

From the Antoniuk [69], the experiments were repeated several times and the results were found reproducible. No bubbles were observed as the liquid, originally at a set temperature level, underwent pressure reduction. Similar results were obtained from temperature reduction experiments provided the liquid temperature did not drop below the freezing point (-98°C).

Experiments, in which the liquid partially froze however, yielded significantly different results. A large number of small bubbles were observed streaming from the surface of the thawing ice. As the melting process went to completion, the bubbles were reduced to a few originating from the bottom surface of the flask and from the outer surface of the mesh screen artery. About a dozen small bubbles were observed trapped inside, the arteries after the ice melted. These bubbles were

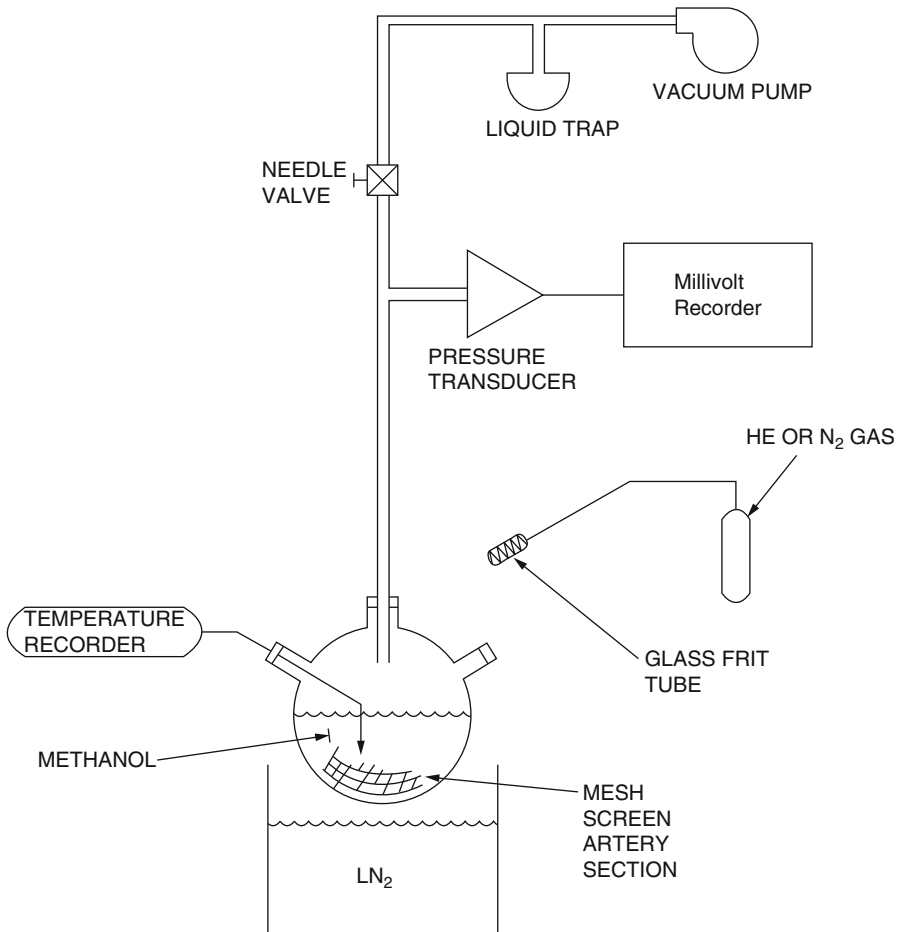


Fig. 3.87 TRW experimental setup

observed later to coalesce forming fewer but larger bubbles which continue to grow. The ultimate size of these bubbles depended on the pressure of the system. For example, at 4 psia the remaining bubbles inside the artery continue to grow for approximately 10 min as the liquid temperature rose from -40 to 0 °C, at which point the size of the bubbles was such that essentially all the liquid in the artery was displaced.

The TRW report on this code was based on experiments were performed with an existing 1.07 m long glass heat pipe. A cross section of this heat pipe is shown in Fig. 3.88. The pipe contains a slab wick with a CTS-type artery attached to one side. A heater and cooling loop are attached to the other side of the wick in the evaporator and condenser sections, respectively. This arrangement permits observations on the behavior of the artery in an operational heat pipe.



Fig. 3.88 Inner and outer fins and grooves of a cylindrical pipe schematic

The heat pipe was gas loaded with a 90 % nitrogen–10 % helium mixture at a pressure equivalent to the conditions in the CTS pipes. The experiments simply involved visually observing the artery behavior as a result of freezing the methanol within it by passing liquid nitrogen through the cooling loop, and subsequently thawing the methanol by terminating the LN2 flow.

As the result of these experiments, freezing of super-saturated methanol in the arteries has been identified as a potential mechanism for bubble formation in the arteries owing to the fact that the ice surface is an excellent source of nucleating sites. For details of his experiment, refer to his report [69].

3.18.3.1 SMLBUB Computer Code Availability

This code is available from the following site:

1. [Galaxy Advanced Engineering](http://www.gaeinc.com) or <http://www.gaeinc.com> where one can purchase a modified version of the code that runs under Windows/PC mode

3.19 COMSOL Multiphysics Software

COMSOL Multiphysics is a finite element analysis, solver and simulation software/FEA software package for various physics and engineering applications, especially coupled phenomena or multiphysics. The package is cross-platform (Windows, Mac, Linux). In addition to conventional physics-based user interfaces, COMSOL Multiphysics[®] also allows for entering coupled systems of partial differential equations (PDEs). The PDEs can be entered directly or using the so-called weak form (see finite element method for a description of weak formulation). Since version 5.0 (2014), COMSOL Multiphysics is also used for creating physics-based apps. These apps can be run with a regular COMSOL Multiphysics license but also with a COMSOL Server license. An early version (before 2005) of COMSOL Multiphysics was called FEMLAB. Recent release of COMSOL is version 5.2 as of the date of this book publication.

Here we show some cooling finned pipe design process where COMSOL Multiphysics[®] was used to present a very general case where this pipe was used for coolers, heaters such as heat pipe, or heat exchangers to increase performance. These fins come in different sizes and designs depending on the application and requirements. When these fins are placed outside the pipe, they increase the heat transfer surface of the pipe so that a cooling or heating external fluids can exchange heat in more efficient way. When they are placed inside the pipe (i.e., grooves inside heat pipe acting as wick), it is the inner fluids that benefits from an increased heat exchange surface. As we said instead of fins, grooves can also enlarge the heat surface, particularly inside the pipe where space is limited. See Fig. 3.88 as below.

In the application, you can customize a long cylindrical pipe with predefined inner and outer fins or grooves to observe and evaluate their cooling effects. Figure 3.88 shows three examples of fins and grooves among those provided by the user interface.

The inner fluid is water, the outer cooling fluid is air, and the pipe is made of copper. However, it is still possible to alter the app to set different materials. After specifying the geometry and operating conditions, the application provides a characterization of the pipe through the following quantities:

- Pipe mass
- Inner volume of the pipe
- Inner and outer heat exchange surfaces
- Heat dissipation rate
- Pressure drop for the inner and outer fluid
- Temperature drop for the inner fluid

Figure 3.89 shows the detail geometry of grooves along with finned pipe based on COMSOL Multiphysics Geometry user interface.

Figure 3.90 below shows the user interface of COMSOL Multiphysics application software.

The different sections for setting the design of the pipe are detailed below.

Pipe

Use this section to specify the dimensions of the pipe itself. The available parameters to manipulate are the **pipe thickness** and the **pipe inner radius**. The **pipe outer radius** is then deduced automatically.

Outer Part

Select between **disk-stacked blades**, **circular grooves**, **helical blade**, **helical grooves**, or **none** for the outer part. According to the selection, size parameters for the fins or grooves can be specified.

Inner Part

For the inner part, select between **none** or **straight grooves**.

Operating Conditions

In this section, define the **air inlet temperature** and **air inlet absolute pressure** for the airflow around the pipe. The **water inlet temperature** is automatically updated

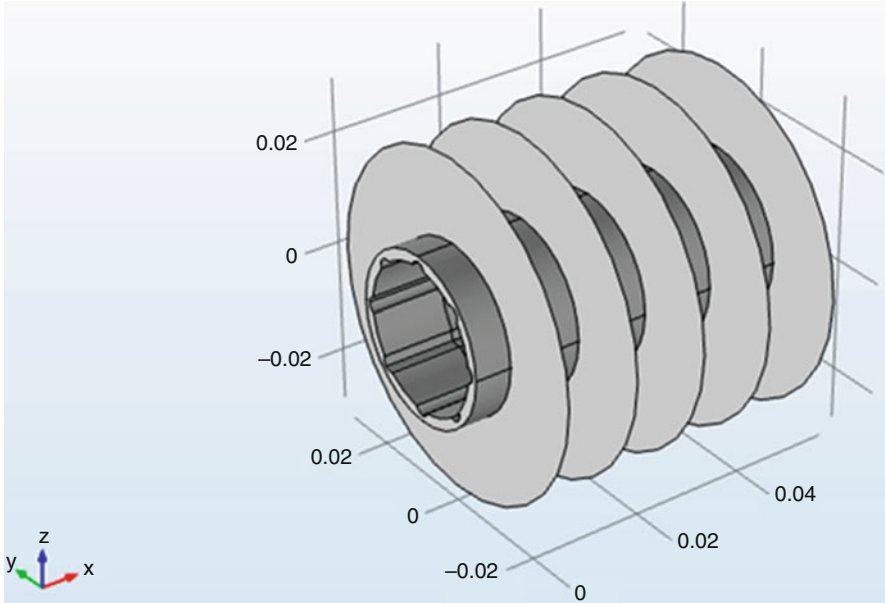


Fig. 3.89 Schematic of geometry of grooves along with finned pipe

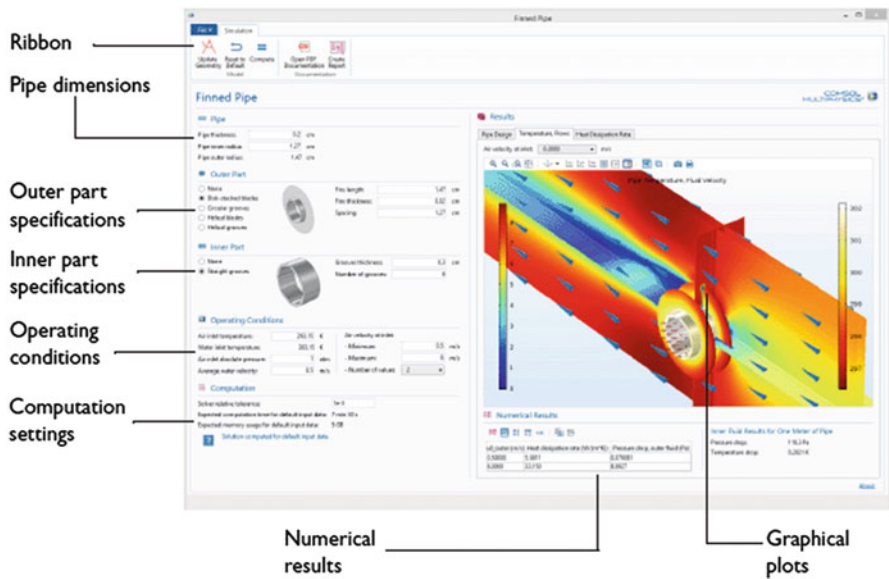


Fig. 3.90 User interface of the application

when the **air inlet temperature** is changed. Define the **average water velocity** for the water flow inside the pipe. The app solves the model for different possible values of velocity for the air flow to analyze its effect on the cooling. Set the **minimum** and **maximum** values for the air velocity range at the inlet, and choose the **number of values** to solve for, between **two** and **ten**.

Computation

Set the solver relative tolerance. The default value provides a good solution at moderate computational costs. This section also displays useful information about computation time and memory consumption.

Results

This section shows several graphical plots and numerical results after computation. The **pipe design** tab displays the geometry according to your custom inputs. At the bottom, information on the mass and dimension of the pipe are provided.

The **temperature flow** tab shows the graphical plot of the temperature in the pipe domains and velocity in water and air domains. Change the values of **air velocity at inlet**, defined beforehand in the **operating conditions** section, to display the corresponding plot. At the bottom, the **Numerical Results** section shows the heat dissipation rate, pressure drops for inner and outer fluids, and temperature drop for the inner fluid.

The **heat dissipation rate** tab draws the curve of the heat dissipation rate with respect to air inlet velocity, in the range specified in the **operating conditions** section.

The Embedded Model

This model consists of a finned and grooved pipe filled with water, which is cooled by the surrounding air. The model makes use of pseudo-periodicity conditions to be able to compute only a small section of the pipe. This provides reliable results if the temperature field along the whole pipe is periodic up to a constant offset and following the geometrical periodicity.

Model Definition

The model solves for a turbulent flow inside and around the pipe. Indeed, the cooling airflow at the exterior of the pipe often reaches high speeds, bringing the problem to the turbulent validity range. Inside the pipe, the water flow already reaches a Reynolds number in the turbulent range from 0.5 m/s.

For heat transfer, the water inlet temperature is 10 K warmer than the air inlet. This ensures that the overall temperature gradient is not too large and material properties in the pipe section remain constant.

To avoid modeling any specific length of pipe, you only solve for a sample of the pipe of 0.5 in. (1.27 cm) that is geometrically periodic. For that sample, pseudo-periodic heat conditions are applied to the opposite extremities. This way, the heat flux is the same at these boundaries but the temperature field has an offset determined by the operating conditions.

Results

The default input data solves for two values of air velocity: 0.5 and 6 m/s. The numerical results for these parameter values are shown in Table 3.12. These results are given for 1 m of pipe.

The default geometry is characterized by the following data (Table 3.13).

Figure 3.91 shows the plot of temperature in the pipe domain and velocity magnitude in the air domain.

Figure 3.92 shows the heat dissipation rate curve with respect to air velocity. The curve is obtained with only two values. For a more significant trend, the model should be solved for more values of air velocity.

The above presentations and figure easily can be produced using COMSOL Multiphysics software application and geometry.

Table 3.12 Numerical results

Air inlet velocity (m/s)	Heat dissipation rate (W/m K)	Pressure drop (air) (Pa)	Pressure drop (water) (Pa)	Temperature drop between pipe extremities
0.5	5.9811	0.079081	118.3	0.2821
6	33.150	8.8927		

Table 3.13 Mass and dimensions of the pipe

Quantity	Value
Pipe mass	1.371 kg
Inner fluid volume (water)	0.5235
Inner heat exchange surface	8.758
Outer heat exchange surface	41.19

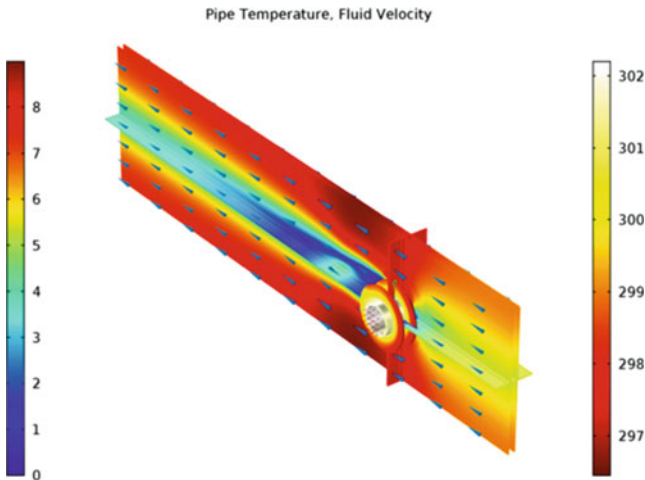


Fig. 3.91 Temperature plot in the pipe domain and velocity magnitude plot in the air domain

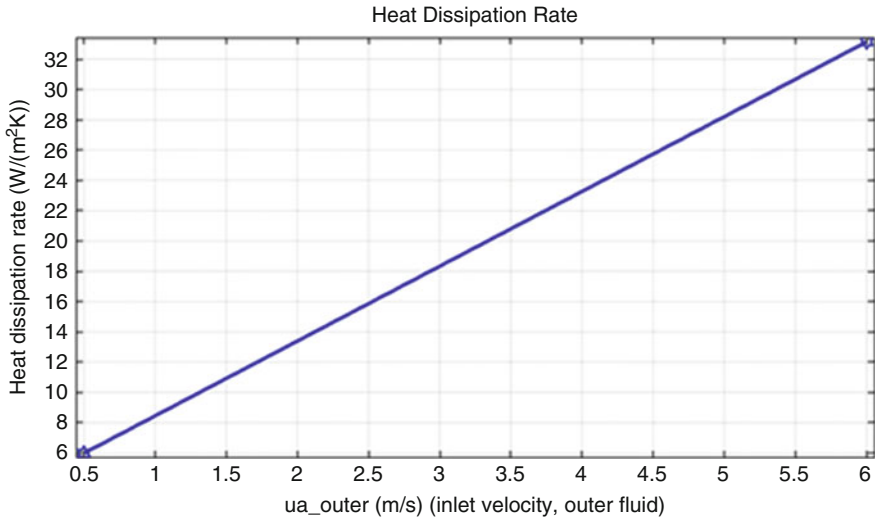


Fig. 3.92 Heat dissipation rate with respect to air velocity

3.19.1 COMSOL Multiphysics Software Availability

The availability and prices for obtaining the software can be inquired from COMSOL Corporation and their web site at <http://www.comsol.com>.

References

1. Chi, S. W. (1971, December). *Mathematical modeling of high and low temperature heat pipes*. George Washington University Final NASA, Grant No. NGR 09-010-070.
2. Chi, S. W. (1970, September). *Mathematical models of cryogenic heat pipes*. Final Report to NASA, Goddard Space Flight Center, Grant No. NGR09-005-071.
3. Bienert, W. B., & Skrabec, E. A. (1972, August). *Heat pipe design handbook*. Dynatherm Corporation. Report to NASA, Contract No., NASA 9-11927.
4. Reay, D. A., & Kew, P. A. (2006). *Heat pipes* (5th ed.). Tarrytown, NY: Butterworth-Heinemann.
5. Chi, S. W. (1976). *Heat pipe theory and practice*. New York: McGraw-Hill.
6. Cotter, T. P. (1965, February). *Theory of heat pipes*. Los Alamos Scientific Laboratory Report LA-3246-MS.
7. Marcus, B. D. (1972, April). *Theory and design of variable conductance heat pipes*. TRW Systems Group, NASA CR-2018.
8. Ribando, R. J. (2004) *View factor for aligned parallel rectangles*. Mechanical and Aerospace Engineering, University of Virginia
9. ASME Boiler and Pressure Vessel Committee. (1965). *ASME boiler and pressure vessel code-Section VIII Unfired pressure vessel*. New York: American Society of Mechanical Engineering.

10. Tien, C. L., & Jun, K. H. (1971). Minimum meniscus radius of heat pipe wick materials. *International Journal of Heat and Mass Transfer*, 14, 1853–1855.
11. Colwell, G. T., Jang, J. H., & Camarda, J. C. (1987, May). *Modeling of startup from the frozen state*. Presented at the Sixth International Heat Pipe Conference, Grenoble, France.
12. Peterson, G. P. (1994). *An introduction to heat pipes—Modeling, testing and applications*. New York: John Wiley & Sons.
13. Faghri, A. (1995). *Heat pipe science and technology*. Washington, DC: Taylor & Francis.
14. Faghri, A., & Harley, C. (1994). Transient lumped heat pipe analysis. *Heat Recovery Systems and CHP*, 14(4), 351–363.
15. Jang, J. H., Faghri, A., & Chang, W. S. (1991). Analysis of the one-dimensional transient compressible vapor flow in heat pipes. *International Journal of Heat and Mass Transfer*, 34, 2029–2037.
16. Carslaw, H. S., & Jaeger, J. C. (1959). *Conduction of heat in solids* (2nd ed.). London: Oxford University Press.
17. Chang, W. S. (1981, March). *Heat pipe startup from the supercritical state*. Ph.D. Dissertation, Georgia Institute of Technology.
18. Colwell, G. T., & Chang, W. S. (1984). Measurement of the transient behavior of a capillary structure under heavy thermal loading. *International Journal of Heat and Mass Transfer*, 27(4), 541–551.
19. Chang, W. S., & Colwell, G. T. (1985). Mathematical modeling of the transient operating characteristic of low-temperature heat pipe. *Numerical Heat Transfer*, 8, 159–186.
20. Colwell, G. T. *Modeling of transient heat pipe operation*. Final Report NASA GRANT NAG-1-392, Period Covered August 19, 1983 through December 31, 1988, Submitted January 15, 1989.
21. Cotter, T. P. (1967, October). Heat pipe startup dynamics. *Proc. IEEE Thermionic Conversion Specialist Conference, Palo Alto, California* (pp. 344–348).
22. Luikov, A. V. (1968). *Analytical heat diffusion theory*. New York: Academic.
23. Silverstein, C. C. (1992). *Design and technology of heat pipes for cooling and heat exchange*. Washington, DC: Taylor and Francis.
24. Pakdemirli, M., & Sahin, A. Z. (2006). A similarity solution of fin equation with variable thermal conductivity and heat transfer coefficient. *Mathematical and Computational Applications*, 11(1), 25–30.
25. Jiji, L. M. (2009). *Heat conduction* (3rd ed.). Berlin: Springer.
26. Nnanna, A. G. A., Haji-Sheikh, A., & Agonafer, D. (2003). Effect of variable heat transfer coefficient, fin geometry, and curvature on the thermal performance of extended surfaces. *Journal of Electronic Packaging, Transactions of the ASME*, 125, 456–460.
27. Lee, H.-L., Yang, Y.-C., & Chu, S.-S. (2002). Transient thermoelastic analysis of an annular fin with coupling effect and variable heat transfer coefficient. *Journal of Thermal Stresses*, 25, 1105–1120.
28. Campo, A., & Salazar, A. (1996). Similarity between unsteady-state conduction in a planar slab for short times and steady-state conduction in a uniform, straight fin. *Heat and Mass Transfer*, 31, 365–370.
29. Kuehn, T. H., Kwon, S. S., & Tolpadi, A. K. (1983). Similarity solution for conjugate natural convection heat transfer from a long vertical plate fin. *International Journal of Heat and Mass Transfer*, 26, 1718–1721.
30. Rozza, G., & Patera, A. T. *The thermal fin (“Tfin”) problem*. In collaboration with D. B. P. Huynh, N. C. Nguyen and, previously, S. Sen and S. Deparis.
31. Holman, J. P. (1986). *Heat transfer* (6th ed.). New York: McGraw-Hill.
32. Nellis, G., & Klein, S. (2008). *Heat transfer* (1st ed.). Cambridge: Cambridge University Press.
33. Marcus, B. D. (1965, May). *On the operation of heat pipes*. TRW Report 9895-6001-TU-000.
34. Brennan, P. J., & Kroliczek, E. J. (1979). *Heat pipe design handbook* (Contract Report No NAS5-23406, Vols. I and II). Washington, DC: National Aeronautics and Space Administration.

35. Asselman, G. A., & Green, D. B. (1973). Heat pipes. *Phillips Technical Review*, 16, 169–186.
36. Eninger, J. E. (1974, August 1). *Computer program grade for design and analysis of graded-porosity heat-pipe wicks*. NASA-CR-137618.
37. Eninger, J. E., & Edwards, D. K. (1976, November). *Computer program grade II for the designed analysis of heat pipe wick*. NASA-CR-137954.
38. Brennan, P. J., & Kroliczek, E. J. (1979, June). *Heat pipe design handbook*. Towson, MD: B & K Engineering, Inc. NASA Contract No. NAS5-23406 Report N81-70113.
39. Tower, L. K. (1992, September). *NASA Lewis steady-state heat pipe code users manual Version 1.0*. Cleveland, OH: NASA Lewis Research Center. NASA TM-105161.
40. Busse, C. A. (1967). Pressure drop in the vapor phase of long heat pipes. *IEEE Conference Record of the Thermionic Conversion Specialist Conference* (pp. 391–398), IEEE.
41. Tower, L. K., & Hainley, D. C. (1989). *An improved algorithm for the modeling of vapor flow in heat pipes*. NASA CR-185179.
42. Tower, L. K. (2000, April). *NASA Glenn steady-state heat pipe code users manual Version 2.0*. Cleveland, OH: NASA Glenn Research Center. NASA TM-2000-209807.
43. McLennan, G. A. (1983, November). *ANL/HTTP: A computer code for the simulation of heat pipe operation*. Argonne National Laboratory, Report No. ANL-83-108.
44. Marcus, B. D. (1972, April). *Theory and design of variable conductance heat pipes*. NASA CR-2018.
45. Soliman, M. M., Grauman, D. W., & Berenson, P. J. (1970). *Effective thermal conductivity of saturated wicks*. ASME Paper No. 70-HT//SpT-40.
46. Ferrel, K. J., & Alleavitch, J. (1970). *Vaporization heat transfer in capillary wick structures*. Chemical Eng., Prog. Symposium Series V66, Heat Transfer, Minneapolis, MN.
47. Glass, D. *Closed form equations for the preliminary design of a heat-pipe-cooled leading edge*. NASA/CR-1998-208962
48. Edelstein, F., & Haslett, R. (1974, August). *Heat pipe manufacturing study*. Final Report prepared by Grumman Aerospace Corp. for NASA No. NAS5-23156.
49. Jen, H. F., & Kroliczek, E. J. (1976). *Grooved analysis program*. Towson, MD: B & K Engineering. NAS5-22562.
50. Nguyen, T. M. (1994, February). *User's manual for groove analysis program (GAP) IBM PC Version 1.0*. OAO Corporation.
51. Skrabek, E. A., & Bienert, W. B. (1972, August). *Heat pipe design handbook* (Parts I and II). Cockeysville, MD: Dynatherm Corporation. NASA CR-1342.
52. Marcus, B. D., Eninger, J. E., & Edwards, D. K. (1976). *MULTIWICK*. Redondo Beach, CA: TRW System Group.
53. Edward, D. K., Fleischman, G. L., & Marcus, B. D. (1973, October). *User's manual for the TRW Gaspipe 2 Program*. Moffet Field, CA: NASA—Ames Research Center. NASA CR-114672.
54. Woloshun, K. A., Merrigm, M. A., & Best, E. D. (1988, November). *Analysis program a user's manual*. Los Alamos National Laboratory. LA-11324-M.
55. Kamotani, Y. (1978, September). *User's manual for thermal analysis program of axially grooved heat pipes (HTGAP)*. NASA-CR-170563.
56. Marcus, B. D., & Fleischman, G. L. *Steady-state and transient performance of hot reservoir gas-controlled heat pipes*. A.S.M.E. Paper No. 70-HT//SpT-11.
57. Bienert, W. (1969). *Heat pipes for temperature control*. Proc: Fourth Intersociety Energy Conversion Engineering Conference, Washington, DC.
58. Antoniuk, D., Edwards, D. K., & Luedke, E. E. (1978, September 1). *Extended development of variable conductance heat pipes*. NASA-CR-152183, TRW-31183-6001-RU-00.
59. Ponnappan, R. *Studies on the startup transients and performance of a gas loaded sodium heat pipe*. Technical Report for Period June 1989, WRDC-TR-89-2046.
60. Myers, G. E. (1987). *Analytical methods in conduction heat transfer* (2nd ed.). Schenectady, NY: Genium Publishing Corp.

61. Scott, S. E. (1983). *MONTÉ—A two-dimensional monte carlo radiative heat transfer code*. M.S. Thesis, Department of Mechanical Engineering, Colorado State University, Fort Collins, CO 80523.
62. Maltby, J. D. (1987). *Three-dimensional simulation of radiative heat transfer by the MonteCarlo method*. M.S. Thesis, Department of Mechanical Engineering, Colorado State University, Fort Collins, CO 80523.
63. Maltby, J. D., & Burns, P. J. (1986). *MONT2D and MONT3D user's manual*. Internal Publication, Department of Mechanical Engineering, Colorado State University.
64. Burns, P. J., & Pryor, D. V. (1989). Vector and parallel Monte Carlo radiative heat transfer. *Numerical Heat Transfer, Part B: Fundamentals*, 16(101), 191–209.
65. Burns, P., Christon, M., Schweitzer, R., Wasserman, H., Simmons, M., Lubeck, O. et al. (1988). Vectorization of Monte Carlo particle transport—An architectural study using the LANL benchmark GAMTEB. *Proceedings, Supercomputing '89*, Reno, NV (pp. 10–20).
66. Maltby, J. D., & Burns, P. J. (1988). *MONT2D and MONT3D user's manual*. Internal Publication, Department of Mechanical Engineering, Colorado State University.
67. Arthur, B., & Shapiro. (1983). FACET—A radiation view factor computer code for axisymmetric, 2D planar, and 3D geometries with shadowing, August, 1983. Lawrence Livermore Laboratory.
68. Maltby, J. D. (1990). *Analysis of electron heat transfer via Monte Carlo simulation*. Ph.D. Dissertation, Department of Mechanical Engineering, Colorado State University, Fort Collins, CO 80523.
69. Antoniuk, D., & Edwards, D. K. (1980). *Depriming of arterial heat pipe: An investigation of CTS thermal excursions*. NASA CR 165153, Final Report August 20, 1980.

Chapter 4

Application of Heat Pipe in Industry

In this chapter we will discuss applications of heat pipes to energy system. We also expand on its applications in space program as well as nuclear industry. We also touch base-up heat pipe applications in electronic manufacturing where the fast central processing units (CPUs) need to be cooled down and how heat pipe can be used as a heat exchanger.

Recently heat pipes have shown very promising results in applications such as thermal energy storage systems and concentrated solar power to produce electricity as part of renewable energy systems as well.

4.1 Application of Heat Pipe in Industry

Grover and his colleagues [1, 2] were working on cooling systems for nuclear power cells for spacecraft, where extreme thermal conditions are found. Heat pipes have since been used extensively in spacecraft as a means for managing internal temperature conditions.

Heat pipes have been applied in many ways since their introduction in 1964 (Vasiliev; Mochizuki et al.) [3, 4]. Depending on their intended use, heat pipes can operate over a temperature range from 4.0 to 3000 K. In all cases, their applications can be divided into three main categories: separation of heat source and sink, temperature equalization, and temperature control. Due to their extremely high thermal conductivity, heat pipes can efficiently transport heat from a concentrated source to a remotely mounted sink. This property can enable dense packing of electronics, for example, without undue regard for heat sink space requirements. Another benefit of the high thermal conductivity is the ability to provide an accurate method of temperature equalization. For example, a heat pipe mounted between two opposing faces of an

The original version of the book was revised. An erratum can be found at DOI [10.1007/978-3-319-29841-2_7](https://doi.org/10.1007/978-3-319-29841-2_7)

orbiting platform will enable both faces to maintain constant with equal temperatures, thus minimizing thermal stresses. The temperature control is a result of the capability of heat pipes to transport large quantities of heat very rapidly. This feature enables a source of varying flux to be kept at a constant temperature as long as the heat flux extremes are within the operating range of the heat pipe.

Heat pipes are extensively used in many modern computer systems, where increased power requirements and subsequent increases in heat emission have resulted in greater demands on cooling system. Heat pipes are typically used to move heat away from components such as CPUs and GPUs (graphics processing units) to heat sinks where thermal energy may be dissipated into the environment.

In solar thermal water heating applications, an evacuated tube collector can deliver up to 40 % more efficiency compared to more traditional “flat-plate” solar water heaters. Evacuated tube collectors eliminate the need for antifreeze additives to be added as the vacuum helps prevent heat loss. These types of solar thermal water heaters are frost protected down to more than $-3\text{ }^{\circ}\text{C}$ and are being used in Antarctica to heat water. Also due to the enormous increase in the global energy demand and possible depletion of conventional energy resources such as fossil fuel, renewable energy resources turned out to be promising options to supply clean and low-cost energy, and heat pipe shows very appropriate and promising apparatus as part of heating and cooling system of such demand.

Heat pipes are used to dissipate heat on the Trans-Alaska Pipeline System. Without them residual ground heat remaining in the oil as well as that produced by friction and turbulence in the moving oil would conduct down the pipe’s support legs. This would likely melt the permafrost on which the supports are anchored. This

Fig. 4.1 Alaska pipeline support legs cooled by heat pipes to keep permafrost frozen



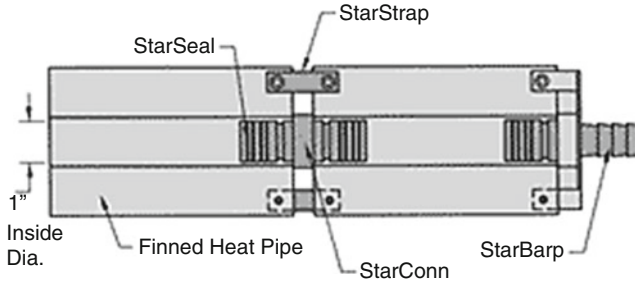


Fig. 4.2 A greenhouse application of finned heat pipe structure

would cause the pipeline to sink and possibly sustain damage. To prevent this each vertical support member has been mounted with four vertical heat pipes (Fig. 4.1).

Heat pipes are also being widely used in solar thermal water heating applications in combination with evacuated tube solar collector arrays. In these applications, distilled water is commonly used as the heat transfer fluid inside a sealed length of copper tubing that is located within an evacuated glass tube and oriented toward the sun.

A company such as TrueLeaf offers fined heat pipe assembly for the greenhouse application using DuoFin shape structure for the condenser side of heat pipe in order to provide incredibly even heating across the width of your greenhouse growing areas. Its unique tapered fin design delivers a combination of convective and radiant heating quietly and efficiently. Having only two fins means that more loops are needed to meet your heat load than with sister product, StarFin. But it also means you never have to clean debris from the fins. Also, the large inside diameter means less pumping energy is required to provide greater evenness than any competitive system (Fig. 4.2).

Below is the illustration of DuoFin assemblies and connectivities produced by TrueLeaf Corporation (Figs. 4.3 and 4.4).

4.2 Overview

In general the applications come within a number of broad groups, each of which describes a property of the heat pipe. These groups are [5]:

- Separation of heat source and sink
- Temperature flattening
- Heat flux transformation
- Temperature control
- Thermal diodes and switches

The high effective thermal conductivity of a heat pipe enables heat to be transferred at high efficiency over considerable distances. In many applications where component cooling is required, it may be inconvenient or undesirable



Fig. 4.3 Finned heat pipe



Fig. 4.4 General use of finned heat pipe

thermally to dissipate the heat via a heat sink or radiator located immediately adjacent to the component. For example, heat dissipation from a high-power device within a module containing other temperature-sensitive components would be affected by using the heat pipe to connect the component to a remote heat sink located outside the module. Thermal insulation could minimize heat losses from intermediate sections of the heat pipe [5].

The second property listed above, temperature flattening, is closely related to source–sink separation. As a heat pipe, by its nature, tends toward operation at a uniform temperature, it may be used to reduce thermal gradients between unevenly heated areas of the body. The body may be the outer skin of a satellite, part of which is facing the sun, the cooler section being in shadow. Alternatively, an array of electronic components mounted on a single pipe would tend to be subjected to feedback from the heat pipe, creating temperature equalization.

The third property listed above, heat flux transformation, has attractions in reactor technology. In some manufacturer such as Thermionics Corporation, for example, the transformation of a comparatively low heat flux, as generated by radioactive isotopes, into sufficiently high heat fluxes capable of being utilized effectively in thermionic generators has been attempted.

The fourth area of application, temperature control, is best carried out using the variable conductance heat pipe. This can be used to control accurately the temperature of devices mounted on the heat pipe evaporator section, while the variable conductance heat pipe found its first major applications in many more mundane applications, ranging from temperature control in electronic equipment to ovens and furnaces [5].

As with any other device, the heat pipe must fulfill a number of criteria before it becomes fully acceptable in applications in industry. For example, in the die-casting and injection molding, the heat pipe has to:

- Be reliable and safe
- Satisfy a required performance
- Be cost-effective
- Be easy to install and remove

Obviously, each application must be studied in its own right, and the criteria vary considerably. A feature of the molding processes, for example, is the presence of high-frequency accelerations and decelerations. In these processes, therefore, heat pipes should be capable of operating when subjected to this motion, and this necessitates development work in close association with the potential users [5].

4.2.1 Cooling of Electronic Components

At present the largest application of heat pipes in terms of quantity used is the cooling of electronic components such as transistors, other semiconductor devices, and integrated circuit packages [5].

There are two possible ways of using heat pipes:

1. Mount the component directly onto the heat pipe.
2. Mount the component onto a plate into which heat pipes are inserted.

4.2.2 *Spacecraft*

Heat pipes, certainly at vapor temperatures up to 200 °C, have probably gained more from developments associated with spacecraft applications than from any other area. The variable conductance heat pipe is a prime example of this “technological fallout.” In the literature can be found details about the following types of application:

- Spacecraft temperature equalization
- Component cooling, temperature control, and radiator design
- Space nuclear power sources:
 - Moderator cooling.
 - Removal of the heat from the reactor at emitter temperature. (Each fuel rod would consist of a heat pipe with externally attached fuel.)
 - Elimination of troublesome thermal gradients along the emitter and collector.

4.2.3 *Energy Conservation*

The heat pipe, because of its effectiveness in heat transfer, is a prime candidate for applications involving the conservation of energy and has been used to advantage in heat recovery systems and energy conversion devices.

Energy conservation is becoming increasingly important as the cost of fuel rises and the reserves diminish, and the heat pipe is proving a particularly effective tool in a large number of applications associated with conservation.

4.2.4 *Heat Pipe Heat Exchanger*

There are a large number of techniques for recovering heat from exhaust air or gas streams or from hot water streams. Details and explanations about heat pipe heat exchangers can be found in this material.

Features of heat pipe heat exchangers that are attractive in industrial heat recovery applications are:

- No moving parts and no external power requirements, implying high reliability.
- Cross-contamination is totally eliminated because of a solid wall between the hot and cold fluid streams.

- Easy to clean.
- A wide variety of sizes are available, and the unit is in general compact and suitable for all.
- The heat pipe heat exchanger is fully reversible—i.e., heat can be transferred in either direction.
- Collection of condensate in the exhaust gases can be arranged, and the flexibility accruing to the use of a number of different fin spacing can permit easy cleaning if required.

The application of heat pipe heat exchangers falls into three main categories:

1. Recovery of waste heat from processes for reuse in the same process or in another, e.g., preheating of combustion air. This area of application is the most diverse and can involve a wide range of temperatures and duties.
2. Recovery of waste heat from a process to preheat air for space heating.
3. Heat recovery in air-conditioning systems, normally involving comparatively low temperatures and duties.

4.2.5 Preservation of Permafrost

One of the largest contracts for heat pipes was placed with McDonnell Douglas Corporation by Alaska Pipeline Service Company for nearly 100,000 heat pipes for the Trans-Alaska pipeline.

The function of these units is to prevent thawing of the permafrost around the pipe supports for elevated sections of the pipeline. Diameters of the heat pipes used are 5 and 7.5 cm, and lengths vary between 8 and 18 m. The system developed by McDonnell Douglas uses ammonia as the working fluid, heat from the ground being transmitted upward to a radiator located above ground level.

4.2.6 Snow Melting and Deicing

An area of application, and one which works in Japan, has been particularly intense. This has been the use of heat pipes to melt snow and prevent icing.

The operating principle of the heat pipe snow melting (or deicing) system is based upon the use of heat stored in the ground as the heat input to the evaporators of the heat pipes.

4.2.7 Heat Pipe Inserts for Thermometer Calibration

Heat pipe inserts have been developed at IKE, Stuttgart, for a variety of duties, including thermocouple calibration. The heat pipes are normally operated inside a conventional tubular furnace. The built-in enclosures provide isothermal

conditions, a necessary prerequisite for temperature sensor calibration. The isothermal working spaces can also be used for temperature-sensitive processes, such as fixed-point cell heating, crystal growing, and annealing.

4.2.8 High-Temperature Heat Pipe Furnace

Under contract from the European Space Agency, IKE developed a high-temperature heat pipe surface, for material processing in a microgravity environment in the temperature range 900–1500 °C.

Recently, also need for high-temperature thermal management is on rise, and for efficient high-temperature (heat source of 300–2000 °C) heat transfer and dissipation, thermal spreading, high-heat flux cooling, and other high-temperature applications such as advanced high-temperature reactor (AHTR) of generation four (GEN-IV), high-temperature heat pipes are in demand for the thermal solution of choice as part of a fully inherent system for heat transfer and safety factors. This demand has been established with the background of heat pipe applications around the 1960s time frame in nuclear reactor thermal management such as liquid-metal fast breeder reactor (LMFBR) research studies in the USA with project such as Clinch River project by Westinghouse Electric Corporation at their advanced reactor Davison by this author around 1970s and finally full production of this reactor in France under Phoenix-II plant.

Today, companies such as Thermacore® with their high-temperature heat pipe technology are offering the use and application of such heat pipes from the ocean floor to lunar surfaces, and they are satisfying the demand requirements with these applications. Aerospace and chemical processing such as annealing, furnace isothermally status, semiconductor material crystal growth, oil shale extraction, and wide range of high-tech electronics are also in need of such high-temperature heat pipes, where the heat dissipation and heat uniformity applications are a must circumstances.

Some of the advantages that are offered by this family of heat pipes are listed below:

- High-power heat transfer capabilities (> 25 kW)
- High-heat flux cooling capability (> 100 kW/cm²)
- High-precision temperature control and rapid temperature recovery
- Isothermality (i.e., equal or constant temperatures) at high temperature
- Uniform material crystal growth
- Thermal-to-electric energy conversion energy savings

Today's cutting-edge technologies need high-temperature heat pipes to deliver the performance their applications require.

4.2.9 Miscellaneous Heat Pipe Applications

To assist the reader in lateral thinking, a number of other applications of heat pipes are listed below:

- Heat pipe roll-bond panels for warming bathroom floors (Japan)
- Heat pipe-cooled dipstick for cooling motorbike engine oil (Japan)
- Passive cooling of remote weather station equipment (Canada)
- Cooling of drills (Russia)
- Thermal control of thermoelectric generators (USA)
- Cooling of gas turbine blades (Czech Republic)
- Thermal control of electric storage heaters (Byelorussia, UK)
- Cooling of semiautomatic welding equipment (Russia)
- Deicing fish farms and ornamental ponds (Romania)
- Heating heavy oil in large tanks (Romania)
- Cooling of soldering iron bit (UK)
- Cooling of bearings for emergency feedwater pumps (UK)
- Cooling of targets in particle accelerators (UK)
- Isothermalization of bioreactors (China)
- Cooling of snubber pins in the synthetic fiber industry (UK)
- Thermal control in electric battery dehumidifiers (USA)
- Car passenger compartment heating
- Domestic warm air heaters (USA)

As far as other applications of heat pipe are concerned, enormous field and usage can be named which are beyond the scope of this book, and readers should do their own investigations and research for further information; however, it is also worth to mention that for efficient data center cooling as part of inherent heat transfer system, computer server microprocessors, CPUs, and other concentrated heat loads can be coupled directly to cooling water (chiller) circuits while keeping water outside the cabinet, and Thermacore's Therma-Bus[®] technology is offering such solution. Therma-Bus gives you the benefits of water as a cooling medium—with much better heat transfer properties than air—without concerns about introducing water to an electronic environment. Improved thermal efficiency (reduced ΔT) also cools major data center loads without active refrigeration.

4.3 Energy-Dependent Boundary Equations

Heat pipe-cooled reactors offer operation redundancy and simplicity in the reactor startup from a frozen state. The redundancy is based on the facts that the reactor could continue to operate with one or more failed heat pipes and has no single-point failure in the removal of its thermal power.

Heat pipe has a long history of more than 40 years up to now and will have more and more application due to demand by market and technology that is available to researcher and designer of this unique thermal device.

A heat pipe-cooled nuclear reactor has been designed to provide 3.2 MW of power to an out-of-core thermionic conversion system. The reactor is a fast reactor to design to operate at a nominal heat pipe temperature of 1675 K. Each reactor fuel element consists of a hexagonal molybdenum block which is bonded along its axis to one end of molybdenum, lithium vapor, heat pipe. The block is perforated with an array of longitudinal holes which are loaded with UO_2 pellets. The heat pipe transfers heat directly to a string of six thermionic converters which are bonded along the other end of the heat pipe. An assembly of 90 such fuel elements forms a hexagonal core. The core is surrounded by a thermal radiation shield, a mal neutron absorber, and a BeO reflector containing boron-loaded control [6]. This study describes the conceptual design of a space nuclear reactor which produces 3.2 MW of power to a 500-kWe out-of-core thermionic conversion system described elsewhere. The reactor is a fast reactor and heat pipe cooled such that each fuel element of the core is directly coupled via a heat pipe to a sting of thermionic converters as shown in Fig. 4.5.

A Heat Pipe-Operated Mars Exploration Reactor (HOMER) providing between 50 and 250 kWe has been proposed for life support, operations, in-situ propellant production, scientific experiments, high-intensity lamps for plant growth, and other activities on Mars mission. It is crucial, since a solar array providing the same

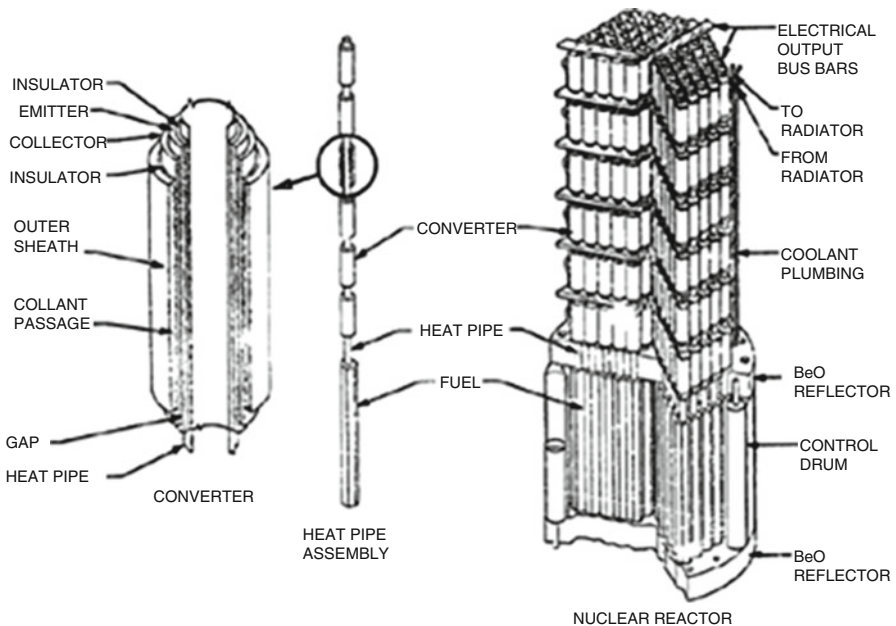


Fig. 4.5 Out of core of thermionic reactor concept [6]

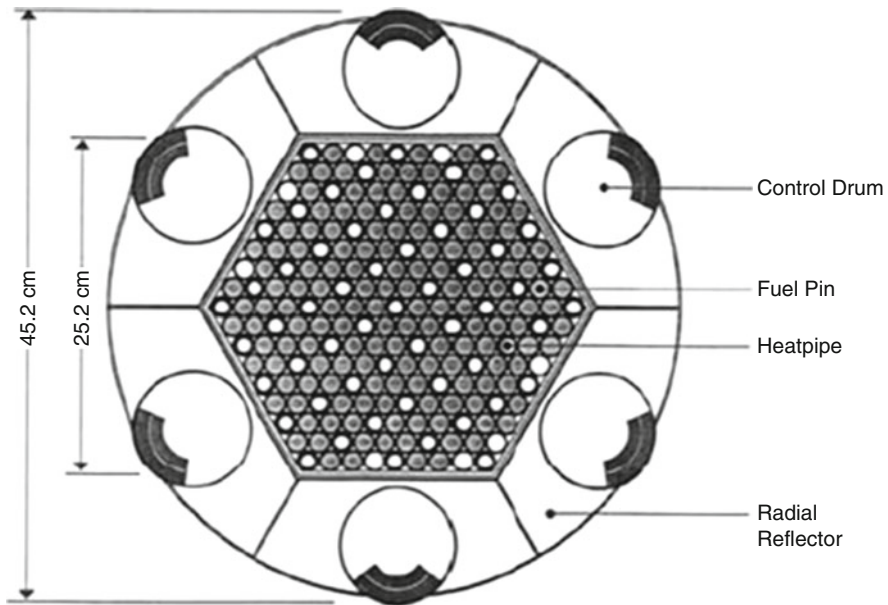


Fig. 4.6 Cross section of heat pipe space reactor of 125-kW power, showing the peripheral control drums [7]

power on Mars would require a surface area of several football fields. In addition environmental side effects such as day and night seasonal variations, geographical sunlight from the sun, and dust storm and other solar phenomena would not affect a fission reactor system. Figure 4.6 shows the core design of such a nuclear power structure which is producing 125 kW of power. The rotating drums around the circumference achieve power-level control. These consist of a neutron absorbing side and a neutron scattering and reflecting side, allowing power control without the need for terrestrial-used control rods. Moving parts are also eliminated by the use of heat pipes transforming heat for rejection by radiation to space without the uses of any mechanical moving parts such as pumps [7].

Major power conversion technique in space where the source is a nuclear heat source is depicted in Fig. 4.7 below.

Figure 4.8 also illustrates chronology of space nuclear power development.

4.4 Heat Pipe in Space

“In 1996, three Los Alamos heat pipes, prototypes of liquid-metal heat pipes to be used in advanced spacecraft, were flown and tested aboard the space shuttle Endeavor. They operated at temperatures exceeding 900 °F and performed flawlessly.” “Heat pipes work well in a zero-gravity environment.” Commercially

Fig. 4.7 Major power conversion techniques in space

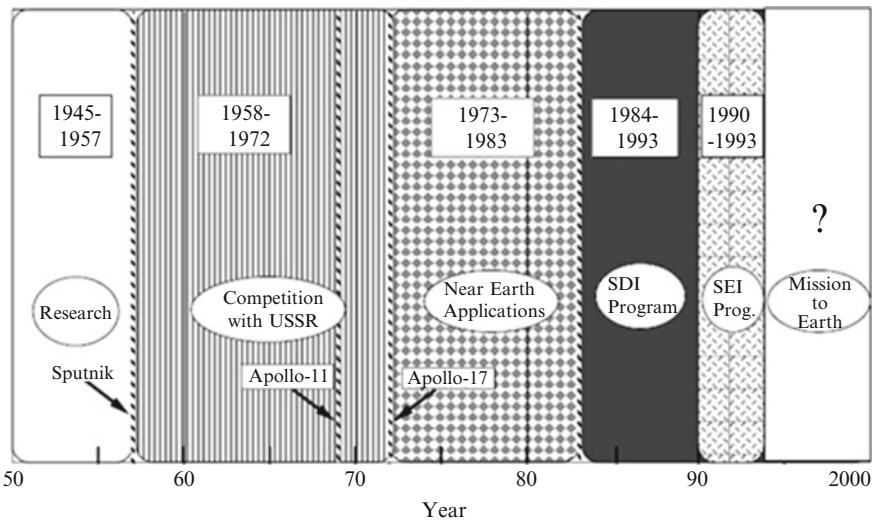
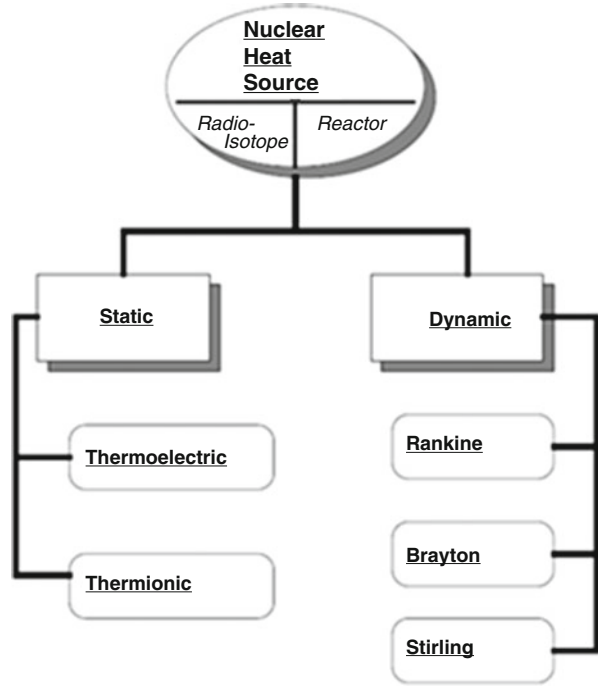


Fig. 4.8 Chronology of space nuclear power development

developed heat pipes operating near room temperature are now routinely used on geostationary communications satellites [8].

High-capacity heat pipe radiator panels have been proposed as the primary means of heat rejection for Space Station Freedom. In this system, the heat pipe would interface with the thermal bus condensers. Changes in system heat load can produce large temperature and heat load variations in individual heat pipes. Heat pipes could be required to start from an initially cold state, with heat loads temporarily exceeding their low-temperature transport capacity. The present research was motivated by the need for accurate prediction of such transient operating conditions. In this work, the cold startup of a 6.7-m long high-capacity heat pipe is investigated experimentally and analytically. A transient thermo-hydraulic model of the heat pipe was developed which allows simulation of partially primed operation. The results of cold startup tests using both constant temperature and constant heat flux evaporator boundary conditions are shown to be in good agreement with predicted transient response [9].

After a gap of several years, there is a revival of interest in the use of nuclear fission power for space missions [10].

While Russia has used over 30 fission reactors in space, the USA has flown only one—the SNAP-10A (System for Nuclear Auxiliary Power) in 1965.

Early on, from 1959 to 1973, there was a US nuclear rocket program—Nuclear Engine for Rocket Vehicle Application (NERVA)—which was focused on nuclear power replacing chemical rockets for the latter stages of launches. NERVA used graphite-core reactors heating hydrogen and expelling it through a nozzle. Some 20 engines were tested in Nevada and yielded thrust up to more than half that of the space shuttle launchers. Since then, “nuclear rockets” have been about space propulsion, not launches. The successor to NERVA is today’s nuclear thermal rocket (NTR) [11].

Another early idea was the US project Orion, which would launch a substantial spacecraft from the Earth using a series of small nuclear explosions to propel it. The project commenced in 1958 and was aborted in 1963 when the atmospheric test ban treaty made it illegal, but radioactive fallout could have been a major problem. The Orion idea is still alive as other means of generating the propulsive pulses are considered.

4.4.1 Radioisotope Systems

So far, radioisotope thermoelectric generators (**RTGs**) have been the main power source for US space work over more than 40 years, since 1961. The high decay heat of plutonium-238 (0.56 W/g) enables its use as an electricity source in the RTGs of spacecraft, satellites, navigation beacons, etc. Heat from the oxide fuel is converted to electricity through static thermoelectric elements (solid-state thermocouples), with no moving parts. RTGs are safe, reliable, and maintenance-free and can

provide heat or electricity for decades under very harsh conditions, particularly where solar power is not feasible.

So far 45 RTGs have powered 25 US space vehicles including Apollo, Pioneer, Viking, Voyager, Galileo, Ulysses, and New Horizons space missions as well as many civil and military satellites. The Cassini spacecraft carries three RTGs providing 870 W of power en route to Saturn. Voyager spacecraft which has sent back pictures of distant planets has already operated for over 20 years and is expected to send back signals powered by their RTGs for another 15–25 years. The Viking and Rover landers on Mars depended on RTG power sources, as will the Mars rovers launched in 2009.

The latest RTG is a 290-W system known as the **GPHS RTG**. The thermal power source for this system is the general-purpose heat source (GPHS). Each GPHS contains four iridium-clad Pu-238 fuel pellets, stands 5 cm tall and 10 cm square, and weighs 1.44 kg. Eighteen GPHS units power one GPHS RTG. The **multi-mission RTG** (MMRTG) will use eight GPHS units producing 2 kW which can be used to generate 100 W of electricity and is a focus of current research.

The **Stirling radioisotope generator** (SRG) is based on a 55-W electric converter powered by one GPHS unit. The hot end of the Stirling converter reaches 650 °C, and heated helium drives a free piston reciprocating in a linear alternator, heat being rejected at the cold end of the engine. The AC is then converted to 55-W DC. This Stirling engine produces about four times more electric power from the plutonium fuel than an RTG. Thus each SRG will utilize two Stirling converter units with about 500 W of thermal power supplied by two GPHS units and will deliver 100–120 W of electric power. The SRG has been extensively tested but has not yet flown.

Russia has also developed RTGs using Po-210; two are still in orbit on 1965 Cosmos navigation satellites. But it concentrated on fission reactors for space power systems. As well as RTGs, radioactive heater units (**RHUs**) are used on satellites and spacecraft to keep instruments warm enough to function efficiently. Their output is only about 1 W and they mostly use Pu-238—typically about 2.7 g of it. Dimensions are about 3 cm long and 2.5-cm diameter, weighing 40 g. Some 240 have been used so far by the USA, and two are in shutdown Russian lunar rovers on the moon. There will be eight on each of the US Mars rovers launched in 2003.

Both RTGs and RHUs are designed to survive major launch and reentry accidents intact, as is the SRG.

4.4.2 Fission Systems: Heat

Over 100 kWe, fission systems have a distinct cost advantage over RTGs. The US SNAP-10A launched in 1965 was a 45-kWt thermal nuclear fission reactor which produced 650 W using a thermoelectric converter and operated for 43 days but was shut down due to a satellite (not reactor) malfunction. It remains in orbit.

The last US space reactor initiative was a joint NASA-DOE-Defense Department program developing the SP-100 reactor—a 2-MWt fast reactor unit and thermoelectric system delivering up to 100 kWe as a multiuse power supply for orbiting missions or as a lunar/Martian surface power station. This was terminated in the early 1990s after absorbing nearly \$1 billion. It used uranium nitride fuel and was lithium cooled.

There was also a Timberwind pebble bed reactor concept under the Defense Dept Multi-Megawatt (MMW) space power program during the late 1980s, in collaboration with DOE. This had power requirements well beyond any civil space program.

Between 1967 and 1988, the former Soviet Union launched 31 low-powered fission reactors in Radar Ocean Reconnaissance Satellites (RORSATs) on Cosmos missions. They utilized **thermoelectric** converters to produce electricity, as with the RTGs. Romashka reactors were their initial nuclear power source, a fast spectrum graphite reactor with 90% enriched uranium carbide fuel operating at high temperature. Then the Bouk fast reactor produced 3 kW for up to 4 months. Later reactors, such as the one on Cosmos-954 which reentered over Canada in 1978, had U-Mo fuel rods and a layout similar to the US heat pipe reactors described below.

These were followed by the Topaz reactors with **thermionic** conversion systems, generating about 5 kWe of electricity for onboard uses. This was a US idea developed during the 1960s in Russia. In Topaz-2 each fuel pin (96% enriched UO_2) sheathed in an emitter is surrounded by a collector, and these form the 37 fuel elements which penetrate the cylindrical ZrH moderator. This in turn is surrounded by a beryllium neutron reflector with 12 rotating control drums in it. NaK coolant surrounds each fuel element.

Topaz-1 was flown in 1987 on Cosmos 1818 and 1867. It was capable of delivering power for 3–5 years for ocean surveillance. Later Topaz was aiming for 40 kWe via an international project undertaken largely in the USA from 1990. Two Topaz-2 reactors (without fuel) were sold to the USA in 1992. Budget restrictions in 1993 forced cancellation of a Nuclear Electric Propulsion Spaceflight Test Program associated with this.

4.4.3 Fission Systems: Propulsion

For spacecraft propulsion, once launched, some experience has been gained with **nuclear thermal** rocket (NTR) propulsion systems which are said to be well developed and proven. Nuclear fission heats a hydrogen propellant which is stored as liquid in cooled tanks. The hot gas (about 2500 °C) is expelled through a nozzle to give thrust (which may be augmented by injection of liquid oxygen into the supersonic hydrogen exhaust). This is more efficient than chemical reactions. Bimodal versions will run electrical systems onboard a spacecraft, including powerful radars, as well as providing propulsion. Compared with nuclear electric

plasma systems, these have much more thrust for shorter periods and can be used for launches and landings.

However, attention is now turning to **nuclear electric** systems, where nuclear reactors are a heat source for electric ion drives expelling plasma out of a nozzle to propel spacecraft already in space. Superconducting magnetic cells ionize hydrogen or xenon, heat it to extremely high temperatures (million °C), accelerate it, and expel it at very high velocity (e.g., 30 km/s) to provide thrust. Research for one version, the Variable Specific Impulse Magnetoplasma Rocket (VASIMR), draws on that for magnetically confined fusion power (tokamak) for electricity generation, but here the plasma is deliberately leaked to give thrust. The system works most efficiently at low thrust (which can be sustained), with small plasma flow, but high-thrust operation is possible. It is very efficient, with 99 % conversion of electric to kinetic energy.

4.4.4 Heat Pipe Power System

Heat pipe power system (HPS) reactors are compact fast reactors producing up to 100 kWe for about 10 years to power a spacecraft or planetary surface vehicle. They have been developed since 1994 at the Los Alamos National Laboratory as a robust and low technical risk system with an emphasis on high reliability and safety. They employ heat pipes to transfer energy from the reactor core to make electricity using Stirling or Brayton cycle converters. Energy from fission is conducted from the fuel pins to the heat pipes filled with sodium vapor which carry it to the heat exchangers and thence in hot gas to the power conversion systems to make electricity. The gas is 72 % helium and 28 % xenon.

The reactor itself contains a number of heat pipe modules with the fuel. Each module has its central heat pipe with rhenium-clad fuel sleeves arranged around it. They have the same diameter and contain 97 % enriched uranium nitride fuel, all within the cladding of the module. The modules form a compact hexagonal core. Control is by six stainless steel-clad beryllium drums each 11- or 13-cm diameter with boron carbide forming a 120° arc on each. The drums fit within the six sections of the beryllium radial neutron reflector surrounding the core and rotate to effect control, moving the boron carbide in or out. Shielding is dependent on the mission or application, but lithium hydride in stainless steel cans is the main neutron shielding.

The **SAFE-400** (Safe Affordable Fission Engine) space fission reactor is a 400-kWt HPS producing 100 kWe to power a space vehicle using two Brayton power systems—gas turbines driven directly by the hot gas from the reactor. Heat exchanger outlet temperature is 880 °C. The reactor has 127 identical heat pipe modules made of molybdenum or niobium with 1 % zirconium. Each has three fuel pins 1-cm diameter, nesting together into a compact hexagonal core 25 cm across. The fuel pins are 70 cm long (fuelled length 56 cm); the total heat pipe length is 145 cm, extending 75 cm above the core, where they are coupled with the heat

exchangers. The core with reflector has a 51-cm diameter. The mass of the core is about 512 kg and each heat exchanger is 72 kg. SAFE has also been tested with an electric ion drive.

A smaller version of this kind of reactor is the **HOMER-15**—the Heat Pipe-Operated Mars Exploration Reactor. It is a 15-kW thermal unit similar to the larger SAFE model and stands 2.4 m tall including its heat exchanger and 3-kWe Stirling engine (see above). It operates at only 600 °C and is therefore able to use stainless steel for fuel pins and heat pipes, which are 1.6-cm diameter. It has 19 sodium heat pipe modules with 102 fuel pins bonded to them, 4 or 6 per pipe, and holding a total of 72 kg of fuel. The heat pipes are 106 cm long and the fuel height is 36 cm. The core is hexagonal (18 cm across) with six BeO pins in the corners. The total mass of reactor system is 214 kg, and the diameter is 41 cm.

4.4.5 Space Reactor Power Systems

In the 1980s the French ERATO program considered three 20-kWe turboelectric power systems for space. All used a Brayton cycle converter with a helium–xenon mix as working fluid. The first system was a sodium-cooled UO₂-fuelled fast reactor operating at 670 °C, the second a high-temperature gas-cooled reactor (thermal or epithermal neutron spectrum) working at 840 °C, and the third a lithium-cooled UN-fuelled fast reactor working at 1150 °C (Table 4.1).

4.4.6 Project Prometheus 2003

In 2002 NASA announced its Nuclear Systems Initiative for space projects, and in 2003 this was renamed Project Prometheus and given increased funding. Its purpose is to enable a major step change in the capability of space missions. Nuclear-powered space travel will be much faster than is now possible and will enable manned missions to Mars.

One part of Prometheus, which is a NASA project with substantial involvement by DOE in the nuclear area, is to develop the Multi-Mission Thermoelectric Generator and the Stirling radioisotope generator described in the RTG.

A more radical objective of Prometheus is to produce a space fission reactor system such as those described above for both power and propulsion that is safe to launch and which will operate for many years. This will have much greater power than RTGs. The power of 100 kW is envisaged for a nuclear electric propulsion system driven by plasma.

The FY 2004 budget proposal was \$279 million, with \$3 billion to be spent over 5 years. This consists of \$186 million (\$1 billion over 5 years) building on last year's allocation plus \$93 million (\$2 billion over 5 years) toward a first flight

Table 4.1 Space reactor power systems [11]

	SNAP-10, USA	SP-100, USA	Romashka, Russia	Bouk, Russia	Topaz-1, Russia	Topaz-2, Russia- USA	SAFE-400, USA
Dates	1965	1992	1967	1977	1987	1992	2007
kWt	45.5	2000	40	<100	150	135	400
kWe	0.65	100	0.8	<5	5-10	6	100
Converter	T ^{electric}	T ^{electric}	T ^{electric}	T ^{electric}	T ^{ionic}	T ^{ionic}	T ^{electric}
Fuel	U-ZrH _x	UN	UC ₂	U-Mo	UO ₂	UO ₂	UN
Reactor mass (kg)	435	5422	455	<390	320	1061	512
Neutron spectrum	Thermal	Fast	Fast	Fast	Thermal	Thermal/epithermal	Fast
Control	Be	Be	Be	Be	Be	Be	Be
Coolant	NaK	Li	None	NaK	NaK	NaK	Na
Core temp. (°C), max	585	1377	1900	?	1600	1900?	1020

mission to Jupiter—the Jupiter Icy Moon Orbiter, expected to launch in 2017 and explore for a decade. Project Prometheus received \$430 million in 2001 budget.

In 2003 NASA's Project Prometheus successfully tested a high-power electric propulsion (HiPEP) ion engine. This operates by ionizing xenon with microwaves. At the rear of the engine is a pair of rectangular metal grids that are charged with 6000 V of electric potential. The force of this electric field exerts a strong electrostatic pull on the xenon ions, accelerating them and producing the thrust that propels the spacecraft. The test was at up to 12 kW, though twice that is envisaged. The thruster is designed for a 7–10-year lifetime with high fuel efficiency and to be powered by a small nuclear reactor.

(On July 14, 2006, at their facility in Racine, WI—Modine Manufacturing Company NYSE: MOD)—a world leader in designing and developing heating and cooling solutions for a diversified group of markets including electronic cooling, automotive, truck, heavy duty and industrial announced that it has delivered, through its wholly owned subsidiary Thermacore International, Inc., high-temperature titanium heat pipes to NASA Glenn Research Center in Cleveland, Ohio. These heat pipes are evaluation prototypes in support of NASA's effort to develop radiator panels for rejecting heat from the power generation systems for long duration space and planetary base missions and could be used on trips to the moon, Jupiter, and points further in space.

The Thermacore heat pipes are intended for use at temperatures up to 250 °C. The delivered prototypes, which are 12.7 mm in diameter and 1.15 m long, are made from titanium and use water as the internal working fluid. These devices, capable of transporting over 500 W, are produced at Thermacore's research and development facilities in Lancaster, Pennsylvania. NASA is pursuing the development of power generation systems capable of producing tens of kilowatts of electrical power for future missions to Jupiter and beyond. The Brayton cycle is the leading power conversion system being evaluated by NASA. Just like all electric generating systems, the unconverted waste heat must be rejected. In this situation, it will be done with large radiator panels that contain heat pipes operating in the temperature range of 20–250 °C. To minimize weight, these heat pipes were constructed from titanium. Heat pipes have been widely accepted in military applications and have high reliability standards.

Spacecraft applications to date have been for heat pipes operating between 200 and 350 K. Consequently, a working fluid that's freezing and boiling points that encompasses this temperature range and has a high latent heat, a low viscosity, and high heat transport capability must be selected. Recent research study by Goddard Space Flight Center (GSFC) has selected ammonia as an appropriate working fluid whose fluid properties meet these criteria. However, for safety reasons, the toxicity of ammonia precludes its use in manned environments such as the shuttle cabin [7]. GSFC has selected aluminum alloys, such as 6061 and 6063, for the container material of the heat pipe because of their long-term compatibility with ammonia (see Table 1.2); heritage; ability to have an extruded axial groove wick structure; ease of fabrication, shaping, and configuring; good thermal compatibility with aluminum radiators and heat sinks; and weldability characteristics.

Mahefkey and Lundberg's [12] paper summarizes the envisioned, future usage of high- and low-temperature heat pipes in advanced Air Force spacecraft. Thermal control requirements for a variety of communications, surveillance, and space defense missions are forecast. Thermal design constraints implied by survivability to potential weapon's effects are outlined. Applications of heat pipes to meet potential low- and high-power spacecraft mission requirements and envisioned design constraints are suggested. A brief summary of past Air Force-sponsored heat pipe development efforts is presented and directions for future development outlined, including those applicable to advanced photovoltaic and nuclear power subsystem applications of heat pipes.

4.5 Space Shuttle Orbiter Heat Pipe Applications

Grumman under contract by NASA launched an investigation that was made to formulate and evaluate heat pipe applications for the space shuttle orbiter. Of the 27 specific applications which were identified, a joint NASA/Grumman evaluation resulted in the selection of five of the most promising ones for prototype development [1].

The primary objectives of this study were to:

- Identify potential heat pipe applications for the space shuttle orbiter
- Evaluate the applications and recommend the most promising ones for further development
- Perform detailed design and analysis on the recommended applications
- Prepare design drawings with necessary material specifications to permit fabrication of prototype hardware for at least three of the recommended applications
- Prepare test plans for performance verification of the three or more prototype applications

The secondary objectives were to:

- Evaluate a general design concept employing "off-the-shelf" heat pipe components to be used in minimizing costs, in the event of an extensive commitment to heat pipe systems
- Create study plans for the development of prototype heat pipe hardware for space station, space shuttle, and common shuttle/station applications (including space radiators)

The formulation process is described in a report prepared by Grumman [1], along with the applications which evolved. The bulk of the discussion deals with the "top" five applications, namely:

- Heat pipe-augmented cold rail
- Avionics heat pipe circuit
- Heat pipe/phase change material modular sink

- Air-to-heat pipe heat exchanger
- Heat pipe radiator for compartment temperature control

The philosophy, physical design details, and performance data are presented for each concept along with a comparison to the baseline design where applicable. A sixth application, heat pipe space radiator for waste heat rejection, was also recommended for prototype development—but its development would be more efficiently handled under a separate contract.

Each of the shuttle subsystems, i.e., structure, propulsion, avionics, power and environmental control, and life support, was reviewed in detail, with possible heat pipe application areas indicated by the heat sources and sinks located throughout the shuttle vehicle. Twenty-seven initial applications were defined, from which 11 were chosen for further design and analysis. The procedure used to evaluate these 11 was based on a better than/worse than comparison with the baseline system for each of six criteria: temperature gradient, capacity margin, power requirements, control requirement, weight, and safety. Because of the lack of factual data, parameters such as cost, maintainability, reliability, durability, and development risk were only evaluated on a secondary basis.

The 11 prime contenders are briefly summarized below:

1. Isothermalization of the leading edge of the wing to lower peak temperature and to increase mission life
2. Wheel well radiators to maintain minimum temperatures sufficient for tire survival by supplying waste heat
3. A design similar to (2) for the air-breathing engine compartments
4. A HP avionics circuit to collect and transfer the thermal load from electronic boxes to the heat transfer system
5. Modular heat sinks for cooling remotely located components without the need for long extensions of the pumped coolant system
6. An adaptation of (5) for the flight/voice recorders located in the tail
7. A modular heat pipe heat exchanger system for adapting air-cooled commercial and military avionics to the shuttle
8. An all-HP radiator system for waste heat rejection
9. A modified version of (8) incorporating a pumped fluid loop header
10. A HP-augmented cold rail capable of absorbing an order of magnitude greater local power density when compared to a simple fluid cold rail
11. A high-temperature heat rejection system for the fuel cells

The preliminary design studies of these prime contenders included a description of the overall system, supporting drawings showing the heat pipe systems and shuttle interfaces, and heat pipe design details including capacity requirements, working fluids, wick design, pipe lengths, and diameters (see Fig. 4.9) shuttle landing.

Further evaluation resulted in 6 of the 11 concepts being selected for detailed design and analysis. These six are noted in Table 4.2, which summarizes the results of the evaluation process.

More details can be found in Alario and Prager's report [1].



Fig. 4.9 The space shuttle Discovery Lands on Kennedy Space Center's Runway 33 Tuesday, April 20, 2010, in Cape Canaveral, Florida

4.6 Heat Pipe in Electronics

All electronic components, from microprocessors to high-end power converters, generate heat, and rejection of this heat is necessary for their optimum and reliable operation. As electronic design allows higher throughput in smaller packages, dissipating the heat load becomes a critical design factor. Many of today's electronic devices require cooling beyond the capability of standard metallic heat sinks. The heat pipe is meeting this need and is rapidly becoming a mainstream thermal management tool [13].

Heat pipes have been commercially available since the mid-1960s. Only in the past few years, however, has the electronic industry embraced heat pipes as reliable, cost-effective solutions for high-end cooling applications. The purpose of this section is to explain basic heat pipe operation, to review key heat pipe design issues, and to discuss current heat pipe electronic cooling applications [14].

Perhaps the best way to demonstrate the heat pipe application to electronic cooling is to present a few of the more common examples. Currently, one of the highest volume applications for heat pipes is cooling the Pentium processors in notebook computers. Due to the limited space and power available in notebook computers, heat pipes are ideally suited for cooling the high-power chips [14].

Fan-assisted heat sinks require electrical power and reduce battery life. Standard metallic heat sinks capable of dissipating the heat load are too large to be incorporated into the notebook package. Heat pipes, on the other hand, offer a high-efficiency, passive, compact heat transfer solution. Three- or 4-mm diameter heat pipes can effectively remove the high heat flux from the processor. The heat pipe spreads the heat load over a relatively large area heat sink, where the heat flux is so low that it can be effectively dissipated through the notebook case to ambient

Table 4.2 Shuttle heat pipe application evaluation [1]

Original 27 candidates	11 Prelim. design studies	Six detail designs
1. TPS leading edge		
2. Landing gear		
3. Avionics HP circuit		
4. Modular sinks		
5. ATR equipment		
6. Flight and voice recorders		
7. HP radiator W/HP header		
8. HP radiator with integral HP/fluid header	TPS leading edge	
9. ECS cold rail	Landing gear	
10. HP radiator for fuel cell	Avionics HP circuit	
11. Air-breathing engine compartment	Modular sinks	
	ATR equipment	HP radiator for compartments
12. OMS LH ₂ boil-off	Flight and voice recorders	HP radiator, waste heat ^a
13. High-intensity lights	HP radiator with HP header	HP circuit, avionics ^b
14. Battery	HP radiator with integral HP/fluid header	HP-augmented cold rail ^b
15. Tracking radar		Modular sink (voice rec) ^b
16. Fluid evaporator	HP-augmented cold rail (high capacity)	Air-cooled equip rack
17. Fuselage TPS, interference heating		
	HP radiator for fuel cell	
18. TPS panel	Air-breathing engine compartment	
19. Control surface pivots		
20. OMS LO ₂ boil-off		
21. Main LO ₂ tank boil-off		
22. C-band directional antenna		
23. Electrical wiring		
24. Hydraulic actuators		
25. APU		
26. LO ₂ natural recirculating system		
27. Water chiller		

^aSelected for study under separate contract

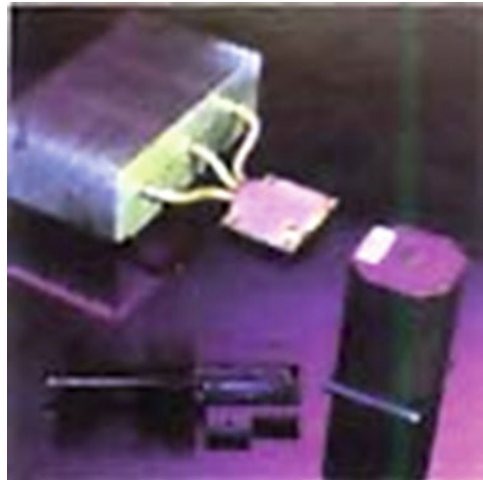
^bSelected for prototype fab dwgs and test plans

air. The heat sink can be the existing components of the notebook, from electromagnetic interference (EMI) shielding under the key pad to metal structural components [14]. Various configurations of notebook heat pipe heat sinks are shown in Fig. 4.10.

Fig. 4.10 Typical notebook heat pipe heat sink [15]



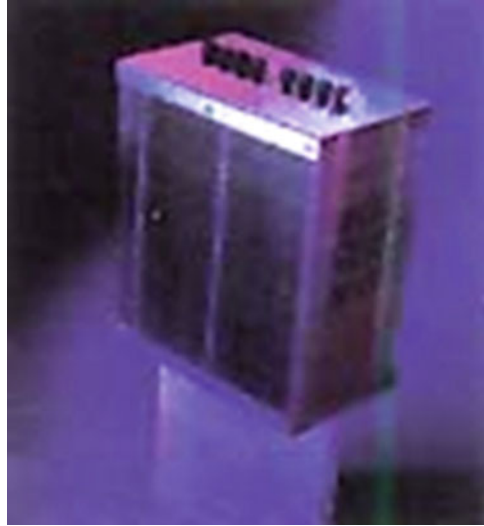
Fig. 4.11 High-end CPU heat pipe heat sink [15]



Typical thermal resistances for these applications at 6–8-W heat loads are 4–6 °C/W. High-power mainframe, mini-mainframe, server and workstation chips may also employ heat pipe heat sinks. High-end chips dissipating up to 100 W are outside the capabilities of conventional heat sinks. Heat pipes are used to transfer heat from the chip to a fin stack large enough to do the convection of the heat to the supplied airstream. The heat pipe isothermalizes the fins eliminating the large conductive losses associated with standard sinks. The heat pipe heat sinks, shown in Fig. 4.11, dissipate loads in the 75–100-W range with resistances from 0.2 to 0.4 °C/W, depending on the available airflow [15].

In addition, other high-power electronics, including silicon-controlled rectifiers (SCRs), insulated-gate bipolar transistors (IGBTs), and thyristors, often utilize heat pipe heat sinks. Heat pipe heat sinks similar to the one shown in Fig. 4.12 are

Fig. 4.12 High-power IGBT heat pipe heat sink [15]



capable of cooling several devices with total heat loads up to 5 kW. These heat sinks are also available in an electrically isolated version where the fin stack can be at ground potential with the evaporator operating at the device potentials of up to 10 kV. Typical thermal resistances for the high-power heat sinks range from 0.05 to 0.1 °C/W. Again, the resistance is predominately controlled by the available fin volume and airflow [15].

4.7 Heat Pipe in Defense and Avionics

Dissipating heat reliably and quickly, for satellite thermal control, is a challenge that grows tougher all the time. Space electronics are steadily becoming more miniaturized, more complex, and more powerful. Increased packaging densities are also limiting the volume available for thermal management systems. The end result, the performance, flexibility, and versatility of thermal management systems, must improve to meet the growing challenge. Plus, “low-maintenance” systems aren’t good enough in space; thermal control must be “no maintenance.” But proven heat pipe technology developed by different companies and designer can meet all these challenges. With a wide range of advanced solid conduction, heat pipe and loop heat pipe technologies are available to meet the need for high performance, system efficiency, and low mass with no moving parts to fail. Companies like Thermacore’s advanced solid conduction solutions, heat pipes, and loop heat pipes are maintenance-free, making them ideal for satellite, military, and aerospace applications.

Military equipment thermal management solutions from Thermacore stand up to the toughest challenges in the world—from submarine electronic cooling and radar electronics in harsh environments to satellite thermal control management in space.



Thermal technology design, development, and manufacturing have helped deliver thousands of solutions that operate in mission-critical applications in the harshest environmental conditions. Thermacore's advanced thermal management technologies are a major source of superior solutions to allow our military equipment customers to overcome the size, weight, and power (SWaP) constraints in current and future generation electronic equipment.

4.7.1 On the Ground

To get a high-performance, lightweight, and compact cooling solution for next-generation transmit/receive modules used in military radar systems, prime contractors throughout the world turn to Thermacore for high-performance cold plate technology. These Thermacore solutions are based on advanced solid conduction (k-Core[®])-embedded heat pipe technology, vapor chamber heat pipe technology, and vacuum-brazed liquid cooling cold plates. These thermal solutions provide high-performance, high-efficiency heat transfer in this space- and weight-constrained application, with heat pipes and k-Core giving cold plates the weight of aluminum with an effective thermal conductivity more than four times that of copper.



Cooling solutions for military ground-based radars use our experience in sealed enclosure cooling technology, providing reliable performance in extreme temperatures, rain, sand, and snow. That includes reliable electronic cooling for communications and target acquisition in tanks and Humvees, where displays and electronics—as well as thermal solutions themselves—face sweltering heat, high humidity, shock, and vibration.

Military electronic cabinet cooling is provided by compact, rugged, and versatile cross flow heat exchangers that resist everything from shock and wind to microorganisms. These military cooling solutions provide superior performance and take advantage of our experience in power electronic heat management.

4.7.2 *On the Sea*

Highly efficient radar electronics and power supply cooling for next-generation naval destroyer radar systems are an area of expertise for Thermacore heat pipes and cold plates. These technologies are specially designed for high thermal performance, low mass, and rugged conditions, including thermal cycling between -40 and 75 °C.



Navy antenna cooling is the mission of the heat pipe assemblies used to reduce heat load on USG-2 naval planar array antenna assemblies (PAAAs). Able to absorb heavy shocks from weather, thermal cycling, and impact, these superior Thermacore liquid cooling systems provide peace of mind for Navy warships all over the world.

Under the sea, nuclear submarine power conversion electronic cooling is provided by embedded heat pipe assemblies and vapor chamber assemblies from Thermacore. Thermacore thermal solutions are also used to protect the power subsystems supporting naval radar platforms. Thermacore heat exchangers are in action cooling nuclear reactor control electronics as well.

4.7.3 *In the Air*

Thermacore patented encapsulated graphite k-Core heat pipes are cooling critical electronic components on the new F-35 Joint Strike Fighter (JSF), providing improved thermal performance over traditional graphite conduction solutions at lower cost.

Loop heat pipes from Thermacore provide highly reliable electro-optics cooling for target acquisition systems, remote wing electronics, and navigational avionics onboard the F-16 fighter aircraft, standing up to extreme temperatures and up to 9 g of force. It's a performance typical of our thermal solutions for aerospace and avionics.



Superior thermal protection of radar systems for US Coast Guard helicopters is the job of Thermacore remote dissipation heat pipe assemblies, combining heat pipes with fins for better overall thermal performance. For thermal management of aircraft electronics under the most severely cold conditions (down to -70°C), designers turn to Thermacore heat pipe assembly solutions to maintain temperatures close to the optimum for avionics operation.

4.7.4 *In Space*

For satellite thermal control and heat transfer, advanced solid conduction, axially grooved low-temperature heat pipes, and loop heat pipe from Thermacore offer the widest variety of high-performance thermal solutions for space applications. Thermacore's k-Core space radiator panels and doublers provide lightweight, high-performance heat spreading. Thermacore's axially grooved low-temperature heat pipes, using ammonia and ethane as working fluids, can be embedded into radiator panels for improving heat spreading within radiator panels over extended lengths. In addition, loop heat pipes from Thermacore offer high total power dissipation ($>2000\text{ W}$) and lightweight (a deployable radiator panel with a weight of $<55\text{ lb}$). Deployable, honeycomb-bonded panel construction enables reliable

performance in the most demanding environment of all—where traditional maintenance is impossible.



4.8 Heat Pipe as Heat Exchanger

The most commonly known and used thermal devices is the heat exchanger, which transfers heat from a hot fluid to a cold one. Heat exchanger is used in a variety of thermal devices ranging from the modern power generation such as nuclear reactor system to domestic heating and air conditioning. There are three basic designs for heat exchangers, as shown in Fig. 4.13, and they are as follows:

1. Parallel flow
2. Counterflow
3. Cross-flow

The effectiveness of heat exchangers ϵ is defined as follow:

$$\epsilon = \frac{Q}{C_{\min}(T_{h_{in}} - T_{c_{in}})} \quad (\text{Eq.4.1})$$

where

Q = the heat transfer rate

C_{\min} = the heat capacity rate defined as the product of specific heat and the mass flow rate of the hot or cold fluid whichever is smaller

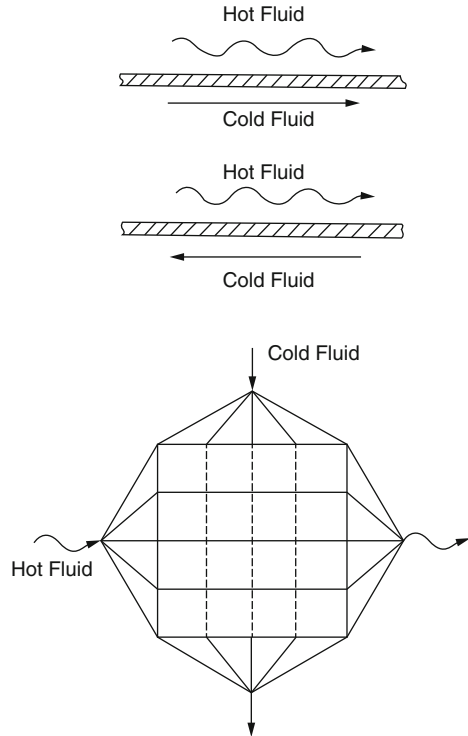
$T_{h_{in}}$ = inlet temperature of the hot fluid

$T_{c_{in}}$ = inlet temperature of the cold fluid

It can be shown theoretically that other things being equal the counterflow heat exchanger effectiveness than either the parallel-flow or cross flow heat exchanger.

Because heat pipes can operate almost near an isothermal mode, i. e., with a very small temperature drop, the effectiveness of heat pipe heat exchanger can be very high. The main heat-flow resistance for a heat pipe heat exchanger is at the interfaces of the heat pipe exterior surfaces and the hot and cold fluids. In order to have reduction in heat-flow resistances, external fins may be provided at the

Fig. 4.13 Types of heat exchange [16]



evaporator and condenser sections of the heat pipe. Excellent heat transfer from the hot fluid to the cold fluid can then be obtained because both the hot and the cold fluids are passed through the coils of finned tubes and the heat is transferred from the hot fluid side to the cold fluid side by the “isothermal” heat pipes. A counterflow heat exchangers using heat pipes is shown in Fig. 4.14 and easily can designed and constructed without any difficulties.

Heat pipe heat exchangers can also take advantage of staggering the finned tubes. Figure 4.15 illustrates a typical arrangement of heat pipe tubes.

A large variety of heat pipe heat exchangers are commercially available at the present time. Technical data provided by manufacturers for their product usually include the thermal effectiveness and the operating temperature ranges [16]. The quoted effectiveness is almost invariably based upon operation in the counterflow mode, and designer of heat pipe heat exchangers should take advantage of the counterflow between the hot and cold fluids.

Design or sizing of a heat pipe heat exchanger involves both the design of the heat pipe and the heat exchanger as a heat transfer device such that it will meet the specified heat duty, pressure drops on both sides, and the heat pipe will work properly in the operating design range [15].

The heat pipe heat exchanger (HPHE) design methodology is illustrated in Fig. 4.16. This design procedure may be characterized by a *case study* method.

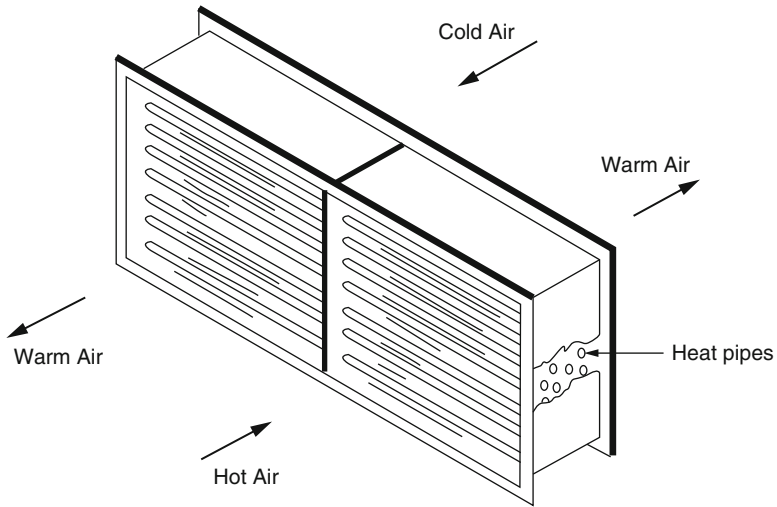
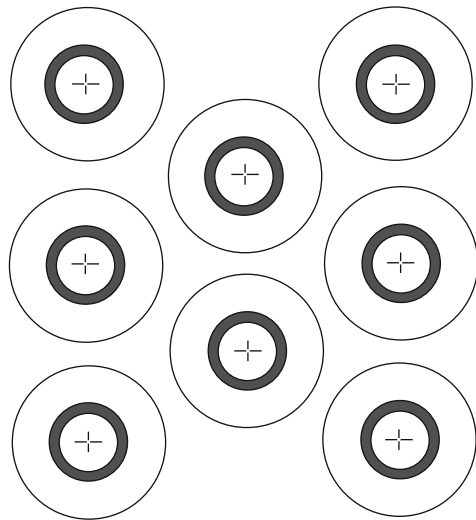


Fig. 4.14 Schematic of a counterflow heat pipe heat exchanger [16]

Fig. 4.15 Illustration of a staging heat pipe tube [16]



It is a complex procedure because of the many qualitative judgments (in addition to the quantitative calculations) that must be introduced [15].

The general characteristic of heat pipe heat exchangers can be illustrated by numerical examples. This may help engineers at the preliminary stage of their design, although the final design should be made after the manufacturer’s data are consulted and analyses are made.

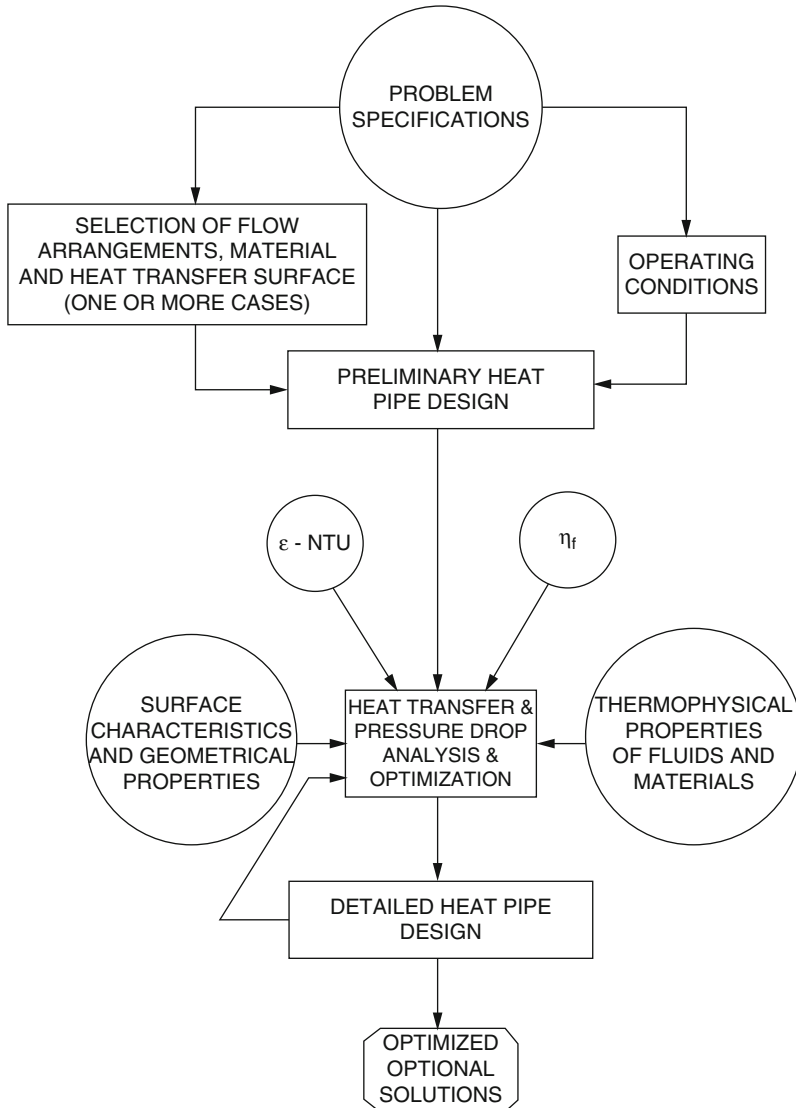


Fig. 4.16 Overall heat pipe heat exchanger thermal and hydraulic design methodology [15]

4.9 Heat Pipe in Residential Building

There so many homes built around the world, and heating, air-conditioning, and hot water supply of these homes are a challenge on annual energy consumption everywhere in the world. A typical home in the mid-region of the USA uses about

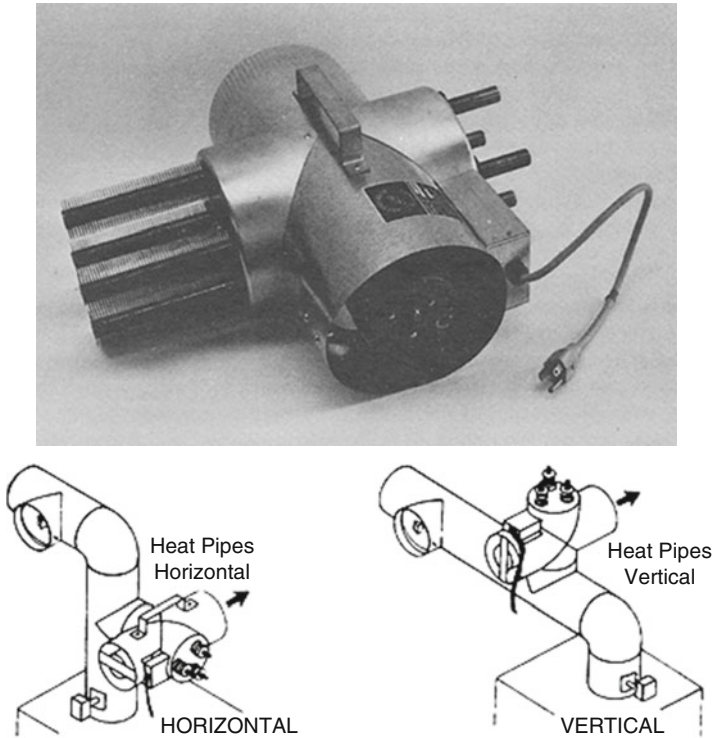


Fig. 4.17 Heat pipe heater for reclaiming heat in flue gas from residential furnaces [16]

200 million BTU (2.1×10^{11} J) per heating season. Hence, there is a great incentive for home energy conservation. Several devices using heat pipes are developed, e.g., heat recovery from furnace flue gas, waste hot water, and fireplace. The temperature of flue gas at the domestic furnace for space heating is about 500°F (533 K), which is about 12% of the energy available from the fuel. In order to reclaim this waste heat, a device using a heat pipe has been developed by companies such as Isothermics, Inc., that is presented in Fig. 4.17 and consists of a heat pipe heater that attaches to the flue pipe above the furnace. A heat made of copper and using water as working fluid are highly recommended for this application. The device uses the gas flue as a heat source; this heat then can be used to heat part or all of the home basement, recreation room, workshop, or laundry room; or a dual duct can be attached to the unit to carry the heat to otherwise chilly spaces inside the house [16].

Houses that have forced air heating can also duct the reclaimed heat to a nearby cold-air return duct in the basement so as to heat up the cold air that comes back to the furnace from the rest of the house, which in return translates to less fuel will be required to heat this air to required temperature for recirculation.

4.10 Heat Pipe Applications in Thermal Energy Storage Systems

Heat pipes and other thermal management systems for renewable energy applications such as in solar, wind, and geothermal can help you design more efficient, more cost-effective, and greener systems.

In concentrated solar power (CSP) applications, uniform heat distribution is crucial for electric power generation efficiency in applications such as Stirling engines and solar panels. Thermacore heat pipe technology, relying on the laws of thermodynamics to spread heat passively, makes uniform heat distribution possible. This eliminates problems such as nonuniform heat fluxes and associated hot spots where two solar mirrors overlap in CSP systems. In addition, Thermacore technologies remove waste heat from solar cells in photovoltaics (PV) solar systems to lower solar cell temperatures and improve PV conversion efficiencies.



For wind power generation thermal solution, heat pipe assemblies could be ideal for cooling power generation subsystem in remote areas where maintenance is difficult.

However due to the enormous increase in the global energy demand and possible depletion of conventional energy resources such as fossil fuels, renewable energy resources turned out to be promising options to supply clean and low-cost energy. The major issue with these sources is their intermittent nature, which causes a gap between energy demand and supply. Most of the studies about renewable energies are focused to improve their efficiency to make them appropriate replace for conventional techniques. Thermal energy storage units can be integrated to renewable power generation systems to alleviate the mentioned temporal mismatch between the energy supply and demand providing power in a dispatchable manner. Employing a phase change medium (PCM) to store energy and taking the advantage of latent heat of fusion increase the energy storage density and reduce the size and cost of the system in comparison to using sensible energy storage. However, the low thermal conductivity of commercially available phase change materials has limited their performance decreasing the heat transfer rate between heat source and PCM and therefore prolongs the melting or solidification processes. Implementing a

passive heat transfer device such as heat pipe is required to enhance the heat transfer rate between the heat source and the phase change material, which increases the efficiency of the system. In this section, we will discuss the application of heat pipes in latent heat thermal energy storage systems with either high or low operating temperatures. For low-temperature applications like domestic hot water production, organic and inorganic heat storage materials, including paraffin, fatty acids, and inorganic salt hydrates with the temperature range of 0–220 °C, can be used as storage media. For high-temperature latent heat thermal energy storage systems which can be integrated in concentrated solar power (CSP) systems, phase change materials are mostly inorganic salts or their eutectic mixtures with operating temperature up to 800 °C. Each of these applications requires specific heat pipe configuration and operating conditions, which will be discussed in the following subsections.

4.10.1 Energy Storage Methods

Design and development of cost-effective energy storage techniques play an important role in achieving levelized cost of energy (LCOE) target of DOE SunShot. Different forms of energy can be stored and some aspect of it are summarized here as following subsections.

4.10.1.1 Electrical Storage

Pumped hydropower storage (PHPS), compressed air energy storage (CAES), and flywheels are different methods in terms of mechanical energy storage. For large-scale utility energy storage, PHP and CAE can be employed, while flywheels are more suitable for intermediate storage [17].

4.10.1.2 Thermal Energy Storage

Thermal energy storage (TES) methods are described as the temporary storage of thermal energy, which occurs at high or low temperatures. Thermal energy storage can be obtained by cooling, heating, melting, solidifying, or vaporizing a material in which the energy becomes available as heat by reversing the process. Using this method provides the opportunity to mitigate environmental impacts and results in more efficient and clean energy systems. The TES methods are classified into three main groups: sensible, latent, and thermochemical.

4.10.1.2.1 Sensible Thermal Energy Storage

In sensible thermal energy storage systems (STESs), the energy is stored as a temperature change of the storage medium. The storage medium can be solid as soil, rock, or liquid like water. The amount of stored heat is the function of the mass of storage material and its specific heat as well as the temperature change as follows:

$$Q = \int_{T_i}^{T_f} mC_p dT \quad (\text{Eq.4.2})$$

where Q is the amount of stored energy, m is the mass of storage medium, and C_p is the specific heat, while T_i and T_f are the initial and final temperature, respectively.

However, if the temperature range changes for the specific heat C_p at constant pressure are infinitesimal, then the simplified form of Eq. (4.2) can be presented as:

$$Q = mC_{pa}(T_f - T_i) \quad (\text{Eq.4.3})$$

In this equation parameter C_{pa} is the average specific heat capacity at constant pressure between the initial T_i and final T_f temperatures, respectively.

Although STESs are possessing simpler design, they disadvantaged by their bigger size and not being capable of working in constant temperature in comparison to latent heat thermal energy storage [18].

4.10.1.2.2 Latent Heat Thermal Energy Storage

Latent heat thermal energy storage (LHTES) systems work based on absorbing and releasing heat as the storage material undergoes a phase change process. In solid–liquid LHTES, the storage capacity can be calculated as:

$$Q = \int_{T_i}^{T_m} mC_p dT + ma_m \Delta H_m + \int_{T_m}^{T_f} mC_p dT \quad (\text{Eq.4.4})$$

where in Eq. (4.4), the symbol of T_m is the melting temperature of the storage medium, a_m is the fraction melted, and ΔH_m is the heat of melting per unit mass.

LHTES benefits from the higher storage density and isothermal operation.

Energy storage media used in latent heat thermal energy storage systems are referred as phase change materials (PCMs). The phase transition can occur from solid to gas, solid to liquid, and liquid to gas [18].

4.10.1.2.3 Thermochemical

The last approach for thermal storage is by means of thermochemical reactions. This storage method has the capability of long-term storage, but its technical complexity and high costs are not compatible with the cost-effective goal [5].

Among the abovementioned thermal heat storage techniques, LHTEs is the most popular since it provides high energy storage density and has the capability of storing energy at constant temperature corresponding to the phase transition temperature of the PCM.

As it was mentioned, phase change in latent heat thermal energy storage systems can be from solid to solid, solid to liquid, and liquid to gas. Solid–solid phase change occurs when a material is transformed from one crystalline to another. These transitions are easy to handle and cost-effective, the lack of liquid material eliminates the risk of leakage, and hence there is no need for encapsulation. The main drawback of these systems is the small heat of fusion. Solid or liquid to gas transitions have high latent heat of transition, but the large volume changes associated with them make the process complex and almost impossible. The smaller volume changes occurring in solid to liquid phase change make them economically and practically attractive as materials for TES systems despite their smaller heat of phase transition [18].

4.10.2 Latent Heat Thermal Storage Materials

The ideal PCM should have the following characteristics:

Thermal properties

- Melting temperature in the desired operating range
- High latent heat of fusion per unit volume
- High specific heat
- High thermal conductivity of both phases

Physical properties

- Small volume change during phase transformation process
- Low vapor pressure at the operating temperature
- Congruent melting of the PCM
- High density

Kinetic properties

- No supercooling
- A high nucleation rate
- An adequate rate of crystallization

Chemical properties

- Long-term chemical stability
- A completely reversible freeze–melt cycle
- Compatibility with the construction materials
- No corrosion influence on the construction materials
- Nontoxic, nonflammable, and nonexplosive to ensure safety

The last important feature is that the large quantity of the PCM should be available at low cost [5].

4.10.3 PCM Classification

A large number of PCMs are available, which are classified and presented in Table 4.3 below.

4.10.3.1 PCMs for Different Thermal Storage Applications

As it can be seen in Table 4.3, the PCMs with the application for thermal energy storages are organic compounds, inorganic salts, and their eutectics. Organic compounds used for PCM are generally paraffin waxes, esters, acids, and alcohols. The salt hydrates, eutectics of inorganic salts, and metals and their eutectics are categorized as inorganic. Those PCMs belonging to organic group usually have low melting points and can only be used for low-temperature applications such as domestic hot water production, direct or heat-pump-assisted space heating, greenhouse heating, solar cooling, etc. [20]. For high-temperature thermal storage, molten salts can be implemented as phase change materials. High-temperature PCM can be used in solar power plants or industrial waste heat recovery systems [21]. Metallic materials have not been popular as other PCMs due to their elevated weight. However, they are good candidates if volume is a priority. The most notable

Table 4.3 Phase change material classification diagram [19]

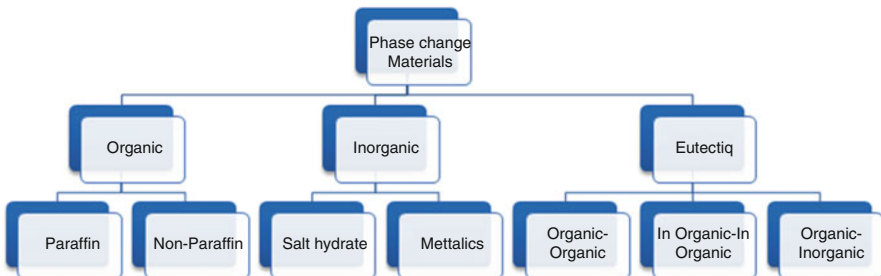


Table 4.4 Inorganic PCMs with melting temperature between 100 and 280 °C

Compound (wt.%)	Melting point (°C)	Latent heat (kJ/kg)	Density (kg/m ³)	Energy density (kJ/m ³)	Thermal conductivity (W/m K)
MgCl ₂ ·6H ₂ O	117	168.6	1450 (liquid, 120 °C)	244,470 (liquid, 120 °C)	0.570 (liquid, 120 °C)
			1569 (solid, 20 °C)	264,533 (solid, 20 °C)	0.694 (solid, 90 °C)
NaNO ₃ –KNO ₃ (50:50)	220	100.7	1920	193,344	0.56
KCl–ZnCl ₂ (68.1:31.9)	235	198	2480	491,040	0.8
LiCl–LiOH (37:67)	262	485	1550	751,750	1.10

Table 4.5 Inorganic PCMs with melting temperature between 280 and 400 °C

Compound (wt.%)	Melting point (°C)	Latent heat (kJ/kg)	Density (kg/m ³)	Energy density (kJ/m ³)	Thermal conductivity (W/m K)
ZnCl ₂	280	75	2907	218,025	0.5
NaNO ₃	308	199	2257	449,143	0.5
NaOH	318	165	2100	346,500	0.92
KNO ₃	336	116	2110	244,760	0.5
NaCl–KCl (58:42)	360	119	2084.4	248,044	0.48
KOH	380	149.7	2044	305,987	0.5

characteristic of metallic materials is their high thermal conductivity, which eliminates the use of thermal conductivity enhancement techniques.

Generally, the materials with the melting temperature below 220 °C are considered as low-temperature materials, while melting temperatures up to 420 °C as medium temperature materials, and melting points greater than 420 °C are classified as high-temperature materials [22]. Some detailed data from common phase change materials are shown in Tables 4.4, 4.5, and 4.6.

Although PCMs possess great benefits, they suffer from different problems and technical difficulties which make the performance fall short out of the expectations and limit their widespread use in practical applications. One of the main drawbacks is the low thermal conductivity of the commercially available PCM which limits the heat transfer rate between the heat source and the PCM. This will result in prolonged melting and solidification processes and the overheating of the heat transfer surface. To address the mentioned issue, different techniques have been suggested. These methods include the use of finned tubes [23, 24], the use of high thermal conductive small particles dispersed in the PCM [25, 26], the microencapsulation of the PCM [27], and the use of highly porous PCM-filled conductive

Table 4.6 Inorganic PCMs with melting temperature above 400 °C

Compound (wt.%)	Melting point (°C)	Latent heat (kJ/kg)	Density (kg/m ³)	Energy density (kJ/m ³)	Thermal conductivity (W/m K)
MgCl ₂ -NaCl (38.5:61.5)	435	351	2480	870,480	N/A
Na ₂ CO ₃ -Li ₂ CO ₃ (56:44)	496	370	2320	858,400	2.09
NaF-MgF ₂ (75:25)	650	860	2820	2,425,200	1.15
MgCl ₂	714	452	2140	967,280	N/A
LiF-CaF ₂ (80.5:19.5)	767	816	2390	1,950,240	1.70 (liquid)
					3.8 (solid)
NaCl	800	492	2160	1,062,720	5.0
Na ₂ CO ₃	854	275.7	2533	698,348	2.0
K ₂ CO ₃	897	235.8	2290	539,982	2.0

material [28]. An alternative approach is embedding of heat pipe inside the PCM to spread the heat provided by heat source throughout the PCM. Latent heat thermal energy storage systems assisted by heat pipes can be implemented in different applications [29–33].

4.10.4 Latent Heat Thermal Energy Storage Systems Assisted by Heat Pipes

In one of the very first studies, Abhat considered the idea of utilizing heat pipe to enhance the PCM melting and solidification rates for solar heating application (see Fig. 4.18). He studied the performance of a latent heat thermal energy storage system assisted by a heat pipe with paraffin PCM. Annular fins were attached to the outer surface of the heat pipe to better spread the heat through the PCM [35].

In another study by Abhat [34], the performance of a modular latent heat thermal energy storage equipped with a finned heat pipe as presented in Fig. 4.19 was studied during charging, discharging, and simultaneous charging and discharging modes. An axially grooved copper–water heat pipe was selected to transport heat of 1000 W over the 3-m length with the maximum temperature difference of 10 K.

The module consists of a container with square cross section with heat pipe located at the center. Section *B* is filled with the PCM and sections *A* and *C* are in contact with the heat transfer fluids [34].

Liu and Ma [36] experimentally studied LHTES with paraffin as PCM ($T_m = 52.1\text{ }^\circ\text{C}$) which was assisted by a gravity-driven heat pipe as shown in Fig. 4.19.

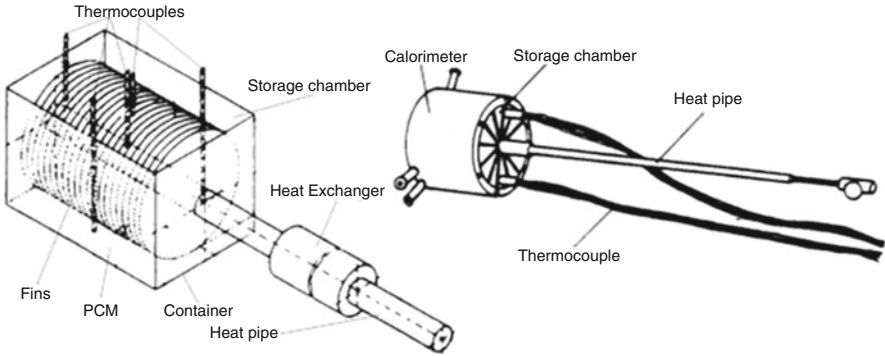


Fig. 4.18 Latent heat thermal storage unit with heat pipe [34]

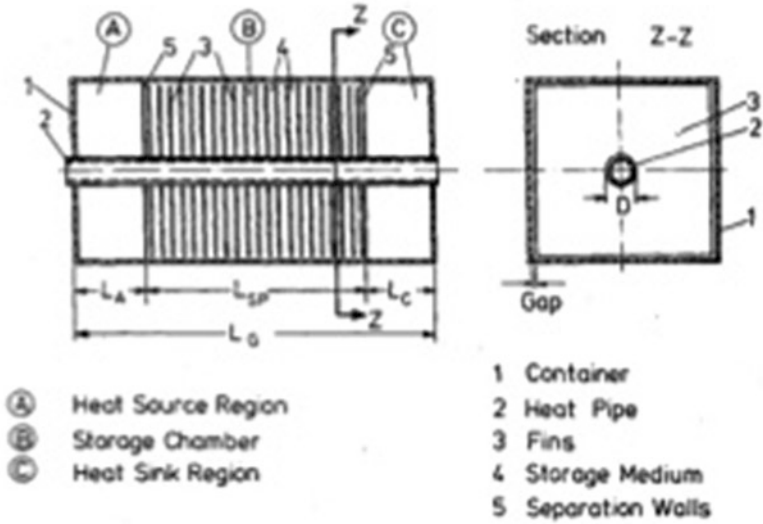


Fig. 4.19 Latent heat thermal energy storage with heat pipe heat exchanger [34]

The effects of heat transfer fluid (HTF) inlet temperature and flow rate on the charging only, discharging only, and simultaneous charging/discharging processes were studied (Fig. 4.20).

Sharifi et al. develop a numerical model to examine the melting of the phase change material in the vertical cylindrical container which is heated by the heat pipe located vertically at the center of the container. The heat pipe condenser is surrounded by the phase change material (PCM) (Fig. 4.21). The performance of the heat pipe integrated system is assessed by comparing the melting fraction at each time to those of assisted by isothermal surface or hot concentric rod or tube. Sodium nitrate (NaNO_3 , $T_m = 580\text{K}$) was chosen as the PCM, and the heat pipe working fluid was selected to be potassium (K, with p_{Sat} at $T_{\text{Sat}} = T_m = 580\text{K}$).

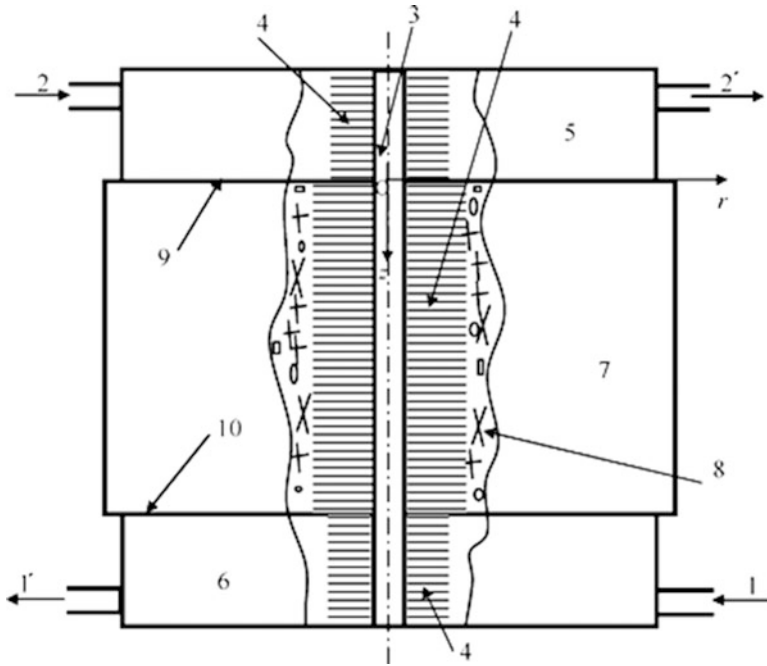


Fig. 4.20 A heat pipe heat exchanger with latent heat thermal storage: the systematic configuration (1) hot fluid in, (1') hot fluid out, (2) cold fluid in, (2') cold fluid out, (3) heat pipes, (4) annular fins, (5) cold fluid-flow passage, (6) hot fluid-flow passage, (7) PCM chamber, (8) PCM, (9) upper separation, and (10) lower separation

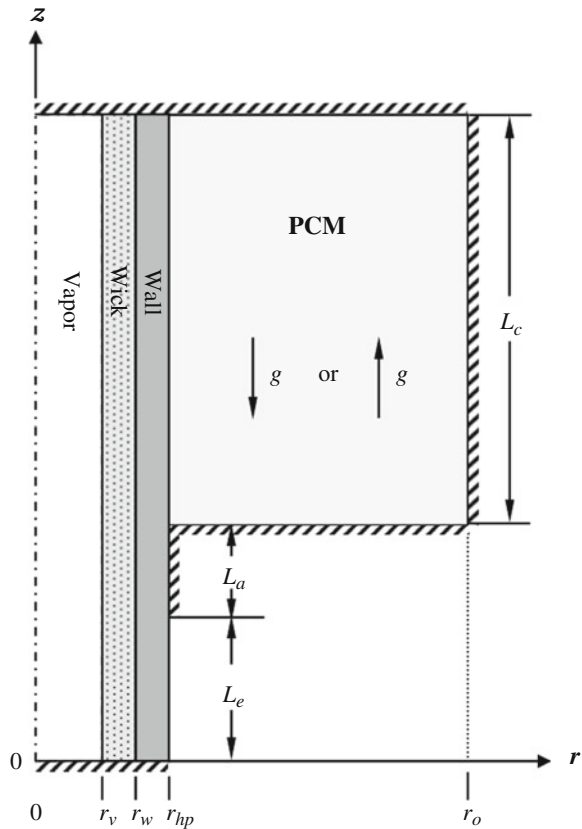
The heat pipe wick and wall material as well as the rod and tube was stainless steel which satisfies the compatibility issue associated with heat pipes.

Later on, Sharifi et al. [31] benefited from embedding the PCM within an aluminum foil matrix to enhance the melting and solidification rate by approximately 200 and 600% relative to the case with heat pipe and no metal foam. *N*-Octadecane was chosen as the PCM which was coupled with a copper–water heat pipe.

Liu et al. presented a novel HP-LHTES in which composite granular solid–liquid PCM was piled up as the porous-medium layer. The PCM was composed of a mixed metal salt and inorganic bentonite which melts over temperature range of 200–250 °C. Naphthalene was selected as heat pipe working fluid. In another study, they used composite granular solid–liquid PCMs compounded by RT100 and high-density polyethylene with phase change temperature of 100 °C. To be compatible with the phase change temperature of the PCM, water was chosen as the working fluid of the heat pipe. Figure 4.21 shows the schematic of fabricated experimental setup.

Tiari et al. conducted a numerical investigation to study the effects of heat pipes on the melting and solidification rate of the PCM enclosed in a square cavity as

Fig. 4.21 Physical model and computational domain for the heat pipe and PCM



shown in Fig. 4.22. The effects of heat pipe spacing and fin length and numbers and the influence of natural convection on the thermal performance of the LHTES unit were examined (see Fig. 4.23).

They have also studied the effect of embedded circular finned heat pipes on the melting of a eutectic mixture of potassium nitrate and sodium nitrate as the PCM in a vertical cylindrical container (Fig. 4.24). Different arrangements of heat pipes were considered.

Figure 4.25 illustrates the effect of heat pipe configuration on PCM liquid fraction evolution during the time at different elevation. As it can be seen, case 3 has provided better spread of heat hence more uniform melting of the phase change material and higher melting rate.

Robak et al. experimentally evaluated the effectiveness of latent heat thermal energy storage systems assisted by heat pipes. To obtain this, the experiment was conducted for (a) a system assisted by heat pipes, (b) a system using fins instead of heat pipes, and (c) a system without heat pipes or fins (benchmark case) for melting and solidification processes. The effectiveness of each scenario was defined as the

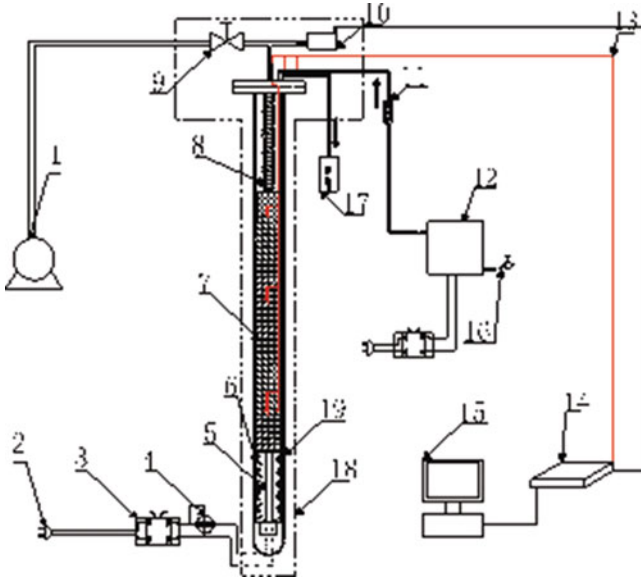


Fig. 4.22 Schematic view of the experimental setup: (1) vacuum pump, (2) power, (3) voltage regulator, (4) power meter, (5) electric heating rod, (6) water, (7) PCM, (8) cooling coil, (9) vacuum valve, (10) pressure sensor, (11) rotor flow meter, (12) electric heater, (13) thermocouple, (14) data acquisition unit, (15) computer, (16) tap, (17) water tank, (18) rubber insulation cotton, and (19) vacuum glass tube

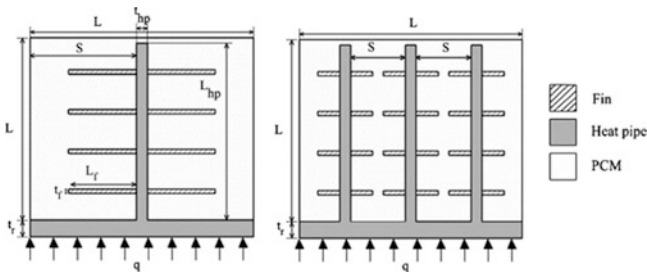


Fig. 4.23 Schematics of the LHTES units with one heat pipe (left) and with three heat pipes (right)

ratio of stored or released energy in cases with heat pipes or fin to the benchmark case:

$$\varepsilon_{HP} = \frac{E_{HP}}{E_{BM}} \quad \varepsilon_F = \frac{E_F}{E_{BM}} \tag{Eq.4.5}$$

where E is the stored or released energy. Also see Fig. 4.26.

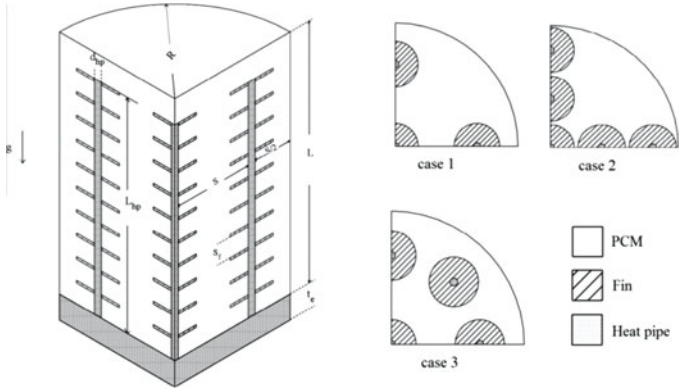


Fig. 4.24 Schematics of heat pipe-assisted thermal energy storage unit and different arrangements of heat pipe

A paraffin, *n*-octadecane ($C_{18}H_{38}$, $T_m = 27.5^\circ C$) of 99 % purity, was used as the PCM which was enclosed in a vertical cylindrical container. During the charging process, the heat was transferred from heat transfer fluid (HTF) to the heat pipe evaporators using a heat exchanger, placed underneath the container. The schematic of the container with embedded heat pipes is shown in Fig. 4.27.

The result showed an increased melting rate of 70 and 50 % for the heat pipe-assisted charging comparing to the cases with no fins or heat pipes and the case with fins, respectively. During the discharging process, the solidification rate was doubled by implementing the heat pipes. It was also reported that the maximum effectiveness associated with the assisted heat pipe unit was around 1.6, while the fin-assisted case only achieved the value of 1.1.

Nithyanandam and Pitchumani [29] developed a numerical procedure utilizing the thermal resistance network model to study the performance of the heat pipe-assisted thermal energy storage system during charging and discharging processes. The effects of the heat pipe and the LHTES system geometry and the LHTES operational conditions were the focus of this study. The system configuration implemented in their study is shown in Fig. 4.28 which includes an array of tubes which are enclosed in a shell. Four heat pipes are mounted on the outer surface of the tube walls (two horizontally oriented and two vertically oriented heat pipes). Two different arrangements can be considered regarding the relative locations of the PCM and the HTF. In case 1, the HTF flows inside the tubes that are encompassed by the PCM, while in case 2 the PCM is placed in the pipes, and the HTF is flowing over the tubes in transverse direction.

The transient operation of the system was investigated applying the thermal resistance network model along with quasi-steady approximation. The developed thermal resistance network is illustrated in Fig. 4.29. The thermal elements E_1 to E_6 belong to heat pipe which are composed of radial conduction for the evaporator (wall, E_1 ; wick, E_2), condenser (wall, E_3 ; wick, E_4), and the axial conduction in the adiabatic section (wall, E_5 ; wick, E_6). The elements E_7 to E_{11} represent the PCM

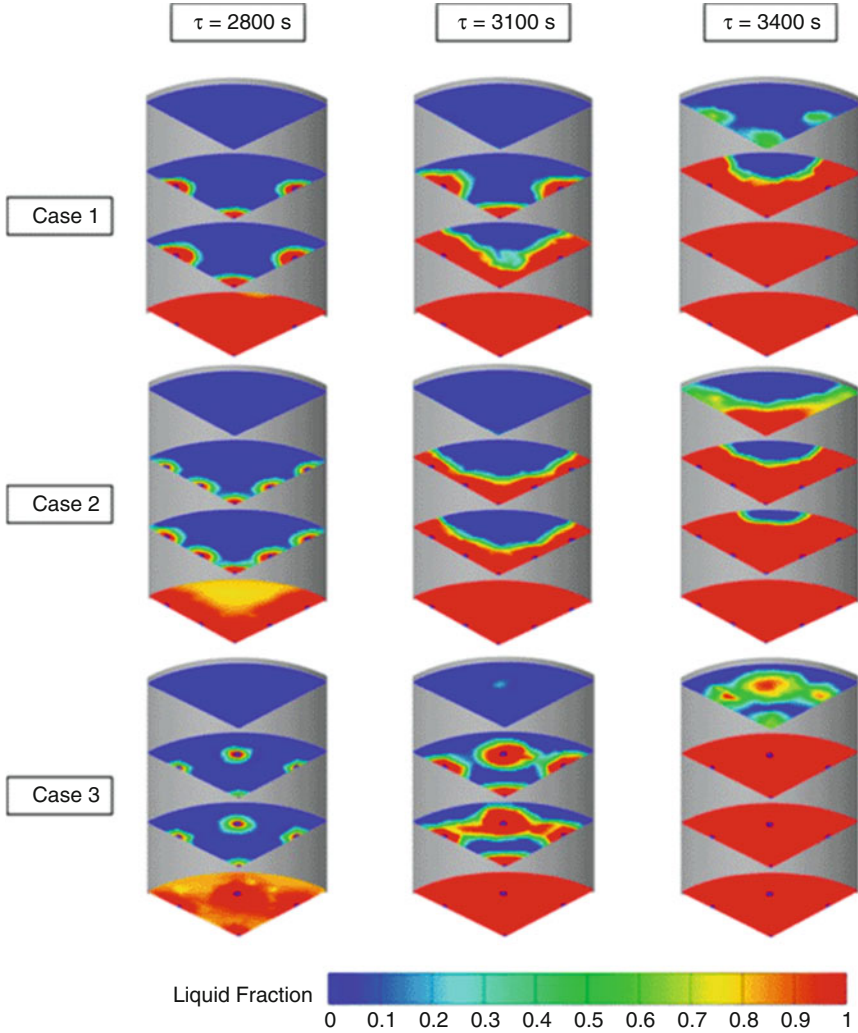


Fig. 4.25 The PCM liquid fraction for studied heat pipe configurations at different elevations

melt (solid) front adjoining the heat pipe, and E_{12} to E_{17} correspond to those of adjoining tube. The thermal resistances associated with vapor flow and evaporation and condensation in the heat pipes are neglected. The HTF temperature change between the tube inlets and its outlets is negligible. The radius of the melt front at the time is assumed to be uniform; however, its advancement is included by the enhancement of thermal conductivity of the liquid PCM. The thermal energy transfer through the heat pipes (the solid lines of the network) and the tube (the dashed lines of the network) occurs between the HTF at temperature T_{HTF} and the

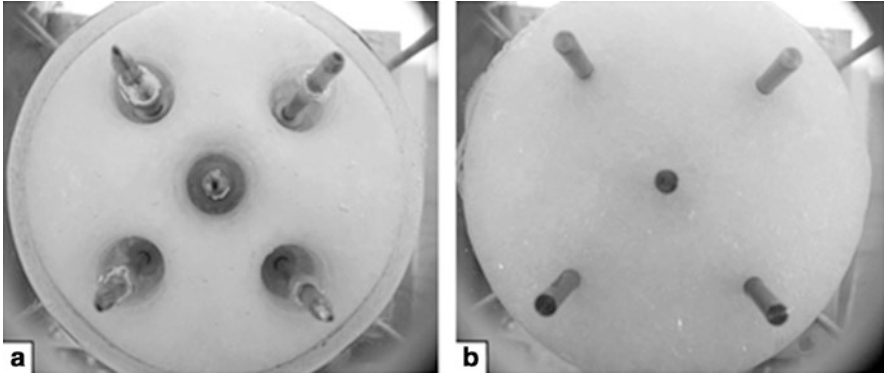


Fig. 4.26 Charging process of TES unit testing by Robak et al. [18]. (a) Heat pipe assisted. (b) Fin assisted

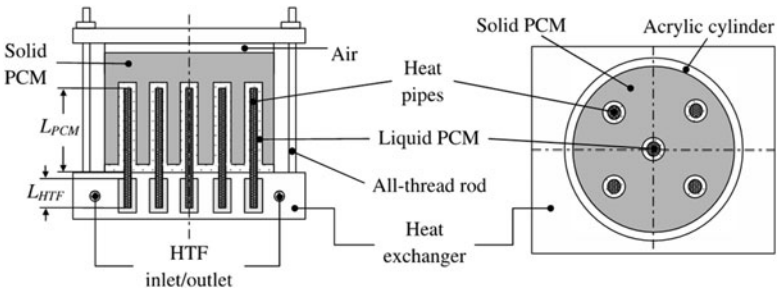
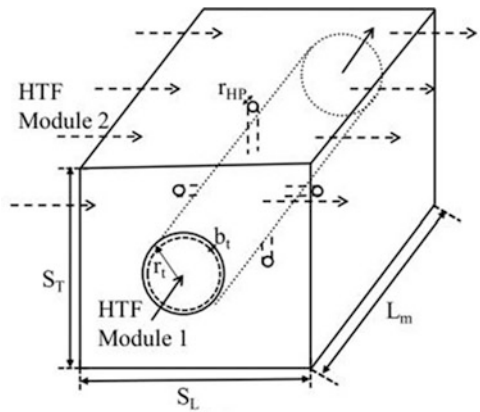


Fig. 4.27 Schematic of the PCM container with embedded heat pipes

Fig. 4.28 Schematic of the flow configuration in module 1 and module 2 of the LHTES system



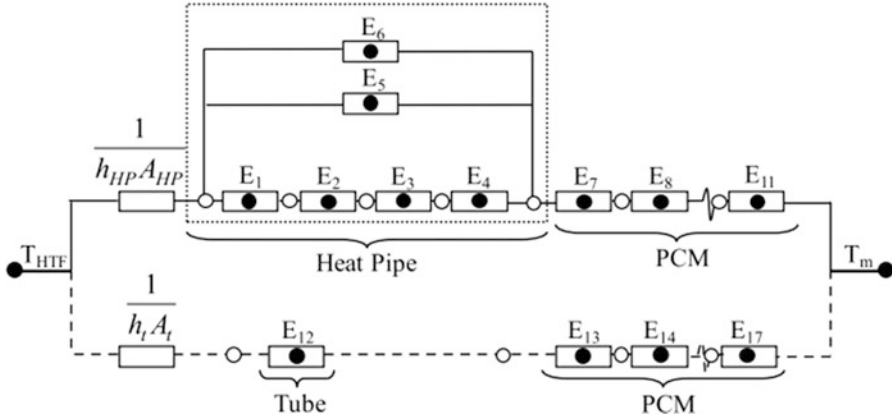


Fig. 4.29 The thermal resistance network of LHTES [29]

liquid (solid) PCM at temperature T_m . For any thermal element, in the network, the energy balance can be written as:

$$\rho_i C_{p,i} V_i \frac{dT_i}{dt} = \left[\frac{T_{i,1} - T_i}{R_{i,1}} - \frac{T_i - T_{i,2}}{R_{i,2}} \right] \tag{Eq.4.6}$$

T_i refers to the surface temperatures at the middle of each element, while $T_{i,1}$ and $T_{i,2}$ are denoting the temperatures at either end of the heat conductor element. The thermal resistances for the heat pipes are explained in Chap. 3.

Surface energy balance is utilized to track the solid–liquid interface of the PCM adjacent to the heat pipe or tube’s external surfaces as follows:

$$\rho \Delta H_f A_{11} \frac{ds_{HP}}{dt} = \pm 2\pi L_{11} k_{11} (T_{11} - T_m) / \ln \left(1 - \frac{L_{11}}{2S_{HP}} \right) \tag{Eq.4.7}$$

$$\rho \Delta H_f A_{17} \frac{ds_{HP}}{dt} = \pm 2\pi L_{17} k_{17} (T_{17} - T_m) / \ln \left(1 - \frac{L_{17}}{2S_{HP}} \right) \tag{Eq.4.8}$$

S is the position of the melt (solid) front and T_m is the melting temperature of PCM. The positive and negative sign should be adopted for charging and discharging, respectively. The physical model was combined with a numerical optimization techniques to maximize the effective rates during charging and discharging. The selected decision variables were HTF mass flow rate, length of the module L_m , outer radius of the tube r_t , length of evaporator and condenser section L_e and L_c of the heat pipe vapor core r_v , and the thickness of the wick of the heat pipes T_w .

In general, the obtained result of this study shows the increase in the HTF mass flow rate, module length, and tube radius decreases the effectiveness of the heat pipe, whereas the longer sections of evaporator and condenser of the heat pipe lead

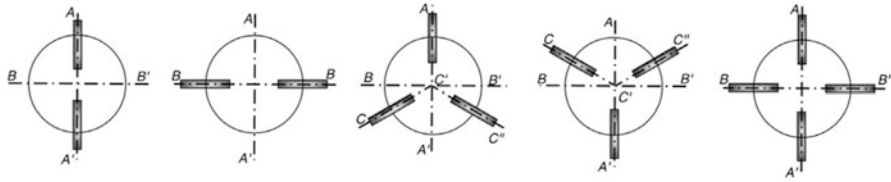


Fig. 4.30 Schematic illustration of the different arrangement of heat pipes [36]

to higher effectiveness. For case 1, the effectiveness of the heat pipes in enhancing the thermal performance of the LTES is significantly higher, while case 2 shows higher effective charging (discharging) rate of the PCM.

The effects of heat pipe configuration were investigated later by combining the simplified thermal resistance network model for heat pipe with three-dimensional numerical model of the HTF and melting/solidification of the PCM. The enthalpy-porosity technique is applied to model the melting and solidification processes within the PCM. Five different arrangements of heat pipe were studied as shown in Fig. 4.30. For the case with two heat pipes, they can be oriented vertically or horizontally. Two and one arrangements are considered for the system with three and four heat pipes, respectively [36].

In order to better understand the effect of heat pipe configurations, the contours of molten PCM during charging are presented here in Fig. 4.31. The arrangement with no heat pipe is served as the basic configuration for comparisons. The solid PCM is colored as the light shaded color, while the molten PCM is represented by the white color. One of the points that should be noted is that as the results of the natural convection within the molten PCM, faster melting of PCM at the top parts is observed compared to the bottom sections. The figure illustrates that the case with four HPs represents higher rates of melting for both modules [36].

In another configuration proposed by Nithyanandam and Pitchumani, the heat pipes are embedded inside a PCM. During charging process, the hot HTF flows into the bottom channel from the right ($x = 0$), and it exchanges heat with the heat pipe evaporator hence the PCM enclosed in the container (see Fig. 4.32). While the discharging occurs, the cold HTF enters the channel located on the top from the right $x = l_d$. In order to provide enough spacing for volumetric expansion of the PCM, the air gap is supplied.

The conservation of energy for the HTF along the channel can be written as

$$\rho_f \Delta H_f \frac{\partial T_f}{\partial t} + \rho_f c_f U_f \frac{\partial T_f}{\partial x} = \dot{Q}_d + N_{HP} \dot{Q}_{HP} \tag{Eq.4.9}$$

where f refers to the HTF and U_f is the velocity of HTF through a single channel. The heat transfer between PCM and HTF can occur either through the channel wall \dot{Q}_d or the heat pipe wall \dot{Q}_{HP} in Fig. 4.33. In Eq. (4.9), N_{HP} represents the number of heat pipes in each control volume. Similar to previous work, the heat exchange between the PCM and HTF through channel walls or heat pipes is described using

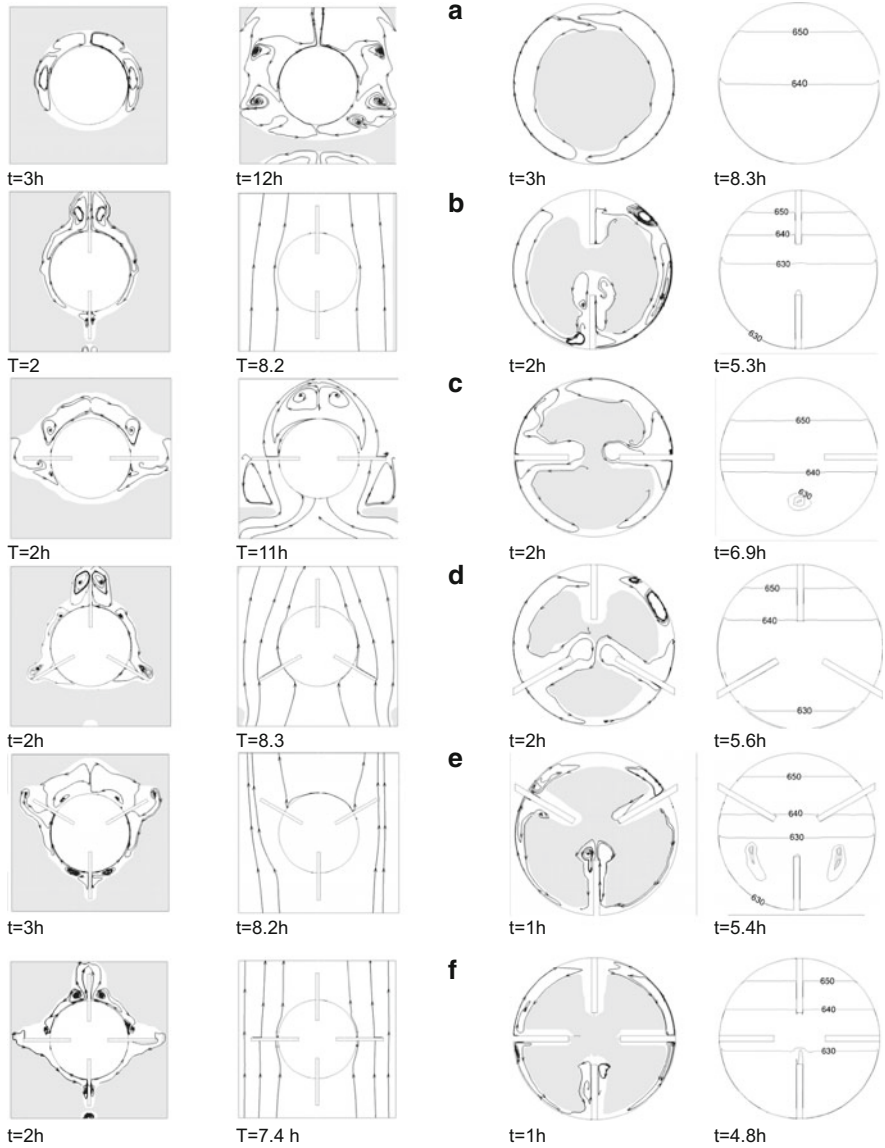


Fig. 4.31 Contours of molten PCM during charging [36]

the thermal resistance network analogy. In this work the energy balance equation for each thermal element mentioned earlier is modified to include the PCM melting:

$$\rho_i C_{p,i} V_i \frac{dT_i}{dt} + p_i h_{sl,i} V_i \frac{dy}{dt} = \left[\frac{T_{i,1} - T_i}{R_{i,1}} - \frac{T_i - T_{i,2}}{R_{i,2}} \right] \quad (\text{Eq.4.10})$$

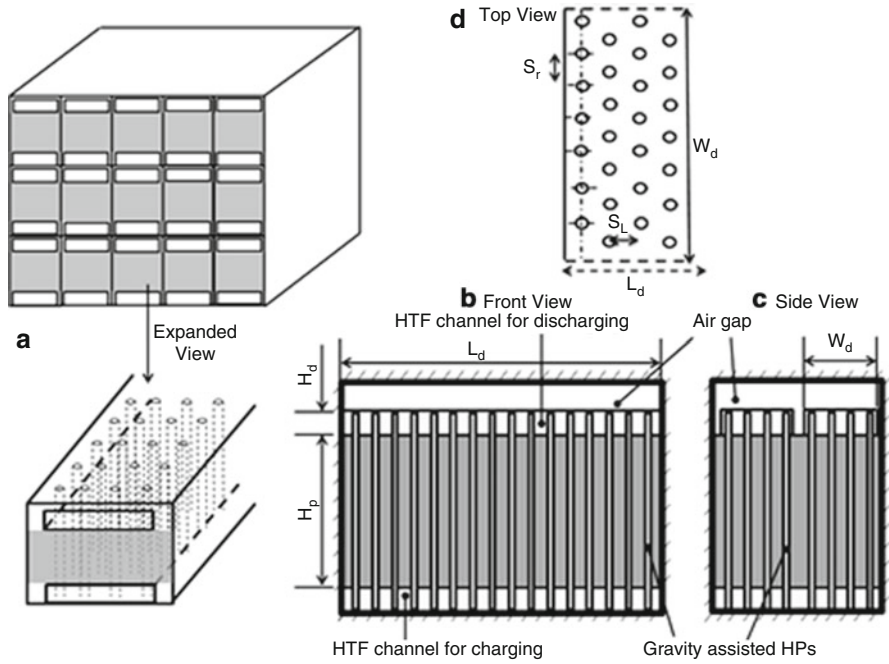
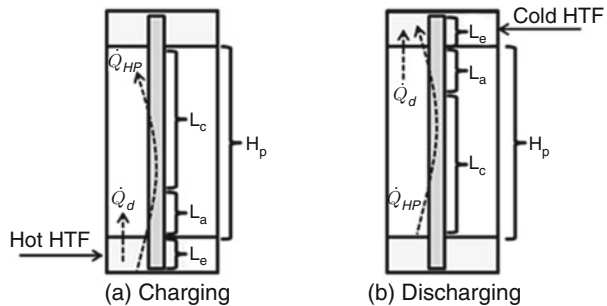


Fig. 4.32 Gravity heat pipes embedded latent thermal energy storage system

Fig. 4.33 Heat transfer pathways during [36]. (a) Charging and (b) discharging of HP-TES system



where γ is the melt fractions of the PCM and the h_{sl} is the latent heat of fraction for the PCM. It should be noted that this term only presents for the PCM thermal elements. The obtained results confirmed that there is an optimal longitudinal spacing between the heat pipes. This can be justified noting that the closer spacing leads to higher storage cost, while larger spacing causes limited heat exchange rate between the PCM and the heat transfer fluid. This study provided the maximum discharging time, the exergetic efficiency, and the minimum storage cost as a function of different operations and the design parameters applied by US Department of Energy SunShot.

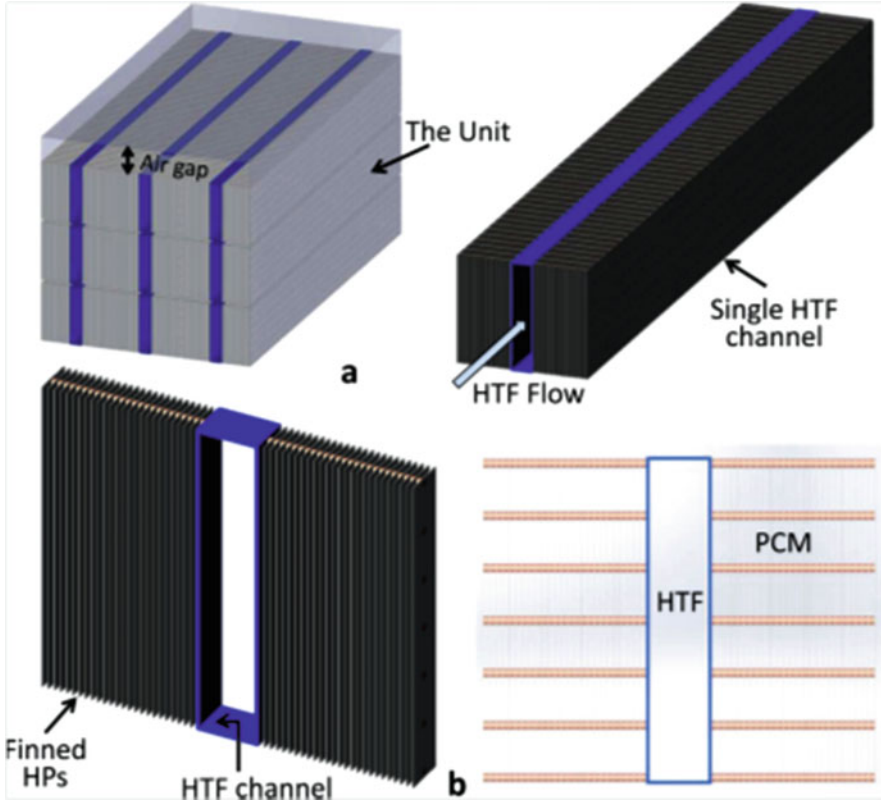


Fig. 4.34 LHTES unit. (a) The proposed design and (b) the unit model cell

Using thermal resistance network, Khalifa et al. evaluated the performance of the high-temperature latent heat storage unit incorporating finned heat pipes. The finned heat pipes were placed in suspension arrangement adjacent to the heat transfer channel to enhance the overall heat conductance of the PCM. A unit model cell of length L_m is shown in Fig. 4.34.

Another advantage of latent heat thermal energy storage systems is their near-isothermal operation which highly qualifies them for power generation systems which require isothermal input such as Stirling engine. Qiu et al. designed and tested the thermal energy storage (TES) system integrated with concentrated solar power. The primary goal of their work was to show the feasibility of the concept. The system was composed of a 3-kW Stirling engine power generator and thermal energy storage system as shown in Fig. 4.35. A different configuration of heat pipe is utilized in order to enhance the system performance, which provided the simultaneous charging and discharging of the phase change material. To aim this, a network of heat pipes was embedded inside the PCM consists of a primary heat pipe and an array of secondary heat pipes. As shown in Fig. 4.34a, during the charging process, the solar energy, which impinges on the evaporator surface of the primary

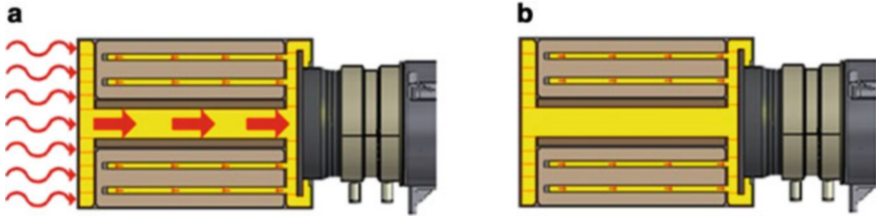


Fig. 4.35 Thermal energy storage module tested by Qui et al. in (a) charging mode and (b) discharging mode

heat pipe, turns the liquid sodium to vapor, which moves toward the heat engine heat receptor where it condenses and releases heat. The excess heat is delivered via the array of secondary heat pipe to charge the phase change material. During the discharging mode, the PCM will solidify, and the released latent heat will be transferred to the heat engine. The testing of the module was performed in two phases: In phase 1, the TES module was charged and discharged, while the helium working fluid of the heat engine was evacuated, and therefore the engine was inoperative. In phase 2, the engine was charged and put in place, and it was running in parallel with charging of the phase change material. The test results revealed that the system performance fell short of the expectations. The shortfall was very likely due to the fact that the condensed liquid could not be returned properly to the evaporator by the heat pipe wick. Another reason could be the secondary heat pipe configurations such as the heat pipe spacing and their number in addition to primary heat pipe geometrical features.

In order to improve the performance of the system, Mahdavi et.al focused on the hydrodynamics and thermal characteristic of the heat pipe. The purpose of their study was to understand the detailed effects of physical and geometrical features, specially secondary heat pipe arrangements on the overall performance of the heat pipe. It was also of interest to find the configurations that provide more uniform heat rejection in the primary condenser to the heat engine which improves the engine efficiency and more uniform phase change of PCM for efficient thermal energy storage. The effects of heat input, the heat transfer to secondary heat pipe in percentage of heat input, the adiabatic section radius, the main condenser thickness, and the secondary heat pipe arrangement were investigated on the temperature distribution of the primary condenser and secondary heat pipes. The results showed that due to the high expansion ratio from adiabatic to primary condenser, the vapor flow leaving the adiabatic section acts similar to a jet which impinges on the main condenser surface and spreads out in radial direction. As the vapor flow proceeds in radial direction, due to interaction of the viscous and inertial forces, several recirculation zones are formed which make the heat pipe performance convoluted. As one can see from Fig. 4.36, the recirculation zone plays a significant role in determining the temperature distribution in main condenser and secondary heat pipe. In order to obtain more uniform temperature distribution, the configuration should be modified to diminish the size and quantity of the vortices. They also

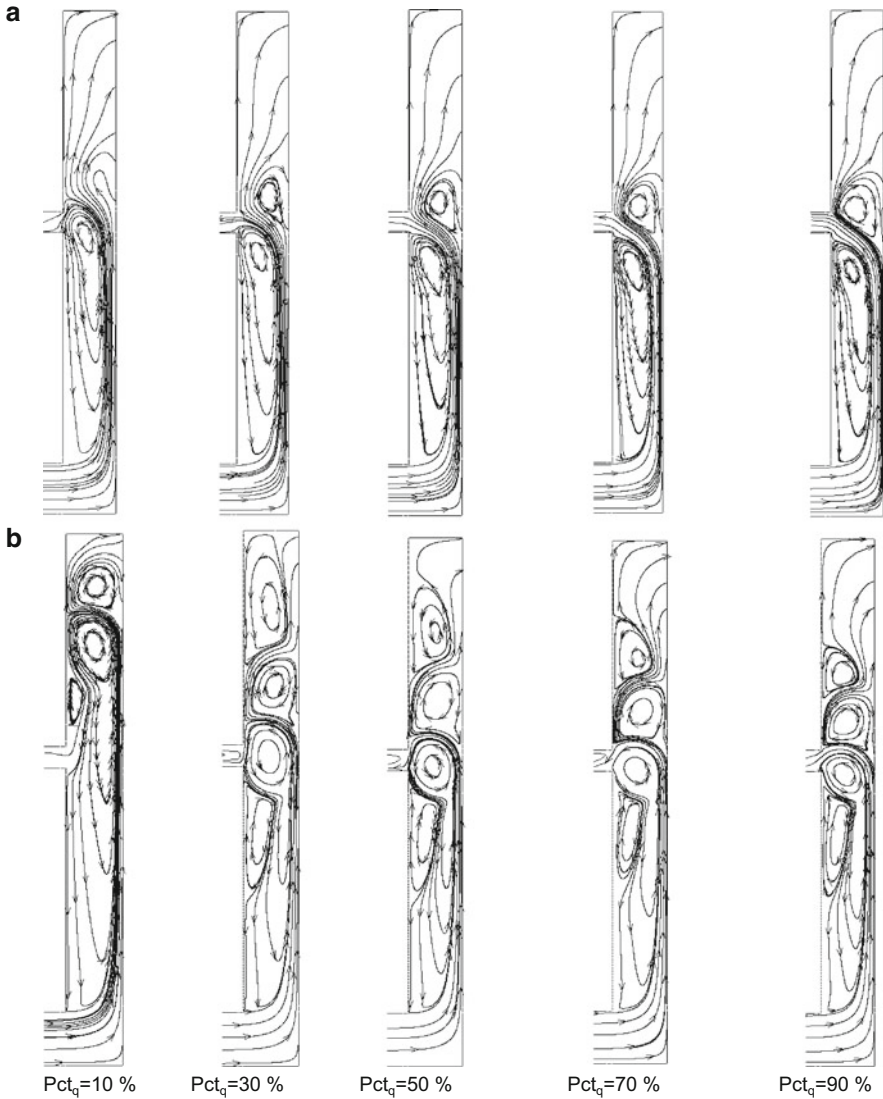


Fig. 4.36 The effect of heat input on the main condenser streamline patterns (a) $Q_e = 1000 \text{ W}$ and (b) $Q_e = 3000 \text{ W}$

studied the effects of condenser's entrance shapes and the adiabatic section location on the uniformity of the temperature distributions of the main condenser. It was concluded that moving the adiabatic section radially outward to the surrounding has significant effect on reducing the size and quantity of the recirculation regions and leads to more uniform temperature distribution.

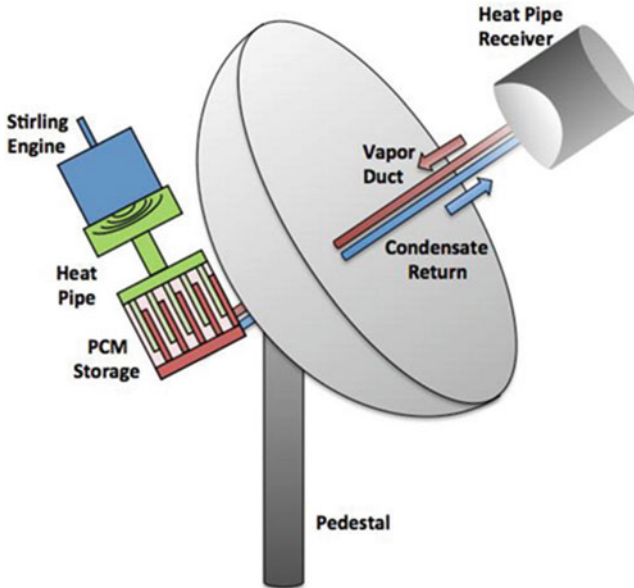


Fig. 4.37 The proposed configuration of heat pipe-assisted LHTES unit with a dish Stirling system

Andraka et al. from Sandia National Laboratories proposed a configuration heat pipe-assisted thermal energy storage system integrated with dish Stirling, shown in Fig. 4.37. In the proposed configuration, the latent heat thermal storage unit and the engine are placed on the rear of the dish instead of being at the focus which enables the power conversion unit to support higher phase change material mass. The thermal energy is transferred from the solar receiver to the storage media, which can be a salt or metallic PCM, via a pumped heat pipe. A second heat pipe isothermally transfers the heat from the PCM to Stirling engine which decreases the exergetic losses of the system and also leads to a higher efficiency.

Shabgard et al. numerically studied the configuration proposed by Andraka et al. to predict the transient response of the storage unit and thermal energy provided for Stirling engine. In order to reduce the computational cost, the HP-PCM unit was simplified to a two-dimensional numerical model. Figure 4.38 shows the three-dimensional and simplified two-dimensional views of thermal energy storage unit. Sodium chloride (NaCl) with melting temperature of 800°C was considered as the PCM, and heat pipe working fluid was sodium. Three operation stages were considered for the study based on time-varying solar irradiance. In the first stage which starts at sunrise and lasts until 9 a.m., all the input thermal energy is used to charge the PCM. The second stage of operation which is simultaneous charging and discharging of the storage unit starts at 9 a.m. and ends at sunset (approximately 7 p. m.). The third stage starts after sunset, during which the stored thermal energy is

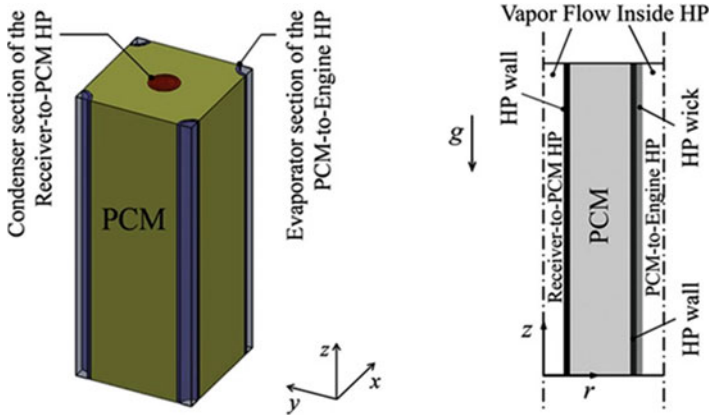


Fig. 4.38 (Left) Three-dimensional schematic of the storage unit showing a receiver to PCM heat pipe and four quarter sections PCM to engine heat pipes. (Right) The simplified two-dimensional model of the system

retrieved to generate power. It was found that the LHTES unit damps the time-dependent variations of solar irradiance and supplies Stirling engine with a relatively smooth thermal energy. It was also shown that the heat pipe spacing plays a significant role in thermal performance of the LHTES system and the system with the minimum heat pipe spacing provides the maximum exergy efficiency.

Malan et al. experimentally and numerically analyzed a concentrated solar power (CSP) system integrated with a heat pipe-assisted latent heat thermal energy storage unit. For the experimental study, a low-temperature storage unit with paraffin as the PCM was built and tested. For the numerical modeling, a high-temperature LHTES unit with a eutectic mixture of KCl and KF ($T_m = 605^\circ\text{C}$) was analyzed which is adapted to simulate a solar tower facility in Meerendal, South Africa, which is part of a project called the *Helio 100*. The experimental study of the test module gave an indication of how the PCM behaves during melting and solidification processes in the specific geometry used for the system. On the other hand, the developed numerical model analyzed the thermal performance of the thermal energy storage system which numerical model analyzed the thermal performance of the thermal energy storage system which gave a more detailed picture about system design and operation modes. They also concluded that additional study is required to deal with corrosion issue on heat pipes and fin surface (see Fig. 4.39).

Naghavi et al. presented a theoretical model for a solar hot water system consisting of an array of evacuated tube heat pipe solar collectors (ETHPSCs) connected to a common manifold filled with phase change material as shown in Fig. 4.40. The heat pipe evaporator is exposed to solar radiation, and the condenser section is inserted into finned sockets welded into the manifold. Therefore the

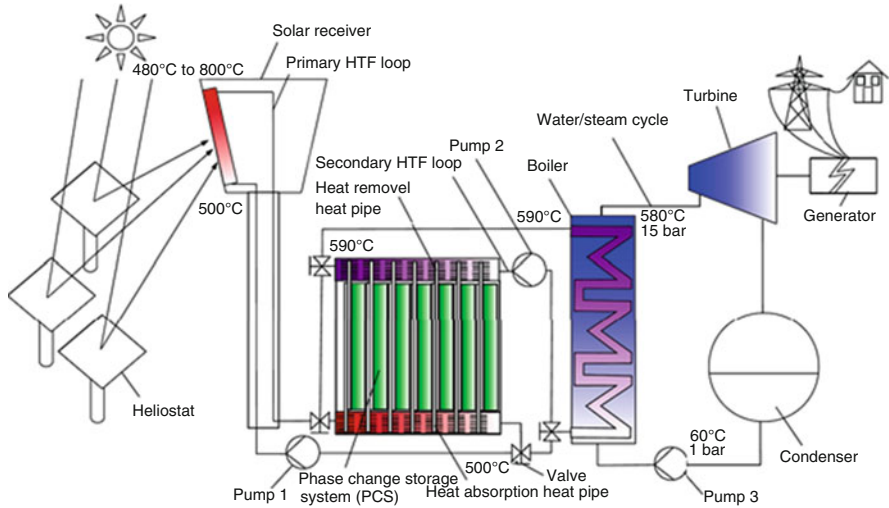
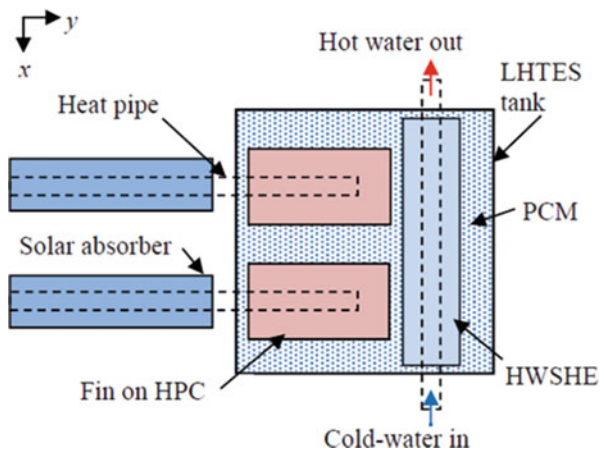


Fig. 4.39 The solar thermal system used for the numerical modeling by Malan et al.

Fig. 4.40 Evacuated tube heat pipe solar collectors



energy received from the sun will be transferred to the PCM via the heat pipe. The heat pipe condenser is equipped with fins to spread heat through the PCM. Domestic cold water will be heated as it flows through the LHTES tank. Figure 4.41 illustrates three different heat transfer processes during charging and discharging.

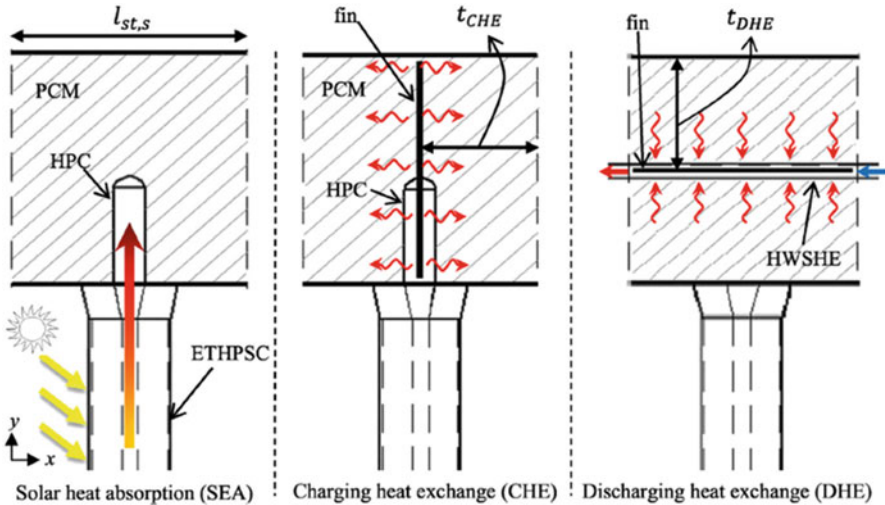


Fig. 4.41 Heat transfer mechanisms in LHTES

References

1. Grover, G. M., Cotter, T. P., & Erickson, G. F. (1964). Structures of very high thermal conductance. *Journal of Applied Physics*, 35(6), 1990–1991.
2. Grover, G. M., Bohdansky, J., & Busse, C. A. (1965). *The use of a new heat removal system in space thermionic power supplies*. European Atomic Energy Community—EURATOM report EUR 2229.
3. Vasiliev, L. L. (2005). Heat pipes in modern heat exchangers. *Applied Thermal Engineering*, 25(1), 1–19.
4. Mochizuki, M., Nguyen, T., Mashiko, K., Saito, Y., Nguyen, T., & Wuttijumnong, V. (2011). A review of heat pipe applications including new opportunities. *Frontiers in Heat Pipes*, 2, 013001.
5. Tranterm web site on Cheaper Heating by Recovering. (2002, January 10). Str. Bisericii Romane no. 27, 500068 Brasov, Romania.
6. Daniel, R. K. (1976). *Heat pipe nuclear reactor for space power*. Los Alamos Scientific Laboratory, LA-UR-76-998, 11th Inter society Energy Conversion Engineering Conference, Sahara Tahoe, state Line, Nevada, September 12–17, 1976.
7. Ragheb, M. (2010). *Space power reactors*. Urbana, IL: University of Illinois.
8. Ranken, W. A., & Lundberg, L. B. (1978). *High temperature heat pipes for terrestrial applications*. International Heat Pipe Conference, 3rd, Palo Alto, Calif., May 22–24, 1978, Technical Papers. (A78-35576 14-34) (pp. 283–291). New York: American Institute of Aeronautics and Astronautics. ERDA sponsored research.
9. Ambrose, J. H., & Holmes, H. R. (Lockheed Missiles and Space Co., Sunnyvale, CA), AB (Lockheed Missiles and Space Co., Sunnyvale, CA). (1991, June). AIAA, Thermophysics Conference, 26th, Honolulu, HI, June 24–26, 1991. p. 7, NASA-supported research.
10. Uranium Information Centre Serving the web since 1995, now part of Australian Uranium Association.
11. Most of the information on subject of Nuclear Reactor in Space comes from this site and user should refer to this site for further consultation. <http://www.world-nuclear.org/info/inf82.html>

12. Mahefkey, T., & Barthelemy, R. R. (1980). *Heat pipe applications for future Air Force spacecraft*. American Institute of Aeronautics and Astronautics, Thermophysics Conference, 15th, Snowmass, Colo., July 14–16, 1980, p. 9.
13. Scott D. Garner P.E., Thermacore Inc., 780 Eden Road, Lancaster PA 17601 USA.
14. Phillips, W. M., Estabrook, W. C., & Hsieh, T. M. (1976). *Nuclear thermionic power system for spacecraft*. Pasadena, CA: Jet Propulsion Laboratory.
15. Shah, R. K., & Giovannelli, A. D. (1988). Heat pipe heat exchanger design theory. In R. K. Shah, E. C. Subbarao, & R. A. Mashelkar (Eds.), *Heat transfer equipment design*. Washington, DC: Hemisphere Publishing.
16. Chi, S. W. (1976). *Heat pipe theory and practice*. New York: Hemisphere Publishing Corporation.
17. Sharma, A., Tyagi, V. V., Chen, C. R., & Buddhi, D. (2009). Review on thermal energy storage with phase change materials and applications. *Renewable and Sustainable Energy Reviews*, 13 (2), 318–345.
18. Pielichowska, K., & Pielichowski, K. (2014). Phase change materials for thermal energy storage. *Progress in Materials Science*, 65, 67–123.
19. Cárdenas, B., & León, N. (2013). High temperature latent heat thermal energy storage: Phase change materials, design considerations and performance enhancement techniques. *Renewable and Sustainable Energy Reviews*, 27, 724–737.
20. Abhat, A. (1983). Low temperature latent heat thermal energy storage: Heat storage materials. *Solar Energy*, 30(4), 313–332.
21. Xu, B., Li, P., & Chan, C. (2015). Application of phase change materials for thermal energy storage in concentrated solar thermal power plants: A review to recent developments. *Applied Energy*, 160, 286–307.
22. Hoshi, A., Mills, D. R., Bittar, A., & Saitoh, T. S. (2005). Screening of high melting point phase change materials (PCM) in solar thermal concentrating technology based on CLFR. *Solar Energy*, 79(3), 332–339.
23. Sciacovelli, A., Gagliardi, F., & Verda, V. (2015). Maximization of performance of a PCM latent heat storage system with innovative fins. *Applied Energy*, 137, 707–715.
24. Wang, W.-W., Wang, L.-B., & He, Y.-L. (2016). Parameter effect of a phase change thermal energy storage unit with one shell and one finned tube on its energy efficiency ratio and heat storage rate. *Applied Thermal Engineering*, 93, 50–60.
25. Jin, Y., Wan, Q., & Ding, Y. (2015). PCMs heat transfer performance enhancement with expanded graphite and its thermal stability. *Procedia Engineering*, 102, 1877–1884.
26. Choi, D. H., Lee, J., Hong, H., & Kang, Y. T. (2014). Thermal conductivity and heat transfer performance enhancement of phase change materials (PCM) containing carbon additives for heat storage application. *International Journal of Refrigeration*, 42, 112–120.
27. Calvet, N., Py, X., Olivès, R., Bédécarrats, J.-P., Dumas, J.-P., & Jay, F. (2013). Enhanced performances of macro-encapsulated phase change materials (PCMs) by intensification of the internal effective thermal conductivity. *Energy*, 55, 956–964.
28. Zhou, D., & Zhao, C. Y. (2011). Experimental investigations on heat transfer in phase change materials (PCMs) embedded in porous materials. *Applied Thermal Engineering*, 31(5), 970–977.
29. Tiari, S., Qiu, S., Mahdavi, M. (2014). Numerical study of finned heat pipe-assisted latent heat thermal energy storage system. *Bulletin of the American Physical Society*, 59.
30. Tiari, M. M., & Qiu, S. (2015). *Analysis of a heat pipe-assisted high temperature latent heat energy storage system using a three-dimensional model*. First Thermal and Fluids Engineering Summer Conference, New York, USA.
31. Sharifi, N., Faghri, A., Bergman, T. L., & Andraka, C. E. (2015). Simulation of heat pipe-assisted latent heat thermal energy storage with simultaneous charging and discharging. *International Journal of Heat and Mass Transfer*, 80, 170–179.
32. Khalifa, A., Tan, L., Date, A., & Akbarzadeh, A. (2014). A numerical and experimental study of solidification around axially finned heat pipes for high temperature latent heat thermal energy storage units. *Applied Thermal Engineering*, 70(1), 609–619.

33. Jung, E. G., & Boo, J. H. (2014). Thermal analytical model of latent thermal storage with heat pipe heat exchanger for concentrated solar power. *Solar Energy*, *102*, 318–332.
34. Abhat, A. (1982). Performance investigation of a long, slender heat pipe for thermal energy storage applications. *Journal of Energy*, *6*(6), 361–367.
35. Abhat, A. (1978). Performance studies of a finned heat pipe latent thermal energy storage system. In F. D. Winter & M. Cox (Eds.), *Sun: Mankind's future source of energy* (pp. 541–546). New York: Pergamon.
36. Liu, Z., & Ma, C. (2002). Numerical analysis of melting with constant heat flux heating in a thermal energy storage system. *Energy Conversion Manage*, *43*, 2521–38.

Chapter 5

Heat Pipe Manufacturing

In this chapter, heat pipe manufacturing methods are examined with the goal of establishing cost-effective procedures that will ultimately result in cheaper and more reliable heat pipes. Those methods which are commonly used by all heat pipe manufacturers have been considered, including envelope and wick cleaning, end closure and welding, mechanical verification, evacuation and charging, working fluid purity, and charge tube pinch-off. Review and evaluation of available manufacturer's techniques and procedures together with the results of specific manufacturing oriented tests have yielded a set of recommended cost-effective specifications which can be used by all manufacturers.

5.1 Manufacturing of Heat Pipes

Key goal of this chapter is to give reader a basic idea of how to develop standardized manufacturing procedures which would assure the reliability of the final product. By evaluating and defining acceptable cleaning procedures, for example, the reliability of a properly fabricated heat pipe will be increased. Moreover, since each manufacturer is currently using essentially independent procedures and are built to different specifications and quality. There is a good deal of duplication of effort in the field; many individual company's procedures have been established iteratively, which is a costly and time-consuming way to develop a technology. This effort, therefore, is only the forerunner of others which will ultimately develop basic heat pipe manufacturing specifications and details for all manufacturers.

Essentially major infrastructure of heat pipe is based on five elements or components which are as follows:

1. Envelope
2. Wick
3. End cap

4. Fill tube
5. Working fluids

Working fluid is introduced into the pipe through the fill tube, which is subsequently sealed by a pinch-off. When heat is applied to a section of the heat pipe (evaporator), the working fluid evaporates, causing a local increase of pressure driving the vapor toward the other end of the pipe (condenser). Cooling this end causes the vapor to condense on the walls of the pipe. Finally, by capillary forces, the working fluid flows back through the wick to the evaporator section. This cycle is repeated as long as heat is supplied to the evaporator and is removed at the condenser. However, if heat is applied to the pipe at a rate higher than the wick can carry, the pipe will fail to function (dry out) [1]. A serious problem with heat pipes is the generation of non-condensable gases which will inhibit their performance. Basically, these gases will accumulate at the cold (condenser) end of the pipe, decreasing the effective conductance of the unit, until the condenser is completely “blocked” and the pipe fails to function. A flowchart of the basic operations involved in manufacturing a heat pipe is presented in Fig. 3.44. A brief summary of the major elements of the manufacturing cycle discussed in this report follows [1].

Details of these components from manufacturing and operation point are discussed below.

5.1.1 Envelope

The envelope may be of any cross section desired by the designer—e.g., circular, square, etc.—and may contain mounting flanges to simplify installation and bent in various shapes. The wick may be grooves extruded into the envelope or may be assemblies—such as Grumman’s spiral artery design—made from fine wire mesh (Fig. 5.1), sintered screen, felt metal slabs, etc. The most common configuration is the round shape. The procedures for determining the tube diameter and the wall thickness have been discussed in Chap. 3, and a great deal of details can be found in Chap. 7 of Chi [2].

Heat pipe manufacturers are rarely concerned with tube manufacturing, because tubes of different materials and sizes are commercially available at reasonable cost. Both seamless and butt-welded tubes may be used as the heat pipe envelope. However, when a tube is cut to the required length, care should be taken so as not to distort the tube ends since this will make it difficult to obtain a strong joint to the end cap. Although round tubes with smooth inside surfaces are common for heat pipe applications, tube with internal fins have also become popular. Several techniques have been developed for production of tubes with internal fins. Kemme [3] was one of the design pioneers to develop the first axial-grooved heat pipes that were formed by milling grooves on a flat plate and then rolling and butt-welding a tube. Today commercially integral fin tubing is now available.

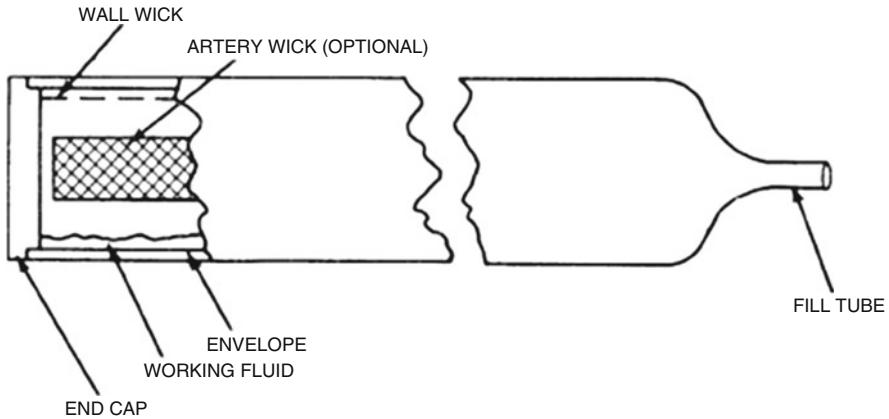


Fig. 5.1 Typical heat pipe components [1]

5.1.2 End Cap

Although a seemingly simple operation, end closure and welding have been a problem for many heat pipe manufacturers. The common concern is porosity or cracks in the weld, which can lead to a loss of the working fluid. To minimize the probability of this failure, inspection should be performed to verify the adequacy of the seal.

Experience and research indicate that it is not uncommon for heat pipes to fail this inspection, requiring that the closure be repaired. A reliable process can lead, therefore, to a “hit-or-miss” manufacturing cycle, where the welding operation is repeated several times to repair a fault. Obviously, these added steps will adversely impact both time and cost budgets. In keeping with the overall objectives of this study, the “optimum” sealing process should be easy to perform, repeatable, require moderately priced equipment, and be reliable and easy to inspect.

The minimum required thickness for heat pipe end cap can be determined by stress analysis as described in Chap. 3, and available computer codes mentioned give you such analysis capabilities. Careful design of the joint for welding is important and plays a great deal to weld end caps. Figure 5.2 shows four types of joint designs and they are named as follows:

- (a) The butt joint
- (b) The lipped butt joint
- (c) The fillet joint
- (d) The lap joint

Dealing with the alignment of these joints is another important step, and among the four kinds, the more difficulty arises with the first one (the butt joints) with respect to the other three. In addition, it should be noted that to obtain a strong, leak-proof welded joint, the end cap must be machined to provide a welded area

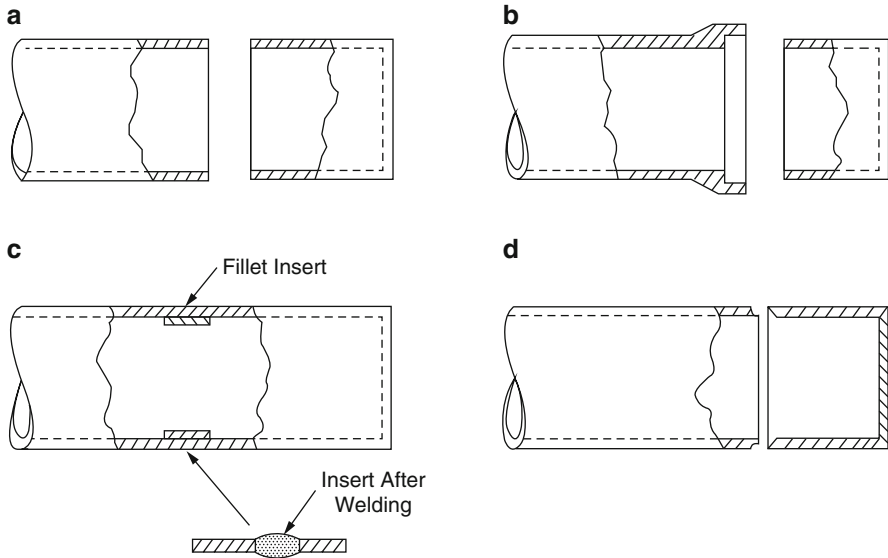


Fig. 5.2 Typical joint design for end cap welding [2]. (a) Butt joint, (b) lipped butt joint, (c) fillet joint, (d) lap joint

thickness, roughly speaking, equal to that of the tube wall [2]. This careful step ensures that both surfaces melt equally resulting in homogeneous fusion.

Detail design of a heat pipe incorporating welded end caps should consider the following points:

- Fusion welding/joining processes result in the best combination of joint strength and leak tightness.
- A fully mechanized fusion welding process should be given preference over a manual process. A mechanized process is significantly more consistent with respect to joint quality, e.g., strength, size of heat-affected zone, and weld bead geometry.
- The use of the aluminum alloy 6061 or the stainless steel alloy 304L eliminates the need for postweld heat treatment, such as a stress relief anneals to prevent either corrosion susceptibility or embrittlement.
- Joint efficiency is a prime consideration. The 304L stainless steel alloy is not heat treatable, and a relatively high joint efficiency in the “as-welded” condition can be obtained. A conservative assumption for this alloy is a weld joint strength that is 85 % (automatic process) or 70 % (manual process) of the minimum strengths guaranteed for the 304L product form in the annealed condition. In the case of the 6061 aluminum alloy, the condition of the material prior to welding and the use of postweld heat treatment must be taken into consideration in establishing weld joint strength.
- The geometry of the weld bead produced by the welding process selected should be known by the designer beforehand since the weld root bead cannot be

machined after welding. An excessively large drop through the root bead can interfere with the operation of the heat pipe. Machining of the crown of the weld bead should be avoided. The removal of the skin material of the weld bead crown may expose interdendritic porosity and result in gas leakage from the heat pipe.

- The use of a square butt joint design is preferable.
- The end cap detail should be designed to be self-aligning during the welding operation. The end cap detail can also provide filler metal to the joint.
- The possible damage to interior details of the heat pipe resulting from welding heat should be considered and, if necessary, determined experimentally.

For more process of end cap welding along with details, reader should refer to Edelstein and Haslett [1] report (Fig. 5.3).

5.1.3 *Fill Tube*

An end cap and fill tube are used to complete the envelope. Working fluid is introduced into the pipe through the fill tube, which is subsequently sealed by a pinch-off. When heat is applied to a section of the heat pipe (evaporator), the working fluid evaporates, causing a local increase of pressure driving the vapor toward the other end of the pipe (condenser). Cooling this end causes the vapor to condense on the walls of the pipe. Finally, by capillary forces, the working fluid flows back through the wick to the evaporator section. This cycle is repeated as long as heat is supplied to the evaporator and is removed at the condenser. However, if heat is applied to the pipe at a rate higher than the wick can carry, the pipe will fail to function (dry out). A serious problem with heat pipes is the generation of non-condensable gases which will inhibit their performance. Basically, these gases will accumulate at the cold (condenser) end of the pipe, decreasing the effective conductance of the unit, until the condenser is completely “blocked” and the pipe fails to function [1].

The fill tube provides the only access to the heat pipe for evacuation and fluid charging, and it too must be closed and sealed. A crimp seal followed by welding has been found to be convenient. For a good crimp, the fill tube must not exceed $\frac{1}{4}$ in. (6.35×10^{-3} m) o.d. Tubes of 1/16-in. (1.59×10^{-3} m) i.d. are often used. Additionally, the thickness of the fill tube wall is also critical for certain materials [2].

5.1.4 *Wick*

If wick structure is an integral part of a heat pipe, e.g., an axial-grooved heat pipe, the operation for the preparation of the wick is not needed. If the wick is formed from wire cloth, e.g., wrapped-screen and artery wicks, the wire cloth must first be

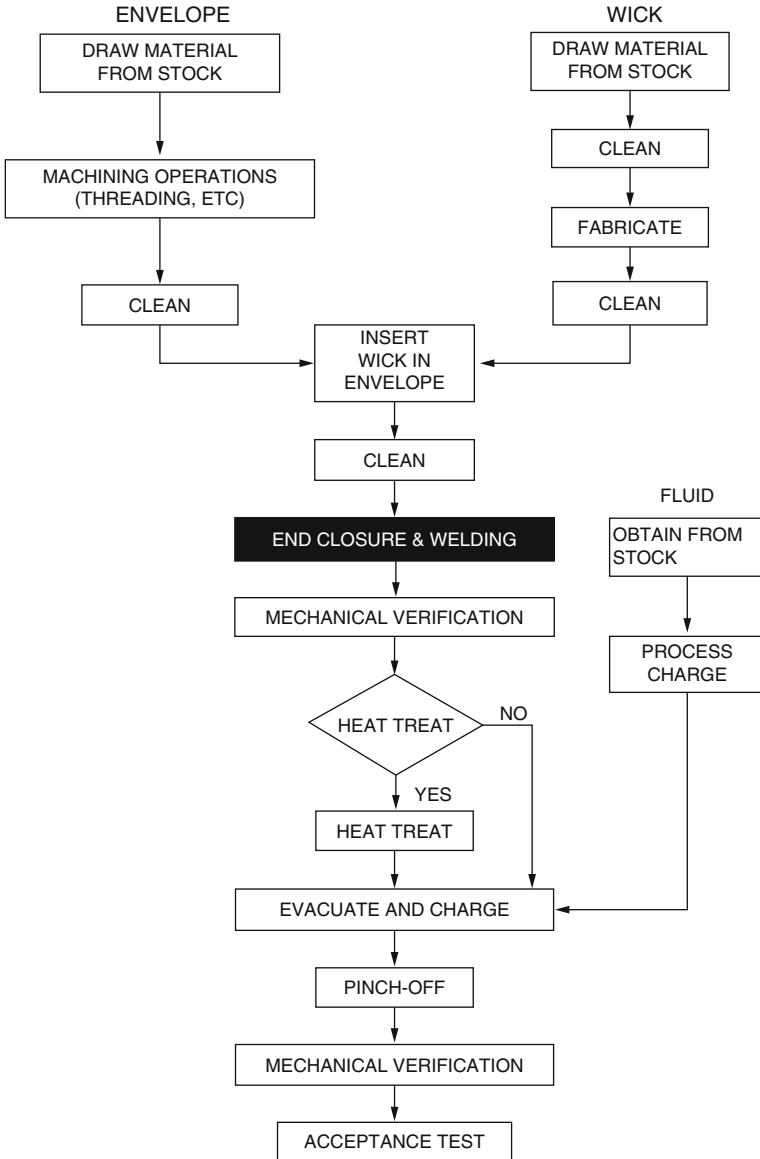


Fig. 5.3 Typical manufacturing steps for welding [1]

cut to the required size. Wire cloth can be difficult to cut accurately, because it is not rigid in the plane of the material. By sandwiching a wire cloth between two flat plates, a wire cloth may be cut along a straight edge [2].

5.1.5 Working Fluid

A heat pipe should not be overfilled or under filled with working fluid. Heat pipe working fluid must be of high quality with minimum impurities gaseous, dissolved solid, or liquid. If these conditions are not met, the designed heat pipe performance may not be reached. Fluid inventory and purification techniques will be discussed below in a section dealing with pipe evacuation and charging [2].

5.2 Heat Pipe Manufacturing Procedures

A flowchart of the basic operations involved in manufacturing of a heat pipe is presented in Fig. 5.4. A bullet topics of the major elements are represented again, and reader can refer to Sect. 3.12.13 for a brief summary of these major elements of the manufacturing cycle discussed in this report. These major elements are as follows:

- Envelope and wick cleaning
- End closure and welding
- Mechanical verification
- Evacuation and charging
- Fluid Parity
- Charge tube pinch-off

Baseline heat pipe manufacturing procedure is summarized and illustrated in Fig. 5.4. Overall restrictions and assumptions unless otherwise specified in the individual manufacturing procedures, the following restrictions or assumptions shall apply [1]:

- Envelope materials considered are aluminum and stainless steel tubing.
- Working fluids are restricted to ammonia, Freon-21, and methanol.
- The pipes are intended for operation in the moderate-temperature range, nominally from -100 to 200 °F (200 to 366 K).
- Typical pipe sizes are approximately 0.5-in. (0.0127 m) diameter and up to about 12 ft (3.6 m) long.
- The procedures described are generally based on small-quantity runs up to approximately 10–20 units. Large-quantity production runs would require more automated operations, the procedures of which might be different from those described here.
- The procedures described are based on a heat pipe manufacturing sequence typical of that shown in Fig. 5.4.

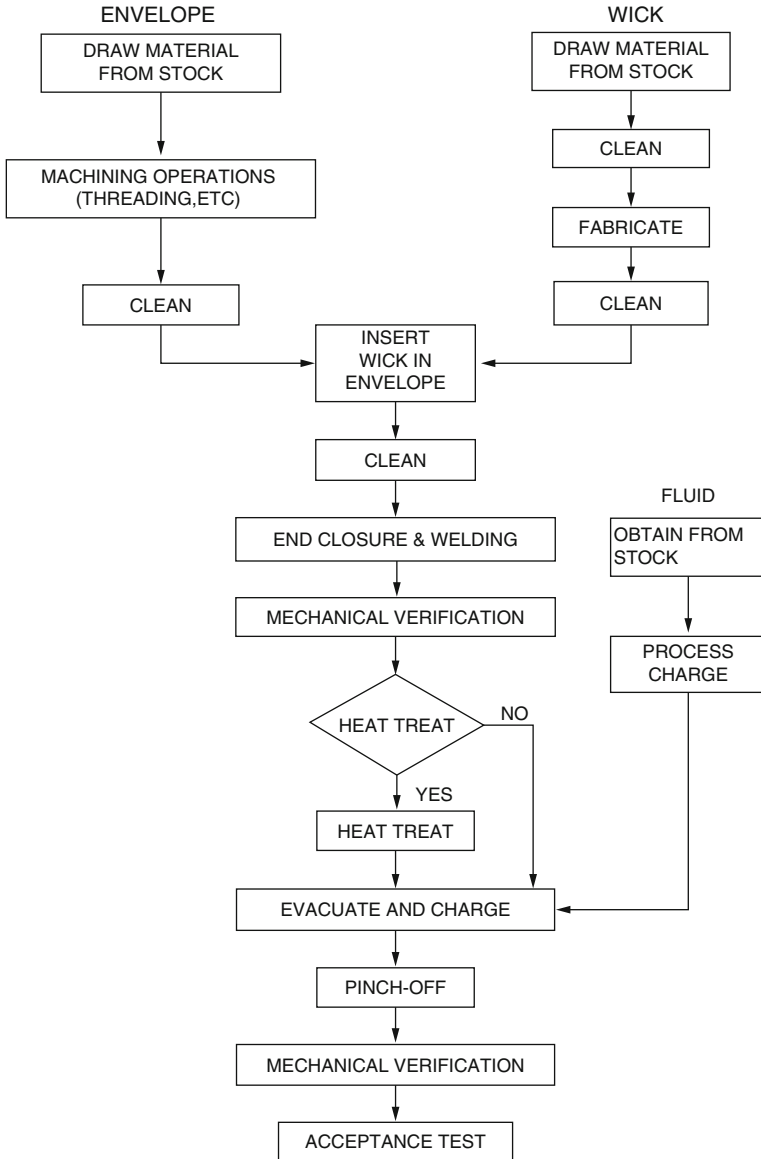


Fig. 5.4 Typical heat pipe manufacturing flowchart [1]

5.3 Cleaning of Parts

Just as extreme care is required in selecting proper heat pipe materials to avoid compatibility problems, cleaning of the component heat pipe parts is critical to avoid similar consequences. Apparently, this is an area in which no accepted standard exists in the industry at the present time [1]. Although there are similarities

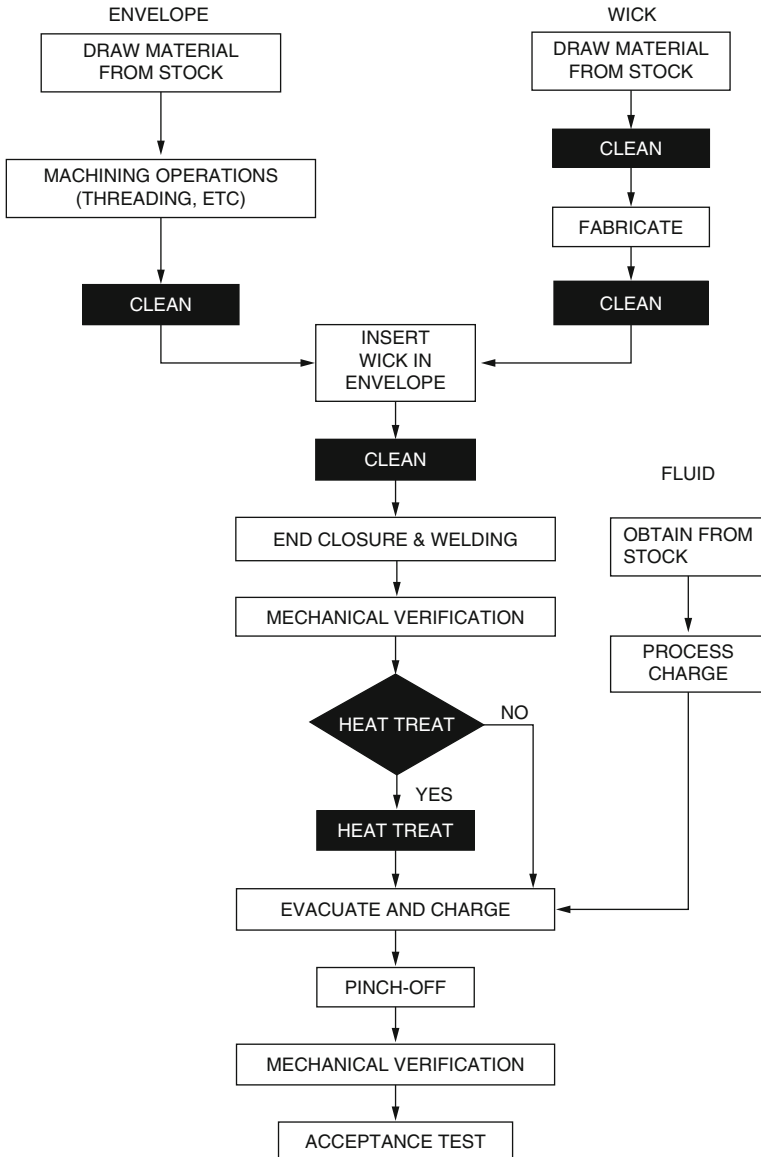


Fig. 5.5 Typical manufacturing steps for cleaning [1]

in the procedures, each manufacturer uses a different process, essentially developed independently. The effectiveness of each process can only be evaluated on the basis of past experience.

As seen in the heat pipe manufacturing cycle in Fig. 5.5, there are many areas where contaminants can be introduced into the heat pipe, i.e., through a dirty wick, dirty envelope, impurities in the working fluid, etc. In fact, every operation not

properly performed can be a source of contamination. This section discusses envelope and wick cleaning and pretreatment for aluminum and stainless steel envelopes and stainless steel wicks. Originally, it appeared that this area should be treated as two topics, wicks, and envelopes. However, during the research effort for this study, it became clear that little wick cleaning information was available. Although most manufacturers were willing to discuss cleaning in general, few were willing to discuss wick cleaning in particular. Each manufacturer considers wick construction and fabrication details as highly proprietary, since it is this element which essentially determines heat pipe performance and separates one company from another. Of the various organizations contacted, therefore, very few were willing to supply information concerning wick cleaning.

Wick cleaning and pretreatment is at least as important as the need for envelope cleaning. Obviously gas generation is just as likely to come from a “dirty” wick as from other improperly cleaned parts. Oil and greases imbedded in either the fine wire mesh or sintered screening material used to construct wicks must be removed to assure proper heat pipe performance. Foreign substances conducive to gas generation might be introduced in the construction process, requiring that a postwick construction cleaning process be designed to remove this impurity. For example, if a copper electrode is used to assemble a wick with tack welds, some copper particles may become imbedded in the stainless steel screen. To remove this material, which is incompatible with ammonia, a nitric acid rinse would be required. However, where possible, it is preferable to eliminate this potential problem by using tungsten electrodes [1].

The heat pipe tube or envelope receives its primary cleaning after dirty operations (such as machining) have been completed. Machining may involve preparing the tube ends for welding, tube bending, and, in some cases, cutting fine circular threads on the inside surface to provide a circumferential wicking surface. An assortment of debris such as metal chips, cutting oil, grease, moisture, etc. can be expected after these operations. The overall cleaning operation, therefore, has a number of aims, namely, to:

- Mechanically remove particulate matter, such as metal chips which may clog capillary and artery surfaces and/or damage these surfaces during subsequent artery insertion.
- Remove water that can cause corrosion, attacking both aluminum and stainless steel, as well as providing a galvanic coupling between the two. Buildup of particulate reaction products, as well as gas generation, is the principal results. Loss of container structural integrity due to crevice corrosion and porosity may also result from the presence of this contaminant.
- Remove contaminants, not necessarily corrosive, but which may impair the heat pipe wicking and fluid properties. Examples of these contaminants are the variety of oils and greases used in metal cutting and removal operations, extruding, forming, etc. These contaminants may coat the internal surfaces and increase the contact angle or may dissolve in the working fluid, changing its transport properties.

- Chemically clean and prepare the surface so as to be nonreactive with subsequent manufacturing environments, the wick, and working fluid.
- Treat the wicking surface in a manner that enhances “wetability” with the working fluid.

Failure to achieve these objectives through either improper procedures or operator error has led to heat pipe problems ranging from performance degradation to complete failure. In one reported incident, for example, water inadvertently left on the inside surface of a threaded aluminum tube was judged to be responsible for failure of a heat pipe to achieve its performance goals. The analysis led to the discovery of huge amounts of aluminum hydroxide on the inside surface which were clogging the radial flow passages.

Contaminants can also chemically react with the wall, wick, or fluid to produce non-condensable gaseous products that block the condenser and decrease heat pipe conductance. In the case of arterial wicks, gas bubbles within the wick can, and have, severely limit the heat transport capacity [3]. On the ATS program, groove failure in a single heat pipe was attributed to embrittlement and porosity caused by the presence of water in a closed pipe during heat treatment [1].

A summary of the foregoing and other problems that can be caused by improper cleaning techniques is as follows:

- Physical clogging of wall and wick capillary surfaces, thereby impairing both heat pipe transport capacity and conductance
- Non-condensable gas generation reducing both heat pipe conductance (loss of condensation area) and transport capacity (bubbles in arterial wicks)
- Decrease in wetability of wick
- Adverse change in fluid properties, such as surface tension, wetting angle, and viscosity
- Loss of structural integrity of container wall due to galvanic corrosion, crevice corrosion, and porosity

Unfortunately, many of these problems cannot be uncovered until the pipe is charged, sealed, and tested. In some cases, a long time can occur until some of these effects are noticed; by then, it is usually too late to provide corrective action. Hence, the objective must be to develop cleaning procedures which will prevent these problems from occurring and produce, therefore, a more reliable product. Moreover, in keeping with the overall aims of this study, the cleaning procedure should also be simple, inexpensive, and as free as possible from human error [1].

Table 5.1 summarizes the procedures currently employed in the heat pipe industry. A brief general description of various cleaning techniques follows, and each manufacturer’s approach will be presented and analyzed. Finally, using this evaluation, recommended cleaning procedures are presented. Note that the procedures used by various manufacturers are typical. If more information is required, it is suggested that the individual company be contacted [1].

To summarize the cleaning procedure for aluminum, copper, and stainless steel, we can show the following [1]:

Table 5.1 Summary of heat pipe cleaning procedures is currently in use [1]

Manufacturer	Envelope cleaning		Wick cleaning (stainless steel)
	Aluminum	Stainless steel	
Dynatherm	<ul style="list-style-type: none"> Solvent Acid 		
NASA/GSFC	<ul style="list-style-type: none"> Solvent Acid 		
Grumman	<ul style="list-style-type: none"> Solvent Alkaline/acid 	<ul style="list-style-type: none"> Solvent Passivation 	<ul style="list-style-type: none"> Solvent Passivation
TRW	<ul style="list-style-type: none"> Solvent Alkaline/acid Ultrasonic 	<ul style="list-style-type: none"> Ultrasonic Vacuum fire 	<ul style="list-style-type: none"> Ultrasonic Vacuum fire
DWDL/MDAC	<ul style="list-style-type: none"> Solvent 		
ESRO/MBB	<ul style="list-style-type: none"> Ultrasonic 		<ul style="list-style-type: none"> Ultrasonic
GE	<ul style="list-style-type: none"> Alkaline/acid 	<ul style="list-style-type: none"> Alkaline/acid 	
University of Stuttgart		<ul style="list-style-type: none"> Ultrasonic Passivation 	
NASA/MSFC	<ul style="list-style-type: none"> Solvent Alkaline/acid 	<ul style="list-style-type: none"> Solvent Alkaline Passivation 	

Table 5.2 Examples of non-etch alkaline cleaners [1]

Material	Concentration	Temperature
Ridoline No. 53 (Amchem Products Co.)	2–10 oz/gal	140–180 °F
Oakite No. 164 (Oakite Products Co.)	2–10 oz/gal	140–180 °F
Kelite Spray White (Kelite Corp)	40–60 % by volume	Ambient
A-38 (Pennwatt Corp)	4–8 oz/gal	160–180 °F

Envelope Cleaning and Pretreatment

• **Assumptions:**

1. Applicable tubing: Aluminum 6061 or 6063 and stainless steel 300 series
2. Tube condition: Threaded, wicked, or otherwise internally machined prior to cleaning
3. Tube size: Typically 0.5-in. (0.0127 m) diameter up to 12 ft (3.6 m) long

• **Materials:**

1. Non-etch alkaline cleaner (refer to Table 5.2).
2. Chromated deoxidizer (refer to Table 5.3).
3. Filtered air.
4. Anhydrous isopropyl alcohol.
5. Dry nitrogen.
6. Passivating solution (refer to Table 5.4).

Table 5.3 Examples of chromated deoxidizer solutions (immersion type) [1]

Material	Concentration	Temperature	Immersion time
Mixture of			
Chromated deoxidizer replenisher No. 17 ^a (Amchem Products Co.)	2–6 oz/gal	Ambient to 120 °F	5–30 min
Nitric acid 42° Be	10–20% by volume		
Mixture of			
Chromated deoxidizer replenisher No. 17 ^a	2–6 oz/gal	Ambient	5–30 min
Sulfuric acid 66' Be	4–7% by volume		

^aDeoxidizer make up No 7 to be used for initial makeup

Table 5.4 Examples of passivating solutions [1]

Material	Concentration	Temperature	Immersion time
Nitric acid	35–65% by volume	Ambient	30 min to 2 h
Mixture of			
Sodium dichromate or potassium dichromate	1–4 oz/gal	Ambient	30 min to 2 h
Nitric acid	15–30% by volume		

• **Procedure—aluminum tubes:**

1. Clean in cold 1,1,1 trichloroethane with bristle brush on wire extension. Periodically clean brush between strokes.
2. Flush internal surface with cold trichloroethane; dry with filtered air and cap pipe ends.
3. Immerse in non-etch alkaline cleaner for 5 min minimum. Refer to Table 5.2 for materials and temperatures.
4. Follow with a 2-min tap water rinse, raising and lowering tube during rinsing.
5. Immerse in chromated deoxidizer. Refer to Table 5.3 for materials, time, and temperature.
6. Follow with a 2-min tap water rinse, raising and lowering tube during rinsing.
7. Thoroughly dry inside surface with forced filtered air.
8. Rinse with anhydrous isopropyl alcohol.
9. Force dry with clean, filtered, and dry nitrogen heated to 160 °F.
10. Cap pipe ends.
11. If applicable, insert artery, rinse with isopropyl alcohol, and dry as in step 9.
12. If heat treatment is required after welding, then:

Evacuate pipe for 4 h at 600 °F and leak check.

Seal evacuated heat pipe.

Perform heat treat operations on sealed pipe.

- **Procedure—stainless steel:**

1. Clean in cold 1,1,1 trichloroethane with bristle brush on wire extension. Periodically clean brush between strokes.
2. Flush internal surface with cold trichloroethane; dry with filtered air and cap pipe ends.
3. Immerse in passivating solution. Refer to Table 5.3 for materials, temperatures, and time.
4. Follow with a 2-min tap water rinse, raising and lowering tube during rinsing.
5. Thoroughly dry inside surface with forced filtered air.
6. Rinse with anhydrous isopropyl alcohol.
7. Force dry with clean, filtered, and dry nitrogen heated to 160 °F.
8. Cap pipe ends. If applicable, insert artery, rinse with isopropyl alcohol, and dry as in step 7.

- **General notes:**

- The cleaning procedure must be as free from operator error as possible, since improperly executed procedures may also lead to unwanted contamination. Training of personnel regarding the cleanliness requirements for heat pipes is mandatory and so are adequate safeguards and inspection points during the steps of the procedure; these must be consistent with good quality assurance practices.
- Do cleaning and charging operations in fairly rapid sequence and in proximity to one another. Avoid storing the pipe for long duration, which increases the likelihood of contamination. Performing these operations near each other lessens the danger of contamination during transportation.

For more details of this operation, reader should refer to Edelstein and Haslett [1] report.

5.4 Assembly of Heat Pipes

The assembly of heat pipe parts includes welding of end caps and fill tube and forming and inserting of wick if applicable. Since parts have been thoroughly cleaned, they should be assembled immediately following the cleaning if practicable. Otherwise, cleaned heat pipe parts should be stored in a clean dry atmosphere to prevent contamination by vapor, smoke, and dust suspended in air. Plastic gloves should be worn while handling parts to prevent contamination by skin oils and acids.

- **Wick Forming and Insertion [4]:**

Manual forming and insertion of wrapped-screen wicks can be accomplished as follows. The assembled wick must not contain wrinkles, and to prevent this, the screen may be wrapped on a cleaned mandrel. The total diameter of mandrel and wrapped screen should be only slightly less than the heat pipe inside diameter, so that the residual stress in the coiled screen will force it against the pipe wall when it is released from the mandrel. Obviously, the screen ends must be even, and the screen must be properly positioned so that the installation of end caps will not interfere with or crush the screen. To ensure physical contact between the screen layers and the pipe wall, a tapered plug or ball may be forced through the wick. A helical spring with an unstretched diameter slightly larger than the wick inside diameter is sometimes used to hold the screen layers in contact. It too can be installed with the aid of a mandrel. In this case, the spring is stretched while it is held by the mandrel. The length of the stretched spring must not greatly exceed that of the installed length or when it is released from the mandrel, axial forces may displace the screen. With the wick properly positioned in the pipe, the end caps are next welded on [2].

- **End Cap Installation [2]:**

End cap installation: If the fill tube is not an integral part of the end cap, it should first be welded to its end cap. End caps with or without a fill tube are usually welded to the pipe ends. High-quality welded joints are required at all seams since porosity or cracks in the weld can lead to a loss of the working fluid. To minimize the probability of this failure, inspections should be performed to verify the adequacy of the seal. A number of welding techniques are available. However, gas torch welding, e.g., using oxyacetylene gases, is generally not recommended, because of the presence of flux. Oxygen and filler metals tend to re-contaminate the cleaned parts. Tungsten inert gas welding (TIG), either manual or automatic, and electron beam welding (EBW) have been found to be satisfactory for heat pipe welding.

The TIG welding is an electric arc welding process using a sharp-tipped tungsten electrode surrounded by an annular shield of inert gas flowing from a torch tip. Filler metals are not generally used for heat pipe welding, but they may be integral parts of the end caps, e.g., the lip of the lipped butt joint shown in Fig. 5.6 can serve as filler metal. In addition this process does not employ a flux. Hence, TIG welding does not contaminate the cleaned heat pipe part. The EB weld is made in a vacuum chamber, and it eliminates the formation of the surface compounds from the metal and air. In addition, the EBW offers minimal heat input with maximum thermal density. It enables one to produce a welded joint with a minimum heat-affected zone, and consequently, the joint properties may approach those of the parent metal. It is, therefore, ideal for heat pipe welding. However, the investment cost in equipment for EBW may exceed that for automatic TIG by over 100 % and that for manual TIG by over 2000 %. Hence, the choice of welding process is dependent upon the availability of the equipment, and the investment in equipment depends greatly upon the quantity of production and the required quality of the products. Nevertheless, TIG and EB welding have been found satisfactory for heat pipe welding [2].

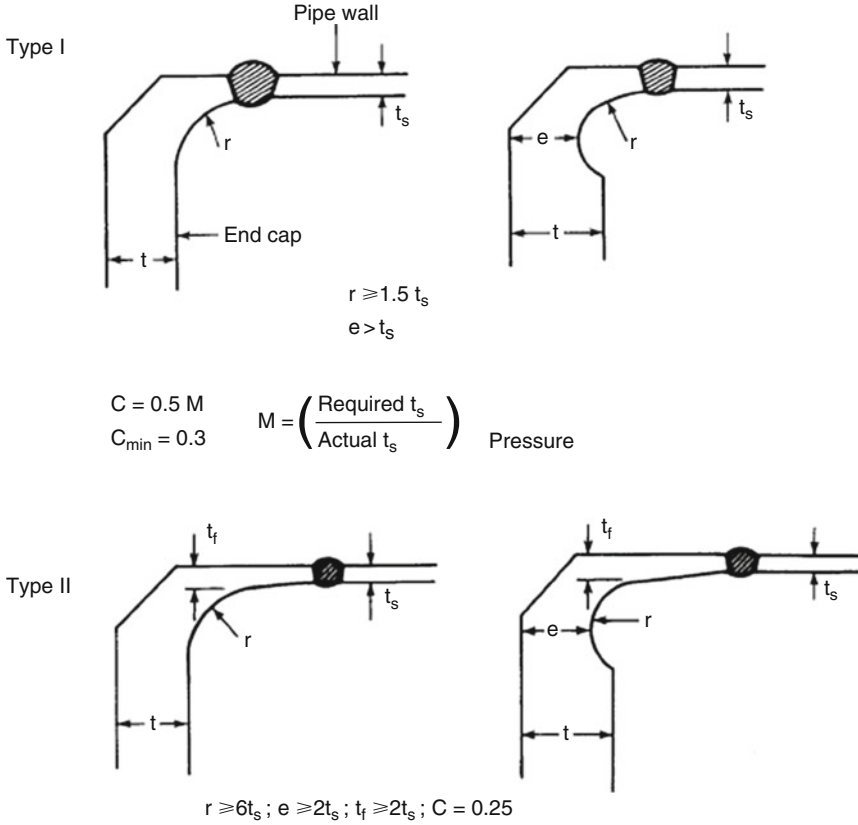


Fig. 5.6 End cap design details [1]

• **End Closure and Welding [1]:**

– End closure design guidelines: Observe the following general guidelines:

Acceptable end cap designs for flat circular heads may be type I or II as shown in Fig. 5.6.

End cap thickness can be determined from Figs. 5.7 and 5.8.

The welded end should have a square butt joint design (see Fig. 5.9).

Self-alignment during welding should be provided, as per the lipped butt joint for stainless steel (Fig. 5.10), the consumable filler insert for aluminum (Fig. 5.11) or an equivalent design.

Full-weld penetration should be achieved.

Machining of the crown of the weld bead should be avoided.

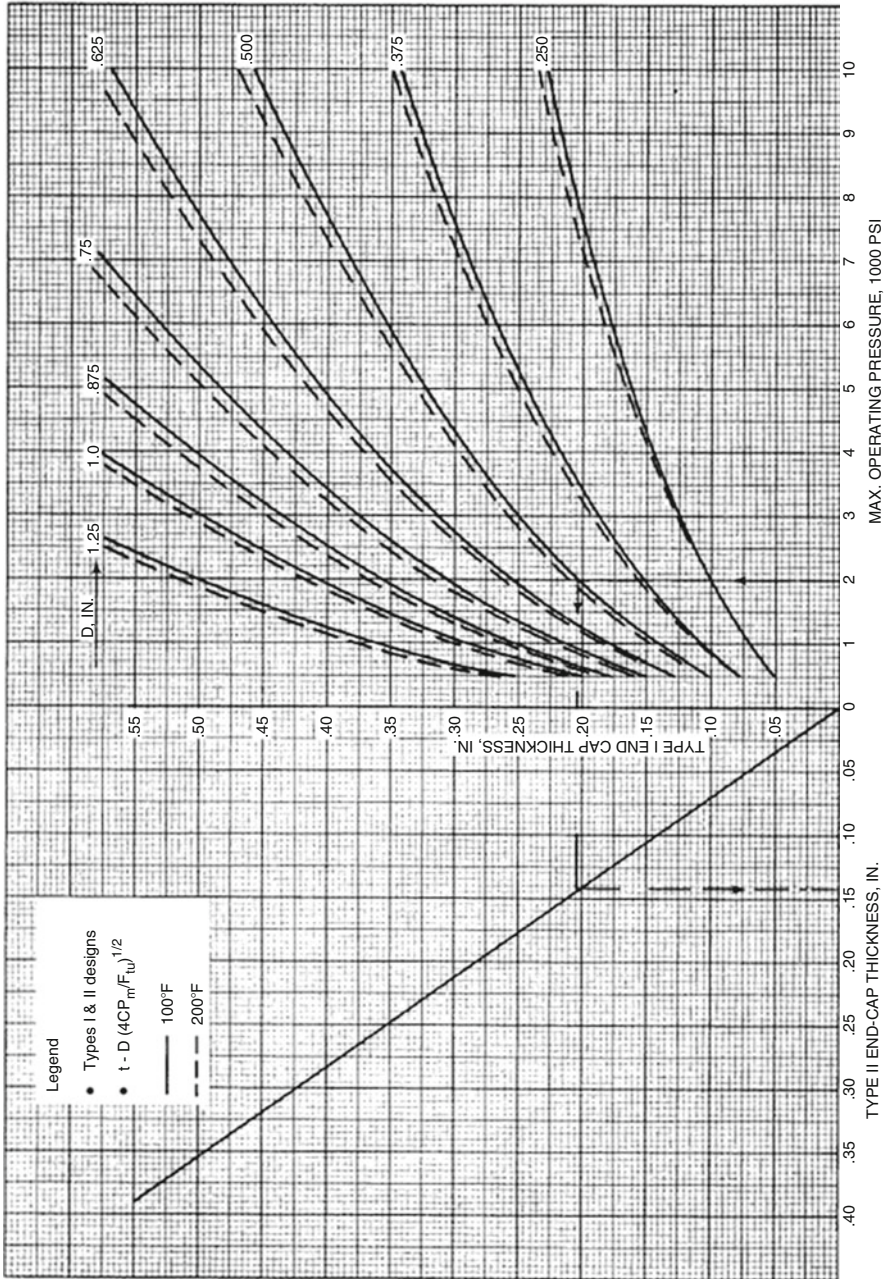


Fig. 5.7 End cap design curve 6061-T6 aluminum (as welded) [1]

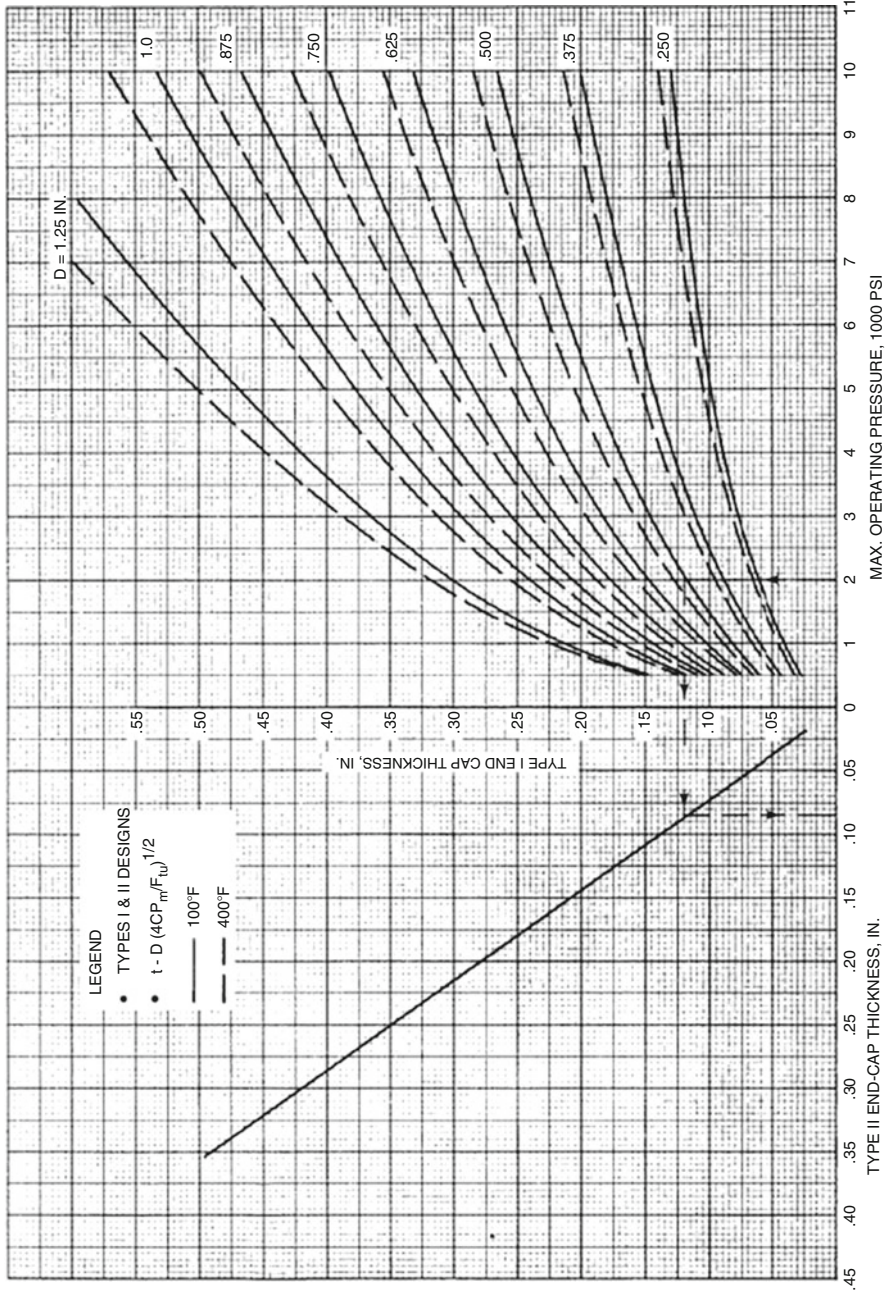


Fig. 5.8 End cap design curves, 304 stainless steel (as welded) [1]

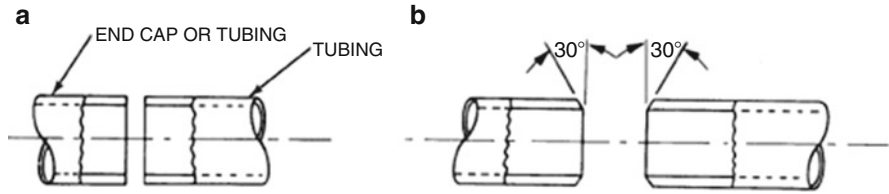


Fig. 5.9 Square butt joint designs [1]. (a) Standard design and (b) single bevel design

Fig. 5.10 Lipped butt joint design [1]

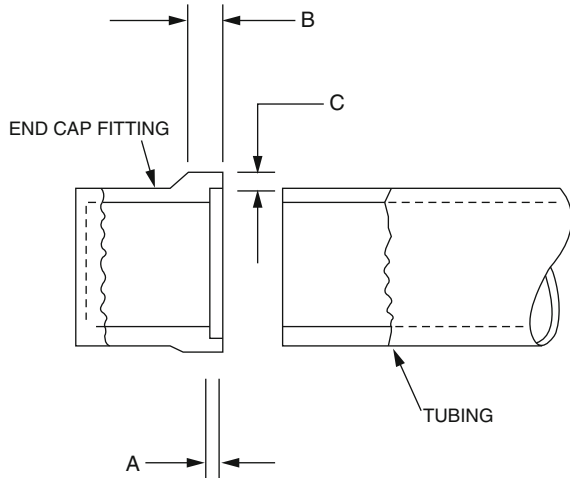
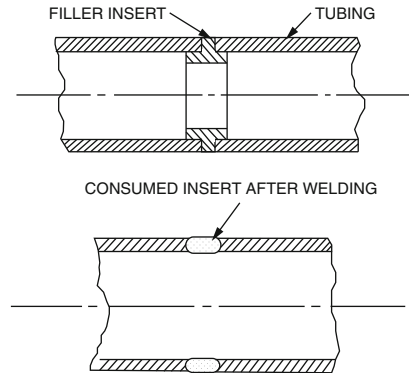


Fig. 5.11 Square butt joint with consumable filler insert [1]



5.4.1 Summary of Assembly of Heat Pipes Procedures

The following is a list of the procedures described above, which should be followed during heat pipe assembly [5]:

1. Select container material.
2. Select wick material and form.

3. Fabricate wick, end caps, etc.
4. Clean wick, container, and end caps.
5. Outgas metal components.
6. Insert wick and locate.
7. Weld end caps.
8. Leak check welds.
9. Select working fluid.
10. Purify working fluid (if necessary).
11. Degas working fluid.
12. Evacuate and fill heat pipe.
13. Seal heat pipe.

It may be convenient to weld the blank end cap before wick insertion, and in cases of sintered and diffusion bonded wicks, the outgassing may be done with the wick in place in the container.

For the manufacturer considering the production of a considerable number of identical heat pipes, for example, 50 or more units following prototype trials, a number of the manufacturing stages may be omitted. Outgassing of metal components may be unnecessary, and it may be found that, depending upon the filling and evacuation procedure used, the fluid degassing may be eliminated as a separate activity [5].

Prior to charging, a heat pipe must be evacuated to remove materials that may subsequently appear as unwanted non-condensable or that chemically react with the working fluid forming undesirable corrosion product.

The non-condensable are due not only to the free gas in the pipe but also to the molecules absorbed on the metal surface. Removal of free gases in the pipe can be done simply by pumping down with a vacuum pump. Removal of absorbed gas requires the evacuation of the pipe at elevated temperatures. The time required to absorb surface contaminants is usually reduced with the increased temperature. However, metals may lose their strength at high temperature [2].

Heat Pipe Assemblies Design Guidelines

Orientation with Respect to Gravity

For the best performance, the application should have gravity working with the system; that is, the evaporator section (heated) should be lower, with respect to gravity, than the condenser (cooling) section. In other orientations where gravity is not aiding the condensed liquid return, the overall performance will be degraded. Performance degradation depends on a number of factors including wick structure, length, and working fluid of the heat pipe along with heat flux of the application. Careful design can minimize the performance loss and allow an accurate prediction performance.

Temperature Limits

Most pipes use water and methanol/alcohol as the working fluids. Depending on the wick structure, pipes will operate in environments with as low as $-40\text{ }^{\circ}\text{C}$. Upper temperature limits depend on the fluid, but $60\text{--}80\text{ }^{\circ}\text{C}$ is the average limit.

Heat Removal

Heat can be removed from the condenser using air cooling in combination with either extrusion, bonded-fin heat sinks, or flat-fin stock. Enclosing the condenser in a cooling jacket allows liquid cooling.

Reliability

Heat pipes have no moving parts and have demonstrated life of over 20 years. The largest contributor to heat pipe reliability comes from control of the manufacturing process. The seal of the pipe, purity of the materials used in the wick structure, and cleanliness of the internal chamber have measurable effect on the long-term performance of a heat pipe. Any leakage will eventually render the pipe inoperable. Contamination of the internal chamber and wick structure will contribute to the formation of non-condensable gas (NCG) that will degrade performance over time. Well-developed processes and rigorous testing are required to ensure reliable heat pipes.

Forming or Shaping

Heat pipes are easily bent or flattened to accommodate the needs of the heat sink design. Forming heat pipes may affect the power handling capability as the bends and flattening will cause a change in fluid movement inside the pipe. Therefore design rules that take into consideration heat pipe configurations and the effect on thermal performance ensure the desired solution performance.

Effects of Length and Pipe Diameter

The vapor pressure differential between the condenser end and the evaporator end controls the rate at which the vapor travels from one end to the other. The diameter and length of the heat pipe also affect the speed at which the vapor moves and must be considered when designing with heat pipes. The larger the diameter, the more cross-sectional area is available to allow vapor to move from the evaporator to the condenser. This allows for greater power-carrying capacity. Conversely, length when in opposition to gravity has a negative effect on heat transport as the rate at which the working fluid returns from the condenser end to the evaporator end is controlled by the capillary limit of the wick which is an inverse function of the length of the pipe. Therefore, shorter heat pipes carry more power than longer pipes when used in application not assisted by gravity.

Wick Structures

Heat pipe inner walls can be lined with a variety of wick structures. The four most common wicks are:

- (a) Groove
- (b) Wire mesh
- (c) Sintered powder metal
- (d) Fiber/spring

The wick structure provides a path for liquid to travel from condenser to the evaporator using capillary action. Wick structures have performance advantages and disadvantages depending on the desired characteristics of the heat sink design. Some structures have low capillary limits making them unsuitable for applications where they must work without gravity assist.

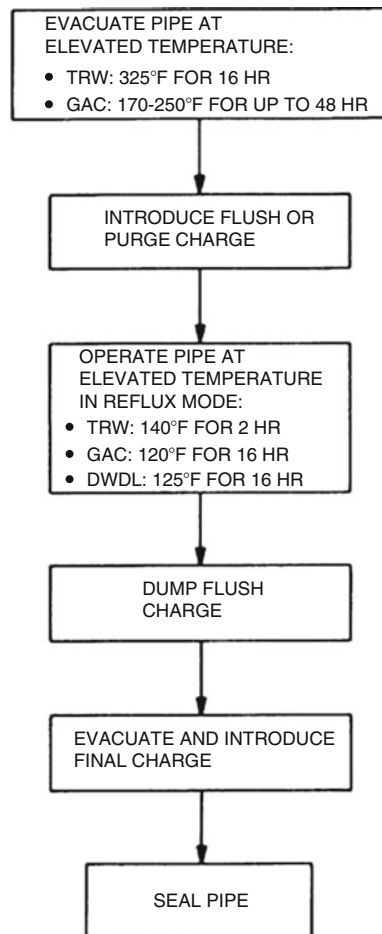
5.5 Evacuation and Charging

Prior to charging, a heat pipe must be evacuated to remove materials that may subsequently appear as unwanted non-condensable. Evacuation and charging are two processes that are closely related.

Figure 5.12 shows a flowchart for the evacuation and charging procedure used by heat pipe manufacturers, e.g., TRW, Grumman, and McDonnell Douglas, as presented by Edelstein and Haslett [1].

Initially, the pipe is evacuated, typically on a 4-in. Veeco pumping station at a station pressure of about 10^{-6} mmHg. Heaters wrapped around the pipe provide the elevated temperatures at which evacuation occurs. A schematic of the setup is shown in Fig. 5.13. The temperatures shown in Fig. 5.12 are representative for aluminum tubes. TRW bakes out at about 325 °F for 16 h, while Grumman bakes

Fig. 5.12 Overall evacuation and procedure used by TRW, Grumman, and DWDL/McDonnell Douglas [1]



Note: Temperatures shown are for aluminum envelopes.

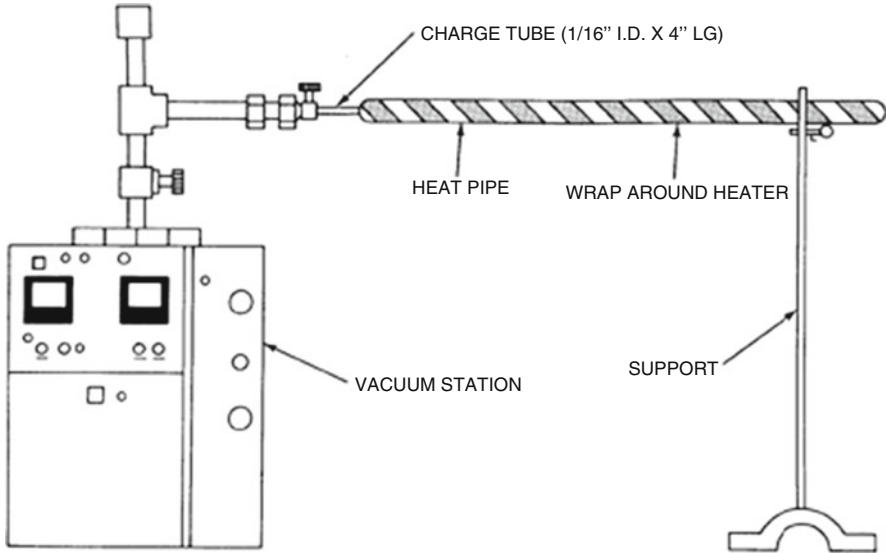


Fig. 5.13 Heat evacuation setup [1]

out at lower temperatures of 170–250 °F but for a longer time of up to 48 h. Although higher evacuation temperatures may be beneficial in removing additional adsorbed molecules, loss of mechanical properties of aluminum can occur at temperatures in the 300 °F range. Figures 5.12 and 5.13 show the effects of elevated temperature exposure on the room temperature ultimate and yield strength of aluminum 6061-T6 [1]. It is seen that loss of strength begins to occur at a temperature of 380 °F for 1/2-h exposure. The close relation between evacuation and charging can be seen in this Fig. 5.12; hence, evacuation and charging are often performed in the same equipment setup.

Typically a 1/16-in. (0.159 cm) i.d. tube, about 4 in. (10:160 cm) long, serves as the charge (pinch-off) tube. Based on the results presented in the previous section, this size tube is mildly restrictive during pump down for 1/2-in. (1.270 cm) d pipes. A technique which avoids the use of a small diameter charge tube will be presented later.

Figure 5.14 shows a possible setup for combined evacuation and charging. A possible procedure is as follows: with valve B closed and valves A and C open, the pipe is first pumped down at the ambient temperature, and then, the pumping is continued while the pipe is heated. The temperature of the heat pipe and the pumping time depend, of course, on the pipe material and its eventual operating temperature as described in the previous paragraph. This process is sometimes called vacuum bake out. After completion of this vacuum bake out process, the pipe is flushed with a small amount of fluid. For this purpose, the fluid in the charge bottle is first heated above the fluid boiling temperature at the pressure of the vacuum system. Momentary opening of valve B then allows a small amount of flush charge to be dumped into the pipe. After the pipe is flushed in this manner once or twice, the pipe is ready for charging [2].

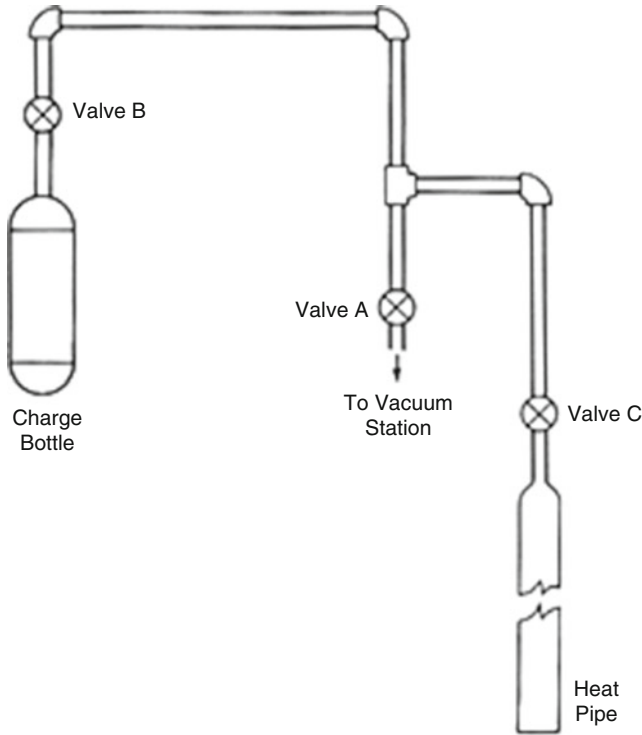


Fig. 5.14 Schematic of equipment for heat pipe evacuation and charging [2]

5.5.1 Fluid Charging

Details of the charging process depend on the state of the working fluid at the ambient temperature. If the fluid is in the gaseous state at room temperature, such as the case for the cryogenic heat pipe fluid, the charge can be introduced from a cylinder containing gas of high quality. The amount of charge can be measured by the gas pressure in the pipe at room temperature. Hence, the charging process consists of closing valve A and opening valves B and C. When the required amount of fluid has been charged into the pipe, valves B and C are closed. The pipe is then ready for pinching off and final sealing.

5.5.2 Fluid Purity and Inventory

Should a manufacturer use almost 99.999 % pure ammonia costing \$40 per pound, or will 99.99 % pure ammonia costing \$2.50 per pound be satisfactory? What impurities are present in the ammonia? How will they affect heat pipe

performance? These are some typical questions asked by both manufacturers and users of heat pipes concerning the requirements for the purity of heat pipe working fluids. These considerations can strongly affect both product reliability and cost [1].

The most prominent manifestation of impurities in a heat pipe is the accumulation of non-condensable gas in the condenser zone, with consequent loss of heat pipe conductance. Depending on the design and operating conditions, the presence of gas may not be serious and may go completely unnoticed. In other cases, significant blockage can occur; for some artery pipes, loss of pumping capacity can result [1].

Impurities may be in the pipe in the form of adsorbed gas molecules even before the working fluid is introduced. It may be brought in during the fluid transfer operation, or it may be present in the fluid itself. Often, the fluid purchased from the supplier may have significantly higher impurity levels than what was nominally specified [1].

Certain techniques are available to purify the fluid to a higher state than it is “as received” from the supplier. Additional cleaning may be necessary to satisfy functional requirements or as a safeguard against uncertain impurity levels in the suppliers fluid [1].

We can now discuss effects of impurities on heat pipe performance. In general, the impurities found in working fluids, such as ammonia, may consist of:

- Gases, such as nitrogen, oxygen, argon, carbon dioxide, carbon monoxide, and methane
- Water
- Miscellaneous materials such as oils, hydrocarbons, and nonvolatile solids

Of the miscellaneous materials, the most detrimental affect on heat pipe performance can be loss of wettability of the wick due to oily residues. As previously mentioned, a significant amount (130 ppm) of an oily contaminant was found in the liquid phase of ammonia and identified to be dioctyl phthalate. These materials, some of which may be soluble in the working fluid, may also adversely affect fluid properties, such as surface tension, wetting angle, and viscosity [1].

The presence of water in an aluminum or stainless steel pipe can cause corrosion, resulting in the loss of structural integrity. However, the quantities of water generally found in working fluids can be minimized by various purification techniques, some of which will be discussed later. The resultant water quantities, in terms of parts per million, are usually small enough so as not to present a serious corrosion loss-of-strength problem, since the corrosive reaction will generally cease when the water is consumed. The reaction products, however, may be far more serious in terms of non-condensable gas generated [1].

Fluid used for the heat pipe must obviously be of high purity. However, non-condensables may be dissolved in the supposedly pure liquids and solids. For example, non-condensables that are transferred to the charge bottle during vapor transfer may be removed by subjecting the fluid to repeated freeze-thaw cycles [1]. A schematic of this processing technique is shown in Fig. 5.15. The fluid is frozen in the charge bottle using, for example, liquid nitrogen for ammonia and ambient air for sodium.

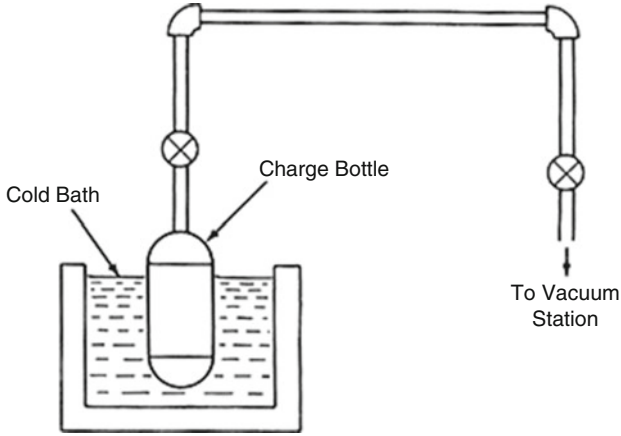


Fig. 5.15 Schematic of fluid purification process [2]

It is also necessary that the heat pipe is neither underfilled nor overfilled with its working fluid. An underfill may result in degradation of its performance. On the other hand, an overfill can result in condenser blockage. If slight overfill can be tolerated, the fluid inventory can be calculated by Eq. (5.1). The fluid inventory calculated by this equation is larger than what is required, because it discounts the meniscus recession. Nevertheless, the depletion of liquid due to this recession is usually negligibly small:

$$m = A_v L_t \rho_v + A_w L_t \varepsilon \rho_l \quad (\text{Eq.5.1})$$

where

m = Fluid inventory.

A_v = Vapor cross-sectional area.

A_w = Wick cross-sectional area.

L_t = Total heat pipe length.

ρ_v = Vapor density at pipe operating temperature.

ρ_l = Liquid density at pipe operating temperature.

ε = Wick porosity.

5.5.3 Analysis of Gas Blockage

In Fig. 5.16, the volume occupied by the non-condensable is, from the ideal gas law is

$$N = n_G R T_G / P_G \quad (\text{Eq.5.2})$$

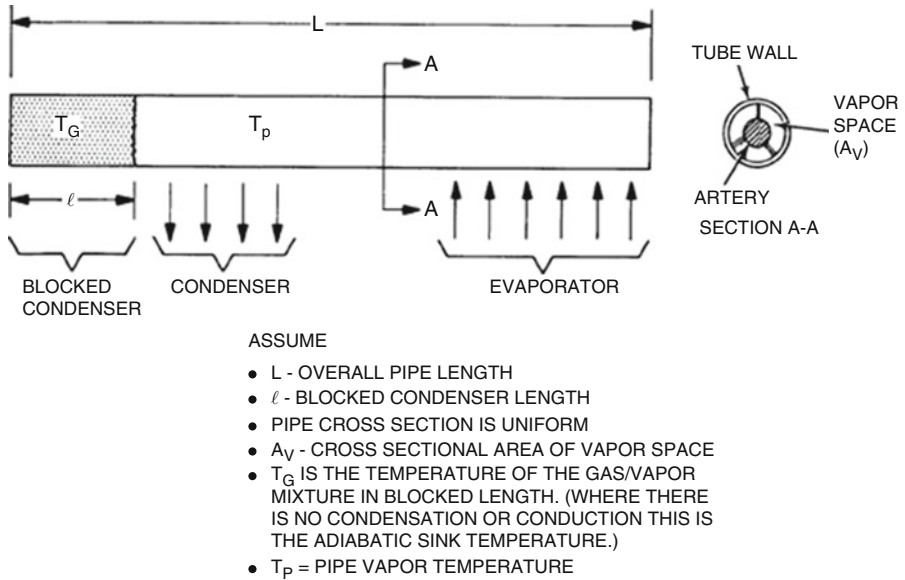


Fig. 5.16 Schematic for analysis of gas blockage [1]

where

n_G = Moles of non-condensable gas in pipe.

R = Gas constant.

T_G = Temperature of the gas/vapor mixture in blocked length.

P_G = Partial pressure of inert gas in length, ℓ

P_G = The difference between the working fluid pressure in the active and inactive portions of the pipe, i.e.,

$$P_G = P(T_p) - P(T_G) \tag{Eq.5.3}$$

where

$P(T_p)$ = Working fluid pressure at temperature T .

$P(T_G)$ = Gas pressure at temperature T .

ℓ = Blocked condenser length.

T_p = Pipe vapor temperature.

From Fig. 5.16, the gas volume can be related to the blocked length by

$$V = A_v \cdot \ell \tag{Eq.5.4}$$

Substituting Eqs. (5.3) and (5.4) in Eq. (5.2) and solving for ℓ yields

$$\ell = \frac{n_G RT_G}{A_v \{P(T_p) - P(T_G)\}} \quad (\text{Eq.5.5})$$

The moles of non-condensables can now be defined in terms of a working fluid impurity level, f ,

$$f = \frac{n_G}{n_p} \quad (\text{Eq.5.6})$$

where

n_p = Moles of working fluid in pipe

n_G = Moles of non-condensable gas in pipe.

f = Mole fraction of non-condensables in working fluid.

Substituting Eq. (5.6) into Eq. (5.5) and dividing by the overall pipe length, L , yields the blockage as a fraction of the total pipe length:

$$\frac{\ell}{L} = \frac{f n_p RT_G}{L A_v \{P(T_p) - P(T_G)\}} \quad (\text{Eq.5.7})$$

If n'_p is defined as the heat pipe charge per unit length, i.e., $n'_p = n_p/L$ then Eq. (5.7) becomes

$$\frac{\ell}{L} = \frac{f n'_p RT_G}{A_v \{P(T_p) - P(T_G)\}} \quad (\text{Eq.5.8})$$

This expression now relates the blockage to the operating conditions T_p and T_G ; to pipe design parameters n_p , A_v and working fluid; and to an impurity level factor, f .

5.5.4 Effect of Heat Pipe Design and Operating Conditions on Gas Blockage

In Fig. 5.17, the pipe blockage is presented as a function of the temperature difference between the operating and nonoperating sections for 0.5-in. (1.270 cm) axial groove ammonia heat pipe. An impurity content, f , of 0.0001 was assumed which is equivalent to 100 ppm (molar). The gases can be considered as being present in the charge fluid or as gas remaining in the pipe after evacuation.

The curve shows that for a fixed temperature difference ($T_p - T_G$), the blockage decreases at higher temperatures. Also, the blocked length increases for small differences in temperature between the pipe and gas temperature (thermal sink), such as, in the case of isothermalizing heat pipes. As an example, consider a 10-ft (3 m) long axial groove/ammonia heat pipe whose temperature (T_p) is 420 °R, attached to a sink (T_G) at 400 °R, i. e., $T_p - T_G = 20^\circ R$. The blockage produced by

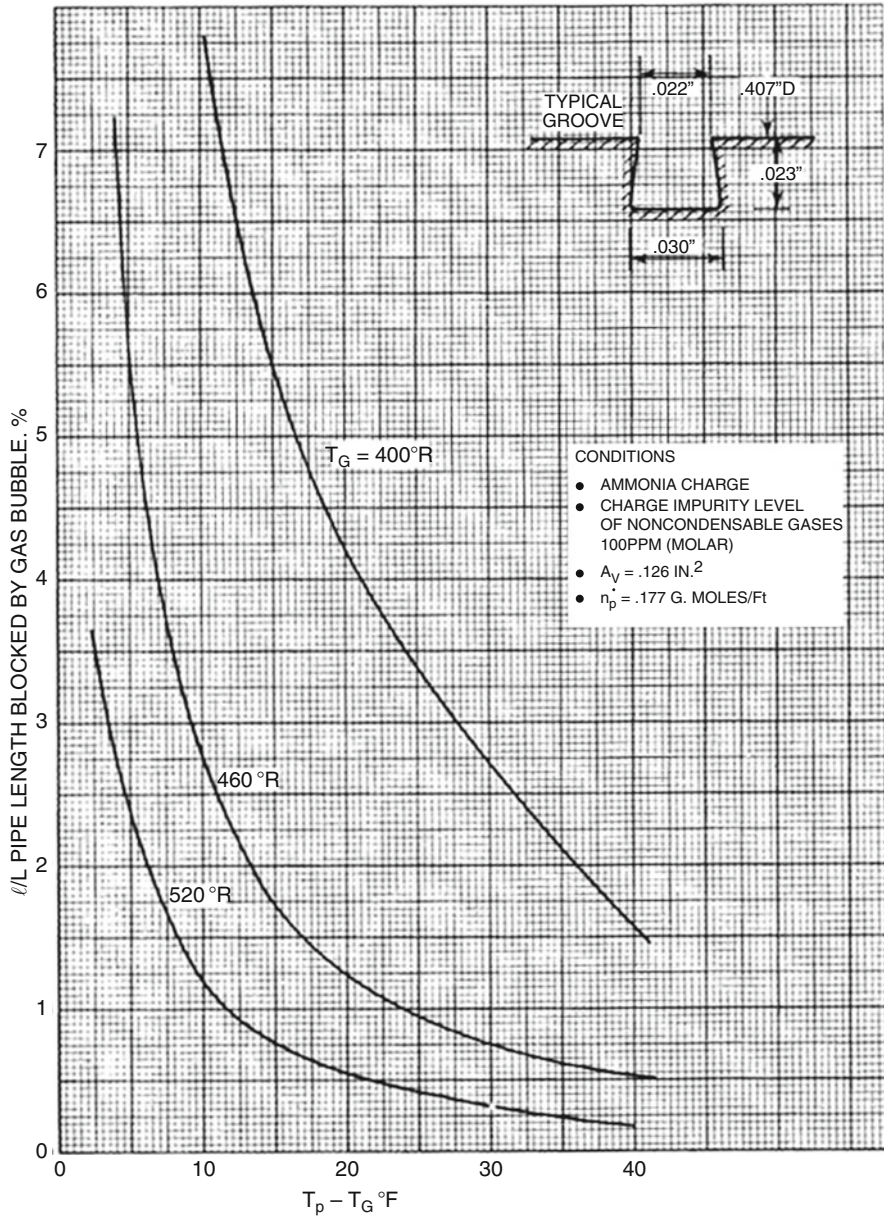


Fig. 5.17 Gas blockage in typical grooved heat pipe [1]

an impurity level of 100 ppm would be 4.2 % or 0.42 ft (5.0 in.) (12.7 cm). For an impurity level of 10 ppm (not shown), the blockage, which is proportional to f , would be 0.50 in. (1.27 cm).

The effect of a different pipe configuration is shown in Fig. 5.18, where a 0.5-in. (1.270 cm) spiral artery design is compared to the 0.5-in. groove design. Because of

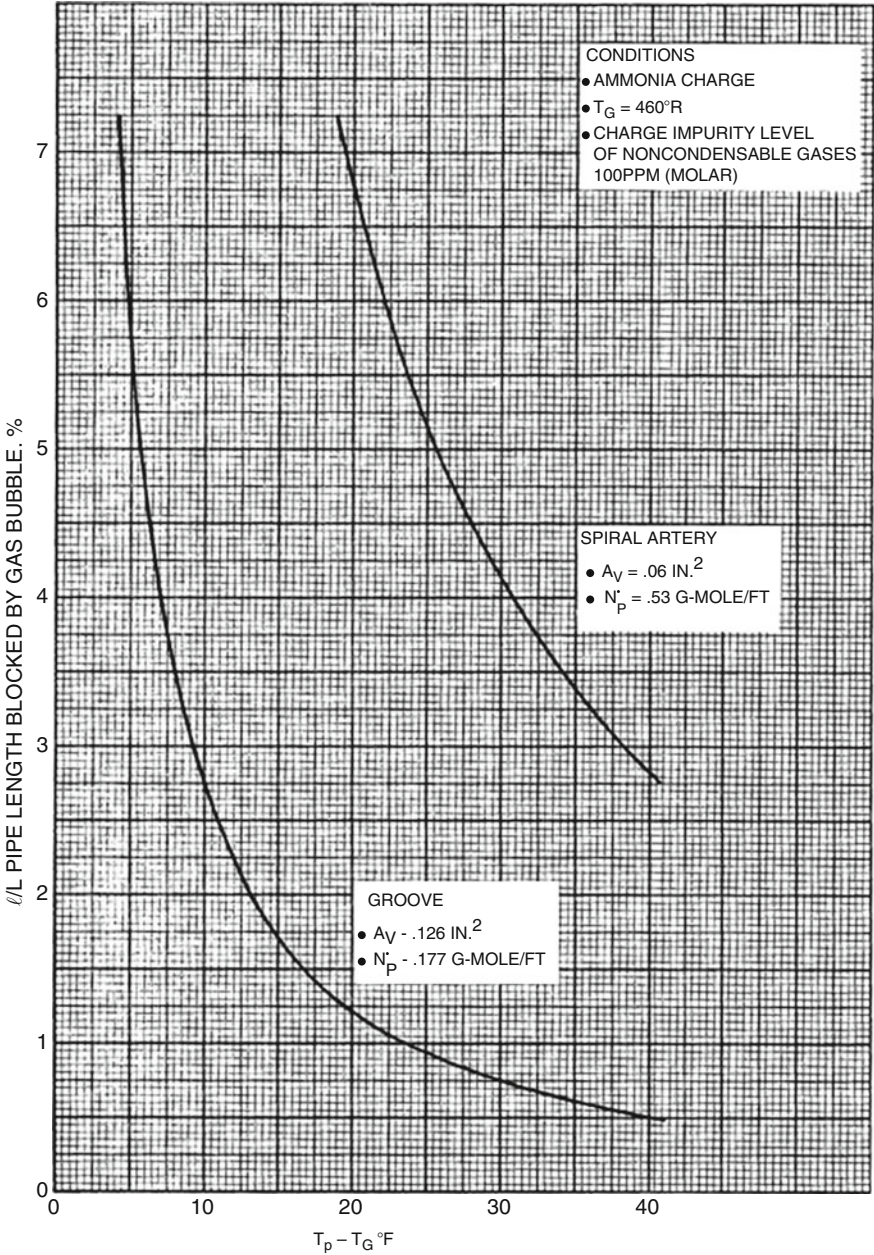


Fig. 5.18 Effect of heat pipe configuration on gas blockage [1]

its smaller vapor space, the spiral design produces a greater blockage than the groove under the same conditions.

The effect of different working fluids is shown in Fig. 5.19. Ammonia, acetone, and Freon-21 are plotted for the 0.5-in. axial groove design. It is seen that ammonia

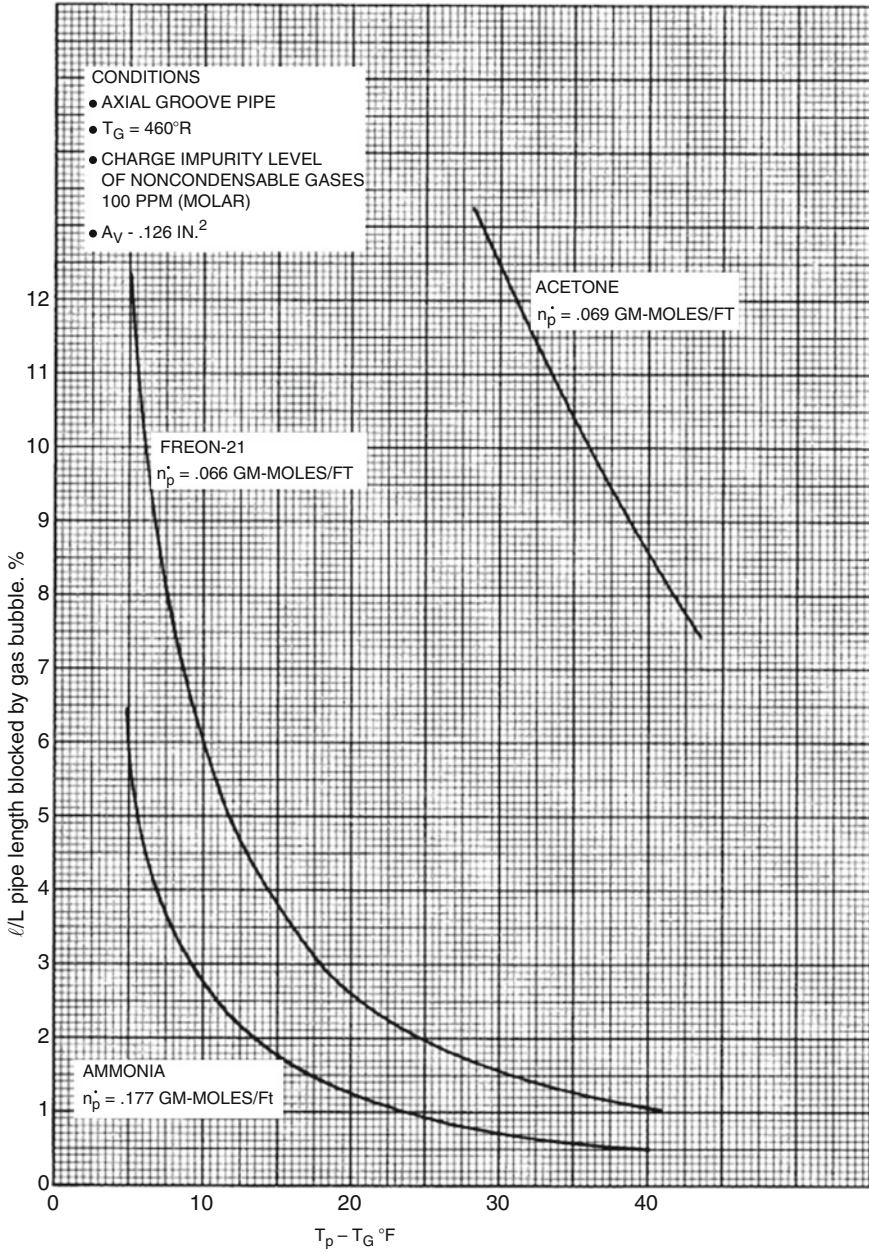


Fig. 5.19 Effect of working fluid on gas blockage [1]

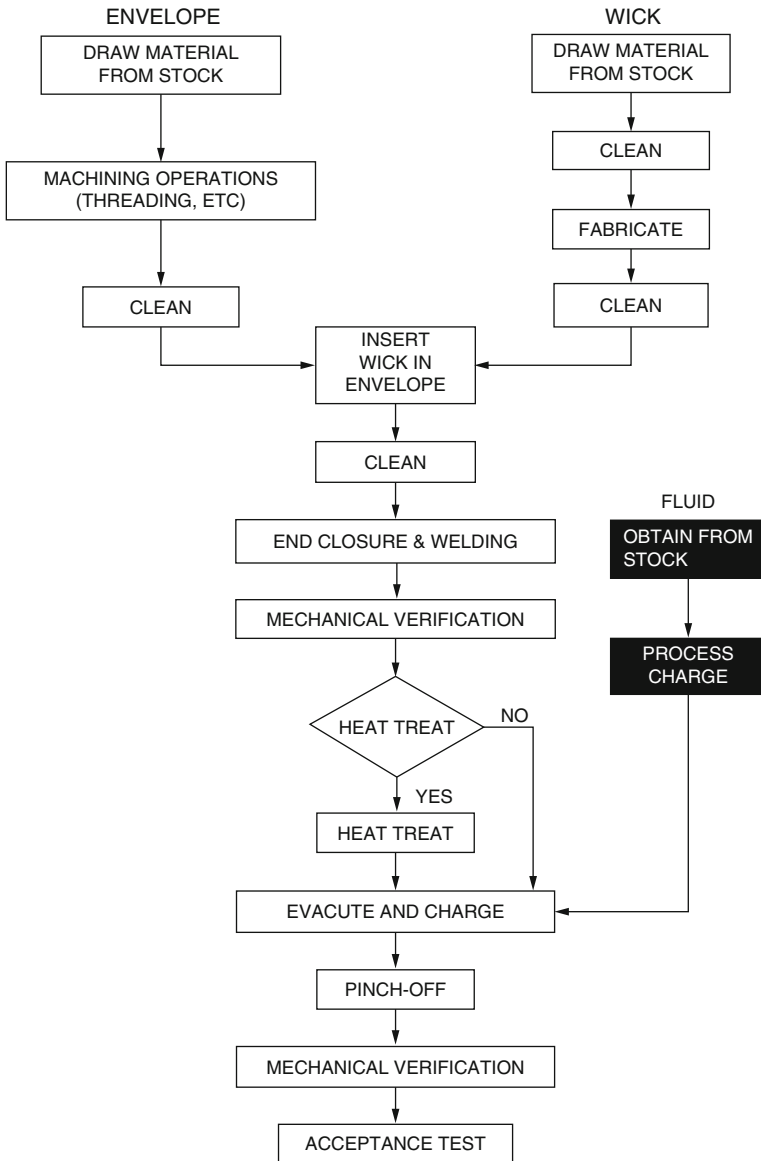


Fig. 5.20 Typical manufacturing steps for charging process [1]

results in a smaller blocked length than acetone or Freon-21. This is because the pressure of ammonia changes more rapidly with temperature than the other fluids. The value of these curves is that it allows the designer, for his particular application, to make a judgment regarding the allowable quantity of gaseous impurities, or conversely, to design the condenser length so as to accommodate some estimated amount of gas that may be present (Fig. 5.20).

5.6 Full Tube Closure

The manufacture of the heat pipe is near its completion with the exception that the pipe is still attached to a closed valve at the fill tube. It is necessary to sever the pipe from the valve and to form a permanent seal at the fill tube. In this process, no gas must enter the pipe and no fluid should be lost from the pipe. A closure technique, which has proved both economical and reliable, consists of:

1. Crimp seal (flatten and pinch) the fill tube to form a temporary leak-proof closure.
2. Sever the valve from the pipe by making a cut in the flattened area of the fill tube on the valve side of the crimp seal.
3. Weld the cut end of the fill tube by TIG or EB welding and remove the crimping tool.

5.7 Heat Pipe Testing Techniques

Per Chi [2], testing of the heat pipe may answer many questions. A simple test on the wetting of the wick and on the absence of leakage will insure that the pipe will operate as a heat pipe. A heat conduction test with an appropriately designed heat source and sink may verify the heat transfer capability and characteristics of the heat pipe. A test on the life of a heat pipe may include recording the performance of sample heat pipes over a long period of time or an accelerated life test may be performed with metallurgical examination of materials over predetermined intervals of time. In addition, tests may be required to answer questions on transient characteristics of the pipe. We will concentrate our discussion of the pipe testing's on verifying the mechanical soundness of the pipe, proper wetting of the wick, and operating characteristics of the pipe.

5.7.1 Mechanical Soundness

A sound structural design that has been properly verified by non-destructive tests is paramount to reliable, long-term heat pipe operation. The ASME pressure vessel code is recommended when specifying allowable design stresses, proof pressure, and burst pressure. Simplified methods are also presented by Edelstein and Haslett [1] for including the stress effects due to internal pressure, end caps, thermal expansion, saddle attachments, pipe bends, and dynamic loading. Cost-effective methods of leak detection for ammonia, Freon, and methanol used during pre-charging and postcharging operations include X-ray examination, pressurization under water, helium detection, and copper sulfate/ethylene glycol (for ammonia) [1].

The pipe must be able to withstand the maximum vapor pressure. For this reason, the pipe envelope and end caps have to be properly designed and joints must be made with high-quality welding before a design and production procedure can be finalized for large-quantity production. Experimental heat pipes may be made and subjected to high vapor pressure by heating the pipe so as to assure that the pipe envelope, the end caps, and the joints will be able to withstand the designed vapor pressure with appropriate margins of safety [2].

5.7.2 Wick Wetting

Unfortunately, many of these problems cannot be uncovered until the pipe is charged, sealed, and tested. In some cases, a long time can occur until some of these effects are noticed; by then, it is usually too late to provide corrective action. Hence, the objective must be to develop cleaning procedures which will prevent these problems from occurring and produce, therefore, a more reliable product. Moreover, in keeping with the overall aims of this study, the cleaning procedure should also be simple, inexpensive, and as free as possible from human error [1].

The simplest way to determine if the working fluid has wet the wick is to oscillate the heat pipe along its axis by hand. If the fluid slugs the end caps, it is fairly obvious that the liquid is riding on the wick in the vapor space. This preliminary test works fairly well for pipes having working fluid in the liquid state at room temperature. However, one can shake the pipe with vigor and break the force of surface tension. Liquid within the vapor space will result. This method is limited to qualitative testing of wick wetting. X-ray radiography may sometimes be used to observe uniformity of the liquid inside the wick or the presence of excessive liquid at the bottom of the pipe [2].

5.7.3 Performance Versification

If a pipe passes the mechanical and wetting tests, it can be assured that the pipe will operate as a heat pipe under favorable conditions. In order to establish pipe performance such as the maximum heat transfer capability and effective thermal conductance of the pipe, tests using the setup illustrated schematically in Fig. 5.21 may be used for the moderate-temperature heat pipe. The pipe may be placed at any desired orientation. The heat is supplied by an electrical tape wound around the evaporator section of the pipe [2].

Either the evaporator or the condenser temperature may be maintained constant regardless of the variation of the rate of heat supply by controlling the water inlet temperature and flow rate. Thermocouples installed along the heat pipe wall measure the axial wall temperature along the pipe at different heat transfer rates, which are indicated by the electrical power input. As the electrical power input is

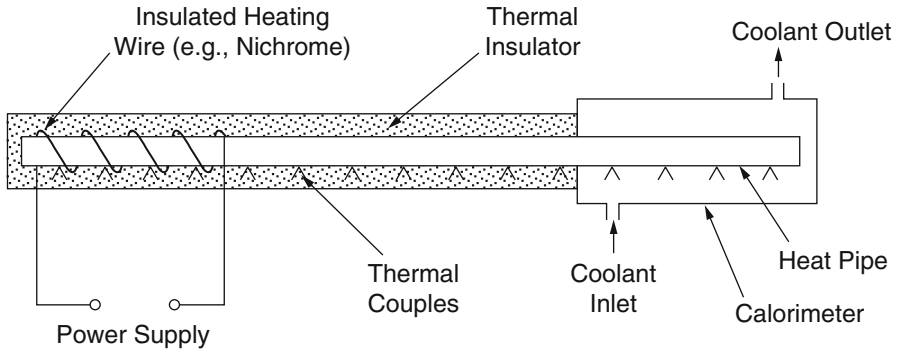


Fig. 5.21 Testing setup for moderate-temperature heat pipe [2]

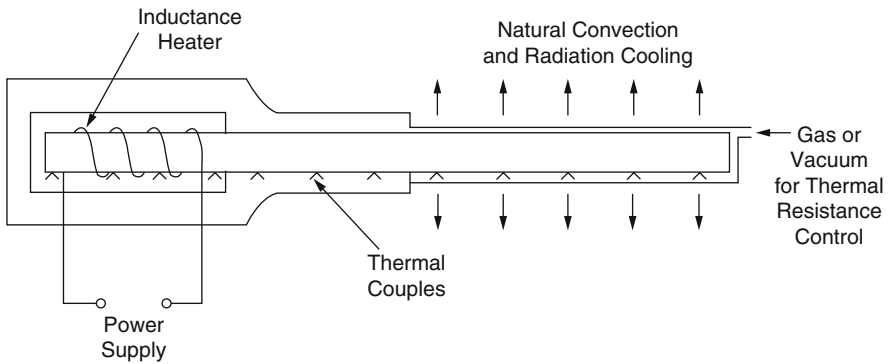


Fig. 5.22 Testing setup for liquid-metal heat pipe [2]

gradually raised to a certain limit, it may be observed that the temperature indicated by the thermocouple at the end of the evaporator rises suddenly above that indicated by other thermocouples at the evaporator. This sudden rise in temperature at the end of an evaporator indicates partial dry out of the evaporator. Hence, both heat transport limit and temperature characteristics of heat pipes may be measured using apparatus shown in Fig. 5.21.

The operating temperature and the heat transfer capability for the liquid-metal heat pipes are usually much higher than those for the moderate-temperature heat pipes. For increasing the power supply capability, the electrical heating tape shown in Fig. 5.21 can be replaced by an electrical induction coil. When this setup is used for testing liquid-metal heat pipes, radiation and natural convection of heat to the atmosphere provide a convenient heat sink. In order to control the pipe operating temperature, the thermal resistance of the condenser section may be controlled by providing a concentric annular gap as shown in Fig. 5.22.

References

1. Edelstein, F., & Haslett, R. (1974, August). *Heat pipe manufacturing study*. Final Report prepared by Grumman Aerospace Corp. for NASA, Contract No. NASS5-23156.
2. Chi, S. W. (1976). *Heat pipe theory and practice*. Washington, DC: Hemisphere Publishing Corporation.
3. Kemme, J. E. (1966, August). *Heat pipe capability experiment*. Los Alamos Scientific Laboratory, Report No. LA-3585-MS.
4. Rhodes Jr., R. A. (1973, October). *Procedures for the construction of a screen wick heat pipe*. A Lecture Note on Heat Pipe, U. S. Army Mobility Equipment R and D Center.
5. Reay, D., & Kew, P. (2006). *Heat pipes theory, design and application* (5th ed.). Amsterdam: Elsevier.

Chapter 6

Other Types of Heat Pipes

In today's market, there are a variety of types of heat pipes in terms of their geometry structure and their function of operations and/or the methods they use to transport heat from the source to the sink or on the other hand from the evaporator to the condenser and bring back the liquid from the condenser to the evaporator. Reay and Kew [1] are presenting a good description of different types of heat pipes along with their application, and the reader can obtain a good knowledge from their book [1]. In Chap. 1 of the book, both constant condenser heat pipe (CCHP) and variable condenser heat pipe (VCHP) types are discussed along with their general applications, and later, a mathematical modeling of heat pipe was presented, following Chaps. 3 and 4. Briefly here both CCHP and VCHP are touched upon again. Readers will be exposed briefly to different types of heat pipes in this chapter although their own research of the market for what type of heat pipe they are looking for and what is their demanding application is highly recommended.

6.1 Other Types of Heat Pipes

Some of the different types of heat pipes that are discussed in this chapter are summarized as follows:

- Variable conductance heat pipes
- Thermal diodes
- Pulsating (oscillating) heat pipes
- Loop heat pipes (LHPs) and capillary pumped loops (CPLs)
- Micro-heat pipes
- Use of electrokinetic forces
- Rotating and revolving heat pipes
- Miscellaneous types—sorption heat pipe (SHP) and magnetic fluid heat pipes

6.2 Thermosyphon

Another relatively simple, passive system, and the most popular solar water heater worldwide is the thermosyphon. Common in Japan, Australia, India, and Israel, they are easily recognizable because the tank must be located directly above the collector.

Thermosyphon systems work on the principal of heat rising. In an open-loop system (for nonfreezing climates only), potable water enters the bottom of the collector and rises to the tank as it warms. In colder climates, an antifreeze solution, such as propylene glycol, is used in the closed solar loop, and freeze-tolerant piping, such as cross-linked polyethylene (PEX), is used for the potable water lines in the attic and on the roof.

Several international manufacturers make thermosyphon systems. The advantage of this system over the batch heater is that solar heat is stored in a well-insulated tank, so hot water can be used any time, without the penalty of overnight losses.

The following illustration includes the primary components of any thermosyphon system (Fig. 6.1).

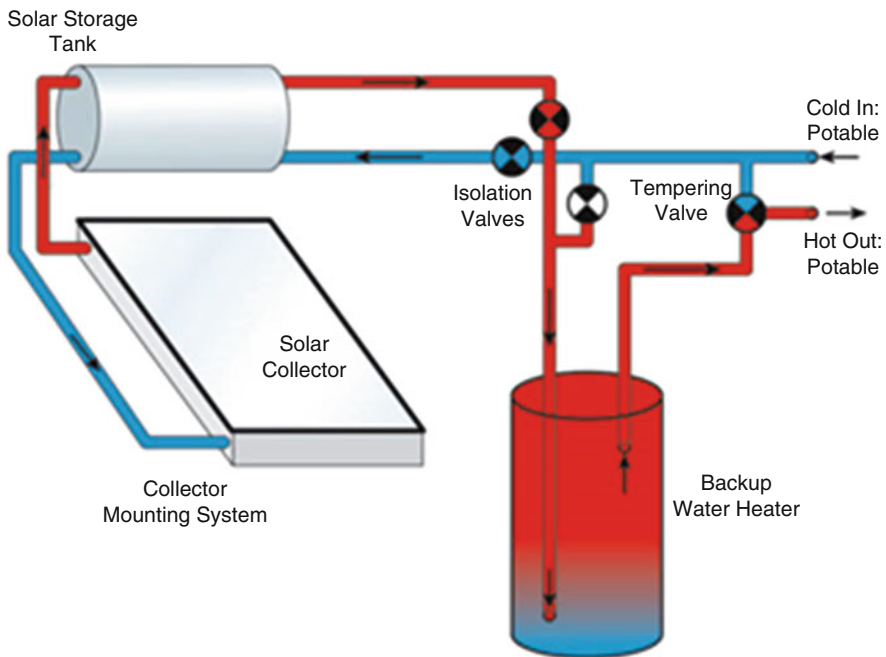


Fig. 6.1 Thermosyphon system

6.3 Loop Heat Pipes/Capillary Pumped Loop

Loop heat pipe thermal solutions are completely passive (minimal moving parts), two-phase heat transfer devices that are bendable, flexible, and routable. They can even operate as thermal diodes to prevent backward heat leak. Ideal for cooling the dispersed control systems found throughout today's military aircraft, Thermacore loop heat pipes can incorporate multiple evaporators and passive/active thermal regulations.

Loop Heat Pipe Advantages

- Totally passive (no external energy required)
- Transports heat up to 75 ft (23 m)
- Broad operating temperature range—for cryogenic to high-temperature applications
- Flexible and flex fatigue resistance (tested to more than 7.5 million flex cycles)
- Resists gravity loads (9g capable), shock, vibration, freeze, and thaw
- Versatile heat load capabilities (for dissipating a few watts or many kW)

6.4 Pulsating Heat Pipes

Pulsating, or oscillating, heat pipes comprise a tube of capillary diameter, evacuated and partially filled with the working fluid. Pulsating heat pipe configurations are shown schematically in Fig. 6.2, and their implementation is shown in Fig. 6.3. Typically, a pulsating heat pipe comprises a serpentine channel of capillary dimension, which has been evacuated, and partially filled with the working fluid. Surface tension effects result in the formation of slugs of liquid interspersed with bubbles of vapor. The operation of pulsating heat pipes was outlined in [2]. When one end of the capillary or evaporator tube is heated, the working fluid evaporates and

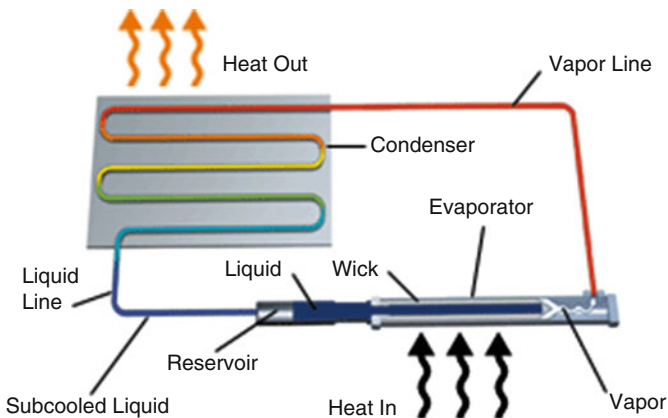


Fig. 6.2 Schematic of loop heat pipe (Courtesy of Thermacore)

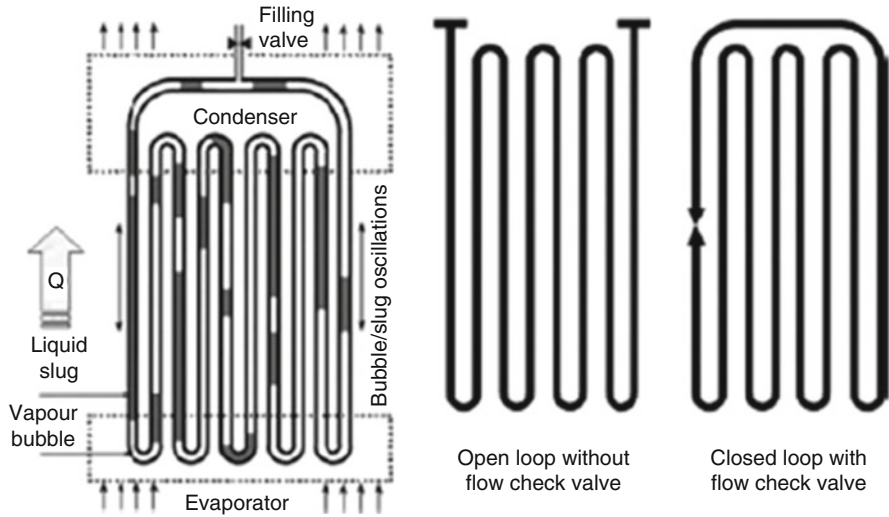


Fig. 6.3 Schematic representation of pulsating heat pipe

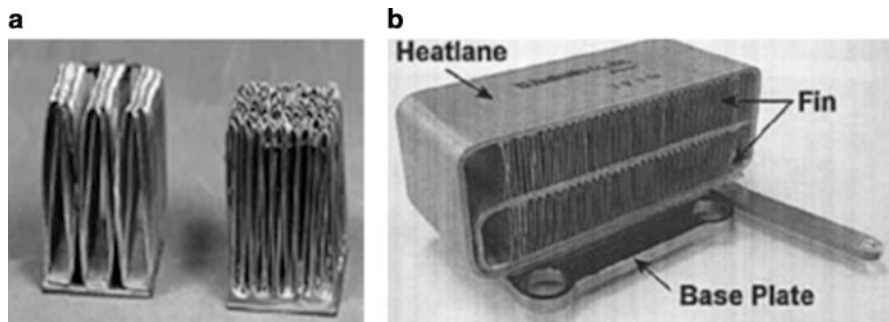


Fig. 6.4 Practical implementation of pulsating heat pipe. (a) Ref. [5], (b) Ref. [6]

increases the vapor pressure, thus causing the bubbles in the evaporator zone to grow. This pushes the liquid toward the low-temperature end or condenser. Cooling of the condenser results in a reduction of vapor pressure and condensation of bubbles in that section of the heat pipe. The rise and collapse of bubbles in the evaporator and condenser section results in an oscillation motion within the tube, respectively [1].

Closed-loop pulsating heat pipes (CLPHPs) perform better than open-loop devices because of the fluid circulation that is superposed upon the oscillations within the loop. It has been suggested that further performance improvements may result from the use of check valves within the loop; however, due to the inherently small nature of the device, it is difficult and costly to install such valves [2–6]. Therefore, a closed-loop device without a check valve is the most practicable implementation of the pulsating heat pipe [1] (Fig. 6.4).

Readers should refer to the book by Reay and Kew [1] for further information on this type of heat pipe.

6.5 Micro-heat Pipes (MHPs)

The theory of micro-heat pipe was introduced by Cotter in 1984. He defined a micro-heat pipe as “so small that the mean curvature of the liquid–vapor interface is comparable in magnitude to the reciprocal of the hydraulic radius of the total flow channel.”

An MHP is a small-scale device with a hydraulic diameter of $100\ \mu$ and a length of several centimeters. It differs from a conventional heat pipe in that it is much smaller, $5\text{--}500\ \mu$ in hydraulic diameter. In general, it does not contain a wick structure to assist the return of the condensate to the evaporator section. It rather uses capillary forces generated in the sharp edges of the pipe’s cross section.

Integrated circuits become faster and more densely packed with transistors. As a result, the power density increases and the heat generated as a by-product becomes more severe. Conventional methods of cooling are not an ideal way to overcome the heat problem so that small-scale and high-performance cooling devices are needed. A simple solution would be using a micro-heat pipe as an integrated part in the silicon substrate of the processors. Currently, the micro-heat pipe is being fabricated using micromachining technology (MEMS) and tested to verify the operation of the micro-heat pipe as a thermal heat spreader (Fig. 6.5).

Computers today have many components as to how fast it can run (Fig. 6.6). One of the components is the processor chip and its ability to cool itself during operations. The technology of computer chips has advanced since the first computer chip dated back in 1978, with 7.14 MHz to the most recent computer chips (for home user) Duo 2 Core with maximum speed of 5.32 GHz (2.66×2) an increased of more than 745 %. The increase is not only from the chip speed but also in power density and power dissipation. From Fig. 6.5, there is a clear increasing trend of the speed of the chip over the last 10 years. There is also an increasing trend in Fig. 6.7 for the power density and in Fig. 6.8 for power dissipation of computer processor chip.

Note that it was almost impossible to find any reference for power density of any chip. Power density graph above was calculated using the power dissipation found divided by the die size of the chip, assuming the die size of the chip is the actual size of the Pentium chip.

Figure 6.7 shows the thermal design power which is also known as the power dissipation. Through much research, the power consumption could not be found. Since the power needed to operate is almost always entirely dissipated in the form of heat and it is assumed that there is no power generated or stored in the chip, the power consumption is therefore closed (or the same) as the power dissipation.

There are many ways to remove heat from laptops. Since laptops are designed to sit on flat surfaces and that the heat is produced from the lower end of the laptop,

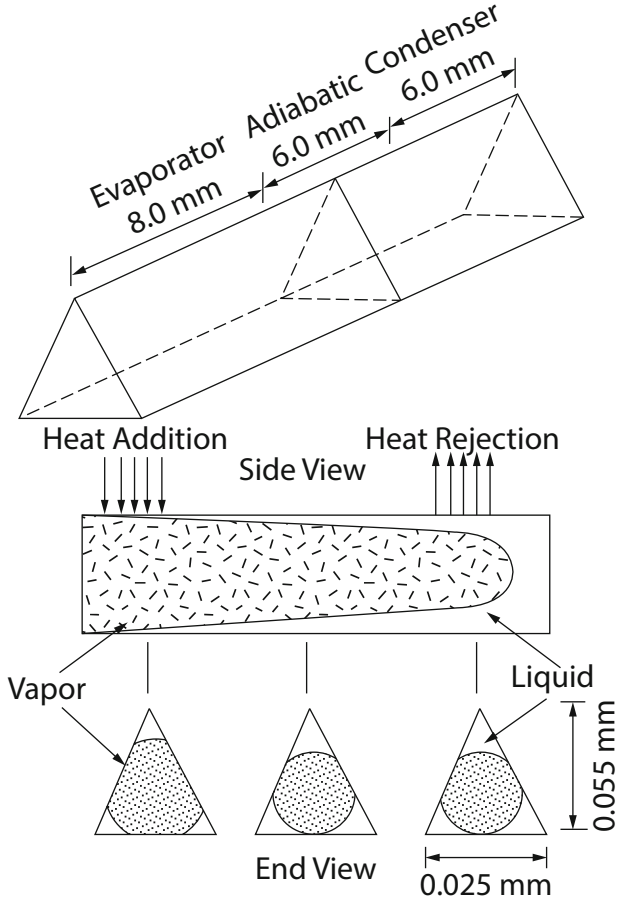


Fig. 6.5 Schematic of micro-heat pipe

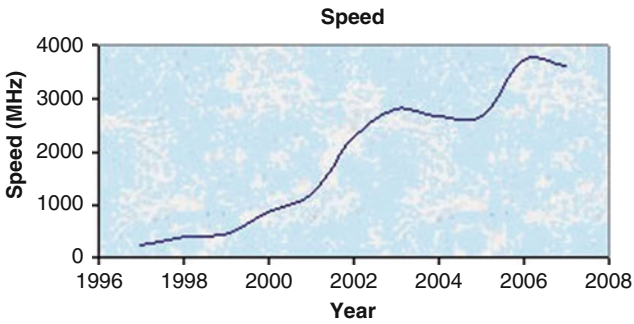


Fig. 6.6 Chip speed

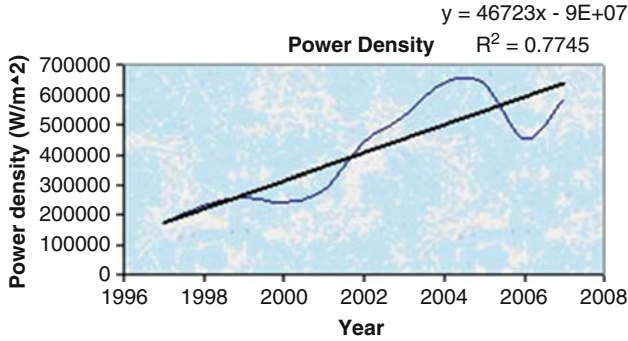


Fig. 6.7 Power density

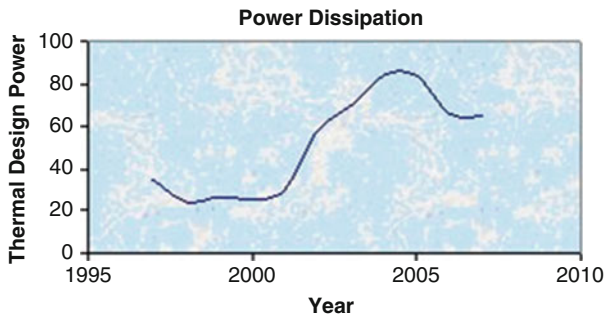


Fig. 6.8 Power dissipation

heat is usually removed by fans. The laptop depended on the cooled air pulled from the bottom of the laptop to cool excess heat. It is very risky to place a laptop on sofas and bed while using them, because this will cause overheating and might damage the internal electronic components. Another way of cooling processors is to use a heat pipe. The heat pipe contains heat transfer fluid in its center. “As the liquid evaporates, it carries heat to the cool end, where it condenses to the hot end.” (Wikipedia). This method is very expensive but at the same time very useful when space is limited.

Figure 6.9 above shows an example of a micro-heat pipe. From this figure, it is shown that the heat pipe is a closed cylindrical pipe (in a vacuum) which contains some sort of liquid. As explained above, the heat would be carried from the “heat in end” to the other end of the pipe with cooler temperature. At the cooled end, the liquid (in steam form) would then condense and release all the heat it carried. This fluid then flows back to the hot end and the whole process repeats. Micro-heat pipe has fast thermal response and is very small. It is very useful in smaller machinery such as a laptop computer and cameras. It is also very dependable and can have a very long lifetime. Figure 6.10 is the newly developed superthin micro-heat pipe.

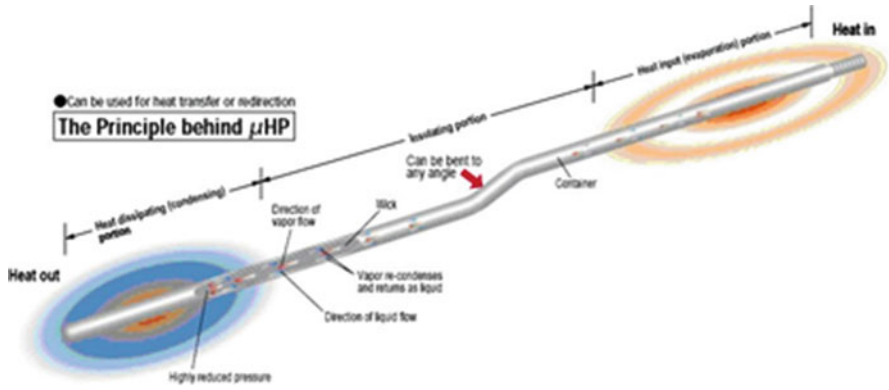


Fig. 6.9 Micro-heat pipe

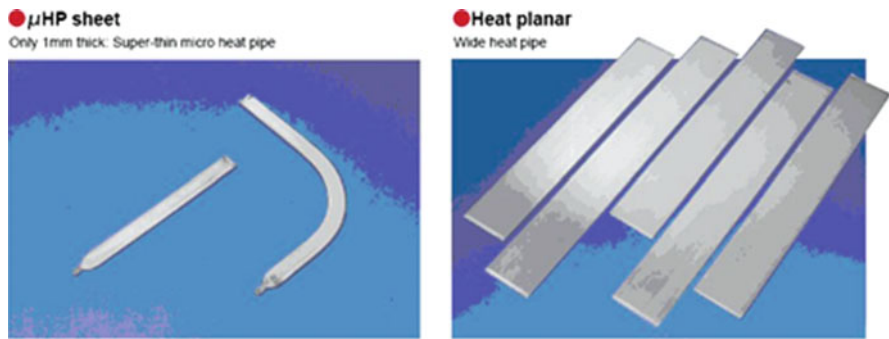


Fig. 6.10 Superthin micro-heat pipe and wide heat pipe

Micro-heat pipe differs from the common fins technology. Although the two uses the same idea, which is to cool off the processor, the fins method is less effective because even though the surface area increases, it cannot transfer heat fast enough to cool the processor. It also requires airflow-free area and fin space. Micro-heat pipe doesn't take much room, and it cools much faster due to the instant phase change in the cooling liquid.

A specific example of micro-heat pipe usage is the ThinkPad T60p notebook by IBM. As technology progresses, there is more and more demand for smaller and thinner laptop; therefore, many newer laptops from HP, Dell, and Fujitsu all use micro-heat pipe technology.

In conclusion, computer processor chip is a very complex subject. It was clear that the speed and power density will increase linearly as technology progresses. It would be interesting to look further into the future to see where technology will take the computer chip in size, shape, and its heat transfer aspect.

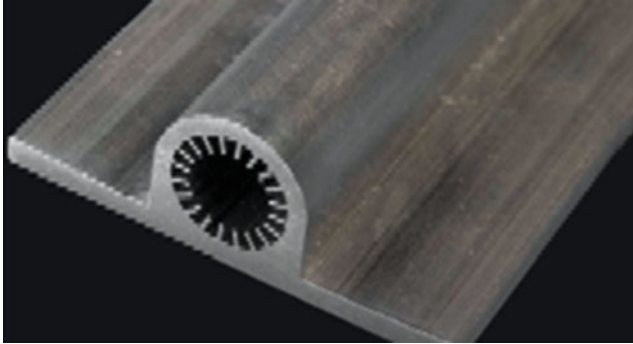


Fig. 6.11 Axial groove extrusion CCHP with integral flange (Courtesy of ACT)

6.6 Constant Conductance Heat Pipes (CCHPs)

Constant conductance heat pipes (CCHPs) are also called *fixed conductance heat pipes* or FCHP. Constant conductance heat pipes transport heat from a heat source to a heat sink with a very small temperature difference. Axial groove capillary wick structures are utilized because of the relative ease of manufacturing (aluminum extrusions) and their demonstrated heritage in spacecraft and instrument thermal control applications. CCHP can transport heat in either direction and is typically used to transfer heat from a specific thermal loads to a radiator panel or as part of an integrated heat pipe radiator panel. Common working fluids include ammonia, propylene, ethane, and water. The optimum fluid charge is determined for the specific application, and the effect of excess fluid charge is determined for both 0-G and 1-G operations. The following chart below compares the model predictions and test data on a specific CCHP (ACT, Advanced Cooling Technologies, Inc.) (Fig. 6.11).

6.7 Variable Conductance Heat Pipes (VCHP)

The early workers in the field of cold-reservoir VCHPs were troubled by vapor diffusion into the reservoir, followed by condensation, even if liquid flow into the gas area had been arrested. It is necessary to wick the reservoir of a cold-reservoir unit in order to enable the condensate to be removed. A good report provided by Berennan and Kroliczek [7] describes various VCHP, and most of this section is copied from their report. The partial pressure of the vapor in the reservoir will then be at the vapor pressure corresponding to its temperature. In principle, a variable heat pipe conductance can be achieved by modulating any one or several of the individual conductances that make up the overall conductance. A number of techniques exist to achieve variable conductance, and they can be grouped into the following four categories:

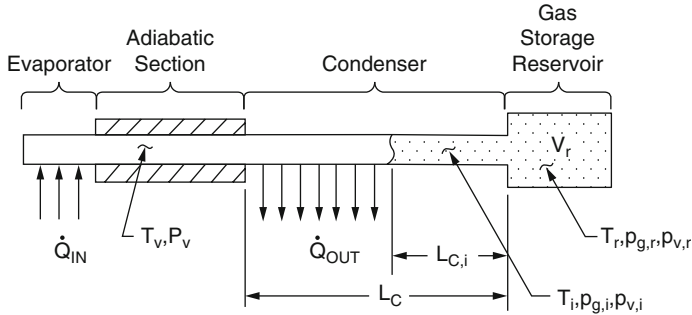


Fig. 6.12 Gas-loaded variable conductance heat pipe [7]

1. Gas-Loaded Heat Pipe

This technique consists of introducing a fixed amount of non-condensable gas into the heat pipe which during operation will form a “plug” which blocks the vapor flow. A schematic of a gas-loaded VCHP is presented in Fig. 6.12. Typically, a reservoir is added to accommodate the gas when “full-on” heat pipe operation is required. As vapor flows from the evaporator to the condenser, it sweeps the non-condensing gas which accumulates in the cold end of the heat pipe. The gas therein forms a barrier to the vapor flow and effectively “shuts off” that portion of the condenser which it fills. The length of the plug and therefore the condenser conductance depend on such factors as the system’s operating temperature, heat source and sink conditions, reservoir size and reservoir temperature, etc. The influence of these parameters as well as the various methods for obtaining gas-loaded VCHP control is discussed in the next section. It should also be noted that gas blockage can also be used to affect diode and switching operations: however, the transients associated with the “shutdown” or “switching” operations can be prohibitive with a gas-loaded system [7].

2. Excess-Liquid Heat Pipe

This approach is analogous to the “gas-loaded” heat pipe except that excess liquid accumulates as a slug in the condenser end rather than a non-condensable gas. The control with this technique tends to be less sensitive to variations in sink conditions (however, the actual designs can be more difficult to implement). Figure 6.13 shows one method for obtaining variable conductance with excess liquid. Again a reservoir is utilized and it is located inside the heat pipe envelope. The effective volume of the reservoir is varied by means of a bellows which contains an auxiliary fluid in equilibrium with its vapor. Adjustment of the bellows to changes in system temperature changes the reservoir volume therein allowing the excess liquid to move into or out of the condenser. Figure 6.14 illustrates a thermal diode heat pipe which utilizes liquid blockage to “shut off” the heat piping action in the reverse direction. In the normal forward mode operation, the excess liquid is swept into the reservoir at the condenser end. When conditions arise (e.g., an increase in sink temperature

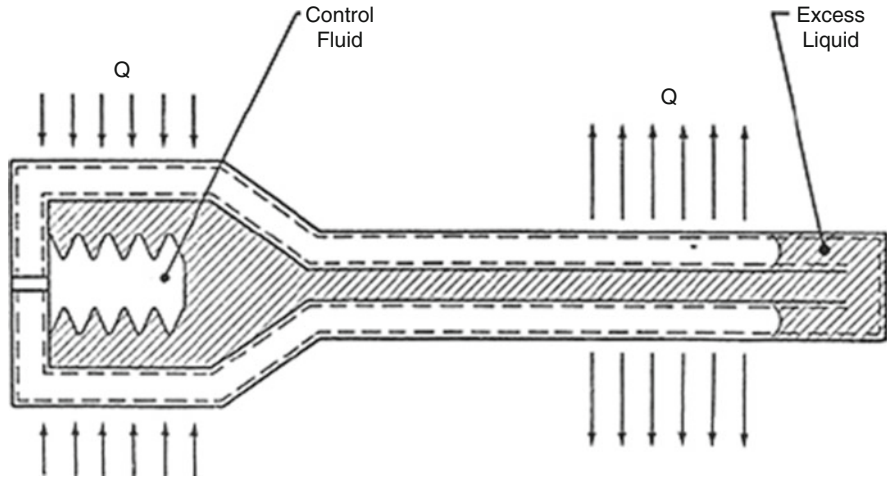


Fig. 6.13 Variable conductance heat pipe [7]

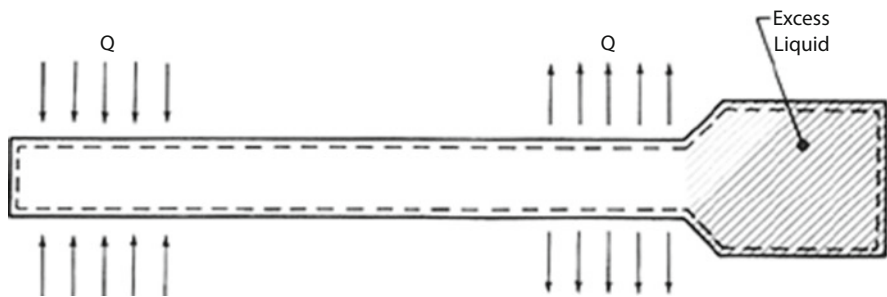


Fig. 6.14 Variable thermal diode heat pipe [7]

due to orbital conditions in space, etc.) which cause the condenser temperature to rise above the evaporator, the direction of vapor flow is reversed. The excess liquid is then driven from the reservoir into the normal evaporator section thus blocking the vapor flow and inactivating that section for heat rejection. Thus, the heat source is insulated from the hot condenser end with the result that the heat piping action is only effective in the forward mode [7].

3. Liquid Flow Control

Liquid flow control involves either interrupting or impeding the condensate return in the wick in order to “dry out” a part or all of the evaporator. This technique achieves control of the evaporator conductance by affecting the circulation of the working fluid and therein creating a hydrodynamic failure in the evaporator section.

Liquid flow control is limited generally to providing “on-off” control for diodes and thermal switches when the heat source is a dissipative one since the hydrodynamic failure will result in a nonuniform temperature distribution at the heat source.

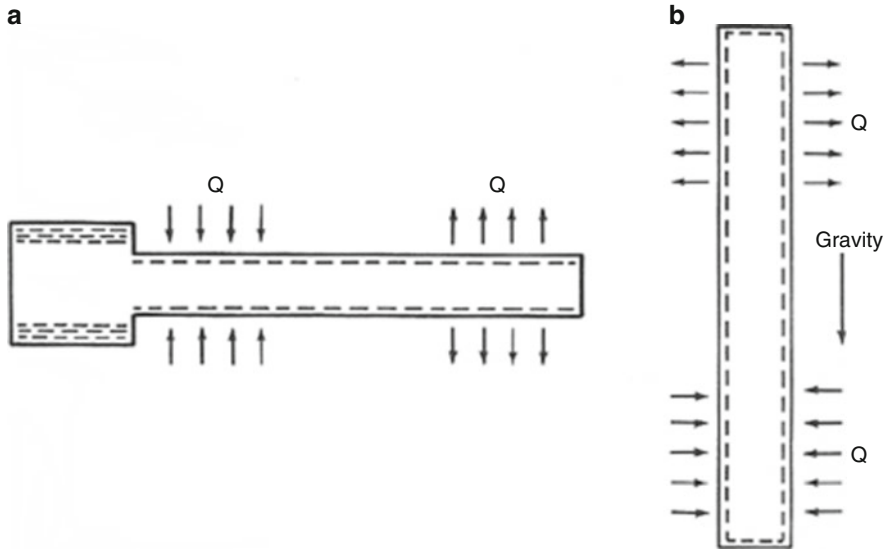


Fig. 6.15 Schematics of liquid flow-modulated heat pipes [7]. (a) Liquid trap diode heat pipe (b) Gravity operated diode heat pipe

However, for fixed temperature sources, continuous modulation of the heat pipe conductance by varying the wick flow resistance is acceptable since partial evaporator dry-out simply results in reduced heat transfer into the pipe.

Figure 6.15a shows a liquid trap diode heat pipe for aerospace application. In this case, a wicked reservoir is located at the evaporator end. This reservoir does not communicate with the main wick; therefore, when the temperature gradient is reversed, liquid evaporates at the hot side of the pipe and then condenses and is trapped within the reservoir. As a result, the wick becomes partially saturated and ultimately the condensate cannot return to the heat input section and the heat piping action is effectively shut “off.”

A gravity-operated diode heat pipe is shown in Fig. 6.15b. Here a reversal of the temperature gradient causes the liquid to collect at the bottom of the pipe where it cannot be pumped back up against the gravitational force.

4. Vapor Flow Control

Vapor flow control involves throttling or interrupting the vapor as it proceeds from the evaporator to the condenser. This creates a pressure drop between the two sections and hence a corresponding temperature drop.

A schematic of a vapor-modulated variable conductance heat pipe is given in Fig. 6.16. A bellows and auxiliary fluid are used to effect the throttling action. An increase in heat load or source temperature causes a rise in the vapor temperature which in turn causes the control fluid to expand and partially close the throttling valve therein creating a pressure differential. This method of control is substantially limited by the fact that the evaporator to condenser pressure differential must not exceed the capillary pressure developed by the fluid/wick combination.

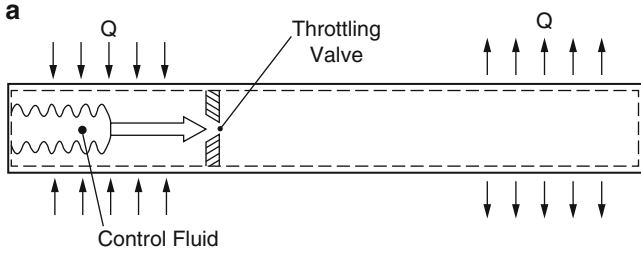


Fig. 6.16 Schematics of vapor flow-modulated heat pipes [7]. Vapor modulated thermal conductance

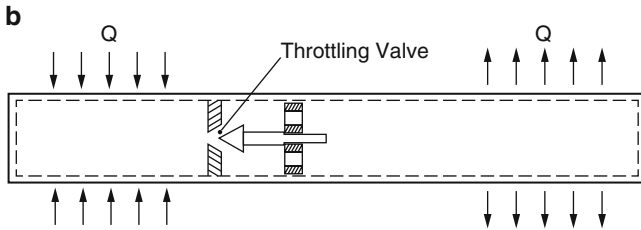


Fig. 6.17 Schematics of vapor flow-modulated heat pipes [7]. Vapor modulated thermal diode

If the valve arrangement is reversed to that shown in Fig. 6.17, a diode action is achieved when conditions arise which reverse the normal temperature gradient [7].

6.7.1 Variable Conductance with Gas-Loaded Heat Pipes

The principle of this technique is the formation of a gas plug at the condenser end of the pipe which prevents vapor from condensing in the part blocked by the gas. This plug is the result of introducing a fixed amount of a non-condensable gas into the heat pipe.

In the absence of circulation of the working fluid (i.e., without heat transport), the gas is uniformly distributed within the vapor space except for a small amount which is dissolved in the liquid phase of the working fluid. During operation, a steady flow of vapor exists from the evaporator to the condenser. The gas is swept by the vapor to the condenser. Unlike the vapor, it does not condense but forms a “plug” at the condenser end of the heat pipe.

Variable conductance variation through the addition of a non-condensable gas is particularly attractive because it accomplishes passive control of the vapor temperature. In a conventional (fixed conductance) heat pipe, the vapor temperature adjusts itself in order to meet the heat rejection requirements for a given sink condition. Thus, if the heat load and/or sink temperature increases, the vapor temperature will also rise.

In a gas-loaded heat pipe, the fixed amount of gas occupies part of the condenser; the length of the gas plug being dependent on the vapor (and sink) temperature. If the heat load is increased, the vapor temperature tends to rise as in the fixed conductance heat pipe.

However, the corresponding increase in vapor pressure of the working fluid compresses the gas plug, thereby increasing the size of the active condenser. This results in a higher conductance which effectively opposes the tendency of the vapor temperature to increase. Similarly, if the heat source and/or sink temperature decreases, the vapor temperature and pressure tend to drop which permits the gas plug to expand, the conductance of the heat pipe to decrease, and the vapor temperature decreases to be minimized. A gas-loaded heat pipe therefore reduces fluctuations of the operating temperature and behaves as a self-controlled VCHP [7] (Fig. 6.18).

6.8 Rotating and Revolving Heat Pipes

An extensive review of rotating and revolving heat pipes has been conducted by Wu and Peterson [8]. In their review, they first defined the difference between rotating and revolving heat pipes, which are sometimes used interchangeably. In rotating or revolving heat pipe, the condensate returned to the evaporator through centrifugal force, and there is no capillary wicks required. These types of heat pipes are used to cool turbine components and armatures for electric motors. Figure 6.19a is an illustration of a rotating heat pipe as the shaft of electric motor, while Fig. 6.19b is an illustration of a revolving heat pipe that rotates around an axis located at some distance from and parallel to the center axis of the pipe similar to the type that might be used to equalize the temperature in a rotating print head drum. The resulting performance characteristics of these two types of heat pipes are quite different and the reader should refer to a book by Peterson for more details [9].

There have been quite a bid of investigations and researches by various scientists around rotation heat pipe, but in the contrast, only limited investigations are in existence around revolving heat pipe, and some references are works by Bontemps et al. [10], Chen and Lou [11], Chen and Tu [12, 13], Keiyou and Maezawa [14], Mochizuki and Shiratori [15], and Niekawa et al. [16]. And in most cases, the speed of revolution was the most important parameter affecting the heat pipe transfer performance very similar to rotating heat pipes (Fig. 6.20).

6.9 High-Temperature Heat Pipes (Liquid-Metal Heat Pipes)

Initially Grover was interested in the development of high-temperature heat pipes, employing liquid-metal working fluids, suitable for supplying heat to the emitters of thermionic electrical generators and removing heat from the collectors of these devices.

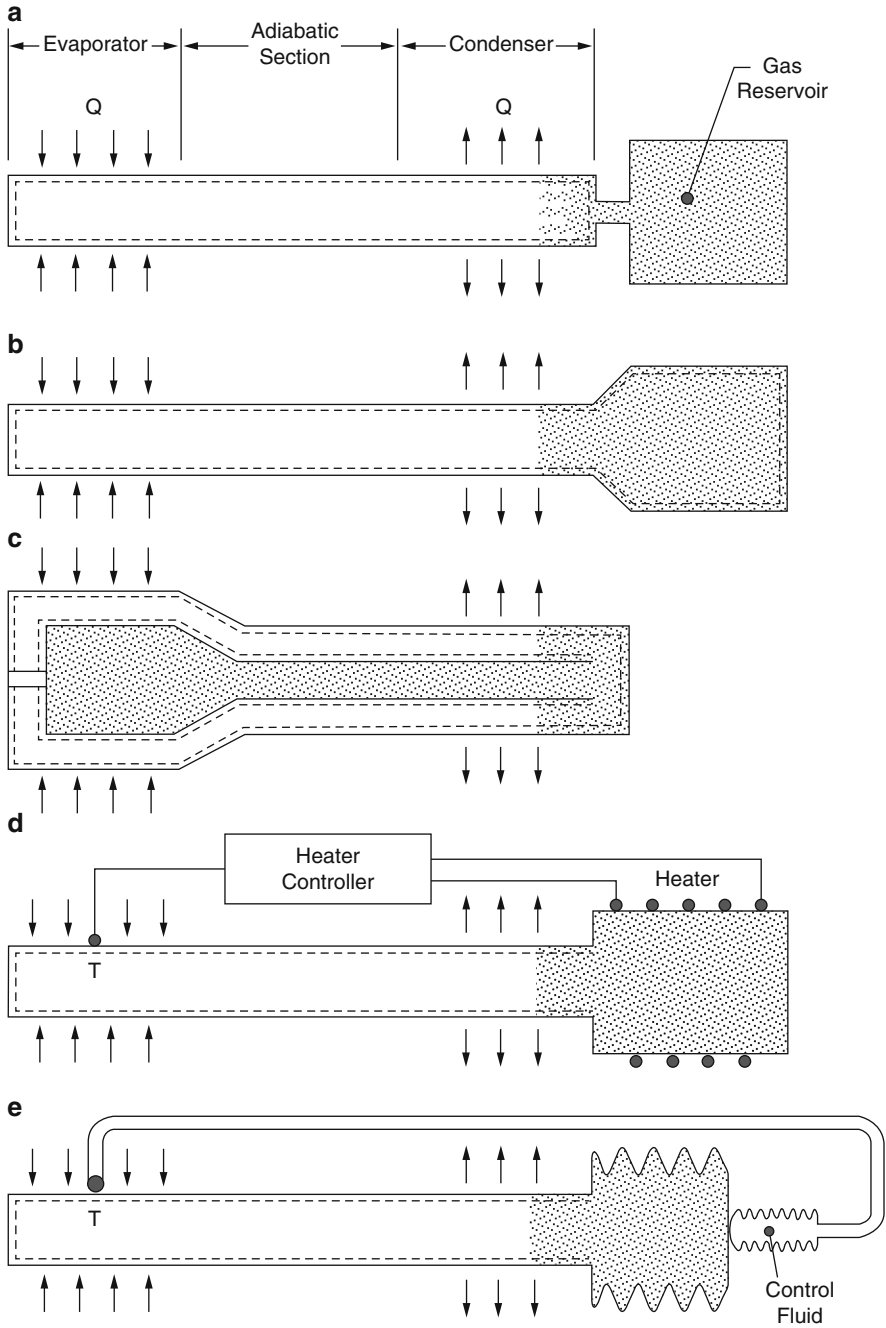


Fig. 6.18 Schematics of gas-loaded heat pipes [7]

Fig. 6.19 Rotating and revolving heat pipes [9]

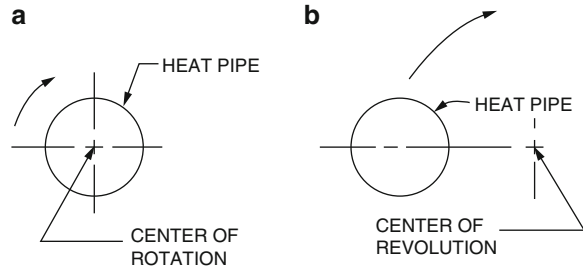
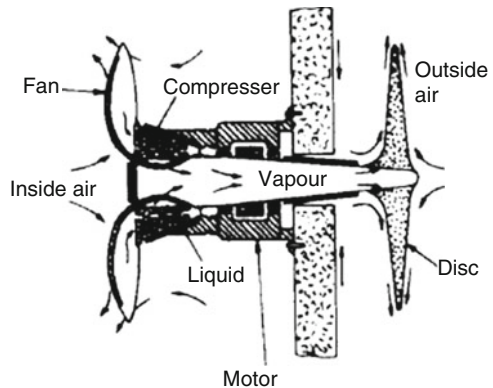


Fig. 6.20 A compact air-conditioning unit based on the wickless rotating heat pipe (Courtesy of NASA) [1]



High-temperature heat pipes are used in a wide variety of applications and service conditions from the ocean floor to geosynchronous orbit. These high-temperature heat pipes have improved processes as mundane as glass making, as industrial as oil-shale extraction, and as high-tech as epitaxial deposition (Fig. 6.21).

It is found that the heat pipe unit potentially offers better heat transfer, lower pressure drop, lower maintenance cost, and possibly lower installation cost for different applications in industry in particular for nuclear power plant and high heat conversion

6.10 Cryogenic Heat Pipes

Most of the work on heat pipes described so far has been associated with liquid-metal working fluids and for lower temperatures water, acetone, alcohols, etc. With the need for cooling detectors in satellite infrared scanning systems, to mention but one application, cryogenic heat pipes began to receive particular attention [17, 18]. The most common working fluid in these heat pipes was nitrogen, which was acceptable for temperature ranges between 77 and 100 K. Liquid oxygen was also used for this temperature range. The Rutherford High Energy Laboratory

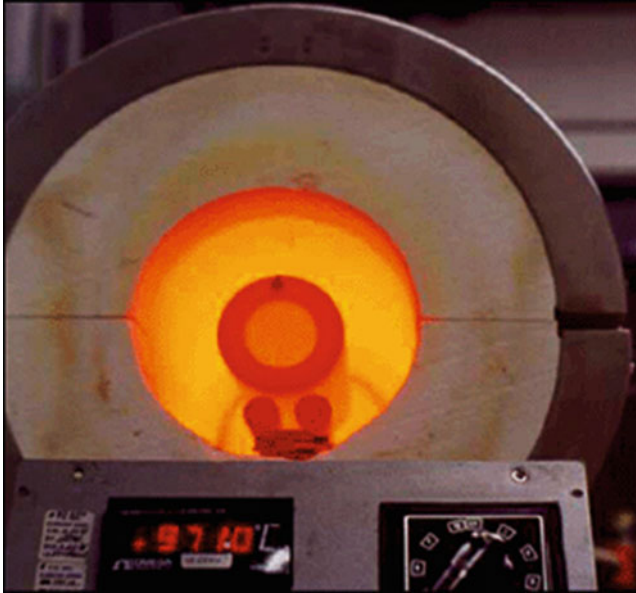


Fig. 6.21 High-temperature heat pipe at 971 °C (Courtesy of Thermacore)

(RHEL) was the first organization in the United Kingdom to operate cryogenic heat pipes [19], liquid hydrogen units being developed for cooling targets at the RHEL.

Long-term life tests on cryogenic heat pipes started a little later than those for higher-temperature units. However, there are comprehensive data from European Space Agency sources [20] on stainless steel (container was type 304L and wick type 316) heat pipes using as working fluids methane, ethane, nitrogen, or oxygen, arising out of tests extending over a period of up to 13 years. The test units were 1 m in length and either 3.2 or 6.35 mm outside diameter. Heat transport capability was up to 5 W m (meaning that the pipe transport 5 W over 1 m, or, e.g., 10 W over 0.5 m), and vapor temperatures 70–270 K. Tests were completed in the mid-1990s [8].

The main outcomes were as follows:

- All pipes retained maximum heat transport capability.
- All pipes maintained maximum tilt capability (capillary pumping demonstration).
- The evaporator heat transfer coefficient remained constant.
- No incompatibility or corrosion was evident in the oxygen and nitrogen pipes.
- Slight incompatibility, resulting in non-condensable gas extending over 1 % of the heat pipe length and therefore affecting condenser efficiency, was noted in the ethane and methane units.

Unlike the oxygen and nitrogen TIG-welded pipes, the ethane and methane units were hard brazed, and the implication is that the gas generation was attributed to

this. Cryogenic heat pipes employing fluids such as liquid air should have special provision for pressure release or be of sufficient strength since they are frequently allowed to rise to room temperature when not in use. The critical pressure of nitrogen is 34 bar [8].

Cryogenic heat pipes should be tested in a vacuum chamber. This prevents convective heat exchange, and a cold wall may be used to keep the environment at the required temperature. As a protection against radiation heat input, the heat pipe, fluid lines, and cold wall should all be covered with super insulation. If the heat pipe is mounted such that the mounting points are all at the same temperature (cold wall and heat sink), it can be assumed that all heat put into the evaporator will be transported by the heat pipe as there will be no heat path to the environment. Further data on cryogenic heat pipe testing can be obtained from [21, 22].

The operating range of cryogenic heat pipes is limited by the comparatively small temperature range between the critical and triple points. Therefore, the wick of a cryogenic heat pipe must have highly effective thermal conductivity and good thermal contact with the internal wall of the pipe. An analysis of the known capillary structures such as metal mesh, felt, cermets, longitudinal grooves, and spiral threads with channels showed that the most preferred capillary structures for cryogenic heat pipes are copper wool, ceramics made of sintered metal particles, and a spiral thread combined with a channel [23].

References

1. Reay, D., & Kew, P. (2006). *Heat pipes theory, design and application* (5th ed.). New York, NY: Butterworth-Heinemann.
2. Polasek, F., & Rossi, L. (1999). Thermal control of electronic equipment and two-phase thermosyphons. In *11th IHPC*.
3. Akachi. (1996). US Patent No. 5490558, United States Patent Office Search. See the following link on the web <http://www.freepatentonline.com/5490558.pdf>
4. Charoensawan, P., Khandekar, S., Groll, M., & Terdtoon, P. (2003). Closed loop pulsating heat pipes, Part A: Parametric experimental investigations. *Applied Thermal Engineering*, 23, 2009–2020.
5. Vogel, M., & Xu, G. (2005, February). Low profile heat sink cooling technologies for next generation cpu thermal designs. *Electronics Cooling 11*(1).
6. Duminy, S. (1998). *Experimental investigation of pulsating heat pipes*. Diploma Thesis, Institute of Nuclear Engineering and Energy Systems (IKE), University of Stuttgart, Germany.
7. Berennan, P. J., & Kroliczek, E. J. (1979, June). Heat pipe design. B & K Engineering Volume I and II. NASA contract NAS5-23406.
8. Wu, D., & Peterson, G. P. *A Review of Rotating and Revolving Heat Pipes*. 1991 National Heat Transfer Conference Paper No. 91-HT-24, Minneapolis, MN, American Society of Mechanical Engineers, New York.
9. Peterson, P. (1994). *An introduction to heat pipes—Modeling, testing and applications*. New York, NY: John Wiley & Sons.
10. Bontemps, A., Goubier, C., Marquet, C., & Solecki, J. C. (1984, May 14–18). Theoretical analysis of a revolving heat pipe. In *Proc. 5th Int. Heat Pipe Conf., Tsukube Science City, Japan* (pp. 274–279).

11. Chen, J., & Lou, Y. S. (1990, May 21–25). Investigation of the evaporation heat transfer in the rotating heat pipe. In *Proc. 7th Int. Heat Pipe Conf., Minsk, USSR*.
12. Chen, J., & Tu, C. (1986). Theoretical and experimental research of condensation heat transfer in parallel rotating heat pipe. In *Int. Heat Pipe Symposium, Osaka, Japan* (pp. 155–165).
13. Chen, J., & Tu, C. (1987, May 25–29). Condenser heat transfer in inclined rotating heat pipe. In *Proc. 6th Int. Heat Pipe Conf., Grenoble, France*.
14. Keiyou, G., & Maezawa, S. (1990, May 21–25). Heat transfer characteristics of parallel rotating heat pipe. In *Proc. 7th Int. Heat Pipe Conf., Minsk, USSR*.
15. Mochizuki, S., & Shiratori, T. (1980). Condensation heat transfer within a circular tube under centrifugal acceleration field. *Transactions of the ASME*, 202, 158–162.
16. Niekawa, J., Matsumoto, K., Koizumi, T., Hasegawa, K., & Kaneko, H. (1981). Performance of revolving heat pipes and application to a rotary heat exchanger. In D. A. Reay (Ed.), *Advances in heat pipe technology* (pp. 225–235). London, England: Pergamon Press.
17. Eggers, P. E., & Serkiz, A. W. (1970). *Development of cryogenic heat pipes*, ASME 70-WA/Ener-1. New York, NY: American Society of Mechanical Engineers.
18. Joy, P. (1970). *Optimum cryogenic heat pipe design*, ASME Paper 70-HT/SpT-7. New York, NY: American Society of Mechanical Engineers.
19. Mortimer, R. (1970, October). *The heat pipe*, Engineering Note-Nimrod/NDG/70-34. Harwell: Rutherford Laboratory, Nimrod Design Group.
20. Van Oost, S., & Aalders, B. (1997, September 21–25). *Cryogenic heat pipe ageing*. Paper J-6, Proceedings of the 10th International Heat Pipe Conference, Stuttgart.
21. Marshburn, J. P. (1973, August). Heat pipe investigations. NASA TN-D-7219.
22. Rice, G., & Fulford, D. (1991). Capillary pumping in sodium heat pipes. In *Proceedings of 7th International Heat Pipe Conference, Minsk, 1990*. New York, NY: Hemisphere.
23. Vasil'ev, L. L., Kiselev, V. G., Litvinets, M. A., & Savchenko, A. V. (2004). Experimental study of heat and mass transfer in a cryogenic heat pipe. *Journal of Engineering Physics and Thermophysics*, 28, 19–21.

Chapter 4

Application of Heat Pipe in Industry

© Springer International Publishing Switzerland 2016
B. Zohuri, *Heat Pipe Design and Technology*,
DOI 10.1007/978-3-319-29841-2_4

DOI 10.1007/978-3-319-29841-2_4

The following references should be listed at the Reference Section of Chapter 4. These are references are cited throughout the content of Chapter 4, and recognition of their material is noted in this errata.

Additional References

38. Z. Liu, Z. Wang, C. Ma, An experimental study on heat transfer characteristics of heat pipe heat exchanger with latent heat storage. Part I: Charging only and discharging only modes, *Energy Conversion and Management*, 47(7-8) (2006) 944-966.
39. Z. Liu, Z. Wang, C. Ma, An experimental study on the heat transfer characteristics of a heat pipe heat exchanger with latent heat storage. Part II: Simultaneous charging/discharging modes, *Energy Conversion and Management*, 47(7-8) (2006) 967-991.
40. N. Sharifi, S. Wang, T.L. Bergman, A. Faghri, Heat pipe-assisted melting of a phase change material, *International Journal of Heat and Mass Transfer*, 55(13-14) (2012) 3458-3469.
41. N. Sharifi, T.L. Bergman, M.J. Allen, A. Faghri, Melting and solidification enhancement using a combined heat pipe, foil approach, *International Journal of Heat and Mass Transfer*, 78 (2014) 930-941.
42. Z. h. Liu, B.-c. Zheng, Q. Wang, S.-S. Li, Study on the thermal storage performance of a gravity-assisted heat-pipe thermal storage unit with granular high-temperature phase-change materials, *Energy*, 81 (2015) 754-765.
43. B. w. Hu, Q. Wang, Z.-H. Liu, Fundamental research on the gravity assisted heat pipe thermal storage unit (GAHP-TSU) with porous phase change materials (PCMs) for medium temperature applications, *Energy Conversion and Management*, 89 (2015) 376-386.
44. S. Tiari, S. Qiu, M. Mahdavi, Numerical study of finned heat pipe-assisted thermal energy storage system with high temperature phase change material, *Energy Conversion and Management*, 89(0) (2015) 833-842.

45. S. Tiari, S. Qiu, M. Mahdavi, Charging and Discharging Process of a High Temperature Latent Heat Thermal Energy Storage System Assisted by Heat Pipe, in: ASME Power & Energy 2015 - ASME 2015 9th International Conference on Energy Sustainability, San Diego, California, USA, 2015.
46. S. Tiari, S. Qiu, Three-dimensional simulation of high temperature latent heat thermal energy storage system assisted by finned heat pipes, *Energy Conversion and Management*, 105 (2015) 260-271.
47. C.W. Robak, T.L. Bergman, A. Faghri, Enhancement of latent heat energy storage using embedded heat pipes, *International Journal of Heat and Mass Transfer*, 54(15-16) (2011) 3476-3484.
48. K. Nithyanandam, R. Pitchumani, Analysis and optimization of a latent thermal energy storage system with embedded heat pipes, *International Journal of Heat and Mass Transfer*, 54(21-22) (2011) 4596-4610.
49. K. Nithyanandam, R. Pitchumani, Computational studies on a latent thermal energy storage system with integral heat pipes for concentrating solar power, *Applied Energy*, 103 (2013) 400-415.
50. K. Nithyanandam, R. Pitchumani, Design of a latent thermal energy storage system with embedded heat pipes, *Applied Energy*, 126 (2014) 266-280.
51. A. Khalifa, L. Tan, A. Date, A. Akbarzadeh, Performance of suspended finned heat pipes in high-temperature latent heat thermal energy storage, *Applied Thermal Engineering*, 81 (2015) 242-252.
52. S. Qiu, R. Galbraith, M. White, Phase change material thermal energy storage system design and optimization, in: ASME 2013 7th International Conference on Energy Sustainability, Minneapolis, Minnesota, USA, 2013.
53. M. Mahdavi, S. Qiu, Mathematical modeling and analysis of steady state performance of a heat pipe network, *Applied Thermal Engineering*, 91 (2015) 556-573.
54. M. Mahdavi, S. Qiu, S. Tiari, Numerical investigation of hydrodynamics and thermal performance of a specially configured heat pipe for high-temperature thermal energy storage systems, *Applied Thermal Engineering*, 81 (2015) 325-337.
55. M. Mahdavi, S. Qiu, Numerical Analysis and Optimization of a Complex Geometry, High Temperature Heat Pipe, First Thermal and Fluid Engineering Summer Conference, TFESC, New York City, USA, (2015).
56. M. Mahdavi, S. Tiari, S. Qiu, Numerical Investigation of the effect of adiabatic section location on thermal performance of a heat pipe network with the application in thermal energy storage systems, *Bulletin of the American Physical Society* 60 (2015).
57. C.E. Andraka, K.S. Rawlinson, N.P. Siegel, Technical Feasibility of Storage on Large Dish Stirling Systems, Sandia National Laboratories, Albuquerque, NM, USA, 2012.
58. H. Shabgard, A. Faghri, T.L. Bergman, C.E. Andraka, Numerical simulation of heat pipe-assisted latent heat thermal energy storage unit for dish-Stirling systems, *Journal of Solar Energy Engineering*, 136(2) (2013) 021025-021025.
59. D.J. Malan, R.T. Dobson, F. Dinter, Solar Thermal Energy Storage in Power Generation Using Phase Change Material with Heat Pipes and Fins to Enhance Heat Transfer, *Energy Procedia*, 69 (2015) 925-936.
60. M.S. Naghavi, K.S. Ong, I.A. Badruddin, M. Mehrali, M. Silakhori, H.S.C. Metselaar, Theoretical model of an evacuated tube heat pipe solar collector integrated with phase change material, *Energy*, 91 (2015) 911-924.

Appendix A: Dimensional Equivalents and Physical Constants

Dimensional Equivalents

Length	1 ft = 12 in. = 30.48 cm = 0.3048
	1 m = 100 cm = 39.37 in. = 3.28 ft
Mass	1 lbm = 0.03108 slug = 453.59 g = 0.45359 kg
	1 kg = 1000 g = 0.06852 slug = 2.205 lbm
Time	1 h = 3600 s
	1 s = 2.778 × 10 ⁻⁴ h
Force	1 lbf = 4.448 × 10 ⁵ dyne = 4.448 N
	1 N = 10 ⁵ dyne = 0.2249 lbf
Angle	1° = 1.745 × 10 ⁻² rad
	1 rad = 57.30°
Temperature	1°F = 1° R = 0.5556° C = 0.5556° K
	1° K = ° C = 1.8° R = 1.8° F
	°F = 1.8° C + 32
	°C = 0.5556 (°F - 32)
	°R = ° F + 459.69
	°K = ° C + 273.16
	°R = 1.8° K
°K = 0.5556° R	
Energy	1 Btu = 777.66 ft lbf = 252 cal = 1.054 × 10 ¹⁰ erg = 1054 J
	1 J = 10 ⁷ erg = 0.239 cal = 0.7375 ft lbf = 9.485 × 10 ⁻⁴ Btu
Power	1 Btu/h = 2.778 × 10 ⁻⁴ Btu/s = 2.929 × 10 ⁶ erg/s = 0.2929 W
	1 W = 10 ⁷ erg/s = 9.481 × 10 ⁻⁴ Btu/s = 3.414 Btu/h
Pressure	1 lbf/ft ² = 6.944 × 10 ⁻³ lbf/in. ² = 4.78.8 dyne/cm ² = 47.88 N/m ²
	1 lbf/in. ² = 144 lbf/ft ² = 68,948 dyne/cm ² = 6894.8 N/m ²
	1 N/m ² = 10 dyne/cm ² = 1.450 × 10 ⁻⁴ lbf/in. ² = 2.089 × 10 ⁻² lbf/ft ²

(continued)

Area	$1 \text{ ft}^2 = 1.44 \text{ in.}^2 = 929 \text{ cm}^2 = 0.0929 \text{ m}^2$
	$1 \text{ m}^2 = 104 \text{ cm}^2 = 1550 \text{ in.}^2 = 10.76 \text{ ft}^2$
Volume	$1 \text{ ft}^3 = 1728 \text{ in.}^3 = 2.832 \times 10^4 \text{ cm}^3 = 0.02832 \text{ m}^3$
	$1 \text{ m}^3 = 10^6 \text{ cm}^3 = 6.102 \times 10^4 \text{ in.}^3 = 35.31 \text{ ft}^3$
	$1 \text{ gal (US liquid)} = 0.13368 \text{ ft}^3 = 0.003785 \text{ m}^3$
Density	$1 \text{ gal (US liquid)} = 0.13368 \text{ ft}^3 = 0.003785 \text{ m}^3$
	$1 \text{ lbm/ft}^3 = 0.03108 \text{ slug/ft}^3 = 1.602 \times 10^{-2} \text{ g/cm}^3 = 16.02 \text{ kg/m}^3$
	$1 \text{ kg/m}^3 = 10^{-3} \text{ g/cm}^3 = 0.00194 \text{ slug/ft}^3 = 0.06242 \text{ lbm/ft}^3$
Viscosity (dynamic)	$1 \text{ lbm/ft h} = 8.634 \times 10^{-6} \text{ slug/ft s} = 4.134 \times 10^{-3} \text{ g/cm s} = 4.134 \times 10^{-4} \text{ kg/m s}$
	$1 \text{ kg/m s} = 10 \text{ g/cm s} = 2.089 \times 10^{-2} \text{ slug/ft s} = 2.419 \times 10^3 \text{ lbm/ft h}$
Thermal conductivity	$1 \text{ Btu/ft h F} = 2.778 \times 10^{-4} \text{ Btu/ft s F} = 1.730 \times 10^5 \text{ erg/cm s K} = 1.730 \text{ W/m K}$
	$1 \text{ W/m K} = 10^5 \text{ erg/cm s K} = 1.606 \times 10^{-4} \text{ Btu/ft s F} = 0.578 \text{ Btu/ft h F}$
Surface tension	$1 \text{ lbf/ft} = 1.459 \times 10^4 \text{ dyne/cm} = 14.59 \text{ N/m}$
	$1 \text{ N/m} = 10^3 \text{ dyne/cm} = 0.06854 \text{ lbf/ft}$
Latent heat of vaporization	$1 \text{ Btu/lbm} = 32.174 \text{ Btu/slug} = 2.32 \times 10^7 \text{ erg/g} = 2.324 \times 10^3 \text{ J/kg}$
	$1 \text{ J/kg} = 10^4 \text{ erg/g} = 1.384 \times 10^{-2} \text{ Btu/slug} = 4.303 \times 10^{-4} \text{ Btu/lbm}$
Heat transfer coefficient	$1 \text{ Btu/ft}^2 \text{ h F} = 5.674 \times 10^3 \text{ erg/cm}^2 \text{ s K} = 5.674 \text{ W/m}^2 \text{ K}$
	$1 \text{ W/m}^2 \text{ K} = 10^3 \text{ erg/cm}^2 \text{ s K} = 0.1762 \text{ Btu/ft}^2 \text{ h F}$

Physical Constants

Gravitational acceleration (standard): $g = 32.174 \text{ ft/s}^2 = 980.7 \text{ cm/s}^2 = 9.807 \text{ m/s}^2$

Universal gas constant: $\bar{R} = 1545.2 \text{ ft lb/mol R} = 1.987 \text{ Btu/lbm mol R} = 8.314 \times 10^7 \text{ erg/g mol K} = 8.314 \times 10^3 \text{ J/kg mol K}$

Mechanical equivalent of heat: $J = 777.66 \text{ ft lbf/Btu} = 4.184 \times 10^7 \text{ erg/cal} = 1 \text{ N m/J}$

Stefan–Boltzmann constant: $\bar{\sigma} = 0.1713 \times 10^{-8} \text{ Btu/ft}^2 \text{ h R}^4 = 5.670 \times 10^{-5} \text{ erg/cm}^2 \text{ s K}^4 = 5.657 \times 10^{-8} \text{ W/m}^2 \text{ K}^4$

Appendix B: Properties of Solid Materials

Most of the content in this section is from Chi “Heat Pipe Theory and Practice” as well as “Heat Pipe Design” from B & K Engineering volumes I and II written by Patrick J. Berennan and Edward J. Kroliczek, published June 1979 under NASA contract NAS5-23406.

In this appendix, properties of solid materials commonly used for heat pipe containers and wicks are summarized and presented in graphical format. The purpose of this appendix is to support the text for what the reader will need to do to design their task and not necessarily fulfill all the requirements that are needed by most common handbooks of this nature. For example, the ultimate tensile strength of materials depends not only on the temperature but also on material processes and treatment. For the presentation of graphics in this appendix, the average properties of the most commonly commercially available materials have been used. For more detailed properties of information and properties of materials, the readers of this text can refer to the following references:

1. *International Critical Table*
E. W. Washington, McGraw-Hill, New York, 1993.
2. *Mechanical Engineers Handbook*
L. S. Marks, McGraw-Hill, New York, 1967.
3. *Cryogenic Engineering*
R. B. Scott, Van Nostrand, Princeton, New Jersey, 1959.
4. *A Compendium of Properties of Materials at Low Temperature*
V. J. Johnson, Wright Air Development Division of Air Research and Development Command, Technical Report 60-56, Part I, July 1960, Part II, October 1960.

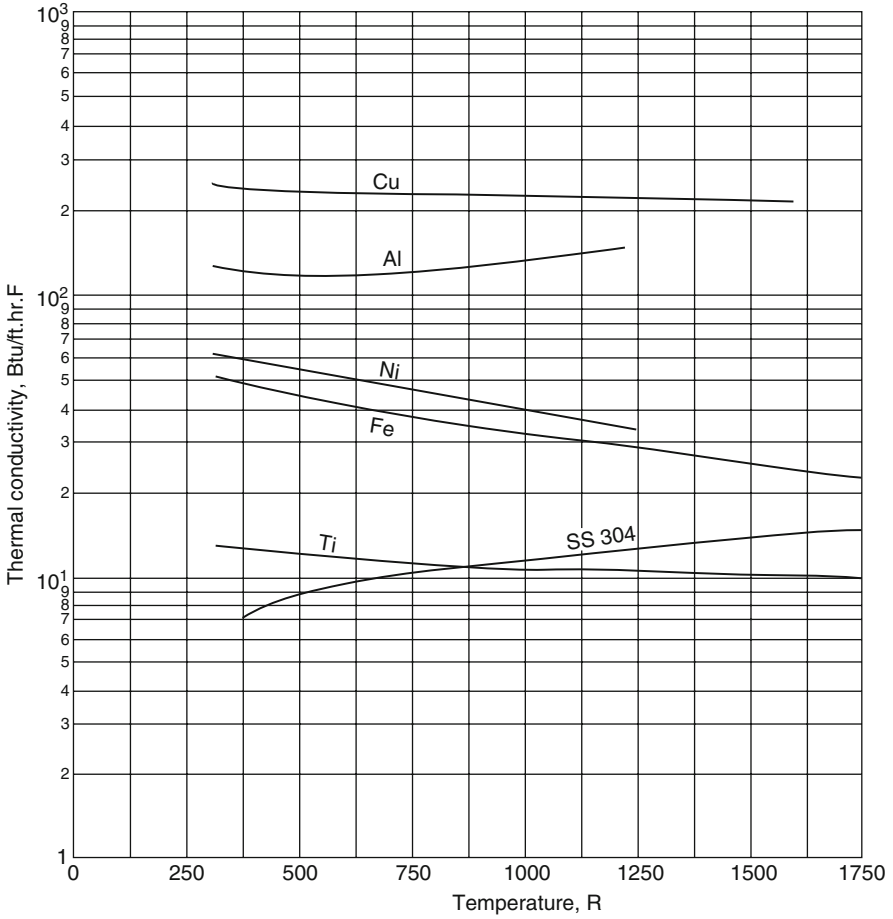


Fig. B.1 Thermal conductivity of several solid materials χ ($^{\circ}\text{R} = 0.556 \text{ }^{\circ}\text{K}$, $1 \text{ Btu/ft}^2\text{h}^{\circ}\text{F} = 1.730 \text{ W/m}^2\text{K}$) [2]

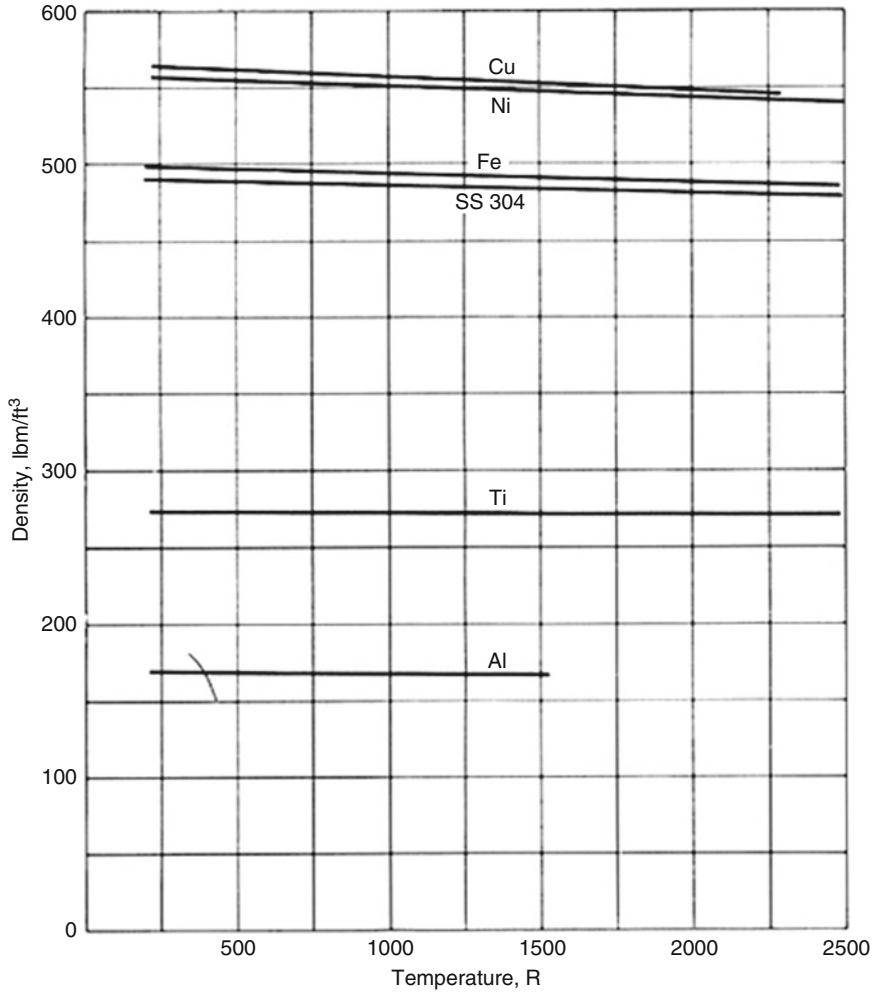


Fig. B.2 Density of several solid materials Chi ($^{\circ}\text{R} = 0.556 \text{ }^{\circ}\text{K}$, $1 \text{ lbm/ft}^3 = 16.02 \text{ kg/m}^3$) [2]

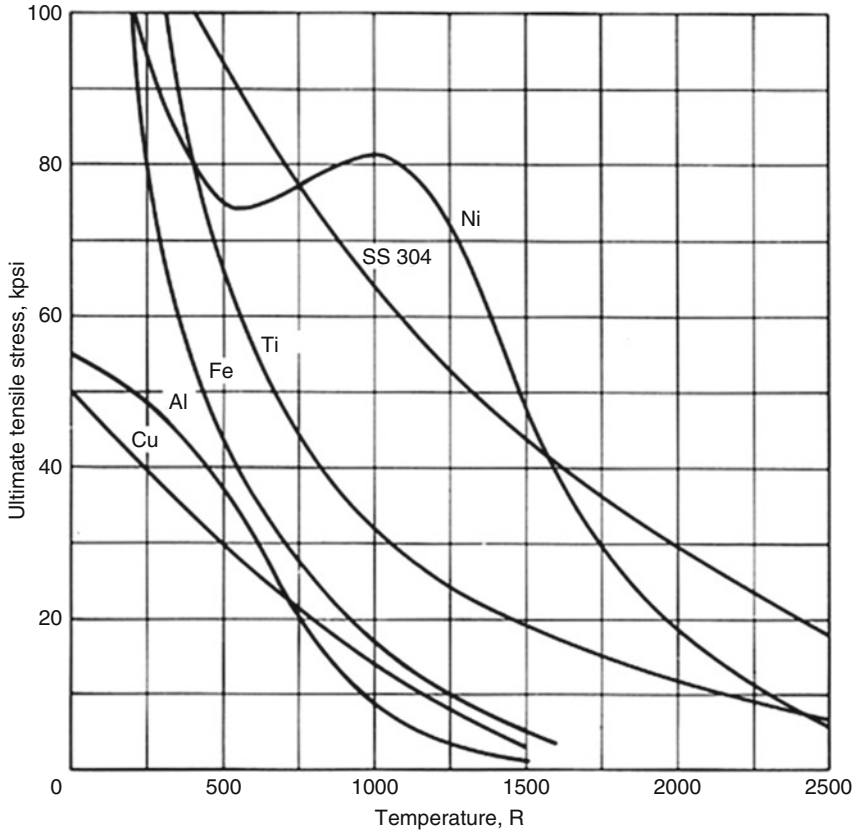


Fig. B.3 Ultimate tensile strength of several solid materials Chi ($1^\circ \text{R} = 0.5556^\circ \text{K}$, $1 \text{ kpsi} = 6.895 \times 10^6 \text{ N/m}^2$) [2]

Composition	Melting Point (K)	Properties at 300 K					Properties at Various Temperatures k (W/m·K) / ρ (kg·K)									
		ρ (kg/m ³)	c_p (J/kg·K)	k (W/m·K)	$\alpha_s \times 10^6$ (m ² /s)		100 K	200 K	400 K	600 K	800 K	1000 K	1200 K	1500 K	200 K	250 K
Aluminum	933	2702	903	237	97.1	302	237	240	231	218						
Pure	755	2770	875	177	73.0	65	163	186	186							
Alloy 2024-T6(4.5% Cu, 1.5% Mg, 0.6% Mn)						473	787	925	1042							
Alloy 195, cast (4.5%Cu)		2790	883	168	68.2	990	301	161	126	106	90.8	78.7				
Beryllium	1550	1850	1825	200	59.2	203	1114	2191	2604	2823	3018	3227	3519			
Cadmium	594	8650	231	96.8	48.4	198	222	242								
Chromium	2118	7160	449	93.7	25.1	159	111	90.9	80.7	71.3	65.4	61.9	57.2	49.4		
Copper						192	384	484	542	581	616	682	779	937		
Pure	1358	8933	385	401	117	482	413	393	379	366	352	339				
Commercial bronze (90%Cu,10%Al)	1293	8800	420	52	14	252	356	397	417	433	451	480				
Phosphor gear bronze (88%Cu,11%Sn)	1104	8780	355	54	17	41	65	74								
Cartridge brass (70%Cu,30%Zn)	1188	8530	380	110	33.9	75	95	137	149							
Constantan (55%Cu,45%Ni)	1439	8920	384	23	6.71	17	19									
Germanium	1211	5360	322	59.9	34.7	237	362									
						232	96.8	43.2	27.3	19.8	17.4	17.4				
						190	290	337	348	357	375	395				
Gold	1336	19300	129	317	127	327	323	311	298	284	270	255				
						109	124	131	135	140	145	155				
Iron																
Pure	1810	1810	447	80.2	23.1	134	94.0	69.5	54.7	43.3	32.8	28.3	32.1			
Ammc(99.75% pure)		7870	447	72.7	20.7	216	384	490	574	680	975	609	654			
						95.6	80.6	65.7	53.1	42.2	32.3	28.7	31.4			
						215	384	490	574	680	975	609	654			

Fig. B.4 Properties of solid materials [3]

Carbon Steels										
Plain carbon($Mn \leq 1\%$, $Si \leq 0.1\%$)										
	7832	434	60.5	17.7	56.7	48.0	39.2	30.0		
					487	559	685	1169		
AISI 1010	7832	434	63.9	18.8	58.7	48.8	39.2	31.3		
					487	559	685	1168		
Carbon-silicon ($Mn \leq 1\%$, $0.1\% < Si \leq 0.6\%$)	7817	446	51.9	14.9	49.8	44.0	37.4	29.3		
					501	582	699	971		
Carbon-manganese-silicon ($1\% < Mn \leq 1.65\%$, $0.1\% < Si \leq 0.6\%$)	8131	434	41.0	11.6	42.2	39.7	35.0	27.6		
					487	559	685	1090		
Chromium(low)steels										
$\frac{1}{2}Cr - \frac{1}{4}Mo - Si$ ($0.18\%C, 0.65\%Cr, 0.23\%Mo, 0.6\%Si$)	7822	444	37.7	10.9	38.2	36.7	33.3	26.9		
					492	575	688	969		
$1Cr - \frac{1}{2}Mo$ ($0.16\%C, 1\%Cr, 0.54\%Mo, 0.6\%Si$)	7858	442	42.3	12.2	42.0	39.1	34.5	27.4		
					492	575	688	969		
$1Cr - V$ ($0.2\%C, 1.02\%Cr, 0.15\%V$)	7836	443	48.9	14.1	46.8	42.1	36.3	28.2		
					492	575	688	969		
Stainless steels										
AISI 302	8055	480	15.1	3.91	17.3	20.0	22.8	25.4		
					512	559	585	606		
AISI 304	1670	7900	477	14.9	3.95	9.2	12.6	19.8	22.6	25.4
					272	402	515	557	582	611
AISI 316	8238	468	13.4	3.48	15.2	18.3	21.3	24.2		
					504	550	576	602		
AISI 347	7978	480	14.2	3.71	15.8	18.9	21.9	24.7		
					513	559	585	606		
Lead	601	11340	129	35.3	24.1	39.7	36.7	34.0	31.4	
					118	125	132	142		
Molybdenum	2894	10240	251	138	53.7	179	143	126	118	112
					141	224	261	275	285	295
Nickel										
Pure	1728	8900	444	90.7	23.0	164	107	80.2	65.6	67.6
					232	383	485	592	530	562
Nichrome (80%Ni,20%Cr)	1672	8400	420	12	3.4	14	16	21		
					480	525	545			
Inconel X-750(73%Ni,15%Cr,6.7%Fe)	1665	8510	439	11.7	3.1	8.7	10.3	13.5	17.0	20.5
					—	372	473	510	546	626
Niobium	2741	8570	265	53.7	23.6	55.2	52.6	58.2	61.3	64.4
					—	—	—	—	—	—
					67.5	72.1	79.1			

Fig. B.5 Properties of solid materials [3]

Composition	Melting Point (K)	P (kg/m ³)	C _p (kJ/kg.K)	Properties at 300K		Properties at Various Temperatures k (W/m-K), (kJ/Kg-K)											
				k (W/m-K)	a _s × 10 ⁶ (m ² /s)	100 K	200 K	400 K	600 K	800 K	1000 K	1200 K	1500 K	200 K	2500 K		
Alloy60Pt-40Rh (60%Pt,40%Rh)	1800	16630	162	47	17.4	52	59	65	69	73	76						
Silicon	1685	2330	712	148	89.2	264	98.9	61.9	42.2	31.2	25.7	22.7					
Silver	1235	10500	235	429	174	444	430	425	412	396	379	361					
Tin	505	7310	227	66.6	40.1	85.2	73.3	62.2									
Titanium	1953	4500	522	21.9	9.32	30.5	24.5	20.4	19.4	19.7	20.7	22.0	24.5				
Tungsten	3660	19300	132	174	68.3	208	186	159	137	125	118	113	107	100	95		
						87	122	137	142	145	148	152	157	167	176		

Fig. B.6 Properties of solid materials [3]

References

1. Berennan, P. J., & Krolczek, E. J. (1979). *Heat pipe design*. From B & K Engineering Volume I and II. NASA contract NAS5-23406.
2. Chi, S. W. (1976). *Heat pipe theory and practice*. New York: McGraw-Hill.
3. Peterson, G. P. (1994). *An introduction to heat pipes—Modeling, testing and applications*. New York: John Wiley & Sons.

Appendix C: Properties of Fluids

Most of the content in this section is from Chi “Heat Pipe Theory and Practice” as well as “Heat Pipe Design” from B & K Engineering Volumes I and II written by Patrick J. Berennan and Edward J. Kroliczek, published in June 1979 under NASA contract NAS5-23406.

Fluid properties relevant to heat pipe performance in this text are presented in this appendix in graphical presentation format for nine working fluids which are:

1. Neon
2. Nitrogen
3. Methane
4. Ammonia
5. Methanol
6. Water
7. Mercury
8. Potassium
9. Sodium

It is often necessary to collect these nine properties for each fluid from different sources. Properties of liquid metal were first compiled by Deverall, Kemme, and Florschuetz and by Frank, Smith, and Taylor. Refer to the following:

1. *Sonic Limitation and Startup Problems of Heat Pipes*

J. E. Deverall, J. E. Kemme and L. W. Florschuetz, Los Alamos National Laboratory, Report LA-4818, September 1970.

2. *Heat Pipe Design Manual*

S. Frank, J. T. Smith and K. M. Taylor, Martin Marietta Corporation, Report MND-3288, February 1967.

Properties of mercury have been compiled by Deverall.

3. *Mercury as a Heat Pipes Fluid*

Deverall, Los Alamos National Laboratory, LA-4300, October 1969.

Properties of modern-temperature fluids have been compiled by:

4. *Heat Pipe Design Handbook*

Bienert and Skrabek and Taylor, Dynatherm Corporation, Report to NASA, Contract No. NAS9-11927, August 1972.

5. *Heat Pipe Design Manual*

S. Frank, J. T. Smith and K. M. Taylor, Martin Marietta Corporation, Report MND-3288, February 1967.

Properties of cryogenic fluids have been compiled by Chi in the following reference along with his computer codes that have been described in Chap. 3.

6. *Mathematical Modeling of Cryogenic Heat Pipes*

S. W. Chi, NASA CR-116175, September 1970.

The above compilations have been the sources of property values used in the preparation of the graphs presented in this appendix.

Also, Reay and Kew [3] are providing a good list of properties of working fluids for the following fluids:

Fluids listed

1. Helium
2. Ammonia
3. Acetone
4. Flutec PP2
5. Heptane
6. Flutec PP9
7. Mercury
8. Potassium
9. Lithium
10. Nitrogen
11. Water
12. High-temperature organics
13. Pentane
14. Cesium
15. Methanol
16. Sodium
17. Ethanol

Properties listed:

Latent heat of evaporation	Vapor dynamic viscosity
Liquid density	Vapor pressure
Vapor density	Vapor-specific heat
Liquid thermal conductivity	Liquid surface tension
Liquid dynamic viscosity	

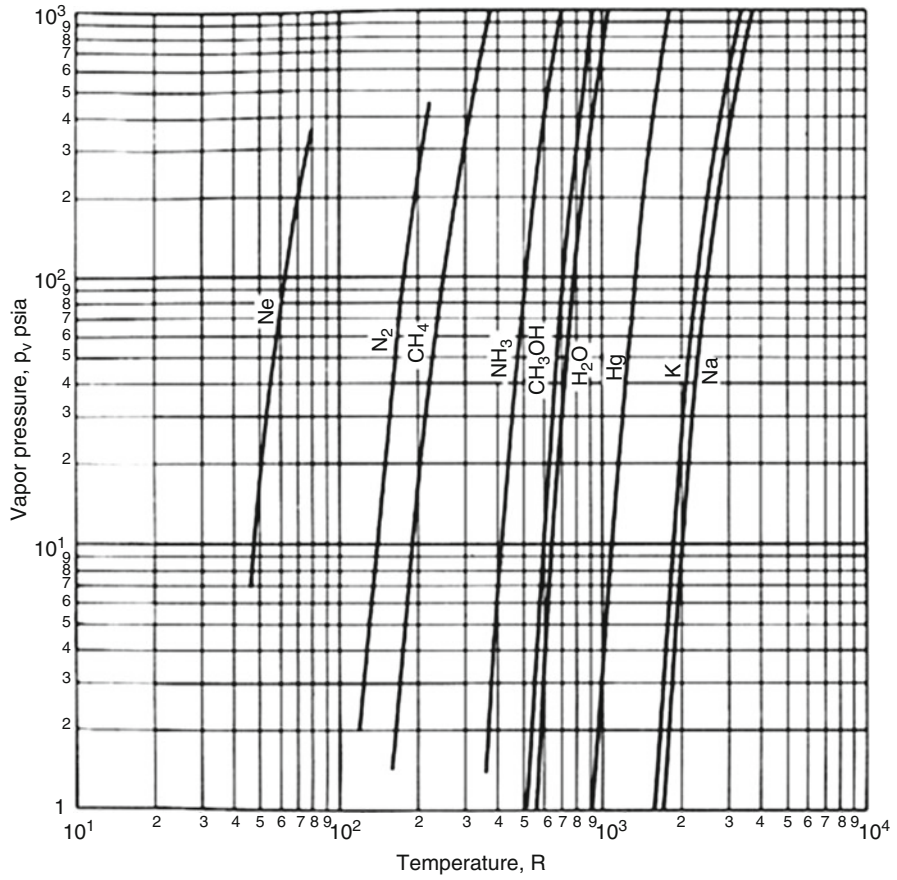


Fig. C.1 Saturation pressure of several heat pipe working fluids Chi [2] ($^{\circ}R = 0.556^{\circ}K$, $1\text{ psi} = 6.895 \times 10^3\text{ N/m}^2$)

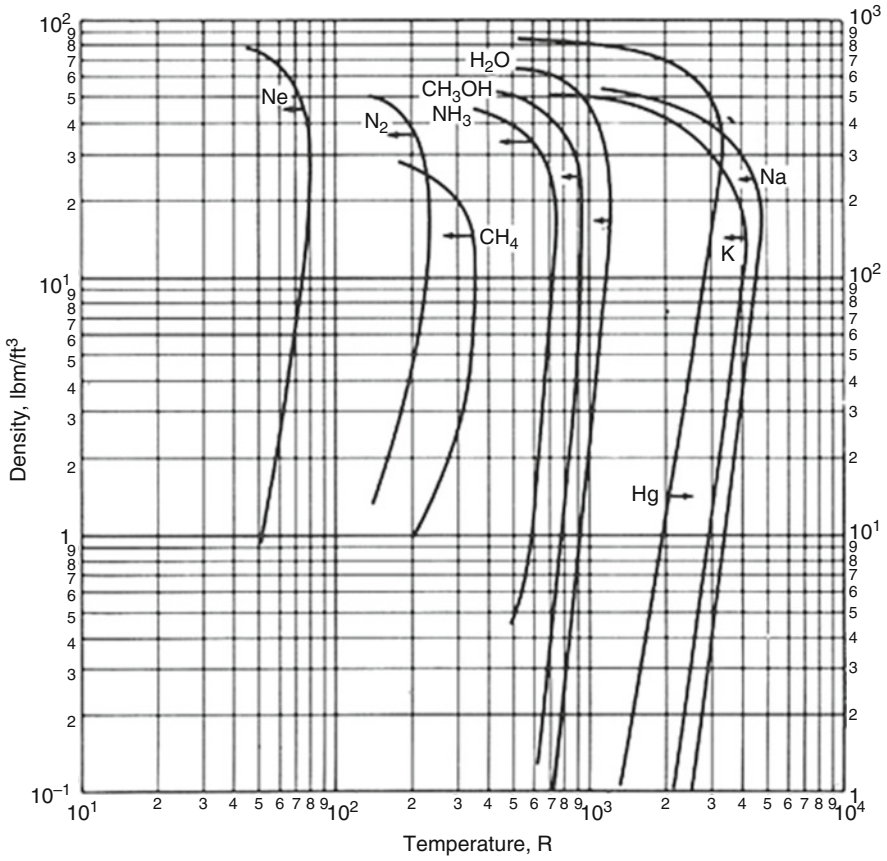


Fig. C.2 Saturation density of several heat pipe working fluids Chi [2] ($1^{\circ} R = 0.5556^{\circ} K$, $1 \text{ lbm/ft}^3 = 1.602 \text{ kg/m}^3$)

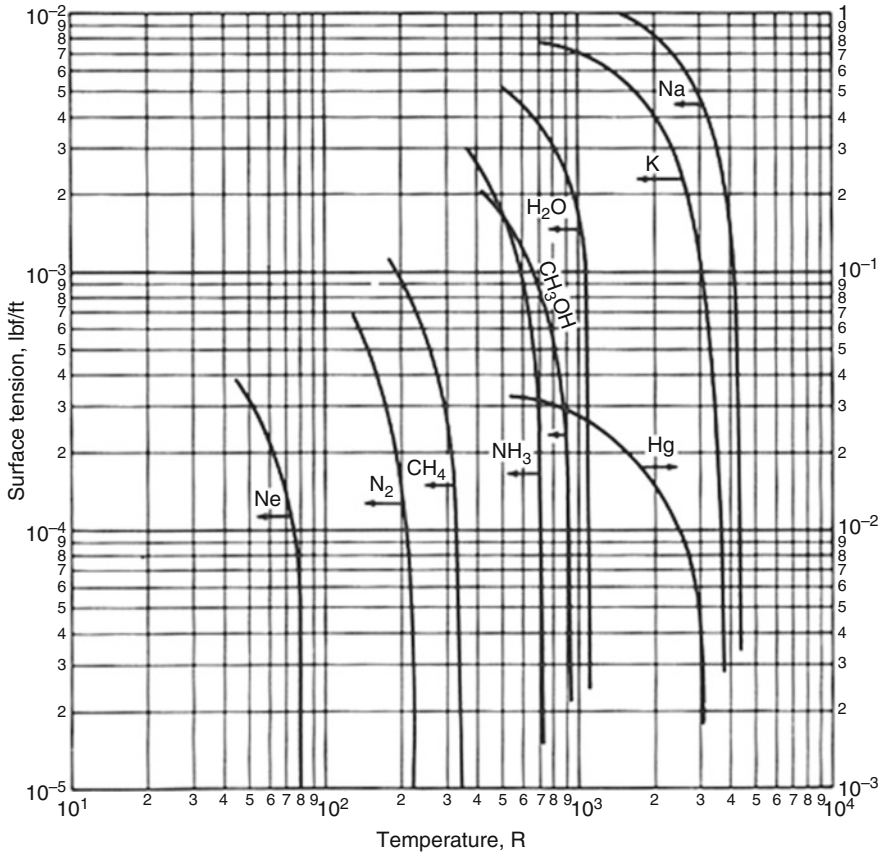


Fig. C.3 Viscosity of several heat pipe working fluids at saturation state Chi [2] ($1^\circ R = 0.5556^\circ K$, $1 \text{ lbf/m h} = 4.134 \times 10^{-4} \text{ kg/m s}$)

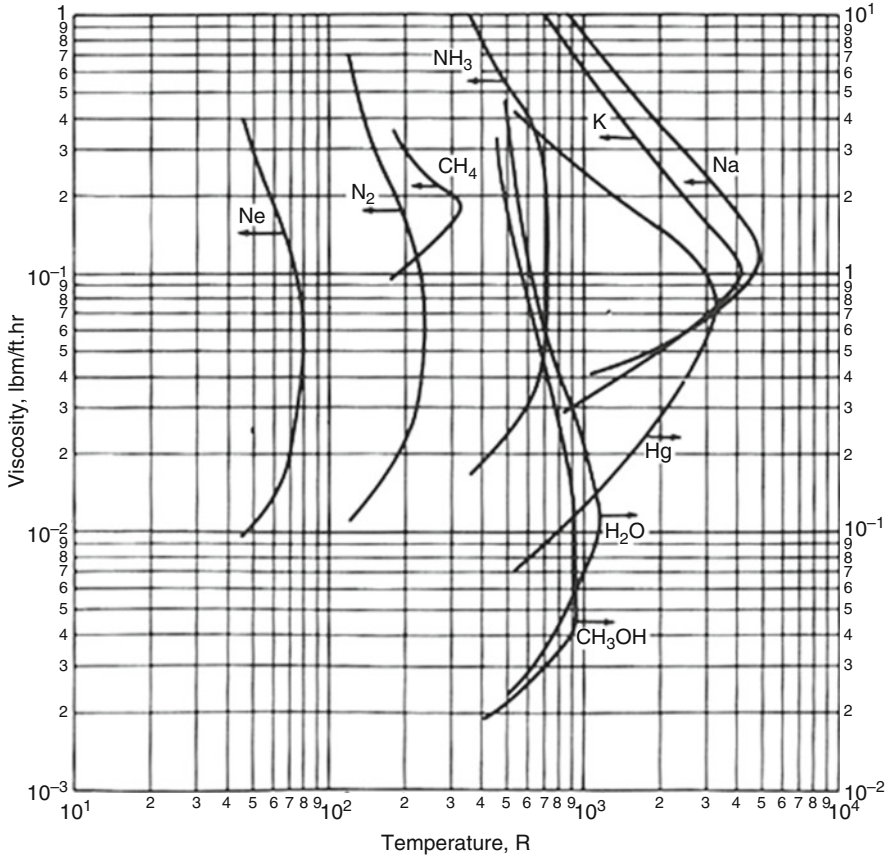


Fig. C.4 Surface tension of saturated liquid for several heat pipe working fluids Chi [2] ($1^{\circ} R = 0.5556^{\circ} K$, $1 \text{ lbf/ft} = 14.59 \text{ N/m}$)

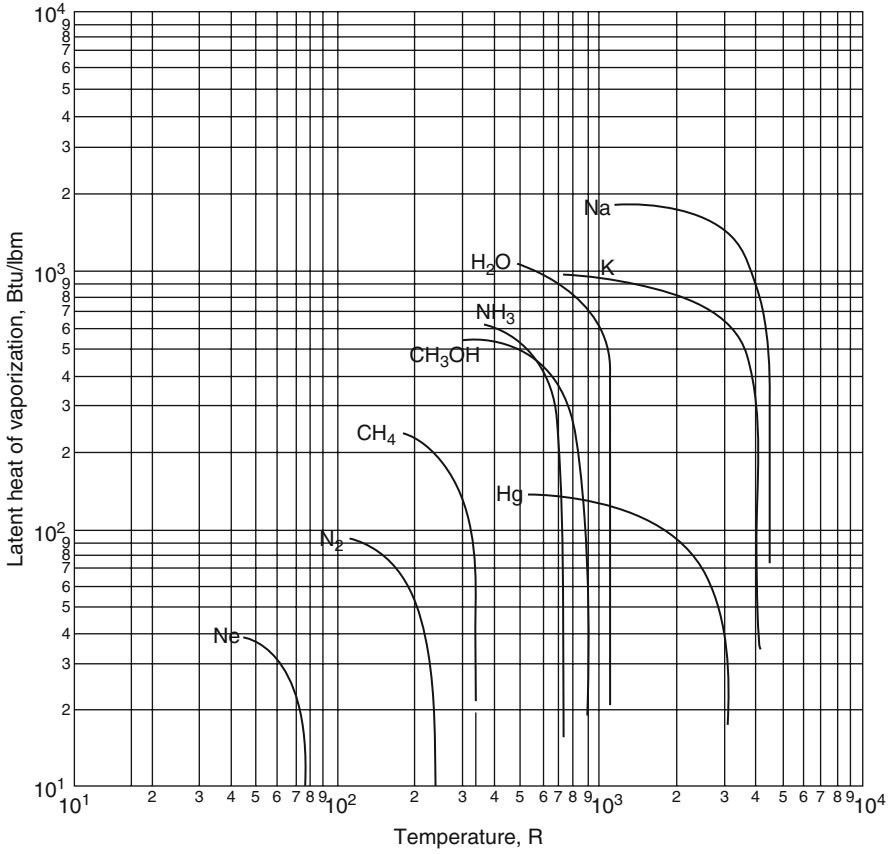


Fig. C.5 Latent heat of vaporization for several heat pipe working fluids Chi [2] ($1^\circ R = 0.5556^\circ K$, $1 \text{ Btu/lbm} = 2.324 \times 10^3 \text{ J/kg}$)

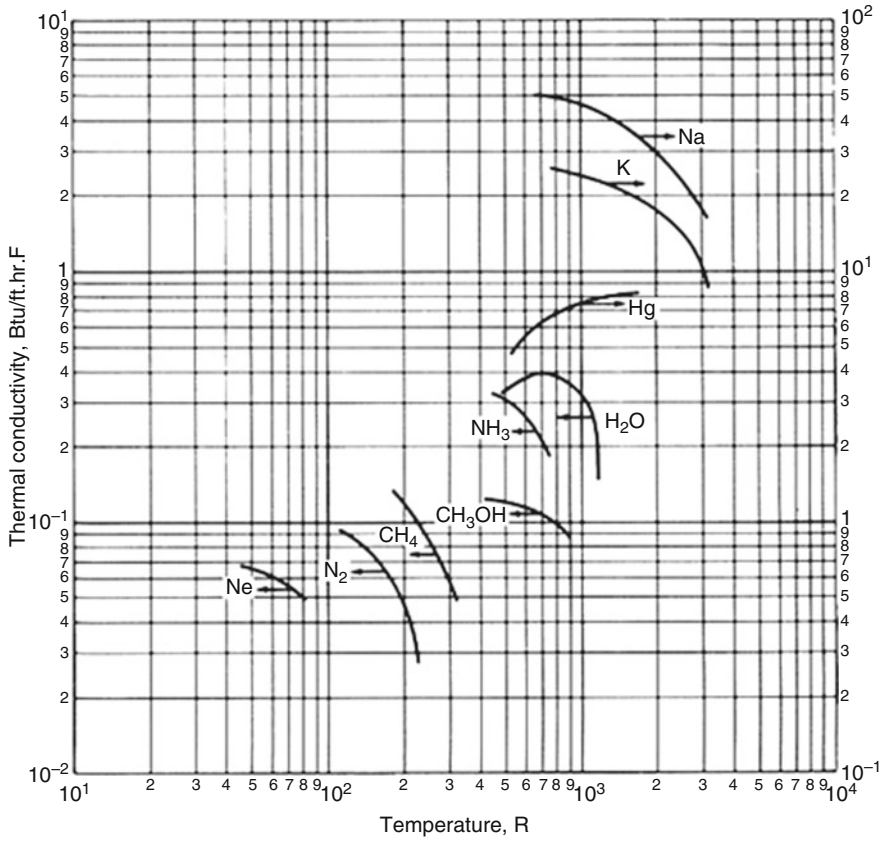


Fig. C.6 Liquid thermal conductivity for several heat pipe working fluids at saturated state Chi [2] ($1^{\circ} R = 0.5556^{\circ} K$, $1 \text{ Btu/ft h F} = 1.730 \text{ W/m K}$)

Helium

Temp °C	Latent heat kJ/kg	Liquid density kg/m ³	Vapour density kg/m ³	Liquid thermal conductivity W/m°C x 10 ⁻²	Liquid viscos. cP x 10 ²	vapour viscos. cP x 10 ³	Vapour press.Bar	Vapour specific heat kJ/kg°C	Liquid surface tension N/m x 10 ³
-271	22.8	148.3	26.0	1.81	3.90	0.20	0.06	2.045	0.26
-270	23.6	140.7	17.0	2.24	3.70	0.30	0.32	2.699	0.19
-269	20.9	128.0	10.0	2.77	2.90	0.60	1.00	4.619	0.09
-268	4.0	113.8	8.5	3.50	1.34	0.90	2.29	6.642	0.01

Nitrogen

Temp °C	Latent heat kJ/kg	Liquid density kg/m ³	Vapour density kg/m ³	Liquid thermal conductivity W/m°C	Liquid viscos. cP x 10 ¹	vapour viscos. cP x 10 ²	Vapour press.Bar	Vapour specific heat kJ/kg°C	Liquid surface tension N/m x 10 ²
-203	210.0	830.0	1.84	0.150	2.48	0.48	0.48	1.083	1.054
-200	205.5	818.0	3.81	0.146	1.94	0.51	0.74	1.082	0.985
-195	198.0	798.0	7.10	0.139	1.51	0.56	1.62	1.079	0.870
-190	190.0	778.0	10.39	0.132	1.26	0.60	3.31	1.077	0.766
-185	183.0	758.0	13.68	0.125	1.08	0.65	4.99	1.074	0.662
-180	173.7	732.0	22.05	0.117	0.95	0.71	6.69	1.072	0.561
-175	163.2	702.0	33.80	0.110	0.86	0.77	8.37	1.070	0.464
-170	152.7	672.0	45.55	0.103	0.80	0.83	1.07	1.068	0.367
-160	124.2	603.0	80.90	0.089	0.72	1.00	19.37	1.063	0.185
-150	66.8	474.0	194.00	0.075	0.65	1.50	28.80	1.059	0.110

Fig. C.7 Working fluid properties of helium [3]

Ammonia

Temp °C	Latent heat kJ/kg	Liquid density Kg/m ³	Vapour density Kg/m ³	Liquid thermal conductivity W/m °C	Liquid viscos.cP	Vapour viscos. cP x 10 ²	Vapour press. Bar	Vapour specific heat kJ/kg °C	Liquid surface tension N/mx 10 ²
-60	1343	714.4	0.03	0.294	0.36	0.72	0.27	2.050	4.062
-40	1384	690.4	0.05	0.303	0.29	0.79	0.76	2.075	3.574
-20	1338	665.5	1.62	0.304	0.26	0.85	1.93	2.100	3.090
0	1263	638.6	3.48	0.298	0.25	0.92	4.24	2.125	2.480
20	1187	610.3	6.69	0.286	0.22	1.01	8.46	2.150	2.133
40	1101	579.5	12.00	0.272	0.20	1.16	15.34	2.160	1.833
60	1026	545.2	20.49	0.255	0.17	1.27	29.80	2.180	1.367
80	891	505.7	34.13	0.235	0.15	1.40	40.90	2.210	0.767
100	699	455.1	54.92	0.212	0.11	1.60	63.12	2.260	0.500
120	428	374.4	113.16	0.184	0.07	1.89	90.44	2.292	0.150

Pentane

Temp °C	Latent heat kJ/kg	Liquid density Kg/m ³	Vapour density Kg/m ³	Liquid thermal conductivity W/m °C	Liquid viscos.cP	Vapour viscos. cP x 10 ²	Vapour press. Bar	Vapour specific heat kJ/kg °C	Liquid surface tension N/mx 10 ²
-20	390.0	663.0	0.01	0.149	0.344	0.51	0.10	0.825	0.01
0	378.3	644.0	0.75	0.143	0.283	0.53	0.24	0.874	1.79
20	366.9	625.5	2.20	0.138	0.242	0.58	0.76	0.922	1.58
40	355.5	607.0	4.35	0.133	0.200	0.63	1.52	0.971	0.37
60	342.3	585.0	6.51	0.128	0.174	0.69	2.28	1.021	0.17
80	329.1	563.0	10.61	0.127	0.147	0.74	3.89	1.050	0.97
100	295.7	537.6	16.54	0.124	0.128	0.81	7.19	1.088	0.83
120	269.7	509.4	25.20	0.122	0.120	0.90	13.81	1.164	0.68

Fig. C.8 Working fluid properties of ammonia [3]

Acetone

Temp °C	Latent heat kJ/kg	Liquid density kg/m ³	Vapour density kg/m ³	Liquid thermal conductivity W/m°C	Liquid viscos. cP	Vapour viscos. cP x 10 ²	Vapour press. Bar	Vapour specific heat kJ/kg°C	Liquid surface tension N/m x 10 ²
-40	660.0	860.0	0.03	0.200	0.800	0.68	0.01	2.00	3.10
-20	615.6	845.0	0.10	0.189	0.500	0.73	0.03	2.06	2.76
0	564.0	812.0	0.26	0.183	0.395	0.78	0.10	2.11	2.62
20	552.0	790.0	0.64	0.181	0.323	0.82	0.27	2.16	2.37
40	536.0	768.0	1.05	0.175	0.269	0.86	0.60	2.22	2.12
60	517.0	744.0	2.37	0.168	0.226	0.90	1.15	2.28	1.86
80	495.0	719.0	4.30	0.160	0.192	0.95	2.15	2.34	1.62
100	472.0	689.6	6.94	0.148	0.170	0.98	4.43	2.39	1.34
120	426.1	660.3	11.02	0.135	0.148	0.99	6.70	2.45	1.07
140	394.4	631.8	18.61	0.126	0.132	1.03	10.49	2.50	0.81

Methanol

Temp °C	Latent heat kJ/kg	Liquid density kg/m ³	Vapour density kg/m ³	Liquid thermal conductivity W/m°C	Liquid viscos. cP	Vapour viscos. cP x 10 ²	Vapour press. Bar	Vapour specific heat kJ/kg°C	Liquid surface tension N/m x 10 ²
-50	1194	843.5	0.01	0.210	1.700	0.72	0.01	1.20	3.26
-30	1187	833.5	0.01	0.208	1.300	0.78	0.02	1.27	2.95
-10	1182	818.7	0.04	0.206	0.945	0.85	0.04	1.34	2.63
10	1175	800.5	0.12	0.204	0.701	0.91	0.10	1.40	2.36
30	1155	782.0	0.31	0.203	0.521	0.98	0.25	1.47	2.18
50	1125	764.1	0.77	0.202	0.399	1.04	0.55	1.54	2.01
70	1085	746.2	1.47	0.201	0.314	1.11	1.31	1.61	1.85
90	1035	724.4	3.01	0.199	0.259	1.19	2.69	1.79	1.66
110	980	703.6	5.64	0.197	0.211	1.26	4.98	1.92	1.46
130	920	685.2	9.81	0.195	0.166	1.31	7.86	1.92	1.25
150	850	653.2	15.90	0.193	0.138	1.38	8.94	1.92	1.04

Fig. C.9 Working fluid properties of acetone [3]

Flutec PP2

Temp °C	Latent heat kJ/kg	Liquid density kg/m ³	Vapour density kg/m ³	Liquid thermal conductivity W/m °C	Liquid viscos. cP	Vapour viscos. cPx10 ²	Vapour Press. Bar	Vapour specific heat kJ/kg°C	Liquid surface tension N/mx10 ²
-30	106.2	1942	0.13	0.637	5.200	0.98	0.01	0.72	1.90
-10	103.1	1886	0.44	0.626	3.500	1.03	0.02	0.81	1.71
10	99.8	1829	1.39	0.613	2.140	1.07	0.09	0.92	1.52
30	96.3	1773	2.96	0.601	1.435	1.12	0.22	1.01	1.32
50	91.8	1716	6.43	0.588	1.005	1.17	0.39	1.07	1.13
70	87.0	1660	11.79	0.575	0.720	1.22	0.62	1.11	0.93
90	82.1	1599	21.99	0.563	0.543	1.26	1.43	1.17	0.73
110	76.5	1558	34.92	0.550	0.429	1.31	2.82	1.25	0.52
130	70.3	1515	57.21	0.537	0.314	1.36	4.83	1.33	0.32
160	59.1	1440	103.63	0.518	0.167	1.43	8.76	1.45	0.01

Ethanol

Temp °C	Latent heat kJ/kg	Liquid density kg/m ³	Vapour density kg/m ³	Liquid thermal conductivity W/m °C	Liquid viscos. cP	Vapour viscos. cPx10 ²	Vapour Press.Bar	Vapour specific heat kJ/kg°C	Liquid surface tension N/mx10 ²
-30	939.4	825.0	0.02	0.177	3.40	0.75	0.01	1.25	2.76
-10	928.7	813.0	0.03	0.173	2.20	0.80	0.02	1.31	2.66
10	904.8	798.0	0.05	0.170	1.50	0.85	0.03	1.37	2.57
30	888.6	781.0	0.38	0.168	1.02	0.91	0.10	1.44	2.44
50	872.3	762.2	0.72	0.166	0.72	0.97	0.29	1.51	2.31
70	858.3	743.1	1.32	0.165	0.51	1.02	0.76	1.58	2.17
90	832.1	725.3	2.59	0.163	0.37	1.07	1.43	1.65	2.04
110	786.6	704.1	5.17	0.160	0.28	1.13	2.66	1.72	1.89
130	734.4	678.7	9.25	0.159	0.21	1.18	4.30	1.78	1.75

Fig. C.10 Working fluid properties of flutec PP2 [3]

Heptane									
Temp°C	Latent heat kJ/kg	Liquid density kg/m ³	Vapour density kg/m ³	Liquid thermal conductivity W/m°C	Liquid viscos.cP	Liquid viscos. cP x10 ²	Vapour press Bar	Vapour specific heat kJ/kg°C	Liquid surface tension N/m x 10 ²
-20	384.0	715.5	0.01	0.143	0.69	0.57	0.01	0.83	2.42
0	372.6	699.0	0.17	0.141	0.53	0.60	0.02	0.87	2.21
20	362.2	683.0	0.49	0.140	0.43	0.63	0.08	0.92	2.01
40	351.8	667.0	0.97	0.139	0.34	0.66	0.20	0.97	1.81
60	341.5	649.0	1.45	0.137	0.29	0.70	0.32	1.02	1.62
80	331.2	631.0	2.31	0.135	0.24	0.74	0.62	1.05	1.43
100	319.6	612.0	3.71	0.133	0.21	0.77	1.10	1.09	1.28
120	305.0	592.0	6.08	0.132	0.18	0.82	1.85	1.16	1.10

Water									
Temp°C	Latent heat kJ/kg	Liquid density kg/m ³	Vapour density kg/m ³	Liquid thermal conductivity W/m°C	Liquid viscos.cP	Vapour viscos. cP x10 ²	Vapour press.Bar	Vapour specific heat kJ/kg°C	Liquid surface tension N/m x 10 ²
20	2448	998.2	0.02	0.603	1.00	0.96	0.02	1.81	7.28
40	2402	992.3	0.05	0.630	0.65	1.04	0.07	1.89	6.96
60	2359	983.0	0.13	0.649	0.47	1.12	0.20	1.91	6.62
80	2309	972.0	0.29	0.668	0.36	1.19	0.47	1.95	6.26
100	2258	958.0	0.60	0.680	0.28	1.27	1.01	2.01	5.89
120	2200	945.0	1.12	0.682	0.23	1.34	2.02	2.09	5.50
140	2139	928.0	1.99	0.683	0.20	1.41	3.90	2.21	5.06
160	2074	909.0	3.27	0.679	0.17	1.49	6.44	2.38	4.66
180	2003	888.0	5.16	0.669	0.15	1.57	10.04	2.62	4.29
200	1967	865.0	7.87	0.659	0.14	1.65	16.19	2.91	3.89

Fig. C.11 Working fluid properties of heptane [3]

Flutec PP9

Temp ^o C	Latent heat kJ/kg	Liquid density kg/m ³	Vapour density kg/m ³	Liquid thermal conductivity W/m °C	Liquid viscos. cP	Vapour viscos. cPx10 ²	Vapour press. Bar	Vapour specific heat kJ/kg °C	Liquid surface tension N/mx10 ²
-30	103.0	2098	0.01	0.060	5.77	0.82	0.00	0.80	2.36
0	98.4	2029	0.01	0.059	3.31	0.90	0.00	0.87	2.08
30	94.5	1960	0.12	0.057	1.48	1.06	0.01	0.94	1.80
60	90.2	1891	0.61	0.056	0.94	1.18	0.03	1.02	1.52
90	86.1	1822	1.93	0.054	0.65	1.21	0.12	1.09	1.24
120	83.0	1753	4.52	0.053	0.49	1.23	0.28	1.15	0.95
150	77.4	1685	11.81	0.052	0.38	1.26	0.61	1.23	0.67
180	70.8	1604	25.13	0.051	0.30	1.33	1.58	1.30	0.40
225	59.4	1455	63.27	0.049	0.21	1.44	4.21	1.41	0.01

High Temperature Organic (Diphenyl-Diphenyl Oxide Eutectic)

Temp ^o C	Latent heat kJ/kg	Liquid density kg/m ³	Vapour density kg/m ³	Liquid thermal conductivity W/m °C	Liquid viscos. cP	Vapour viscos. cPx10 ²	Vapour press. Bar	Vapour specific heat kJ/kg °C	Liquid surface tension N/mx10 ²
100	354.0	992.0	0.03	0.131	0.97	0.67	0.01	1.34	3.50
150	338.0	951.0	0.22	0.125	0.57	0.78	0.05	1.51	3.00
200	321.0	905.0	0.94	0.119	0.39	0.89	0.25	1.67	2.50
250	301.0	858.0	3.60	0.113	0.27	1.00	0.88	1.81	2.00
300	278.0	809.0	8.74	0.106	0.20	1.12	2.43	1.95	1.50
350	251.0	755.0	19.37	0.099	0.15	1.23	5.55	2.03	1.00
400	219.0	691.0	41.89	0.093	0.12	1.34	10.90	2.11	0.50
450	185.0	625.0	81.00	0.086	0.10	1.45	19.00	2.19	0.03

Fig. C.12 Working fluid properties of flutec PP9 [3]

Mercury									
Temp°C	Latent heat kJ/kg	Liquid density kg/m ³	Vapour density kg/m ³	Liquid thermal conductivity W/m°C	Liquid viscos.cP	Vapour viscos. cP x10 ²	Vapour press Bar	Vapour specific heat kJ/kg°C	Liquid surface tension N/m x 10 ²
150	308.8	13230	0.01	9.99	1.09	0.39	0.01	1.04	4.45
250	303.8	12995	0.60	11.23	0.96	0.48	0.18	1.04	4.15
300	301.8	12880	1.73	11.73	0.93	0.53	0.44	1.04	4.00
350	298.9	12763	4.45	12.18	0.89	0.61	1.16	1.04	3.82
400	296.3	12656	8.75	12.58	0.86	0.66	2.42	1.04	3.74
450	293.8	12508	16.80	12.96	0.83	0.70	4.92	1.04	3.61
500	291.3	12308	28.60	13.31	0.80	0.75	8.86	1.04	3.41
550	288.8	12154	44.92	13.62	0.79	0.81	15.03	1.04	3.25
600	286.3	12054	65.75	13.87	0.78	0.87	23.77	1.04	3.15
650	283.5	11962	94.39	14.15	0.78	0.95	34.95	1.04	3.03
750	277.0	11800	170.00	14.80	0.77	1.10	63.00	1.04	2.75

Caesium									
Temp°C	Latent heat kJ/kg	Liquid density kg/m ³	Vapour density kg/m ³ x 10 ²	Liquid thermal conductivity W/m°C	Liquid viscos. cP	Vapour viscos. cP x10 ²	Vapour press Bar	Vapour specific heat kJ/kg°C x 10	Liquid surface tension N/m x 10 ²
375	530.4	1740	0.01	20.76	0.25	2.20	0.02	1.56	5.81
425	520.4	1730	0.01	20.51	0.23	2.30	0.04	1.56	5.61
475	515.2	1720	0.02	20.02	0.22	2.40	0.09	1.56	5.36
525	510.2	1710	0.03	19.52	0.20	2.50	0.16	1.56	5.11
575	502.8	1700	0.07	18.83	0.19	2.55	0.36	1.56	4.81
625	495.3	1690	0.10	18.13	0.18	2.60	0.57	1.56	4.51
675	490.2	1680	0.18	17.48	0.17	2.67	1.04	1.56	4.21
725	485.2	1670	0.26	16.83	0.17	2.75	1.52	1.56	3.91
775	477.8	1655	0.40	16.18	0.16	2.28	2.46	1.56	3.66
825	470.3	1640	0.55	15.53	0.16	2.90	3.41	1.56	3.41

Fig. C.13 Working fluid properties of mercury [3]

Potassium

Temp °C	Latent heat kJ/kg	Liquid density kg/m ³	Vapour density kg/m ³	Liquid thermal conductivity W/m ² °C	Liquid viscos. cP	Vapour viscos. cP × 10 ²	Vapour press. Bar	Vapour specific heat kJ/kg °C	Liquid surface tension N/m × 10 ²
350	2093	763.1	0.002	51.08	0.21	0.15	0.01	5.32	9.50
400	2078	748.1	0.006	49.08	0.19	0.16	0.01	5.32	9.04
450	2060	735.4	0.015	47.08	0.18	0.16	0.02	5.32	8.69
500	2040	725.4	0.031	45.08	0.17	0.17	0.05	5.32	8.44
550	2020	715.4	0.062	43.31	0.15	0.17	0.10	5.32	8.16
600	2000	705.4	0.111	41.81	0.14	0.18	0.19	5.32	7.86
650	1980	695.4	0.193	40.08	0.13	0.19	0.35	5.32	7.51
700	1969	685.4	0.314	38.08	0.12	0.19	0.61	5.32	7.12
750	1938	675.4	0.486	36.31	0.12	0.20	0.99	5.32	6.72
800	1913	665.4	0.716	34.81	0.11	0.20	1.55	5.32	6.32
850	1863	653.1	1.054	33.31	0.10	0.21	2.34	5.32	5.92

Sodium

Temp °C	Latent heat kJ/kg	Liquid density kg/m ³	Vapour density kg/m ³	Liquid thermal conductivity W/m ² °C	Liquid viscos. cP	Vapour viscos. cP × 10	Vapour press. Bar	Vapour specific heat kJ/kg °C × 10	Liquid surface tension N/m × 10 ²
500	4370	828.1	0.003	70.08	0.24	0.18	0.01	9.04	1.51
600	4243	805.4	0.013	64.62	0.21	0.19	0.04	9.04	1.42
700	4090	763.5	0.050	60.81	0.19	0.20	0.15	9.04	1.33
800	3977	757.3	0.134	57.81	0.18	0.22	0.47	9.04	1.23
900	3913	745.4	0.306	53.35	0.17	0.23	1.25	9.04	1.13
1000	3827	725.4	0.667	49.08	0.16	0.24	2.81	9.04	1.04
1100	3690	690.8	1.306	45.08	0.16	0.25	5.49	9.04	0.95
1200	3577	669.0	2.303	41.08	0.15	0.26	9.59	9.04	0.86
1300	3477	654.0	3.622	37.08	0.15	0.27	15.91	9.04	0.77

Fig. C.14 Working fluid properties of potassium [3]

Lithium

Temp °C	Latent heat kJ/kg	Liquid density kg/m ³	Vapour density kg/m ³	Liquid thermal conductivity W/m°C	Liquid viscos.cP	Vapour viscos. cP × 10 ²	Vapour press. Bar	Vapour specific heat kJ/kg°C	Liquid surface tension N/m × 10 ²
1030	20500	450	0.005	67	0.24	1.67	0.07	0.532	2.90
1130	20100	440	0.013	69	0.24	1.74	0.17	0.532	2.85
1230	20000	430	0.028	70	0.23	1.83	0.45	0.532	2.75
1330	19700	420	0.057	69	0.23	1.91	0.96	0.532	2.60
1430	19200	410	0.108	68	0.23	2.00	1.85	0.532	2.40
1530	18900	405	0.193	65	0.23	2.10	3.30	0.532	2.25
1630	18500	400	0.340	62	0.23	2.17	5.30	0.532	2.10
1730	18200	398	0.490	59	0.23	2.26	8.90	0.532	2.05

Fig. C.15 Working fluid properties of lithium [3]

References

1. Berennan, P. J., & Kroliczek, E. J. (1979). *Heat pipe design*. From B & K Engineering Volume I and II. NASA contract NAS5-23406.
2. Chi, S. W. (1976). *Heat pipe theory and practice*. New York: McGraw-Hill.
3. Reay, D., & Kew, P. (2006). *Heat pipes theory, design and application* (5th Ed.). Oxford: Butterworth-Heinemann.

Appendix D: Different Heat Pipe Design Examples

Different design examples from different resources and references are presented in this appendix to help the reader to have better understanding and approach to design a heat pipe under different conditions and functional requirement while heat pipe is operating under normal condition.

Design Example 1

This example is part of The Effects of Transverse Vibration on the Performance of an Axial Groove Wick Heat Pipe, Master's thesis, By Kenneth A. Carpenter, December 1994. Defense Technical Information Center under **Accession Number:** ADA289349

An experimental investigation was performed to determine the effects of transverse vibrations on the performance of an ammonia–aluminum axial groove wick heat pipe. Theoretical calculations predicted performance degradation due to the working fluid being shaken out of the upper capillary grooves.

A bench top shaker was used to apply transverse, sinusoidal vibrations of 30, 35, and 40 Hz, corresponding to peak acceleration amplitudes of 1.84 g, 2.50 g, and 3.27 g, respectively. Maximum heat throughput, $Q_{sub\ max}$, of the vibrating heat pipe was measured. A comparison of these values and static $Q_{sub\ max}$ values indicated degradation in heat pipe performance. A mean performance deterioration of 27.6 W was measured for the 1.84 g case, an average degradation of 12.9 % from static heat pipe performance. At 2.50 g peak acceleration, the degradation rose to 37.3 W, an average decrease of 14.8 % from static performance. An average deterioration in performance of 28.1 % was recorded for the 3.27 g case. This amounted to a mean performance degradation of 69.3 W. The results of this investigation revealed that transverse, sinusoidal vibrations have a detrimental impact on the performance of an ammonia/axial groove wick heat pipe. Further, the performance degradation increases with increasing vibration peak acceleration amplitude.

Heat Pipe Geometry

Heat pipe performance is as much a function of the wick geometry as it is a function of the working fluid. The heat pipe for this experiment was supplied by Dynatherm Corporation. It was an axial groove wick heat pipe of extruded aluminum. For a working fluid, the heat pipe groove was charged with 8.6 g of anhydrous ammonia. Figure D.1 shows the tested heat pipe in cross section, while Table D.1 presents critical heat pipe dimensions. The tested heat pipe is shown in profile in Fig. D.2 and includes the dimensions for the evaporator, adiabatic, and the condenser sections

Heat Transport Limits

All heat pipes are constrained by four operating heat transport limits. These are the sonic limit, the entrainment limit, the capillary limit, and the boiling limit. The heat transport limits are functions of the heat pipe geometry, the working fluid properties, and the heat pipe operational environment. This last category includes heat pipe inclinations, heat pipe section lengths, and other external influences.

Fig. D.1 Heat pipe cross-sectional drawing

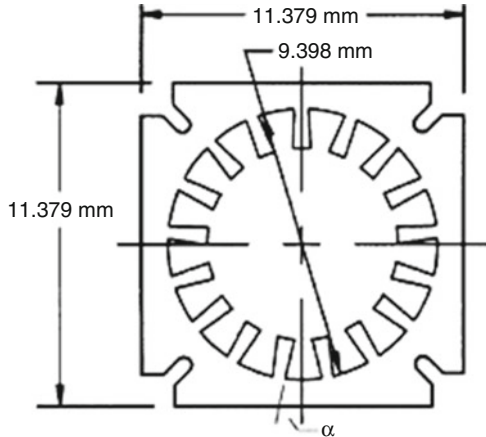


Table D.1 Heat pipe cross-sectional parameters

Land thickness (bottom)	t_1	0.020 in.	0.508 mm
Groove opening (top)	w	0.025 in.	0.635 mm
Groove opening (bottom)	w_b	0.048 in.	1.219 mm
Groove depth	δ	0.055 in.	1.397 mm
Groove angle	α	13.9°	0.2426 rad
Number of grooves	n	17	17

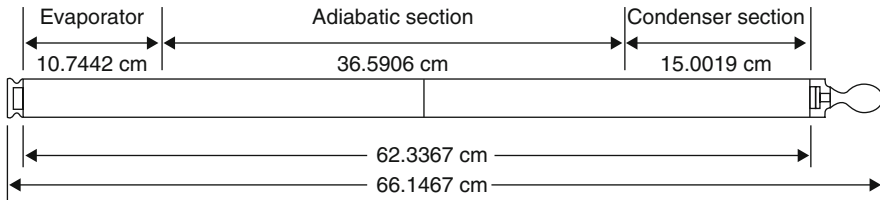


Fig. D.2 Heat pipe profile view

Table D.2 Theoretical heat transport limits

T_{op}	$Q_{S,max}$	$Q_{e,max}$	$Q_{c,max}$	$Q_{b,max}$
Operating temperature (°C)	Sonic limit (W)	Entrainment limit (W)	Capillary limit (W)	Boiling limit (W)
40	99,050	529.29	289.09	18.22
50	124,740	543.15	263.78	12.69
60	158,550	554.04	234.78	8.58
70	202,230	558.36	202.64	5.63
80	256,760	551.02	168.05	3.59

The complete explanations and derivations for the heat transport limits of the tested heat pipe are provided below. Table D.2 is a representation of the theoretical operating limits of the tested heat pipe. Column 1 of this table gives the heat pipe operating temperature, which is the temperature of the adiabatic section of the heat pipe. The remaining columns give the values for the four heat transport limits at the various operating temperatures. An examination of Table D.2 reveals that for the anticipated operating temperature range of 40–80 °C, the boiling limit was expected to constrain the maximum heat transport of the test article since it has the lowest heat transport value for the entire operating range. However, as Chi points out [2], the boiling limit of a heat pipe must be verified experimentally.

Experimental investigation showed the theoretical boiling limit to be overly conservative. This agrees with the findings of Brennan and Krolczek [1]. They point out that boiling limit models are very conservative.

In their work, they found that the theoretical boiling limit could be an order of magnitude lower than the actual boiling limit. The true heat transport limit in the operating temperature range of 40–80 °C proved to be the capillary limit.

Heat pipes are subject to four different heat transport limits, depending upon the portion of the operational range in which they are being used. These limits are, from the lowest operating temperature to the highest, as follows: sonic limit, entrainment limit, capillary limit, and boiling limit. Table D.2 is a summary of the four abovementioned limits, and they are summarized as follows.

Sonic Limit Analysis

When the vapor leaving the evaporator, or if there exists an adiabatic section, reaches the sonic limit, then Eq. (2.20) (or Eq. (D.1) here) can be used and is presented here again. This equation for the sonic heat transport limit was first derived by Levy [3] and is known as the Levy equation. Chi has reproduced the derivation of this equation as well [2]:

$$Q_{S_{max}} = A_v \rho_0 \lambda \left[\frac{\gamma_0 R_v T_0}{2(\gamma_0 + 1)} \right]^{1/2} \quad (\text{Eq.D.1 (or Eq.2.20)})$$

where

- $Q_{S_{max}}$ = Sonic heat transport limit (W).
- A_v = Vapor core cross-sectional area (m²).
- ρ_0 = Vapor density at stagnation temperature (kg/m³).
- λ = Latent heat of vaporization (J/kg).
- γ_0 = Specific gas constant.
- R_v = Vapor gas constant (J/kg K)
- T_0 = Stagnation temperature (K).

The sonic heat transport limit for this heat pipe example is represented in Fig. D.3.

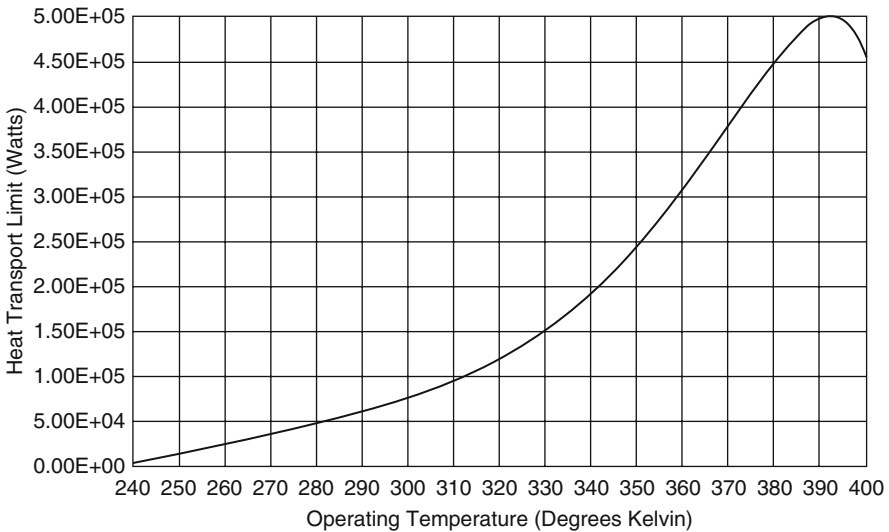


Fig. D.3 Sonic heat transport limit

Entrainment Limit Analysis

The entrainment limit is a result of the interactions of the vapor stream and the liquid stream. The interface between these opposite flowing streams is a mutual shear layer. If the relative velocity between the two streams is great enough, liquid droplets will be torn from the liquid stream and become entrained in the vapor stream [1]. When this occurs, evaporator wick dryout follows rapidly [2]. Chi derives the equation for computing the entrainment heat transport limit:

$$Q_{e_{max}} = A_v \lambda \left[\frac{\sigma \rho_v}{2r_{h,s}} \right]^{1/2} \tag{Eq.D.2}$$

where

$Q_{e_{max}}$ = Entrainment heat transport limit (W).

A_v = Vapor core cross-sectional area (m²)

λ = Latent heat of vaporization (J/kg).

σ = Surface tension coefficient (N/m).

ρ_v = Vapor density (kg/m³).

$r_{h,s}$ = Hydraulic radius of wick at vapor/wick interface (m).

The entrainment heat transport limit for the heat pipe used in this experiment is represented in Fig. D.4.

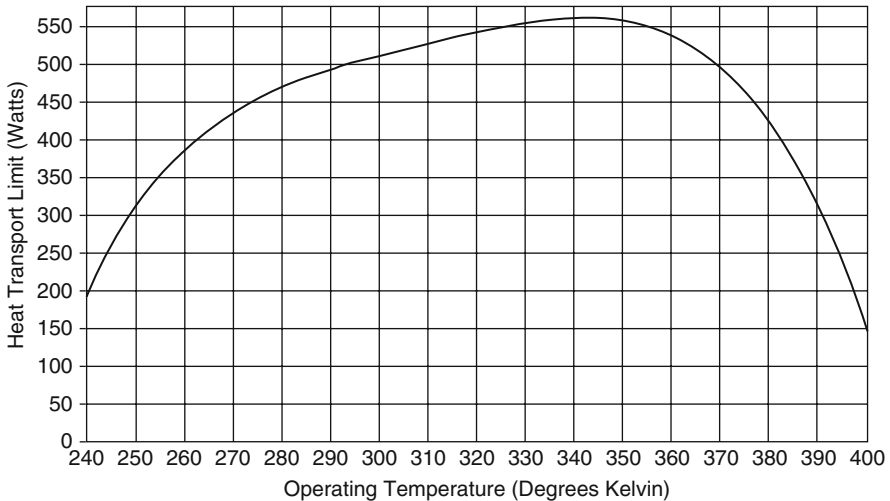


Fig. D.4 Entrainment heat transport limit

Capillary or Wick Limit Analysis

The capillary limit occurs when liquid is evaporating more rapidly than capillary forces can replenish the liquid. This condition results in local wick dryout and increased wall temperatures [1]. Chi [2] has derived the equations for determining the capillary or wick heat transport limit:

$$Q_{c_{\max}} = \frac{(QL)_{c_{\max}}}{\left(\frac{1}{2}L_c + L_a + \frac{1}{2}L_e\right)} \quad (\text{Eq.D.3})$$

with

$$(QL)_{c_{\max}} = \frac{\left(\frac{2\sigma}{r_c} - \Delta P_{\perp} - \rho_l g L_t \sin \Phi\right)}{(F_l + F_v)} \quad (\text{Eq.D.4})$$

where

$$F_l = \frac{\mu_l}{K A_w \rho_l \lambda} \quad (\text{Eq.D.5})$$

and

$$F_v = \frac{(f_v Re_v) \mu_v}{\left(2r_{h_v}^2 A_v \rho_v \lambda\right)} \quad (\text{Eq.D.6})$$

where

$Q_{c_{\max}}$ = Capillary heat transport limit (W).

L_c = Length of condenser section (m).

L_a = Length of adiabatic section (m).

L_e = Length of evaporator section (m).

L_t = Total length of the heat pipe (m).

σ = Surface tension coefficient (N/m).

r_c = Effective pore radius (m).

r_h = Hydraulic vapor radius.

ΔP_{\perp} = Hydrostatic pressure perpendicular to pipe axis (N/m²).

ρ_l = Liquid density (kg/m³).

ρ_v = Vapor density (kg/m³).

λ = Heat of vaporization (J/kg).

Φ = Heat pipe inclination (radians).

g = Gravitational force (9.81 m/s²).

F_l = Liquid frictional coefficient.

F_v = Vapor frictional coefficient.

μ_l = Liquid viscosity (kg/m s).

- μ_v = Vapor viscosity (kg/m s).
 K = Effective wick permeability (m^{-2}).
 f_v = Vapor drag coefficient.
 Re_v = Reynolds number.
 A_w = Wick cross-sectional area (m^2).

For this example, some simplifications can be made to Eq. (D.4). Since there is no connection between the grooves in the tested heat pipe, the hydrostatic pressure term, ΔP_{\perp} , is zero. The heat pipe was maintained in a nearly horizontal position throughout the test; therefore, the pipe inclination angle, Φ is zero. These simplifications reduce Eq. (D.4) to

$$(QL)_{\text{cmax}} = \frac{\left(\frac{2\sigma}{r_c}\right)}{(F_l + F_v)} \quad (\text{Eq.D.7})$$

The effective wick permeability used in Eq. (D.5) is a function of the wick geometry. For the axial groove wick used in this study, the equation for the effective wick permeability of the trapezoidal shaped groove is assumed by Brennan and Krolczek [1]:

$$K = 0.435 \left\{ \frac{(w\delta + \delta^2 \tan \alpha)^{1/2}}{w^{0.2} \left[\frac{2\delta}{\cos \alpha (1 - \sin \alpha) + w} \right]^2} \right\} \quad (\text{Eq.D.8})$$

where

- K = Effective wick permeability (m^{-2}).
 w = Groove width at the inner radius (m).
 δ = Groove depth (m).
 α = Groove angle ($^{\circ}$).

The capillary or wick heat transport limit for the heat pipe used in this example is shown below (Fig. D.5);

Boiling Limit Analysis

The boiling limit results when the heat flux density is great enough to cause the saturation vapor pressure at the interface between the wick and the wall to exceed the liquid pressure at the same point. When this occurs, vapor bubbles form in the liquid stream. These bubbles cause hot spots and restrict liquid circulation, leading to wick dryout [2]. The heat transport limit at which this occurs is known as the boiling limit. Chi derives the equation for computing the boiling heat transport limit:

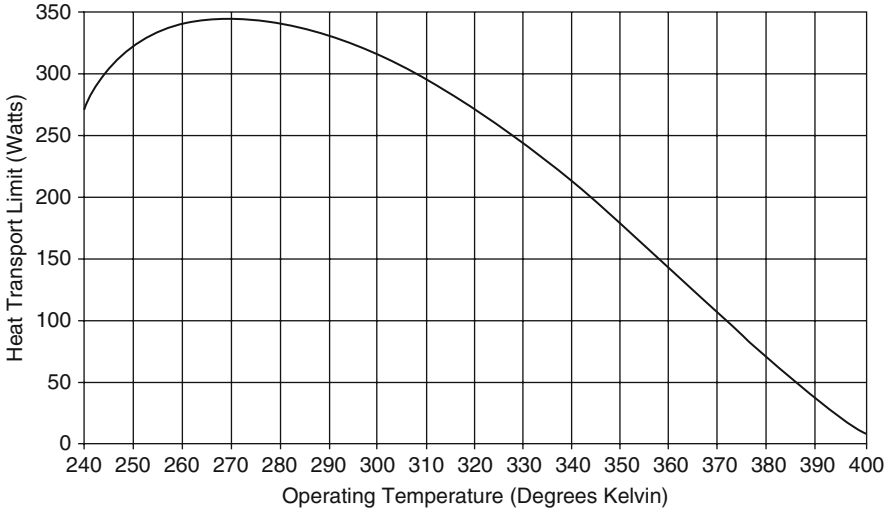


Fig. D.5 Capillary or wick heat transport limit

$$Q_{b_{\max}} = \frac{2\pi L_e k_e T_v}{\lambda \rho_v \ln(r_i/r_v)} \left(\frac{2\sigma}{r_n} - P_c \right) \quad (\text{Eq.D.9})$$

where

$Q_{b_{\max}}$ = Boiling heat transport limit (W).

L_e = Evaporator section length (m).

k_e = Effective thermal conductivity of the liquid or saturated wick matrix (W/m K).

T_v = Vapor temperature (K).

λ = Latent heat of vaporization (J/kg).

ρ_v = Vapor density (kg/m³).

r_i = Inside radius of pipe (m).

r_v = Vapor core radius (m).

σ = Surface tension coefficient (N/m).

r_n = Boiling nucleation radius (m).

P_c = Capillary pressure (N/m²).

The effective thermal conductivity, K_e , used in Eq. (D.9) is highly dependent upon the wick geometry. Chi gives the equation for finding the effective thermal conductivity of an axially grooved heat pipe;

$$k_e = \frac{wk_1(0.185w_f k_w + \delta k_1) + (w_f k_1 k_w \delta)}{(w + w_f)(0.185w_f k_w + \delta k_1)} \quad (\text{Eq.D.10})$$

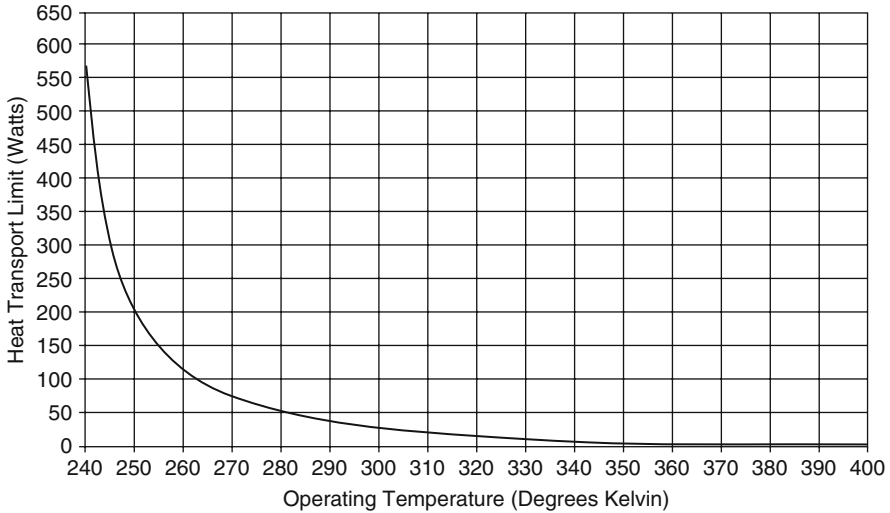


Fig. D.6 Boiling heat transport limit

where

w_f = Groove fin thickness (m).

w = Groove width (m).

δ = Groove depth (m).

k_l = Liquid thermal conductivity (W/m K).

k_w = Wall thermal conductivity (W/m K).

The radius of nucleation, r , used in Eq. (D.9) is also a function of the boiling surface [2]. A wide range of values for r have been reported. Chi gives typical nucleation radii of 254–2540 nm, while Silverstein reports values ranging from 1 to 7 μm (Silverstein [3] Page 162). A third source, Brennan and Krociczek, give typical nucleation radii of 1–10 μm [1]. Brennan and Krociczek also point out that the boiling limit model is very conservative. Even using their lower limit for nucleation radius, they've found that the model boiling limit can easily be an order of magnitude lower than the actual measured boiling limit. The boiling limit for the heat pipe used in this experiment, using Chi's lower limit of 254 nm, is represented in Fig. D.6.

Note: Recommended Values for Nucleation Site Radius [3]. It is reasonable to assume that the nucleation site radius in properly fabricated and conditioned heat pipes lies within the range of 1–7 μm . A value of 3 μm is suggested for preliminary design purpose.

Evaluation of this Example

The heat transport for this investigation was based on an anticipated heat pipe operating temperature of 313–353 K (40–80 °C). Based on the theoretical curves shown in Figs. D.3, D.4, D.5, and D.6, the boiling heat transport limit is expected to

be the performance-limiting condition for the tested heat pipe. This is based on the boiling limit having the lowest heat transport capability over the expected operating temperature range.

Design Example 2

This example is given by **Larry W. Swanson** [4].

Heat Transfer Research Institute College Station, Texas

Design a water heat pipe to transport 80 W of waste heat from an electronic package to cooling water. The heat pipe specifications are:

1. Axial orientation—Complete gravity-assisted operation (condenser above the evaporator; $\Psi = 180^\circ$).
2. Maximum heat transfer rate—80 W.
3. Nominal operating temperature—40 °C.
4. Inner pipe diameter—3 cm.
5. Pipe length—25-cm evaporator length, 50-cm adiabatic section, and 25-cm condenser length.

The simplest type of wick structure to use is the single-layer wire mesh screen wick shown in the table below. The geometric and thermophysical properties of the wick have been selected as (this takes some forethought):

- $d = 2.0 \times 10^{-5} \text{ m}$
- $w = 6.0 \times 10^{-5} \text{ m}$
- $\frac{1}{2N} = r_c = 1/2(2.0 \times 10^{-5} + 6 \times 10^{-5}) = 4.0 \times 10^{-5} \text{ m}$
- $\varepsilon = 1$
- $k_{\text{eff}} = k_1 = 0.630 \text{ W/m K}$
- $t_w = 1.0 \times 10^{-3} \text{ m}$
- $K = \frac{r_w^2}{12} = \frac{(1 \times 10^{-3})^2}{12} = 8.33 \times 10^{-8} \text{ m}^2$

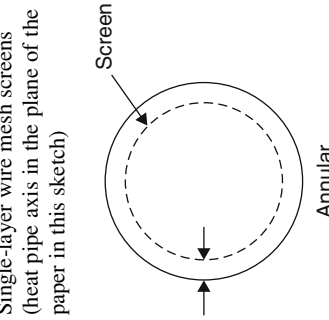
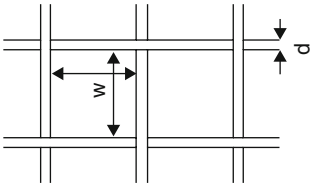
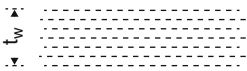
The other heat pipe geometric properties are:

- $r_v = r_i - t_w = 0.015 - 0.001 = 0.014 \text{ m}$
- $l_{\text{eff}} = \frac{0.25+0.25}{2} + 0.5 = 0.75 \text{ m}$
- $L_t = 0.25 + 0.50 + 0.25 = 1.0 \text{ m}$
- $A_w = \pi(r_i^2 - r_v^2) = \pi[(0.015)^2 - (0.014)^2] = 9.11 \times 10^{-15} \text{ m}^2$
- $A_v = \pi r_v^2 = \pi(0.014)^2 = 6.16 \times 10^{-4} \text{ m}^2$

The thermophysical properties of water at 40 °C are (see Table D.3):


- $\rho_l = 992.1 \text{ kg/m}^3$
- $\rho_v = 0.05 \text{ kg/m}^3$
- $\sigma_1 = 2.402 \times 10^6 \text{ J/kg}$


Table D.3 Physical properties of wick structure

	Wick type ^a	Thermal conductivity	Porosity	Minimum capillary radius	Permeability
<p>Single-layer wire mesh screens (heat pipe axis in the plane of the paper in this sketch)</p>  <p>Screen</p> <p>Annular</p>		$k_{\text{eff}} = k_e$	$\epsilon = 1$	$r_c = 1/(2N)$	$K = \frac{d^2 \epsilon^2}{12}$
<p>Annular</p> <p>$1/N = d + w$</p> <p>$N =$ number of apertures per unit length</p>  <p>t_w</p>	<p>Multiple wire mesh screens, plain or sintered (screen dimensions as for single layers illustrated above)</p>	$k_{\text{eff}} = \frac{k_e [k_e + k_s - (1 - \epsilon)(k_e - k_s)]}{k_e + k_s + (1 - \epsilon)(k_e - k_s)}$	<p>Estimated from</p> $\epsilon = 1 - (\pi N d)/4$	$r_c = 1/(2N)$	$k = \frac{d^2 \epsilon^2}{122(1 - \epsilon)^2}$

(continued)

Table D.3 (continued)

	Wick type ^a	Thermal conductivity	Porosity	Minimum capillary radius	Permeability
	Unconsolidated packed spherical particles (d = average particle diameter) Plain Sintered	Thermal conductivity $k_{\text{eff}} = \frac{k_e [2k_e + k_s - 2(1 - \epsilon)(k_e - k_s)]}{2k_e + k_s + (1 - \epsilon)(k_e - k_s)}$ $k_{\text{eff}} = \frac{k_e [2k_s + k_e - 2\epsilon(k_s - k_e)]}{2k_s + k_e + \epsilon(k_s - k_e)}$	Estimated from (assuming cubic packing) $\epsilon = 0.48$	$r_c = 0.21d$	$k = \frac{d^2 \epsilon^2}{150(1 - \epsilon)^2}$
					$k = C_1 \frac{y^2 - 1}{y^2 - 1}$ where

	Sintered metal fibers (d = fiber diameter)		$k_{\text{eff}} = \varepsilon^2 k_c (1 - \varepsilon)^2 k_s + \frac{4\varepsilon(1 - \varepsilon)k_c k_s}{k_c + k_s}$	Use manufacturers data	$r_c = \frac{d}{2(1 - \varepsilon)}$	$y = 1 + \frac{C_2 d^2 \varepsilon^3}{(1 - \varepsilon)^2}$
						$C_1 = 6.0 \times 10^{-10} \text{ m}^2$ $C_2 = 3.3 \times 10^7 \text{ l/m}^2$

Revised from Peterson, G.P., *An Introduction to Heat Pipes: Modeling, Testing, and Applications*, John Wiley & Sons, New York, 1994

^aThe axis of the pipe and direction of fluid flow are normal to the paper

^bThese wicks are positioned so that the layers follow the contours of the inner surface of the pipe wall

- $\mu_l = 6.5 \times 10^{-3} \text{ kg/m s}$
- $\mu_v = 1.04 \times 10^{-4} \text{ kg/m s}$
- $P_v = 7000 \text{ Pa}$
- $h_{fg} = 2.402 \times 10^6$ is the latent heat of vaporization for water at the range of -40 to $+40$ °C.

The various heat transfer limitations can now be determined to ensure that the heat pipe meets the 80 W heat transfer rate specification. The vapor pressure (viscous limitation) limitation is:

$$Q_{vp_{\max}} = \frac{\pi r_v^4 h_{fg} \rho_v P_v}{12 \mu_v l_{\text{eff}}}$$

$$Q_{vp_{\max}} = \frac{\pi(0.014)^4 (2.402 \times 10^6)(0.05)(7000)}{12(1.04 \times 10^{-4})(0.75)}$$

$$= 1.08 \times 10^5 \text{ W}$$

The sonic limitation is

$$Q_{s_{\max}} = 0.474 A_v h_{fg} (\rho_v P_v)^{1/2}$$

$$Q_{s_{\max}} = 0.474 (6.16 \times 10^{-4}) (2.402 \times 10^6) [(0.05)(7000)]^{1/2}$$

$$= 1.31 \times 10^4 \text{ W}$$

The entrainment limitation is:

$$Q_{e_{\max}} = A_v h_{fg} \left[\frac{\rho_v \sigma_l}{2r_{\text{cave}}} \right]^{1/2}$$

$$Q_{e_{\max}} = (6.16 \times 10^{-4}) (2.402 \times 10^6) \left[\frac{(0.05)(0.07)}{2(4.0 \times 10^{-3})} \right]^{1/2}$$

$$= 9.979 \times 10^3 \text{ W}$$

Noting that $\cos \Psi = 1$, the capillary limitation is:

$$Q_{c_{\max}} = \left[\frac{\rho_l \sigma_l h_{fg}}{\mu_l} \right] \left[\frac{A_w K}{l_{\text{eff}}} \right] \left(\frac{2}{r_{c,e}} - \left[\frac{\rho_l}{\sigma_l} \right] g L_t \cos \Psi \right)$$

$$Q_{c_{\max}} = \left[\frac{(992.1)(0.07)(2.402 \times 10^6)}{6.5 \times 10^{-3}} \right] \left[\frac{(9.11 \times 10^{-5})(8.33 \times 10^{-8})}{0.75} \right]$$

$$\times \left[\frac{2}{4.0 \times 10^{-5}} + \frac{992.1}{0.07} 9.8(1.0) \right]$$

Finally the boiling limitation is:

$$Q_{b_{\max}} = \frac{4\pi l_{\text{eff}} T_v \sigma_v}{h_{fg} \rho_l \ln(r_i/r_v)} \left(\frac{1}{r_n} - \frac{1}{r_{c,e}} \right)$$

$$Q_{b_{\max}} = \frac{4\pi(0.75)(0.63)(313)(0.07)}{(2.402 \times 10^6)(992.1) \ln\left(\frac{0.015}{0.014}\right)} \left[\frac{1}{2.0 \times 10^{-6}} - \frac{1}{4.0 \times 10^{-5}} \right]$$

$$= 0.376 \text{ W}$$

All of the heat transfer limitations, with the exception of the boiling limitation, exceed the specified heat transfer rate of 80 W. The low value of 0.376 for the boiling limitation strongly suggests that the liquid will boil in the evaporator and possibly cause local dry spots to develop. The reason the liquid boils is that the effective thermal conductivity of the wick is equal to the conductivity of the liquid, which is very low in this case. Because the liquid is saturated at the vapor–liquid interface, a low-effective thermal conductivity requires a large amount of wall superheat, which, in turn, causes the liquid to boil. This problem can be circumvented by using a high-conductivity wire mesh or sintered metal wick, which greatly increases the effective conductivity. It should be noted, however, that because porous wicks have lower permeabilities, the capillary limitation should be lower as well. Let us try a sintered particle wick made of copper with the following properties (see Table D.3):

- $d = 1.91 \times 10^{-4} \text{ m}$
- $r_c = 0.21d = 4.0 \times 10^{-5} \text{ m}$
- $\varepsilon = 0.48$
- $K = \frac{(1.91 \times 10^{-4})(0.48)}{150(1-0.48)^2} = 2.07 \times 10^{-10} \text{ m}^2$
- $K_1 = 400 \text{ W/m K}$ (Copper)
- $K_1 = 0.630 \text{ W/m K}$ (Water)
- $k_{\text{eff}} = \frac{400 \left[2(400+0.63-2(0.48)(400-0.63)) \right]}{2(400)+0.63+0.48(400-0.63)} = 168 \text{ W/m K}$

All other geometric and thermophysical properties are the same. The heat transfer limitations affected by the change in wick structure are the capillary and boiling limitations. The sintered metal wick produces a capillary limitation of

$$Q_{c_{\max}} = \left[\frac{(992.1)(0.07)(2.402 \times 10^6)}{6.5 \times 10^{-3}} \right] \left[\frac{9.1 \times 110^{-5}(2.07 \times 10^{-10})}{0.75} \right]$$

$$\times \left[\frac{2}{4.0 \times 10^{-5}} + \frac{992.1}{0.07}(9.8(1.0)) \right] = 122 \text{ W}$$

The boiling limitation for the sintered wick is

$$Q_{b_{\max}} = \frac{4\pi(0.75)(168)(313)(0.07)}{(2.402 \times 10^6)(992.1)\ln\left(\frac{0.015}{0.014}\right)} \left[\frac{1}{2.0 \times 10^{-6}} - \frac{1}{4.0 \times 10^{-5}} \right]$$

$$= 100 \text{ W}$$

This design now meets all the specifications defined in the problem statement. More points can be calculated to reveal that for the anticipated operating temperature range of -40 to $+40$ °C, the boiling limit was expected to constrain the maximum heat transport of the test article since it has the lowest heat transport value for the entire operating range. This will allow one to plot all the limiting operation of this heat in order to come up with best optimum design and envelope of operating range where under that the heat up pipe operates according to its spec. See Example 1.

Design Example 3

This example is given by **G. P. Peterson** [5].

G. P. Peterson: An Introduction to Heat Pipes—Modeling, Testing, and Applications, John Wiley & Sons, Inc., 1994.

A simple horizontal copper–water heat pipe is to be constructed from a 1.5-cm internal diameter, 0.75-m-long tube to cool an enclosed electrical cabinet as shown in Fig. D.7. The evaporator and condenser lengths of the heat pipe are 0.25 m each,

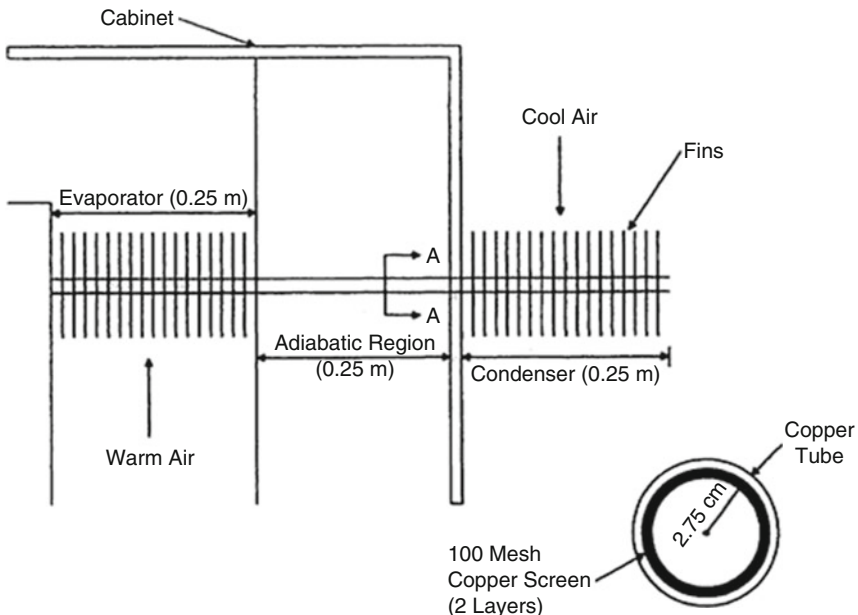


Fig. D.7 Sketch of copper–water heat pipe of Example 3 [5]

and the wicking structure consists of two layers of 100-mesh copper screen. The maximum heat transport capacity of the heat pipe is estimated to be 20 W and to occur at an adiabatic vapor temperature of 30 °C:

1. If the working fluid is water and is assumed to fully wet the wicking structure, will this heat pipe be adequate?
2. What happens to the maximum transport capacity if the wetting angle is increased to 45 °C due to poor cleaning?

Solutions

First it is necessary to summarize the physical parameters and known information for this application:

Wick geometry
$N = 100 \text{ in.}^{-1} = 3937 \text{ m}^{-1}$ (Mesh number)
$d_w = 0.0045 \text{ in.} = 1.143 \times 10^{-4} \text{ m}$ (Wire diameter)
Spacing = $d_w = 1.143 \times 10^{-4} \text{ m}$ (Assume)
Fluid properties at 30 °C
$\lambda = 2425 \times 10^3 \text{ J/kg}$ (Latent heat of vaporization)
$\rho_\ell = 995.3 \text{ kg/m}^3$ (Working liquid density)
$\rho_v = 0.035 \text{ kg/m}^3$ (Vapor density)
$\mu_\ell = 769 \times 10^{-6} \text{ N s/m}^2$ (Working liquid absolute viscosity)
$\mu_v = 70.9 \times 10^{-6} \text{ N s/m}^2$ (Vapor absolute viscosity)
$\sigma = 70.9 \times 10^{-3} \text{ N/m}$

Next, calculate the vapor diameter:

$$\begin{aligned}
 d_v &= d - 2 \text{ (Two Layers + Two Space)} \\
 &= 0.015 - 2[4(1.143 \times 10^{-4})] \\
 &= 0.0141 \text{ m}
 \end{aligned}$$

To evaluate the maximum heat transport capacity, the capillary limit must be evaluated. This is represented by Eq. (2.8):

$$(\Delta P_c)_m \geq \int_{L_{\text{eff}}} \frac{\partial P_v}{\partial x} dx + \int_{L_{\text{eff}}} \frac{\partial P_l}{\partial x} dx + \Delta P_{e_{\text{phase}}} + \Delta P_{c_{\text{phase}}} + \Delta P_{\perp} + \Delta P_{\parallel}$$

where

$(\Delta P_c)_m$ = Maximum capillary pressure difference generated within capillary wicking structure between wet and dry points.

$$\int_{L_{\text{eff}}} \frac{dP_v}{dx} dx = \text{Vapor pressure drop (Eq. 2.55).}$$

$$\int_{L_{\text{eff}}} \frac{dP_l}{dx} dx = \text{Liquid pressure drop (Eq. 2.38).}$$

$\Delta P_{\text{e phase}} =$ Pressure gradient across phase transition in evaporator.

$\Delta P_{\perp} = \rho_1 g d_v \cos \psi$ Normal hydrostatic pressure (Eq. 2.8a)

$\Delta P_{\parallel} = \rho_1 g L \sin \psi$ Axial hydrostatic pressure (Eq. 2.8b).

Assuming that one-dimensional flow and the wet point are at the end of the condenser yields,

$$\int_{L_{\text{eff}}} \frac{dP_v}{dx} dx = \Delta P_v = \left(\frac{C(f_v \text{Re}_v) \mu_v}{2(r_{\text{hv}})^2 A_v \rho_v \lambda} \right) L_{\text{eff}} q \quad (\text{Eqs. 2.55 and 2.55a})$$

$$\int_{L_{\text{eff}}} \frac{dP_l}{dx} dx = \Delta P_l = \left(\frac{\mu_l}{K A_w \rho_l \lambda} \right) L_{\text{eff}} q \quad (\text{Eqs. 2.38 and 2.38a})$$

$$\left. \begin{aligned} \Delta P_{\perp} &= \rho_1 g d_v \cos \psi = \rho_1 g d_v \\ \Delta P_{\parallel} &= 0 \end{aligned} \right\}$$

For horizontal heat pipe where $\psi = 0$, then $\sin \psi = 0$.

ψ is the inclination angle of heat pipe in respect to horizontal frame of reference.

Utilizing Eq. (2.7a) and (2.7b), we can write:

$$(\Delta P_c)_m = \frac{2\sigma \cos \theta}{r_c} \quad \text{where } r_c = \frac{1}{2N}$$

Thus Eqs. (2.8a and 2.8b) takes the form of

$$\frac{2\sigma \cos \theta}{r_c} = \left(\frac{C(f_v \text{Re}_v) \mu_v}{2(r_{\text{hv}})^2 A_v \rho_v \lambda} \right) L_{\text{eff}} q + \left(\frac{\mu_l}{K A_w \rho_l \lambda} \right) L_{\text{eff}} q + \rho_1 g d_v$$

Next it is necessary to find the capillary radius r_c from Table 2.1.

$$r_c = \frac{1}{2N} = \frac{1}{2(3937)} = 1.27 \times 10^{-4} \text{ m}$$

The vapor space area of A_v is then given by the following relationship:

$$A_v = \frac{1}{4} \pi (d_v)^2 = \frac{1}{4} \pi (0.0141 \text{ m})^2 = 1.56 \times 10^{-4} \text{ m}^2$$

The liquid flow area A_l is given by the following relationship:

$$A_l = \frac{1}{4} \pi (d^2 - d_v)^2 = \frac{1}{4} \pi [(0.015 \text{ m})^2 - (0.014 \text{ m})^2] = 1.057 \times 10^{-5} \text{ m}^2$$

And the wick permeability K can be calculated from Table 2.2 as follows;

$$K = \frac{d_1^2 \varepsilon^3}{122(1 - \varepsilon)^2} \quad \text{where} \quad \varepsilon = 1 - \frac{1.05\pi N d_1}{4}$$

$$\varepsilon = 1 - \frac{1.05\pi N d_1}{4} = 1 - \frac{1.05\pi(3937)(1.143 \times 10^{-4})}{4} = 0.629$$

And as a result for permeability K , we have

$$K = \frac{d_1^2 \varepsilon^3}{122(1 - \varepsilon)^2} = \frac{(1.143 \times 10^{-4})^2 (0.629)^3}{122(1 - 0.629)^2} = 1.94 \times 10^{-10} \text{ m}^2$$

Because, at this point, it is not known if the vapor flow is laminar or turbulent or compressible or even incompressible; it is necessary to, as a first approximation, assume laminar, incompressible flow situations, which means $f_v \text{Re}_v = 16$ and $C = 1.0$ in Eq. (2.55a). Substituting these and the other values from above into modified Eqs. (2.8a and 2.8b) that is shown above, we have:

$$\frac{2(70.9 \times 10^{-3}) \cos \theta^\circ}{1.27 \times 10^{-4}} = \frac{1.0(16)(9.29 \times 10^{-6})(0.50)q}{2(0.00705)^2(1.56 \times 10^{-4})(0.035)(2425 \times 10^3)}$$

$$+ \frac{(769 \times 10^{-6})(0.50)q}{(1.94 \times 10^{-10})(2.057 \times 10^{-5})(2425 \times 10^3)(995.3)}$$

$$+ 995.3(9.81)(0.0141)$$

or

$$1116.5 = 0.0565q + 25.1q + 137.7$$

Solving for q yields,

$$q = \frac{1116.5 - 137.7}{0.0565 + 39.9}$$

or the value which represents the maximum axial heat transfer that heat pipe can transport prior to reaching the capillary limit is given by

$$q_m = 24.5 \text{ W}$$

Next, the assumption of laminar, incompressible flow must be verified. This can be done by evaluating the Reynolds number:

$$\begin{aligned} \text{Re} &= \frac{4\dot{m}}{\pi d_v \mu} = \frac{4q}{\pi d_v \mu \lambda} = \frac{4(24.5)}{\pi(0.0141)(2.29 \times 10^{-6})(2425 \times 10^3)} \\ &\Rightarrow \text{Re} = 97.9 \end{aligned}$$

This value of Reynolds number validates the laminar flow assumption. For uniform mass addition (vaporization) and uniform mass removal (condensation), the L_{eff} is given by

$$L_{\text{eff}} = 0.5L_e + L_a + 0.5L_c$$

Finally, the Mach number must be calculated to verify the assumption of incompressible flow as follows:

$$\begin{aligned} \text{Mach} &= \frac{v_m}{c} = \frac{\dot{m}/A_v}{\sqrt{\gamma RT_v}} = \frac{4q/(\lambda \pi d_v^2)}{\sqrt{\gamma RT_v}} \\ &= \frac{4(38.91)/\left((2425 \times 10^3)\pi(0.0141)^2\right)}{\left[(1.22)(461.89(30 + 273))\right]^{1/2}} \\ &= \frac{0.1028}{431.4} = 2.38 \times 10^{-4} = 0.3 \Rightarrow \text{Incompressible flow} \end{aligned}$$

Because the original assumptions are valid, the maximum heat transport capacity is equal approximately to 24.5 W.

If θ approaches to 45° due to poor cleaning, then the maximum capillary pressure becomes

$$(\Delta P_c)_m = \frac{2\sigma \cos \theta}{r_c} = \frac{2(70.9 \times 10^{-3}) \cos 45^\circ}{1.27 \times 10^{-4}} = 789.5 \text{ Pa}$$

and $q_m = 15.98 \text{ W}$ or 66% of q_m with $\theta = 0^\circ$

The preceding example illustrates the procedure for finding and estimating the maximum transport capacity as determined by the capillary limit and assumption was that the heat pipe is horizontal, which may not always be the case of somebody application.

Design Example 4

This example is given by **G. P. Peterson** [5].

G. P. Peterson: An Introduction to Heat Pipes—Modeling, Testing, and Applications, John Wiley & Sons, Inc., 1994.

For the heat pipe of Design Example 3, determine the effects of tilt angle (evaporator elevated above the condenser) on the heat pipe performance. What is the maximum tilt angle at which heat pipe will still operate?

Solutions

If ΔP_{\parallel} is no longer equal to zero, then the capillary limit is represented by (Fig. D.8 and Table D.4)

$$(\Delta P_c)_m \geq \int_{L_{\text{eff}}} \frac{\partial P_v}{\partial x} dx + \int_{L_{\text{eff}}} \frac{\partial P_l}{\partial x} dx + \Delta P_{\perp} + \Delta P_{\parallel}$$

At 30 °C, these terms are equal to

$$1116.5 = 0.0565q + 39.9q + 137.7 + \rho_l g L \sin \psi$$

or

Fig. D.8 Evaporator elevation vs. heat transport capacity of Example 4 [5]

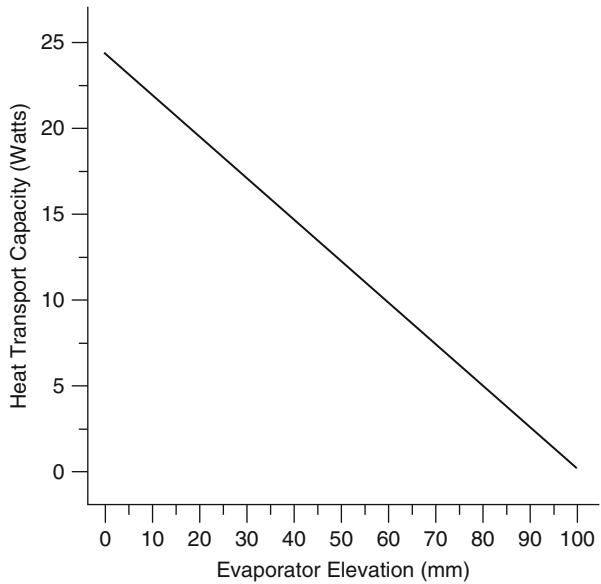


Table D.4 Heat pipe data for different inclined angles of Example 4 [5]

ψ (°)	$h = L \sin \psi$ (cm)	q_m (W)
0	0	24.5
1	1.31	21.28
2	2.62	18.18
3	3.92	14.89
4	5.23	11.70
5	6.54	8.52
6	7.83	5.33
7	9.14	2.16
8	10.43	–

$$978.8 = 39.96q + 995.3(9.81)(0.75) \sin \psi$$

$$\Rightarrow q_m = \frac{978.8 - 7323 \sin \psi}{39.96}$$

The maximum angle at which the heat pipe will still operate occurs when $q_m = 0$ or $\psi = 7.68^\circ$ ($h = 10.02$ cm). However, to still transfer the required thermal load of 20 W, the tilt angle must be less than approximately 1.4° .

Note: ΔP_\perp will not change for small angles of ψ since $\cos \theta \simeq 1.0$ (e.g. $\cos 7^\circ = 0.993$).

In addition to determine the effect of tilt angle on the transport capacity, variations in the mean operating temperature may also have a significant impact on the transport capacity. While in practice, it is difficult to estimate what this value will be, the capillary transport limit can be estimated for a reasonable temperature range, allowing the designer to determine if the design is appropriate.

Design Example 5

This example is given by **G. P. Peterson** [5].

G. P. Peterson: An Introduction to Heat Pipes—Modeling, Testing, and Applications, John Wiley & Sons, Inc., 1994.

For the heat pipe described in Design Example 3, determine the effects of the capillary limit of varying the adiabatic vapor temperature over a range of 10–120 °C.

Solutions

Variations in the adiabatic vapor temperature will cause corresponding changes in the properties of the working fluid. This in turn will affect the performance and the capillary limit. The basic equation is

$$\frac{2\sigma \cos \theta}{r_c} = \left(\frac{C(f_v \text{Re}_v)\mu_v}{2(r_{h_v})^2 A_v \rho_v \lambda} \right) L_{\text{eff}} q + \left(\frac{\mu_l}{K A_w \rho_l \lambda} \right) L_{\text{eff}} q + \rho_l g d_v$$

which in terms of the fluid properties reduces to

$$\frac{2\sigma}{1.27 \times 10^{-4}} = \frac{1(16)\mu_v(0.5)q}{2(0.0075)^2(1.56 \times 10^{-4})\rho_v\lambda} + \frac{\mu_1(0.50)}{(1.94 \times 10^{-10})(2.057 \times 10^{-5})\rho_1\lambda} + \rho_1(9.81)(0.0141)$$

or

$$1.575 \times 10^4 \sigma = \left(4.546 \times 10^8 \frac{\mu_v}{\rho_v\lambda} + 1.25 \times 10^{14} \frac{\mu_1}{\rho_1\lambda} \right) q + \rho_1(0.138)$$

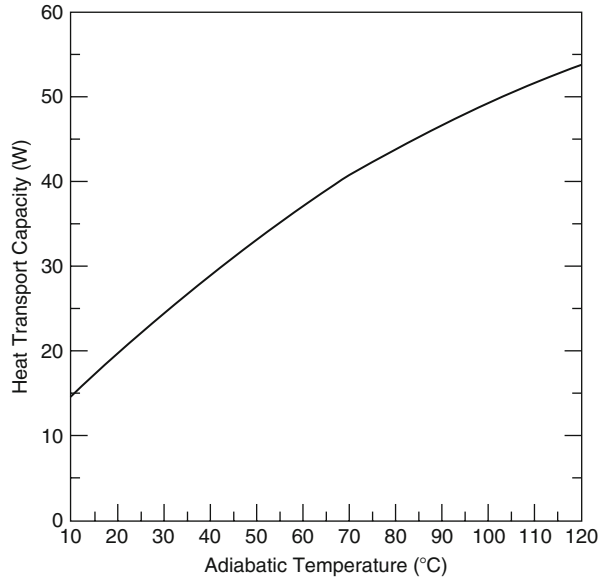
Simplifying yields

$$q = \frac{(1.575 \times 10^4)\sigma - (0.138)\rho_1}{(4.56 \times 10^8)(\mu_v/\rho_v\lambda) + (1.25 \times 10^{14})(\mu_1/\rho_1\lambda)}$$

The results as a function of temperature can be calculated and tabulated as follows.

T	λ (kJ/kg)	σ (N/m)	ρ_v (kg/m ³)	ρ_l (kg/m ³)	μ_v (N s/m ²)	μ_l (N s/m ²)	ΔP_e (Pa)	$\Delta P_l/q$ (Pa/w)	$\Delta P_{\sqrt{q}}$ (Pa/w)	ΔP^+ (Pa)	q (W)
10	2478.0	0.075	0.006	1000.0	82.9×10^{-7}	14.2×10^{-4}	1181.3	71.6	0.191	138.0	14.5
20	2453.8	0.073	0.0173	999.0	88.5×10^{-7}	10.0×10^{-4}	1149.8	51.0	0.095	137.86	19.8
40	2406.5	0.069	0.051	993.1	96.6×10^{-7}	6.51×10^{-4}	1086.8	34.1	0.036	137.05	27.8
60	2358.4	0.066	0.130	983.3	105.0×10^{-7}	4.63×10^{-4}	1039.5	25.0	0.016	135.7	36.0
80	2308.9	0.063	0.293	971.8	113.0×10^{-7}	3.51×10^{-4}	992.3	19.55	0.008	134.1	43.9
100	2251.2	0.059	0.597	958.8	121.0×10^{-7}	2.79×10^{-4}	929.3	16.2	0.004	132.3	49.2
120	2202.2	0.055	1.121	943.4	128.0×10^{-7}	2.3×10^{-4}	866.3	13.8	0.002	130.2	53.3

Fig. D.9 Plot of heat transport capacity versus adiabatic temperature



or shown graphically (Fig. D.9).

The preceding examples illustrate the effects the gravitational environment and operating temperature can have on the capillary limit of heat pipes, but as mentioned previously, this is only one of the several limits encountered during the design and operation of heat pipes. The following example illustrates the modeling procedures for finding the other limitations outlined in Chap. 2.

Design Example 6

This example is given by **G. P. Peterson** [5].

G. P. Peterson: *An Introduction to Heat Pipes—Modeling, Testing and Applications*, John Wiley & Sons, Inc., 1994.

In addition to the capillary limit, it is also necessary in many applications to determine the capillary, sonic, boiling, and entrainment limits as function of mean operating temperature and the tilt angle of the heat pipe described in Design Example 3. Assume a round copper–water heat pipe with an overall length of 25.4 mm; a finned condenser section 9.39 mm long; an evaporator section 11.81 mm long, constructed from 3.2-mm diameter copper tubing with a wall thickness of 0.9 mm; a wicking structure constructed from phosphor bronze wire mesh (No. 325) with a wire diameter of 0.0355 mm; and a condenser section with a series of ten fins approximately 6-mm square, 0.2 mm thick, at a spacing of 1 mm. These limits can be found as follows.

Solutions

The thermophysical properties of the working fluid are summarized below.

Operating temperature (K)	ρ_l	ρ_v	μ_l	μ_v	k_{eff}	σ	λ
298.15	996.92	0.024	9.47×10^{-4}	1.03×10^{-5}	0.605	7.29×10^{-2}	2.347
323.15	996.92	0.083	5.5×10^{-4}	1.116×10^{-5}	0.640	6.93×10^{-2}	2.324
348.15	974.50	0.247	3.93×10^{-4}	1.119×10^{-5}	0.657	6.20×10^{-2}	2.254
373.15	960.72	0.580	2.82×10^{-5}	1.28×10^{-5}	0.680	5.84×10^{-2}	2.1

where

ρ_l = Liquid density (kg/m³)

ρ_v = Vapor density (kg/m³)

μ_l = Liquid viscosity (kg/m s)

μ_v = Vapor viscosity (kg/m s)

σ = Surface tension (N/m)

k_{eff} = Thermal conductivity (W/m K)

For screen mesh, the capillary radius can be found in Table 2.1 as follows:

$$r_c = \frac{1}{2N} = \frac{1}{2(12,795.25)} = 3.91 \times 10^{-5} \text{ m}$$

The maximum capillary pressure can be found in Eq. (2.10) as follows:

$$P_{\text{Capillary}_{\text{max}}} = \frac{2\sigma}{r_c} \text{ (N/m}^2\text{)}$$

The normal hydrostatic pressure can be found in Eq. (2.8a) as follows:

$$\Delta P_{\perp} = \rho_l g d_v \cos \psi \text{ (N/m}^2\text{)}$$

The axial hydrostatic pressure can be found in Eq. (2.28b) as follows:

$$\Delta P_{\parallel} = \rho_l g L \sin \psi \text{ (N/m}^2\text{)}$$

And the maximum effective pumping pressure can be expressed as

$$P_{p,m} = P_{c,m} - \Delta P_{\perp} - \Delta P_{\parallel}$$

Using these expressions, the contributions of each of the pressure terms can be summarized in tabular form as shown below.

Operating temperature (K)	σ	$P_{c,m}$	ΔP_+	$\Delta P_{ }$	$P_{p,m}$
298.15	7.29×10^{-2}	3728.90	12.21	0	3716.70
232.15	6.93×10^{-2}	3544.76	12.10	0	3532.66
348.15	6.20×10^{-2}	3171.35	11.94	0	3159.41
373.15	5.84×10^{-2}	2987.21	11.77	0	2975.44

Other intermediate values that must be evaluated are as follows:

Wick cross-sectional area: $A_w = \frac{1}{4}\pi(d_i^2 - d_v^2) = 2.9 \times 10^{-7} \text{ m}^2$

Wick porosity, $\varepsilon = 1 - \frac{1}{4}\pi S N d = 0.625$ (Table 2.2, Eq. (2.53), where a wick crimping factor $S = 1.05$ is used).

Wick permeability, $K = d^2 \left[t^3 / 122(1 - t)^2 \right] = 2 \times 10^{-11} \text{ m}^2$ (Table 2.2, Eq. (2.52)).

Liquid frictional coefficient, $F_l = \frac{\mu_l}{K A_w \rho_l}$ (Eq. 2.44).

Vapor core cross-sectional area, $A_v = \frac{1}{4}\pi d_v^2 = 1.277 \times 10^{-6} \text{ m}^2$.

Vapor core hydraulic radius, $r_{h_v} = \frac{1}{2}d_v = 0.000625 \text{ m}$.

Drag coefficient, $(f_v \text{Re}_v) = 16$ (circular vapor flow passage).

Vapor frictional coefficient, $F_v = \frac{(f_v \text{Re}_v)\mu_v}{2r_{h_v}^2 A_v \rho_v \lambda}$ (Eq. 2.59).

Assuming that phase transition pressure is almost 0, then, we have

$$\Delta P_{\text{Ph}} \sim 0$$

The governing equation becomes

$$P_c = F_l L_{\text{eff}} q + F_v L_{\text{eff}} q + \Delta P_{\perp} + \Delta P_{||} + \Delta P_{\text{Ph}}$$

The friction factors can be summarized as follows:

Temperature (K)	F_c	F_v	$(qL)_{c,m}$	$q_{c,m}$
298.15	69,782.83	3052.10	0.0510	3.45
323.15	41,287.91	965.68	0.0836	5.65
348.15	30,848.13	335.50	0.1013	6.85
373.15	23,182.43	168.66	0.1275	8.61

Computing the effective length as

$$L_{\text{eff}} = 0.5L_c + L_a + 0.5L_e = 0.0148 \text{ m}$$

The transport capacity can be found as a function of length or in terms of the total power:

$$(q_{c,m}L) = \frac{P_{p,m}}{F_l + F_v} (\text{W m}) \quad \text{or} \quad (q_{c,m}L) = \frac{q_{c,m}L}{L_{\text{eff}}}$$

Using a similar approach, the individual pressure terms and transport capacities can be determined for tilt angles of 15° as follows.

Temperature (K)	$P_{c,m}$	ΔP_{\perp}	ΔP_{\parallel}	$P_{p,m}$
298.15	3728.90	11.79	63.26	3653.85
323.15	3544.76	11.69	62.71	3470.36
348.15	3171.35	11.53	31.84	3097.98
373.15	2987.21	11.38	60.96	2914.87

Temperature (K)	$q_{c,m}L$	$q_{c,m}$
298.15	0.0502	3.39
323.15	0.0821	5.55
348.15	0.0993	6.71
373.15	0.1249	8.44

And for tilt angles of 45° can be determined as follows.

Temperature (K)	$q_{c,m}L$	ΔP_{\perp}	ΔP_{\parallel}	$P_{p,m}$
298.15	3728.90	8.64	172.64	3547.62
323.15	3544.76	8.56	171.14	3365.06
348.15	3171.35	8.44	168.75	2994.16
378.15	2987.21	8.32	166.37	2812.52

Temperature (K)	$q_{c,m}L$	$q_{c,m}$
298.15	0.0487	3.29
323.15	0.0796	5.38
348.15	0.0960	6.48
373.15	0.1205	8.14

Sonic Limit

The sonic limit can be found in Eq. 2.20:

$$Q_{s,max} = A_v \rho_0 \lambda \left[\frac{\gamma_0 R_v T_0}{2(\gamma_0 + 1)} \right]^{1/2} \quad (\text{W})$$

Vapor molecular weight $M = 18$

Vapor specific heat ration $\gamma_0 = 1.33$

Universal gas constant $\tilde{R} = 8.314 \times 10^3 \text{ J/kg mol K}$

Vapor constant $R_v = \frac{8.314 \times 10^3}{18} = 462 \text{ J/kg K}$

Temperature (K)	$q_{s,m}$
298.15	13.70
323.15	48.85
348.15	146.36
373.15	344.76

Boiling Limit

The boiling limit can be found in Eq. 2.96;

$$Q_{b,max} = \frac{2\pi L_e k_{eff} T_v}{\lambda \rho_v \ln(r_i/r_v)} \left(\frac{2\sigma}{r_n} - P_{c,m} \right)$$

where $P_{c,m}$ is the capillary pressure in the wicking structure or, if $P_c < P_{c,m}$ the maximum capillary pressure found earlier, and the nucleation radius r_n is in the range $2.54 \times 10^{-5} - 2.54 \times 10^{-7}$. The effective conductivity of the saturated wick, k_{eff} can be found in

$$k_{eff} = \frac{k_i(k_i+k_w-(1-\varepsilon)(k_i-k_w))}{k_i+k_w(1-\varepsilon)(k_i-k_w)}$$

where $L_e = 0.0118$ m and $r_n = 2.54 \times 10^{-7}$ m or

$k_w = 402$ W/m K.

Temperature (K)	k_{eff}	$q_{b,m}$
298.15	1.327	2797.53
323.15	1.404	890.54
348.15	1.441	305.24
373.15	1.491	140.35

Entrainment Limit

The entrainment limit can be estimated using Eq. (2.34)

$$Q_{e,max} = A_v \lambda \left[\frac{\sigma \rho_v}{2r_{h,w}} \right]^{1/2}$$

where the wick surface pore hydraulic radius is $r_{h,w} = \frac{1}{2N} - \frac{d}{2} = 2.13 \times 10^{-5}$ m

Temperature (K)	$q_{c,m}$
298.15	18.45
323.15	33.13
348.15	52.44
373.15	75.56

Viscous Limit

Finally the viscous limit can be estimated using Eq. 2.109:

$$Q_{\text{vapor,max}} = \frac{\pi r_v^4 h_{fg} \rho_{v_e} P_{v_e}}{12 \mu_{v_e} l_{\text{eff}}}$$

where $(f_v \text{Re}_v) = 16$ and

Temperature (K)	$P_v(\text{N/m}^2)$	$q_{v,m}$
298.15	3293	42.93
323.15	12,349	219.25
348.15	37,290	760.72
373.15	101,350	2095.25

The five limits can be represented graphically as a function of the mean adiabatic or operation temperature as shown below (Fig. D.10).

As shown above, this configuration is a capillary limit over the entire temperature range.

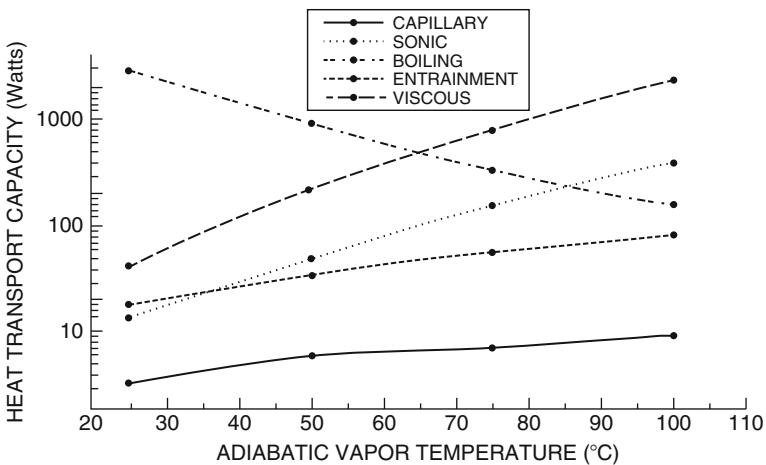


Fig. D.10 Heat transport capacity versus adiabatic vapor temperature

Note: It is important to note that in order to determine the actual heat transport capacity in the preceding Example 6 from Peterson [5], the mean operating temperature or adiabatic vapor temperature must be known, a priori, which is not usually the case.

There are many more examples following this one in Peterson's book [5] that is recommended for the reader to refer to it.

References

1. Berennan, P. J., & Kroliczek, E. J. (1979). *Heat pipe design*. From B & K Engineering Volume I and II. NASA contract NAS5-23406.
2. Chi, S. W. (1976). *Heat pipe theory and practice*. New York: McGraw-Hill.
3. Silverstein, C. C. (1992). *Design and technology of heat pipes for cooling and heat exchange*. Washington, DC: Taylor and Francis.
4. Swanson, L. W. Heat Transfer Research Institute College Station, Texas. *The CRC Handbook of Mechanical Engineering* (2nd Ed., Handbook Series for Mechanical Engineering).
5. Peterson, G. P. (1994). *An introduction to heat pipes—Modeling, testing and applications*. New York: John Wiley & Sons.

Index

A

Aavid Engineering, 20
Advanced High Temperature Reactor (AHTR), 342
Aligned Parallel Rectangles, 242
American Society of Mechanical Engineering (AMSE), 189
Assembly of heat pipe parts, 408
ATS-6, 36
Axial Power Rating (APC), 20
Axial Reynolds Number, 67, 68

B

Bessel functions, 240
Biot (Bi) number, 238
Bouk fast reactor, 349
Butt joints, 397

C

Capillary limit, 88, 139
Capillary pressure, 57
Capillary Pumped Loop (CPL), 10, 289
Charging heat pipe, 414
Cleaning techniques, 405
Closed Loop Pulsating Heat Pipes (CLPHP), 434
Coaxial Cylinders, 242
Coaxial Parallel Disks, 242
Compressed Air Energy Storage (CAES), 369
Computer Aided Design (CAD), 288
Concentrated Solar Power (CSP), 369, 390
Condenser, 79

Constant Conductance Heat Pipe (CCHP), 12, 13, 431, 439
Cullimore & Ring Technologies (C&R), 287

D

Data Center Cooling, 343
Design Guidelines, 20
Designed Analysis of Heat-Pipe Wicks, 261
Diffusivity, 220
Dirty envelope, 403
Dirty wick, 403
Dropwise Condensation, 75

E

Eddying motions, 66
Electro-Magnetic Interference (EMI), 357
End cap installation, 409
End closure design guidelines, 410
ERATO program, 351
ERIDAN 214, 36
ESRO (the IKE Institute in Stuttgart), 36
Evacuated Tube Heat Pipe Solar Collectors (ETHPSC), 390
Evaporator, 79

F

First Law of Thermodynamics, 71
Fixed Conductance, 185
Fixed Conductance Heat Pipe (FCHP), 12, 13
Fluid Integrator (FLUINT), 287
Forced convection, 73
Free convection, 73

French National Center for Space Research, 36
Fully Inherent, 342
Furukawa Electric, 229

G

Gas gap, 78
General Purpose Heat Source (GPHS), 348
GFW (Dornier), 36
Goddard Space Flight Center (GSFC), 353
Graphics User Interface (GUI), 288

H

Heat Pipe Assemblies, 20
Heat Pipe Heat Exchanger (HPHE), 364
Heat Pipe Operated Mars Exploration Reactor (HOMER), 344
Heat Transfer Coefficient, 231
Heat Transfer Fluid (HTF), 375, 379, 382, 383
Heat Transfer Unit NTU, 272
High Power Electric Propulsion (HiPEP), 353
HOMER-15 - the Heat Pipe Operated Mars Exploration Reactor, 351
Hughes (Hughes), 36

I

Insulated Gate Bipolar Transistors (IGBT's), 358

K

Kinematic viscosity, 65
Kolmogorov length scale, 65

L

Laminar flow, 64, 65, 96
Latent Heat Thermal Energy Storage (LHTES), 370, 371, 374, 376, 379, 390
Levelized Cost of Energy (LCOE), 369
Liquid Controlled Heat Pipe (LCHP), 13
Liquid Metal Fast Breeder Reactors (LMFBR), 342
Liquid Transport Factor, 30
Liquid-Vapor Interface, 219
Log Mean Temperature Difference, 231
Loop Heat Pipe (LHP), 10, 34, 121, 289

M

Mach number, 80
Manufacturing cycle, 401
Maximum capillary pressure, 61
Maximum Expected Operating Pressures (MEOP), 31
Maximum heat transport rate, 81
Mesh screen, fiberglass, 261
Multi-Mission RTG (MMRTG), 348

N

NaK coolant, 349
NASA/Ames (Hughes), 36
NASA/GSFC (Grumman and TRW), 36
Non-Condensable Gas (NCG), 23, 28, 49, 414
Non-Operating Thermal Environment, 258
Nuclear electric systems, 350

O

OAO-III, 36
Ocean Reconnaissance Satellites (RORSATs), 349
Ocean Thermal Energy Conversion (OTEC), 233

P

Partial Differential Equations (PDEs), 220, 326
Performance degradation, 405, 414
Perpendicular Rectangles with a Common Edge, 242
Phase Change Materials (PCMs), 368, 370–372, 374–377, 379, 383, 385–387, 389, 390
Photovoltaics (PV), 368
Pipe blockage, 422
Prandtl number, 236
Pumped Hydro-Power storage (PHPS), 369

R

Radioactive Heater Units (RHUs), 348
Radioisotope Thermoelectric Generators (RTGs), 347
Reciprocity, 243
Reduced Basis (RB), 240
Reynolds Number, 65
Romashka reactors, 349

S

SABCA, 37
SAFE-400 space fission reactor, 350
Seamless and butt welded, 396
Sensible Thermal Energy Storage Systems (STES), 370
Silicon Controlled Rectifiers (SCR's), 358
Skylab, 36
Small Business Innovation Research (SBIR), 288
Sound structural design, 427
Spiral artery design, 396
Steady-State Design, 212
Steady-State mode, 209
Stirling Radioisotope Generator (SRG), 348
Surface tension, 52

T

Thermal Energy Storage (TES), 369, 371, 386
Timberwind pebble bed reactor, 349
Tokamak, 350
Topaz reactors, 349
Total thermal capacity, 217
Turbulent flow, 64
Two Phase Flow, 68
Two-Dimensional analyses, 233

U

U.S. Department of energy SunShot, 385

V

Vapor pressure, 415
Vapor-pressure limitation, 133
Variable Conductance, 185
Variable Conductance Heat Pipe (VCHP), 12–14, 16, 28, 49, 431
Variable Cryogenic Heat Pipe, 213
Variable Specific Impulse Magneto plasma Rocket (VASIMR), 350
Ventilating, and Air Conditioning (HVAC), 2
Viscous limitation, 82, 133

W

Weber number, 86
Wick structure, 201, 255
Wicking limit, 88
Wick-liquid dynamics, 68
Working fluid, 399

Y

Young-Laplace equation, 52, 57, 58